

This Document  
Reproduced From  
Best Available Copy

AD-A013 073

METHODS FOR AIRCRAFT STATE AND PARAMETER  
IDENTIFICATION

Advisory Group for Aerospace Research  
and Development

Prepared for:

North Atlantic Treaty Organization

May 1975

DISTRIBUTED BY:

**NTIS**

National Technical Information Service  
U. S. DEPARTMENT OF COMMERCE

TV  
224106

(1)  
AGARD-CP-172

AGARD-CP-172

AD A013073

AGARD  
ADVISOR GROUP FOR AEROSPACE RESEARCH & DEVELOPMENT

BOULEVARD DE LA LIBERTE 100 PARIS 12 FRANCE

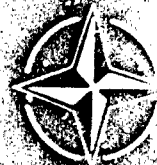
AGARD CONFERENCE PROCEEDINGS No. 172

on

# Methods for Aircraft State and Parameter Identification

12-19-1975  
Jr

NORTH ATLANTIC TREATY ORGANIZATION



Reproduced by  
NATIONAL TECHNICAL  
INFORMATION SERVICE  
U.S. Department of Commerce  
Springfield, VA. 22151

DISTRIBUTION AND AVAILABILITY

## **REPRODUCTION QUALITY NOTICE**

**This document is the best quality available. The copy furnished to DTIC contained pages that may have the following quality problems:**

- **Pages smaller or larger than normal.**
- **Pages with background color or light colored printing.**
- **Pages with small type or poor printing; and or**
- **Pages with continuous tone material or color photographs.**

**Due to various output media available these conditions may or may not cause poor legibility in the microfiche or hardcopy output you receive.**

☐ **If this block is checked, the copy furnished to DTIC contained pages with color printing, that when reproduced in Black and White, may change detail of the original copy.**

AD-A 013 073

REPORT DOCUMENTATION PAGE			
1. Recipient's Reference	2. Originator's Reference AGARD-CP-172	3. Further Reference	4. Security Classification of Document UNCLASSIFIED
5. Originator	Advisory Group for Aerospace Research and Development North Atlantic Treaty Organization 7 rue Ancelle, 92200 Neuilly sur Seine, France		
6. Title	Methods for Aircraft State and Parameter Identification		
7. Presented at	NASA Langley Research Center, Hampton, Virginia. U.S.A.		
8. Author(s) Various	9. Date May 1975		
10. Author's Address Various	11. Pages 436		
12. Distribution Statement	This document is distributed in accordance with AGARD policies and regulations, which are outlined on the Outside Back Covers of all AGARD publications.		
13. Keywords/Descriptors Fighter aircraft Transport aircraft Supersonic transports Vertical takeoff aircraft	Short takeoff aircraft Helicopters Systems engineering Mathematical models	14. UDC  629.73.05:629.735	
15. Abstract  Twenty-nine papers and comments are contained in these Proceedings. Several discuss and compare results obtained with different parameter identification techniques applied to specific fighter aircraft at high angles of attack, subsonic and supersonic transports, VTOL and STOL aircraft, and helicopters. Special problem areas such as systems modelling with high internally-generated fluctuations, aircraft state estimation in non-steady flight and parameter identification for non-linear aerodynamic regimes are covered. The sessions at the Specialists' Meeting were titled mathematical models, instrumentation and filters, flight test techniques, analysis of flight test data, rotorcraft parameter identification and selected topics.			

PRICES SUBJECT TO CHANGE



AGARD-CP-172

NORTH ATLANTIC TREATY ORGANIZATION  
ADVISORY GROUP FOR AEROSPACE RESEARCH AND DEVELOPMENT  
(ORGANISATION DU TRAITE DE L'ATLANTIQUE NORD)

AGARD Conference Proceedings No.172  
METHODS FOR AIRCRAFT STATE AND  
PARAMETER IDENTIFICATION

Papers presented at a Specialists' Meeting of the Flight Mechanics Panel of AGARD held at  
NASA Langley Research Center, Hampton, Virginia, USA on 5-8 November 1974.

## THE MISSION OF AGARD

The mission of AGARD is to bring together the leading personalities of the NATO nations in the fields of science and technology relating to aerospace for the following purposes:

- Exchanging of scientific and technical information;
- Continuously stimulating advances in the aerospace sciences relevant to strengthening the common defence posture;
- Improving the co-operation among member nations in aerospace research and development;
- Providing scientific and technical advice and assistance to the North Atlantic Military Committee in the field of aerospace research and development;
- Rendering scientific and technical assistance, as requested, to other NATO bodies and to member nations in connection with research and development problems in the aerospace field;
- Providing assistance to member nations for the purpose of increasing their scientific and technical potential;
- Recommending effective ways for the member nations to use their research and development capabilities for the common benefit of the NATO community.

The highest authority within AGARD is the National Delegates Board consisting of officially appointed senior representatives from each member nation. The mission of AGARD is carried out through the Panels which are composed of experts appointed by the National Delegates, the Consultant and Exchange Program and the Aerospace Applications Studies Program. The results of AGARD work are reported to the member nations and the NATO Authorities through the AGARD series of publications of which this is one.

Participation in AGARD activities is by invitation only and is normally limited to citizens of the NATO nations.

The content of this publication has been reproduced directly from material supplied by AGARD or the authors.

Published May 1975

Copyright © AGARD 1975

629.73.05:629.735

National Technical Information Service is authorized to reproduce and sell this report.



*Printed and edited by Technical Editing and Reproduction Ltd  
Harford House, 7-9 Charlotte St, London, W1P 1HD*

## PREFACE

The Flight Mechanics Panel Specialists' Meeting on "Method for Aircraft State and Parameter Identification" was held so that flight test engineers and pilots, handling qualities and simulation experts, and aircraft and flight control system designers could share their understanding, knowledge and experience in the area of aircraft systems identification.

Although the essential aircraft characteristics can be partially predicted with rather satisfactory accuracy by means of theoretical calculations and wind-tunnel measurements, the demand for more precise, experimentally determined aircraft flight mechanics parameters has increased. These characteristics can lead to a mathematical aircraft model with which investigations may be made of specific flight conditions of interest. This approach can significantly reduce the amount of flight testing required and consequently can decrease testing time and costs as well as increase test safety.

The requirements for exact and reliable stability and control coefficients are based on the following applications:

- (i) Proving the flying qualities as specified by the aircraft users and improving the flight vehicles themselves.
- (ii) Optimizing the design of automatic control and stability augmentation systems. The stability and control characteristics of the vehicle in which these systems are to be applied must be known accurately before the desired optimization can be mechanized.
- (iii) Producing the baseline data needed for flight simulations. This applies to either basic computer simulations, to fixed and moving base ground simulators or to in-flight simulations. Testing organizations, industry and the users of flight vehicles are intensely interested in this application.
- (iv) Providing data for comparisons with results from purely analytical aircraft modeling techniques and wind-tunnel measurements.
- (v) Improving testing and data evaluation methods in general. The necessity for this application is based on current economic considerations and the fact that results from prototype testing contribute more and more to production decisions.

The Specialists' Meeting indicated that in recent years several new identification procedures have evolved for obtaining aircraft parameters from in-flight measurements. These approaches have been successfully applied to conventional (winged) aircraft and are practical techniques. The Specialists' Meeting further confirmed that assumptions which are widely used to simplify the mathematical model of the basic aircraft are acceptable. In this regard, it is well-known that conventional aircraft, even at extreme conditions in their flight envelopes, usually possess distinctive characteristic modes of motions with different frequencies (short-period, phugoid, Dutch roll and spiral modes) and that these modes normally can be identified and separated fairly easily.

The parameter identification problem becomes a much more complicated task when applied to large and slender-body aircraft for which the elastic deformations at high dynamic pressures can no longer be neglected. For helicopters, simplifying assumptions are, in general, considerably more difficult to make due to the strong coupling of the rigid body degrees-of-freedom and because of the different flexible motions introduced by the rotor blades. An additional problem in parameter identification for helicopters lies in the shortness of the test period which can be recorded due to the inherent instability of these vehicles. This is one of the reasons why, up until this time, relatively little work has been accomplished in identification of rotorcraft characteristics.

The papers presented at the Specialists' Meeting offer an excellent overview of the present state-of-the art of systems identification in relation to flight testing. It was found that interest is concentrated primarily in a few procedures; namely, in the relatively easy analysis methods such as the time vector, regression analysis and frequency response techniques or in the more advanced maximum-likelihood method with its developments. It can be concluded that with the application of the more advanced methods, the ever progressive mathematical development is leading to a continuously increasing requirement for computation time. On the other hand, a certain inertia exists among users whose experience exists in applying any one of these procedures and who wish to continue working with that specific technique for the time being. It was frequently noted during the discussions at the Specialists' Meeting that a person with a good physical understanding of the problem could often obtain, with a simplified procedure, results as good as those obtained by a person with a more complicated approach but little insight into the physical problem. Further, it was noted that the quality of the results could be increased not only by improving the flight test analysis method but also through the application of optimum input signals and improved flight test instrumentation.

At the final round table discussion of the Specialists' Meeting it was concluded that at the present time linear stability and control derivatives can be determined from flight test data in a routine manner using either simple or sophisticated methods. Nevertheless, the application of parameter identification techniques to each flight test program must be considered individually depending on the goals or objectives of that testing. Further, problems can develop rapidly when the linearity assumptions for the aerodynamic model are no longer valid, such as in situations with flow separation at high angles of attack or unsteady aerodynamics due to quick responsive control

surfaces. Finally, there was a strong plea to increase the confidence level of the aircraft parameters derived from flight tests by demonstrating their repeatability through the use of different maneuvers, control system inputs and turbulence inputs.

**P.HAMEL**  
Member  
Flight Mechanics Panel

**William AIKEN, Jr**  
Member  
Flight Mechanics Panel

<b>PREFACE</b>	<b>Page</b> iii
 <b><u>SESSION I - MATHEMATICAL MODELS</u></b>	
<b>MODELLING OF SYSTEMS WITH A HIGH LEVEL OF INTERNAL FLUCTUATIONS</b> by J.G.Jones	<b>Reference</b>  1
<b>IDENTIFICATION OF NON-LINEAR AERODYNAMIC STABILITY AND CONTROL PARAMETERS AT HIGH ANGLE OF ATTACK</b> by B.J.Eulrich and E.G.Rynaski	 2
<b>METHODS USED FOR OPTIMIZING THE SIMULATION OF "CONCORDE S.S.T." USING FLIGHT TEST RESULTS</b> by J.Tardy	 3
<b>APPLICATION OF A NEW CRITERION FOR MODELING SYSTEMS</b> by L.W.Taylor, Jr	 4
 <b><u>SESSION II - INSTRUMENTATION AND FILTERS</u></b>	
<b>A MONTE CARLO ANALYSIS OF THE EFFECTS OF INSTRUMENTATION ERRORS ON AIRCRAFT PARAMETER IDENTIFICATION</b> by W.H.Bryant and W.F.Hodge	 5
<b>ADVANCED FLIGHT TEST INSTRUMENTATION: DESIGN AND CALIBRATION</b> by R.J.A.W.Hosman	 6
<b>A COMPLEMENTARY FILTERING TECHNIQUE FOR DERIVING AIRCRAFT VELOCITY AND POSITION INFORMATION</b> by F.R.Niessen	 7
<b>SENSORS AND FILTERING TECHNIQUES FOR FLIGHT TESTING THE VAK 191 AND VFW 614 AIRCRAFT</b> by W.E.Seibold	 8
 <b><u>SESSION III - FLIGHT TEST TECHNIQUES</u></b>	
<b>DESIGN AND EVALUATION OF A SYMMETRIC FLIGHT-TEST MANOEUVRE FOR THE ESTIMATION OF LONGITUDINAL PERFORMANCE AND STABILITY AND CONTROL CHARACTERISTICS</b> by H.W.Klingeld	 9
<b>DETERMINATION OF STABILITY DERIVATIVES FROM FLIGHT TEST RESULTS - COMPARISON OF FIVE ANALYTICAL TECHNIQUES</b> by H.Wünnenberg, H.Friedrich, U.von Meier and H-J.Munser	 10
<b>FIVE IDENTIFICATION METHODS APPLIED TO FLIGHT TEST DATA</b> by J-P.Chaquin	 11
<b>STATUS OF INPUT DESIGN FOR AIRCRAFT PARAMETER IDENTIFICATION</b> by R.K.Mehra and N.K.Gupta	 12
<b>INPUT DESIGN FOR AIRCRAFT PARAMETER IDENTIFICATION: USING TIME-OPTIMAL CONTROL FORMULATION</b> by R.T.N.Chen	 13
<b>DETERMINATION OF AERODYNAMIC DERIVATIVES FROM TRANSIENT RESPONSES IN MANOEUVRING FLIGHT</b> by A.J.Ross	 14

<b>ADVANCEMENT IN PARAMETER IDENTIFICATION AND AIRCRAFT FLIGHT TESTING</b> by R.A.Burton	<b>Page</b> 15
---------------------------------------------------------------------------------------------	-------------------

#### SESSION IV – ANALYSIS OF FLIGHT TEST DATA

<b>PRACTICAL ASPECTS OF USING A MAXIMUM LIKELIHOOD ESTIMATOR</b> by K.W.Illiff and R.E.Maine	16
<b>DETERMINATION OF AIRCRAFT DERIVATIVES BY AUTOMATIC PARAMETER ADJUSTMENT AND FREQUENCY RESPONSE METHODS</b> by M.Marchand and R.Koehler	17
<b>A COMPARISON AND EVALUATION OF TWO METHODS OF EXTRACTING STABILITY DERIVATIVES FROM FLIGHT TEST DATA</b> by P.W.Kirsten	18
<b>ESTIMATION OF THE AIRCRAFT STATE IN NON-STEADY FLIGHT</b> by J.A.Mulder	19
<b>DETERMINATION OF STABILITY DERIVATIVES FROM FLIGHT TEST RESULTS BY MEANS OF THE REGRESSION ANALYSIS</b> by H.Friedrich	20
<b>MODEL STRUCTURE DETERMINATION AND PARAMETER IDENTIFICATION FOR NON-LINEAR AERODYNAMIC FLIGHT REGIMES</b> by W.E.Hall, Jr, N.K.Gupta and J.S.Tyler, Jr	21

#### SESSION V – ROTORCRAFT PARAMETER IDENTIFICATION

<b>IMPORTANCE OF HELICOPTER DYNAMICS TO THE MATHEMATICAL MODEL OF THE HELICOPTER</b> by W.F.White, Jr	22
<b>ESTIMATES OF THE STABILITY DERIVATIVES OF A HELICOPTER AND A V/STOL AIRCRAFT FROM FLIGHT DATA</b> by D.G.Gould and W.S.Hindson	23
<b>ROTORCRAFT DERIVATIVE IDENTIFICATION FROM ANALYTICAL MODELS AND FLIGHT TEST DATA</b> by J.A.Molusis	24
<b>ROTOR SYSTEMS RESEARCH AIRCRAFT (RSRA) – REQUIREMENTS FOR, AND CONTRIBUTIONS TO, ROTORCRAFT STATE ESTIMATION AND PARAMETER IDENTIFICATION</b> by G.W.Condon	25
<b>COMMENTS ON COMPUTATION OF AIRCRAFT FLIGHT CHARACTERISTICS</b> by C.L.Livingston	26

#### SESSION VI – SELECTED TOPICS

<b>THE EFFICIENT APPLICATION OF DIGITAL IDENTIFICATION TECHNIQUES TO FLIGHT DATA FROM A VARIABLE STABILITY V/STOL AIRCRAFT</b> by J.V.Lebacqz	27
<b>PARAMETER ESTIMATION OF POWERED-LIFT STOL AIRCRAFT CHARACTERISTICS INCLUDING TURBULENCE AND GROUND EFFECTS</b> by R.C.Wingrove	28
<b>ESTIMATION OF ELASTIC AIRCRAFT AERODYNAMIC PARAMETERS</b> by R.C.Schwanz and W.R.Wells	29

## MODELLING OF SYSTEMS WITH A HIGH LEVEL OF INTERNAL FLUCTUATIONS

by

J.C. Jones  
 Royal Aircraft Establishment  
 Bedford, England

## SUMMARY

This paper is concerned with systems with a high level of internally-generated fluctuations. The problem of modelling the structure of such systems is discussed and some problems in parameter identification are reviewed.

The systems considered typically have two types of behaviour, determined by the magnitude of a controlling parameter which influences stability. For a finite range of parameter values the system is stable and its structure may be described by a deterministic set of differential equations. If not subjected to external disturbances the system will achieve a state of equilibrium. At some 'critical' value of the parameter, however, the system becomes unstable and beyond this boundary the system no longer achieves a state of equilibrium but may exist (as a result of nonlinearities) in a steady state typified by continuous fluctuations. This state may either be described as a regular limit-cycle type of oscillation or may be essentially random in nature.

Practical examples include aircraft buffeting and wing-rocking, forms of fluctuating motion which occur respectively in structural and rigid-body modes. In these examples aircraft incidence may be regarded as the controlling parameter and the fluctuating motion is associated with the existence of extensive areas of separated flow at high incidence.

Another example of aeronautical interest, whose structure falls into the type considered, is the standard human-pilot model in which the internal fluctuations are represented by a 'remnant'. An example is discussed which illustrates problems that can arise in the identification of this type of system when operating as part of a closed loop.

## 1. PRELIMINARY

Aircraft buffeting and wing-rocking under high-g manoeuvre conditions are instances of system behaviour characterized by a high level of internally-generated fluctuations, associated with the characteristic unsteadiness of separated flow<sup>1,2</sup>. As aircraft speed is increased from subsonic into the transonic range, the angle of attack at which these undesirable features occur tends to decrease; indeed, at transonic speeds steady conditions may not exist even in the case of flight at 1 g (straight and level in the mean). Since such forms of fluctuating motion clearly have an adverse effect on the manoeuvre capability of high performance aircraft, it is of great practical interest to be able to understand and predict these characteristics; thus methods for aircraft state and parameter identification need to be developed to cover such situations. In contrast to flight at lower angles of attack and relatively low speeds, where the forms of the relevant mathematical models are relatively well understood and research interest lies largely in the development of improved methods for the identification of the parameters in prescribed equations, conditions of high angle-of-attack and/or transonic speeds require further work on the formulation and validation of theoretical model structures, as a preliminary to parameter identification. It is to this problem of formulating appropriate model structures that the present paper is largely orientated.

Current interest in aircraft buffeting is largely concerned with manoeuvres of combat aircraft at high subsonic speeds, where the existence of shock-induced separations plays a primary role. A related problem, mainly associated with work on high performance compressor and helicopter blades, is the oscillatory motion of a stalled airfoil in such a manner that the nature of the flow separation differs at different instants in the cycle, possibly switching from attached to separated flow or from a leading-edge to a trailing-edge stall. This phenomenon, known as stall-flutter, is usually associated with a marked torsional (pitching) airfoil motion. The affinity between buffeting and stall-flutter has been discussed by Fung<sup>3</sup> who pointed out that there may be situations where it is difficult to make the distinction.

We shall be concerned with overall 'systems' which comprise a dynamically-responding wing in association with a flow field which may be separated. In particular, we shall consider situations where such a system becomes unstable, where the loss of stability may involve the mutual interaction between wing and flow field or may be purely hydrodynamic, manifesting itself in the latter case by the growth to macroscopic magnitudes of disturbances in the (usually separated) flow field. The systems considered are often found to have two types of behaviour, determined by the value of a controlling parameter, such as angle-of-attack or airspeed, which influences stability. For a finite range of parameter values the system, if not subjected to external disturbances, remains in a state of equilibrium typified by constant values of its state variables. At some critical value of the controlling parameter (a 'bifurcation' value<sup>4</sup>), however, the system becomes unstable and beyond this value it no longer achieves a state of equilibrium but may exist, as a result of nonlinearities, in a steady state of continuous fluctuation. Such a fluctuating state may in some cases be modelled mathematically as a regular limit-cycle oscillation, or it may be essentially random in nature.

A basic feature of such fluctuating systems is the interaction between the fluid motion, involving separated flow, and the motion of the wing surface. We distinguish between two cases, differing in the nature of this interaction. The first we refer to as a FORCED VIBRATION. This consists of an irregular random motion in which 'turbulent' pressure fluctuations which are independent of wing motion produce an aerodynamic driving force, the consequent motion of the wing producing an additional, additive, motion-dependent pressure field. The appropriate analytical model in this case is 'non-autonomous', involving a random forcing term explicitly expressible as a function of time. The theoretical model describing the wing motion, for a prescribed random force of excitation, may often take the form of linear equations.

However, nonlinearity plays an essential role in an overall view of the situation as it dominates the process of energy transfer, within the airflow, by which energy is extracted from the mean flow and channelled into the fluctuations of the aerodynamic driving force.

The second case we refer to as **NONLINEAR FLUTTER**. Here, more-or-less regular oscillations of a stalled wing occur, in which the time-varying pressure field is essentially determined by the past history of wing motion. The appropriate analytical model is 'autonomous' and involves no significant terms explicitly expressed as functions of time. This type of motion is also known as a limit-cycle, and a non-linear analytical model is essential. It includes stall-flutter as a particular case. In contrast to 'forced vibration', the nonlinear mechanism of energy transfer from the mean airflow now involves the motion of the wing in addition to the unsteady motion of the air. The essential distinction between the two phenomena is that in the former case we may say that the wing motion is 'forced' by the fluctuating flow field, whereas in the latter case the joint motion of wing and flow field arises as a mutual interaction.

In some situations the amplitude of wing motion is a relevant parameter, motion of small amplitude leaving the turbulent fluctuations in the separated flow similar to those that would occur in the flow past a rigid wing but leading to an additive, motion-dependent, pressure field. As the amplitude of wing motion is increased, however, the possibility arises of the 'entrainment' of the larger-scale irregular flow fluctuations into a deterministic relationship with the wing motion. This type of resonance is of course most likely if the frequency of wing motion (Strouhal number) is close to some natural frequency of vorticity shedding in the separated flow.

Whilst it is customary to regard wing structural buffeting as an aerodynamically forced vibration, in which the forcing term can in principle be obtained from measurements on a rigid wing, more basic research is required to determine the limits of applicability of this approach. Even in cases where the buffeting wing is appropriately regarded as aerodynamically forced, the relationship between the forces on the structurally-responding wing and on a geometrically similar but rigid wing is not necessarily straightforward. In particular, there is the possibility that the motion of the wing may interfere with the non-linear process by which energy is transferred from the mean flow to the fluctuating fluid motion and thus modify the statistical characteristics of the aerodynamic exciting force. The clarification of these topics is of considerable practical importance in that they determine the circumstances in which rigid wind-tunnel models may be used as the basis for estimation of intensity of buffeting of full-scale aircraft.

An analogous problem concerning the choice of appropriate theoretical model occurs in connection with wing-rocking. Should a state of steady wing-rocking be regarded as aerodynamically forced or in terms of limit-cycle oscillations of a closed-loop system whose motion remains bounded through the action of amplitude-dependent nonlinear forces? In the latter case a unified treatment of wing-rocking and the divergent motions known as 'wing-dropping' and 'nose-slice' may be possible, the distinction arising primarily in the nature of the (nonlinear) forces at large amplitude, stabilising in the case of wing-rocking but not in the other cases. An important area of current work is the determination of appropriate characteristics that may be identified using wind-tunnel models to indicate the onset of wing-rocking of the full-scale aircraft. Two types of criterion are possible, one based on the appearance of a significant random **FLUCTUATING** component in the aerodynamic forces (or moments) and the other, based on the **MEAN** component of the aerodynamic forces, indicating either a loss of dynamic stability for small perturbations about some high-lift equilibrium condition, or a loss of equilibrium due to asymmetry. For example, one might expect the appearance of fluctuating forces or moments on a rigidly-mounted wind-tunnel model to correlate in general with a dynamic situation appropriately modelled as an aerodynamically forced vibration. Conversely, we might expect the measurement of mean aerodynamic forces that indicate a loss of dynamic stability or equilibrium to correlate with a dynamic divergence or, under the action of appropriate amplitude-dependent forces, with fluctuating motion of the limit-cycle, or non-linear flutter, type. However, exceptions to this association of onset criteria with types of dynamic motion can occur. For instance, the appearance of random fluctuating forces on a rigidly-mounted model may correlate with a dynamic situation in which the fluctuations in the flow field become deterministically related to wing motion, leading to nonlinear flutter. Moreover, it is quite possible for the two types of criterion to be satisfied simultaneously, fluctuating aerodynamic forces occurring in conjunction with destabilising changes in the mean force or moment curves.

Another example of aeronautical interest, where the theoretical model of a system is required to represent spontaneous fluctuations in addition to the response to external inputs, is the standard human-pilot model<sup>5</sup> in which the internal fluctuations are represented by a 'remnant'. This remnant, or internal noise source, can be due to such things as sampling effects and random errors of judgement or may be partly an intentional signal injected by the pilot as a means of monitoring the response of the controlled system. An example will be discussed which illustrates the problems that can arise in the identification of this type of system when it is coupled into a 'closed-loop' (as the human pilot is coupled to the system he controls).

## 2. MATHEMATICAL MODELS

### 2.1 GENERAL OUTLINE

A common element of the buffeting and wing-rocking phenomena discussed in the previous section is the interaction between the unsteady fluid motion, involving separated flow, and the motion of the wing. In this section we clarify the ways in which a mathematical formulation of these and related phenomena may be made.

We begin by considering the influence of time-varying boundary conditions, applied at the surface of a wing, upon a rotational flow field. Two cases can be distinguished:



## (a) Random flow field

Substantially different flow time histories follow from nominally identical realisations of the boundary conditions. Thus, corresponding to given boundary conditions, there exists a whole family of compatible flow fields. Quantitative analysis is concerned with statistical properties, such as means and correlations, of such a family.

## (b) Deterministic flow field

The flow field at any instant depends uniquely upon the past history of boundary conditions. A separated flow field of this type depends upon the orderly shedding of vorticity from the boundary.

In the above distinction between random and deterministic flow fields the time-varying boundary conditions may either be externally imposed, by forcing the wing to follow some prescribed time history, or may arise through the structural response of the wing to aerodynamic forces. In the latter case the wing motion becomes one of the unknowns in the dynamic equations and we have a 'closed-loop' interaction.

The interaction between fluid motion and wing motion may be described in 'systems analysis' terms (Fig.1). The simplest 'closed-loop' system representation arises when the flow field is deterministic, depending uniquely upon the past history of wing motion. As illustrated in Fig.1a there are in this case two independent deterministic relationships between the wing motion and the aerodynamic force (a generalised force, appropriate to the mode of response in question, taking the form of a weighted integral of pressures over the structure). One relationship is obtained from the equations of motion of the structure; and since the flow field is uniquely dependent upon the past history of wing motion we can, in principle, deduce a second relationship between wing motion and aerodynamic force from the equations of motion for the fluid. The joint time variation of wing motion and aerodynamic force may then be deduced as that compatible with these two independent relationships. The closed-loop system may be referred to as 'autonomous' or 'self-excited' and the motion takes the form of a limit cycle. Whilst the structural response can often be adequately defined using linear equations, the fact that two INDEPENDENT functional relationships exist between aerodynamic force and wing motion requires that the aerodynamic feedback loop be non-linear (we exclude the trivial case where the closed loop fluctuations take the form of sinusoidal oscillations of a linear system in neutral equilibrium). We will refer to all such types of motion as NONLINEAR FLUTTER.

A particular type of autonomous oscillation, the case of single-degree-of-freedom flutter, has been discussed in some detail by Lambourne<sup>6</sup>. Many examples of this phenomenon can be described approximately by a second-order differential equation in which a nonlinear damping, or in-quadrature, term is negative for small amplitudes but positive for large amplitudes. One simple example of such motion concerns the behaviour of smoke stacks and has been described by Scruton<sup>7</sup>. The representation of such behaviour using differential equations with amplitude-dependent rate terms is, however, in general an oversimplification based on the assumption that a single sinusoidal harmonic dominates the motion. More generally, the past history of motion needs to be taken explicitly into account because of its effect on the aerodynamic force through the current distribution of vorticity in the fluid. In this situation the system cannot be described by differential equations, integral terms with respect to time being required. Such representations, involving forces dependent upon the past history of motion, may be given a unified treatment using the theory of 'functionals'. This point of view is adopted, in particular, in Refs.8 and 9. Its practical value lies largely in the clarification of the significance of various approximations. For example, the usual treatment of aircraft stability in terms of 'aerodynamic derivatives' may be derived from a formulation in terms of functionals by means of a Taylor series expansion of the functions involved. Alternatively, we record that some success has been obtained<sup>10,11</sup> by making use of an approximation in which integral terms, representing time-lag effects, are concentrated into one single time lag.

A second representation of the interaction between fluid motion and wing motion arises in the case where the flow field is random, differing flow time-histories following from identical realisations of wing motion. The appropriate system formulation then takes the form illustrated in Fig.1b where two components of aerodynamic force are shown separated, one determined by, and one independent of, wing motion. Two particular cases of this formulation may be distinguished. In the first case the combination (indicated in Fig.1b by a dashed line) of structural response and motion-dependent aerodynamic force forms a stable system which, left to itself, would settle down to a state of equilibrium. In conjunction with the motion-independent component of aerodynamic force this is the FORCED VIBRATION model for the interaction. The motion-dependent aerodynamic force may be linear or nonlinear. In the second case the feedback loop itself produces self-excited oscillations (for which nonlinearity of the motion-dependent aerodynamic force is an essential condition) and we have the situation of an essentially autonomous system disturbed by random noise. Whilst this latter theoretical model is at present little used in practice it is required conceptually if we wish to consider a continuous transition between aerodynamically forced vibration and nonlinear flutter.

In practical applications of the forced-vibration model (Fig.1b) the motion-dependent force is generally taken to be linear. In addition, several further assumptions are often made which require critical examination. For example, it is usually assumed that the aerodynamic excitation, or motion-independent aerodynamic force, is relatively wide-band with a power spectral density that is approximately constant over the effective bandwidth of response. As reviewed in Refs.1 and 2, this assumption enables the total damping of the closed-loop system to be simply deduced from the power spectrum (or autocorrelation function) of wing motion (Fig.1b). A method commonly proposed to obtain the power spectrum of aerodynamic excitation is to make measurements on a rigid (non-moving) wing with identical geometry. However, the assumption that the aerodynamic excitation of the structurally responding system is the same as the aerodynamic force on a rigid (and rigidly-mounted) wing is itself a further hypothesis. For, whilst the aerodynamic excitation of the system illustrated in Fig.1b is 'motion-independent' in the sense that it may be regarded as an 'external noise generator', the STATISTICAL PROPERTIES (such as power spectral density) of this force may in principle depend on the mean amplitude of structural motion. This possibility appears to have been first discussed in Ref.12. Since we cannot necessarily simply relate the aerodynamic forces on the responding wing illustrated in Fig.1b to forces measured on a rigid wing (or for

that matter relate the forces on two structurally-responding wings with differing structural properties) the question arises as to how the separation into 'motion-dependent' and 'motion-independent' components of aerodynamic force may be made conceptually. The only measurable quantities on the responding wing are the fluctuating pressures on the structure, which may in principle be integrated to give the total aerodynamic force, and the structural motion. However, nothing about the decomposition of aerodynamic forces can be learnt from the relationship (e.g. cross-correlation) between total aerodynamic force and wing motion, as this relationship is completely determined by the transfer function representing the response of the structure (Fig.1b). A similar comment applies to the cross-correlation of wing motion and individual fluctuating pressures at points on the wing: such a cross-correlation function in general depends on a combination of the 'transfer function' representing the motion-dependent aerodynamic pressure field and the transfer function representing the structure (see Ref.2). Consequently, in principle, the only way to separate the motion-dependent and motion-independent components of aerodynamic force on a structurally-responding wing is to introduce an external 'test-signal' (such as an additional force, Fig.2). Such a signal must be large enough to produce measurable components both in total aerodynamic force and in wing motion, and yet, in order not to change the quantities being measured, not so large as to significantly alter the mean amplitude of wing motion. As described in section 6 (see equation (17)) the aerodynamic transfer function relating the motion-dependent aerodynamic force to the motion of the wing may then in principle be identified as a ratio of cross-spectra. (Note: if the system is in fact linear, this method will quantitatively identify it. If it is nonlinear, the method will identify<sup>5</sup> the best linear fit, in a mean-square error sense, or 'linear describing function'.) It should be emphasised that the use of a test signal has been introduced here as a conceptual device, to show that meaningful definitions of the two components of aerodynamic force are possible. It is not suggested as a practical experiment, because of both the difficulty of introducing and measuring such additional forces in wind-tunnel tests and the uncertainties introduced in the integration of fluctuating pressures to obtain generalised aerodynamic forces.

If we do make the assumption that the aerodynamic excitation may be obtained from measurements on a rigid wing and are also able to obtain numerical estimates for the motion-dependent aerodynamic force (of which, in the case of wing flexible response, the most significant component is usually aerodynamic damping) the forced-vibration model provides the basis of a method for predicting the amplitude of the closed-loop response on the basis of rigid-wing measurements (see Refs.1 and 2). It is therefore also of practical importance to know whether the existence of separated flow significantly affects motion-dependent forces such as aerodynamic damping. There is now substantial evidence<sup>1,13,28</sup> that there may be a significant change of damping under these circumstances. For example, in the case of wing structural buffeting at high subsonic speeds measurements indicate<sup>1</sup> relatively large increases in aerodynamic damping around the buffet - onset condition. A possible mechanism to explain this phenomenon, in terms of the (quasi-static) variation with wing incidence of the area over which a leading-edge suction force acts, has been proposed in Ref.13.

## 2.2 SOME RELEVANT MODELS FROM MECHANICS, PHYSICS AND ELECTRICAL ENGINEERING

As a guide to the range of theoretical models that are available to represent systems with a high level of internal fluctuations we briefly review in this section some concepts and equations from mechanics, physics and electrical engineering.

The simplest equation of randomly forced motion arises in physics in the Langevin form of the theory of Brownian motion, where the velocity of a particle suspended in a viscous fluid obeys the equation of motion

$$m \frac{dv}{dt} = -\zeta v + F(t) \quad , \quad (1)$$

where  $\zeta$  is a friction coefficient and  $F(t)$  is a fluctuating force associated with the thermal motion of molecules. The ensemble average of the fluctuating force is zero, and its second moment is given (employing standard notation) by the fluctuation-dissipation theorem

$$\langle F(t)F(t') \rangle = 2k_B T \zeta \delta(t - t') \quad . \quad (2)$$

In the elementary theory of Brownian motion,  $F(t)$  is assumed to be a Gaussian process, so that it is fully determined by the mean value and second moment. The relationship (2) between  $\zeta$  and  $F(t)$  derives from the fact that both  $\zeta$  (damping) and  $F$  (excitation) arise from collisions with surrounding molecules.

More generally, the evolution of a set of dynamical variables  $\{a_k\}$  has been described by a (linear) generalised set of Langevin equations of the form

$$\frac{d}{dt} a_k = \sum_l \Omega_{kl} a_l - \int_{-\infty}^t ds \sum_l \phi_{kl}(t-s) a_l(s) + F_k(t) \quad , \quad (3)$$

where  $F_k(t)$  is again a fluctuating force with zero mean. The 'memory' kernels  $\phi_{kl}$  describe the current effect of the past history of the system and in the generalised theory of transport coefficients<sup>14</sup> are related to the  $F_k(t)$  by an extension of equation (2). We may introduce frequency dependent coefficients  $\gamma_{kl}(\omega)$  by:

$$\gamma_{kl}(\omega) = \int_0^{\infty} dt \exp(-i\omega t) \phi_{kl}(t) .$$

When the memory of the system is short, or

$$\phi_{kl}(t) \approx 2\gamma_{kl}\delta(t) ,$$

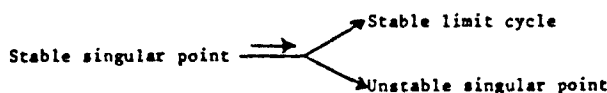
then the resulting  $\gamma_{kl}(\omega)$  are approximately independent of frequency and the set of equations (3) takes the 'Markovian' (or memory-less) form

$$\begin{aligned} \frac{d}{dt} a_k &= \sum_l (\Omega_{kl} - \gamma_{kl}) a_l + F_k(t) , \\ &= \sum_l A_{kl} a_l + F_k(t) . \end{aligned} \quad (4)$$

In the above, it is assumed that the sets of equations (3) and (4) represent stable systems. Thus, if the excitation terms  $F_k(t)$  are dropped, the motion of the system decays and a state of equilibrium is achieved.

The next step is to assume that the coefficients  $\Omega_{kl}$ ,  $\phi_{kl}$ ,  $A_{kl}$  are dependent upon a controlling parameter  $\lambda$  which influences stability. For a finite range of parameter values the system is assumed to be stable and its structure is described by the above sets of (integro-) differential equations. At some 'critical' magnitude of the parameter,  $\lambda_0$ , however, let us assume that the system becomes unstable.

The value  $\lambda = \lambda_0$  is then known as a 'bifurcation value' of the parameter<sup>4</sup>. (More generally, a sequence of bifurcations  $\lambda = \lambda_0, \lambda_1, \lambda_2, \dots$  may be defined.) As  $\lambda$  passes through the value  $\lambda_0$  a qualitative change occurs in the behaviour of the system. On the assumption that when  $\lambda > \lambda_0$ , the subsequent motion remains bounded, one possibility is that, instead of decaying to a state of equilibrium ( $F_k = 0$ ) or fluctuating about the equilibrium state under the influence of forces of excitation ( $F_k \neq 0$ ), the system oscillates in a regular limit-cycle. A standard example, from electrical engineering, is the electron tube oscillator. In the simplest case of *soft* self-excitation<sup>4</sup>, the bifurcation then occurs as follows. If the parameter  $\lambda$  (in this case the parameter is the coefficient of mutual inductance between anode and grid circuits) is sufficiently small ( $\lambda < \lambda_0$ ) the circuit operates as an amplifier and, if there is no signal, one has the state of rest. If  $\lambda$  increases up to the bifurcation value  $\lambda = \lambda_0$  the circuit is just on the threshold between two modes of operation. For  $\lambda > \lambda_0$  a self-sustained oscillation appears and its amplitude begins to grow with  $\lambda$ . Minorsky<sup>4</sup> illustrates the passage of  $\lambda$  through its bifurcation value  $\lambda = \lambda_0$  by the following scheme:



which justifies the term 'bifurcation'.

The phenomenon of *hard* self-excitation is similar except that the limit cycle appears suddenly as soon as the boundary  $\lambda = \lambda_0$  is crossed; that is, its amplitude does not grow steadily from zero with increasing  $\lambda$  as in the 'soft' case.

More generally, bifurcation is possible from two types of stable equilibrium state. One possibility is that for values of  $\lambda < \lambda_0$ , in the neighbourhood of the bifurcation value, the perturbations about the stable equilibrium state correspond to complex values of the normal mode frequencies. The equilibrium state is then a stable 'focus'; the loss of stability at  $\lambda = \lambda_0$  is associated with loss of damping and is referred to as 'flutter'. With appropriate nonlinearities, for  $\lambda > \lambda_0$  the system may approach in time a periodic state (limit-cycle) whose characteristics are independent of the initial conditions. The bifurcation then takes the particular form



The other possibility is that, for values of  $\lambda < \lambda_0$  in the neighbourhood of the bifurcation value, the imaginary part of the relevant root vanishes. The equilibrium state is then a node. The loss of stability is in this case associated with loss of stiffness and the condition at  $\lambda = \lambda_0$  corresponds to onset of 'divergence'. With appropriate nonlinearities a stable equilibrium state may however exist for values of  $\lambda > \lambda_0$  (as in the buckling of struts). A characteristic of such an equilibrium state is its asymmetry; in some cases we find two 'mirror-image' stable states (cf. the buckled state). We can again use the terminology of 'soft' and 'hard' modes depending upon whether or not the bifurcation corresponds to the establishment of nonlinear equilibrium configurations with continuously growing amplitude as  $\lambda$  increases beyond the value  $\lambda_0$ . In the case of a conservative system the soft mode case may be described by the continuous appearance of a pair of 'potential wells' (Fig.3).

In our discussion of 'bifurcation from a focus', we stressed the importance of nonlinearity for the establishment of a steady fluctuating state of limit-cycle form. Mention should also be made of the possible influence of hysteresis on the existence of such an oscillation. For example, Lambourn<sup>15</sup> has described a type of limit-cycle, in the context of oscillations occurring with aircraft control surfaces in transonic flow, where hysteresis in the form of 'switching' between two states of the flow field, plays an essential role. This example is interesting as it describes a mechanism whereby divergence from an unstable node (i.e. loss of stiffness) can lead to a state of oscillation. This mechanism, which depends on the existence of asymmetric 'buckled' states which are statically stable but dynamically unstable, is in fact closely related to the flutter of buckled panels described in Ref.16.

In the above discussion of bifurcations and their possible consequences, we have ignored excitation terms such as the  $F_k(t)$  in equations (3) and (4). However, even if the  $F_k(t)$  are of small amplitude, their existence will have a significant influence when  $\lambda$  approaches a bifurcation value  $\lambda_0$ , in the sense that a microscopic input to the system will lead to a macroscopic response. For instance, in physical systems undergoing a phase transition, one often finds a dynamical mode the frequency of which goes to zero at the transition and a soft mode appears. The existence of such a soft mode is intimately related to the occurrence of 'critical' fluctuations of macroscopic amplitude. Moreover, for values of  $\lambda$  only slightly larger than  $\lambda_0$ , the existence of such fluctuations can lead to the mean state 'jumping' from one equilibrium configuration to another (e.g. between the two potential wells in Fig.3). The probability distribution for the state of such a system could thus be bi-modal with high probability densities near the two equilibrium configurations and relatively low elsewhere.

Another possible effect of the inclusion of excitation terms  $F_k(t)$  is the 'triggering-off' of a 'hard' mode before  $\lambda$  has in fact reached the bifurcation value  $\lambda_0$ . This phenomenon is associated with the fact that for hard modes the range of amplitudes, in the vicinity of the equilibrium point, for which the system is stable is limited and tends to zero as  $\lambda \rightarrow \lambda_0$ . The existence of the excitation terms  $F_k(t)$  may thus serve to 'push the system over the edge' for a value of  $\lambda < \lambda_0$ .

Lastly, we briefly consider the theoretical modelling of systems performing autonomous closed-loop oscillations in the presence of an additional source of random excitation which produces perturbations about the basic limit cycle. In particular, we draw attention to the fact that, in cases where the basic limit cycle may be described by (nonlinear) differential equations, quantitative analogies exist<sup>17</sup> between the probability distributions for the state of the system and the distributions for memory-less linear systems excited by random noise, such as those described by equations (4). Furthermore, just as a linear system may become unstable as a controlling parameter  $\lambda$  passes through a bifurcation value  $\lambda_0$ , leading to a qualitatively different mode of operation of which a limit-cycle is one possibility, so a limit cycle may itself become unstable at some subsequent bifurcation value  $\lambda_1 > \lambda_0$ , leading to further qualitative changes in system behaviour. In the presence of additive noise, systems performing autonomous oscillations can exhibit 'critical' fluctuations (analogous to those described earlier) in the vicinity of such bifurcation values. Ref.17 refers to recent examples from physics and electronics where dissipative systems performing autonomous oscillations have bifurcation phenomena which are entirely analogous to ordinary phase transitions and which may be accompanied by soft modes and critical fluctuations.

The basic equations describing the operation of such an oscillating system in the presence of noise have been presented by Stratonovich<sup>18</sup>, who relates the probability distributions for amplitude and phase to the corresponding distributions applicable to linear systems of the type defined by equation (4). The latter, having no memory effects, are known as Markov processes; for such systems, provided that the correlation time of the noise excitation  $F_k(t)$  is extremely short, the evolution of the state of the system from a known initial value may be determined as a time-dependent (conditional) probability distribution. This conditional probability distribution can be found as the solution of a related partial-differential equation known as a FOKKER-PLANCK equation (although alternative techniques do exist and have been used in the context of transient aircraft buffeting<sup>19</sup>). What Stratonovich<sup>18</sup> showed is that the Fokker-Planck method also applies to the time evolution of fluctuations in amplitude and phase of a nonlinear oscillator under the influence of external noise. In particular, the probability distributions describing fluctuations in amplitude and phase about a steady-state limit cycle may be found. This result is relevant to the possible future generalisation of methods of parameter identification to cover the situation of systems modelled by 'noisy' limit-cycles.

In the light of the above outline of available theoretical models, we will in the following sections go on to consider separately buffeting associated with the structural response of a flexible wing and aircraft rigid-body motions influenced by the existence of separated flow.

### 3. STRUCTURAL BUFFETING OF A FLEXIBLE WING

In the case of structural buffeting of a flexible wing it is usual to assume that a linear 'forced vibration' model, with aerodynamic excitation obtainable from rigid-wing measurements, is applicable. Then the model equation takes the form of equation (4), where the excitation  $F_k(t)$  arises as a result of the unsteady state of the flow field, associated with existence of separated flow. Taking wing angle-of-attack to be the controlling parameter ( $\lambda$  in the previous section), it is assumed that no bifurcation associated with the loss of stability of the system represented by this model equation occurs within the angle of attack range considered. However, it should be noted that the onset of buffeting, represented in the model by the growth to macroscopic magnitude of the exciting force  $F_k(t)$ , may itself be regarded as a form of generalised bifurcation within the subsystem consisting solely of the flow field (note that the associated 'loss of stability' then refers to the hydrodynamic instability of separated flow and is independent of the motion of the wing).

In this section we review the manner in which the forced vibration theoretical model may be applied to the phenomenon of buffeting. Before doing so, however, we emphasise that the limits of applicability of this approach are in need of further experimental clarification, particularly by the comparison of fluctuating pressures and forces on structurally-rigid and flexible wind-tunnel models of wings of similar geometry (a discussion of this comparison is presented in Refs.1 and 2). It is likely that the applicability of this theoretical model will be limited at high-subsonic and transonic speeds in the case of flexible

modes which cause significant wing-incidence variations, as there is evidence<sup>25</sup> that oscillatory wing motion may in such situations couple in a nonlinear manner with fore-and-aft motion of the shock wave leading to a form of nonlinear flutter (requiring a limit cycle representation). For a wing at small sweep angles, this suggests that the model will probably be valid for wing bending but possibly not for wing-torsion modes. In the case of a highly-swept wing the situation is less clear-cut, as the bending and torsion modes may each contribute significantly to wing incidence changes.

The forced vibration linear analytical model for response in a flexible mode may be expressed in terms of a generalised co-ordinate  $Z(t)$ , representing the displacement in that mode, and a generalised aerodynamic excitation  $x(t)$  assumed to have no feedback from wing motion (see Fig.4).  $Z(t)$  should be multiplied by the mode shape to obtain the displacement at an arbitrary point on the wing. The aerodynamic excitation  $x(t)$  has a power-spectrum which depends on cross-spectra of fluctuating pressures over all pairs of points on the wing, weighted by mode shape. The power spectral density  $\phi_x(f)$  of  $x(t)$  is assumed to be approximately constant in the neighbourhood of the mode natural frequency  $f_0 = \omega_0/2\pi$ . When relating measurements on a model in a wind tunnel to full scale, assumptions have to be made concerning the appropriate scaling factors. On the hypothesis that Reynolds number effects are negligible, the mean-square fluctuating force  $x^2$  scales like  $(qS)^2$ , where  $q$  is dynamic pressure and  $S$  wing area, and the appropriate length and velocity parameters for scaling frequency are a geometric length (e.g. mean wing chord  $\bar{c}$ ) and true airspeed  $V$ .

On this basis the power spectral density of aerodynamic excitation may be expressed<sup>2</sup> in the form

$$\phi_x = \frac{E^2 \bar{c}^2}{V} (qS)^2, \quad (5)$$

where  $E$  is a non-dimensional aerodynamic parameter, a function only of wing incidence, Mach number and Reynolds number.

The response in the single-degree-of-freedom mode is defined by the differential equation:

$$m_1 \ddot{Z} + 2m_1 \zeta \omega_0 \dot{Z} + m_1 \omega_0^2 Z = x(t). \quad (6)$$

By standard state-space techniques this second-order equation in one dynamic variable may be replaced by two first-order equations involving two dynamic variables (e.g.  $Z$  and  $\dot{Z}$ ) and thus cast into the form of equation (4).

In equation (6),  $m_1$  is the equivalent (generalised) mass of the mode, given by

$$m_1 = k_1 m \quad (7)$$

where  $m$  is the total mass of the aircraft and  $k_1$  is a non-dimensional quantity that depends on wing geometry, mode shape, and mass distribution. The undamped natural frequency  $\omega_0$  (in  $\text{rad s}^{-1}$ ) is assumed to be independent of aerodynamic forces (stiffness and inertia). This simplifying approximation, together with the neglect of aerodynamic coupling between modes, appears on the basis of experimental data to be acceptable in many practical buffeting situations. It assumes, of course that we are well away from any boundaries of conventional flutter.  $\zeta$  (equation (6)) is the total damping ratio,

$$\zeta = \zeta_a + \zeta_s$$

where  $\zeta_a$  is aerodynamic damping ratio and  $\zeta_s$  is structural damping ratio (this assumption of a viscous type of structural damping simplifies, but is not essential to, the analysis).

The aerodynamic damping ratio is given by

$$2m_1 \zeta_a \omega_0 = k_2 a_1 \rho V S, \quad (8)$$

where  $a_1$  is effective lift-curve slope (evaluated at the non-dimensional mode frequency  $n_0 = f_0 \bar{c}/V$ ).  $k_2$  is a non-dimensional quantity that depends on mode shape.  $\rho$  is air density.

The term  $m_1 \omega_0^2$  in equation (6) represents the structural stiffness.

Then a power-spectral density (PSD), analysis gives the root-mean-square acceleration associated with the mode as

$$\sigma_{\ddot{Z}} = \frac{1}{2\sqrt{2}} \left( \frac{\bar{c} \omega_0}{V \zeta} \right)^{\frac{1}{2}} \frac{q E}{(m_1/S)} \quad (9)$$

It follows from equation (9) that the non-dimensional aerodynamic excitation parameter  $E$  is given by

$$E = 2\sqrt{2} \left( \frac{V}{\bar{c} \omega_0} \right)^{\frac{1}{2}} \left( \frac{m_1}{S} \right)^{\frac{1}{2}} \left( \frac{\zeta}{q} \right)^{\frac{1}{2}} \quad (10)$$

The quantity  $\zeta \sigma_z / q$  thus appears as a useful measure of aerodynamic excitation derivable from measured acceleration response and total damping ratio. Equation (9) illustrates the quantities required in a theoretical buffeting prediction method based, for example, on wind-tunnel measurements. For an aircraft flying at given wing loading, speed and altitude, the aerodynamic-dependent quantities are  $E$  and  $\zeta$ .

One method for the evaluation of  $E$  involves the measurement of fluctuating pressures on relatively rigid wind-tunnel models and the derivation of the generalised force by means of cross-correlation techniques<sup>25,26,27</sup>. Alternatively,  $E$  may be derived from wind-tunnel tests on the basis of equation (10) using models for which the relevant mode shape is approximately correct (note that fully-scaled aeroelastic models are not necessary). To obtain  $E$  from equation (10), wind-tunnel measurements of  $\sigma_z$  and total damping ratio are required, together with a knowledge of mode natural frequency  $\omega_0$  and generalised mass  $m_1$ .

The other quantity required in a buffeting prediction method, based on equation (9), is the value of the total damping ratio appropriate to the full-scale aircraft. As described in section 2.1, the investigation of effects of separated flow on the aerodynamic component  $\zeta_a$  of damping ratio is a subject of current research.

Perhaps the most promising approach to the problem of predicting aerodynamic damping, for use in conjunction with the forced-vibration model of buffeting, equation (6), is that based on the use of static experimental data as an input, as suggested in Ref.13. Qualitative agreement with measured changes in damping of the wing-bending mode in the vicinity of buffet onset have been shown using this approach, although good quantitative predictions have still to be demonstrated.

The least-well understood aspect of structural buffeting of a flexible wing concerns the response in wing torsion modes at high-subsonic and transonic speeds. There is substantial evidence that fore-and-aft shock motion tends to couple with torsional oscillations of the wing, providing a strong mechanism by which the flow fluctuations occurring on a rigidly-mounted wing might be fundamentally modified. Indeed, if the flow-field essentially 'locks-in' to the wing torsional motion, the forced-vibration type of analytical model for buffeting (equation (6) or, more generally, equation (4)) is no longer appropriate and the phenomenon becomes a type of nonlinear flutter. The appropriate model then takes the form of a limit cycle, probably with a significant amount of additive noise (an analytical model described at the end of section 2.2). This is an area where considerable further work remains to be done.

#### 4. FLUCTUATING RIGID-BODY MOTIONS OF AN AIRCRAFT

##### 4.1 INTRODUCTORY REMARKS

We turn now to aircraft fluctuating motion, associated with wing separated flow, in rigid-body response modes. The frequencies involved are lower than those associated with airframe flexible response, and can have a direct effect on the controllability of an aircraft and the ability to hold an accurate flight path. From the pilot's point of view, whereas aircraft flexible response may be said to influence 'ride-quality', rigid-body fluctuating motion also adversely influences 'handling-characteristics'. The most important example of rigid-body response in this context is the lateral fluctuating motion known as 'wing-rocking' which is known to have a detrimental effect on air-to-air tracking capability. In some situations, however, longitudinal rigid-body motion plays a significant role, either in the form of predominantly longitudinal motions or by coupling with the lateral degrees of freedom.

In the following, we illustrate the use of the mathematical models of fluctuating motion outlined in section 2 for the separate cases of predominantly longitudinal and lateral aircraft response.

##### 4.2 LONGITUDINAL MOTION

Pilot descriptions of aircraft fluctuating motion at high lift include the expressions 'bounce' and 'porpoising'. These refer to types of longitudinal motion at frequencies primarily influenced by aircraft rigid-body modes. The former is a description of a type of motion perceived as fluctuations at about 2-3 Hz in normal acceleration. The latter, porpoising, probably involves both normal acceleration and pitching motion and takes place at a rather lower frequency.

From the pilot's point of view there is probably no clear distinction between the types of motion mentioned above and aircraft buffeting that takes place primarily through the response of the flexible structure. However, for the purposes of theoretical analysis, the appropriate response mode for calculations of buffeting intensity (in terms of normal acceleration) depends upon the frequency range in which the response is to be evaluated. In section 3 we showed how buffeting can be modelled as wing flexible response. However, if we are concerned with response fluctuations at frequencies below that of the first wing-bending mode (say below about 7 Hz on a combat aircraft) it is more appropriate to consider aircraft rigid-body motion. Moreover, if we are concerned with buffeting in the vicinity of the nodes of the first wing-bending mode (and the pilot may sit at a point where the amplitude of wing-bending response is relatively small), a significant part of the energy in the frequency range up to approximately 10 Hz could appear as a rigid-body motion.

A simple approximation to longitudinal rigid-body aircraft motion may be derived by neglecting pitching motion and considering the response in heave (translation) only. Fig.5 illustrates the block diagram for the heaving motion (of an aircraft with mass  $m$  and wing area  $S$ ) modelled in this manner (a special case of Fig.1b). The total aerodynamic force  $G(t)$  is expressed as the sum of two components, a fluctuating aerodynamic excitation  $F(t)$  having no feedback from aircraft motion, and an aerodynamic damping contribution expressed in terms of lift slope ' $a$ '. The corresponding differential equation is

$$m \frac{dw}{dt} + \rho V S a w = F(t) \quad (11)$$

where  $w(t)$  is aircraft heaving velocity. This simple first order equation is a particular instance of equation (4). The equivalent transfer function equation describing the effect of  $F(t)$  on normal acceleration  $\dot{w}(t)$  is

$$\dot{w} = \frac{B}{As + B} F, \quad (12)$$

where  $s = d/dt$

$$A = m$$

$$B = \rho V S a.$$

A 'break frequency', related to the time constant of the above first order equation is given by

$$\bar{f} = \frac{1}{2\pi} \frac{B}{A}. \quad (13)$$

For frequencies above  $\bar{f}$ , the effect of damping on the heaving acceleration  $dw/dt$  becomes small. Moreover, the effect of unsteady aerodynamics reduces the influence of damping still further at high frequencies. On the assumption that the power spectral density  $\phi_F$  of  $F$  is constant over the frequency range of interest, and introducing a dimensionless parameter  $E$ , dependent only on flow geometry, we may write

$$\phi_F = \frac{c}{V} E^2 (qS)^2. \quad (14)$$

The root-mean-square intensity of acceleration corresponding to an arbitrary fixed pass band above frequency  $\bar{f}$  then satisfies the proportionality:

$$\begin{aligned} \sigma_{\dot{w}} &\sim \frac{1}{A} \sigma_F \\ &\sim \left(\frac{c}{V}\right)^{\frac{1}{2}} \frac{qE}{m/S}. \end{aligned} \quad (15)$$

As a numerical example, we take a typical small military aircraft, say

$$\begin{aligned} m/s &= 60 \text{ lb ft}^{-2} \\ \text{lift slope } a &= 4.0 \\ \text{Mach number} &= 0.7 \\ \text{altitude} &= 10000 \text{ ft} \end{aligned}$$

then

$$\bar{f} \approx 0.2 \text{ Hz}.$$

At frequency  $\bar{f}$  the effect of damping is to reduce the amplitude of fluctuating acceleration to about 66% of its value without damping. However, at frequencies above 1 Hz, the acceleration amplitude is at least 97% of its undamped value. Thus, in situations in which heaving motion makes a significant contribution to buffeting intensity, for example at positions very close to wing-bending nodes at frequencies in the range 1-10 Hz, the effect of aerodynamic damping is negligible and buffeting intensity satisfies equation (15). A particular consequence is that at a given value of  $E$ , for example for flight at constant incidence on the assumption that Reynolds number effects are negligible, the buffeting response, at fixed Mach number and within a fixed frequency range, is directly proportional to excitation and hence to  $q$ , and thus at constant true airspeed varies linearly with air density  $\rho$ . Allowing for changes in airspeed with altitude the variation is approximately with  $\rho^{1.2}$ . This contrasts with the case of response in a flexible mode, where buffeting intensity at constant airspeed is proportional to  $\rho^{\frac{1}{2}}$ ; allowing for changes in airspeed with altitude this becomes  $\rho^{0.6}$ .

The analysis presented in this section is the rigid-body equivalent of the forced-vibration type of analysis used for wing structural response in section 3. However, it should be noted that in the case of aircraft rigid-body motion it is more likely that the effects of nonlinear mean aerodynamic forces become significant. In particular, the regularity of the 'porpoising' motion suggests that the possibility of a limit-cycle (nonlinear flutter), in which the periodic fluctuations in the flow field become coupled deterministically to the motion of the wing, cannot be ruled out.

#### 4.3 LATERAL MOTION

The principal undesirable rigid-body motions in the context of handling characteristics of combat aircraft at high lift are the wing-rocking, wing-dropping, and nose-slice phenomena already referred to. Wing-rocking should be distinguished from wing-dropping and nose-slice in that, whilst the latter two may present a major hazard, possibly leading to loss of an aircraft in extreme circumstances, wing-rocking should generally be regarded more in terms of nuisance, degrading weapon aiming accuracy but not necessarily limiting sustained manoeuvres. Whereas wing-dropping and nose-slice are relatively well understood phenomena, taking the form of a divergence associated with loss of lateral or directional stability (bifurcation at a node), the provision of an appropriate theoretical model for wing-rocking is an outstanding problem. A principal objective is a means for relating the dynamic motion of the full-scale aircraft to measurements that can be made using rigidly-mounted wind-tunnel models.

Two basic types of analytical model exist for wing-rocking, analogous to the systems illustrated in Figs. 1a and 1b, one representing an autonomous oscillation, or limit-cycle, and the other an aerodynamically forced response. If wing-rocking takes the form of an autonomous oscillation, the system is unstable over a limited range of amplitudes, but constrained to motion of finite amplitude through the existence of

nonlinear aerodynamic forces. (We use the expression 'unstable' (above) in a broad sense to cover both dynamically-unstable equilibrium configurations and asymmetrical configurations which are not even in static equilibrium.)

The simplest analytical models for the case of autonomous oscillations exclude hysteresis and/or time-lag effects and are related to bifurcation from a focus (change from positive to negative damping). If it is required to model conditions of sustained wing-rock, in which the oscillations continue with approximately constant amplitude, a nonlinear model is called for. It may be necessary to include a source of additive noise as a means of introducing small perturbations about the basic limit cycle. If, however, it is required to model conditions of transient wing-rock, terminated by the pilot reducing the aircraft angle-of-attack, then it may be sufficient to employ linear equations (with negative damping) to describe the rate of growth of the amplitude of oscillations. The existence of additive noise is again likely to distort the oscillatory motion, particularly in the initial phase when the amplitudes are small. Tests with wind-tunnel models are in principle capable of predicting the onset of this class of motions through the indication of a loss of aerodynamic damping. For this application, the aerodynamic measurements should be made on a complete model so as to include effects of wing separated flow on the rear-fuselage or tail. However, the prediction of the nature of the motion subsequent to initial oscillations is much more difficult. If it is desired to predict the complete wing-rocking motion as an autonomous oscillation then the aerodynamic forces (including those dependent on aircraft rates of motion) need to be known as functions of aircraft angular displacements, and account should also be taken of the possible existence of hysteresis, for instance in rolling-moment measurements. This type of prediction has not as yet been attempted, and indeed it is clear that a complete analysis would be one of some complexity.

The alternative possibility is that wing-rocking takes the form of an aerodynamically-forced vibration, excited by fluctuating aerodynamic forces which are independent of wing motion. Fluctuating rolling- and yawing-moments have in the past been observed on rigidly-mounted wind-tunnel models, but it is not known under what circumstances coupling (locking-in) between flow field and motion takes place in the corresponding dynamic situation. On the assumption that significant random force or moment components persist throughout the motion, the analytical model then resembles in general structure that used to describe buffeting (section 3), an aerodynamic excitation force, analogous to  $F_k(t)$  in equation (4), producing fluctuations in the response of an essentially stable system. A variant of this model occurs in the case of 'critical fluctuations of a soft mode' (section 2), where the approach to a condition of disappearing stiffness leads to an amplification of the forced response.

Experience with a range of high-performance aircraft over the past few years has provided a wide variety of illustrations of the types of phenomena outlined above. Examples include loss of lateral stiffness (bifurcation from a node), due largely to changes in the  $n_y$  derivative, leading to 'yaw-off' or 'nose-slice', loss of Dutch roll damping (due for instance to changes in the  $l_p$  and  $n_p$  derivatives) leading to wing-rock<sup>20</sup> (bifurcation from a focus), and a case of wing-rock where no loss of stability is apparent from the measured stability derivatives and the phenomenon has thus been regarded as a 'forced' motion, associated with a randomly fluctuating wing flow-field. It is clear that no single parameter, or combination of parameters, can provide a measure for aircraft handling qualities at high angle of attack. In some cases the phenomenon of wing-rock is regarded by pilots as non-repeatable, in the sense that the same aircraft flown by the same pilot in apparently the same conditions may or may not exhibit wing-rock. The explanation may be that rolling-moment behaviour is sensitive to small changes in sideslip angle of which the pilot is not aware. A further complication is the effect on stability of pilot control inputs. For example, in the absence of control forces the parameter controlling Dutch roll stiffness is  $n_y - \sin \alpha \dot{l}_y / i_x$ , known as 'dynamic  $n_y$ '. However, the use of ailerons by the pilot, in an attempt to keep wings level, can lead to divergence at a lower angle of attack on account of the yawing moments introduced by aileron deflections.

## 5 RELATED TOPICS

The concepts used in prescribing appropriate analytical models for the fluctuating motion of a wing in the presence of separated flow are applicable in a more general range of situations. An instructive example is that of a circular cylinder, transverse to the mean-flow direction, shedding a regular vortex street. In the case of a rigidly-mounted cylinder, despite the high degree of order in the vorticity distribution, we have an example of a 'random' flow field, since the phase of the flow fluctuations is not determined by the boundary conditions. However, if the cylinder is mounted on elastic supports so that it is free to respond dynamically in a direction transverse to the flow, the phase of the flow fluctuations may become deterministically related to the cylinder motion if the structural stiffness is chosen so that the cylinder natural frequency lies sufficiently close to the vortex shedding frequency. When this phenomenon occurs, the coupled motion is appropriately regarded as a limit cycle and measurements of pressures and forces on the rigidly-mounted cylinder cannot be sensibly related to the motion of the dynamically-mounted cylinder by 'forced-response' calculations.

In the above situation we may say that the cylinder is 'structurally responding'. A related experiment may be performed in which the cylinder is 'externally forced', by means of imposed constraints, to perform sinusoidal oscillations of prescribed amplitude and frequency. Again, if the amplitude of motion is sufficiently large, and the forcing frequency (Strouhal number) lies in the neighbourhood of the natural vortex-shedding frequency, the phase of the flow fluctuations may become controlled by the cylinder motion. These are extreme examples of the phenomenon that a changeover from a 'random' to a 'deterministic' flow field, and a corresponding necessary change in the nature of associated dynamic response calculations, can occur as the mean amplitude of structural motion increases.

Brief mention may be made here of the related topic (in that it involves flow fluctuations and wing motion) of panel vibration. Instead of fluid motion involving separated flow, the problem usually studied involves the motion of a panel in the presence of a fluctuating turbulent boundary layer. A commonly used procedure is to measure fluctuating pressures on a rigid panel, and to use these in conjunction with aerodynamic damping estimates to calculate the motion of a flexible panel as an aerodynamically-forced response. Alternatively, the panel oscillations sometimes occur as nonlinear flutter. These alternatives have been discussed in Ref.21. In the latter case the larger-scale boundary-layer fluctuations, which are



random on the rigid panel, become coupled deterministically to the panel motion. The theory of Landahl<sup>22</sup>, in which the large-scale turbulence components in a boundary layer on a rigid wall are calculated as the most lightly damped eigenmodes of the associated linear stability problem, suggests that a form of non-linear coupling could arise in which the large scale fluctuating components in the turbulent flow past a flexible panel are related to the eigenmodes of the linear stability problem including wall flexibility. This is only to suggest possibilities, however, as the theory for large-scale turbulence fluctuations has not yet reached any generally accepted form, a fact which serves to emphasise that the type of problem discussed in this paper can at present only be treated by semi-empirical analytical theories.

## 6. PARAMETER IDENTIFICATION FOR SYSTEMS WITH A HIGH LEVEL OF INTERNAL FLUCTUATIONS

### 6.1 GENERAL REMARKS

The main purpose of this section is to serve as a reminder of the pitfalls that can arise in the process of parameter identification if a system with internal fluctuations is treated, as regards the relationship between system 'input' and 'output', as if it were deterministic. More precisely, we shall be concerned with parameter identification for a system that is coupled, in a closed-loop manner, to other dynamic components. The general situation is illustrated in Fig.6 where the system whose parameters we wish to identify, system A, is coupled to a second system B. From the point of view of system A the function of time  $e(t)$  is the 'input' and  $c(t)$  the 'output'. We shall consider only the most straightforward case where system A can be represented by a linear transfer function  $P$  (or equivalent set of ordinary differential equations) together with a source of internal fluctuations  $n(t)$ . As illustrated in Fig.6 the second system B (also assumed to be linear) may itself contain an internal source of fluctuations,  $i(t)$ . Two practical realisations of the general situation illustrated in Fig.6 will be discussed. Firstly, we note the resemblance between Fig.6 and Figs.1b, 4 and 5. In these cases the parameters (to be identified) of system A are aerodynamic force coefficients, and the noise source  $n(t)$  arises from the randomly fluctuating separated flow field. The coupled system B then represents the elastic (Fig.4) or dynamic (Fig.5) response of a wing. From the viewpoint of system A, the input  $e(t)$  describes the motion of the wing in the mode of interest, and the output  $c(t)$  represents the associated generalised force arising as a (possibly weighted) integral of aerodynamic pressure fluctuations. In this context, we have not previously considered the case where the system B also contains a source of fluctuations; such a source occurs, for example, if the wing motion  $e(t)$  contains a component independent of aerodynamic forces, for instance due to mechanical vibration arising from the aircraft propulsive system.

The second example concerns the theoretical representation of a human controller, or operator, performing a single-axis closed-loop control task. For some applications it is sufficient to represent the human operator by a linear transfer function, or describing function, together with a noise source or 'remnant'. The overall situation is then as illustrated in Fig.6, with system A corresponding to the human operator and system B to the system he is controlling. We will consider an example in which it is desired to identify the human operator parameters when controlling a system with rate response.

### 6.2 REVIEW OF THEORETICAL RESULTS

Consider first of all the open-loop situation illustrated in Fig.7. Since the loop is open, the internal noise source  $n(t)$  is uncorrelated with the input signal  $e(t)$ . In this case we have<sup>5</sup>

$$P = \frac{\phi_{e,c}}{\phi_{e,e}} \quad (16)$$

where  $\phi_{e,c}$  is the cross spectral density of the signals  $e(t)$  and  $c(t)$  and  $\phi_{e,e}$  is the power spectral density of  $e(t)$ .

Next consider the closed-loop situation illustrated in Fig.6. In this case, one way of determining the linear transfer function  $P$  is from the ratio of two cross spectral densities<sup>5</sup>

$$P = \frac{\phi_{i,c}}{\phi_{i,e}} \quad (17)$$

Note, however, that this formula requires the measurement of the signal  $i(t)$  and is only valid within the frequency range of  $i(t)$ . Outside this range the formula (17) for  $P$  becomes indeterminate. Suppose now that in the closed-loop case we define the transfer function analogous to that given by equation (16):

$$P' = \frac{\phi_{e,c}}{\phi_{e,e}} \quad (18)$$

Then<sup>5</sup>,  $P'$  is the linear transfer function which, with input  $e(t)$ , minimises the mean-square difference between its output and  $c(t)$ . In this sense it is the 'best linear transfer function' from  $e$  to  $c$ . This result will be important when we come to consider the analogue matching technique for parameter identification (section 6.4).

The next step is to relate  $P'$  to the transfer functions  $P$  and  $S$  of systems A and B respectively (Fig.6). We first consider two special cases in which  $e(t)$  and  $c(t)$  are deterministically related. Fig.8a illustrates the case where system A contains no source of internal fluctuations, i.e.  $n(t) = 0$ . In this case we have

$$c = Pe \quad (19)$$

(where the right hand side can be interpreted as either a product in the frequency domain or a convolution in the time domain). Since  $P'$  is the 'best linear transfer function' from  $e$  to  $c$  we evidently have

in this case

$$P' = P. \quad (20)$$

Alternatively, Fig. 8b illustrates the case where the second system B contains no source of fluctuations and may thus be completely represented by a (linear) transfer function  $S$ . The overall coupled system is thus excited by the internal fluctuations of system A. Then we have

$$e = Sc$$

or equally

$$c = \frac{1}{S} e. \quad (21)$$

By the argument used to obtain equation (20) we have in this case (provided that the transfer function  $1/S$  is physically realizable):

$$P' = \frac{1}{S}. \quad (22)$$

Equations (20) and (22) are in fact special cases of a general result applicable<sup>5,23</sup> when both internal noise sources  $n(t)$  and  $i(t)$  are non-vanishing:

$$P' = \frac{\{\phi_{ee}\}_i}{\phi_{ee}} P + \frac{\{\phi_{ee}\}_n}{\phi_{ee}} \frac{1}{S}, \quad (23)$$

where  $\{\phi_{ee}\}_i$  and  $\{\phi_{ee}\}_n$  are those components of the spectral density of  $e$  which are correlated with  $i$  and  $n$  respectively. The form that  $P'$  takes in a particular example is discussed in section 6.4.

From the above general analysis we see that, when a system with a significant level of internal fluctuations is coupled into a closed loop, it is not in general possible to identify its parameters in the usual manner from records of its 'input' and 'output'. The result of such an operation is to identify the parameters of the transfer function  $P'$  which in general (equation (23)) depends both upon the parameters of the system of interest and upon the properties of the remainder of the loop.

### 6.3 CONTRAST BETWEEN STRUCTURALLY-RESPONDING AND EXTERNALLY-FORCED WING MOTION

As an illustration of the way in which the relation between 'input' and 'output' of a system with internal fluctuations can depend upon the manner in which it is coupled into a closed-loop, we consider the aerodynamic force associated with the motion of a wing under conditions of separated flow. The system 'input' is the motion of the wing and the 'output' is the aerodynamic force, obtained as a weighted integral of aerodynamic pressures. The mutual interaction between such a system and the structural response of a wing is an essential part of the phenomenon of buffeting (Fig. 4). In cases where the wing motion arises entirely as a result of aerodynamic forces we will refer to the wing motion as 'structurally-responding' (Fig. 9b). This situation should be contrasted with that which occurs when the time history of wing motion is externally imposed by means of additional forces (as a wing surface might be forced to follow some prescribed time history in a wind-tunnel experiment). The relationship between wing motion and the resulting aerodynamic force (weighted integral of aerodynamic pressures) is then as illustrated in Fig. 9a, the result of externally-imposed constraints being to destroy any influence of the aerodynamic pressure field (and the associated aerodynamic force) on wing motion. In such a case we will refer to the wing motion as 'externally-forced'.

As either type of wing motion may occur in wind-tunnel experiments it is instructive to contrast the relationships between wing motion and aerodynamic force (or pressure field) in the two cases. The principle result is that, provided the buffeting response takes the form of a forced vibration (in contrast to nonlinear flutter) the statistical characteristics of fluctuating pressures (and associated aerodynamic forces) are fundamentally different even for identical time histories of wing motion.

For, in the case of externally-forced wing motion, the ensemble (family) of fluid motions corresponding to a given time history of wing motion consists of all those flow field compatible with the boundary conditions imposed by the wing surface velocities (Fig. 9a). In the case of a structurally-responding wing, however, there is a smaller ensemble of compatible fluid motions consisting of that subset of flow fields which satisfy IN ADDITION the relation between aerodynamic force and wing motion imposed by the equation for structural response (Fig. 9b). Since the aerodynamic force is obtained as an integral over the wing involving pressure fluctuations and mode shape, in the case of a structurally-responding wing there is an additional integral constraint enforced on the ensemble of possible flow fields. A particular consequence is the difference in statistical properties of the fluctuating pressure fields, and associated aerodynamic forces, on externally-forced and structurally-responding wings. This difference was illustrated by means of a numerical example in Refs. 1 and 2. In this example  $Z(t)$  represents the motion of a wing and  $y(t)$  the associated total aerodynamic force when the wing is structurally responding in an elastic mode (as in Fig. 4). The power spectra of  $Z(t)$  and  $y(t)$  are illustrated in Fig. 10. It can be seen that whilst  $\phi_Z$  has a peak at the resonant frequency of the mode,  $\phi_y$  has a corresponding region of low spectral density (a 'notch' in the spectrum) associated with the mutual cancellation of the aerodynamic forcing and damping fields.

Suppose now that the wing is constrained, by means of externally-imposed forces as in Fig. 9a, to reproduce the time history  $Z(t)$ . The power spectrum  $\phi_Z$  will thus be unaltered. However,  $Z(t)$  will now be completely uncorrelated with the random component of aerodynamic force ( $x(t)$  in Fig. 4). It can then be shown<sup>1,2</sup> that the spectrum  $\phi_{\bar{y}}$  of the resulting aerodynamic force  $\bar{y}(t)$  (obtained as a weighted integral of fluctuating pressures) differs from  $\phi_y$  as illustrated in Fig. 10, having a peak related to that in  $\phi_Z$ .

In Ref.2 the consequences of the above result for the interpretation of fluctuating pressure measurements from full-scale flight tests and wind-tunnel experiments are discussed. It is concluded<sup>2</sup> that the interpretation of flight-test measurements is complicated by the delicate phase-balance existing between the spatially-overlapping aerodynamic excitation and response fields (including aerodynamic damping). It is also suggested<sup>2</sup> that considerably more information may be obtained from wind-tunnel tests if fluctuating pressures on structurally-responding wings and on rigid wings with similar geometry are compared.

From the point of view of parameter identification, perhaps the most significant consequence<sup>2</sup> of the above analysis is that information concerning the aerodynamic transfer function, and in particular aerodynamic damping (Fig.4), can NOT be obtained (e.g. by cross-correlation) from the time histories of wing motion and the associated aerodynamic pressure fields measured on a structurally-responding buffeting wing.

#### 6.4 HUMAN OPERATOR CONTROLLING A SYSTEM WITH RATE RESPONSE

We consider the situation illustrated in Fig.6 with system A corresponding to the human operator and system B to the system he is controlling. Thus  $P$  is the operator describing function, or transfer function, and  $n(t)$  the pilot 'remnant', or noise source, due to such things as sampling effects or random errors of judgement of the 'error'  $e(t)$ . Alternatively,  $n(t)$  can be partly an intentional signal injected by the operator as a means of monitoring the system response.

$S$  is the transfer function of the system response to control signal  $c(t)$ . For instance, if we assumed that the control of aircraft bank angle can be regarded as a single-loop task then we could interpret the quantities in Fig.6 as follows:  $i(t)$  is the bank angle response to gusts, i.e. the time history of bank angle that would result if no attempt were made to control.  $e(t)$  is the actual bank angle in the controlled case.  $c(t)$  is pilot stick-force, related to aileron deflection.  $S$  is the transfer function of aircraft response to pilot stick force. The pilot attempts to produce a bank-angle response to stick force which opposes  $i(t)$  thus keeping  $e(t)$ , the actual bank angle, small.

Methods of parameter identification that have been used in the past to define the human operator in terms of  $P$  and  $n(t)$  include

- (a) cross power spectral analysis
- (b) adaptive analogue model.

Advantages that have been claimed for the latter method are that it saves computational effort and that it can be used for non-stationary processes, possibly in real time. The method of application is to assume a model  $P^*$  with several variable parameters. The error signal  $e(t)$  is fed to the model which proceeds to adapt itself (by means of auxiliary loops) so as to minimise some functional such as the mean square difference (averaged over some fixed time) between its own output  $c^*(t)$  and that,  $c(t)$ , of the human operator. Within the limitations of the assumed model form, the model is thus designed to adapt to the 'best' linear transfer function from  $e$  to  $c$ , in a mean-square error sense. We are concerned here with clarifying the effect of pilot 'remnant' or random noise  $n(t)$  on the adapted state of the (deterministic) model.

As described in section 6.2, the best linear transfer functions from  $e$  to  $c$  in a mean-square error sense is in fact  $P'$ , as given by equation (23). The model will thus adapt itself so as to give the best fit of its assumed form to the linear transfer function  $P'$ .

A theoretical treatment of the case of a human operator controlling a system with rate response has been given by Durand and Jex<sup>24</sup>, whose results we quote here. The theoretical model is very simplified but appears to be consistent with the main features of existing experimental data.

Durand and Jex's theoretical model is as follows<sup>24</sup>. The closed-loop system is as illustrated in Fig.6. The system response is given by

$$S = - \frac{K_c}{s(T_R s + 1)} \quad T_R = 0.4 \text{ s} \quad (24)$$

(The negative sign arises because the output from  $S$  opposes the signal  $i(t)$ .) The assumed form for the describing function of the human operator is taken to be

$$P = \frac{K_p}{T_p s + 1} \quad T_p = 0.1 \text{ s} \quad (25)$$

where  $T_p$  represents a time lag.

The power spectrum of the input disturbance  $i(t)$  is taken to be as illustrated in Fig.11 with constant power  $I^2$  per unit band up to a cut-off frequency  $\omega_i$  taken to have the value  $\omega_i = 1 \text{ rad/s}$ . The operator's noise  $n(t)$  is assumed to be proportional to his gain  $K_p$  and is taken in the form

$$n(t) = K_p N(t) \quad (26)$$

where  $N(t)$  is assumed to have constant power  $N^2$  per unit band up to a sharp cut-off at  $\omega_n = 10 \text{ rad/s}$ . The input disturbance to noise power ratio is taken to be  $I^2/N = 30$ . The results to be discussed are not, in fact, very sensitive to the exact form of the operator noise, the only basic property being that it has considerably greater bandwidth than the input noise. In practice the exact form of noise will probably vary to quite a large extent from operator to operator.

The assumed input spectra lead to a theoretical error spectrum (Fig.12) having two distinct peaks: one at  $\omega_i$  and one at the closed-loop natural frequency. As the operator increases his gain  $K_p$  to reduce the external input errors, the assumed form of pilot noise implies that the noise errors increase. In fact there will exist a theoretically optimum gain  $K_p$  which minimizes the overall mean square error. The resulting closed-loop frequency and damping ratio corresponding to this optimum gain turn out<sup>24</sup> in this case to take values 3.3 rad/s and 0.2 respectively. This damping ratio is rather low but the above parameter values are not inconsistent with existing experimental data. The corresponding components of the error spectrum are illustrated in Fig.12. Note that the power in the error signal at around the closed loop natural frequency is due to operator noise and is uncorrelated with the external disturbance input. In general, of course, the input power spectrum would not be cut-off as sharply as shown in Fig.11 and as a result the components of  $\Phi_{ee}$  would not be as distinct as in Fig.12. The low frequency peak would be much less sharp and between the peaks would be a region where the contributions of  $\{\Phi_{ee}\}_i$  and  $\{\Phi_{ee}\}_n$  were of equal importance.

Consider now the behaviour of the adaptive analogue model in this case. As explained earlier, the model will adapt itself so as to give the best fit of the assumed model form to  $P'$ , where  $P'$  is given by equation (23). It can be seen that in this case we have

$$P' = \begin{cases} \frac{K_p}{T_p s + 1} & 0 < \omega < \omega_i \\ \frac{s(T_R s + 1)}{K_c} & \omega_i < \omega < \omega_n \end{cases} \quad (27)$$

According to the (idealised) theory of Ref.24, this is the transfer function to which the 'pilot analogue model' would adapt.

In practice, the input spectrum  $\Phi_{ii}$  (Fig.11) would not be cut off so sharply and hence  $i(t)$  would have some energy at frequencies above  $\omega_i$ . Thus  $P'$ , equation (23), would contain some contribution from  $P$  in the frequency range  $\omega > \omega_i$ . Nevertheless, in the neighbourhood of the closed-loop natural frequency it is likely that the dominant term in  $P'$  would still be the contribution from  $1/S$ . We conclude that the parameters in the analogue model which most strongly influence response at the closed loop natural frequency will tend to adapt so as to give a good match, not to the human operator transfer function  $P$  but to the inverse of the transfer function  $S$  of the controlled system. A more detailed discussion is presented in Ref.23, where it is argued that there will be a particularly strong influence of  $1/S$  on lead terms (i.e. coefficients proportional to  $s$  in the numerator) in the assumed analogue model.

## 7 CONCLUDING REMARKS

We have discussed a variety of systems characterized by their high level of internally-generated fluctuations, and reviewed the problem of formulating appropriate theoretical model structures for such systems.

Practical examples include aircraft buffeting and wing-rocking, where the fluctuations are associated with the unsteady behaviour of separated flow. The importance of understanding these phenomena lies in the fact that modern high-performance aircraft often have to operate in such states in order to fully exploit their manoeuvre flight-envelope. Applications of theoretical models of the phenomena include planning and interpretation of appropriate wind-tunnel tests, as a basis for prediction of full-scale behaviour, and programming of ground-based simulations of manoeuvring conditions.

The mutual interaction between a dynamically-responding wing and a separated flow field can take two forms: in one the wing motion is 'forced' by the fluctuating flow field, in the other the joint motion of wing and flow field arises as a mutual interaction. The distinction is that in the former the nonlinear process of energy transfer from the free stream to the fluctuations is predominantly a flow-field phenomenon, the response of the wing possibly modifying but not fundamentally interfering with this process; in the latter case the nonlinear energy transfer mechanism depends fundamentally on the coupling between flow field and wing motion.

We have stressed the desirability of correctly modelling the manner in which system behaviour changes as some controlling parameter, such as wing incidence, is continuously varied. Of particular importance are conditions where the behaviour of the system undergoes a basic qualitative change, for instance from a nonfluctuating to a fluctuating state. Mathematically such qualitative changes are represented by 'bifurcations' in the state of the model. From a generalised point of view such bifurcations may be associated with a loss of stability either of the coupled flow-field/responding-wing combination (as in classical flutter) or of the flow field in isolation (i.e. a purely hydrodynamic instability, independent of wing motion, leading to fluctuating flow conditions). Another important phenomenon that can occur as the controlling parameter, say wing incidence, is continuously increased is the 'locking-in' of previously random flow fluctuations so as to have a deterministic relationship to wing motion. Thus 'buffeting' can become transformed to 'nonlinear flutter'.

An important element in the application of such modelling concepts to practical situations is the planning and interpretation of appropriate experiments. In this context there is an important role to be played by 'diagnostic' experiments, whose purpose is to investigate the qualitative characteristics of the system, i.e. to find the appropriate model structure. We have elsewhere<sup>2</sup> discussed such qualitative use of measurements of fluctuating pressures in studies of buffeting and wing-rocking.

Lastly, we have emphasised that the identification of a system from its 'input' and 'output' is a questionable procedure when the system has a high level of internal fluctuations and is operating as part of a closed loop. In such a situation it may be necessary to inject a measurable 'test-signal' to

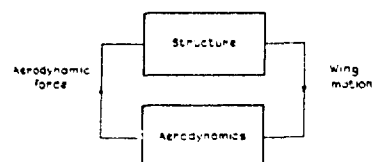
separate the characteristics of the system under investigation from those of the systems comprising the rest of the loop.

## REFERENCES

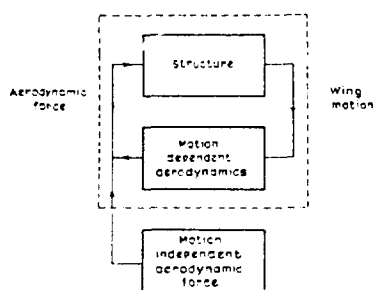
1. J.G. Jones      The dynamic analysis of buffeting and related phenomena.  
AGARD Specialists Meeting on Fluid Dynamics of Aircraft Stalling, Lisbon  
AGARD CP 102 (1972)
2. J.G. Jones      A survey of the dynamic analysis of buffeting and related phenomena.  
RAE Technical Report 72197 (1973)
3. Y.C. Fung      An introduction to the theory of aeroelasticity.  
John Wiley (1955)
4. N. Minorsky      Nonlinear oscillations.  
D. Van Nostrand (1962)
5. D. Graham  
D. McRuer      Analysis of nonlinear control systems.  
John Wiley (1961)
6. N.C. Lambourne      Flutter in one degree of freedom.  
Manual of aeroelasticity, Part V, Chap.5, AGARD
7. C. Scruton      On the wind-excited oscillations of stacks, towers and masts.  
National Physical Laboratory, Paper 16 (1963)
8. M. Tobak      On nonlinear longitudinal dynamic stability.  
AGARD Flight Mechanics Panel, Cambridge, England (1966)
9. R.E.D. Bishop  
R.K. Burcher  
W.G. Price      The uses of functional analysis in ship dynamics.  
Proc. Roy. Soc. Lond. A, 332 (1973)
10. L.E. Ericsson  
J.P. Reding      Unsteady airfoil stall.  
NASA CR-66787 (1969)
11. L.E. Ericsson      Comments on unsteady airfoil stall.  
J. Aircraft, Vol. 4, No. 5 (1967)
12. A.G. Rainey  
T.A. Byrdsong      An examination of methods of buffeting analysis based on experiments with wings  
of varying stiffness.  
NASA TND-3 (1959)
13. L.E. Ericsson      Dynamic effects of shock-induced flow separation.  
AIAA Paper No. 73-308 (1973)
14. H. Mori      Progr. Theor. Phys. 33, (423) (1965)
15. N.C. Lambourne      On certain types of self-excited oscillation occurring with aircraft control  
surfaces in transonic flow.  
National Physical Laboratory Aero Report 1191.  
ARC 27852 (1966)
16. S.C. Dixon      Application of transtability concept to flutter of finite panels and experimental  
results.  
NASA Technical Note TN D-1948 (1963)
17. R. Landauer  
J.W.F. Woo      The steady state far from equilibrium. Phase changes and entropy of fluctuations.  
In 'Statistical Mechanics, New concepts, problems and applications'.  
University of Chicago Press (1972)
18. R.L. Stratonovich      Topics in the theory of random noise.  
Vol II, Trans, R.A. Silverman, Gordon and Breach (1967)
19. J.K. Zbrozek  
J.G. Jones      Transient buffet loads on wings.  
J. Sound Vib, 5 (2) (1967)
20. A.J. Ross      Determination of aerodynamic derivatives from transient responses in manoeuvring  
flight.  
AGARD Flight Mechanics Panel Specialists Meeting on Methods for Aircraft State  
and Parameter Identification.  
NASA Langley, Hampton, Virginia (1974)
21. E.H. Dowell      Noise or flutter or both?  
J. Sound Vib. 11 (2) (1970)
22. M.T. Landahl      A wave-guide model for turbulent shear flow.  
J. Fluid Mech. 29 (1967)
23. J.G. Jones      A note on the model matching technique for the measurement of human operator  
describing functions.  
RAE Technical Report 65290 (1965)
24. T.S. Durand  
M.R. Jex      Handling qualities in single-loop roll tracking tasks: theory and simulator  
experiments.  
ASD-TDR-62-507 (1962)
25. D.B. Benepe  
A.M. Cunningham Jr.  
W.D. Durmyer      A detailed investigation of flight buffeting response at subsonic and transonic  
speeds. General Dynamics Convair Aerospace Division, AIAA Paper (to be  
published)

## REFERENCES (concluded)

26. C. Hwang  
W.S. Pi      Transonic buffet behaviour of Northrop F-5A aircraft.  
Northrop Corporation. Presented to 38th AGARD Structures and Materials Panel Meeting, Washington (1974)
27. H. John      Critical review of methods to predict the buffet penetration capability of aircraft.  
Messerschmitt-Bolkow-Blohm GMBH. 38th AGARD Structures and Materials Panel Meeting, Washington (1974)
28. L.L. Erickson      Transonic single-mode flutter and buffet of a low aspect ratio wing having a subsonic airfoil shape.  
NASA TN D-7346 (1974)



a Closed loop, autonomous



b Closed loop, general case

Fig.1 Systems analysis relating aerodynamic force and wing motion

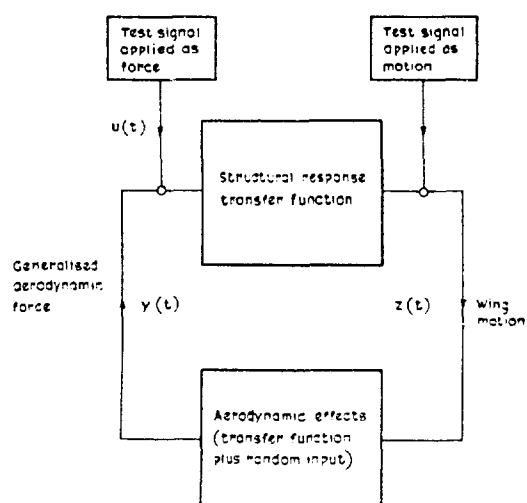
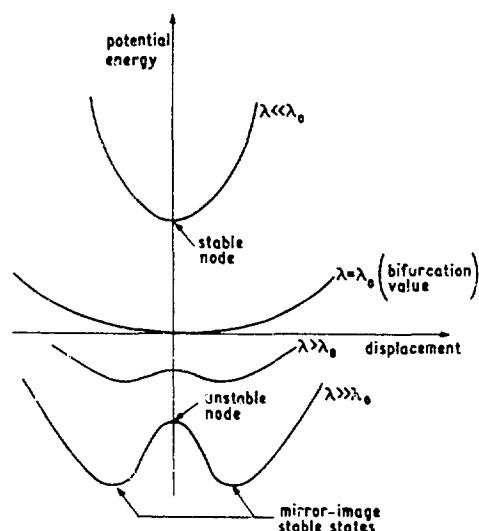


Fig.2 Use of externally-applied test signal to separate components of aerodynamic force



The vertical displacement of the curves is introduced to keep them from intersecting and obscuring each other.

Fig.3 Soft mode bifurcation from stable node into mirror-image stable states defined by 'potential wells'

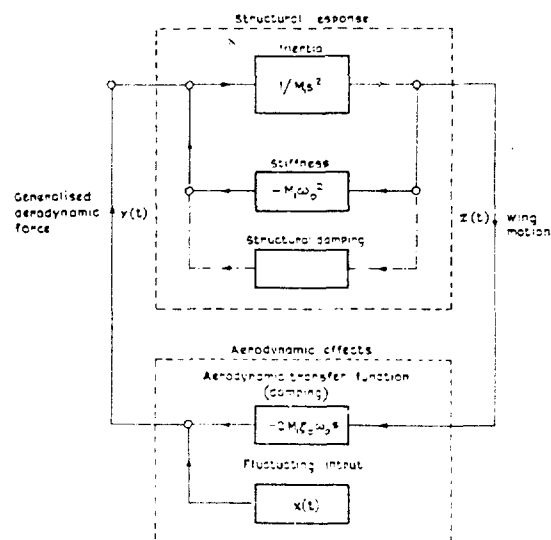


Fig.4 Forced-vibration model of structural buffeting, representing response in a flexible mode

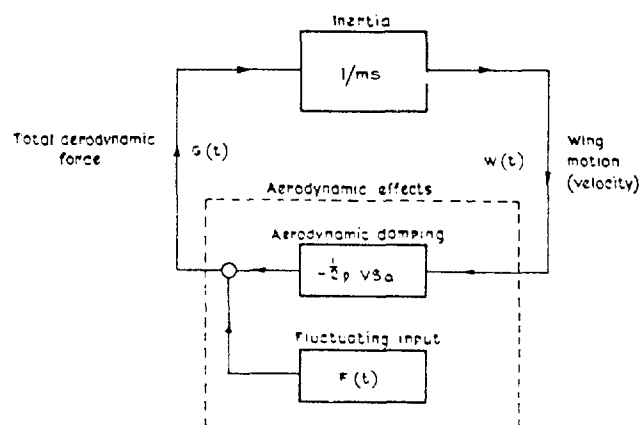


Fig.5 Forced-vibration model for 'buffeting' associated with rigid-body heave mode

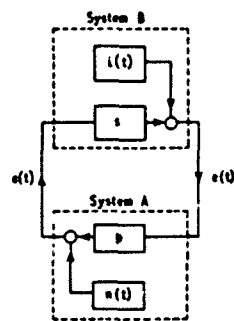


Fig.6 Closed-loop situation

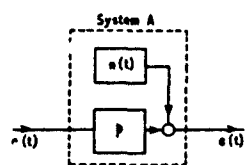


Fig.7 Open-loop situation

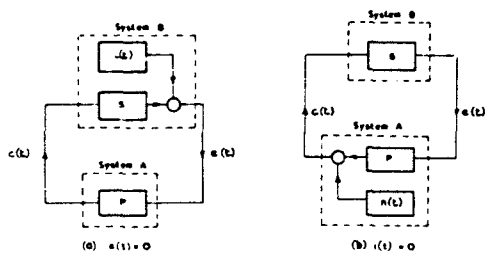
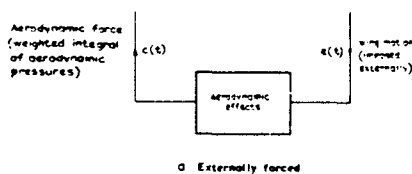
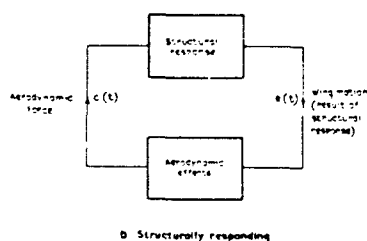


Fig.8 Two special cases



a Externally forced



b Structurally responding

Fig.9 Contrast between: structurally-responding and externally-forced wing motion

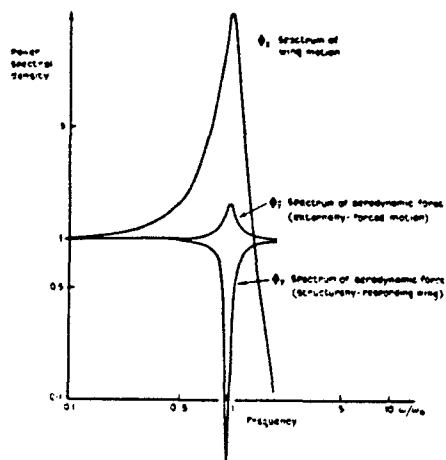


Fig.10 Power spectra of aerodynamic forces on externally-forced and structurally-responding wings

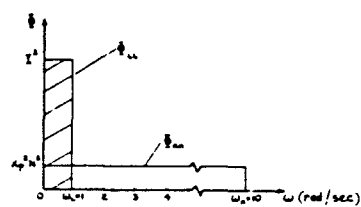


Fig.11 Input spectra

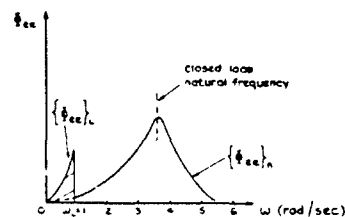


Fig.12 Error spectrum  $\hat{\Phi}_{ee} = \{\hat{\Phi}_{ee}\}_i + \{\hat{\Phi}_{ee}\}_n$



# IDENTIFICATION OF NONLINEAR AERODYNAMIC STABILITY AND CONTROL PARAMETERS AT HIGH ANGLE OF ATTACK\*

By

B. J. Eulrich and E. G. Rynaski  
Calspan Corporation  
Buffalo, New York 14221

## ABSTRACT

This paper describes a procedure for the estimation of the nonlinear aerodynamic stability and control coefficients at high aircraft angles of attack. It is based on a nonlinear, iterated Kalman filter/fixed-point smoother identification algorithm and a least square equation error method. Key ingredients for successful identification are the mathematical model, instrumentation system, control inputs and the identification algorithm. The major emphasis here is placed on the use of the identification procedure in analyzing high angle of attack flight data.

Specifically, model form and initial estimates are established from wind tunnel data using series expansions to represent the nondimensional force and moment coefficients for selected ranges of angle of attack. This high dimensional representation is reduced by: (i) preprocessing the flight data using the instrumentation system model and the six-degree-of-freedom aircraft kinematic equations to perform optimal state estimation and hence decrease the effects of instrumentation errors; and (ii) separating the six equations of motion into two separate four-degree-of-freedom systems; one for extracting the longitudinal coefficients and the other for the lateral-directional coefficients.

Specific problems associated with the identification procedure at high angles of attack and parameter identifiability problems caused by poorly conditioned flight data are reviewed. Selection of the coordinate system for the aircraft model, the determination of the initial covariance estimates and the measurement and process noise statistics required to use the iterated Kalman technique are discussed. The results and problems of identifying the F-4E high angle of attack aerodynamic characteristics from records taken during the Air Force acceptance tests of this aircraft are presented. These results are in the form of time history matches and comparisons of the estimated coefficients with wind tunnel data.

## INTRODUCTION

Effective solutions to the problem of inadvertent departure and subsequent post-stall gyrations of modern, high performance aircraft are dependent upon an accurate description of the aerodynamic characteristics of the vehicle at high angles of attack. This paper describes a systematic procedure for the estimation or identification of the significantly nonlinear aerodynamic stability and control coefficients at high angles of attack. The actual post-stall gyration time histories of an F-4E are used to verify the identification techniques used. The results are extensively described in Reference 1.

The key ingredients for successful identification are a suitable form of mathematical model, the accuracy and adequacy of the instrumentation system, the control inputs or excitation to the airframe and, finally, the identification algorithm used to extract the unknown coefficients of the aerodynamic and instrumentation models. This paper discusses all these aspects of the identification process, but emphasizes the efficiency of the nonlinear, iterated Kalman filter/fixed point smoothing identification algorithm for obtaining accurate results.

Special attention is given to the description and identification of the instrumentation system used during the flight testing of the aircraft and to techniques for reducing the dimensionality problem of simultaneously identifying the aerodynamic parameters of all six equations of motion of the F-4E aircraft.

The results are in the form of time history matches and comparisons of the extracted aerodynamic coefficients with wind tunnel estimates. The functional dependency of the nondimensional stability and control parameters on angle of attack of the full scale airplane was found to compare favorably with data obtained in two separate wind tunnels.

This paper is organized as follows. The identification problem at high angles of attack is first reviewed and the identification procedure and algorithms used are briefly presented. This is followed by a description of the system models employed and some general comments relating to the identification. Sample results are then presented using the F-4E high angle of attack flight data.

## AIRCRAFT IDENTIFICATION AT HIGH ANGLES OF ATTACK

Aircraft parameter identification is associated with the extraction of stability and control parameters from flight test data in the form of time history responses of the aircraft and applied control inputs. It is well known that the ability to extract stability and control parameters from flight test data depends upon many elements related to both the theory of identification and the very practical matter of flight test experience, but four major ingredients predominate. These four ingredients are:

1. Mathematical modeling
2. Instrumentation
3. Maneuvers or experiment design
4. Identification algorithms

\* This work was supported under Contract No. F33615-72-C-1248, Air Force Flight Dynamics Laboratory, Wright-Patterson Air Force Base, Ohio.

The first three are illustrated in Figure 1, which is a conceptual block diagram of the actual aircraft and the general model used for parameter identification purposes. The equations of motion of the aircraft are written in the conventional, but general form:

$$\dot{x} = f(x, p, u) + w(t), \quad x(t_0) = x_0 \quad (1)$$

$$y_i = h(x_i, p, u_i) + v_i, \quad i = 1, \dots, N$$

where

$x$  = state vector for the aircraft and associated dynamical system

$p$  = unknown parameter vector

$u$  = control input vector such as  $\delta_3, \delta_2, \delta_r$

$y_i$  = measurement vector of sensor outputs at discrete time points

$f(), h()$  = functional form of aircraft and measurement system model

and  $w(t)$  and  $v_i$  are zero mean, Gaussian white noise vectors which represent errors in the formulation of the model (that is, missing terms, unknown inputs, etc.) and the inherent random error in the instrumentation, respectively. The first equation in Equation (1) is commonly referred to as the dynamical model of the system to be identified, or the equations of motion of the aircraft if sensor/control system dynamics are neglected, and the second equation the measurement system. The unknown constant parameter vector to be identified from the control inputs and noisy sensor outputs satisfies

$$\dot{p} = 0 \quad (2)$$

where  $p$  can contain unknown aircraft initial conditions, aerodynamic parameters, and instrumentation errors such as constant biases, for example. Given the first three ingredients--that is, the model, the instrumentation and the proper maneuvers (e.g., control inputs) to insure that the unknown parameters are identifiable from the measurements--then the identification technique(s) can be successfully used to obtain these unknowns. In fact, if the instrumentation is complete, very accurate and noise-free, if the model form can adequately represent the motions of the aircraft without significant error, and if all the degrees of freedom of motion of the aircraft are properly excited to allow for unique identifiability of the unknown parameters, then some of the simplest, straightforward identification techniques can be used to accurately obtain the stability and control parameters of the vehicle. Before outlining the specific problems and our approach associated with identification at high angles of attack, the identification techniques used will first be discussed.

#### Identification Algorithms:

The identification algorithms used here are a classical least squares (LS) linear regression method and a locally iterated Kalman filter/fixed-point smoothing algorithm (IKF/FP). This technique is explained more fully in Appendix V of Reference 1 and a more complete documentation is available in References 2 and 3.

The LS method is a simple and efficient technique which is used to establish the initial model form and to provide a set of initial parameter estimates and a set of approximate variances of these estimates for initializing the IKF, if so desired. Once the model form  $f()$  is chosen, this method minimizes the error in satisfying the equations with respect to the unknown parameter vector ( $p$ ) in the equation. That is,  $w(t)$  in Equation (1) is minimized with respect to  $p$  and consequently, it is called an equation error method. This method also provides an indication as to the adequacy of the model form and the identifiability of the parameters representing the model. The structural form of  $f()$ , which is one of the key problems at high angles of attack, is established with the use of the LS technique as a guide by visual observation of the fit and by adjusting the model form so as to minimize the estimate of the variance of the equation error,  $w(t)$ . This estimate is equal to the sum of squares of the error in the fit divided by the numbers of degrees of freedom, that is, the number of data points used minus the number of unknown parameters being identified.

The restrictions of this technique, as it is used here, are that:

1. All measurements of  $\ddot{x}$  (aircraft accelerations) and  $x$  must be available.
2. The estimates are biased if the state measurements ( $x$ ) are noisy; that is, if  $v_i \neq 0$  in Equation (1).

Once  $f()$  has been established, to account for both equation error (process noise  $w(t)$ ) and instrumentation error ( $v_i$ ), the identification problem is transformed to a nonlinear filtering problem by augmenting the aircraft state equations with the parameter vector model, Equation (2). The problem can then be viewed as one of fixed-point smoothing, that is, estimating both the unknown parameters and the initial condition of the aircraft from the data. With this as a starting point, the estimation philosophy may then be divided into two major groups: Bayesian and non-Bayesian. The difference between these groups is that Bayesian philosophy can take into account a priori information about the data of unknowns, whereas non-Bayesian does not. The Bayesian philosophy assumes that the entire information available to an estimator is contained in the a posteriori density function; that is, the density function of the unknowns given the data.

With the Bayesian philosophy, two estimation criteria can be considered:

1. The minimum variance or minimum mean squared error criterion; the resulting estimator is the conditional mean, that is, the expected value of the a posteriori density function, or
2. Maximum likelihood (Bayesian) or most probable estimate, which is the mode of the a posteriori density function.

The development of the identification algorithm used for the research described in this paper is documented in Reference 2. Using a mean square error criterion, the resulting recursive algorithm is a form of nonlinear, iterated Kalman filter/fixed-point smoother. The nonlinear filter used is a form of an extended Kalman filter utilizing a "local iteration" scheme between successive measurements to reduce

the errors in linearizing the  $f(x, \rho, u)$  and  $h(x, \rho, u)$  functions by improving the reference trajectory. This improvement is accomplished by smoothing each measurement data point backwards in time one point and re-linearizing. In addition, the outputs of the filter at each data point can be used in a fixed-point smoothing algorithm to produce a better smoothed estimate of the aircraft initial condition.

This technique is both a response error and an equation error minimization technique under the usual Gaussian assumptions in the error sources. That is, the technique adjusts the parameters of the model so as to minimize the "weighted" errors between both the measured responses (accelerations included) and the error in formulating the equations of motion of the airplane. The weighting in the measurements is selected to be compatible with the accuracy of the instrumentation and recording system, whereas the weighting of the equation error is compatible with the error in the mathematical model of the airplane. These error sources are commonly referred to as the measurement and process noise, respectively.

The selection of these noise statistics in particular is an iterative process which is carried out in practice by observing the residual sequences (measurement data minus predicted measurements) of the filtering operation and adjusting the statistics as required to force consistency between the predicted and actual dispersion of the residuals. If the model is correct (implies both form and statistics used), the actual dispersions of the residuals should be zero mean, white and consistent with the theoretically calculated statistics. The residuals and the final covariance matrix in the algorithm also serve as additional checks on the adequacy of the model form and accuracy and identifiability of the parameter estimates.

Besides the form of the model and the noise statistics, two additional pieces of information are required to perform the identification with the IKF. These are the initial estimates of the parameters and states and the variance of the initial estimate ( $P_0$ ). These can be obtained using wind tunnel data and a knowledge of the aircraft being identified or else by the LS initial estimates. In practice,  $P_0$ , which represents the initial uncertainty of these estimates, is usually adjusted to ensure that the final parameter estimates are not affected by its value. This is accomplished by increasing the magnitude of  $P_0$  until the initial estimates have no effect on the final values.

#### Specific Problems and Identification Procedure:

In relation to the major ingredients for successful identification outlined above, there are four additional problems which increase the difficulties in identifying nonlinear stability and control characteristics in the post-stall high angle of attack flight regime. These are associated with:

1. The complexity and uncertainty of the aerodynamic model(s) required,
2. the gross or large maneuver requirements,
3. the instrumentation, and
4. the short time duration of maneuvers where one particular model is applicable.

The first three requirements lead to a very high dimensional (and, therefore, a computationally demanding) identification problem because of the large number of unknown parameters needed to represent the model accurately. The fourth item further compounds the problem because the relatively unstable and uncontrollable nature of the aircraft in this flight regime could force the aircraft to traverse the angle of attack range of interest rather quickly, thereby providing only short time-duration records if the aircraft maneuvers are not first carefully planned. The approach taken here was to reduce the dimensionality of the identification problem by separating the overall problem into separate lower dimensional problems, the solutions of which are computationally practical. The three areas of concern and the approach taken are discussed below.

First, the aircraft model, that is, the functional forms of  $f(\cdot)$  and  $h(\cdot)$  in Equation (1), must be selected to adequately represent the aircraft motions to be measured. The model should contain all of the terms of significance that contribute to the forces and moments on the airframe. This includes kinematic terms, inertia coupling, gravitational, thrust, engine gyroscopic effects and aerodynamic forces and moments. The aerodynamic forces and moments in this flight regime are highly nonlinear functions of several variables and a Taylor's series representation of the aerodynamics, where the constant coefficients in these expansions are the unknown parameters to be identified, can contain a large number of terms that can be candidates for logical inclusion in the model.

In order to reduce the number of terms, three approaches can be taken to the problem of identification of high angle of attack ( $\alpha$ ) aerodynamics. They can be described as:

- fixed point identification
- complete range identification
- limited range identification

Fixed point identification, where the small perturbation equations of motion about a trim or reference flight condition may be applicable, has the favorable feature of using simple linear models with a small number of parameters to identify. However, its major drawback for high angle of attack identification is that the model is good only for very short periods of time, too short to get meaningful identification results. Stability derivatives change very rapidly at high angles of attack, so a fixed point identification would only be good for a very small range of  $\alpha$ . Compounded with this drawback is the fact that the airplane may be highly unstable at high angles of attack so that the airplane cannot be held at a particular  $\alpha$  for any significant length of time.

The complete angle of attack range approach to identification overcomes the problems of using a linear model at fixed points to describe a highly nonlinear system. Using the complete range approach, an analytical aerodynamic model complex enough to describe the aircraft at all angles of attack can be developed. There would be no need to try to hold an unstable airplane at a constant angle of attack. However, there is the problem of having too complex a model. To adequately define the complete aerodynamics of an aircraft from normal cruise  $\alpha$  through post stall maneuvers may require more than 150 parameters. The practicalities

and economics of enabling an identification technique to handle such a large model precluded the possibility of taking this approach.

A limited range of angle of attack identification, where the model is applicable for a selected range of angle of attack, for example, is a practical compromise between the above two approaches. With this approach an analytical model is chosen to adequately represent the aerodynamics for selected ranges of angle of attack, sideslip angle, Mach number, and altitude. The ranges are selected on the basis of wind tunnel data and the available flight test data within the candidate ranges. Hopefully, enough data will be available in each range so that the unknown parameters can be accurately extracted and that only the parameter values change for different ranges of Mach number and altitude, not the model form. After identification of the aerodynamics at different ranges of angle of attack, a complete model can be pieced together to define the aerodynamics of the aircraft for the full range of  $\alpha$ .

The latter approach was considered the only one feasible for this program because of the flight data base available. The aerodynamics to be identified were expressed in aircraft body axis, nondimensional form instead of stability axes for two reasons:

1. The extracted coefficients could be compared directly to the wind tunnel data which was presented in the body axis system, and
2. the force coefficients ( $C_x$ ,  $C_y$  and  $C_z$ ) in the body axis system are directly related to the individual body fixed linear acceleration measurements ( $n_x$ ,  $n_y$  and  $n_z$ ).

Taylor's series expansion were used to represent these nondimensional coefficients, where the coefficients of the expansion are the unknown parameters to be identified, because the resulting analytical forms are readily amenable for use in the present identification algorithms.

The following assumptions were also made:

1. Power effects were included in the aerodynamic coefficients to be estimated.
2. The mass, moments of inertia, and center of gravity of the aircraft are known precisely.
3. The aircraft is rigid and no turbulence or wind effects are present.
4. Mach effects for  $M < .5$  and hysteresis effects due to flow separation are negligible.
5. Angle of attack and sideslip angle rate effects are included in the appropriate rotary derivatives.
6. Control surface deflections are measured perfectly.
7. The actual complexity of the aerodynamics (that is, the number of terms and the functional dependence of the variables) is no greater than the wind tunnel data indicates, especially for the static coefficients.

The other two areas which increase the dimensionality of the problem are the instrumentation system and the modeling of gross maneuvers which requires a complete six-degree-of-freedom representation of the aircraft. Even with the limited range identification approach, the number of unknown parameters to be concurrently identified is still extremely large. The measurement system,  $h(x, \rho, u)$  in Equation (1), must be modeled and if instrumentation inconsistencies or bias errors are present in addition to the random error,  $v_i$ , these errors will degrade the accuracy of the estimated aerodynamic parameters if not taken into consideration (References 3, 4 and 5). If these effects are modeled and identified simultaneously with the aerodynamic parameters, it will be extremely difficult to separate errors in the instrumentation from errors caused by incorrectly representing the aerodynamics.

This consideration is especially important for high angle of attack testing, since the large full scale ranges required of the instrumentation and large aircraft maneuvers accentuate these errors. To alleviate this difficulty, and consequently reduce the number of parameters to be concurrently identified, instrumentation consistency checks and error estimation can first be performed using the aircraft kinematic equation and measurement system model with the iterated Kalman filter/fixed-point smoother. The equations, which are given in Table I and discussed below, are the six-degree-of-freedom kinematic equations of the aircraft with the body-fixed airframe linear accelerometers and rate gyros used in the manner of a strapped down inertial measuring unit. This mechanization allows for the extraction of instrumentation biases from the flight data and the optimal state estimation of the aircraft trajectory ( $V, \alpha, \beta, \phi, \theta$ ) using the Kalman filter to further reduce the effects of measurement noise. In addition, an automatic procedure is thereby provided to optimally transform angle of attack and sideslip angle measurements at the boom to those at the center of gravity of the aircraft and to estimate the aircraft initial conditions. It should be noted that if angular acceleration sensors ( $\dot{p}, \dot{q}, \dot{r}$ ) are available, which was not the case, then an optimal estimate of the aircraft rotational rates ( $p, q, r$ ) can also be easily obtained by simply expanding the instrumentation consistency check equations to model these additional measurements.

To further reduce the computational burden, when employing the iterated Kalman filter, the six-degree-of-freedom equations of motion of the aircraft were separated into two separate four-degree-of-freedom systems; one for extracting the longitudinal coefficients ( $C_x, C_z$  and  $C_m$ ) and the other for the lateral-directional coefficients ( $C_L, C_n$ , and  $C_y$ ). These equations and a discussion on the choice of coordinate system used are given in the following section.

In summary, the overall identification procedure is illustrated in block diagram form in Figure 2. It can be summarized by the following five steps:

1. Model form is initially determined from wind tunnel data by representing the nondimensional aerodynamic force and moment coefficients by Taylor's series expansion for selected ranges of angle of attack, Mach number, and sideslip angle. The constant coefficients in these expansions represent the unknown parameters to be extracted from the flight data.

2. The six-degree-of-freedom aircraft kinematic equations and measurement system model are mechanized in the iterated Kalman filter/fixed-point smoother (IKF/FP) to identify instrumental errors in the form of biases, aircraft initial conditions, and generate an optimal state estimate of the aircraft trajectory ( $V, \alpha, \beta, \phi, \theta$ ). This procedure separates the identification of instrumentation errors from the identification of aerodynamic parameters and reduces the effects of measurement noise contaminating the air data and attitude measurements.
3. The results of step 2 are used to compute the six total nondimensional aerodynamic forces and moments exerted on the aircraft using the corrected rate and acceleration measurements and computed thrust and engine gyroscopic characteristics. Angular accelerations ( $\dot{p}, \dot{q}, \dot{r}$ ) are obtained from angular rate measurements ( $p, q, r$ ). Candidate model forms selected from step 1 above are used in the least squares (LS) identification technique to identify the parameters in the aerodynamic model forms by minimizing the error in satisfying the aerodynamic equations with respect to the unknown parameters in the equations. The error in the fit and the normalized regressor in the technique provide an approximate indication as to the adequacy of the candidate models and identifiability of the unknown parameters from the flight data.
4. The results from step 3, tempered with the values for the coefficients from the wind tunnel data, provide a priori estimates of the model form and initial parameters and covariance estimates for the IKF identification technique. Model structure verification is done with the aid of the residual sequences in the Kalman filter. If the model is accurate, and the instrumentation errors are truly zero mean, these residuals are zero mean and random. The final covariance matrix serves as a check on the accuracy and identifiability of the resulting parameter estimates.
5. Model verification, the last step, is performed by building up an aerodynamic model base which can be used in a simulation to predict the time histories of flight data in the flight regimes of applicability. This, of course, represents the true test as to the accuracy of the extracted parameters.

#### SYSTEM MODELS FOR IDENTIFICATION

A total of three models were used in the iterated Kalman filter/fixed-point smoother identification algorithm. These were the aircraft kinematic equations and measurement system for the identification of instrumentation errors and generation of state estimates of the aircraft trajectory and two separate four DOF systems: one for extracting the longitudinal coefficients ( $C_x, C_y$  and  $C_m$ ) and the other for extracting the lateral-directional coefficients ( $C_L, C_n$  and  $C_y$ ).

#### Aircraft Kinematic Equations:

The six-degree-of-freedom aircraft kinematic equations and measurement systems used for the identification of instrumentation errors are given in Table I with appropriate definitions. The kinematic equations are written in the aircraft body axes systems with three linear inertial velocities ( $u, v, w$ ), one linear position ( $h$ ) and the three Euler angles ( $\theta, \phi, \psi$ ) as state variables. Forcing inputs to these equations are measured time histories of the linear accelerations ( $n_x, n_y, n_z$  corrected to the c.g.) and the rotational rates ( $p, q, r$ ). Errors in these measurements are modeled as constant biases (for example,  $n_{x_b}, n_{y_b}, n_{z_b}, p_b, q_b, r_b$ ) to be identified. Since the linear accelerations and rate gyro measurements are contaminated with random measurement noise, the use of these measurements in the kinematic equation introduces process noise or equation error into the dynamical system and consequently makes the system model stochastic. These noise inputs are accounted for by the  $w_i, i = 1, \dots, 6$  noise terms in the equation.

Seven parameters are modeled in the measurement system. These include true airspeed ( $V_m$ ), boom vane angle of attack ( $\alpha_m$ ) and sideslip angle ( $\beta_m$ ) with the appropriate corrections, altitude ( $h_m$ ) and the three Euler angles ( $\theta_m, \phi_m, \psi_m$ ). Bias errors are included in all measurements to be identified in addition to scale factor errors in the air data measurements to model possible airflow effects. Auxiliary equations are included to generate optimal state estimates of  $V, \alpha, \beta$  (at the c.g.) for use during the identification of the aerodynamic coefficients. Other common sources of sensor errors, such as time lags in  $h_m$ , for example, were not modeled completely but were accounted for in the bias parameters and random noise terms. The units used are self-explanatory.

Note that all the instrumentation is assumed perfectly aligned to the aircraft reference body axis and that the major source of errors are treated as biases in the measurements in addition to the random noise terms. The rectangular body axis coordinate system ( $u, v, w$ ) was used instead of the nonorthogonal system ( $V, \alpha, \beta$ ) because the accelerometer biases appear linearly in the dynamical system and the  $\alpha, \beta$  vane measurement models are less complicated in the  $u, v, w$  system.

The instrumentation consistency check equations as given in Table I contain two approximations. These are associated with neglecting the effects of random errors (noise) in the rate gyro measurements in accounting for airplane rotation rates in the  $\alpha_{V_m}$  and  $\beta_{V_m}$  measurement models and the linear acceleration corrections to the center of gravity. Modeling these noise terms would make the process and measurement noise statistics correlated and the measurement noise nonstationary and extremely complex. Errors in neglecting these effects were never fully investigated, but they are small for reasonable levels of rate gyro measurement noise.

However, if angular acceleration sensors are available, the errors caused by the above approximations can be eliminated by simply including three angular acceleration equations in the dynamical model and adding the rate gyro measurements to the measurement system. This will also eliminate the modeling of rate biases ( $p_b, q_b, r_b$ ) and the  $w_4, w_5$ , and  $w_6$  process noise terms in the dynamic model. In addition, an optimal estimate can now be generated for the aircraft rotational rates,  $p, q$ , and  $r$ . The additions required to the equations of Table I when angular acceleration measurements are available are given in Equation (3) on the following page.

Dynamical Model:

$$\begin{aligned}\dot{p} &= \dot{p}_m + \dot{p}_b + w_7 \\ \dot{q} &= \dot{q}_m + \dot{q}_b + w_8 \\ \dot{r} &= \dot{r}_m + \dot{r}_b + w_9\end{aligned}\quad (3a)$$

Measurement System:

$$\begin{aligned}p_m &= p + p_b + v_8 \\ q_m &= q + q_b + v_9 \\ r_m &= r + r_b + v_{10}\end{aligned}\quad (3b)$$

$\dot{p}_b$ ,  $\dot{q}_b$  and  $\dot{r}_b$  are the unknown angular acceleration bias parameters and  $w_7$ ,  $w_8$ , and  $w_9$  the random component of noise on the respective measurements.

#### Four-Degree-of-Freedom Longitudinal and Lateral-Directional Models:

As indicated above, the representation of the aircraft characteristics in the post-stall flight regime when large maneuvers are encountered for identification purposes requires a six-degree-of-freedom (DOF) nonlinear equations-of-motion model and at least two kinematic relationships to describe the evolution of the roll and pitch Euler angles. Further, the use of Taylor series expansions to adequately represent all six aerodynamic force and moment coefficients over a large enough range of angle of attack (as dictated by the flight data being used), leads to a very high-dimensional and, therefore, a computationally demanding identification problem.

To circumvent the high degree of dimensionality, the identification problem was reduced by separating the equations of motion into two systems, one for extracting the longitudinal coefficients ( $C_x$ ,  $C_z$ , and  $C_m$ ) and the other for extracting the lateral-directional coefficients ( $C_y$ ,  $C_n$  and  $C_l$ ), with cross-coupling turns entering similarly to the control inputs. The systems of equations used are given in Tables II and III respectively, along with appropriate definitions.

The force equations in both systems are written in the nonorthogonal coordinate system ( $V, \alpha, \beta$ ), instead of the rectangular body axis system ( $u, v, w$ ), because the dynamic equations and the measurement system are the most linear with respect to the state variables for this system. This is the case because the time history responses of  $V, \alpha, \beta$  are measured directly ( $\alpha$  and  $\beta$  at the c.g. are available as state estimates from the instrumentation consistency checks) and more importantly because the aerodynamic forces and moments are expressed as functions of  $\alpha$  and  $\beta$ , so that auxiliary calculations are not required. Both systems are also four-degree-of-freedom, instead of the conventional three. The lift and side force degrees of freedom are included in both sets of equations because the aerodynamic forces and moments are strong functions of both  $\alpha$  and  $\beta$ ; particularly  $\alpha$ . Due to large attitude maneuvers, the roll and pitch Euler angles are also included in both systems. All aerodynamic coefficients are in the body axis reference system. Although the aircraft state estimates from the instrumentation consistency checks serve to reduce the bias inherent in the LS estimates, it should be noted that their use as measurements in the IKF invalidates the assumption of independent measurement noise.

The equations are fairly general and no simplifying assumptions, such as small angle approximation, for example, have been made to limit their range of applicability, except that  $|\theta| < 90^\circ$ . In addition, to further reduce the number of parameters to be concurrently identified, the  $n_x$  linear accelerometer measurement can be used to account for the x-force contribution ( $C_x$ ) to the longitudinal equations and similarly the  $n_y$  accelerometer measurement can account for the y-force contribution ( $C_y$ ) in the lateral-directional model. The analytical representation of a force or moment coefficient, for example, the  $C_{m_3}$  static moment coefficient of Table II, is given by the typical expression

$$C_{m_3}(\alpha, \beta) = C_{m_0} + \sum_i C_{m_{\alpha(i)}} \alpha^{(i)} + \sum_j \sum_i C_{m_{\alpha(i)\beta(j)}} \alpha^{(i)} \beta^{(j)}$$

where  $\alpha^{(i)}$ ,  $\beta^{(j)}$  represent the  $i^{\text{th}}$  power of  $\alpha$  and the  $j^{\text{th}}$  power of  $\beta$ , respectively. The  $\alpha$  and  $\beta$  effects are lumped with the rotary derivatives due to their linear dependency. That is, the effects or sensitivity of the measured responses of the airplane to a variation in  $C_{m_2}$  or  $C_{m_{\alpha}}$ , for example, would be almost identical.

In both models, the linear acceleration measurements are first corrected to the c.g. using the appropriate transformation. Forcing inputs to the longitudinal model (Table II) include the stabilator control ( $\delta_s$ ), effective roll control ( $\delta_a$ ), thrust ( $T_x, T_z$ ), thrust moment ( $m_{y_r}$ ) and air density ( $\rho$ ). Cross-coupling inputs are measured roll and yaw rate ( $\dot{p}_m, \dot{r}_m$ ) and side acceleration ( $n_{y.c.g.}$ ). For the lateral-directional model (Table III), forcing inputs are the rudder control ( $\delta_r$ ), effective roll control ( $\delta_a$ ), thrust ( $T_y$ ), thrust moment ( $m_{x_r}, m_{y_r}$ ) and the cross-coupling inputs are measured pitch rate ( $\dot{q}_m$ ), airspeed ( $V_m$ ), and linear accelerations ( $n_{x.c.g.}, n_{y.c.g.}$ ).

It should also be noted that by including the cross-coupling and other forcing terms in the dynamic equations (thru the use of the measured time histories of the linear accelerations and the rotational rates) inherently leads to the introduction of process noise into the model. That is, these inputs are in error by an amount equal to the measurement noise on their sensor outputs and consequently, this error is introduced into the dynamical system model as process noise. The identical situation occurs with the kinematic equations used for instrumentation consistency checking as described in the preceding subsection.

The process noise introduced this way is lumped into the  $w_i$ ,  $i = 1, \dots, 6$  noise terms which are assumed zero-mean, white Gaussian uncorrelated stationary noise processes. An approximate lower bound

for the variances of  $w_i$  can be calculated as follows:

For the longitudinal model, let

$$\begin{aligned} n_{x_m} &= n_x + n_{x_n} \\ p_m &= p + p_n \\ r_m &= r + r_n \\ n_{y_m} &= n_y + n_{y_n} \end{aligned} \quad (4)$$

where  $n_{x_n}$ ,  $p_n$ ,  $r_n$  and  $n_{y_n}$  are zero-mean white Gaussian measurement noise. Substituting Equation (4) into the dynamical model equations given in Table II, assuming  $\cos \beta = 1$  and eliminating terms of second order (for example  $p_n r_n \approx 0$ ), it can be shown that

$$\begin{aligned} w_1 &= n_{x_n} \cos \alpha + n_{y_n} \sin \beta \\ w_2 &= I_3 (r p_n + p r_n) + 2 I_4 (p p_n - r r_n) - \frac{h_{x_2}}{I_y} r_n \\ w_3 &= \left( \frac{57.3}{V} \right) \sin \alpha n_{x_n} - \tan \beta (p_n \cos \alpha + r_n \sin \beta) \\ w_4 &= - \left( \frac{57.3}{V} \right) \cos \alpha \sin \beta n_{x_n} + p_n \sin \alpha - r_n \cos \alpha + \frac{57.3}{V} n_{y_n} \\ w_5 &= p_n + \cos \phi \tan \theta r_n \\ w_6 &= - \sin \phi r_n \end{aligned} \quad (5)$$

if all other possible equation error is assumed equal to zero. From Equation (5) it can be readily seen that  $w_i$ ,  $i = 1, \dots, 6$  are correlated and nonstationary even though  $n_{x_n}$ ,  $p_n$ ,  $r_n$  and  $n_{y_n}$  are uncorrelated and stationary. However, two additional approximations were made:

1.  $w_i$ ,  $i = 1, \dots, 6$ , were made stationary by choosing constant reference values for  $\alpha$ ,  $\beta$ ,  $V$ ,  $r$ , and  $p$ . The reference values are, of course, dependent upon the flight record being analyzed.
2. Neglect all cross correlations between  $w_i$ ,  $i = 1, \dots, 6$ .

With the above approximations, Equation (5) can now be used to calculate the variances for  $w_i$  given the noise statistics for  $n_{x_n}$ ,  $p_n$ ,  $r_n$  and  $n_{y_n}$ . A similar set of equations can be derived for the lateral-directional model.

The errors introduced by the addition of process noise into the dynamical model and the above approximations are small in comparison to other possible error sources, such as model form, for example. Of course, the smaller the measurement errors in these sensors, the more accurate the approximations.

#### GENERAL COMMENTS

Before presenting the identification results, this section will review (briefly) some of the symptoms and causes of identifiability problems, which can occur with poorly conditioned data, and the indicators available in the identification algorithm to detect these potential problems. Additionally, combining results from two or more flight records and computing the accuracy of estimated total coefficient, for example  $C_m(\alpha)$ , is presented.

Parameter identifiability is concerned with the ability to identify the associated parameters of the model from the flight data, for it is intuitively obvious that those parameters which have no effect on the data cannot be identified. Identifiability also relates to whether the parameters themselves can be identified separately or whether they can only be identified as part of a linear combination. Most identification problems are those related to the identifiability of the parameter set and are usually the result of the use of poorly conditioned data caused by the application of an improper control input.

Stated formally (Reference 2), a nonstochastic system, linear or nonlinear, is identifiable if and only if the sensitivity vector functions of the measurements with respect to the unknown parameters representing the system are nontrivial (nonzero) and linearly independent. This, of course, is equivalent to saying that small changes in each parameter must produce a change in the measured responses of the aircraft and these changes must be a different type for each parameter. For a linear system, this implies all the natural modes of the system must be excited and the control inputs must be linearly independent among themselves and also linearly independent of the state variables. If these conditions are met, the accuracy of the parameter estimates are also functions of the level of measurement noise present and the data record length, i.e., the signal to noise ratio in the output measurements.

In practice, unrealistic parameter estimates are usually obtained whenever the sensitivity of the output measurements to changes in these parameters is small (low signal to noise ratio) or else there is strong dependency between the sensitivities of several parameters. These problems are readily identified in the IKF identification algorithm by comparing the size of the diagonal elements in the final covariance matrix ( $P_f$ ) with the size of the diagonal elements of the initial covariance matrix ( $P_0$ ) and by observing the size of the off-diagonal correlation coefficients in the normalized  $P_f$  matrix; large values, for example

greater than .9, indicate potential problems. Two possible solutions to these problems are to use a priori weighting with  $\hat{\rho}_0$  or to fix one or more of the parameters in the group which show high correlation at the "best guess" values (e.g., wind tunnel values). A priori weighting is accomplished by reducing the magnitude of the initial parameter variance in  $\hat{\rho}_0$  so as to reflect a more accurate initial parameter estimate and hence weight the initial estimate more heavily. If information is available from other flight records, it can be incorporated in this fashion. However, if the model form is adequate, the parameters which exhibit high sensitivity in the measurements and are not correlated with other parameters, usually are extracted relatively accurately even if other groups of parameters are highly correlated. Model adequacy is determined from the residual sequences.

For the nonlinear aircraft identification problem, it was observed that relatively large correlations usually existed between the parameter estimates making up a particular lumped coefficient (e.g.,  $C_{m\dot{\alpha}}(\omega)$ ). If large correlations did not exist between the parameter estimates representing different lumped coefficients, this "internal correlation" did not appear to be a particular problem. This internal correlation was expected and is usually present between the parameters in polynomial representations. Also, if the number of terms in the series representing a particular coefficient is not adequate for the range of angle of attack being considered, the resulting extracted coefficient tends to match the actual coefficient only in the range of angle of attack where most of the data and excitation occur. An additional difficulty occurs when the data record length in which the aircraft excitation occurs is short, as an asymptotically convergent solution is then not possible. In this case, extremely unrealistic coefficient values in certain ranges of angle of attack may be obtained.

Associated with each estimated coefficient are their second control moments or variances which are computed using the final covariance matrix of the parameter estimates from the identification algorithm. These variances represent a band of uncertainty associated with the estimated coefficient which must be taken into consideration when comparing the estimated coefficient to wind tunnel data or when combining estimates from different flight records. Coefficient estimates combined from different flight records, which traversed different ranges of  $\alpha$  and  $\beta$ , must be done on a point by point basis at discrete values of  $\alpha$  and  $\beta$ . Coefficients estimated over a particular range of  $\alpha$  and  $\beta$ , where a low order polynomial representation was used for this particular range, cannot be expected to predict outside this range.

## RESULTS

Extensive application of the identification procedure for the extraction of the nonlinear aerodynamic stability and control parameter of the F-4E aircraft from flight test data is reported in Reference 1. A few of these results are presented below.

The majority of low speed wind tunnel data used to obtain the initial model representation was obtained from two NASA reports (References 6 and 7) and accompanying data tabulations from a series of tests in the Langley Full-Scale Wind Tunnel. For comparison purposes, data was also obtained from References 8 and 9. Data from Reference 8 will be referred to as Ames data, although the rotary derivatives were actually obtained from a set of Langley results.

The flight data is from the Stall/Near-Stall Investigation of the F-4E aircraft (Reference 10) which was conducted at Edwards Air Force Base. Specifically, the results from two flight records are presented, both of which are for the 10 to 23 degree angle of attack range at Mach numbers between .4 and .47. One record, called Record 9, had primarily a longitudinal stabilator pulse type input applied and the other, labeled Record 10, had aileron pulse type inputs applied with very little rudder excitation. All data were recorded at a common sample rate of 10 samples per second and time de-skewed to a common reference time point using linear interpolation. The measurements consisted of the standard flight parameters and certain engine parameters. All three aircraft body reference inertial attitudes, angular rates and linear accelerations were available in addition to air data measurements from nose boom mounted range of attack and angle of sideslip vanes and a pitot-static head. Special calculations, needed for Mach number, true airspeed, air density and an estimate of engine thrust, for example, were also performed.

Angular accelerations were derived from the angular rates using digital filtering techniques and a modified spline function computer program, the details of which are given in Reference 1. These derived accelerations are used, along with the linear accelerometer measurements and other flight parameters, to generate the nondimensional aerodynamics force and moment time histories for use with the LS identification technique.

Prior to the extraction of the aerodynamic parameters, instrumentation consistency checks were performed. Consistent biases in all three rate measurements, the  $\dot{\alpha}$  and  $\dot{\beta}$  linear accelerometers, pitch attitude and angle of attack were identified. All biases were within the expected accuracy of the instrumentation, except for the angle of attack vane which was reading approximately three degrees too high. As an example, comparisons between the flight data and predicted responses for Record 10, using the kinematic model of Table I, without and with biases, are given in Figures 3 and 4, respectively. Crosses represent the flight data and solid traces are the predicted responses. The improvement is readily apparent.

Record 9 has very good aircraft excitation and control input ( $\delta_e$ ) for identification of the longitudinal coefficients ( $C_x$ ,  $C_z$  and  $C_m$ ) but very little lateral-directional excitation. The results of the identification using this record are given in Figures 5, 6 and 8. Figure 5 shows a comparison of the non-dimensional force and moment time histories ( $C_x$ ,  $C_z$  and  $C_m$ ) with those computed using the estimated coefficients from the LS techniques. The resulting model consisted of 21 parameters--6 to represent the  $C_x$  coefficient, 6 for the  $C_z$  coefficient and the remaining 9 for the  $C_m$  coefficient. Two parameters,  $C_{\dot{\alpha}}/\delta_a$  and  $C_{\dot{\beta}}/\delta_\beta$ , were held fixed at the wind tunnel values because of the small  $\delta_a$  input. Updating the model with the iterated Kalman filter identification technique produced the response comparisons given in Figure 6. These are the time history comparisons between the flight data and the predicted responses using the identified coefficients in the four-degree-of-freedom model given in Table II. Crosses represent flight data and solid traces, the predicted responses. The comparisons are excellent. The residuals, which are



not shown, also indicate an adequate model. These results were expected, since this record is considered good for identification purposes.

Figure 8 presents the identified coefficients from both the LS and IKF, overlaid on the wind tunnel coefficients for comparison. The wind tunnel data (Langley and Ames) are presented in the form of hand faired plots to the actual test data points for convenience and are representative for  $-15^\circ \leq \beta \leq 15^\circ$ .

The static  $C_L$  versus  $\alpha$  curve agrees almost exactly with the wind tunnel data.  $C_m$  showed a positive .03 shift from the wind tunnel data which is consistent with the least squares results and the positive increment in the extracted  $C_{Y\dot{\beta}}$ . This is also consistent with the increased moment effectiveness of the elevator ( $C_{m\delta_e}$ ). The static  $C_x$  versus  $\alpha$  curve showed a positive .05 shift or approximately 2300 pounds less drag or more thrust than the wind tunnel data indicated. Less damping in pitch,  $C_{m\dot{\alpha}}$ , was also obtained. An attempt was also made to identify a cubic  $C_m$  versus  $\alpha$  derivative, to see if the form of  $C_m$  would more closely approximate the wind tunnel data. The result was a  $C_{m\alpha^3}$  term that was almost zero. In general, all coefficients identified were very reasonable and the forms of the static aerodynamics for this angle of attack range appear to be similar to what the wind tunnel data predicts.

Similar results are presented for Record 10 in Figures 5, 7 and 9. These figures show the LS comparisons to  $C_L$ ,  $C_n$  and  $C_y$  time histories, the response comparisons using the four-degree-of-freedom lateral-directional model, and the coefficients identified overlaid on the wind tunnel data, respectively. As seen from Figures 5 and 7, this record has very little rudder deflection and yaw rate, implying that the rudder derivatives and the yaw rate derivatives and dynamic cross derivatives would not be identifiable. Indeed, these parameters had to be held fixed at the wind tunnel values. The results are fair, indicating the poor maneuvers in this record for identification purposes.

#### CONCLUDING REMARKS

The identification procedure described in this paper is demonstrated to be an adequate and accurate procedure for the identification of nonlinear aerodynamic stability and control parameters of an aircraft at high angles of attack if properly followed. Model definitions from wind tunnel data, selected range of angle of attack flight, separation of instrumentation and aerodynamic models, and partial decoupling of longitudinal and lateral-directional equations of motion to reduce the dimensionality problem are all shown to help considerably in reaching the final result of accurate parameter identification.

The results described in this paper also demonstrate the need for close cooperation between the flight test and flight data analysis engineers. A carefully designed instrumentation complement is essential. A series or set of control inputs specifically oriented towards the enhancement of vehicle parameter identifiability is also very important to the objective of obtaining accurate and useful results. Adequate identification algorithms exist now; future emphasis should be directed toward experiment design, for this is where the more significant improvements in parameter identification are likely to be obtained in the future.

#### REFERENCES

1. B. J. Eulrich and N. C. Weingarten, Calspan Corporation, "Identification and Correlation of the F-4E Stall-Post-Stall Aerodynamic Stability and Control Characteristics from Existing Test Data," 1973, Report No. AK-5126-F-1.
2. R.T.N. Chen, B.J. Eulrich, and J.V. Lebacqz, Calspan Corporation, "Development of Advanced Techniques for the Identification of V/STOL Aircraft Stability and Control Parameters," 1971, Report No. BM-2820-F-1.
3. R. T. N. Chen and B. J. Eulrich, "Parameter and Model Identification of Nonlinear Systems Using a Suboptimal Fixed-Point Smoothing Technique." Paper presented at the 1971 Joint Automatic Control Conference, August 1971.
4. D. DiFranco, Calspan Corporation, "In-Flight Parameter Identification by the Equations-of-Motion Technique--Application to the Variable Stability T-33 Airplane," 1965, Report No. TC-1921-F-3.
5. John A. Sorenson, NASA, "Analysis of Instrumentation Error Effects on the Identification Accuracy of Aircraft Parameters," 1972, Report No. CR-112121.
6. E. L. Anglin, NASA, "Static Force Test of a Model of a Twin-Jet Fighter Airplane for Angles of Attack from  $-10^\circ$  to  $110^\circ$  and Sideslip Angles from  $-40^\circ$  to  $40^\circ$ ," 1971, Report No. TN D-6425.
7. S. B. Grafton and C. E. Libbey, NASA, "Dynamic Stability Derivatives of a Twin-Jet Fighter Model for Angles of Attack from  $-10^\circ$  to  $110^\circ$ ," 1971, Report No. TN D-6091.
8. C. C. Brady, W. A. Moran, and Resenstein, M.L., McDonnell Douglas Corporation, "Model F-4 Spin Evaluation Program," 1969, Report No. MDC A0005, Vol. I and II.
9. W. J. Bonine, et al., McDonnell Douglas Corporation, "Model F/RF-4B-C Aerodynamic Derivatives," 1971, Report No. MDC-R-9842, Revision K.
10. C. E. McElroy, et al., Air Force Flight Test Center, Edwards AFB, California, "Stall/Near Stall Investigation of the F-4E Aircraft," 1970, Report No. FTC-SD-70-20.

TABLE I  
KINEMATIC EQUATIONS FOR INSTRUMENTATION CONSISTENCY CHECKS

Dynamical Model:

$$\begin{bmatrix} \dot{u} \\ \dot{v} \\ \dot{w} \\ \dot{h} \end{bmatrix} = \begin{bmatrix} 0 & r+r_b & -(q+q_b) & 0 \\ -(r+r_b) & 0 & p+p_b & 0 \\ q+q_b & -(p+p_b) & 0 & 0 \\ \sin\theta & -\sin\phi\cos\theta & -\cos\phi\cos\theta & 0 \end{bmatrix} \begin{bmatrix} u \\ v \\ w \\ h \end{bmatrix} + \begin{bmatrix} -\sin\theta & n_x \\ \cos\theta\sin\phi & n_y \\ \cos\theta\cos\phi & n_z \\ 0 & 0 \end{bmatrix} \begin{bmatrix} n_x \\ n_y \\ n_z \\ n \end{bmatrix} + \begin{bmatrix} 0 & -w & v \\ w & 0 & -u \\ -v & u & 0 \\ 0 & 0 & 0 \end{bmatrix} \begin{bmatrix} w_4 \\ w_5 \\ w_6 \\ 0 \end{bmatrix} + \begin{bmatrix} w_1 \\ w_2 \\ w_3 \\ 0 \end{bmatrix} + \begin{bmatrix} \text{c.g.} \\ \text{corrections} \\ \text{for} \\ n_x, n_y, n_z \end{bmatrix}$$

Inherent Process Noise

$$\begin{bmatrix} \dot{\phi} \\ \dot{\theta} \\ \dot{\psi} \end{bmatrix} = \begin{bmatrix} 1 & \sin\phi\tan\theta & \cos\phi\tan\theta \\ 0 & \cos\phi & -\sin\phi \\ 0 & \sin\phi/\cos\theta & \cos\phi/\cos\theta \end{bmatrix} \begin{bmatrix} p+p_b & +w_4 \\ q+q_b & +w_5 \\ r+r_b & +w_6 \end{bmatrix}$$

Inherent Process Noise

Measurement System:

$$V_m = (1+V_g)(u^2+v^2+w^2)^{1/2} + V_b + v_1, \quad \alpha_{V_m} = (1+\alpha_g)\tan^{-1}\left(\frac{w-(q+q_b)L_{z_b}}{u}\right) + \alpha_{V_b} + v_2$$

$$\beta_{V_m} = (1+\beta_g)\tan^{-1}\left(\frac{v+(r+r_b)L_{z_b}-(p+p_b)L_{y_b}}{u}\right) + \beta_{V_b} + v_3$$

$$h_m = h + h_b + v_4, \quad \phi_m = \phi + \phi_b + v_5, \quad \theta_m = \theta + \theta_b + v_6, \quad \psi_m = \psi + \psi_b + v_7$$

Forcing Inputs:

$p, q, r, n_x, n_y$  and  $n_z$  measurements

Definitions and Notes:

Subscripts  $b$  - Bias parameters to be identified

Subscripts  $g$  - Scale factor parameters to be identified

$w_1, w_2, w_3$  - Zero mean, white Gaussian process noise, introduced because of measurement noise contaminating  $n_x, n_y, n_z$  measurements

$w_4, w_5, w_6$  - Zero mean, white Gaussian process noise, introduced because of measurement noise contaminating  $p, q, r$  measurements

$v_i$  - Zero mean, white Gaussian measurement noise

$L_{x_b}, L_{y_b}, L_{z_b}$  - Locations of  $\alpha$  and  $\beta$  vanes from the c.g. along  $x, y, z$  body axes

TABLE II  
FOUR-DEGREE-OF-FREEDOM LONGITUDINAL MODEL

Dynamical Model:

$$\dot{V} = \left[ (b_3 V^2 C_{x_s} + b_4 V C_{x_d} + \frac{T_x}{m}) \cos\alpha + (b_3 V^2 C_{y_s} + b_4 V C_{y_d} + \frac{T_y}{m}) \sin\alpha \right] \cos\beta - g \sin\tau + g n_{y_m} \sin\beta + w_1$$

$$\dot{q} = b_1 V^2 C_{m_s} + b_2 V C_{m_d} + I_3 p_m \cdot r_m + I_4 (r_m^2 - p_m^2) - \frac{h_{1x}}{I_y} r_m + \frac{m_{4r}}{I_y} + w_2$$

$$\dot{\alpha} = \frac{1}{\cos\beta} \left\{ (b_3 V C_{y_s} + b_4 C_{y_d} + \frac{1}{V} \frac{T_y}{m}) \cos\alpha - (b_3 V C_{x_s} + b_4 C_{x_d} + \frac{1}{V} \frac{T_x}{m}) \sin\alpha \right\} + g \\ + \frac{1}{\cos\beta} \frac{g}{V} (\sin\theta \sin\alpha + \cos\theta \cos\phi \cos\alpha) - (p_m \cos\alpha + r_m \sin\alpha) \tan\beta + w_3$$

$$\dot{\beta} = -\sin\beta \left\{ (b_3 V C_{x_s} + b_4 C_{x_d} + \frac{1}{V} \frac{T_x}{m}) \cos\alpha + (b_3 V C_{y_s} + b_4 C_{y_d} + \frac{1}{V} \frac{T_y}{m}) \sin\alpha \right\} \\ + \frac{g}{V} (\sin\theta \cos\alpha - \cos\theta \cos\phi \sin\alpha) + \frac{g}{V} (n_{y_m} + \cos\theta \sin\phi) \cos\beta + p_m \sin\alpha - r_m \cos\alpha + w_4$$

$$\dot{\phi} = p_m + (q \sin\phi + r_m \cos\phi) \tan\theta + w_5, \quad \dot{\theta} = q \cos\phi - r_m \sin\phi + w_6, \quad \text{for } |\theta| < 90^\circ$$

where  $\sin\tau = (\cos\alpha \sin\theta - \sin\alpha \cos\phi \cos\theta) \cos\beta - \sin\theta \cos\theta \sin\beta$

TABLE II Cont.

Measurement System:

$$\begin{aligned} V_m &= V + v_1, & \phi_m &= \phi + v_2, & \alpha_m &= \alpha + v_3, & \beta_m &= \beta + v_4, & \theta_m &= \theta + v_5, & \psi_m &= \psi + v_6, \\ \dot{\eta}_{\phi m} &= \frac{1}{g} (b_3 V^2 C_{\phi_3} + b_4 V C_{\phi_4} + \frac{T_{\phi}}{m}) + v_7, & \dot{\eta}_{\alpha m} &= \frac{1}{g} (b_5 V^2 C_{\alpha_5} + b_6 V C_{\alpha_6} + \frac{T_{\alpha}}{m}) + v_8 \end{aligned}$$

Control or Forcing Inputs:  $S_s, S_a, T_x, T_y, m_{y_T}, \rho$ Cross-Coupling Inputs:  $\dot{\psi}_m, \dot{\psi}_m, \eta_{y_m}$  (at c.g.)

Definitions:

- $d's$  - Dimensionalizing terms which may also be a function of air density  
 $I_x, I_y$  - Function of moment of inertia  
 $C_{x_0}, C_{y_0}, C_{\eta_{xy}}$  - Static Force or Moment Aerodynamic Coefficient; functions of parameters to be identified  
 $C_{x_d}, C_{y_d}, C_{\eta_{yd}}$  - Dynamic or Rotary Aerodynamic Coefficients; functions of parameters to be identified  
 $w_i, v_i$  - Zero mean, white Gaussian process and measurement noise  
 $T_x, T_y$  - Thrust force along x and y body axes  
 $m_{y_T}$  - Thrust moment around y axis

TABLE III

FOUR-DEGREE-OF-FREEDOM LATERAL-DIRECTIONAL MODEL

Dynamical Model:

$$\begin{aligned} \dot{p} &= d_1 V^2 C_{p_1} + d_2 V C_{p_2} + d_3 V^2 C_{p_3} + d_4 V C_{p_4} + I'_x m_{x_T} + I'_{xy} m_{y_T} + (I_x r + I_z p + I'_{xz} h_{I_x}) q_m + w_1 \\ \dot{r} &= d_5 V^2 C_{r_1} + d_6 V C_{r_2} + d_7 V^2 C_{r_3} + d_8 V C_{r_4} + I'_{xy} m_{x_T} + I'_y m_{y_T} + (I_y r - I_z p + I'_{yz} h_{I_y}) q_m + w_2 \\ \dot{\beta} &= \frac{g}{V} \left\{ \left[ (\sin \theta - \eta_{\psi m}) \cos \alpha - (\cos \theta \cos \phi + \eta_{\phi m}) \sin \alpha \right] \sin \beta + \cos \theta \sin \phi \cos \beta \right\} \\ &\quad + \cos \beta (d_9 V C_{\beta_9} + d_{10} C_{\beta_{10}} + \frac{1}{V} \frac{T_y}{m}) + p \sin \alpha - r \cos \alpha + w_3 \\ \dot{\alpha} &= \frac{g}{V \cos \beta} \left\{ (\sin \theta - \eta_{\psi m}) \sin \alpha + (\cos \theta \cos \phi + \eta_{\phi m}) \cos \alpha \right\} - (p \cos \alpha + r \sin \alpha) \tan \beta + q_m + w_4 \\ \dot{\phi} &= p + (q_m \sin \theta + r \cos \theta) \tan \theta + w_5, & \dot{\theta} &= q_m \cos \theta - r \sin \theta + w_6, & \text{for } |\theta| < 90^\circ \end{aligned}$$

Measurement System:

$$\begin{aligned} p_m &= p + v_1, & r_m &= r + v_2, & \beta_m &= \beta + v_3, & \alpha_m &= \alpha + v_4, & \phi_m &= \phi + v_5, & \psi_m &= \psi + v_6, \\ \dot{\eta}_{\phi m} &= \dot{\phi} + v_7, & \dot{\eta}_{\alpha m} &= \dot{\alpha} + v_8, & \eta_{y_m} &= \frac{1}{g} (d_{11} V^2 C_{y_5} + d_{12} V C_{y_6} + \frac{T_y}{m}) + v_9 \end{aligned}$$

Control or Forcing Inputs:  $S_r, S_\delta, S_\delta, T_y, \rho, m_{x_T}, m_{y_T}$ Cross-Coupling Inputs:  $q_m, v, \eta_{x_m}, \eta_{y_m}$  (at c.g.)

Definitions:

- $d's$  and  $I's$  - Dimensionalizing terms which may also be a function of air density  
 $C_{x_0}, C_{y_0}, C_{\eta_{xy}}$  - Static Aerodynamic Coefficients; function of parameters (and states) to be identified  
 $C_{x_d}, C_{y_d}, C_{\eta_{yd}}$  - Dynamic or Rotary Aerodynamic Coefficients; functions of parameters (and states) to be identified  
 $T_y$  - Thrust force along y-body axis  
 $m_{x_T}, m_{y_T}$  - Thrust moment around x, y body axes  
 $w_i, v_i$  - Zero mean, white Gaussian process and measurement noise

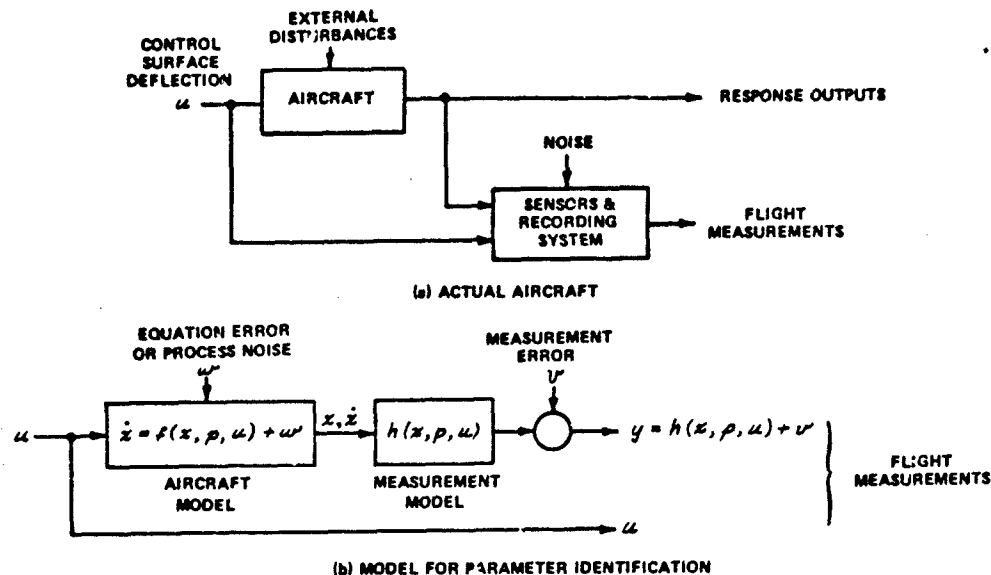


FIGURE 1 BLOCK DIAGRAM OF ACTUAL AIRCRAFT SYSTEM AND MODEL FOR PARAMETER IDENTIFICATION

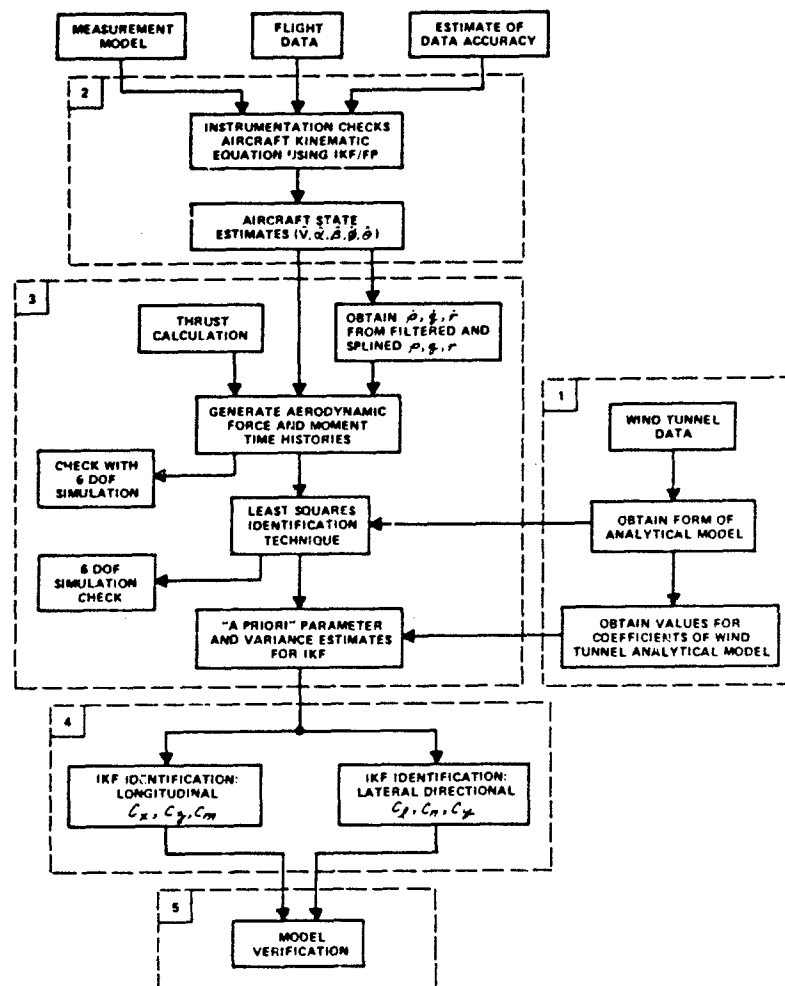


FIGURE 2 BLOCK DIAGRAM OF GENERAL IDENTIFICATION PROCEDURE

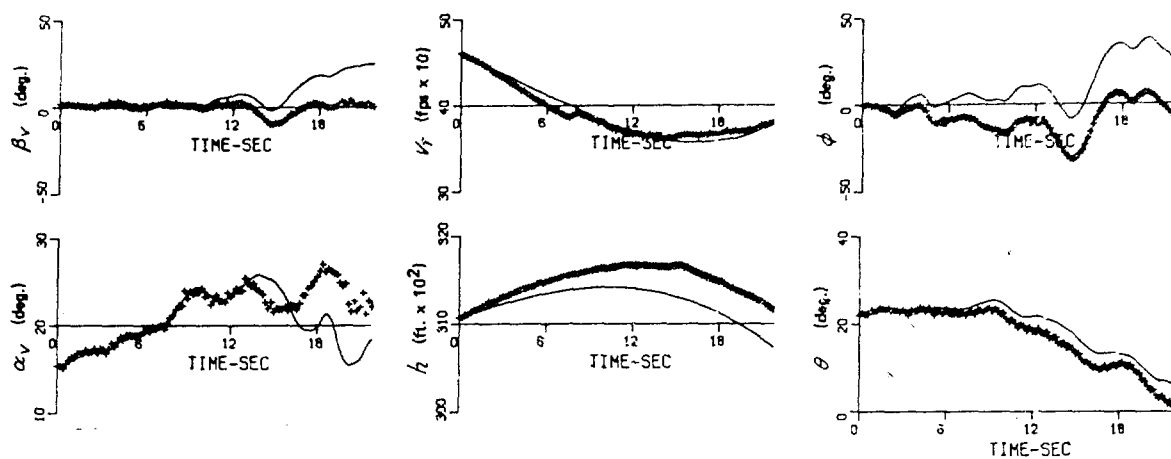


FIGURE 3 COMPARISON OF FLIGHT DATA WITH RESPONSES GENERATED FROM THE KINEMATIC EQUATIONS WITH NO BIASES - RECORD 10

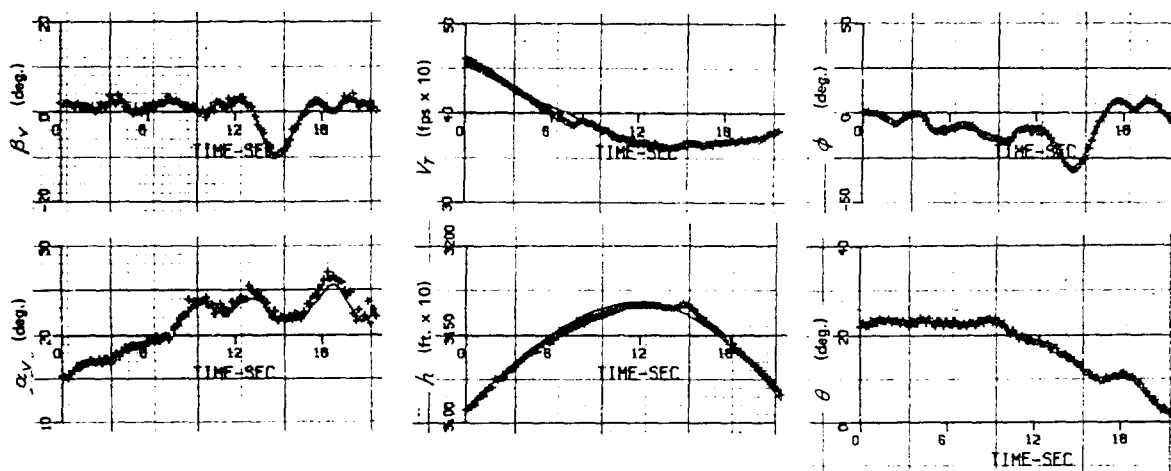


FIGURE 4 COMPARISON OF FLIGHT DATA WITH RESPONSES GENERATED FROM THE KINEMATIC EQUATIONS WITH IDENTIFIED  $n_{x_b}$ ,  $n_{z_b}$ ,  $p_b$ ,  $q_b$ ,  $r_b$ ,  $\alpha_{v_b}$ ,  $\theta_b$  BIASES - RECORD 10

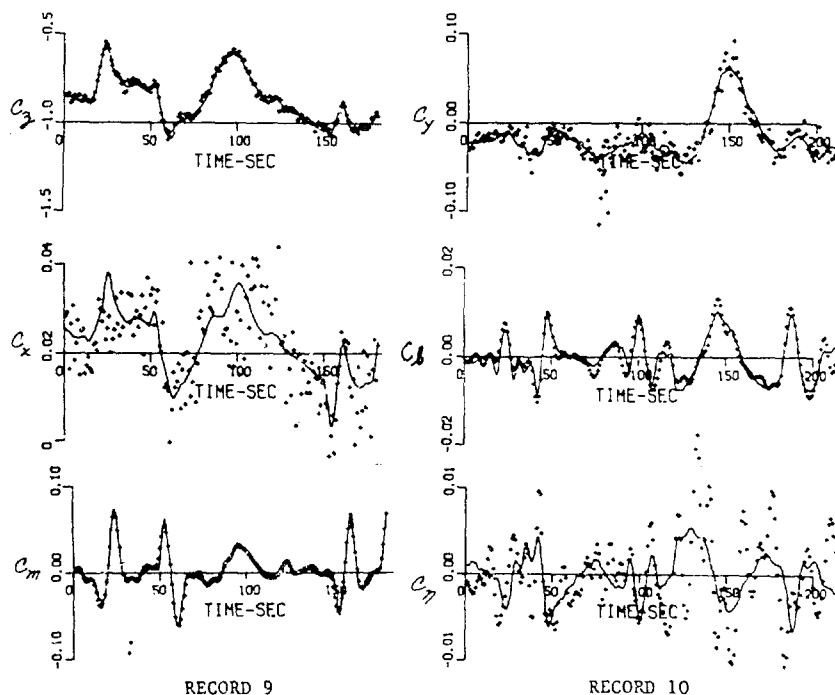


FIGURE 5 LEAST SQUARES FORCE AND MOMENT COMPARISONS WITH FLIGHT DATA

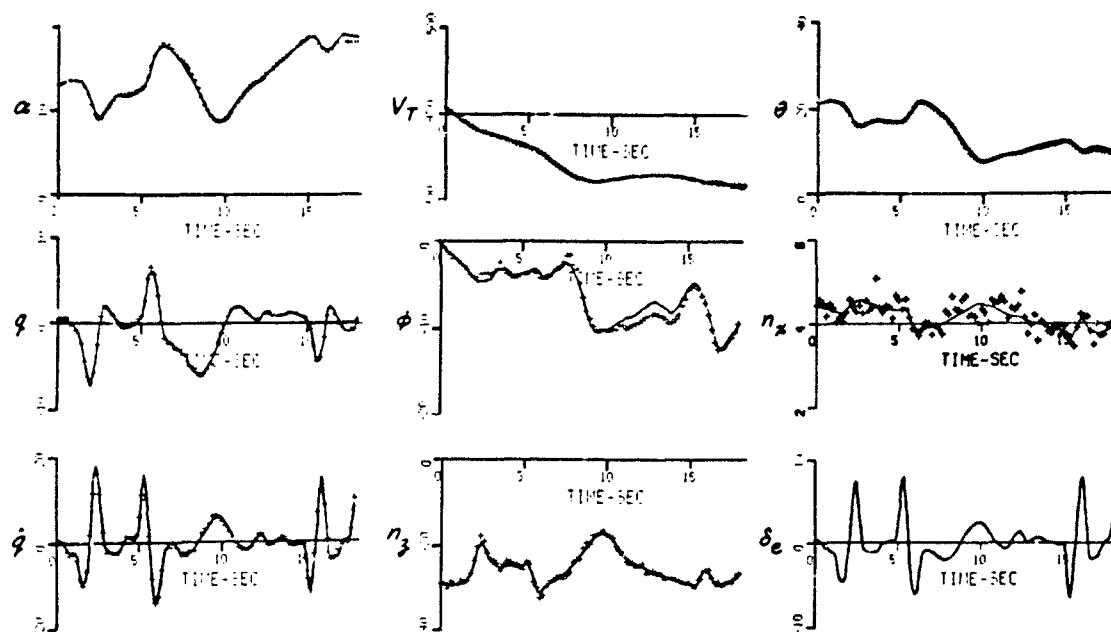


FIGURE 6 RESPONSE COMPARISONS WITH FLIGHT DATA AND KALMAN RESULTS - RECORD 9, LONGITUDINAL

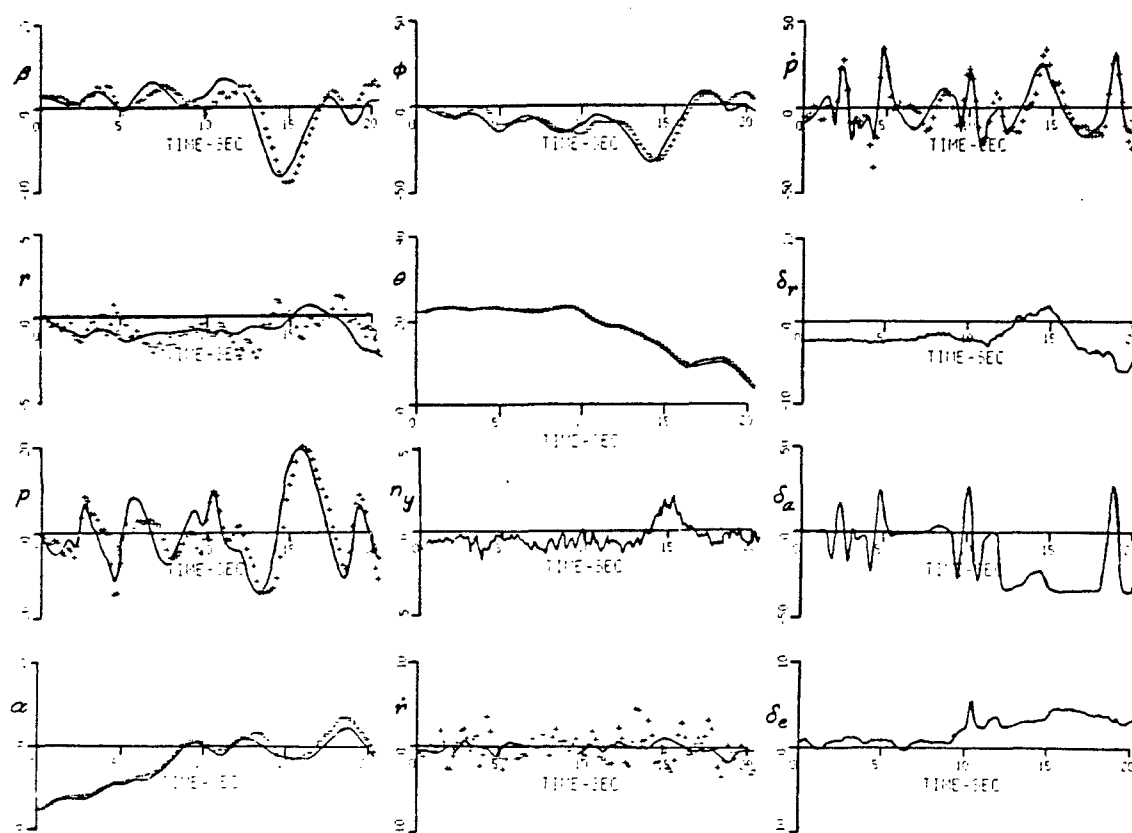


FIGURE 7 RESPONSE COMPARISONS WITH FLIGHT DATA AND KALMAN RESULTS - RECORD 10, LATERAL-DIRECTIONAL

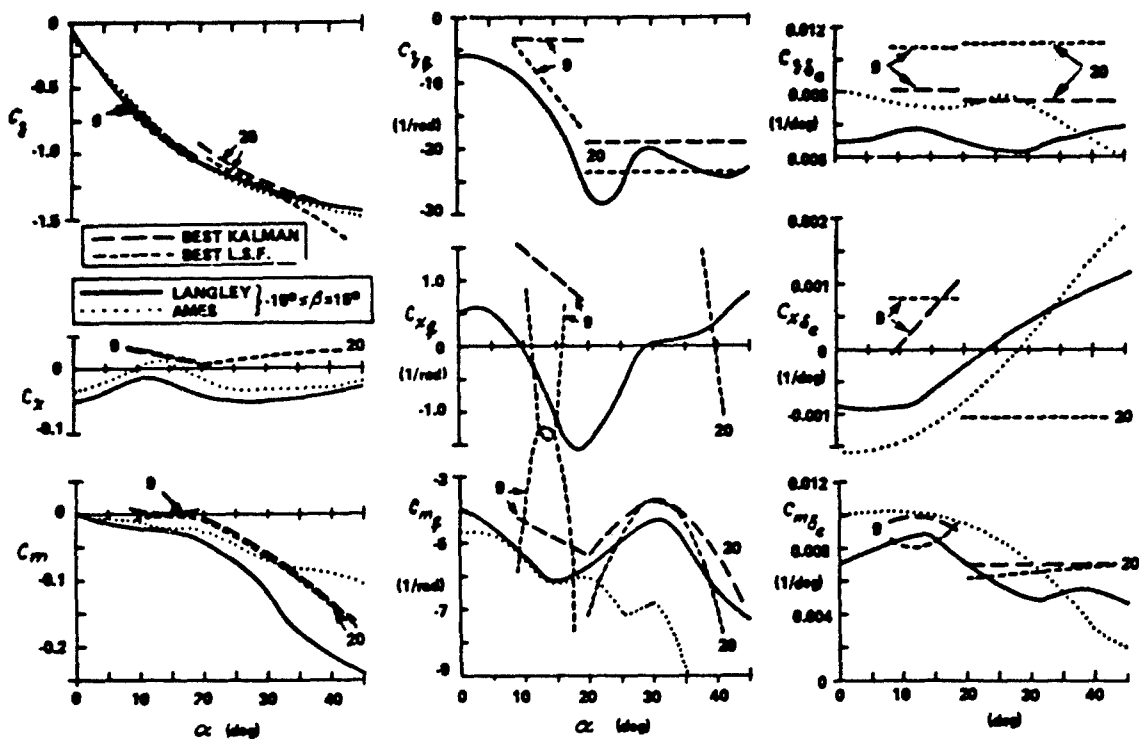


FIGURE 8 IDENTIFIED COEFFICIENTS VERSUS WIND TUNNEL VALUES - RECORDS 9 AND 20, LONGITUDINAL

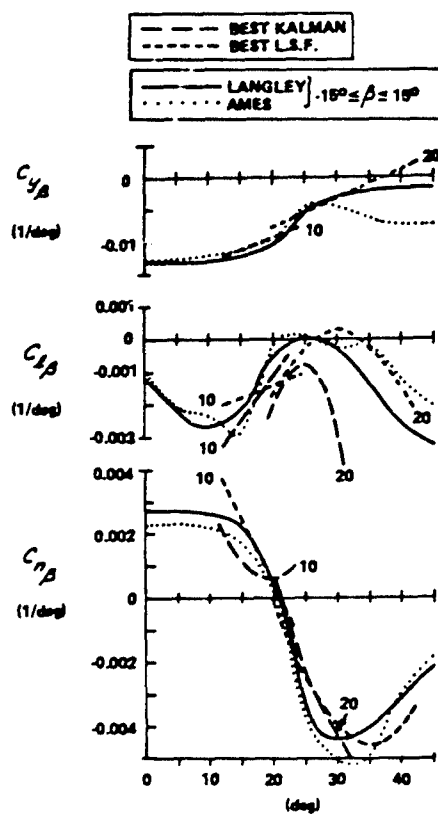


FIGURE 9 IDENTIFIED COEFFICIENTS VERSUS WIND TUNNEL VALUES - RECORDS 10 AND 20, LATERAL-DIRECTIONAL

METHODS USED FOR OPTIMIZING THE SIMULATION OF "CONCORDE S.S.T."  
USING FLIGHT TEST RESULTS

by

Jacques TARDY  
Ingénieur Bureau d'Etudes  
AEROSPATIALE  
316, route de Bayonne  
B.P. 3153 - 31 053 TOULOUSE CEDEX.  
FRANCE

### INTRODUCTION

The elaborate calculation means provided by a simulator were used very early in the design of CONCORDE. Different simulators of more and more sophisticated design, were installed from a fixed base analog simulator to the present simulator which we shall describe later.

This simulator is used for various design purposes :

- development studies for the aircraft and its systems : handling qualities, flying controls, various piloting aids, failure research
- flight test preparation and crew training
- crew work load studies
- studies for introducing CONCORDE into air traffic in liaison with EUROCONTROL
- preparation for aircraft certification, examination of requirements and participation in certification for the most critical conditions to be tested in flight, testing very low probability failures or investigations in the extreme regulatory atmospheric conditions.

### DESCRIPTION OF THE AEROSPATIALE CONCORDE SIMULATOR (See Fig. 1).

The geometry of the cabin is as similar as possible to the preproduction/production aircraft, not only for an instrument point of view, but also for warning lights, seats and flying controls. The cabin is mounted on a 3° of freedom platform, with pitch, roll and elevation (Redifon system). A screen onto which is projected a colour picture filmed by a cine camera in front of a mock-up of TOULOUSE airport and surrounding contry, is installed on the same platform. The cine camera follows the movements of the aircraft and gives the picture which the pilot would see in the windscreen of his aircraft (G P S System).

The calculation means used comprise :

- a HONEYWELL DDP 224 digital computer with 32 000 words
- a RED 5 000 analog computer
- an interface unit
- a Boolean computer.

The engineers who follow the tests have the following recording apparatus available :

- 2 course tracers
- 5 eight-track recorders
- 1 photographic recorder.

It is possible to follow the main parameters available to the pilot on an instrument panel, from the control station. A television screen reproduces the picture projected on the pilot's screen.

Failures are introduced from the control station, from which the crew work resulting from these failures and the functional condition of the systems can be followed.

The following simulations have been carried out and can operate simultaneously :

- aerodynamics and flight mechanics
- engines and associated systems
- air intake logic conditions
- electrical power generation
- fuel
- hydraulics
- air conditioning
- de-icing
- manometrics
- navigation - radic aids
- warning systems.

The pilot controls (wheel control column, pedals, throttle) are identical to those on the aircraft. The same applies to all the mechanical controls which affect the impressions of the pilot :

- artificial force restoring devices, linkages down to the servo-control relays (used as servo actuators in automatic control mode).

The other items in the manual or automatic control channels can either be simulated on an analog computer, or be real aircraft items. The following items can also be introduced into the control channel.

- all the mechanical controls as far as the control surfaces by means of a system which electrically connects the simulator controls to the controls of the flying control test rig which is comprised of aircraft equipment and parts,
- most of the detectors : rate gyros and inertia platform (attitudes only) by means of a 3 axis servo-board - air data computer via servo pressure generators etc ...
- all the automatic flying aid and autopilot computers.



## METHODS USED FOR IMPROVING SIMULATION

### 1. Aerodynamics

Owing to the importance of the design work carried out on the simulator, one of the major problems was to maintain this computation means in a configuration as similar as possible to the aircraft as we know it. This caused considerable complication for simulation. The mathematical model used before first flight was deduced essentially from wind tunnel testing, aero-elasticity calculations and engine rig testing. After the first flight of the prototype, the simulator was modified almost continuously after analysis of the flight recordings. This analysis was made in several ways. During the exploration of the flight envelope, a rapid analysis was required for flight safety. It was necessary to ensure not only that the controllability and stability characteristics remained at adequate levels, but also that there was no tendency for them to deteriorate to a level which could prove dangerous. This rapid analysis only gave a first approximation of possible modifications to be made to the simulator. Representation of the aircraft required a more complete examination of the mathematical model. The methods used were different according to the parts of the model which we wished to improve. For this purpose, we used digital programmes which were independent of the simulator but which used the same equations. These programmes can be divided into two groups :

- the first group is comprised of the programmes which are only partial copies of the mathematical model of the simulator. They are used to reproduce the inputs to which the aircraft is subjected, and we modify the model until identical responses are obtained.
- the other group is comprised of programmes which automatically look for the changes to be made to the numerical values of the model so as to minimise the differences between responses from the aircraft and responses from the model.

We are kept informed of flight results by a large amount of recording equipment installed on the aircraft. For these studies, we have used quasi-static recordings on magnetic tapes or time histories from the same tapes.

### Longitudinal equations

The most generally used method for optimising longitudinal equations is the method based on use of the programmes in the first group since the automatic methods available are based on A PRIORI knowledge of the shape of the model. We have been led to modify the longitudinal equations to introduce a larger number of parameters or introduce them with a different formulation. Although it is true to say that we experienced no big problems with the lift equation, such was not the case with the pitching moment equation. We had to introduce effects connected with aircraft weight, c.g. location, and variations of this c.g. location with fuel movement during manoeuvres in addition to the parameters determined from wind tunnel testing such as atmosphere, undercarriage or nose effects. This precise simulation is required, for instance, for studying controllability at c.g. limits. For certain studies, we have determined additional parameters to enable us to simulate the effects of in-flight thrust reversal, engine failure, or thermal deformation of the aircraft after supersonic cruise.

All these parameters were obtained by a comparative analysis of flight test results. First of all they were programmed on the computer, and their numerical values adjusted by successive approximations. The same method was used to develop engine effects using a digital programme (a copy of the simulator programme) to obtain thrusts and the characteristic air intake factors which we then introduced into the flight mechanics programme. This method enabled us to simulate the evolution of the various parameters during aircraft acceleration or deceleration. Pitch efficiencies and damping derivatives were changed little except in transonic conditions. These transonic adjustments were determined by reproducing deflections per g in static conditions and responses to elevator deflections in dynamic conditions. An accelerated analysis of these programmes was then developed. Aircraft responses and model responses are superposed on a cathode ray screen. A block diagram of this method is given in figure 2. Some identifications were made based on responses to elevator deflections using the gradient method which we shall describe later. With these successive approximations we thus achieved a satisfactory mathematical model. It is certainly not optimum but it enables us to represent aircraft characteristics so accurately that we were able to use the simulator to study handling qualities and more particularly to determine manoeuvrability at c.g. limits, which requires great accuracy of simulation.

### Lateral equations

The shape of the mathematical model in lateral mode has never changed so it was possible to use automatic methods.

### TIME VECTOR METHOD

During flight envelope exploration, we required a simple and quick method of determining the trends of the main parameters and checking that future flights would still be safe. To achieve this, we generally used the time vector method. With this method starting from the response of a system released in unstable conditions, one can determine certain parameters of the corresponding mathematical model.

Let us assume a second order system the damping of which is less than the critical damping :

$$(1) \quad \begin{cases} \frac{dx}{dt} = a_1 x + b_1 y \\ \frac{dy}{dt} = a_2 x + b_2 y \end{cases}$$

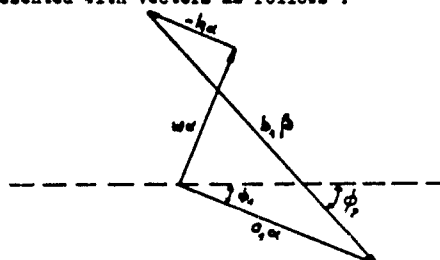
Let us now assume that the system is released with initial conditions  $x_0, y_0$ .  $x$  and  $y$  can then be expressed as a function of time, as follows :

$$\begin{cases} x = \alpha e^{-kt} \sin(\omega t + \phi_1) \\ y = \beta e^{-kt} \sin(\omega t + \phi_2) \end{cases}$$

If  $x$  and  $y$  are replaced by their value in the system (1), we obtain :

$$(2) \quad \begin{cases} \alpha [\omega \cos(\omega t + \phi_1) - k \sin(\omega t + \phi_1)] = a_1 \alpha \sin(\omega t + \phi_1) + b_1 \beta \sin(\omega t + \phi_1) \\ \beta [\omega \cos(\omega t + \phi_2) - k \sin(\omega t + \phi_2)] = a_2 \alpha \sin(\omega t + \phi_1) + b_2 \beta \sin(\omega t + \phi_2) \end{cases}$$

Each equation can then be represented with vectors as follows :



Factors  $\alpha$ ,  $\beta$ ,  $\phi_1$ ,  $\phi_2$ ,  $\omega$  can be determined from aircraft time histories and  $a_1$ ,  $b_1$  and  $a_2$ ,  $b_2$  can then be determined from the drawing of the polygons.

This method is implemented fairly rapidly. Unfortunately, it is extremely dependent on precise phase determination. Furthermore, it does not allow all the parameters of the model to be determined; the values of some of these parameters have to be assumed and it is easily applicable only for a badly damped oscillatory system if the input is not harmonic.

This very simple method was used much more during flight envelope exploration than for mathematical model development. It only provides a first approximation of the evolution of the parameters.

#### GRADIENT METHOD

To identify the aircraft in lateral conditions, we have often used the method called the gradient method. We shall only give a few explanations of this means of identifying the aircraft here, a complete development is given in the appendix. This method consists of comparing the responses of the aircraft (object) with the calculated response (model) over a given portion of flight time and modifying the model according to a function  $\theta$  of the difference between the two responses (see fig. 3).

For  $\theta$  we have chosen the integral quadratic difference :

$$\theta = \int_0^T \sum_{j=1}^n \theta_j (S_{ja} - S_{jm})^2 dt$$

where  $T$  is the duration of the flight portion.

$S_a$  are the aircraft state vector coordinates ; i. e. the parameters defining aircraft response.

$S_m$  are the model state vector coordinates.

$\theta_j$  is a weighting factor which enables the same relative precision to be maintained in output identification.

The coordinates of the gradient of  $\theta$  are calculated in the space of the  $n$  parameters of the model, and we thus determine a preferential direction of search to minimise  $\theta$ .

Progression towards the optimum value of  $\theta$  is also subject to certain calculation constraints to avoid oscillations around the optimum point.

We are also able to maintain only a priority subspace in the space of the factors to be determined. This principle was used to perfect the programme developed at AEROSPATIALE. It appeared desirable to deal first of all with the parameters which are most sensitive to the force to be identified, by giving them theoretical values (wind tunnel tests and aerelasticity calculations) as initial values and calculating the minimum of  $\theta$  in the subspace of these parameters. The parameters as a whole are then dealt with, at a second stage, and the initial values of the sensitive parameters are then the values determined previously.

Owing to lack of time, it has not been possible to study the inputs which favour the determination of certain parameters and we have therefore identified responses with the conventional deflections encountered in flight in roll and yaw (Cf. fig. 4 and 5).

This method provides quite a good identification of model responses to aircraft recordings. The parameters present a varying degree of scatter, when they are identified in similar flight conditions. This is due to their facility of determination by the inputs considered (Cf. fig. 6). So, roll and yaw sideslip derivatives can be determined quite accurately by this method. On the other hand, crossed damping derivatives have considerable scatter, and the same is true for lateral force equation terms.

The results of this programme are therefore known with a certain accuracy. We attempt to confirm them by reproducing the deflection recorded on the aircraft with a 6 degree of freedom programme, but above all by calculating balanced deflections in steady sideslip. These calculations enable us to choose the values of the parameters in the ranges of uncertainty found by the gradient method.

The simulator gives rise to an additional problem owing to its reduced capacity data storage. Aerodynamic curves must thus be introduced with a minimum number of points, which implies representing them as kinked lines. We must then check that this does not appreciably modify the desired response evolution. Rapid implementation of programmes displaying the responses on a screen is very useful for this study. These methods enable us to follow the evolutions of the aircraft, at least in the flight envelope explored.

This problem is one of the major problem implied by the identification of an aircraft for a simulator. It is always possible to identify one response of the aircraft in specific flight conditions but for a simulator it is necessary to have a model as simple as possible which is valid from ground effect up to cruise conditions.

We have only mentioned here the optimisation methods generally used at AEROSPATIALE, but some tests have been carried out with the modified NEWTON-RAPHSON method with which we have obtained satisfactory results.

Research is in hand to adapt the "least squares method" and the "KALMAN filter method", but neither of these methods has yet proved satisfactory.

#### Hinge moments

Control surface hinge moments are also simulated. Before first flight we had a mathematical model based on wind tunnel test results and aeroelasticity calculations. This model was very complicated and we experienced much difficulty in modifying it to obtain the hinge moments measured on the aircraft. We therefore decided to review the whole problem and realized that a much simpler conventional model could give just as good results. This factor adjustment was made in successive approximations or by using smoothing techniques, but it would also have been possible to adapt the gradient method.

#### Difficulty in perfecting a mathematical model

It is difficult to say if one of the methods we used is better than another. Both have their advantages and disadvantages. However, the mistake we certainly made was to start with a complicated model and try to improve it to achieve the same results as those achieved during aircraft testing. We now think that it would have been preferable to start with an aerodynamic model based on wind tunnel data and aeroelasticity calculations in which only the main effects were kept. This technique was applied for hinge moment calculations only, but we have been able to see that it considerably reduced the time required for perfecting the model.

### 2. Engines

It was also necessary to simplify engine programming for computer capacity reasons. A complete simulation is made of the bare engine (flange to flange) that is the engine as in the manufacturer's brochure; we then make corrections to include air intake and nozzle effects using the complete performance calculation program. These corrections are for gross thrust, intake momentum drag and free stream tube area (this quantity intervenes in aerodynamics).

Our objective is not to use the simulator for performance calculations, but simply to have performance data such that handling qualities studies are not affected. We therefore try to use realistic performance on the simulator. To improve this performance, we have sometimes had to modify drag values for instance, in order to reproduce aircraft climb performance or aircraft maximum altitudes. Similarly, instead of using the complicated calculation used by the engine manufacturers in their brochure for a windmilling engine, we have introduced the ratings measured on the aircraft.

Engine adjustments were nevertheless very limited, for when the control amplifiers are simulated, engine ratings can be simulated quite well, at least in steady conditions.

We experienced some problems with engine calculation stability and dynamic responses, but we solved them by internal engine calculation time lags.

### 3. Fuel

The fuel transfer system on CONCORDE is complex, with several transfer possibilities. CONCORDE has 13 separate tanks, and in non automatic mode it is possible to transfer fuel from one tank to any of the others.

The first programme carried out on the simulator was very complicated since it took pump characteristics and pipe pressure drops into account. Although this simulation was extremely complex, it was not perfect and proved very difficult to improve because of its complexity. We therefore only introduced the intertank fuel flows measured on a test rig, and only retained the normal transfer procedures. These fuel flows, programmed in this way, can easily be modified when the measurements made on the aircraft show that this is necessary.

### RESULTS OBTAINED AND POSSIBILITIES OFFERED BY THE SIMULATOR

The CONCORDE simulator has been in use for 8 years for CONCORDE development purposes. It has amply contributed to the development of this aircraft, the good handling qualities of which are recognized by all the pilots who have been at the controls.

It has enabled the number of control system development flights to be reduced considerably and has contributed to the good progress and safety of test flying. To achieve this, it has always been necessary to keep it to a standard as close as possible to the aircraft.

Design work is now completed and the simulator is used for aircraft certification. For that, we had to demonstrate to the certification Authorities beforehand that the simulator showed conformity with the aircraft.

## APPENDIX

## GRADIENT METHOD

Let	-	$\beta_a$	$\beta_m$	$r_a$	$\phi_a$	be the aircraft state variables (object)
	-	$\beta_n$	$\beta_m$	$r_n$	$\phi_n$	be the model state variables
	-	$\delta_p$	$\delta_r$			be the disturbances
	-	$\left\{ \begin{array}{cc} C_{Y\beta} & C_{Yp} \\ C_{L\beta} & C_{Lp} \\ C_{N\beta} & C_{Np} \end{array} \right\}$	$\left\{ \begin{array}{cc} C_{Yr} & C_{Y\delta_r} \\ C_{Lr} & C_{L\delta_r} \\ C_{Nr} & C_{N\delta_r} \end{array} \right\}$			be the parameters to be identified

In the following test, we shall call  $C$  any one of the 15 parameters to be identified.

## STATE EQUATIONS

Constant factor linearised flight mechanics equations :

$$(1) \quad \begin{cases} \frac{d\beta_m}{dt} = \beta_a (\beta_m, p_m, r_m, \phi_m, C, \dots, \delta_p, \delta_r) \\ \frac{d\beta_n}{dt} = \beta_a (\beta_m, p_m, r_m, \phi_m, C, \dots, \delta_p, \delta_r) \\ \frac{dr_n}{dt} = \beta_a (\beta_m, p_m, r_m, \phi_m, C, \dots, \delta_p, \delta_r) \\ \frac{d\phi_m}{dt} = \beta_a (\beta_m, p_m, r_m, \phi_m, C, \dots, \delta_p, \delta_r) \end{cases}$$

## INTEGRAL QUADRATIC CRITERION FOR IDENTIFICATION

$$(2) \quad \theta = \int_0^T \left[ \theta_1 (\beta_a - \beta_n)^2 + \theta_2 (p_a - p_n)^2 + \theta_3 (r_a - r_n)^2 + \theta_4 (\phi_a - \phi_n)^2 \right] dt$$

$\theta_i$  are the weighting factors which allow the weight which seems to be the most logical in the identification to be matched with each output.

## PRINCIPLE OF THE METHOD

We must look for the direction of variations to be adopted for each factor  $C$  so as to minimise  $\theta$ , by calculating

$$(3) \quad \frac{d\theta}{dC} = -2 \int_0^T \left[ \theta_1 (\beta_a - \beta_n) \frac{\partial \beta_n}{\partial C} + \theta_2 (p_a - p_n) \frac{\partial p_n}{\partial C} + \dots \right] dt$$

$$\text{We write} \quad \frac{\partial \beta_n}{\partial C} = U_{\beta C} \quad \frac{\partial p_n}{\partial C} = U_{pC} \quad \frac{\partial r_n}{\partial C} = U_{rC} \quad \frac{\partial \phi_n}{\partial C} = U_{\phi C}$$

$$\text{We calculate} \quad \frac{d}{dt} (U_{\beta C}) = \frac{d}{dt} \left( \frac{\partial \beta_n}{\partial C} \right) \quad \dots$$

and obtain, by reversing the order of the derivations

$$\frac{d}{dt} (U_{\beta C}) = \frac{\partial}{\partial C} \left( \frac{d\beta_n}{dt} \right) \quad \dots$$

Referring to the state equations (1) we can then write

$$\begin{cases} \frac{d}{dt} (U_{\beta C}) = \frac{\partial \beta_a}{\partial C} + \frac{\partial \beta_a}{\partial \beta_m} \frac{\partial \beta_m}{\partial C} + \frac{\partial \beta_a}{\partial p_m} \frac{\partial p_m}{\partial C} + \frac{\partial \beta_a}{\partial r_m} \frac{\partial r_m}{\partial C} + \frac{\partial \beta_a}{\partial \phi_m} \frac{\partial \phi_m}{\partial C} \\ \frac{d}{dt} (U_{pC}) = \frac{\partial \beta_a}{\partial C} + \frac{\partial \beta_a}{\partial \beta_m} \frac{\partial \beta_m}{\partial C} + \frac{\partial \beta_a}{\partial p_m} \frac{\partial p_m}{\partial C} + \dots \\ \frac{d}{dt} (U_{rC}) = \frac{\partial \beta_a}{\partial C} + \frac{\partial \beta_a}{\partial \beta_m} \frac{\partial \beta_m}{\partial C} + \dots \\ \frac{d}{dt} (U_{\phi C}) = \frac{\partial \beta_a}{\partial C} + \frac{\partial \beta_a}{\partial \beta_m} \frac{\partial \beta_m}{\partial C} + \dots \end{cases}$$

If we replace  $\frac{\partial \hat{p}_n}{\partial C}$ ,  $\frac{\partial \hat{r}_n}{\partial C}$ ,  $\frac{\partial \hat{r}_n}{\partial C}$ ,  $\frac{\partial \hat{\phi}_n}{\partial C}$  by  $U_{pc}$ ,  $U_{pc}$ ,  $U_{rc}$ ,  $U_{\phi c}$  for each factor C,

We obtain a system of 4 differential equations called an associated system. Resolution of this system enables us to obtain  $U_{pc}$ ,  $U_{pc}$ ,  $U_{rc}$ ,  $U_{\phi c}$  which we transfer to equation (3) to obtain, by integration  $\frac{\partial \theta}{\partial C}$

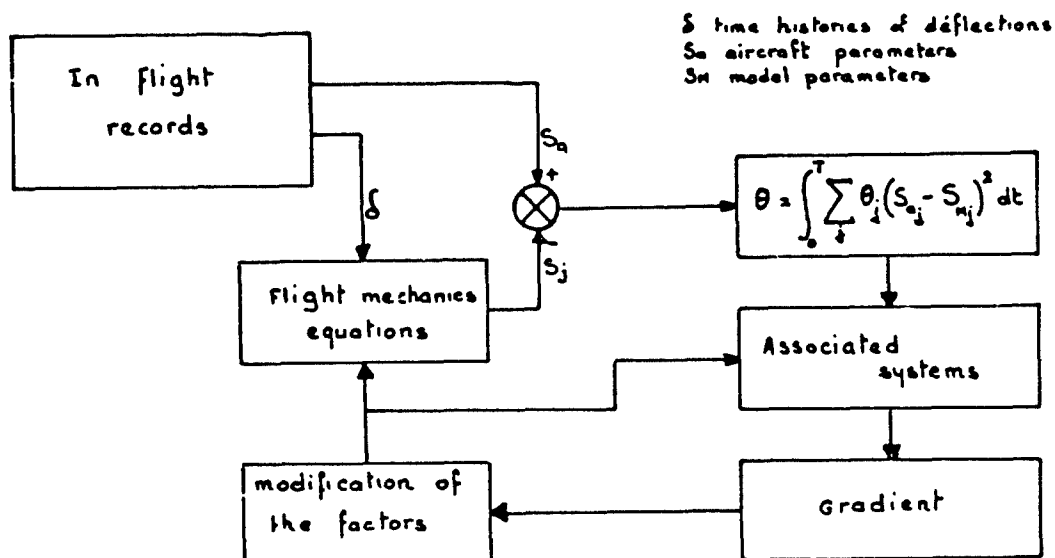
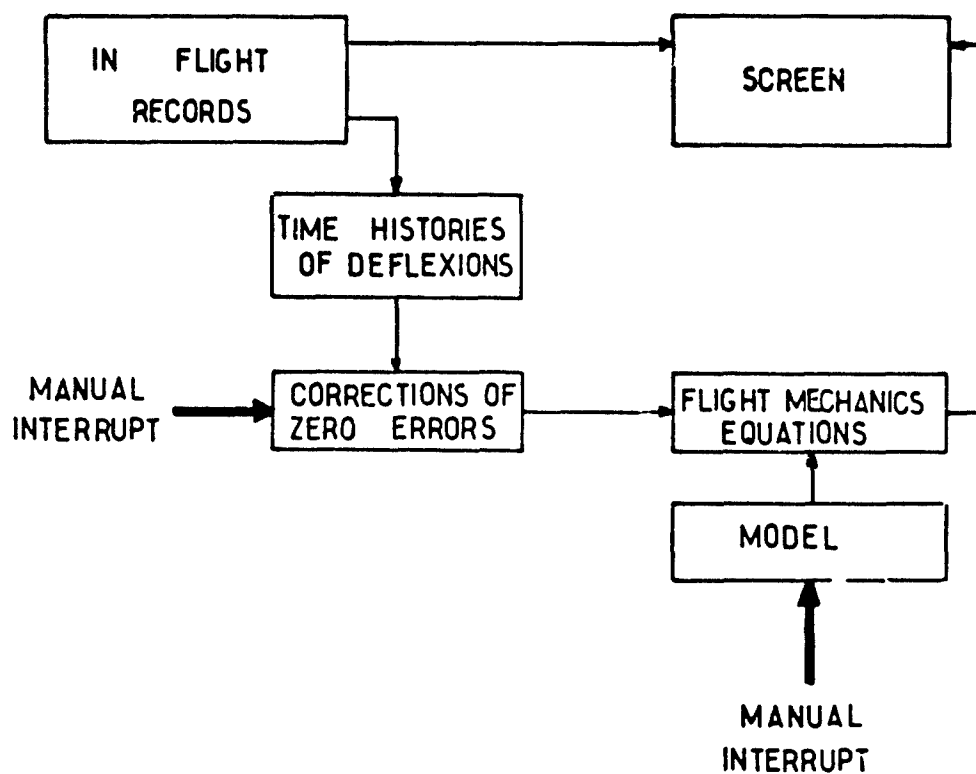
From this, we deduce the value to be adopted for C at a step  $n + 1$

$$C_{n+1} = C_n + \gamma_c \left( \frac{\partial \theta}{\partial C} \right)_n$$

$\gamma_c$  is the gain of the loop on each of the parameters to be identified ; it also allows priority identification of the parameters which are most sensitive to the force considered. In addition, on completion of identification, when  $\theta_n$  and  $\theta_{n+1}$  are on either side of the minimum of the criterion, the convergence is achieved by dichotomy.

This method is based on the assumption that the only minimum of the criterion  $\theta$  in the space of factors C containing the initial point is the optimum required. If this were not so, there would be a risk of stopping at a local minimum, in which case we would obtain erroneous factors C.





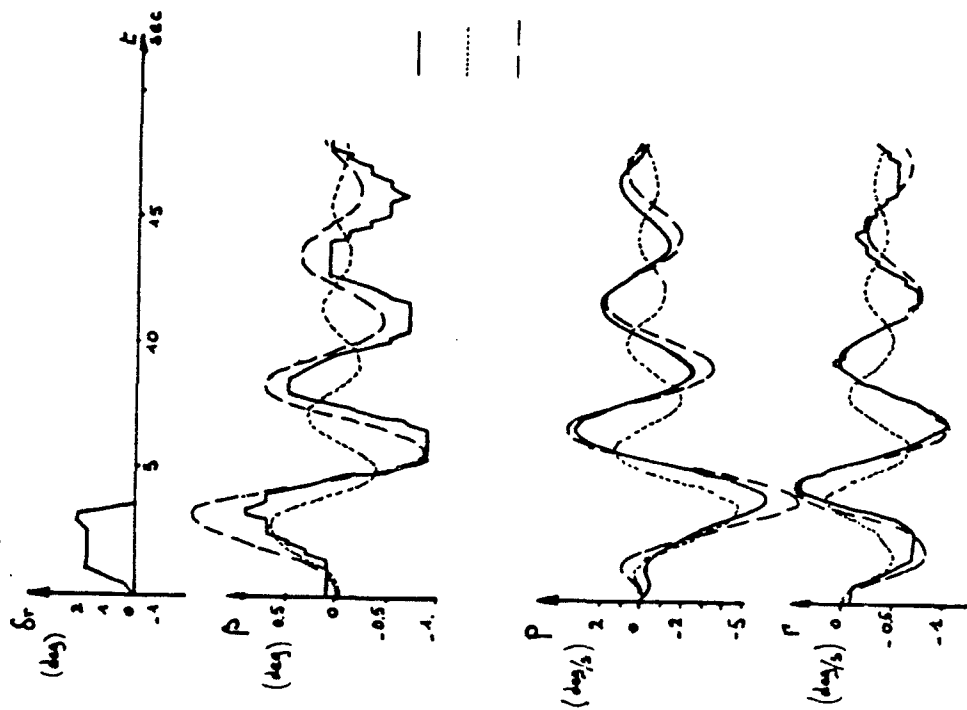
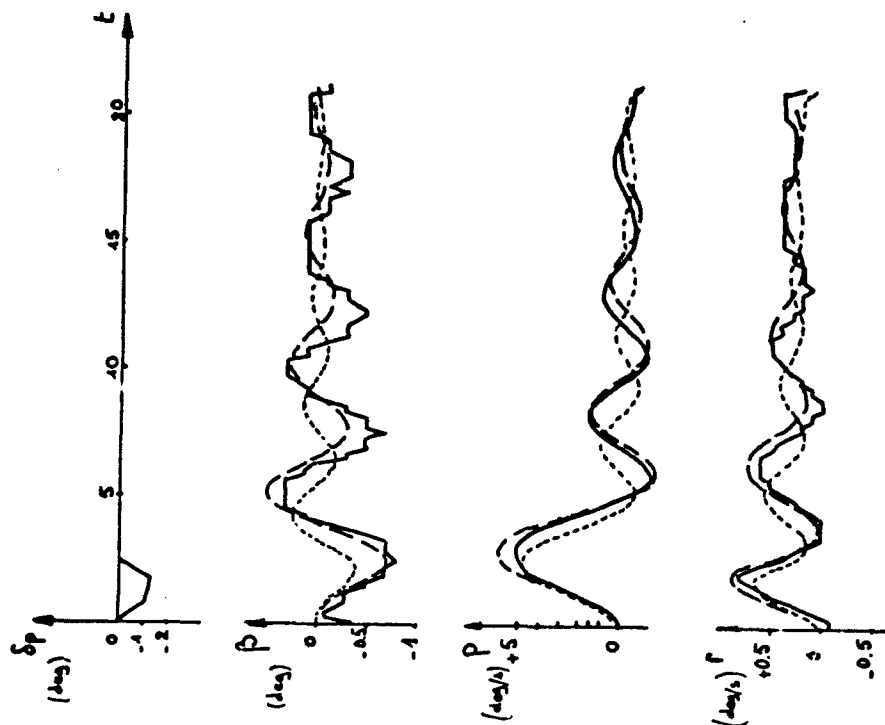


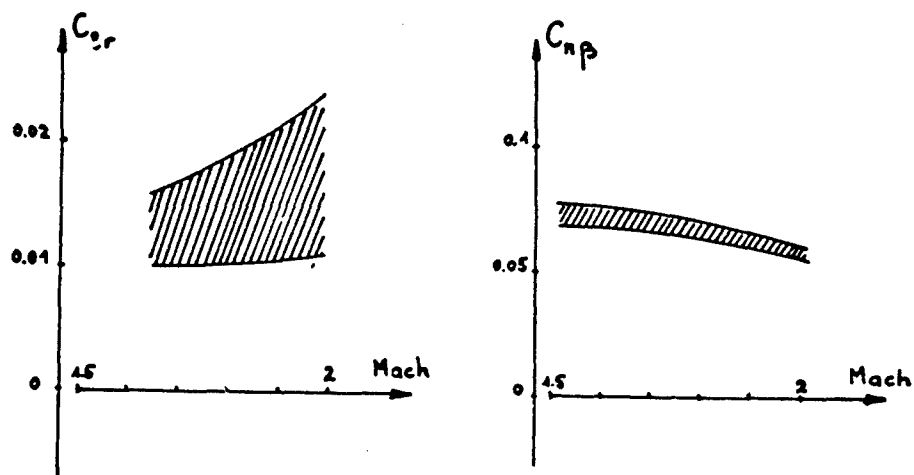
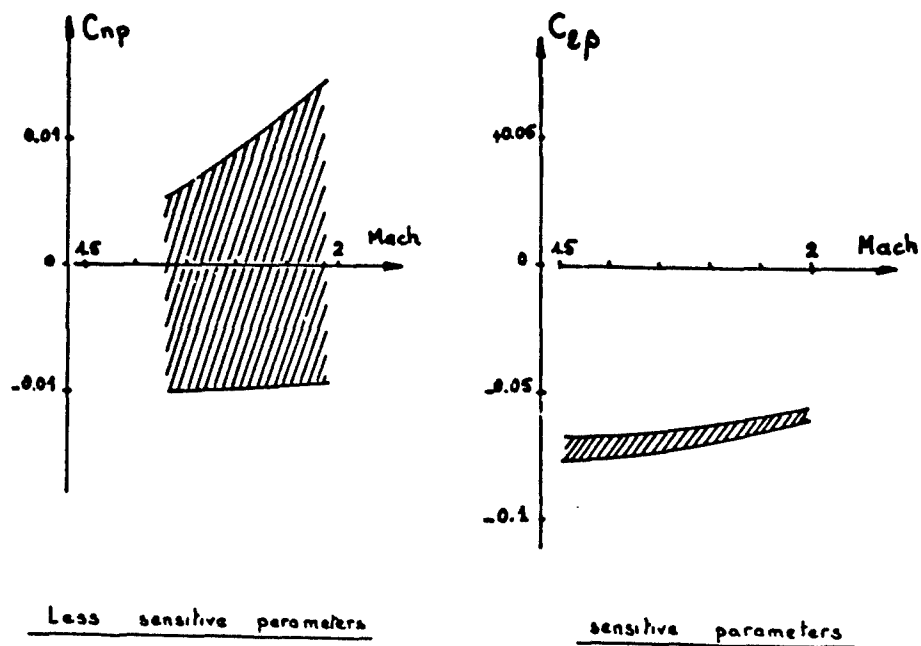
FIG 4



IDENTIFICATION BY "GRADIENT METHOD"

FIG 5





IDENTIFICATION BY GRADIENT METHOD

FIG 6

## APPLICATION OF A NEW CRITERION FOR MODELING SYSTEMS

by  
Lawrence W. Taylor, Jr.  
NASA Langley Research Center  
Hampton, Virginia

## SUMMARY

A new criterion has been proposed for modeling systems which promises to be useful in deciding how complex a model should be. The criterion is based on the expected model response error instead of the error in fitting the data used for estimating the model parameters. The new criterion also does not require withholding data to be used exclusively for testing. There remains, however, the difficulty of testing a large number of candidate models that correspond to the combinations of terms used in the dynamic equations. In this paper, a computational approach is suggested which greatly reduced the computations required in searching for the best model. In the suggested approach the gradient of the response with respect to the model coefficients is held fixed and numerous combinations of terms are assessed. After determining the most promising candidate model, the gradient is updated and the process is repeated. This procedure gives greater assurance that the best model is selected and does not rely on the analyst's judgment.

## DISCUSSION

One interesting problem arises in modeling systems when the analyst does not know the exact form and the particular terms in the dynamic equations which are most suitable for his purposes. Consequently, the analyst must test a number of candidate models and obtain parameter estimates for each. He is then confronted with the problem of choosing one of them with little or no basis on which to base his selection. It is tempting to use a model with many parameters since it will fit the measured response error best. Unfortunately, it is often the case that a simpler model would be better for predicting the system's response. This is because the fewer number of unknown parameters could be estimated with less uncertainty. An example of using an excessive number of model parameters is given in Figure 1 of this paper which is based on results of Reference 1. Although the fit error decreased as the number of terms in the model was increased, the more complex models were poorer at predicting response, as is indicated by the upper curve. It was only after the modeling process was repeated with an expanded data base that the more complex models were better at predicting response as is shown in Figure 2. One test that can be used is to segregate the response data available into a portion for estimating the model parameters and a portion for testing the resulting model. An improvement on this approach is given in Reference 2 which enables the use of the entire data base for modeling by replacing the test by the calculation of the expected response error of such a test.

The analyst still faces the difficulty of testing a large number of model candidates if he wishes to be certain a particular model is best. In Reference 3, it is suggested that the eigenvalues of the information matrix be used to decide which eigenvectors be used as constraints on the model parameters. Although this procedure will aid convergence, the solution obtained is not satisfactory for many applications. Because of the discrete manner in which the constraints are applied, the solution becomes a function of the initial values of the model parameters. Another disadvantage is that the model complexity is never reduced but equals that of the most complex model considered. A search of all possible model candidates is considered to be a better alternative, but is thought to have a computational cost that is prohibitive. It is the purpose of this paper to apply the new criterion of Reference 2 in a way that (1) automates model making by testing all possible candidate models for the smallest expected model error, and (2) arranges the calculations in a way to greatly reduce the computational cost.

## THE MODELING PROBLEM

The modeling or systems identification problem of determining the parameters of a linear, constant-coefficient dynamic model will be considered from two viewpoints, (1) given the model except for not knowing the values of its parameters, and (2) given a large number of candidate models to consider. The conditional maximum likelihood estimate is used in which the noise error covariance matrix is known. A modified Newton-Raphson technique is used to express changes in the estimated model parameters.

## Problem Statement

The problem considered is that of determining the values of certain model parameters which are best with regard to a particular criterion, if the input and noisy measurements of the response of a linear, constant-coefficient system are given. The system to be identified is defined by the following equations:

$$\dot{x} = Ax + Bu \quad (1)$$

$$y = Fx + Gu + b \quad (2)$$

$$z = y + n \quad (3)$$

where

x state vector  
u control vector

$y$  calculated response variable  
 $b$  constant-bias vector  
 $n$  noise vector, assumed to be Gaussian, uncorrelated  
 $z$  measured response variable

The unknown parameters will form a vector  $c$ . The matrices  $A$ ,  $B$ ,  $F$ , and  $G$  and the vectors  $b$  and  $x(0)$  are functions of  $c$ .

#### KNOWN MODEL FORMAT

The modeling problem is straightforward if we assume the model is known except of the values of its parameters. One criterion that is often used in systems identification is the mean-square difference between the measured response and that given by the model. A cost function which is proportional to the mean-square error can be written as

$$J = \sum_{i=1}^N (z_i - y_i)^T D_1 (z_i - y_i) \quad (4)$$

where  $D_1$  is a weighting matrix and  $i$  is a time index. The summation approximates a time integral. The estimate of  $c$  is then

$$\hat{c} = \text{ARG MIN}_c (J) \quad (5)$$

which means that vector  $c$  which minimizes the cost function  $J$ . If we linearize the calculated response  $y$  with respect to the unknown parameter vector  $c$ :

$$y_i = y_{i0} + \nabla_c y_i (c - c_0) \quad (6)$$

where

$y_{i0}$  nominal response calculated by using  $c_0$   
 $\nabla_c y_i$  gradient of  $y$  with respect to  $c$   
 $c_0$  nominal  $c$  vector

Substituting  $y_i$  into the expression for  $J$  and solving for the value of  $c$  which minimized  $J$  yields

$$\hat{c} = c_0 + \left[ \sum_{i=1}^N \nabla_c y_i^T D_1 \nabla_c y_i \right]^{-1} \left[ \sum_{i=1}^N \nabla_c y_i^T D_1 (z_i - y_{i0}) \right] = Q^{-1} \sum_{i=1}^N \nabla_c y_i^T D_1 (z_i - y_{i0}) \quad (7)$$

Because the inverted expression occurs repeatedly we will denote it as  $Q$ .

If this relationship is applied iteratively to update the calculated nominal response and its gradient with respect to the unknown parameter vector, the minimum-response error estimate  $\hat{c}$  will result. The method has been called quasi-linearization, repetitive least squares, and modified Newton-Raphson. The latter seems more appropriate since  $Q$  approximates the second gradient of  $J$  in the Newton-Raphson formulation. The flow chart of Figure 3 depicts this procedure when the model format is known.

#### UNKNOWN MODEL FORMAT

An analyst never knows with certainty what model is best suited for his purposes because it depends not only on the model's use but also on the response data available for determining its parameters. Models having excessive complexity should not be used when simpler ones would provide more accurate response estimates. The analyst must test the possible candidates to be certain which is best for its intended purpose. For the purpose of this discussion it will be assumed that the model's intended use is to predict the response of a system and that a meaningful measure of the model's performance is a weighted mean-square error.

#### A CRITERION FOR COMPARING CANDIDATE MODELS

The development of the new criterion of Reference 2 is repeated in the following discussion. The weighted mean-square response error which was minimized by the minimum response error estimate was:

$$J = \sum_{i=1}^N (z_i - y_i)^T D_1 (z_i - y_i)$$

Let us denote the weighted mean-square response error which corresponds to testing the model's performance in predicting the system's response as:

$$J^1 = \sum_{i=1}^N (z_i^1 - y_i)^T D_1 (z_i^1 - y_i)$$

Where  $z^1$  is measured response data that is not part of  $z_1$  which is used to determine the model parameters. It is convenient to consider the input,  $u$ , to be identical in both cases.

The criterion suggested for comparing candidate models is the expected value of  $J^1$ . If it is possible to express the expected value,  $E\{J^1\}$ , in terms not involving actual data for  $z^1$ , then a considerable saving in data can be made and improved estimates will result from being able to use all available data for establishing the model parameter values.

Let us examine first, the expected value of the fit error with respect to the data used to determine estimates of the unknown parameters.

We can express the response error as:

$$z - y = y_{\text{true}} + n - y = y_{\text{true}} + n - y_{\text{true}} - \nabla_c y (\hat{c} - c_{\text{true}}) = n - \nabla_c y (\hat{c} - c_{\text{true}})$$

It has been assumed that (1) the response can be linearized with respect to the model parameters over the range in which they are in error, and (2) the gradient  $\nabla_c y$  is constant over the same range.

The expected value of the fit error,  $E\{J_1\}$ , because:

$$E\{J\} = E\left\{\sum_{i=1}^N (z_i - y_i)^T D_1 (z_i - y_i)\right\} = E\left\{\sum_{i=1}^N n - (\nabla_c y_i) (\hat{c} - c_{\text{true}})^T D_1 (n - (\nabla_c y_i) (\hat{c} - c_{\text{true}}))\right\}$$

Expanding we get:

$$E\{J\} = E\left\{\sum_{i=1}^N n_i^T D_1 n_i\right\} - 2E\left\{\sum_{i=1}^N n_i^T D_1 (\nabla_c y_i) (\hat{c} - c_{\text{true}})\right\} + E\left\{\sum_{i=1}^N (\hat{c}^T - c_{\text{true}}^T) \nabla_c^T y_i D_1 (\nabla_c y_i) (\hat{c} - c_{\text{true}})\right\}$$

If a maximum likelihood estimate is used, or if the minimum mean-square response error estimate is used with a weighting equal to the measurement error covariance matrix, then we can write:

$$D_1 = M^{-1}$$

$$\hat{c} = c_{\text{true}} + \left[ \sum_{i=1}^N \nabla_c y_i^T M^{-1} \nabla_c y_i \right]^{-1} \left[ \sum_{i=1}^N \nabla_c y_i^T M^{-1} n_i \right]$$

again linearization is assumed and it is noted that:

$$z_i - y_{\text{true},i} = n_i$$

After substituting we get:

$$E\{J\} = E\left\{\sum_{i=1}^N n_i^T M^{-1} n_i\right\} - 2E\left\{P^T Q^{-1} P\right\} + E\left\{P^T Q^{-1} Q Q^{-1} P\right\} = E\left\{\sum_{i=1}^N n_i^T M^{-1} n_i\right\} - E\left\{P^T Q^{-1} P\right\}$$

Next, let us examine expected fit error  $E\{J\}$  of a model used to predict response measurements,  $z^1$ , which are independent of the data  $z$ , used to determine the estimates of the model.

We can again express the expected fit error as:

$$E\{J^1\} = E\left\{\sum_{i=1}^N n_i^1 T D_1 n_i^1\right\} - 2E\left\{\sum_{i=1}^N n_i^1 T D_1 \nabla_c y_i (\hat{c} - c_{\text{true}})\right\} + E\left\{\sum_{i=1}^N (\hat{c}^T - c_{\text{true}}^T) \nabla_c^T y_i D_1 \nabla_c y_i (\hat{c} - c_{\text{true}})\right\}$$

Note that the only difference between the above expression and that obtained earlier for  $E\{J\}$  is that the noise vector is  $n^1$  instead of  $n$ . The same expression can be used for  $\hat{c}$  as before:

$$\hat{c} = c_{\text{true}} + \left[ \sum_{i=1}^N \nabla_c^T y_i M^{-1} \nabla_c y_i \right]^{-1} \left[ \sum_{i=1}^N \nabla_c^T y_i M^{-1} n_i \right]$$

Substituting the above expression for  $\hat{c}$ , and  $M^{-1}$  for  $D$ , we get:

$$E\{J^1\} = E\left\{\sum_{i=1}^N n_i^1 T M^{-1} n_i^1\right\} - 2E\left\{\sum_{i=1}^N n_i^1 T M^{-1} \nabla_c y_i Q^{-1} \sum_{i=1}^N \nabla_c^T y_i M^{-1} n_i\right\} + E\left\{P^T Q^{-1} P\right\}$$

Where  $P$  and  $Q$  are defined as before. Since the noise vector,  $n^1$  and  $n$  are uncorrelated, that is:

$$E\left\{n_i^1 n_i^T\right\} = 0 \text{ for all } i \neq j$$

Then the second term is zero.

Since the noise vectors  $n_i$  and  $n_i^1$  are assumed to have the same covariance matrix,  $M$ , we can write:

$$E \left\{ \sum_{i=1}^N n_i^1 T M^{-1} n_i^1 \right\} = \text{TRACE} \left[ E \left\{ \sum_{i=1}^N n_i^1 T M^{-1} n_i^1 \right\} \right] = \text{TRACE} \left[ E \left\{ \sum_{i=1}^N n_i^1 n_i^{1T} \right\} M^{-1} \right] = \text{TRACE} [N I] = Nr$$

Where  $N$  is the number of time samples and  $r$  is the number also

$$E \left\{ \sum_{i=1}^N n_i^1 T M^{-1} n_i^1 \right\} = Nr$$

We can now express  $E(J^1)$  in terms of  $E(J)$  as:

$$E(J^1) = E(J) + 2E(P^T Q^{-1} P)$$

Examining the second term:

$$E(P^T Q^{-1} P) = E \left\{ \sum_{i=1}^N n_i^1 T M^{-1} \nabla_c y_i Q^{-1} \sum_{j=1}^N \nabla_c^T y_j M^{-1} n_j^1 \right\}$$

After taking the trace of the scalar and reordering the vectors we get:

$$E(P^T Q^{-1} P) = \text{TRACE} \left[ E \left\{ \sum_{i=1}^N \sum_{j=1}^N n_j n_i^T M^{-1} \nabla_c y_i Q^{-1} \nabla_c^T y_j M^{-1} \right\} \right]$$

Because the noise is uncorrelated at unlike times the term simplifies to:

$$E(P^T Q^{-1} P) = \text{TRACE} \left[ \sum_{i=1}^N \nabla_c y_i Q^{-1} \sum_{j=1}^N \nabla_c^T y_j M^{-1} \right]$$

Finally, we have that the expected fit error for the case of testing the model's prediction of the system's response as:

$$E(J^1) = J + 2 \text{TRACE} \left\{ \sum_{i=1}^N \nabla_c y_i Q^{-1} \sum_{j=1}^N \nabla_c^T y_j M^{-1} \right\}$$

Since it is available, the actual fit error,  $J$ , is used instead of its expected value. The intent of the new criterion,  $E(J^1)$ , is that it be used instead of  $J$  in determining the level of model complexity that is best.

#### APPLYING THE NEW CRITERION TO ALL POSSIBLE CANDIDATE MODELS

Although it is a great help to have a criterion for comparing candidate models, there remains a problem of an excessive number of candidate models. Figure 4 illustrates the large number of candidate models that result from the combinations of unknown parameters that can be used for an example model with as many as 23 terms. The total number of possible candidate models that results from the combination of terms exceeds 8 million. Consequently, the calculations involved become an economic consideration. As the maximum number of unknown parameters increases, the number of possible candidate models rapidly becomes astronomical.

One can do several things to reduce the computations involved in assessing a large number candidate models, particularly if all possible combinations of terms are considered. First, it is essential to hold fixed the gradient  $\nabla_c y$ . Next, it is useful to express the new modeling criterion,  $E(J^1)$  as:

$$E(J^1) = J + 2 \text{TRACE} \left[ \sum_{j=1}^N \nabla_c^T y_j M^{-1} \sum_{i=1}^N \nabla_c y_i Q^{-1} \right]$$

By rearranging terms it is now possible to compute all but  $Q^{-1}$  in advance. One can also take advantage of a "bordering" technique to express  $Q^{-1}$  of a model in terms of that for a model with one less term, that is:

If  $Q_m^{-1}$  is the inverse of the information matrix for candidate model  $m$ , the inverse of the information matrix  $Q_{m+1}^{-1}$  for a model having one additional term is:

$$Q_{m+1}^{-1} = \begin{bmatrix} Q_m^{-1} + Q_m^{-1} b c b^T Q_m^{-1} & -Q_m^{-1} b (c - b^T Q_m^{-1} b) \\ -(c - b^T Q_m^{-1} b) b^T Q_m^{-1} & c - b^T Q_m^{-1} b \end{bmatrix}$$

Because of symmetry of both  $Q_m^{-1}$  and  $Q_{m+1}^{-1}$ , only  $2n^2 - 2n$  additional multiplications are required to form  $Q_{m+1}^{-1}$  compared to  $n^3$  if one starts from scratch. For example of looking at all possible combinations of a 25-term model, the multiplications involved in forming over 8 billion inverses is reduced from 14.4 trillion to 2.12 trillion, a savings of 85 percent.

The following procedure is suggested to realize these savings:

1. Determine values of the model parameters using all terms being considered.
2. Preserve the information matrix,  $Q$ , of step 1.
3. Compute and preserve the matrix

$$\sum_{j=1}^M v_c^T y_j H^{-1} \sum_{i=1}^M v_c y_i \text{ of step 1.}$$

4. Starting with terms taken singly, then pairs, and so forth, form the inverse of the corresponding information matrix using the bordering technique.
5. Select the appropriate rows and columns of the matrix of step 3 which correspond to the set of terms being considered.
6. Form the trace of the product of the matrices in steps 4 and 5. Either order may be used for the multiplication.
7. Preserve the models having the lowest value of expected fit error,  $E(J^1)$ .

The flow chart of Figure 5 depicts this procedure as it relates to the modeling problem when the format is unknown.

#### CONCLUDING REMARKS

The analyst often faces the problem of selecting a model's level of complexity in addition to determining the model's unknown parameters. If a model is selected solely on the basis of fit error or a likelihood function, the model will probably be less accurate in predicting system response than a simpler one.

Several models of varying complexity should always be examined and at least tested by predicting system response measurements not used in determining the unknown model parameters. Unfortunately, this form of test requires reserving part of the total data for testing only.

A new criterion is developed by expressing the expected fit error that would result from testing a model. The new modeling criterion enables using all of the data for determining the unknown model parameters.

A problem exists because of the large number of possible candidate models caused by the numerous combination of terms. The example which involved up to 23 unknown parameters corresponds to over 8 million candidate models or combinations of parameters. A procedure has been suggested which reduces by 85 percent the computation effort involved. The problem, however, of efficiently searching for the best candidate model remains an area worthy of attention.

#### REFERENCES

1. Taylor, Lawrence W., Jr.: "Nonlinear Time — Domain Models of Human Controllers." Hawaii International Conference on System Sciences, Honolulu, Hawaii. January 29-31, 1968.
2. Taylor, Lawrence W., Jr.: "A New Criterion for Modeling Systems." Symposium on Parameter Estimation Techniques and Applications in Aircraft Flight Testing. Edwards, California, April 1973. Also presented at the Fifth IFIP Conference on Optimization Techniques. Rome, Italy, May 1973.
3. Mehra, Raman K., and Stepner, David E.: "Maximum Likelihood Identification and Optimal Input Design for Identifying Aircraft Stability and Control Derivatives." NASA CR-2200, March 1973.

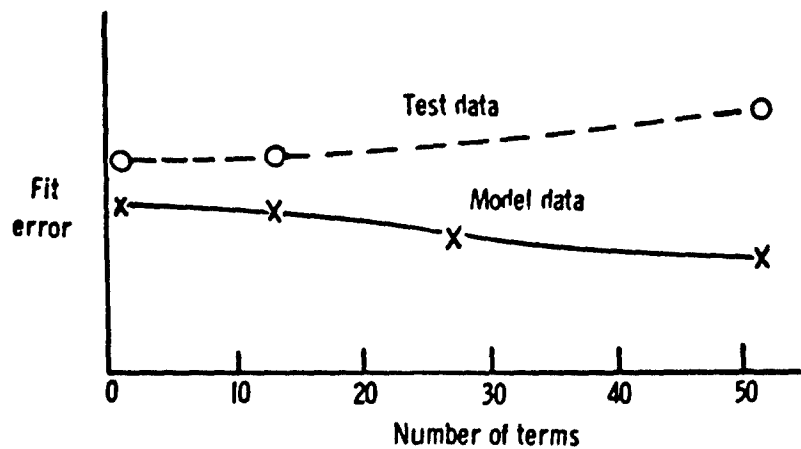


Figure 1. Comparison of fit error on data used to determine model parameter values with that using test data.  $T = 60$  seconds.

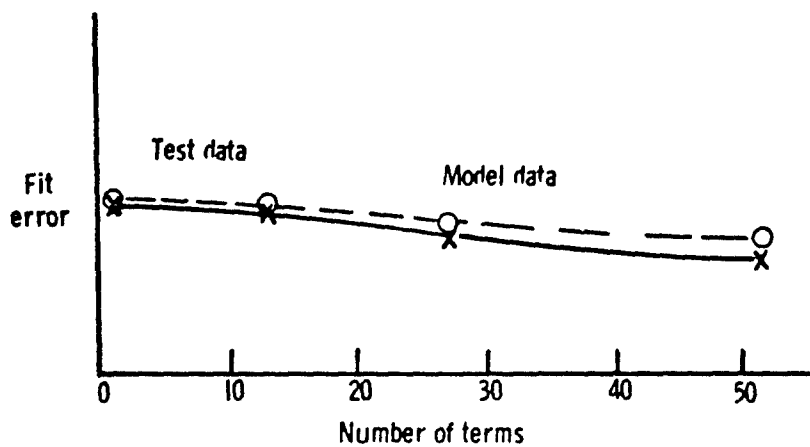


Figure 2. Comparison of fit error on data used to determine model parameter values with that using test data.  $T = 240$  seconds.

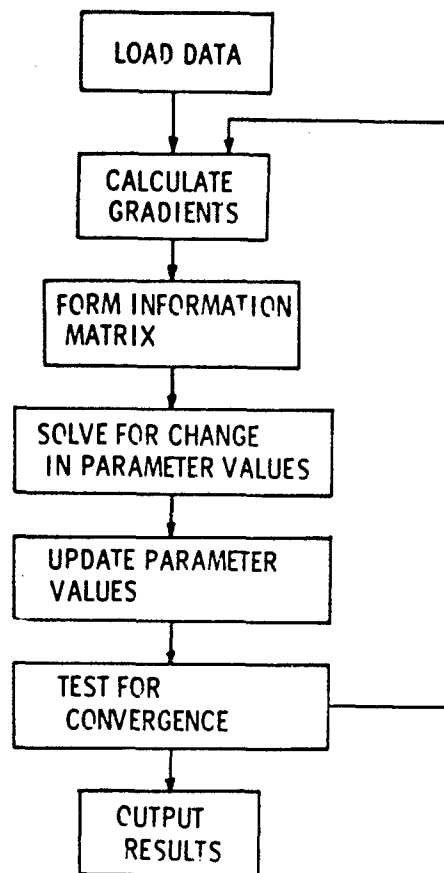


Figure 3. Flow chart for "known" model format.



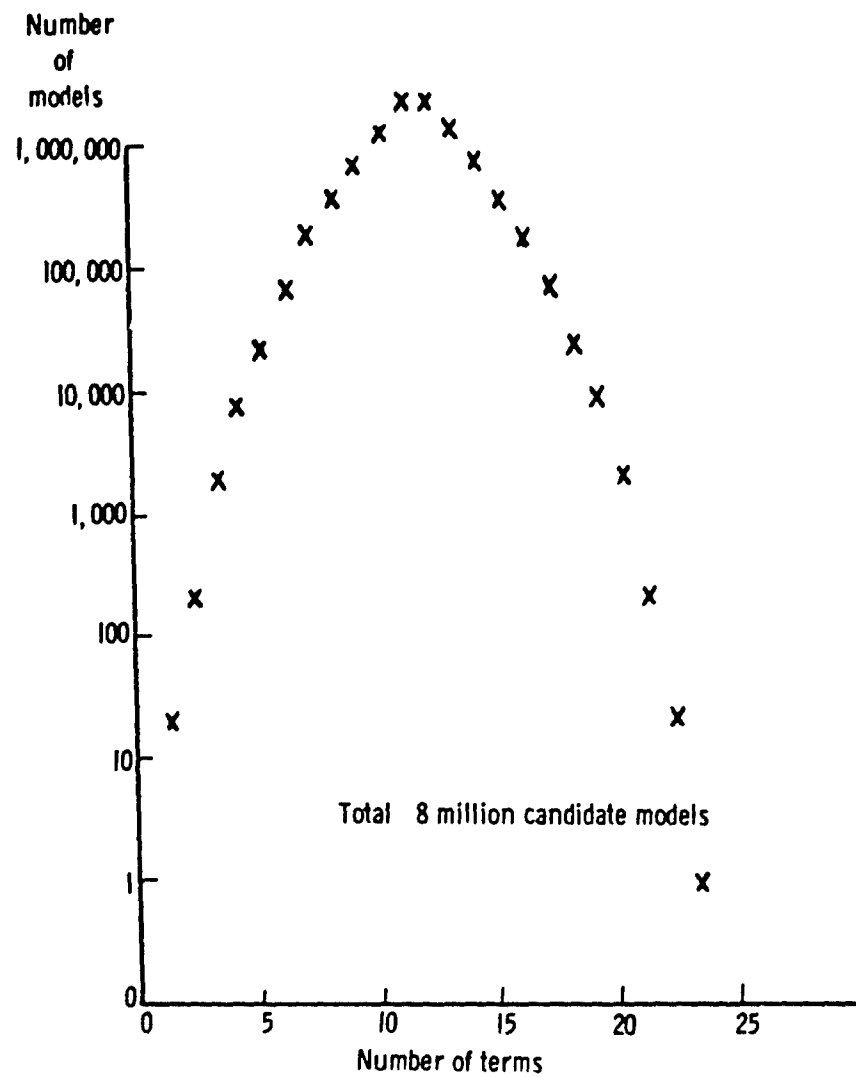


Figure 4. Number of candidate model due to combinations of terms in the dynamic equations.

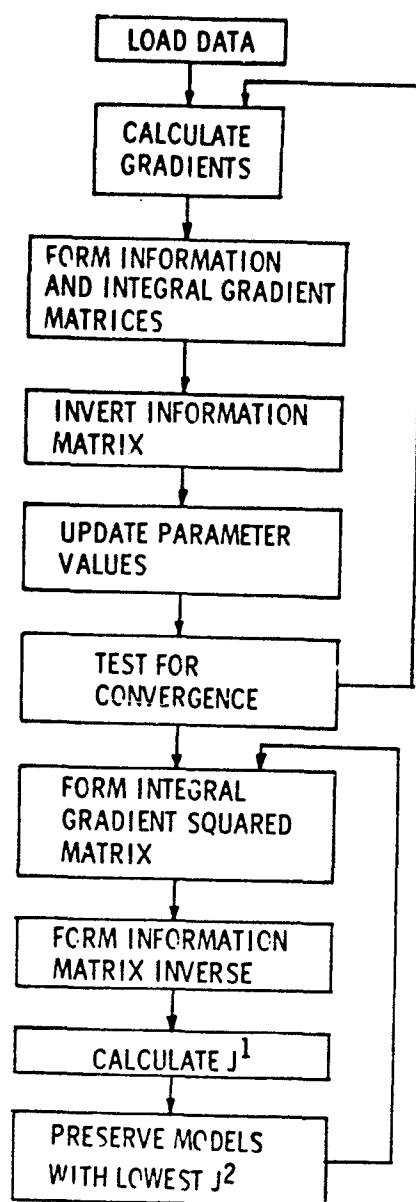


Figure 5. Flow chart for unknown model format.

# A MONTE CARLO ANALYSIS OF THE EFFECTS OF INSTRUMENTATION ERRORS ON AIRCRAFT PARAMETER IDENTIFICATION

by

Wayne H. Bryant and Ward F. Hodge  
NASA Langley Research Center  
Hampton, Virginia 23665

## SUMMARY

An output error estimation algorithm was used to evaluate the effects of both static and dynamic instrumentation errors on the estimation of aircraft stability and control parameters. A Monte Carlo analysis, using simulated cruise flight data, was performed for a high-performance military aircraft, a large commercial transport, and a small general-aviation aircraft. The effects of variations in the information content of the flight data, resulting from two different choices of control input maneuvers, were also determined.

The results indicate that unmodeled instrumentation errors can cause inaccuracies in the estimated parameters which are comparable to their nominal values. However, the corresponding perturbations to the estimated output response trajectories and characteristic equation pole locations appear to be relatively small. The magnitudes of these perturbations to the estimated parameters, output response trajectories, and characteristic equation pole locations, for both longitudinal and lateral response modes, can vary appreciably with different classes of aircraft, and with the information content of the flight data used. Control input errors and angular accelerometer lags were found to be most significant of the instrumentation errors evaluated, and the perturbations they produce are much larger than those arising from the combined effects of static errors and white noise in the output response measurements.

Although comprehensive data regarding parameter accuracy are not available without an exhaustive study, results for specific cases can be readily obtained using the error analysis algorithm described here.

## INTRODUCTION

One of the important tasks associated with current efforts to improve the estimates of stability and control derivatives obtained from flight data is to evaluate the effects of unmodeled errors in the measurements. The estimated quantities may be used in a variety of applications each with its own accuracy requirements, and the measurement system and flight maneuvers used may be specified primarily for other purposes. For these reasons, it is desirable to be able to evaluate the effect of a given instrumentation set on the accuracy of estimated stability and control parameters, and conversely, to determine an instrumentation set which will permit the parameters for a specific aircraft to be identified to a desired level of accuracy. Largely because of the difficulty in specifying parameter accuracy requirements and the existence of less powerful computational facilities, suitable error analysis algorithms for this purpose have appeared only recently. Two such algorithms, based on the minimization of output response errors, are described in Reference 1. The first one furnishes statistics of the resulting parameter inaccuracies through the use of sensitivity coefficients in an ensemble technique, and the other provides the statistics by means of a Monte Carlo analysis of simulated flight data.

Reference 1 also reports an initial investigation using the ensemble algorithm to determine the suitability of presently utilized instrumentation. This study assumed typical instrumentation, cruise flight conditions, and included the effects of static instrumentation errors only (such as biases, scale factors, misalignments, center-of-gravity uncertainty, and vane corrections). The results, together with those presented in Reference 2, indicated that these error sources can cause much larger parameter inaccuracies than those attributed to white noise in the output response measurements alone.

The results contained in Reference 3 and this report extend the overall investigation in several respects. A principal objective of these studies was to evaluate the effects of additional error sources such as those arising from instrumentation dynamics and measurements of control inputs. The simulated data algorithm (Monte Carlo) was used for this purpose, since these errors cannot be handled by the ensemble algorithm without introducing approximations which have not yet been evaluated. As stability and control derivatives are often estimated from flight data obtained for other purposes that may not require the full excitation of the aircraft modes, results were obtained for two different input maneuvers. Further data were obtained to determine how much the results change with different classes of aircraft for one input maneuver and identical instrumentation sets. In order to provide a more complete evaluation, the effects of parameter inaccuracies caused by unmodeled instrumentation errors on the output response trajectories, and characteristic equation pole locations were also determined. Lastly, a sensitivity analysis was performed to qualitatively identify the dominant error sources.

## METHOD OF ANALYSIS

### Simulated Data Error Analysis Algorithm

The process of estimating stability and control derivatives by minimizing an appropriate quadratic performance function  $J(p)$  provides a natural approach for analyzing the effects of unmodeled errors in the measurement data  $y_m$ . The essential feature of the simulated data concept is that the increase in

parameter inaccuracies caused by unmodeled instrumentation errors are obtained simply as the differences between the assumed true values of the parameters, and those estimated from simulated flight data which contain the unmodeled errors. The algorithm used for this purpose is that of Reference 4, which minimizes the output response error using the discrete performance index

$$J(p) = \sum_{i=1}^N (y_{m1} - \hat{y}_1)^T R^{-1} (y_{m1} - \hat{y}_1) \quad (1)$$

where  $y_1$  is the estimated response,  $R^{-1}$  is a weighting matrix, and the product is summed over the number of data points ( $N$ ) in the measured trajectory. The estimated parameters  $\hat{p}$  are solved for using the modified Newton-Raphson algorithm

$$\hat{p}_{j+1} = \hat{p}_j + \Delta \hat{p}_j = \hat{p}_j + \left[ \sum_{i=1}^N \left( \frac{\partial \hat{y}_i}{\partial p} \right)^T R^{-1} \left( \frac{\partial \hat{y}_i}{\partial p} \right) \right]^{-1} \left[ \sum_{i=1}^N \left( \frac{\partial \hat{y}_i}{\partial p} \right)^T R^{-1} (y_{m1} - \hat{y}_1) \right] \quad (2)$$

The convergence criteria used for the present study was  $|\Delta \hat{p}_j| \leq |0.01 \hat{p}_j|$  simultaneously for each parameter.

#### Aircraft Equations

The equations of motion used to represent the aircraft dynamics in the present study are:

$$\begin{bmatrix} \Delta \dot{\theta} \\ \Delta \dot{q} \\ \Delta \dot{w} \\ \Delta \dot{u} \end{bmatrix} = \begin{bmatrix} 0 & 1 & 0 & 0 \\ 0 & M_q & M_w & M_u \\ -g \sin \theta_0 & V \cos \alpha_0 & Z_w & Z_u \\ -g \cos \theta_0 & -V \sin \alpha_0 & X_w & X_u \end{bmatrix} \begin{bmatrix} \Delta \theta \\ \Delta q \\ \Delta w \\ \Delta u \end{bmatrix} + \begin{bmatrix} 0 \\ M_{\delta_e} \\ Z_{\delta_e} \\ 0 \end{bmatrix} \begin{bmatrix} \Delta \delta_e \end{bmatrix} \quad (3)$$

for the longitudinal mode and

$$\begin{bmatrix} \Delta \dot{\beta} \\ \Delta \dot{p} \\ \Delta \dot{r} \\ \Delta \dot{\phi} \end{bmatrix} = \begin{bmatrix} Y_{\beta} \sin \alpha_0 - \cos \alpha_0 g \cos \theta_0 / V \\ L_{\beta}^* & L_p^* & L_r^* & 0 \\ N_{\beta}^* & N_p^* & N_r^* & 0 \\ 0 & 1 & \tan \theta_0 & 0 \end{bmatrix} \begin{bmatrix} \Delta \beta \\ \Delta p \\ \Delta r \\ \Delta \phi \end{bmatrix} + \begin{bmatrix} Y_{\delta_a} & Y_{\delta_r} \\ L_{\delta_a}^* & L_{\delta_r}^* \\ N_{\delta_a}^* & N_{\delta_r}^* \\ 0 & 0 \end{bmatrix} \begin{bmatrix} \Delta \delta_a \\ \Delta \delta_r \end{bmatrix} \quad (4)$$

for the lateral directional mode. The short-period equations are obtained from (3) by eliminating the state  $\Delta u$  and all its factors. The unknown parameters estimated in the longitudinal mode are  $M_q, M_w, M_u, M_{\delta_e}, Z_{\delta_e}, Z_w, Z_u, X_w$ , and  $X_u$ . In the short-period mode,  $M_q, M_w, M_u, M_{\delta_e}$ , and  $Z_{\delta_e}$  are estimated and in the lateral mode  $Y_{\beta}, Y_{\delta_a}, Y_{\delta_r}, L_{\beta}^*, L_p^*, L_r^*, L_{\delta_a}^*, L_{\delta_r}^*, N_{\beta}^*, N_p^*, N_r^*, N_{\delta_a}^*, N_{\delta_r}^*$ , and  $L_r^*$  are estimated. Aircraft considered in the study were the DC-8, the F4-C, and Cessna 172. This selection permits the evaluation of a high-performance aircraft, a large transport, and a small general-aviation aircraft.

#### Measurement Equations

The ideal measurement equations are represented as

$$y = H(p) x + D(p) u \quad (5)$$

where  $x$  and  $u$  are the state and control vectors and  $H(p)$  and  $D(p)$  are the state and control observation matrices, respectively.

The simulated longitudinal measurements are:

- (1) Pitch attitude ( $\theta$ )
- (2) Pitch rate ( $q$ )
- (3) Angle of attack ( $\alpha$ )
- (4) Longitudinal velocity ( $u$ )
- (5) Longitudinal acceleration ( $n_x$ )
- (6) Normal acceleration ( $n_z$ )
- (7) Pitch acceleration ( $\dot{q}$ )

In the short-period mode, longitudinal velocity and acceleration are not used. In the lateral mode, the simulated measurements are:

- (1) Angle of sideslip ( $\beta$ )
- (2) Roll rate ( $p$ )
- (3) Yaw rate ( $r$ )
- (4) Roll attitude ( $\phi$ )
- (5) Lateral acceleration ( $n_y$ )
- (6) Roll acceleration ( $\dot{p}$ )
- (7) Yaw acceleration ( $\dot{r}$ )

These measurements are corrupted by errors which are modeled in the following order:

$$y_I = T y + b \quad (6)$$

where  $T$  is a matrix of scale factor, cross-coupling, and misalignment errors, and  $b$  represents measurement biases. State measurement lags are modeled as

$$\dot{y}_L = \Gamma_y^{-1} (y_I - y_L) \quad (7)$$

where  $\Gamma_y$  is a diagonal matrix of measurement time constants. The simulated flight data measurements are then obtained by adding white noise at each time point

$$y_m = y_L + w \quad (8)$$

In a similar fashion, control surface position measurement errors are modeled as

$$u_I = T_c u + b_c \quad (9)$$

where  $T_c$  is a matrix of scale factor errors, and  $b_c$  are measurement biases. Control measurement lags are included as

$$\dot{u}_L = \Gamma_c^{-1} (u_I - u_L) \quad (10)$$

with  $\Gamma_c$  a diagonal matrix of measurement system time constants. The simulated control measurement is obtained by adding white noise as

$$u_m = u_L + w_c \quad (11)$$

and is used in the development of the estimated state measurements. A more detailed description of the measurement models can be found in Reference 3.

#### Monte Carlo Computations

The statistics of the measurement errors appearing in the preceding equations are assumed in Table I (Refs. 1 and 6) to be given by zero-mean 1 $\sigma$  values, which are used in conjunction with a pseudo-random number generator to simulate a number of sets of  $y_m$  and  $u_m$ . Following the simulation procedure employed in References 1 and 2, the sensor location errors ( $\epsilon_{ax}$ ,  $\epsilon_{az}$ ,  $\epsilon_{vx}$ ) and the elements of  $\Gamma_y$  and  $\Gamma_c$  are treated as constants which remain at their tabulated 1 $\sigma$  values for all sets of  $y_m$  and  $u_m$  generated. The elements of  $w$  and  $w_c$  are given new random values at each time point of every set of  $y_m$  and  $u_m$ , while the values for all remaining error sources are regenerated once for each such set to simulate random biases. A corresponding set of parameter estimates  $\hat{p}$  are computed using Equation (2), and the resulting estimation errors  $\Delta\hat{p}$  are formed by subtracting the assumed true parameter values,  $p$ . Means and variances of  $\Delta\hat{p}$  are then calculated.

Further computations are made to permit evaluating the effects of the  $\Delta\hat{p}$  on the estimates of the output response trajectories and the open-loop characteristic equation pole locations. Statistics of the former, for each discrete value of time, are calculated using all sets of data generated. Computations of all quantities were generally based on 50 such data sets; however, in some cases as few as 25 sets were used with satisfactory results. An interval of 0.1 second was used for both the integration step size and the data sampling rate. Since the short-period roots of the longitudinal characteristic equation become real for some of the  $\Delta\hat{p}$ , scatter diagrams are used to indicate the distribution of these quantities.

#### RESULTS AND ANALYSIS

The Monte Carlo analysis of the effects of unmodeled instrumentation errors outlined in the introduction was based on simulated flight data, generated from the aircraft parameters and cruise flight conditions listed in Table II (Refs. 7, 8, 9) and the two sets of control input maneuvers plotted in Figure 1. These choices permit examining the effects of independently varying the information content of the simulated response measurements and the type of aircraft, and facilitate comparisons with similar results presented in References 1 and 2. The effects of the unmodeled error sources were evaluated in three groups or error cases for each control input or aircraft type. These error cases correspond to progressively adding white measurement noise (case 0), static measurement errors (case 1), and dynamic lags and control input errors (case 2) to the simulated data. The analysis presented includes results for both the longitudinal short-period and lateral-directional response modes. Lastly, sensitivity computations were performed to identify the dominant error sources.

Although the results presented are not exhaustive, they are representative of those that can be obtained through the use of the error analysis programs described here and in Reference 1 for specific combinations of aircraft type, instrumentation set and error level, and the control input selection.

#### Error Analysis

In order to extend and make possible direct comparisons with the results for the ensemble algorithms given in References 1 and 2, those for the present study also were generated mainly for the F4-C aircraft (see Table II) using the input maneuvers designated as sequence 1 in Figures 1(a) and 1(b). The effects of the unmodeled instrumentation errors on the estimated aircraft parameters are analyzed, then the corresponding perturbations to the output response trajectories and characteristic pole locations are discussed.

**Stability and Control Derivatives.** The statistics of the errors in the estimated aircraft parameters, for both the short-period and lateral response modes, are presented in Figure 2 for each of the three error cases. This information is expressed in terms of percentage deviation from the assumed true value of each such derivative presented, and includes the mean and standard deviation for every element of the resulting  $\Delta\hat{p}$ . For Figure 2, and all subsequent plots of a similar nature, the mean and standard deviation of each plotted quantity are respectively denoted by cross hatched and solid bars as indicated.

In generating the data plotted in Figure 2, the estimation errors for the longitudinal derivatives  $\hat{R}_u$ ,  $\hat{X}_u$ ,  $\hat{Z}_u$ , and  $\hat{X}_w$  associated with the phugoid, and the lateral derivatives  $\hat{Y}_{\delta a}$  and  $\hat{Y}_{\delta r}$ , were found to be very large. Since the phugoid period for the F4-C aircraft is roughly 22 times the 15-second data sampling interval used, the results for  $\hat{R}_u$ ,  $\hat{X}_u$ ,  $\hat{Z}_u$ , and  $\hat{X}_w$  were judged to be inaccurately determined because of insufficient information, and only those for the derivatives retained in the short-period approximation are presented. The values for  $\hat{Y}_{\delta a}$  and  $\hat{Y}_{\delta r}$  were omitted for the same reason, but these two derivatives were allowed to vary in the estimation process.

Reference to Figure 2 shows that the static errors added by case 1 cause much larger parameter inaccuracies than those due to white measurement noise alone (case 0). The case 1 errors produce biases in most of the elements of  $\Delta\hat{p}$  for both response modes which are comparable to their respective standard deviations. These biases proved to be mainly a consequence of modeling  $\epsilon_{ax}$ ,  $\epsilon_{az}$ , and  $\epsilon_{vx}$  as constant errors (see Table I), and not the result of any statistical inaccuracy that could be attributed to the number of data sets used.

Comparisons of the Monte Carlo results presented in Figure 2 with those obtained using the ensemble algorithm generally indicated good agreement, but were limited to cases 0 and 1 since case 2 was not evaluated in References 1 and 2. With the exception of some of the weaker derivatives, the differences amounted to only a few percent in both the mean and random components of  $\Delta\hat{p}$ . The results for case 2 show that dynamic lags and control input errors can cause much larger inaccuracies in the estimated derivatives than the combined effects of white noise and static errors in the response measurements.

The effects of initial state errors were also evaluated; however, the resulting changes in  $\Delta\hat{p}$  proved to be very small (about equal to those for case 0) so that the utility of estimating them would seem questionable for either case 1 or case 2. Since the results for case 1 imply that the contributions to  $\Delta\hat{p}$  from the biases in the response measurements are small compared to those from the dynamic lags and control input errors, the value of estimating the output biases also appears doubtful. Assuming they are present in the flight data, estimating case 2 error sources would therefore seem to offer better prospects for reducing inaccuracies in the estimated derivatives.

One additional aspect of the computations that should be mentioned is that  $\left(\frac{\partial \hat{p}}{\partial p}\right)^T R^{-1} \left(\frac{\partial \hat{p}}{\partial p}\right)$  remained almost unchanged for all three error cases, so that the inverse of this matrix is not indicative of the error covariance matrix  $E[\Delta\hat{p} \Delta\hat{p}^T]$  except for case 0. Furthermore, the elements of  $\Delta\hat{p}$  contain biases which are comparable to their respective standard deviations for both cases 1 and 2 as previously noted.

**Output Response Trajectories.** The effects of the  $\Delta\hat{p}$  on the resulting output response trajectories are illustrated by the time history curves presented in Figure 3. Plotted for each element of the short-period and lateral output vectors are the assumed true response (based on the Table II parameter values), and the means and standard deviations of both the measured and estimated response. Only the curves for case 2 are plotted since those for cases 0 and 1 exhibit almost no deviation from the true trajectories. These results show that the perturbations to the response trajectories are not very severe, however, their importance depends on the particular application.

Reference to Figure 3 indicates that the largest perturbations for both response modes occur for the attitude angles, and increase to fairly large values over the 15-second interval plotted. This propagation results from the effects of the  $\Delta\hat{p}$  on the integration of the aircraft equations of motion. Inspection of Equation (3) for the short-period mode shows that the errors in  $\hat{R}_q$ ,  $\hat{R}_w$ , and  $\hat{R}_{\delta e}$  directly affect the integration of  $\Delta\hat{q}$ . The resulting inaccuracy in  $\Delta\hat{q}$  is in turn propagated by the integration of  $\Delta\hat{\theta}$ , so that the effect on the pitch attitude error  $\Delta\hat{\theta}$  is twofold. Equation (4) for the lateral mode indicates that the roll attitude error  $\Delta\hat{\phi}$  results from a similar double perturbation of the errors in  $\hat{L}_{\delta a}^*$ ,  $\hat{L}_{\delta r}^*$ ,  $\hat{L}_{\delta a}$ , and  $\hat{L}_{\delta r}$  by the integration of  $\Delta\hat{\beta}$  and  $\Delta\hat{\delta}$ . The perturbations to the attitude angles  $\Delta\hat{\theta}$  and  $\Delta\hat{\phi}$  thus depend on the errors in these eight derivatives, which all increase appreciably between cases 1 and 2 (see Fig. 2).

The relative positions of the  $\hat{y}$  and  $y_m$  time histories plotted in Figure 3 further indicate the effects of the unmodeled instrumentation errors on the fit between the estimated and measured response curves, which appears to be generally good except for the attitude angles  $\Delta\hat{\theta}$  and  $\Delta\hat{\phi}$ . The estimated response curves (except that for  $\Delta\hat{\phi}$ ) exhibit negligible biases, but their standard deviations are larger than those for the corresponding measured curves. This behavior is opposite to that observed for cases 0 and 1, and may be due to process noise introduced in Equations (3) and (4) by the addition of control input errors (case 2) which degrades parameter estimates obtained with the modified Newton-Raphson algorithm (see Ref. 10).

**Characteristic Equation Pole Locations.** The s-plane representation is employed for the scatter diagrams presented in Figure 4 to illustrate the effects of the  $\Delta\hat{p}$  on the resulting characteristic equation pole locations. The plotted pole locations for both response modes were calculated using data points for each set of  $\hat{p}$  used in generating Figures 2 and 3. The results for the different poles are denoted by plotting symbols as shown, and their assumed true locations (based on the Table II parameter values) are indicated by arrows. As was the case with Figure 3, only the results for case 2 are presented since those for cases 0 and 1 also showed very little departure from the true values. While the perturbations to the characteristic equation pole locations do not appear to be much more severe than those for the response trajectories, their importance again should be judged by the application.

To determine which of the  $\Delta \hat{p}$  cause the majority of the bias and scatter seen in Figure 4, the equations used to determine pole locations were evaluated with only one parameter at a time set first to its estimated mean value, then to its estimated mean  $\pm 1\sigma$  value. The following table shows which errors were found to have the greatest effect on the indicated movement of the poles.

Mode	Axis	Derivatives affecting pole motion
Short period	$i\omega$ - bias and scatter	$M_y$
	$\sigma$ - bias and scatter	$M_q$
Lateral Dutch roll	$i\omega$ - bias	$L^*$
	$i\omega$ - scatter	$L^*, N^*, N^*$
	$\sigma$ - bias	$L^*, N^*, N^*$
	$\sigma$ - scatter	$L^*, N^*, N^*$
Roll subsidence	$\sigma$ - bias and scatter	$L^*, P$

Reference to Figure 2 again shows that the errors in those derivatives which dominate the resulting perturbations increase appreciably between cases 1 and 2.

#### Effect of Control Input Maneuver

To determine how the results presented in Figures 2, 3, and 4 might vary for an alternate choice of control inputs corresponding data were generated using the input maneuvers designated as sequence 2 in Figures 1(c) and 1(d). The sequence 2 inputs for both response modes are comprised of ordinary short doublet pulses, and were chosen to provide a comparison with results for maneuvers of the type often used in actual flight tests. As evident from Figure 1, these inputs differ both in form and duration from those for sequence 1 which consist of doublets augmented with trailing step pulses.

To facilitate comparisons of the parameter estimation errors for the two sets of input maneuvers, the ratio of  $\Delta \hat{p}$  for sequence 2 to that for sequence 1,  $\frac{\Delta \hat{p}_2}{\Delta \hat{p}_1}$ , is plotted in Figure 5 for each of the short-period and lateral derivatives. The actual  $\Delta \hat{p}_2$  percentage values can easily be obtained by multiplying  $\Delta \hat{p}_1$  by  $\frac{\Delta \hat{p}_2}{\Delta \hat{p}_1}$  if desired. For example, the values of  $\Delta \hat{p}_1$  and  $\frac{\Delta \hat{p}_2}{\Delta \hat{p}_1}$  for the mean error in  $L^*$  (from Figs. 2 and 5) are respectively about 20 percent and 0.5, which give 10 percent as the value of the mean error in  $L^*$  for sequence 2.

Except for the ratios of the mean errors in some of the lateral derivatives for case 0 (which are inaccurately formed because of the smallness of the numbers involved), the fact that the values for most of the  $\frac{\Delta \hat{p}_2}{\Delta \hat{p}_1}$  ratios plotted in Figure 5 are nearly unity indicates essentially the same magnitude  $\Delta \hat{p}$  errors for both sets of inputs. Even though the aircraft response differs substantially, as evident from the corresponding state variable time histories also plotted in Figure 1, the increase in information content afforded by the use of sequence 1 did not result in any appreciable decrease in  $\Delta \hat{p}$ . Thus, the information content of the response data does not appear to be deficient for either set of input maneuvers. While the assumed true response trajectories for the two sets of inputs also exhibit the differences just noted, the magnitudes and overall characteristics of the resulting perturbations are essentially the same for each corresponding element of  $\hat{y}$ . The two sets of characteristic equation pole locations show similar scatter patterns, which is consistent with the fact that the parameter estimation accuracy remained almost unchanged. Because of the limited additional information they contribute, the response trajectories and pole location plots for sequence 2 are not presented for either response mode.

#### Instrumentation Error Effects for Different Aircraft Classes

To determine how the effects of unmodeled instrumentation errors might vary for different aircraft using the same control input and identical instrumentation sets, the previous computations were repeated using the parameters and nominal flight conditions for the large transport (DC-8) and the light general-aviation aircraft (C-172) also listed in Table II. These data include results for both the short-period and lateral response modes, and were generated using the sequence 1 input maneuvers. The ratio of the  $\Delta \hat{p}$  for the

DC-8 and the C-172 to that for the F4-C aircraft,  $\frac{\Delta \hat{p}_{DC-8}}{\Delta \hat{p}_{F4-C}}$  and  $\frac{\Delta \hat{p}_{C-172}}{\Delta \hat{p}_{F4-C}}$ , were formed in the same manner as  $\frac{\Delta \hat{p}_2}{\Delta \hat{p}_1}$  to facilitate comparisons of the results for the three types of aircraft. The values of  $\frac{\Delta \hat{p}_{DC-8}}{\Delta \hat{p}_{F4-C}}$  are presented in Figures 6(a) and 6(b), and those for  $\frac{\Delta \hat{p}_{C-172}}{\Delta \hat{p}_{F4-C}}$  in Figures 6(c) and 6(d). No results for  $\Delta \hat{p}_{\delta_e}$

are included in Figure 6(c), since the assumed true value for this derivative was zero for the C-172 aircraft (see Table II). As with Figure 5, some of the case 0 ratios are inaccurate, however, these results are of minor importance as the elements of  $\Delta \hat{p}$  for each of the three aircraft are all very small for case 0 anyway.

The  $\frac{\Delta \hat{p}_{DC-8}}{\Delta \hat{p}_{F4-C}}$  ratios plotted in Figures 6(a) and 6(b) indicate that the elements of  $\Delta \hat{p}$  for the DC-8 and F4-C aircraft are about the same for the short-period mode, but are larger for most of the DC-8 lateral

derivatives. The corresponding values of  $\frac{\Delta \hat{p}_{C-172}}{\Delta \hat{p}_{F4-C}}$  presented in Figures 6(c) and 6(d) exhibit even larger differences between the two sets of parameter estimation errors for each response mode. These results indicate that the effects of unmodeled instrumentation errors on  $\hat{p}$  can vary appreciably for different classes of aircraft.

The perturbations to the output response trajectories for the DC-8 and C-172 also exhibited much the same overall characteristics as those for the F4-C aircraft, and the plots for these curves were therefore omitted for the same reason as those for sequence 2. The corresponding characteristic equation pole location plots for case 2, however, are presented in Figure 7. Comparisons of Figures 4 and 7 indicate that the pole location errors for the DC-8 and C-172 are very similar to those for the F4-C aircraft, except those for the C-172 short-period poles exhibit a much larger scatter pattern. Evaluations of the pole location equations similar to those performed in conjunction with Figure 4 showed the increased scatter to be caused mainly by  $\Delta R_y$  and  $\Delta Z_y$  which are much larger for the C-172 than for either the DC-8 or F4-C aircraft. The effects of the errors in these derivatives are further manifested by the short-period roots of the longitudinal characteristic equation becoming real for five of the 50 sets of pole locations plotted in Figure 7(c); however, examination of the output response trajectories for these five sets showed no appreciable differences from the rest. Because of the high short-period damping factor for the C-172 (0.92 for the assumed true values), the estimation algorithm has difficulty in determining accurate values for the derivatives, and instrumentation errors compound this difficulty. However, the algorithm still estimates a set of derivatives that closely represents the observed output responses.

#### Identification of Dominant Error Sources

The remaining objective of the present study was to qualitatively identify which of the error sources dominate the resulting perturbations plotted in Figures 2, 3, and 4. The initial phase of this process showed that, while  $\Delta \hat{p}$  for error case 1 is much larger than that for case 0, neither white noise nor static errors in  $y_m$  proved to have much effect on either the estimated response trajectories or characteristic equation pole locations. These error sources thus appeared to be relatively unimportant, indicating that the perturbations to the output measurements  $\hat{y}$  and pole locations  $\hat{s}$  evident in Figures 3 and 4 are produced mainly by the effects of the dynamic lags and control input errors.

The addition of only dynamic lags to case 1 was found to produce negligible changes in the random components of  $\Delta \hat{p}$  for both the short-period and lateral derivatives, but the magnitudes of the mean or bias components generally increased. Results generated by including the individual elements of  $\Gamma_y$  and  $\Gamma_c$  one at a time indicated that these changes are produced principally by the pitch accelerometer and elevator position transducer lags for the short-period mode, and by the roll accelerometer and aileron position transducer for the lateral mode. Further analysis showed that the biases in the pole locations evident in Figure 4 are noticeably affected by these lags, while the corresponding  $\hat{y}$  trajectories remain essentially unchanged. Except for the effects of static bias errors in the lateral control input measurements, as discussed in the following paragraph, the resultant biases in  $\Delta \hat{p}$  (Fig. 2) and (Fig. 4) for case 2 proved to be caused mainly by the two dominant lags for each response mode. While the effects of dynamic lags do not appear to be very large for the cutoff frequencies represented by the time constants listed in Table I, these values are near a threshold such that the biases they produce may increase rapidly if onboard filtering below these frequencies is employed.

The random components of  $\Delta \hat{p}$  and  $\Delta \hat{y}$  and the scatter in  $\hat{s}$  for case 2 thus were traced to the static control input errors. By adding these error sources to case 1 one at a time, as was done with the lags, the elevator white noise and the aileron bias were found to be the dominant static control measurement errors for the short-period and lateral modes, respectively. This procedure further indicated that the random parts of the perturbations evident in Figures 2, 3, and 4 are caused mainly by these error sources. As mentioned previously,  $b_{\delta_a}$  also contributes to the resultant biases in  $\Delta \hat{p}$ ,  $\Delta \hat{y}$ , and  $\hat{s}$  for the lateral mode. These biases are most noticeable in the roll attitude trajectory (Fig. 3(b)), and the root location for the roll subsidence time constant (Fig. 4(b)). While only results for the F4-C aircraft are discussed, the dominant error sources were determined to be the same for all three aircraft.

#### CONCLUSIONS

The results from a Monte Carlo analysis of the effects of unmodeled flight instrumentation errors on the estimation of aircraft stability and control derivatives indicate the following conclusions:

1. Aircraft derivatives estimated from flight data, obtained with existing instrumentation, may be in error by amounts which are comparable to their respective nominal values. The effects of these errors on the corresponding estimates of the output response trajectories and characteristic equation pole locations do not appear to be very severe, however, their importance depends on the particular application.
2. The perturbations to the estimated parameters, response trajectories, and pole locations contributed by dynamic lags (particularly those for the angular accelerometers) and control input errors are much larger than those arising from white noise and static errors in the response data combined.
3. The effects of initial state errors and output measurement biases also are comparatively small, so that the utility of estimating them would seem questionable particularly if the flight data contain dynamic lags or control input errors.
4. While some exceptions may be noted, the magnitudes of the resulting parameter estimation errors can vary appreciably for different classes of aircraft with some tendency to be largest for light aircraft and smallest for heavy transports.



# REFERENCES

1. Sorenson, John A.: Analysis of Instrumentation Error Effects on the Identification Accuracy of Aircraft Parameters. NASA CR-112121, 1972.
2. Sorenson, J. A., Tyler, J. S., Jr., and Powell, J. David: Evaluation of Flight Instrumentation for the Identification of Stability and Control Derivatives. Preprint 72-963, Am. Inst. Aeron. and Astronaut., September 1972.
3. Bryant, Wayne H., and Hodge, Ward F.: Effects of Instrumentation Errors on the Estimation of Aircraft Stability and Control Derivatives. NASA TN D-7647, April 1974.
4. Illiff, Kenneth W., and Taylor, Lawrence W., Jr.: Determination of Stability Derivatives From Flight Data Using a Newton-Raphson Minimization Technique. NASA TN D-6579, 1972.
5. Hodge, Ward F., and Bryant, Wayne H.: Monte Carlo Analysis of Inaccuracies in Estimated Aircraft Parameters Caused by Unmodeled Flight Instrumentation Errors. NASA TN D-7712, 1974.
6. Hill, R. W., Clinkenbeard, I. L., and Bolling, N. F.: V/STOL Flight Test Instrumentation Requirements for Extraction of Aerodynamic Coefficients. Tech. Rept. APTDL-TR-68-154, Vought Aeronautics Div., LTV Aerospace Corp., December 1968.
7. Anon.: Aerodynamic Derivatives of F/RP-4B-C. MAC 9842, McDonnell Aircraft Corp., February 1964.
8. McRuer, Duane, Ashkenas, Irving, and Graham, Dunston: Aircraft Technology, Inc., August 1968. Appendix A, Stability Derivatives and Transfer Function Factors for Representative Aircraft.
9. Leisher, L. L., and Walter, H. L.: Stability Derivatives of Cessna Aircraft. Rept. 1356, Res. Dept., Cessna Aircraft Co., May 1957.
10. Stepner, David E., and Mehra, Raman K.: Maximum Likelihood Identification and Optimal Input Design for Identifying Aircraft Stability and Control Derivatives. NASA CR-2200, 1972.

TABLE I. STANDARD DEVIATIONS OF NOMINAL INSTRUMENTATION ERRORS  
(From Reference 1, except as noted)

Instrument	Subscript	Bias & noise (b)	Scale factor (w)	Sensor location (c)	c.g. location (e)	Misalignment (Y)	Time constant <sup>1</sup> (T)
Gyros							
Pitch attitude	$\theta$	0.150°	0.005	-	-	-	0.333 s
Roll attitude	$\phi$	.500°	.005	-	-	-	.333 s
Pitch rate	q	.100°/s	.005	-	-	-	.333 s
Roll rate	p	.100°/s	.005	-	-	0.60°	.333 s
Yaw rate	r	.100°/s	.005	-	-	.60°	.333 s
Accelerometers							
Forward	$n_x, a_x^2$	.005 g	.005	0.305 m	-	.60°	.100 s
Normal	$n_z, a_z^2$	.005 g	.005	.305 m	-	.60°	.100 s
Lateral	$n_y$	.0005 g	.005	-	-	-	.100 s
Pitch	$\dot{q}$	.100°/s <sup>2</sup>	.005	-	-	-	.333 s
Roll	$\dot{p}$	.100°/s <sup>2</sup>	.005	-	-	.60°	.333 s
Yaw	$\dot{r}$	.100°/s <sup>2</sup>	.005	-	-	.60°	.333 s
Airflow							
$\alpha$ - vane	$\alpha, v_\alpha^2$	.100°	.005	.305 m	-	-	.333 s
$\beta$ - vane	$\beta$	.050°	.005	-	-	-	.333 s
Pitot tube	u	.305 m	.005	-	-	-	1.000 s
Control surface position potentiometer							
Elevator	$\delta_e$	.100°	.005	-	-	-	.500 s
Aileron	$\delta_a$	.100°	.005	-	-	-	.500 s
Rudder	$\delta_r$	.100°	.005	-	-	-	.500 s
Airframe center of gravity							
Forward	xcg	-	-	-	0.152 m	-	-
Normal	zcg	-	-	-	.152 m	-	-

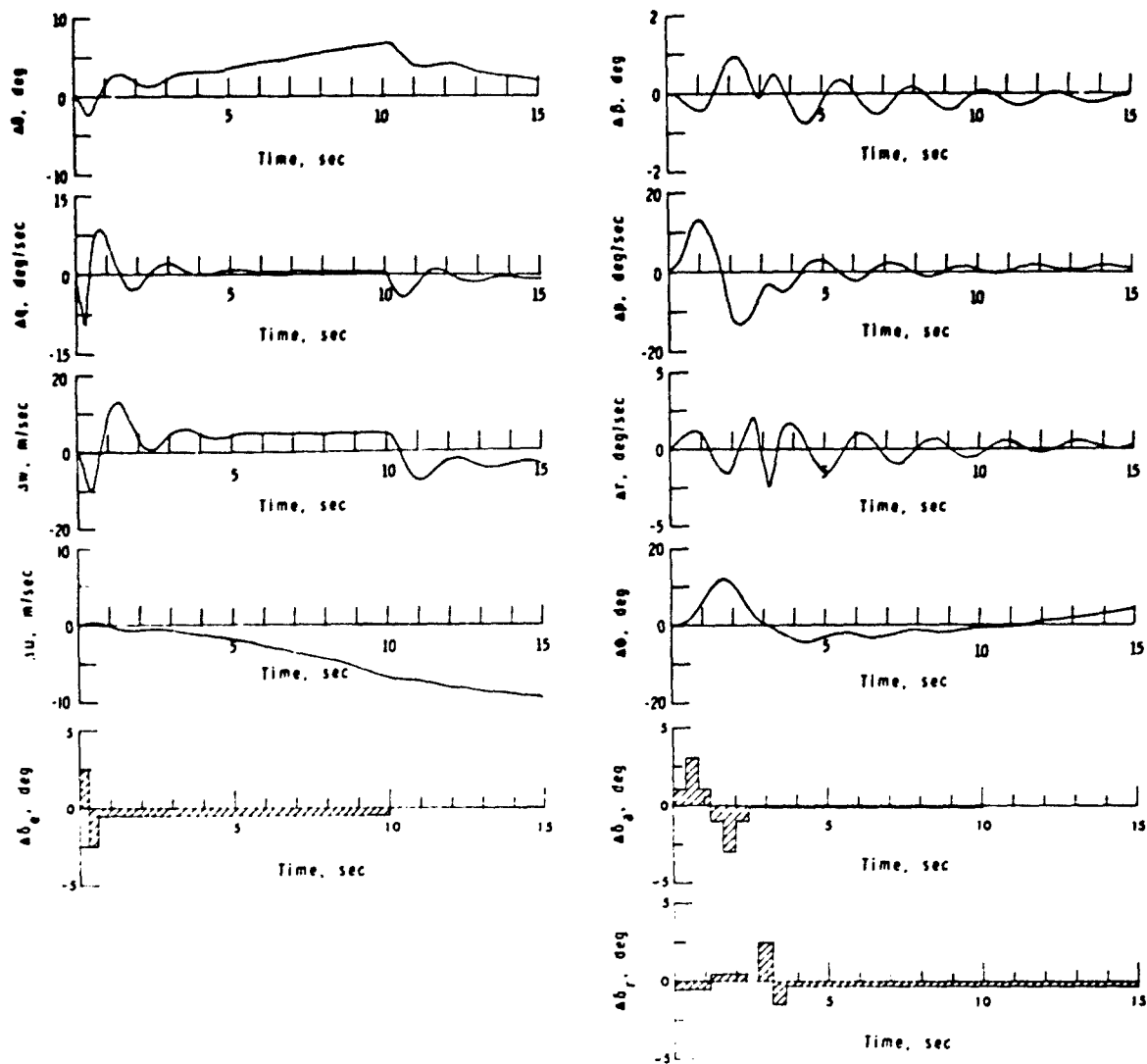
<sup>1</sup>Reference 6.

<sup>2</sup>Subscript applies to sensor location only.

TABLE II. REFERENCE TRAJECTORIES AND STABILITY AND CONTROL DERIVATIVES

	Aircraft		
	F4-C <sup>1</sup>	DC-8 <sup>2</sup>	C-172 <sup>3</sup>
Reference trajectory			
V, m/s	252.2	251.2	54.5
$\alpha_o$ , degrees	2.6	0	-0.7
$\theta_o$ , degrees	2.6	0	-0.6
Altitude, m	6096.0	10058.4	1524.0
Longitudinal			
Mq, s <sup>-1</sup>	-0.7192	-0.9240	-6.7346
Mw, 1/s-m	-0.0338	-0.0364	-0.1664
Zw, s <sup>-1</sup>	-0.7624	-0.8060	-2.0702
Mu, 1/s-m	-0.0015	-0.0026	-0.0020
Zu, s <sup>-1</sup>	-0.0617	-0.0735	-0.3844
Xu, s <sup>-1</sup>	-0.0070	0.0140	-0.0427
Xw, s <sup>-1</sup>	.0273	.0043	.0702
M <sub>oe</sub> , 1/s <sup>2</sup> -rad	-16.2100	-4.5900	-24.3809
Z <sub>oe</sub> , m/s <sup>2</sup> -rad	-21.7514	-10.5461	0
Lateral			
y <sub>B</sub> , s <sup>-1</sup>	-0.1569	-0.0868	-0.1630
L <sub>B</sub> <sup>*</sup> , s <sup>-1</sup>	-15.9779	-4.4103	-23.2641
N <sub>B</sub> <sup>*</sup> , s <sup>-2</sup>	6.5630	2.1405	5.5036
L <sub>p</sub> <sup>*</sup> , s <sup>-1</sup>	-1.6084	-1.1812	-11.5311
N <sub>p</sub> <sup>*</sup> , s <sup>-1</sup>	-0.0997	-0.0204	-1.3632
L <sub>r</sub> <sup>*</sup> , s <sup>-1</sup>	.3840	.3343	2.6918
N <sub>r</sub> <sup>*</sup> , s <sup>-1</sup>	-0.3432	-0.2281	-1.2138
y <sub>oa</sub> , 1/s-rad	-0.0034	0	0
L <sub>oa</sub> <sup>*</sup> , 1/s <sup>2</sup> -rad	10.8972	2.1102	53.7865
N <sub>oa</sub> <sup>*</sup> , 1/s <sup>2</sup> -rad	.7063	-0.0652	.2103
y <sub>or</sub> , 1/s-rad	.0246	.0222	0
L <sub>or</sub> <sup>*</sup> , 1/s <sup>2</sup> -rad	2.5431	.5490	.9974
N <sub>or</sub> <sup>*</sup> , 1/s <sup>2</sup> -rad	-3.9028	-1.1644	-6.1719

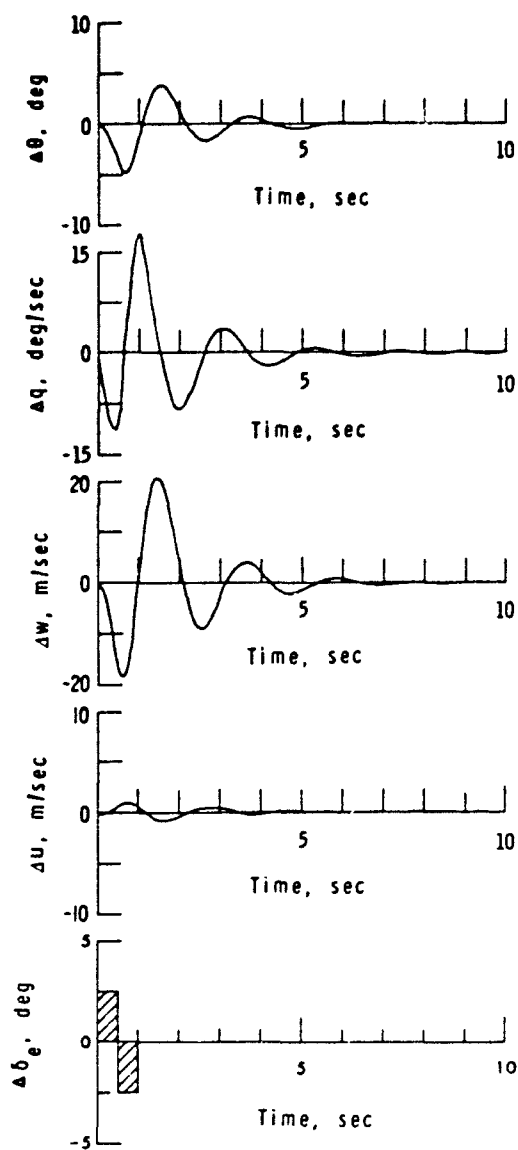
<sup>1</sup>Reference 7.<sup>2</sup>Reference 8.<sup>3</sup>Reference 9.



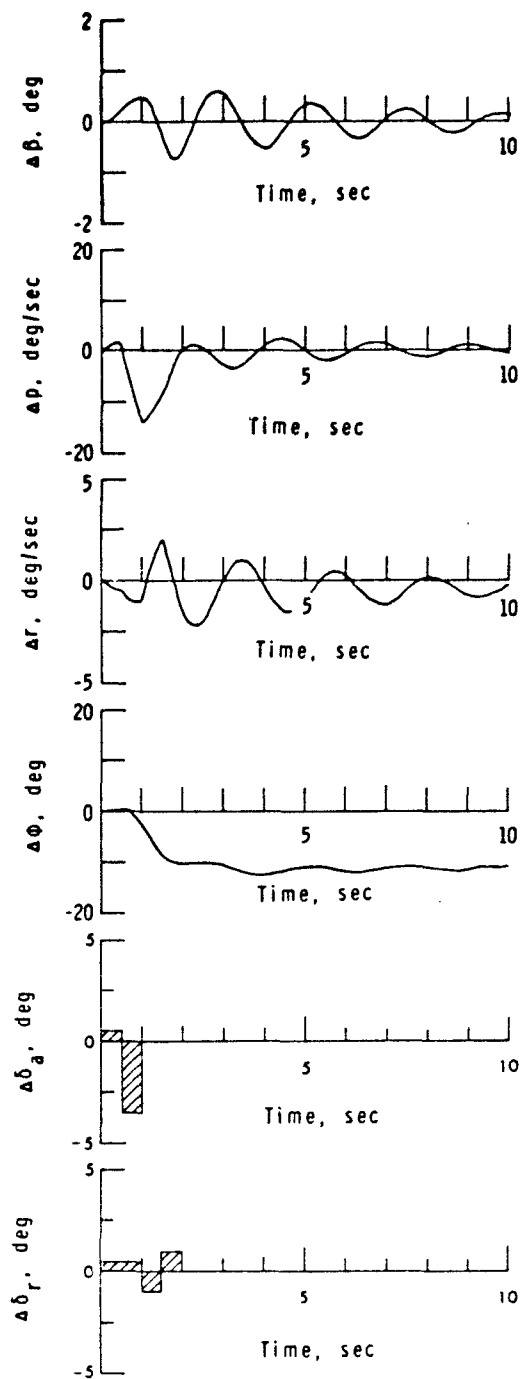
(a) Longitudinal mode. Sequence 1.

(b) Lateral-directional mode. Sequence 1.

Figure 1. Control-input maneuvers and resulting state variable-response trajectories for the F4-C.

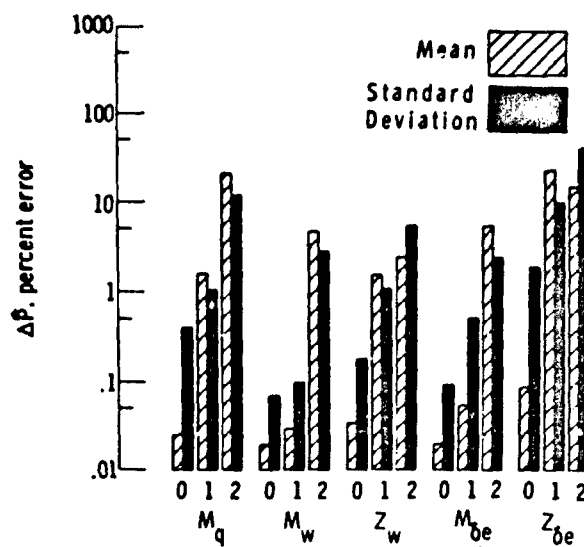


(c) Longitudinal mode. Sequence 2.

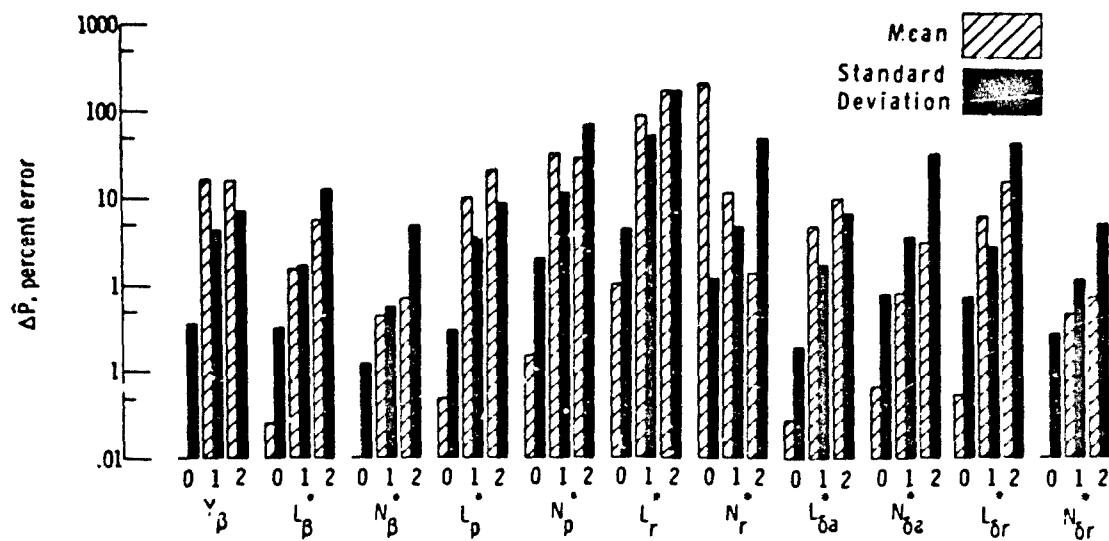


(d) Lateral directional mode. Sequence 2.

Figure 1. Concluded.

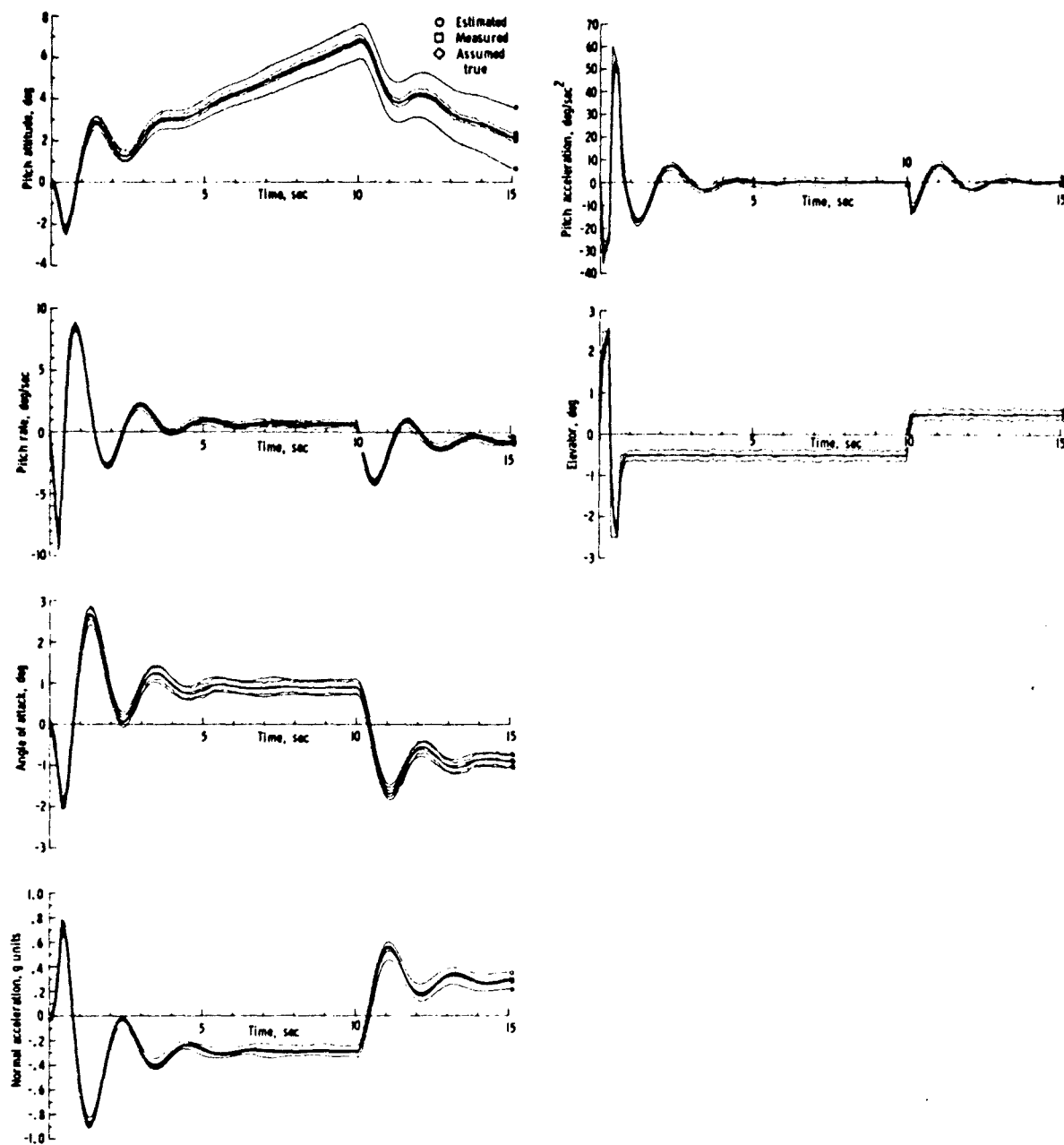


(a) Short-period mode.



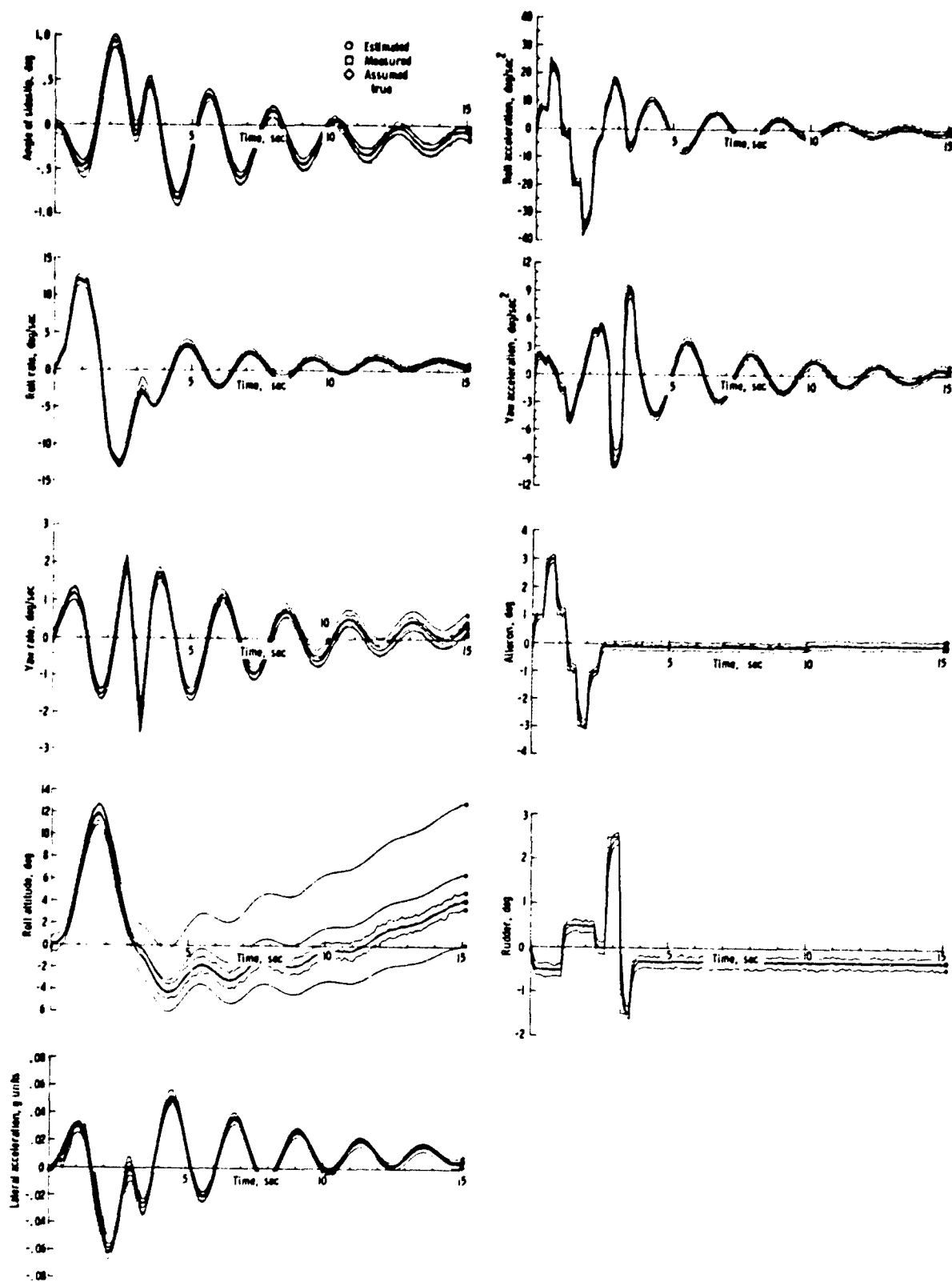
(b) Lateral-directional mode.

Figure 2. Errors in estimated parameters for the F4-C.



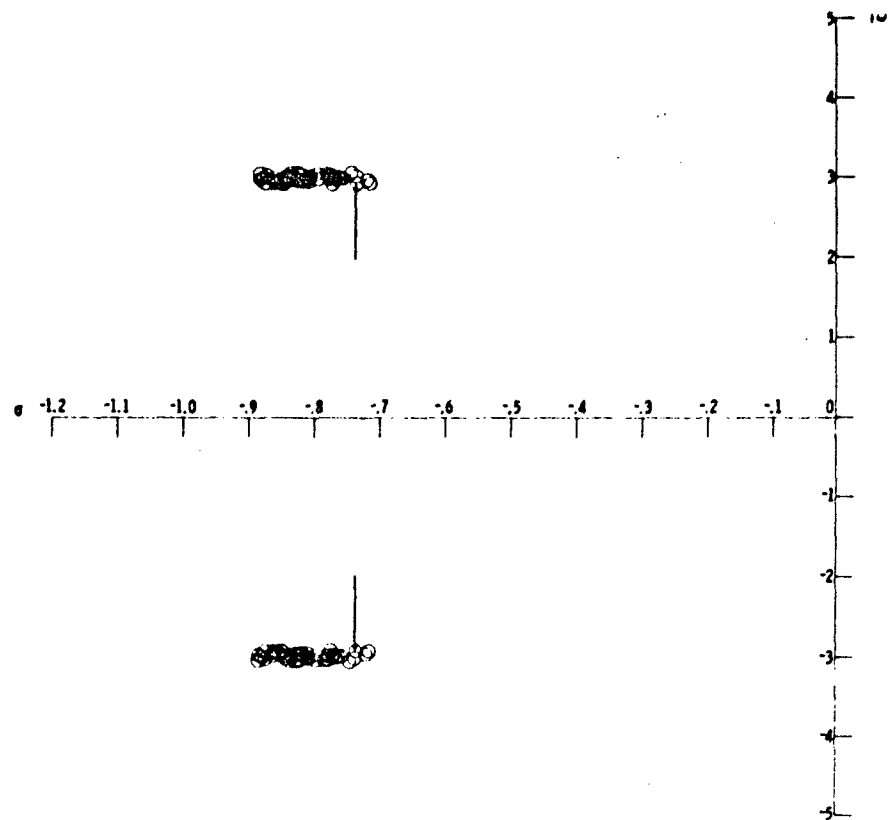
(a) Short-period measurements.

Figure 3. Estimated, measured, and assumed true output-response trajectories for the F4-C.

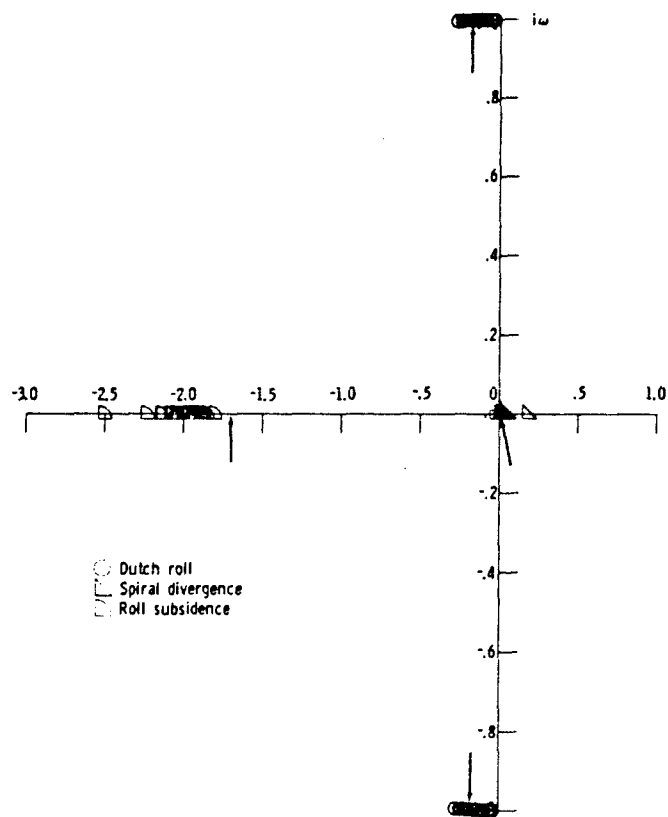


(b) Lateral-directional measurements.

Figure 3. Concluded.



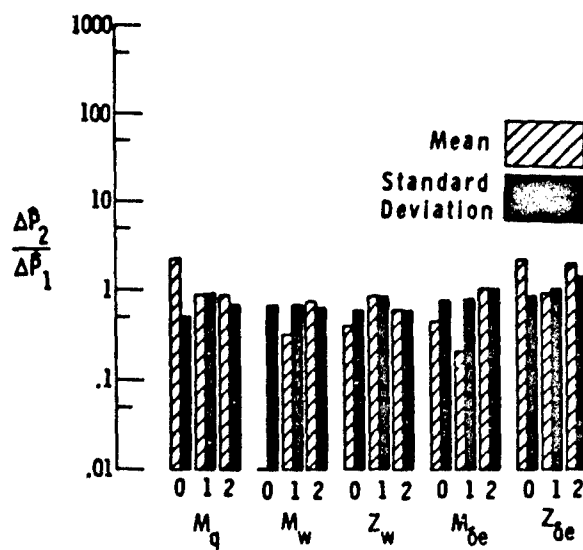
(a) Short-period mode.



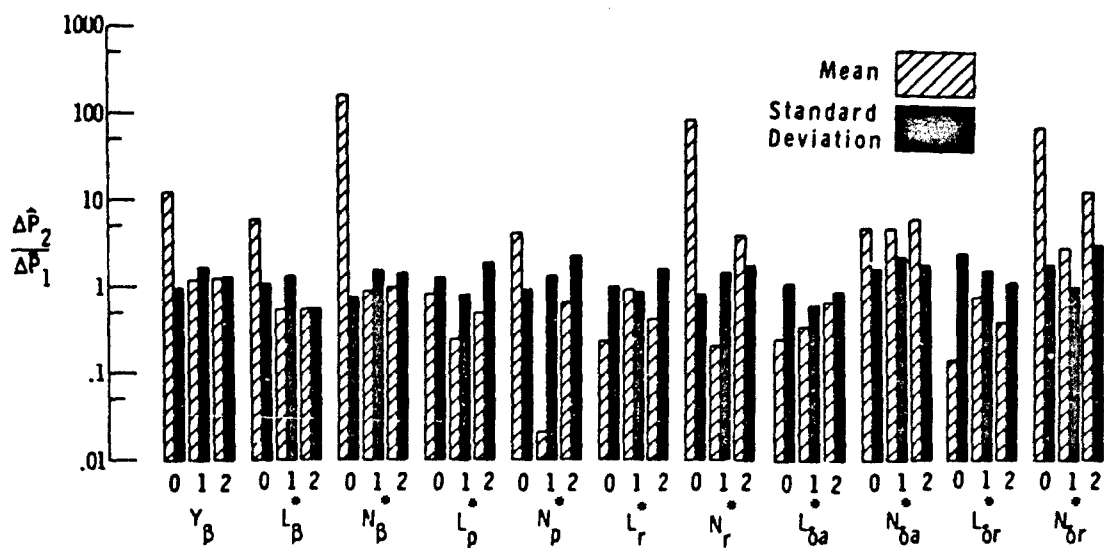
(b) Lateral-directional mode.

Figure 4. Estimated characteristic equation pole locations for the F4-C aircraft.



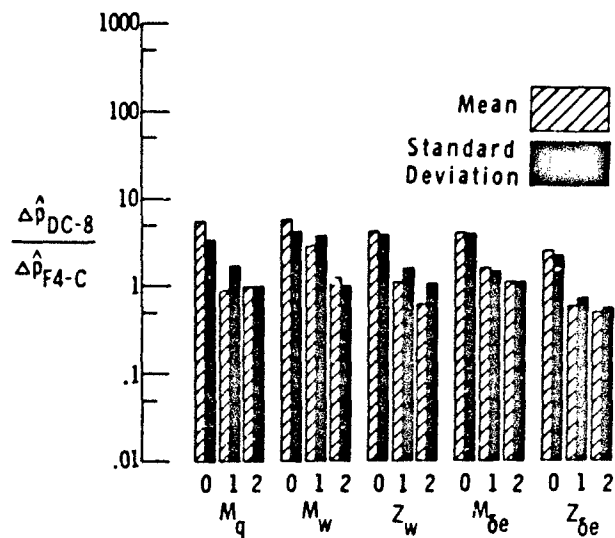


(a) Short-period mode.

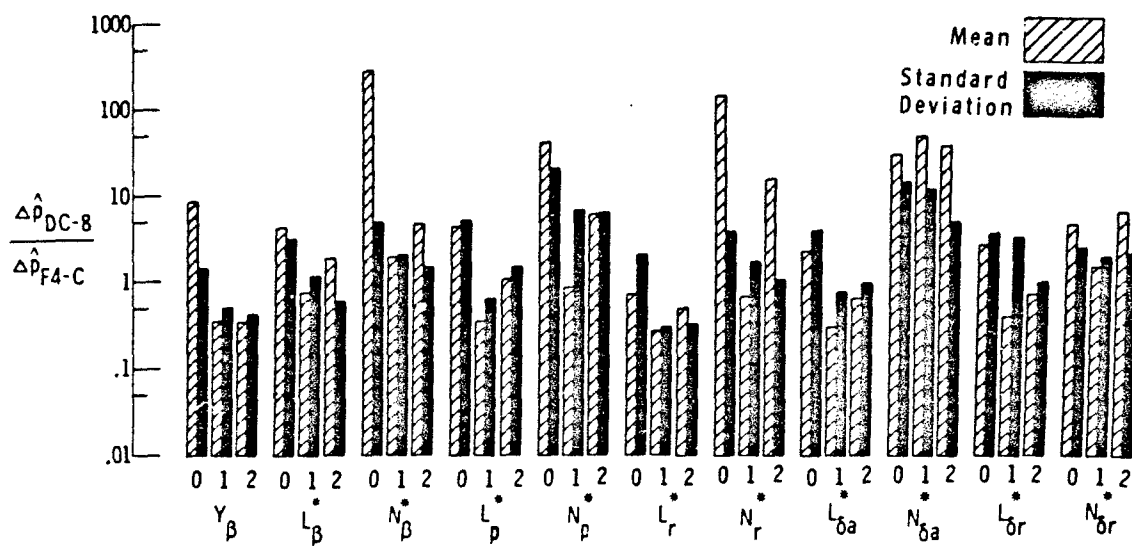


(b) Lateral-directional mode.

Figure 5. Effect of control-input maneuver for the F4-C.

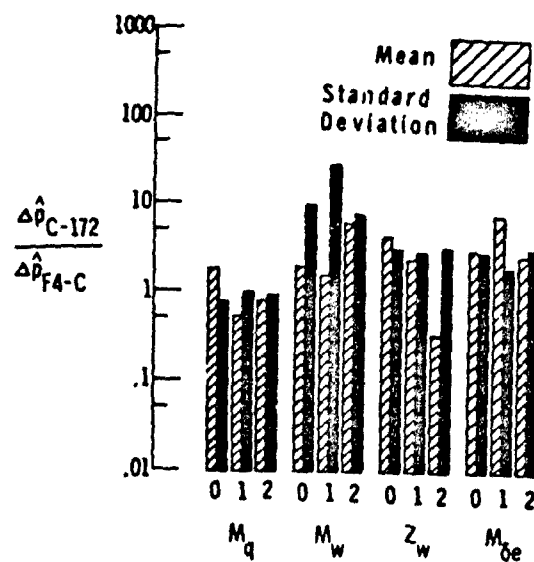


(a) Short-period (DC-8) mode.

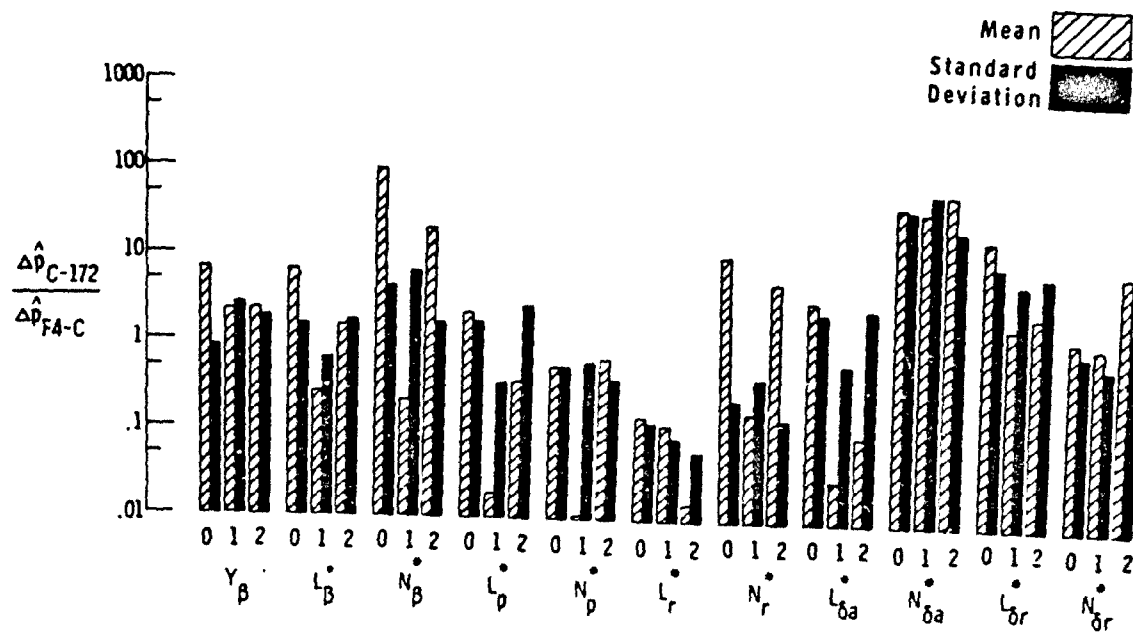


(b) Lateral-directional (DC-8) mode.

Figure 6. Comparison of parameter estimation errors for the DC-8 and the C-172 with those for the F4-C.

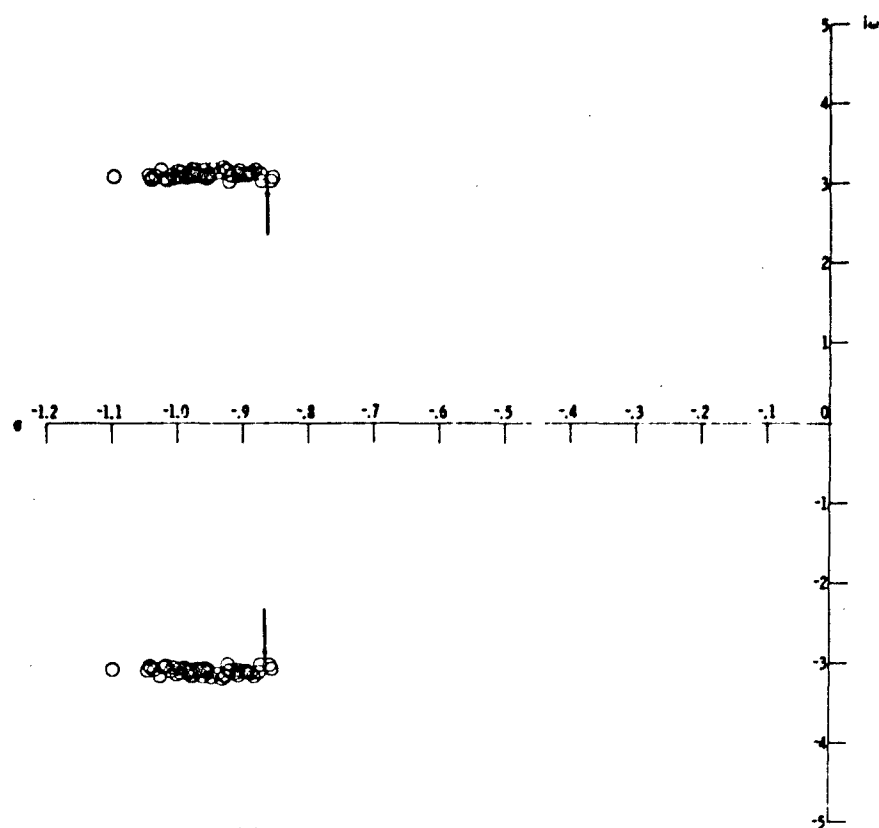


(c) Short-period (C-172) mode.

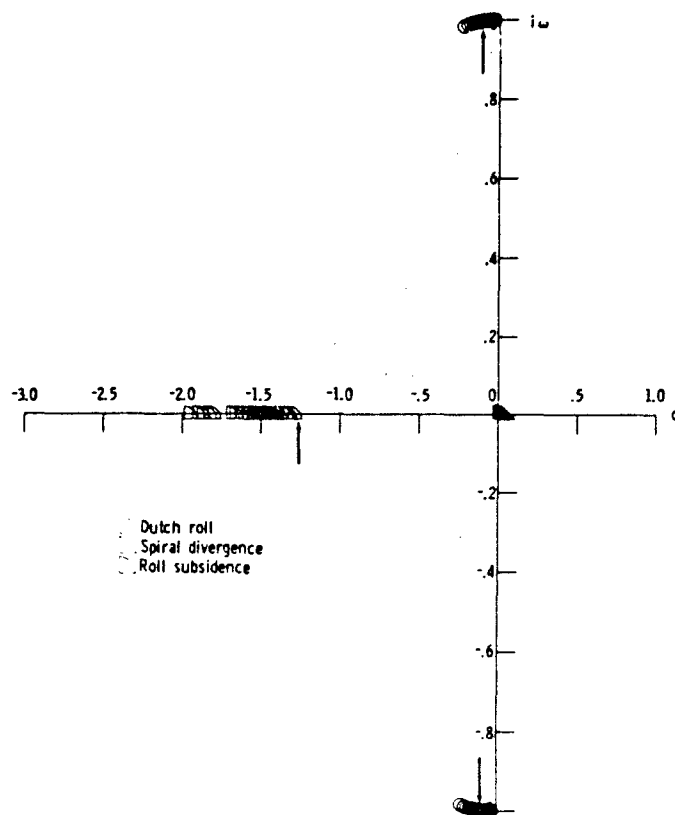


(d) Lateral-directional (C-172) mode.

Figure 6. Concluded.

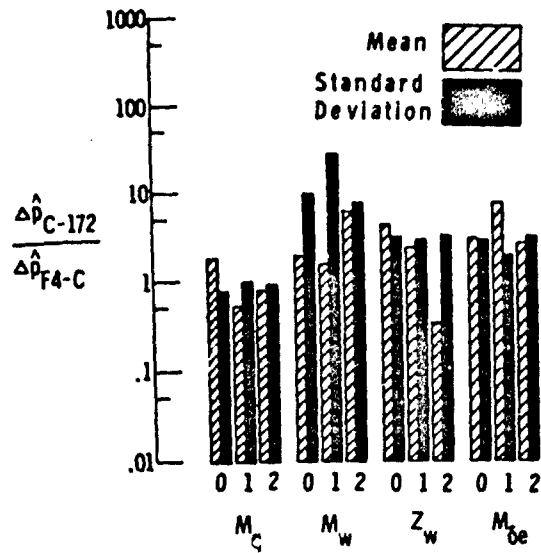


(a) Short-period (DC-8) mode.

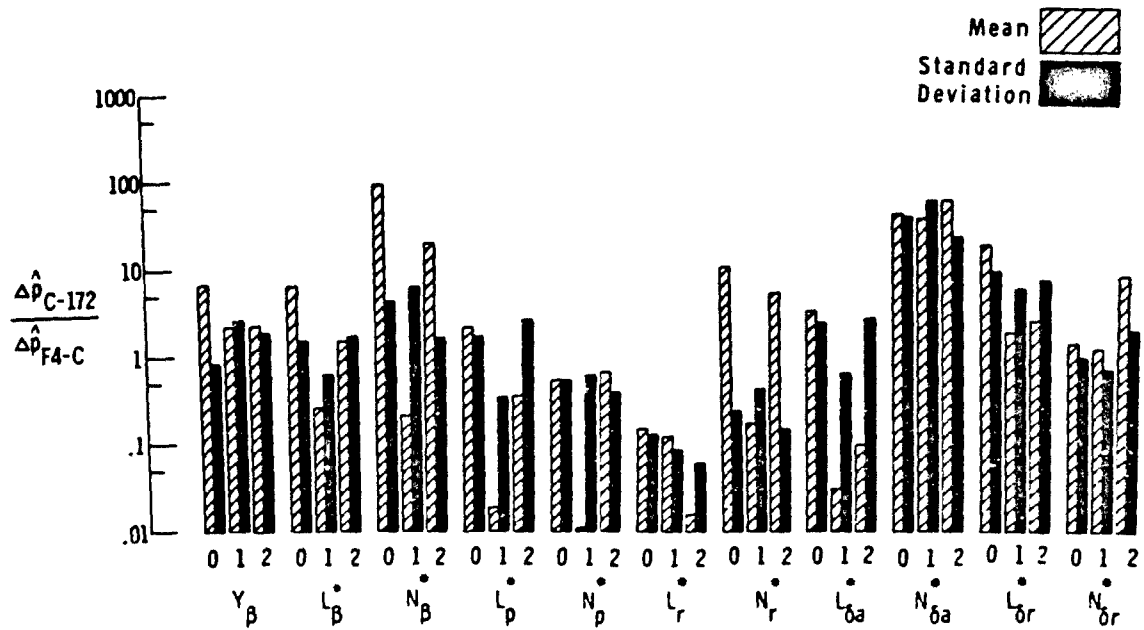


(b) Lateral-directional (DC-8) mode.

Figure 7. Estimated characteristic equation pole locations for the DC-8 and C-172 aircraft.

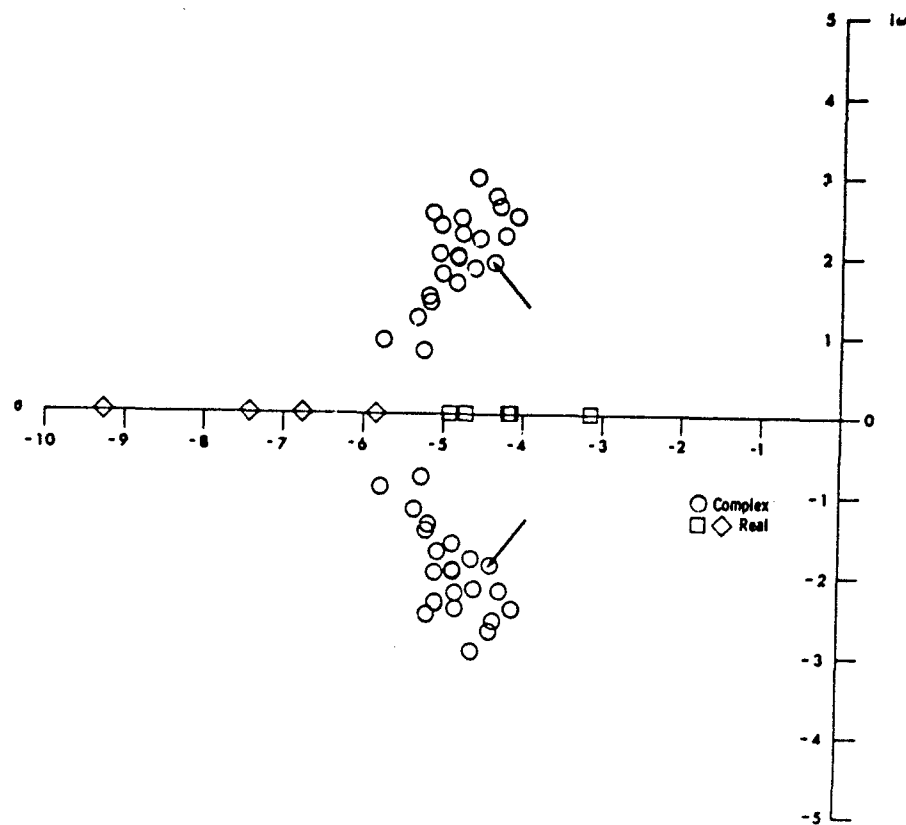


(c) Short-period (C-172) mode.

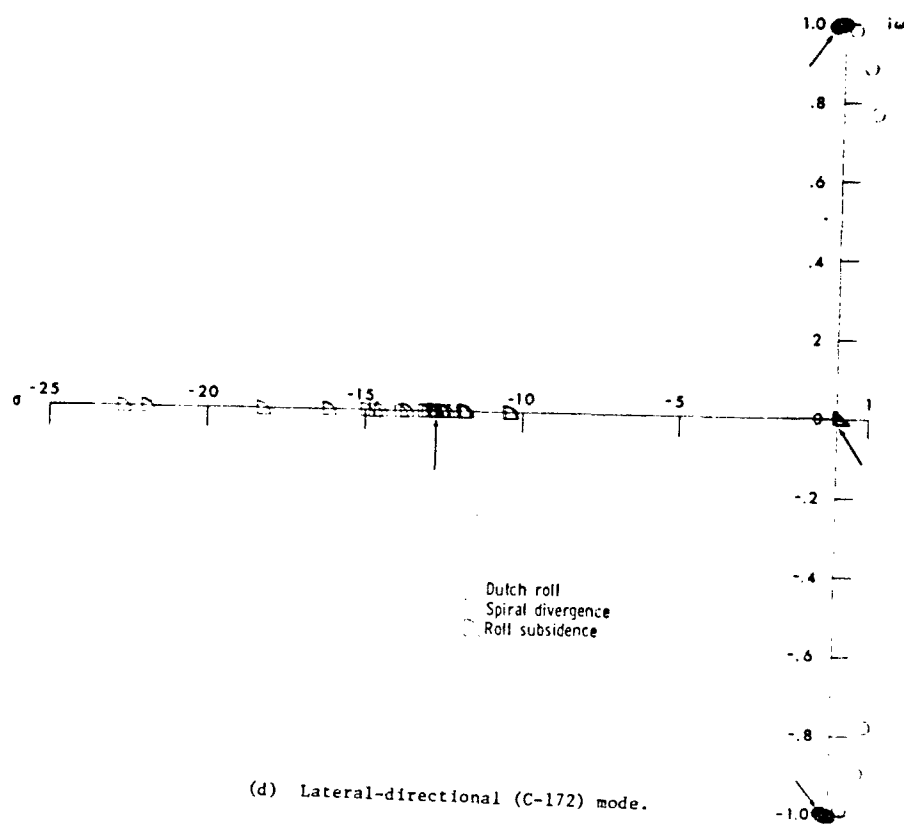


(d) Lateral-directional (C-172) mode.

Figure 6. Concluded.



(c) Short-period (C-172) mode.



(d) Lateral-directional (C-172) mode.

Figure 7. Concluded.

## ADVANCED FLIGHT TEST INSTRUMENTATION: DESIGN AND CALIBRATION

by

R.J.A.W. Hosman

Department of Aeronautical Engineering  
Delft University of Technology  
Delft, The Netherlands

### SUMMARY

From november 1973 till april 1974 a series of flight tests with a Hawker Hunter Mk.7 aircraft was performed to determine the performance as well as stability and control characteristics from measurements during non-steady symmetric manoeuvres. The instrumentation system used in these tests will be described briefly in this paper. In the description of the layout of the system the following subjects will be treated in more detail.

1. The choice of the specifications for the transducers as related to the desired accuracy of the characteristics of the aircraft to be determined. Special attention will be given to the methods applied to meet these specifications, especially for the pressure transducers.
2. The calibration program to determine the characteristics of the transducers in the statistical format, to apply modern system theory to the analysis of the flight measurements.

### 1. INTRODUCTION

A method to determine performance as well as stability and control characteristics from accurate measurements in non-steady flight has been developed at the Department of Aeronautical Engineering of the Delft University of Technology during the last decade. The De Havilland Canada DHC-2 Beaver laboratory aircraft, owned and operated by the Delft University, has been used for the experimental evaluation of the flight test method developed. Experimental results have been published in Refs. 1 and 2. Recently an additional flight test program has been carried through in close cooperation with the National Aerospace Laboratory using a Hawker Hunter Mk.7 as test aircraft. See Fig. 1. This flight test program was aimed at application of the method to flight testing a high performance aircraft so as to enable further evaluation. A brief outline of the flight test method applied will be given prior to presenting a description of the instrumentation system, the design specifications and the performance achieved.

The flight test method applied is based on deduction of aircraft performance as well as stability and control characteristics from measurements obtained during a nominally symmetric non-steady manoeuvre. The manoeuvre is characterized by a nearly constant acceleration of the aircraft from low to high speed in a time interval of about 200 seconds. At more or less equal time intervals the aircraft is forced to oscillate about the lateral axis by manually controlled oscillations of the elevator. Characteristic time histories of several variables are shown in Fig. 2. The non-steady manoeuvre is described in more detail in Ref. 3.

Stability and control characteristics are derived from measurements obtained during the aircraft's oscillations. Aircraft performance and the polar drag curve are determined from the quasi-stationary parts between the oscillations.

A two step procedure is applied for flight test data reduction. See Fig. 3. First of all the aircraft's flightpath is reconstructed with the aid of Maximum Likelihood or Kalman Filtering methods from the measurements recorded. See Refs. 4 and 5. Results obtained processing the Hawker Hunter flight test measurements are presented in Ref. 6.

Secondly aircraft performance as well as stability and control characteristics are derived from flight-path reconstruction results.

The instrumentation system used for the flight tests mentioned above will now be discussed. Specifications of the transducers incorporated in the system will be presented. Finally the calibration program required for determination of the measurement channel input-output relations as well as the measurement error statistics will be described. The results achieved will be compared with the specifications desired.

### 2. DESCRIPTION OF THE INSTRUMENTATION SYSTEM

The system was built at the Department of Aeronautical Engineering of the Delft University of Technology and was based on the experience obtained during the non-steady flight test programs with the Beaver in 1967 and 1968. See Refs. 1 and 2. This experience, however, was limited to the instrumentation of low speed aircraft and was extended with the experience of the National Aerospace Laboratory, which guaranteed a solid basis for the instrumentation of the Hawker Hunter laboratory aircraft.

The Beaver flight test program, see Refs. 4, 5 and 10, showed that several aircraft state variables had to be determined with great accuracy (r.m.s. errors less than 0.01% of full range) to obtain accurate aircraft performance characteristics.

The transducers of the system can be divided into four groups:

1. Transducers to determine the flightpath of the aircraft
  - a. three accelerometers aligned along the X, Y and Z axes of the aircraft's body frame of reference.
  - b. two rate gyro's measuring rate of pitch and rate of yaw.
  - c. two attitude gyro's measuring bank angle and heading angle.
  - d. one absolute- and three differential pressure transducers used to measure static and dynamic pressures.
  - e. an angle of attack vane and a temperature probe.

2. Transducers to determine engine thrust.
  - a. two differential pressure transducers to measure static and total pressure in the jetpipe.
  - b. sensors for measurement of E.G.T. and engine r.p.m.
3. Transducers to measure elevator and stabilizer angles.
4. Transducers to determine the position error correction of the static part of the nose boom.

All transducers mentioned are summarized in Table 1.

A simplified block diagram of the flight test instrumentation system is shown in Fig. 4. The data logging part of the system is capable of measuring and recording 19 variables, each at a sample frequency of 20 samples per second. This system is described in Ref. 7.

The transducers were mounted in the aircraft's fuselage, the data logging part was carried in the inboard pylon tank of the port wing. The operator's panel was placed at the starboard side of the instrument panel of the dual cockpit.

#### 2.1 The specifications of the transducers.

The specifications used for transducer selection were based mainly on the experience obtained from the flight test programs with the Beaver aircraft. The impact of the measurement error model used for flight test data analysis on the transducer specification requirements will be discussed prior to presenting instrumental specifications.

The inaccuracy of a transducer basically depends on the design of the transducer and the environmental operational conditions. A number of error sources can be mentioned. Non-linearity, hysteresis, sensitivity for interfering inputs, etc. The effects of these error sources on the achievable measurement accuracy can be expressed in a rather simple model. See Refs. 8 and 9. This model contains two different error types.

First of all the systematic errors. The systematic errors are assumed to be constant during a short period of time (duration of one non-steady manoeuvre). The systematic errors to be considered here have the same effect as and indeed will often be due to zeroshifts.

Secondly the random errors which can be considered as measurement noise.

The accuracy of the transducers depends on both errors. The bias errors of the differential pressure transducers, however, can be determined in flight by short circuiting the pertaining pneumatic circuits prior to and after each flight test manoeuvre. This feature enables the application of model matching techniques for flightpath reconstruction and estimation of the bias errors of the inertial transducers. See Refs. 4, 5 and 10. However, in these references it has been shown that the bias error of the accelerometer aligned along the aircraft's longitudinal axis can be determined only with insufficient accuracy. For that reason an extremely accurate accelerometer exhibiting negligible zeroshifts has been incorporated in the flight test instrumentation system, to sensing the aircraft's longitudinal acceleration.

To further improve the achievable flightpath reconstruction accuracy more accurate differential pressure transducers were needed than those available on the market when designing the instrumentation system. However, the measurement accuracy of the pressure transducers could be considerably augmented by careful stabilization of the environmental operational conditions. This goal could be achieved mounting all differential pressure transducers in one specially designed box. In Table 2 the specifications of the transducers are presented.

#### 2.2. The pressure transducer box

Pressure transducers are sensitive to temperature changes and accelerations in the direction perpendicular to the membrane. In particular differential pressure transducers designed for a relatively small measuring range tend to show large zeroshifts in course of time. These errors could be attenuated by the following precautions.

The seven differential pressure transducers were mounted in one box. This pressure transducer box was installed in the ammunition bay of the aircraft.

The temperature inside the box was maintained at  $43 \pm 1^\circ \text{C}$  by a thermostat combined with effective isolation of the box. To decrease the time constant of the temperature control system, forced ventilation with a small fan was applied. See Fig. 5.

The non-steady manoeuvre is considered as nominally symmetric. Asymmetric deviations were consequently assumed small. The acceleration sensitive axes of the differential pressure transducers have therefore been installed parallel to the Y-axis of the aircraft's body frame of reference. The acceleration sensitivity of the pressure transducers is of the order of 2 - 6 % of full range per g. The results of the flight test program showed accelerations in Y direction being less than 0.05 g. Consequently corrections for acceleration induced errors could be omitted.

The systematic errors could be corrected for by measuring the output of the transducers at zero input before and after the manoeuvre. Zero input can be obtained by short circuiting the transducer with the aid of a valve. Time averaging the output voltage thus obtained provides a mean voltage magnitude representative of the zero shift. Six electro mechanically driven valves have been used for short circuiting. A scheme of the entire pneumatic circuit is given in Fig. 6.

To obtain further improvement of the performance of the transducers some additional precautions were taken.

The non-linearities of the transducers were determined by calibration and consequently corrected for.



The static pressure inside the box was used as reference pressure for the differential pressure transducers. To stabilize the reference pressure a damper was installed. See Fig. 6.

As pressure transducer amplifiers are temperature sensitive, these amplifiers were also mounted in the pressure transducer box.

The results of the calibration program to be described in the next chapter, will show that the precautions discussed above gave a considerable improvement of the accuracy of the transducers.

One of the variables to be measured accurately to enable flightpath reconstruction is the altitude variation  $\Delta h$ . See Refs. 4, 5 and 10. The method used to measure this quantity needs some explanation. The altitude variation  $\Delta h$  is computed according to:

$$\Delta h = - \frac{\Delta p}{\rho g} \quad (1)$$

where  $\Delta p$  is the static pressure variation relative to the static pressure at manoeuvre initiation. Determination of  $\Delta h$  may thus be seen to require the measurement of the change of static pressure. This measurement is performed with the aid of a differential pressure transducer coupled to a thermosflask. See Fig. 5 and 6. When the valve shown in Fig. 6 is closed at manoeuvre initiation the corresponding reference pressure is stored in the flask. Consequently reference pressure variations can be measured with the differential pressure transducer  $\Delta p_1$ . Static pressure variation can then be determined according to:

$$\Delta p = \Delta p_1 + \Delta p_4 \quad (2)$$

See Fig. 6.

The accuracy with which the change of static pressure  $\Delta p$  can be measured depends on the differential pressure transducers applied and the stability of the pressure in the thermosflask. A temperature variation of  $1^\circ \text{C}$  in the flask induces a pressure variation of 0.3 %. Such a pressure variation equals an altitude variation of about 25 meters.

To stabilize the temperature in the flask the heat capacity inside the flask had to be augmented and the isolation had to be improved. The flask was therefore filled with 150 grams of steelwool. This material had the additional advantage of fast heat exchange with the air. The isolation of the flask was improved by plastic foam. See Fig. 5. A small electric heater mounted inside the thermosflask was required to maintain equal temperature in- and outside the flask during the warm-up period of the pressure transducer box. A second thermosflask was used to prevent cold air from entering into the measurement flask during fast descents of the aircraft. This flask was also filled with steelwool and provided with a temperature control unit.

Taking account of the design described above it was expected that the temperature inside the thermosflask could be kept within a range of  $\pm 0.03^\circ \text{C}$  during a period of 5 minutes which is long enough for one manoeuvre.

### 3. TESTING AND CALIBRATION OF THE INSTRUMENTATION SYSTEM

Testing and calibration of an instrumentation system in advance of a flight test program provides both a final check on the proper operation of the whole system and the relations between input and output of the measuring chains. Calibration after completion of the flight tests is necessary to have a check on possible changes in the characteristics of the transducers.

If Kalman filtering or corresponding techniques are used for flight path reconstruction from flight test data detailed knowledge concerning measurement error statistics is required. This knowledge cannot be gained from one single calibration. In this Chapter it will be shown that combination of the data of all calibrations carried out during the flight test program provides additional knowledge about the measurement error statistics.

Before discussing the calibration program some data of the test program of the instrumentation system will be given.

#### 3.1. Testing the instrumentation system.

To have a check on the proper operation of the system under the environmental conditions which could arise during the flight tests all components were tested before the calibration. The temperature was varied between  $+25^\circ$  and  $-30^\circ \text{C}$ . The pressure was varied corresponding to an altitude change from zero to 30,000 ft. Acceleration changes in all directions of  $\pm 1g$  were applied. Modifications of data logging system components had to be made in order to meet the system specifications.

Due to lack of the possibility to test the system when changing all environmental conditions at the same time, the pressure transducer box and later the whole system were tested in the Beaver laboratory aircraft up to an altitude of 20,000 ft.

The performance of the pressure transducer box satisfied the required specifications. When the temperature was varied from  $+25$  to  $-30^\circ \text{C}$  the maximum temperature deviation inside the box after one hour was  $3.2^\circ \text{C}$ . Due to this low outside temperature of the pressure transducer box the rate of change of the pressure inside the thermosflask was found to correspond to an altitude variation rate of 1.5 ft/min one hour after the decrease of the outside temperature.

During the test flight in the Beaver laboratory aircraft, which lasted three hours, a maximum temperature change inside the box of  $1.5^\circ \text{C}$  was observed.

### 3.2. The calibration program.

An instrument calibration program was accomplished to determine the respective input-output relations of the measuring chains of the system and to obtain information about the systematic and random errors of each measuring chain. All transducers were calibrated twice prior to flight testing, once during flight testing and twice posterior to flight test program completion. All data points of the five calibrations were combined and used to determine the input-output relations of the transducers and to determine the error model.

Successive calibrations of a particular transducer under constant conditions will always differ in some respect.

Calibrating transducers inputs  $Y$ , measured in engineering units, are related to output voltages  $X$ . If the inverse relation is expressed in terms of a polynomial

$$Y = a_0 + a_1 X + a_2 X^2 + \dots + a_m X^m \quad (3)$$

then the deviation of a calibration data point  $\Delta Y$  is defined by

$$\Delta Y = Y - a_0 - a_1 X - a_2 X^2 - \dots - a_m X^m \quad (4)$$

Differences between the results of successive calibrations can be found comparing the polynomial coefficients  $a_0, a_1, \dots, a_m$  and comparing the corresponding r.m.s. magnitudes of the data point deviations.

Combining the data of several calibrations and fitting one curve through all that data, the differences between the calibrations can be shown by a plot of the deviations  $\Delta Y$  versus the corresponding values of  $Y$ . Such a plot of a differential pressure transducer is given in Fig. 7.

When the data of successive calibrations are combined the r.m.s. magnitude of the deviations  $\Delta Y$  will increase with increasing number of calibrations. The r.m.s. magnitude will be larger than the r.m.s. of the deviations  $\Delta Y$  of only one calibration. See Fig. 8. The increase shown can be caused by:

1. different systematic errors occurring during different calibrations;
2. time dependent variations of transducer gradients;
3. different realizations of random measurement noise.

A general description of the calibration procedure applied and the calibration standards used will be presented prior to discussing the results.

Due to the high resonance frequency of most transducers and the comparatively small bandwidth of the variables, static calibration was considered to be adequate. See Ref. 2. Except for the thermometers,  $T$  and E.G.T., all the calibration curves were determined by calibration of the entire measuring chain, so as to improve the accuracy of the calibration curve. As described in Ref. 11 third order polynomial were fitted through the calibration data by using regression analysis. In case of the accelerometers a more extended formula was used to correct for misalignment and cross-axis sensitivity. The three accelerometers were calibrated together relative to the frame axes of the accelerometer box. See Fig. 9. The following equations were used:

$$\begin{aligned} A_x &= a_0 + a_1 e_x + a_2 e_x^2 + a_3 e_x^3 + a_4 e_y + a_5 e_z + a_6 e_x e_y \\ A_y &= b_0 + b_1 e_y + b_2 e_y^2 + b_3 e_y^3 + b_4 e_x + b_5 e_z + b_6 e_x e_y \\ A_z &= c_0 + c_1 e_z + c_2 e_z^2 + c_3 e_z^3 + c_4 e_x + c_5 e_y + c_6 e_x e_y \end{aligned} \quad (5)$$

where  $e_x, e_y$  and  $e_z$  are the output voltages of the accelerometers.

The calibration polynomials of the differential pressure transducers were modified to eliminate the zero input related output, related to the zero shift during the calibration.

$$\Delta p = c_0 + c_1 (e_p - e_{p_0}) + c_2 (e_p - e_{p_0})^2 + c_3 (e_p - e_{p_0})^3 \quad (6)$$

wherein:

- $p$  = the input of the differential pressure transducer
- $e_p$  = the output
- $e_{p_0}$  = the output related to zero input during the calibration

The following standards are used for the calibration of the rate gyro's accelerometers and the pressure transducers.

1. A rotary, tiltable indexing table (Optical Measuring Tools, England) for calibration of accelerometers between  $-1 g$  and  $+1 g$ .
2. A rate of turn table (Genisco Inc., U.S.A.) for calibration of rate gyro's and accelerometers above  $1 g$ .
3. A tilting piston pressure gauge (Delft University of Technology) used for calibration of differential pressure transducers in a range of  $0 - 250 \text{ kgf/m}^2$ .
4. A primary pressure standard (Consolidated Electrodynamics Corp., U.S.A.) for calibration of absolute and differential pressure transducers with a range larger than  $250 \text{ kgf/m}^2$ .

### 3.3. Calibration results.

The calibration program yields for each instrument the coefficients of the pertaining calibration polynomial as well as the r.m.s. value of the data point deviations  $\Delta Y$ . The r.m.s. value of the deviations of all transducers are listed in table 3. Two r.m.s. values are given for each transducer. The first r.m.s. value  $\sigma(\Delta Y)_1$  is the mean of the r.m.s. values of the deviations obtained from each calibration. The second r.m.s. value  $\sigma(\Delta Y)_2$  is the r.m.s. of the deviations obtained when one polynomial is fitted to the data of the 5 calibrations.

With these data it is possible to compare the specifications of the transducers given in table 2 and the pertaining characteristics derived from the calibrations made.

The results of some transducers will be discussed next:

#### The pitch rate gyro.

In Fig. 10 a plot of the deviations of 5 calibrations is given. From table 3 it is clear that the r.m.s. value of the deviations of 5 combined calibrations  $\sigma(\Delta Y)_2$  is three times larger than  $\sigma(\Delta Y)_1$  from one calibration. This is caused mainly by the torquer characteristics of the rate gyro used. However, the zero-shift is very small. According to table 3 the random error is within the specifications.

#### The accelerometers.

The deviations of the calibrations of the accelerometer in X direction are plotted in Fig. 11. This transducer showed small gradient variations, whereas measurement noise expressed in the r.m.s. value of the deviations  $\sigma(\Delta A_x)_2$  is smaller than specified. The same holds for the accelerometers in Y and Z direction.

#### Pressure transducers.

The differential pressure transducers behave entirely different from the transducers discussed above. As shown in Table 1 two different types of differential pressure transducers were used in the system:

1. Three ACB H 5010 differential pressure transducers for the lowest pressure ranges ( $\pm 170 \text{ kgf/m}^2$ ).
2. Four Statham PM6TC transducers for the medium and high pressure ranges ( $\pm 500$  up to  $\pm 17.000 \text{ kgf/m}^2$ ).

In section 2.1. it was assumed that to improve the performance of the pressure transducers it was necessary to measure the zero input related output during flight to eliminate the effect of the zero shift on measurement accuracy. In addition a number of precautions were taken to improve the environment of the transducers.

The low pressure transducers  $\Delta p_s$ ,  $\Delta p_j$  and  $\Delta p_t$  exhibit large zero shifts as shown in Fig. 12a for  $\Delta p_s$ . When fitting one single calibration curve through the data of 5 calibrations considerable differences arise depending on the corrections are made for the zeroshifts. See Fig. 12b and Table 3. The three identical ACB transducers exhibit a remarkably large differences in measurement accuracy.

The three high pressure transducers  $q_c$ ,  $\Delta p_s$  and  $\Delta p_t$  do not show a clear zero shift, but rather a change of the gradient. In Fig. 13 the deviations of  $q_c$  are plotted. Remarkable in this figure is the change of the gradient with time which was also found for  $\Delta p_s$  and  $\Delta p_t$ . Comparing the r.m.s. values  $\sigma(\Delta Y)_2$  with and without zeroshift correction only small differences are found for these three transducers. See Table 3.

The Statham transducer used to measure the change of the reference pressure  $\Delta p$  exhibits both a zero shift and a small gradient variation. See Fig. 14. Correction for the zero shift yields the largest relative improvement of the r.m.s. value  $\sigma(\Delta Y)_2$  of the deviations. In spite of the much larger range of  $\Delta p$  ( $\pm 500 \text{ kgf/m}^2$ ) as compared to the range of the ACB transducers ( $\pm 170 \text{ kgf/m}^2$ ) the measurement noise has a r.m.s. magnitude of the same order. See Table 3.

The r.m.s. magnitude  $\sigma(\Delta Y)_2$  of the measurement noise of all differential pressure transducers has an order of magnitude of 0.1 to 0.2 % of the range of the transducers, which is smaller than was expected.

Essential parameters for flightpath reconstruction are the measured altitude variation  $\Delta h$  as well as the airspeed  $V$ . Accuracies achievable when deriving these quantities from pressure measurements recorded in flight can now be estimated.

The error in the altitude variation  $\Delta h$  is mainly dependent on the error in the measurement of the static pressure variation.  $\Delta p = \Delta p_s + \Delta p_t$ . Assuming that the errors in the measurements of  $\Delta p_s$  and  $\Delta p_t$  are independent, the noise of  $\Delta p$  can be easily computed from the data in Table 3.  $\sigma \Delta p = 1.06 \text{ kgf/m}^2$ . This value is equivalent to 0.8 m altitude change at zero altitude and 1.6 m at an altitude of 20.000 ft.

Due to the non-linear relation between the true airspeed  $V$  and the dynamic pressure  $q_c$  and taking account of the non-normal distribution function characterising the statistics of the error in the measurements of  $q_c$ , see Fig. 13, it is not possible to give an estimate of the r.m.s. of the error in the measured true airspeed  $V$ . As far as the influence of an error in  $q_c$  on the true airspeed is concerned, it is possible to determine the effect of an error in  $q_c$  on the true airspeed for a given value of the airspeed and the altitude.

Using the maximum errors in Fig. 13 of  $q_c$  due to the gradient change with time, the error  $\Delta V$  can be determined for different values of the true airspeed  $V$  and the altitude  $h$ .

$V$	$h$	$\Delta V \text{ max}$
130 m/sec	20.000 ft	0,5 m/sec
250 m/sec	20.000 ft	0,3 m/sec

From these data it is evident that the variation of the gradient of  $q_c$  does not have much influence on the accuracy of the true airspeed.

#### 4. SUMMARY AND CONCLUSIONS

In this paper an instrumentation system for flight tests in non-steady flight is described. Amongst others the system comprises several high accuracy transducers and a high quality data logging system. The results of the calibration program described show that:

1. An instrumentation system with an overall accuracy in the order of 0.01 % has been realized such in accordance with prespecified tolerances.
2. An improvement of accuracy of differential pressure transducers can be achieved by correcting the zero shifts and improving the environmental conditions of the transducers.
3. One single calibration has been shown to provide insufficient information to determine the statistical characteristics of the measurement noise.

#### 5. REFERENCES

1. O.H. Gerlach, "Determination of performance and stability parameters from non-steady flight test manoeuvres", S.A.E.-paper 700236, Soc. of Autom. Eng., Inc., New York, 1970.
2. O.H. Gerlach, "The determination of stability derivatives and performance characteristics from dynamic manoeuvres", AGARD Conference Proceedings, No. 85, AGARD, 1972.
3. H.W. Kleingeld, "Design and evaluation of a symmetric flight test manoeuvre for estimation of performance, stability and control characteristics", National Aerospace Laboratory, Miscellaneous Paper 74-029, 1974.
4. J.A. Mulder, "Aircraft performance measurements in non-steady flights", Conference Proceedings of the 3rd IFAC Symposium "Identification and System Parameter Estimation", The Hague/Delft, the Netherlands, 1973.
5. H.L. Jonkers, "Application of the Kalmanfilter to flightpath reconstruction, including estimation of instrumental bias errors from flight test data", Delft University of Technology, Department of Aeronautical Engineering, Report VTH-162, to be published.
6. J.A. Mulder, "Estimation of the aircraft state in non-steady flight", Delft University of Technology, Department of Aeronautical Engineering, Memorandum M-221, 1974.
7. H.L. Jonkers, J.A. Mulder, K. van Woerkom, "Measurements in non-steady flight: Instrumentation and analysis", Proceedings of the 7th International Aerospace Instrumentation Symposium, Cranfield, England, 1972.
8. V. Klein, "Evaluation of the basic performance characteristics of an instrumentation system", Cranfield Institute of Technology, Cranfield Report Aero No. 22, Cranfield, 1973.
9. J. Idrac, "Metrological characteristics of a measuring channel", AGARD Flight Test Instrumentation Series, Volume I on Basic Principles of Flight Test Instrumentation Engineering, AGARDograph No. 160, 1974.
10. R.J.A.W. Hosman, "A method to derive angle of pitch, flightpath angle and angle of attack from measurements in non-steady flight", Delft University of Technology, Department of Aeronautical Engineering, Report VTH-156, 1971.
11. O.H. Gerlach, "The application of regression analysis to the evaluation of instrument calibrations", AGARD Conference Proceedings, No. 32, 1967.

#### ACKNOWLEDGEMENT

The author wishes to acknowledge the contributions of mr. K. van Woerkom, who was responsible for the design and construction of the instrumentation system and who took an active part in the execution of the instrument calibration program. The author likes to thank mr. H.E. Jonkers for his careful reading of the manuscript.

Table 1. Transducers used in the instrumentation system.

channel number	measured variable	transducer type	range
1	q rate of pitch	Honeywell GC87	$\pm 23^\circ/\text{sec}$
2	$A_x$ specific force along X-axis	Donner model 4810	$\pm 10 \text{ m/sec}^2$
3	$A_y$ specific force along Y-axis	Donner model 4310	$\pm 5 \text{ m/sec}^2$
4	$A_z$ specific force along Z-axis	Donner model 4810	$\pm 100 \text{ m/sec}^2$
5	$\psi$ change in heading	Sperry 53A	-
6	r rate of yaw	S.F.I.M. I 14	$\pm 7^\circ/\text{sec}$
7	n engine speed	D.U.T.	0 - 8200 r.p.m.
8	T temperature	Rosemount Model 102	-100 to $+200^\circ \text{C}$
9	$\Delta p_4$ $P_c - P_{\text{ref}}$	ACB H 5010	$\pm 200 \text{ kgf/m}^2$
10	$\Delta p_5$ $P_s - P_{\text{ref}}$	ACB H 5010	$\pm 200 \text{ kgf/m}^2$
11a	$\Delta p_6$ $P_c - P_s$	ACB H 5010	$\pm 200 \text{ kgf/m}^2$
11b	E.G.T. exhaust gas temperature	Bell and Howell 187A-80	0 - $1200^\circ \text{C}$
12	$\Delta p_1$ $P_1 - P_{\text{ref}}$	Statham PM6TC	$\pm 700 \text{ kgf/m}^2$
13a	$\alpha$ angle of attack	N.L.R.	$\pm 30^\circ$
13b	$\Delta p_{s_j}$ $P_{s_j} - P_{\text{ref}}$	Statham PM6TC	$\pm 7000 \text{ kgf/m}^2$
14	$\Delta p_{t_j}$ $P_{t_j} - P_{\text{ref}}$	Statham PM6TC	$\pm 17.500 \text{ kgf/m}^2$
15	$\delta_e$ elevator angle	D.U.T.	-9 to $+21^\circ$
16	$P_{\text{ref}}$ reference pressure	Kelvin Hughes KTG 1902	0 - $11.000 \text{ kgf/m}^2$
17	$q_c$ $P_t - P_{\text{ref}}$	Statham PM6TC	$\pm 7000 \text{ kgf/m}^2$
18	$\varphi$ bank angle	Sperry HGU-B	$\pm 90^\circ$
19	$i_h$ elevator trim angle	D.U.T.	$\pm 25^\circ$

$P_1$   $P_{\text{ref}}$  at manoeuvre initiation  
 $P_c$  static pressure at the trailing cone  
 $P_s$  static pressure at the nose boom static port  
 $P_t$  free stream total pressure  
 $P_{s_j}$  static pressure at nozzle exit  
 $P_{t_j}$  total pressure at nozzle exit

Table 2. Desired input range and accuracy of the transducers.

channel number	measured variable	input range	desired accuracy	
			zeroshift	rms error
1	q	$\pm 23^\circ/\text{sec}$	0.004	$0.009^\circ/\text{sec}$
2	$A_x$	$\pm 10\text{m}/\text{sec}^2$	0.005	$0.004\text{ m}/\text{sec}^2$
3	$A_y$	$\pm 5\text{m}/\text{sec}^2$	0.01	$0.002\text{ m}/\text{sec}^2$
4	$A_z$	$-15\text{ to }45\text{ m}/\text{sec}^2$	0.05	$0.012\text{ m}/\text{sec}^2$
5	$\psi$	$\pm 90^\circ$		$1^\circ$
6	r	$\pm 7^\circ/\text{sec}$	0.07	$0.07^\circ/\text{sec}$
7	n	0 - 8200 rpm		8 rpm
8	T	$\pm 50^\circ\text{ C}$		$0.1^\circ\text{ C}$
9	$\Delta p_4$	$\pm 170\text{ kgf}/\text{m}^2$		$1.7\text{ kgf}/\text{m}^2$
10	$\Delta p_5$	$\pm 170\text{ kgf}/\text{m}^2$		$1.7\text{ kgf}/\text{m}^2$
11a	$\Delta p_6$	$\pm 170\text{ kgf}/\text{m}^2$		$1.7\text{ kgf}/\text{m}^2$
11b	E.G.T.	$0-750^\circ\text{ C}$		$4^\circ\text{ C}$
12	$\Delta p_1$	$\pm 500\text{ kgf}/\text{m}^2$		$5\text{ kgf}/\text{m}^2$
13a	$\alpha$	$\pm 30^\circ$		$0.3^\circ$
13b	$\Delta p_{sj}$	$-3000\text{ to }+7000\text{ kgf}/\text{m}^2$		$50\text{ kgf}/\text{m}^2$
14	$\Delta p_{ej}$	0 - 17,000 $\text{kgf}/\text{m}^2$		$85\text{ kgf}/\text{m}^2$
15	$\delta_e$	$-9\text{ to }+21^\circ$		$0.1^\circ$
16	$p_{ref}$	0 - 11,000 $\text{kgf}/\text{m}^2$		$22\text{ kgf}/\text{m}^2$
17	$q_e$	0 - 5000 $\text{kgf}/\text{m}^2$		$25\text{ kgf}/\text{m}^2$
18	$\varphi$	$\pm 20^\circ$		$0.2^\circ$
19	$i_h$	$\pm 2.5^\circ$		$0.05^\circ$

Table 3. Calibration results: the runs of the calibration data point deviations.

channel number	measured variable	number of calibrations	$\sigma(\Delta Y)_1$ *	$\sigma(\Delta Y)_2$ not corrected for zeroshift	$\sigma(\Delta Y)_2$ corrected for zeroshift	$\frac{\sigma(\Delta Y)_2}{\text{input range}}$
1	q °/sec	5	0.0022	0.0061		0.013 Z
2	A <sub>x</sub> m/sec <sup>2</sup>	5	0.0016	0.0026		0.013 Z
3	A <sub>y</sub> m/sec <sup>2</sup>	5	0.0010	0.0015		0.015 Z
4	A <sub>z</sub> m/sec <sup>2</sup>	5	0.0042	0.0074		0.012 Z
5	ψ °	4	0.063	0.12		0.06 Z **
6	r °/sec	4	0.017	0.043		0.31 Z
7	n rpm	4	1.2	1.2		0.015 Z
8	T ° C	4	0.018	0.036		0.036 Z
9	Δp <sub>4</sub> kgf/m <sup>2</sup>	5	0.57	1.00	0.82	0.24 Z
10	Δp <sub>5</sub> kgf/m <sup>2</sup>	5	0.39	0.67	0.41	0.12 Z
11a	Δp <sub>6</sub> kgf/m <sup>2</sup>	5	0.53	1.00	0.56	0.17 Z
11b	EGT ° C	3	1.1	2.6		0.35 Z
12	Δp <sub>1</sub> kgf/m <sup>2</sup>	5	0.41	2.3	0.67	0.067 Z
13a	α °	4	0.034	0.19		0.32 Z
13b	Δp <sub>8j</sub> kgf/m <sup>2</sup>	5	3.2	11.	8.3	0.083 Z
14	Δp <sub>12j</sub> kgf/m <sup>2</sup>	5	11.	19.	20.	0.12 Z
15	δ <sub>e</sub> °	5	0.036	0.079		0.26 Z
16	p <sub>ref</sub> kgf/m <sup>2</sup>	5	3.4	5.9		0.054 Z
17	q <sub>c</sub> kgf/m <sup>2</sup>	5	1.4	5.4	5.6	0.11 Z
18	φ °	4	0.033	0.058		0.15 Z
19	i <sub>h</sub> °	5	0.0088	0.039		0.78 Z

\*  $\sigma(\Delta Y)_1$  and  $\sigma(\Delta Y)_2$  are defined in section 3.3

\*\* only the synchro of the heading gyro was calibrated.

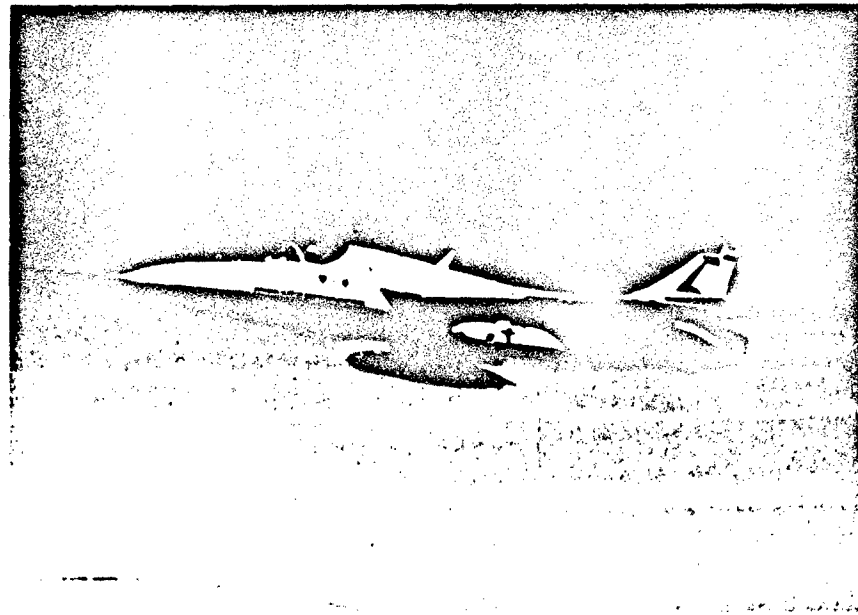


Fig. 1 The Hawker Hunter Mk.7 laboratory aircraft



Fig. 3 Flow-diagram of analysis of test data.

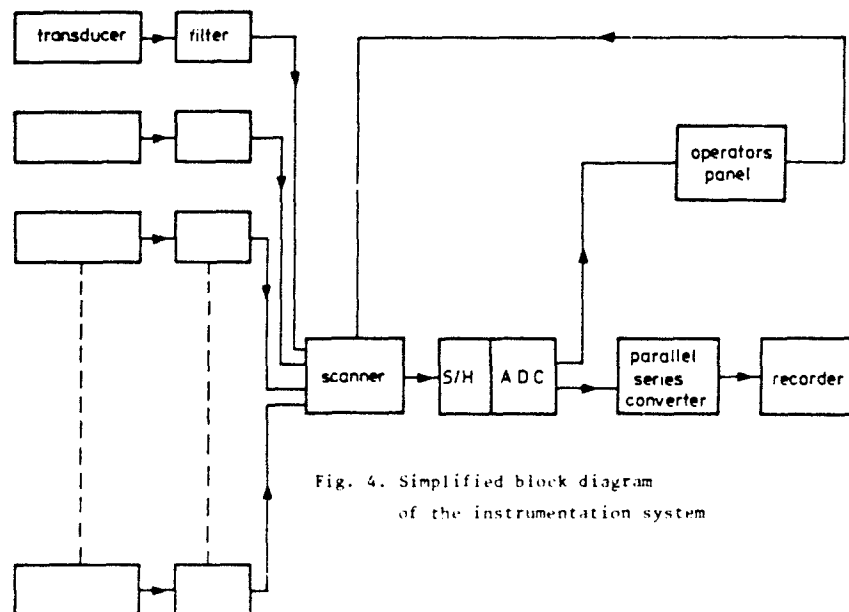


Fig. 4. Simplified block diagram of the instrumentation system



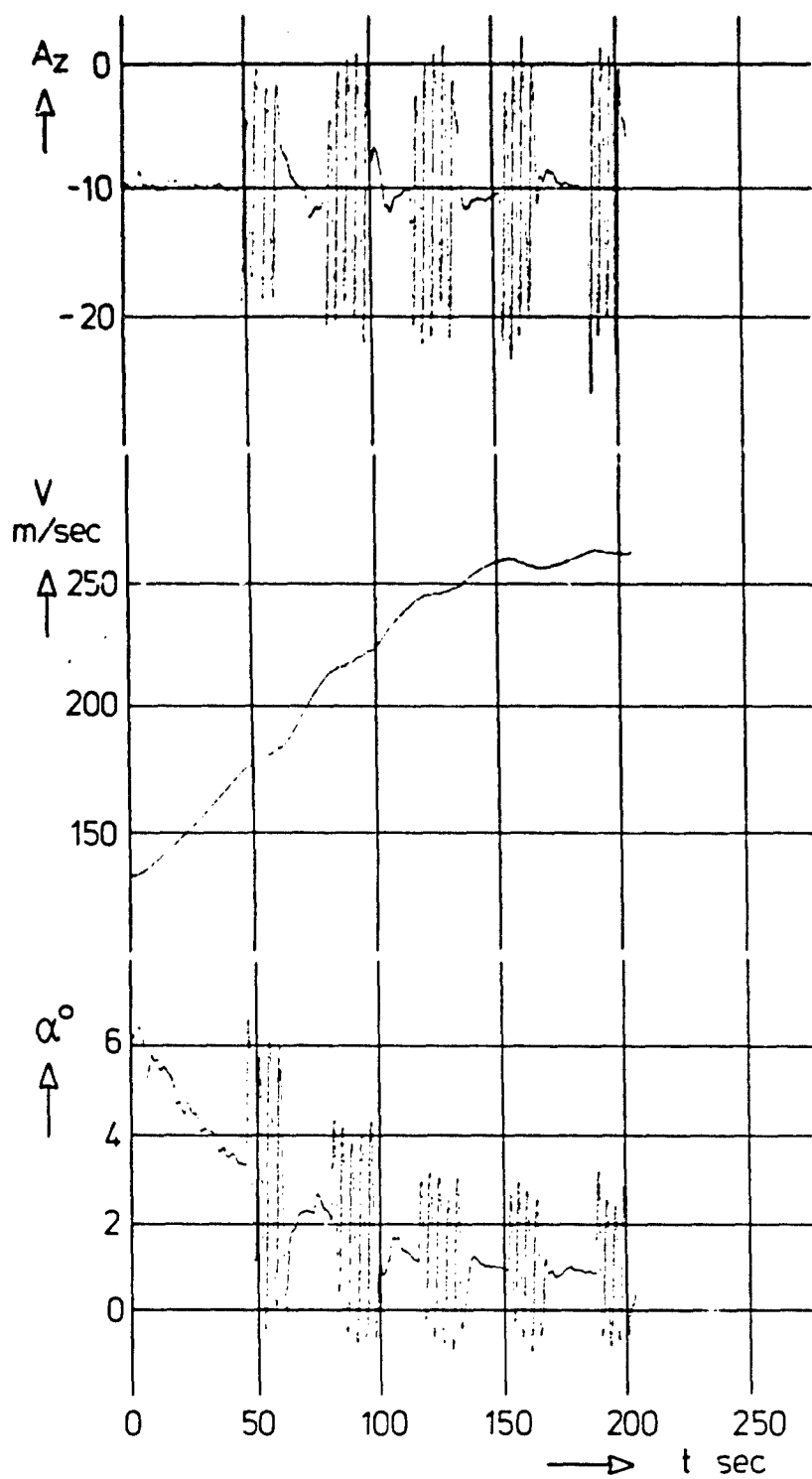


Fig. 2 The angle of attack  $\alpha$ , the airspeed  $V$  and the specific force along the Z-axis during a non-steady manoeuvre

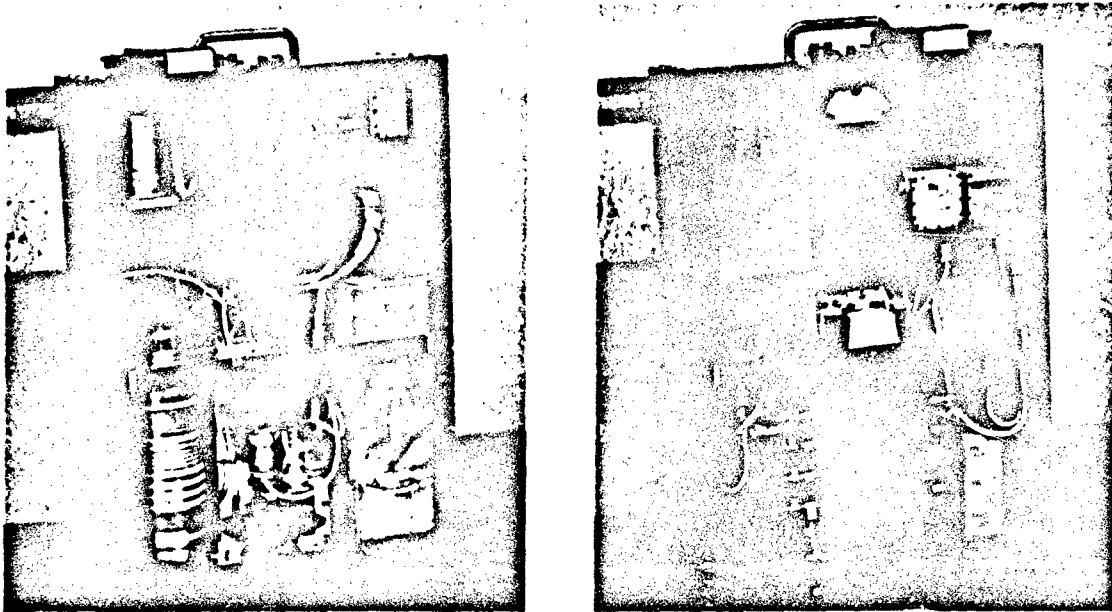


Fig. 5 The front and rear side of the pressure transducer box

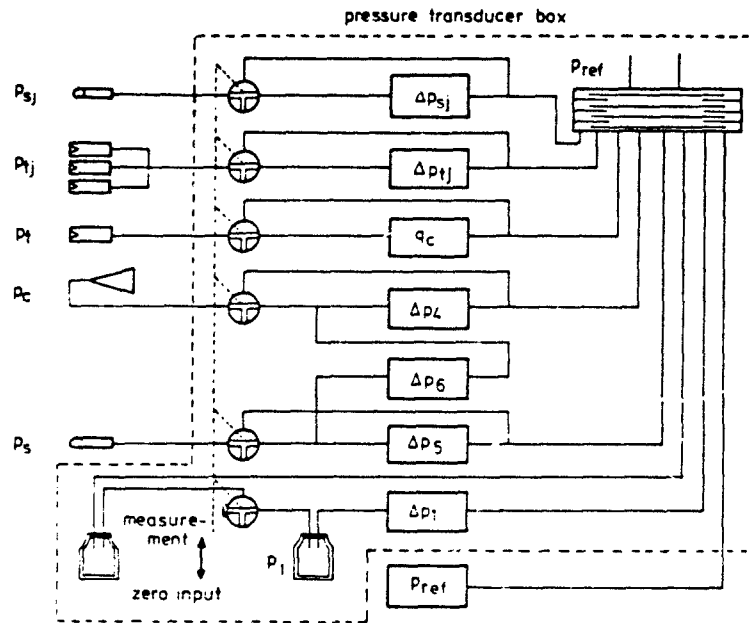


Fig. 6 Connection scheme of the pressure transducers

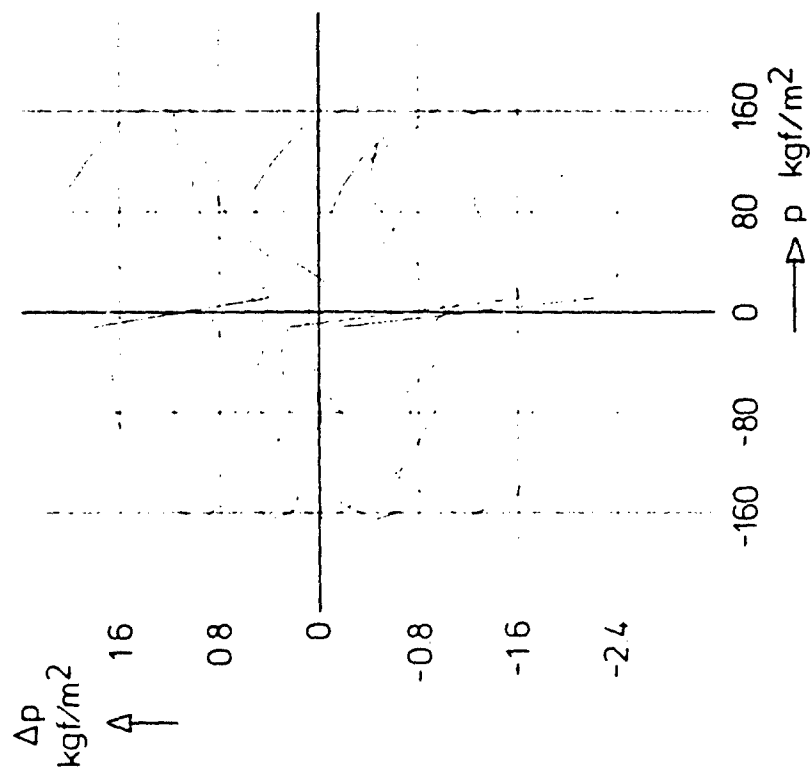


Fig. 7 Datapoint deviation of five combined calibrations of a differential pressure transducer

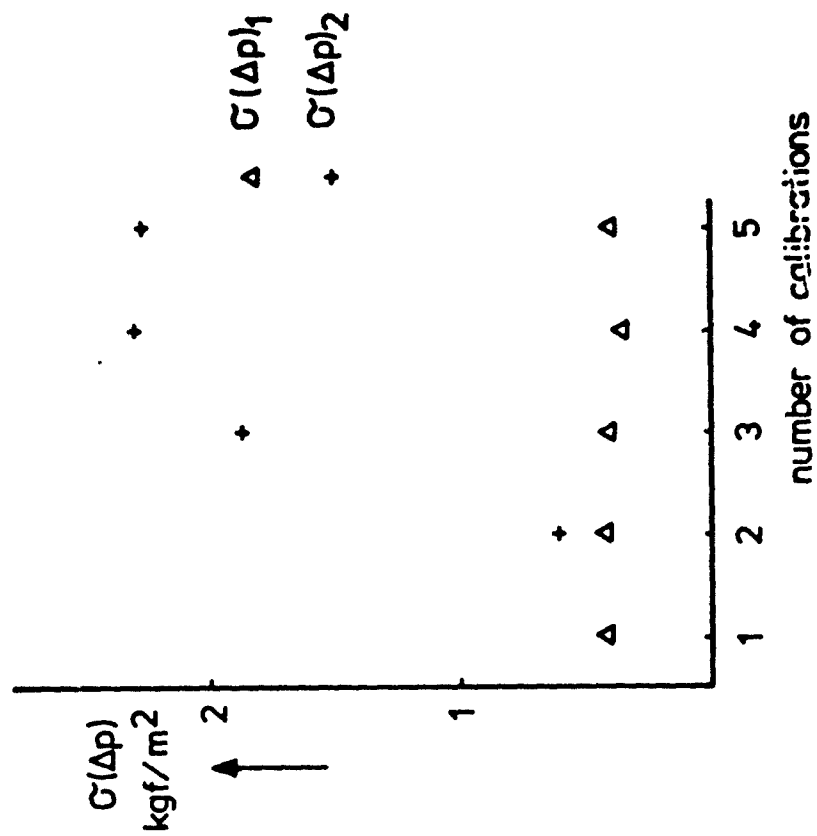


Fig. 8 The rms values  $\sigma(\Delta p)_1$  and  $\sigma(\Delta p)_2$  of five calibrations of a differential pressure transducer

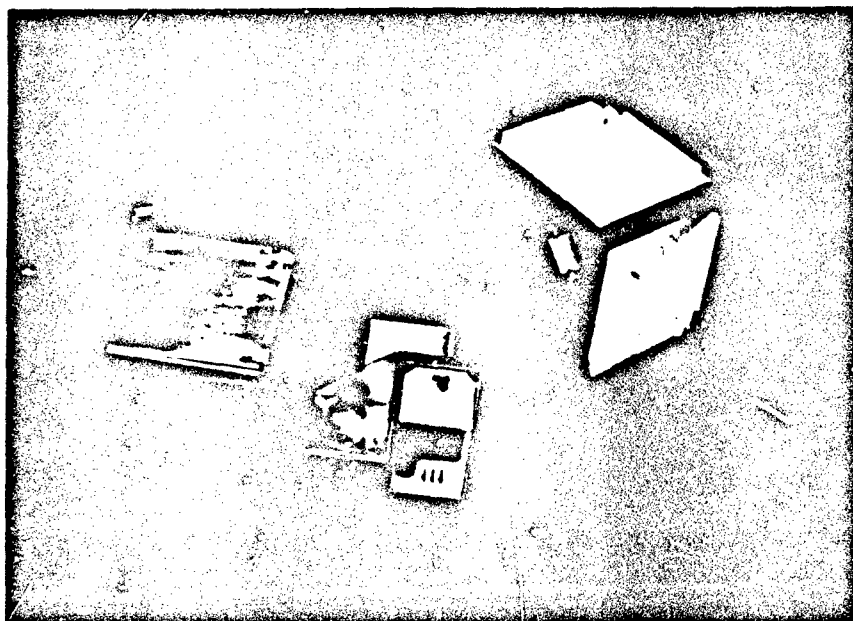


Fig. 9 The accelerometer box

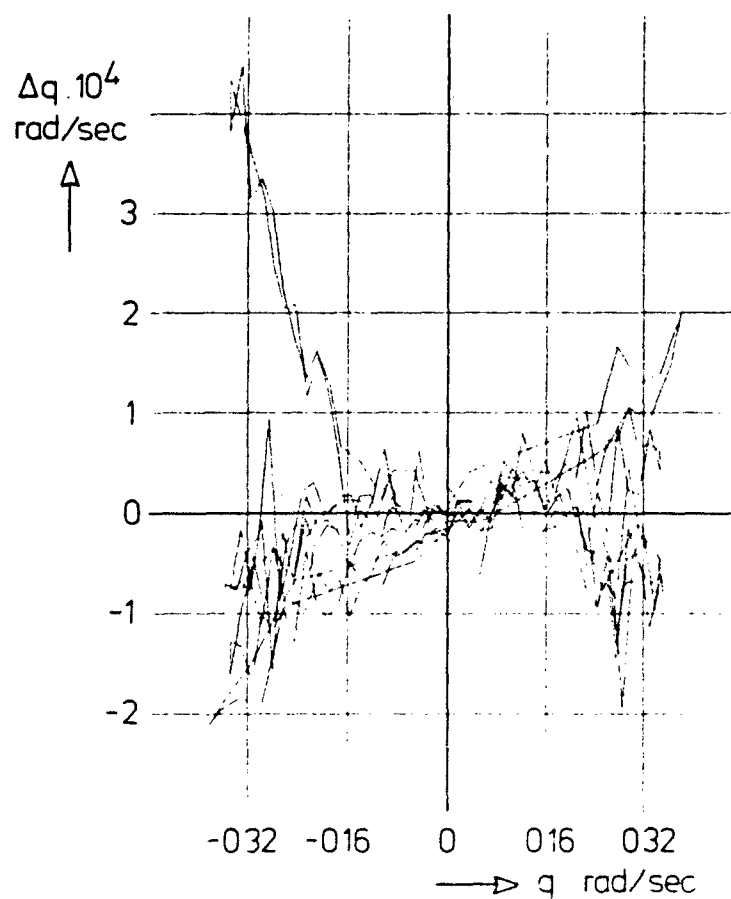


Fig. 10 Deviation curves of five combined calibrations of the rate of pitch gyro

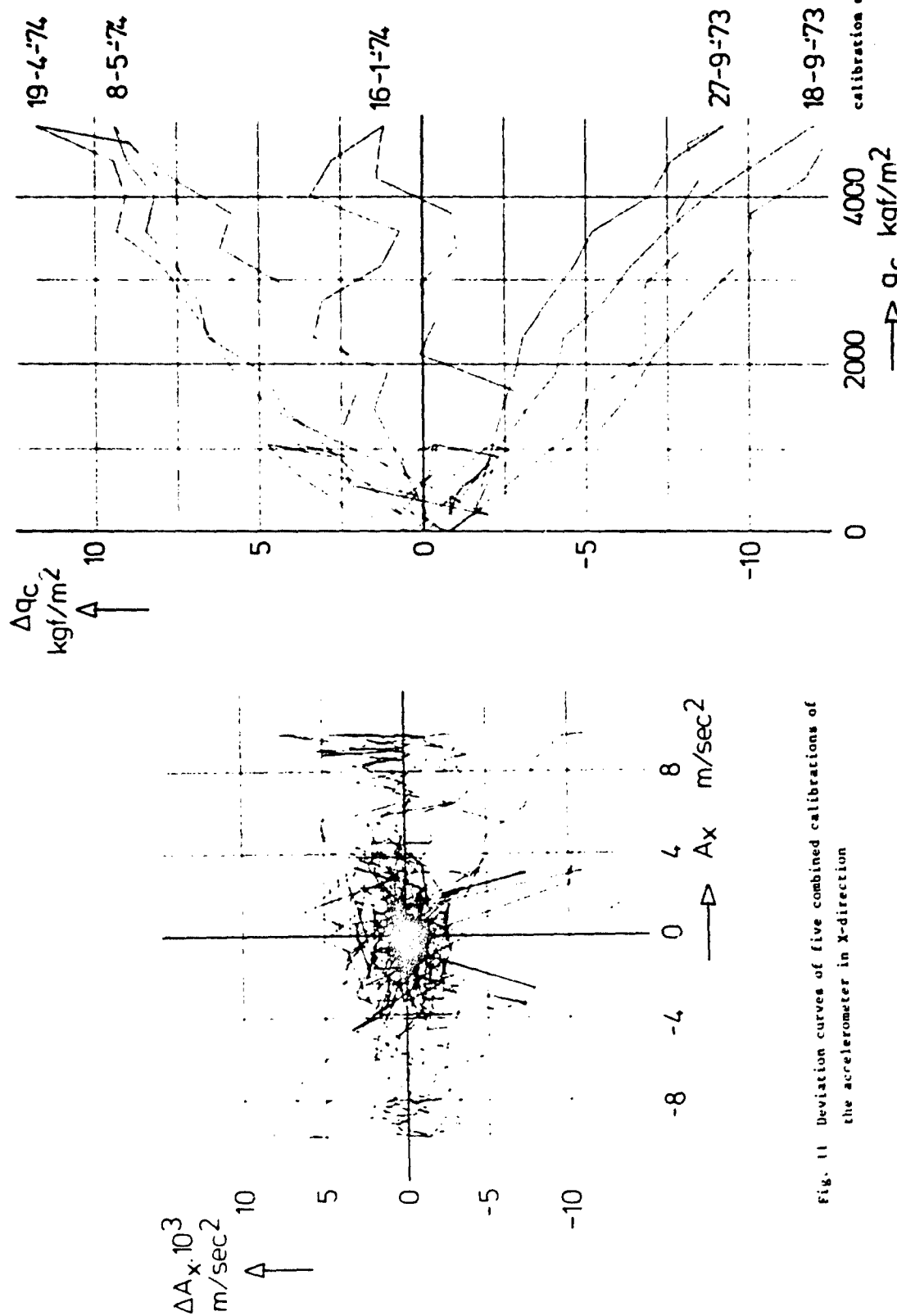


Fig. 11 Deviation curves of five combined calibrations of the accelerometer in X-direction

Fig. 13 The effect of gradient shift on the deviation curves of five calibrations of the differential pressure transducer  $q_c$

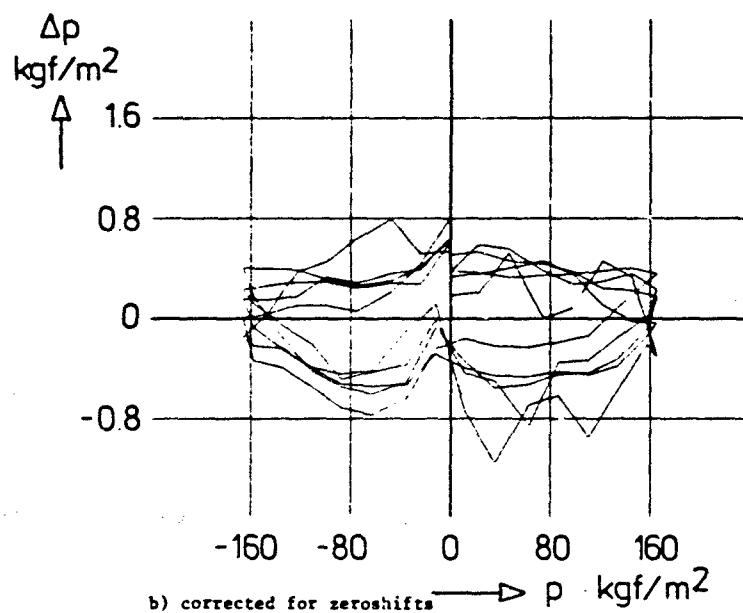
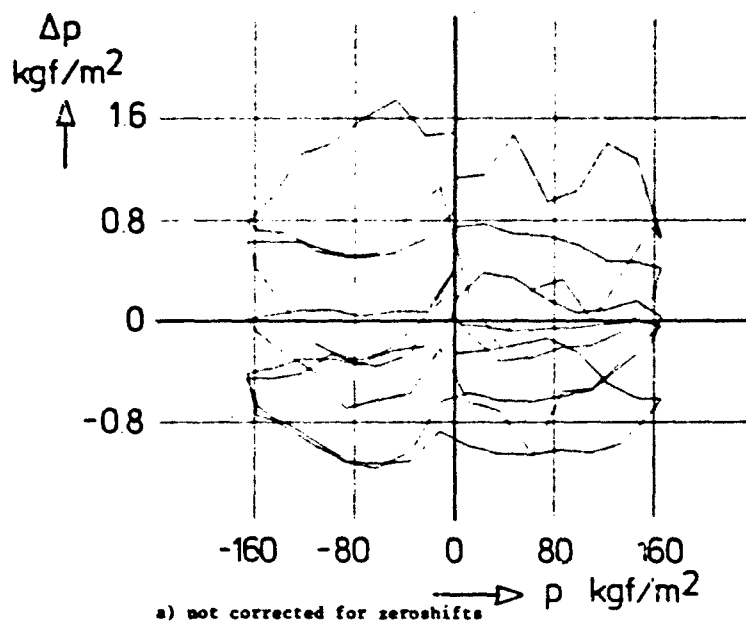
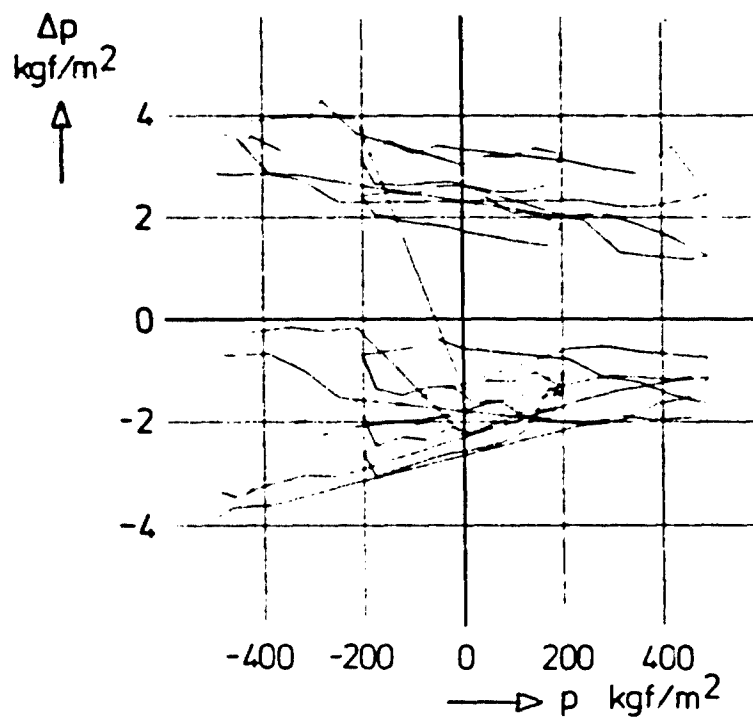
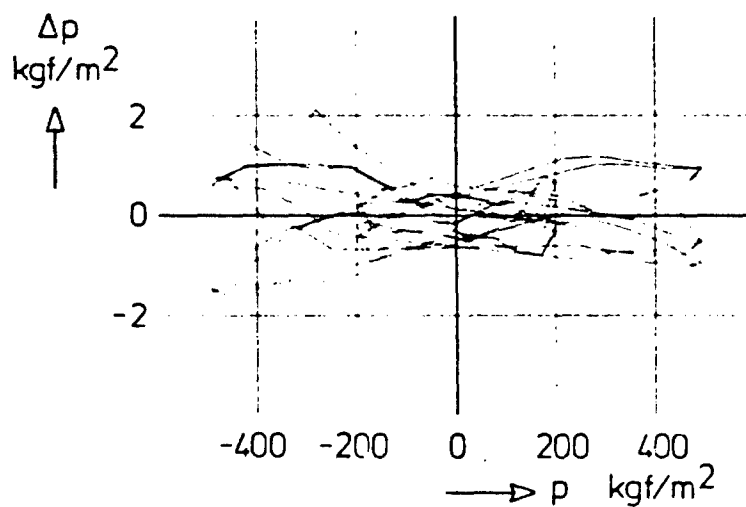


Fig. 12 Deviation curves of five combined calibrations of the differential pressure transducer  $\Delta p_5$



a) not corrected for zeroshifts



b) corrected for zeroshifts

Fig. 14 The effect of zeroshift and gradientshift on the deviation curves of five calibrations of the differential pressure transducer  $\Delta p_1$

# A COMPLEMENTARY FILTERING TECHNIQUE FOR DERIVING AIRCRAFT VELOCITY AND POSITION INFORMATION

by

Frank R. Nissen  
NASA Langley Research Center  
Hampton, Virginia 23665

## SUMMARY

In a VTOL instrument approach and landing research program at the Langley Research Center, there was a requirement for ground-referenced velocity and position information, without noise or lag. Radar position information, which was contaminated with noise, was telemetered to the aircraft; in addition to smoothing the position signal, the components of velocity, which were not measured, had to be derived.

An onboard navigation system which employed complementary filtering was developed to provide the velocity and position information. The inputs to the mix filter included both acceleration inputs, which provided high-frequency position and velocity information, and radar position inputs, which provided the low-frequency position and velocity information. Onboard aircraft instrumentation, including attitude reference gyros and body-mounted accelerometers, was used to provide the acceleration information. An in-flight comparison of signal quality and accuracy showed good agreement between the complementary filtering system and an aided inertial navigation system. Furthermore, the complementary filtering system was proven to be satisfactory in control and display system applications for both automatic and pilot-in-the-loop instrument approaches and landings.

## SYMBOLS

Values are given in both SI and U.S. Customary Units. The measurements and calculations were made in U.S. Customary Units.

A, B, C	Matrices
$a_x, a_y, a_z$	Body-mounted accelerometer outputs, m/sec <sup>2</sup> (ft/sec <sup>2</sup> )
b, c	Single column matrices or vectors
g	Gravity constant, 9.8 m/sec <sup>2</sup> (32.2 ft/sec <sup>2</sup> )
K	Gain matrix
k	Element of gain matrix
R	Riccati equation matrix solution
s	Laplacian operator
t	Time, sec
u	Control input vector
v	Input noise vector
w	Measurement noise vector
X, Y, Z	Displacement in runway reference coordinate frame (see Fig. 6), m (ft)
$\ddot{x}_b, \ddot{y}_b, \ddot{z}_b$	Inertial accelerations in aircraft reference coordinate frame (see Fig. 6), m/sec <sup>2</sup> (ft/sec <sup>2</sup> )
x	State vector
y	Output vector
ζ	Damping ratio
θ	Pitch attitude, positive nose upward, rad
$\sigma_v^2$	Variance of input signal noise
$\sigma_w^2$	Variance of measurement signal noise
τ	Time constant, sec
φ	Roll attitude, positive right wing down, rad



$\theta$  Yaw attitude, positive nose right, rad

$\omega_n$  Undamped natural frequency, rad/sec

### Superscript

T Matrix transpose

A dot over a symbol indicates a derivative with respect to time. A circumflex ( $\hat{\phantom{x}}$ ) denotes an estimated value.

## INTRODUCTION

In a VTOL instrument approach and landing research program at the Langley Research Center, there was a requirement for ground-referenced velocity and position information, without noise or lag. This information was needed for implementation of advanced control and display concepts. Radar position information, which was contaminated with noise, was telemetered to the aircraft; in addition to smoothing the position signal, the components of velocity, which were not measured, had to be derived. Over the course of the flight-test program, three different techniques were used to obtain this information — approximate differentiation and filtering, an aided inertial navigation system, and complementary filtering.

The development of the system which employed complementary filtering and its subsequent performance in flight are described in this paper. The complementary filtering system computed ground-referenced acceleration from onboard sensors and combined this information with the noisy radar position signals on a weighted-frequency basis to obtain satisfactory position and velocity information. The complementary filter used fixed gains which were based not only on signal noise characteristics, but also on other practical aspects such as instrument and computation accuracies.

The use of this system represents a practical application of the complementary filtering technique. Furthermore, being based on classical estimation theory, it is of interest since it illustrates the application of that theory. Finally, the system concept itself is noteworthy because it could be used for the approach and landing guidance problem, as an alternative to more complex systems such as inertial or Doppler navigation systems.

## FLIGHT-TEST PROGRAM

An onboard navigation system employing complementary filters was developed for a flight-test program at the Langley Research Center in which a CH-46 helicopter was used to investigate control and display concepts for VTOL instrument flight. These investigations have been reported in References 1-3. The test helicopter, shown in Figure 1, was equipped with an electronic flight control system, electromechanical displays including a three-axis VTOL flight director, and onboard general-purpose analog computers, by which advanced control and display concepts were mechanized. The basic instrument task included acquisition of runway center line and glide path, deceleration to a hover, and a vertical landing. While the emphasis of the investigations was on manual approaches, with the pilot actively in the control loop, automatic approaches were also performed to demonstrate that the guidance control laws which had been developed could be used as well for that purpose. Position and velocity information without lag or objectionable noise was required since this information was sent directly into the controls for automatic approaches through the guidance control laws and was displayed to the pilot through a three-axis VTOL flight director and other indicators.

The evaluation pilot's control panel is shown in Figure 2. The engine instruments, pitch- and roll-attitude indicator, needle-ball, airspeed, barometric altitude, and vertical speed indicator were standard instruments. The remaining indicators were driven by the onboard computers and, specifically, the command needles and deviation needles on the attitude director indicator, the moving map, and the radar altimeter were driven by position and velocity signals from the onboard navigation system. Typical sensitivities which were used for the various display indicators are given in Table I.

Over the course of the flight-test program, three different onboard navigation system configurations were employed to obtain aircraft position and velocity. Each configuration relied on a ground-based precision tracking radar to provide position information to the aircraft via telemetry. The onboard navigation systems, which received this position information, had to provide both position and velocity information for guidance. The onboard system configurations which were used included the following:

- (1) Approximate differentiation and filtering
- (2) An inertial navigation system with periodic radar position updates
- (3) Complementary filtering whereby radar position information was continuously mixed with acceleration information obtained from onboard sensors

### Precision Radar

Aircraft position was sensed by a precision tracking radar system, located at Wallops Flight Center, Virginia, where the flight tests were performed. A photograph of the precision tracking radar system is shown in Figure 3. The position of the aircraft was sensed directly in terms of slant range and azimuth and elevation angles of the radar antenna. This information was transformed into rectangular coordinates in the runway reference frame and transmitted to the aircraft by means of telemetry.

The radar was K-band, with an antenna beamwidth of approximately  $0.5^\circ$ . A passive reflector was mounted on the nose of the aircraft to provide a specific point for the radar to track. The limits of the radar tracking antenna were  $30^\circ$  in elevation and  $\pm 45^\circ$  in azimuth. The accuracy of the radar was approximately  $0.02^\circ$  for the azimuth and elevation angles and 3 m (10 ft) or 1 percent (whichever is greater) for slant range.

### Onboard Navigation Systems

As reported in References 1 and 2, the first series of tests were conducted with a  $\pm 10$ -volt analog computer used to filter the radar position information because of radar and telemetry noise. The telemetry unit was an FM unit with  $\pm 10$ -volt discriminator outputs. Velocity information was obtained by approximate differentiation of the position signals. This approach, even with maximum tolerable filtering, resulted in considerable noise from velocity signals which, in turn, caused the flight director command needles to "jitter." These random needle fluctuations were found to be quite objectionable.

An inertial navigation system with periodic radar-position updates was used for the steep-angle approach work reported in Reference 3. The system, formerly a Gemini spacecraft inertial navigation system, was modified so that the radar position data could be used to update the navigation outputs. The radar signals were sampled and digitized at a ground station at 1-second intervals and transmitted to the aircraft by means of a digital telemetry link. The position and velocity outputs from the digital computer were converted to analog form, and then routed to the onboard analog computers. In general, the signal outputs were of sufficiently high quality in terms of both accuracy and noise level to be used for the flight director display application. However, this system was quite complex, which made it difficult and costly to maintain and operate, and it weighed approximately 350 kg (800 lb).

Lastly, a system using a complementary filtering technique was used to provide accurate position and velocity outputs with low-noise content. A detailed description of this system and its development are presented in subsequent sections of the paper. Briefly, this system featured a second-order complementary filter with inertial-acceleration inputs as well as the radar-position inputs. The inertial-acceleration inputs provided short-term position and velocity information, while radar-position inputs provided the long-term position and velocity information. Onboard sensors, including attitude reference gyros and body-mounted accelerometers, were used to provide the inertial acceleration information. Since only the high-frequency content of the onboard inertial acceleration information was relied on in this application, the relatively crude inertial information was adequate. This system was used for the constant-attitude deceleration profile tests and the automatic approach tests, also described in Reference 3.

### THEORETICAL BACKGROUND

#### Differentiation of Position Information

There are inherent problems in differentiating position information to obtain velocity information, because of signal noise. Of course, position and velocity information which is to be used in display or control system applications must be practically noise free. Figure 4 shows the transfer function for approximate differentiation. Notice that approximate differentiation inherently introduces a first-order lag equal to the time constant,  $\tau$ . Since the effect of filtering or lagging a signal used in a closed-loop control system is to reduce the stability of the system, it is desirable to keep the lag,  $\tau$ , as small as possible. On the other hand, by reference to the time response, it can be seen that high-frequency noise on the input signal will be amplified by a factor of  $1/\tau$ . Thus, from this standpoint, it is necessary that  $\tau$  be large, preferably greater than 1.0, in order to reduce the noise contained by the input signal.

A trade off has to be made between lag and noise level but, frequently, an acceptable trade off cannot be made. Figure 5 is a plot of velocity versus position which was recorded at the precision tracking radar facility. The velocity information was derived by approximate differentiation of the radar's position signal using a time constant,  $\tau$ , of 0.5 second. Since this computation was performed at the ground station, the position signal was not contaminated with telemetry system noise. Even so, it can be seen from Figure 5 that the derived velocity signal has noise with a peak-to-peak amplitude on the order of 3.0 to 6.0 m/sec (10 to 20 ft./sec). Since the noise on the derived velocity signal varies inversely with  $\tau$ , this noise could be reduced to a minimum of 1.5 to 3.0 m/sec (5 to 10 ft./sec) assuming that a time constant as large as 1.0 second could be tolerated, but even this level of noise would be clearly unacceptable. As indicated by this example, differentiation of position information alone was not capable of providing acceptable velocity information.

#### Complementary Filtering Technique

The complementary filtering technique combines acceleration with position data to determine low-noise estimates of both velocity and position. The coordinate frames of reference which were used in measuring aircraft acceleration and position are depicted in Figure 6. Figure 7 is a block diagram representation of the complementary filter. It is noted that the form of the filter for this particular estimation problem is identical to that of a Kalman filter. The part of the system drawn with solid lines (Fig. 7) represents the high-frequency computation of velocity and position, based on aircraft acceleration. Since acceleration is integrated directly to obtain velocity and position, there is no lag. Note also that the mix filter provides a position estimate as well as a velocity estimate. As drawn with dashed lines (Fig. 7), the difference between the estimated position and the position measured by the tracking radar is fed back as a correction to both the velocity estimate and the acceleration input. In contrast to approximate differentiation, the velocity estimate is the output of an integrator which attenuates the noise component of the position input and also of the accelerometer input. For additional information, Table II contains transfer functions which indicate the response of each of the estimator outputs to individual acceleration and position inputs.

The selection of the complementary filter gains was based on the general steady-state Kalman filter solution for this particular estimation problem. Given the noise properties of the inputs, the Kalman filter solution provides the gains for an optimal estimator in the sense that the estimates will have minimum variance noise. The results of the general solution for the gains for this particular form of filter are discussed here, and a more detailed treatment of the solution is given in the Appendix.

The gains  $k_1$  and  $k_2$  can be expressed in terms of the familiar second-order parameters  $\zeta$  and  $\omega_n$  as  $k_1 = 2\zeta\omega_n$  and  $k_2 = \omega_n^2$ . The damping ratio was found to be constant and the undamped natural frequency was determined to be a function only of the ratio of accelerometer noise to position noise

$$\zeta = \frac{\sqrt{I}}{2} = 0.707$$

$$\omega_n = \sqrt{\sigma_v / \sigma_a}$$

It is important to note that the solution is dependent only on the relative noise between the inputs and not on the absolute noise levels. It is possible, of course, that if the absolute noise levels were extremely high, the filter would provide estimates which could be unacceptably noisy.

#### FLIGHT-TEST VALIDATION OF COMPLEMENTARY FILTERING SYSTEM

##### System Description

A photograph of the components of the onboard navigation system which used complementary filtering is shown in Figure 8. The onboard sensors which were used included three body-mounted accelerometers, a vertical gyro for pitch and roll attitude, and a directional gyro for heading. These sensors were part of the research aircraft instrumentation package and had previously been used for recording and for control system applications. The 10-volt analog computer which was used to perform all the necessary onboard computations was housed in a box which normally remained closed.

As shown by the block diagram of the system in Figure 9, the computations included correcting the body-mounted accelerometers for the effect of gravity and resolving the accelerations into components along the runway reference coordinates. Several approximations were made to minimize computational requirements, based on the assumption of small pitch and roll angles during the final approach and landing maneuver for the research tests.

The body-mounted longitudinal and lateral accelerometers were corrected for the effects of gravity by using the sine of pitch and roll angles from the onboard vertical gyro

$$\bar{X}_h = a_x - g \sin \theta$$

$$\bar{Y}_h = a_y + g \sin \phi$$

The normal accelerometer was corrected for effects of gravity by assuming small pitch and roll angles

$$\bar{Z}_h = a_z - g \cos \theta \cos \phi$$

$$\bar{Z}_h = a_z - g$$

In resolving the accelerations along the body axes into the runway reference coordinate frame, it was assumed that the aircraft would at all times be approximately in a level attitude so that

$$\bar{X} = \bar{X}_h \cos (\psi - \psi_0) - \bar{Y}_h \sin (\psi - \psi_0)$$

$$\bar{Y} = \bar{X}_h \sin (\psi - \psi_0) + \bar{Y}_h \cos (\psi - \psi_0)$$

$$\bar{Z} = \bar{Z}_h$$

The horizontal accelerations were resolved by using a sine-cosine resolver driven by a directional gyro synchro output. A differential synchro input was incorporated to permit selection of any desired runway-reference heading  $\psi_0$ . The three position signals  $\bar{X}$ ,  $\bar{Y}$ , and  $\bar{Z}$  were obtained from the precision tracking radar, as described in a previous section. The 10-volt analog computer was used to perform all the above computations onboard the aircraft; and Figure 10, the analog computer schematic, shows the details of these computations and indicates the scaling which was used.

It is noted that if the accelerometers were slaved to vertical so that the longitudinal and lateral accelerometers would indicate true horizontal accelerations and the normal accelerometer would indicate true vertical accelerations, then the need to correct the longitudinal and lateral accelerometers for effects of gravity would be eliminated and would make the rest of the computations valid for other than small pitch and roll angles. This was not done, however, for the system described herein.

The complementary-filter gains which were used corresponded to a natural frequency of  $\omega_n = 0.45$  rad/sec with a settling time constant of 12.5 seconds, based on the time to settle within 2 percent of steady state. These gains were selected so that the time constant would be long enough that noise from the radar position signal would be satisfactorily attenuated, but short enough that errors which would result from inaccuracies associated with the acceleration information would be kept small.

##### Flight-Test Results

As discussed above, the complementary filtering system was developed for use in a VTOL instrument approach and landing research program. The modification of the recording system that was necessary to obtain the data presented here was restricted in order that the data could be obtained in a timely manner, without impeding the main research program. For this reason, data were obtained for only  $\bar{X}$  and  $\bar{Y}$  in one instance, and for only  $\bar{X}$  in another instance. Nevertheless, the axes that were selected for documentation were the axes with the least desirable scale factors and, consequently, represent the worst case rather than the best.

Figures 11 and 12 show the input and output signal noise characteristics for the complementary filtering system. These data were recorded separately for X and Y during hovering flight near the landing area. These data were obtained by an FM magnetic tape recording system and were later sampled at a rate of 100 Hz during the data-reduction process. Longitudinal acceleration was not recorded during these tests; however, its signal noise characteristics were very similar to those of the lateral accelerometer. The noise on the position output was greatly reduced compared to the noise on the position input signal, which had a peak-to-peak amplitude of approximately 30.5 m (100 ft). The noise on the position input signal was mostly due to telemetry noise, which was nearly 1 percent of full scale. The accelerometer signal noise, mainly due to aircraft structural vibration, was also essentially eliminated by the integration process within the filter, as evidenced by the low-noise velocity estimate. It was determined that the signal noise contributed by the analog computer components themselves, which was related to computer scaling, resulted in approximately 0.06 m/sec (0.2 ft/sec) peak-to-peak noise for the velocity estimate for X, for which the scaling problem was most severe. This level of computer-generated noise therefore accounted for nearly all the noise observed on the velocity output; hence, the complementary filter essentially eliminated the effects of both acceleration and position measurement noise.

A comparison in accuracy was made in flight between the complementary filtering system and the inertial navigation system with periodic radar position updates, mentioned in a previous section. Baseline performance data on the inertial navigation system are contained in Reference 4, whereas details of this system's navigation computations, including the update logic, are described in Reference 5. Both systems relied on the precision tracking radar for long-term position and velocity information; the complementary filtering system received continuous position information, whereas the aided inertial navigation system received position updates at 1.0-second intervals. Without updates, the position-error drift rate of the inertial navigation system was approximately 2.0 nautical miles per hour. For comparison, the position-error drift rate of the complementary filtering system, without position feedback, was estimated to be on the order of 100 to 200 nautical miles per hour. This high drift rate was mainly due to approximations which were made in resolving the accelerations and also was a result of computer scaling limitations. However, Figures 13 and 14 show the close agreement obtained between the outputs of the two systems during a decelerating approach to hover and during a hovering maneuver, respectively. From Figure 14, it can be seen that the velocity outputs agree within about 0.30 m/sec (1.0 ft/sec).

In addition to the results discussed above, the six position and velocity outputs of the complementary filtering system were found to be satisfactory for both control and display applications in the VTOL instrument approach and landing research program for which the system was developed. As noted previously, displays driven by these outputs consisted of a flight director indicator, a horizontal-situation moving-map display, lateral and vertical flight-path error needles, rising runway needle, and simulated radar altimeter. Again, Figure 2 illustrates the display panel configuration while Table I indicates typical display sensitivities which were used. The guidance computer, which provided pitch, roll, and power flight director display commands, also provided similar commands to the control system in the automatic approach mode. The VTOL landing approach task in these tests involved acquisition of the runway center line, capture of the glide path, deceleration to a hover, vertical descent, and touchdown. The entire sequence could be accomplished either manually, with the pilot centering the flight director commands, or automatically. Signal noise was not apparent either in the display movements or, while in the automatic mode, in the control actuator motions. The accuracy of the complementary filtering system enabled tracking of the approach path and speed profiles with a high degree of precision. Figures 15 and 16, from Reference 3, show manual and automatic tracking performance, respectively, for decelerating instrument approaches along a 6° glide path.

#### CONCLUDING REMARKS

An onboard navigation system employing complementary filters was developed for use in a VTOL approach and landing research program at the Langley Research Center. The system used onboard conventional aircraft instrumentation in combination with landing guidance system signals to provide acceptable position and velocity information for landing approach guidance. Based on the development of this system, the following conclusions were drawn:

1. Straightforward differentiation of landing guidance system signals, alone, did not provide adequate velocity information for use in either controls or displays since differentiation tended to amplify the noise.
2. The complementary filtering system was effective in providing estimates of aircraft position and velocity state information, without appreciable noise and without lag. Flight data indicated that accelerometer and radar position signal noise, approximately  $1.2 \text{ m/sec}^2$  ( $4 \text{ ft/sec}^2$ ) and 30.5 m (100 ft) double-amplitude noise, respectively, had been greatly reduced by the complementary filter, which provided a velocity estimate with only 0.06 m/sec (0.2 ft/sec) double-amplitude noise. Furthermore, an in-flight comparison of signal quality and accuracy between the complementary filtering system and an aided inertial navigation system showed agreement within 0.30 m/sec (1.0 ft/sec) for the velocity outputs.
3. The concept of combining onboard acceleration information with telemetered radar position information to provide useful landing guidance system signals was validated through the use of such a system in the VTOL approach and landing research program for which the system was developed. The VTOL approach task included acquisition of the runway center line, capture of the glide path, deceleration to a hover, and a vertical descent to touchdown. The task was accomplished both manually, with the pilot centering flight director commands, and automatically, with the flight director command signals sent directly into the controls.

## APPENDIX — FIXED-GAIN SOLUTION FOR COMPLEMENTARY FILTERING

The general Kalman filter solution, obtained from Reference 6, is outlined below. The plant dynamics are expressed as:

$$\dot{\underline{x}} = \underline{A}\underline{x} + \underline{B}\underline{u}$$

with measured outputs

$$\underline{y} = \underline{C}\underline{x} + \underline{w}$$

The input and output measurement noise characteristics are specified by the correlation matrices  $\underline{Q}$  and  $\underline{P}$ , respectively. The Kalman filter gain matrix, for the stationary case, is found from

$$\underline{K} = \underline{R}_0 \underline{C}^T \underline{P}^{-1}$$

where  $\underline{R}_0$  is the steady-state solution of the matrix Riccati equation

$$\dot{\underline{R}} = \underline{A}\underline{R} + \underline{R}\underline{A}^T - \underline{R}\underline{C}^T \underline{P}^{-1} \underline{C}\underline{R} + \underline{B}\underline{Q}\underline{B}^T$$

For the complementary filtering problem, as shown in Figure 17, the acceleration input is regarded as a control input and, as a single input, is a scalar; therefore, the  $\underline{B}$  matrix is reduced to a column matrix or vector  $\underline{b}$ . Similarly, there is only one measured output; therefore, the  $\underline{C}$  matrix becomes a row matrix  $\underline{c}^T$ .

$$\dot{\underline{x}} = \underline{A}\underline{x} + \underline{b}\underline{u}$$

where  $\underline{A} = \begin{bmatrix} 0 & 1 \\ 0 & 0 \end{bmatrix}$  and  $\underline{b} = \begin{bmatrix} 0 \\ 1 \end{bmatrix}$

$$\underline{y} = \underline{c}^T \underline{x} + \underline{w}$$

where  $\underline{c} = \begin{bmatrix} 1 \\ 0 \end{bmatrix}$

The correlation matrices  $\underline{Q}$  and  $\underline{P}$  are reduced to the scalar quantities  $\sigma_v^2$  and  $\sigma_w^2$ . The matrix Riccati equation, therefore, becomes

$$\dot{\underline{R}} = \underline{A}\underline{R} + \underline{R}\underline{A}^T - \underline{R}\underline{c} \left( \frac{1}{\sigma_w^2} \right) \underline{c}^T \underline{R} + \underline{b} \left( \sigma_v^2 \right) \underline{b}^T$$

The steady-state solution is found by setting  $\dot{\underline{R}} = 0$ . Taking each element of  $\underline{R}$ ,

$$\dot{r}_{11} = 0 = r_{21} + r_{12} - \left( \frac{1}{\sigma_w^2} \right) r_{11}^2$$

$$\dot{r}_{12} = 0 = r_{22} - \left( \frac{1}{\sigma_w^2} \right) r_{11} r_{12}$$

$$\dot{r}_{21} = 0 = r_{22} - \left( \frac{1}{\sigma_w^2} \right) r_{21} r_{11}$$

$$\dot{r}_{22} = 0 = - \left( \frac{1}{\sigma_w^2} \right) r_{21} r_{12} + \sigma_v^2$$

By using the fact that the  $\underline{R}$  matrix is symmetric and that  $r_{21} = r_{12}$ , these equations can be reduced to

$$0 = 2r_{12} - \left( \frac{1}{\sigma_w^2} \right) r_{11}^2$$

$$0 = r_{22} - \left( \frac{1}{\sigma_w^2} \right) r_{12} r_{11}$$

$$0 = - \left( \frac{1}{\sigma_w^2} \right) r_{12}^2 + \sigma_v^2$$

From these equations, the steady-state values for the elements of  $\underline{R}$  have been found to be

$$\underline{R}_0 = \begin{bmatrix} r_{11} & r_{12} \\ r_{21} & r_{22} \end{bmatrix} = \begin{bmatrix} \sqrt{2} \sigma_v^{1/2} \sigma_w^{3/2} & \sigma_v \sigma_w \\ \sigma_v \sigma_w & \sqrt{2} \sigma_v^{3/2} \sigma_w^{1/2} \end{bmatrix}$$

The gains are obtained from

$$\begin{bmatrix} k_1 \\ k_2 \end{bmatrix} = R_c \begin{pmatrix} 1 \\ \sigma^2 \end{pmatrix}$$

and result in  $k_1 = \sqrt{2} \sqrt{\sigma_v/\sigma_w}$  and  $k_2 = \sigma_v/\sigma_w$ . By expressing the gains as  $k_1 = 2\zeta\omega_n$  and  $k_2 = \omega_n^2$ , it may be shown that  $\omega_n = \sqrt{\sigma_v/\sigma_w}$  and  $\zeta = \sqrt{2}/2 = 0.707$ .

#### REFERENCES

1. Kelly, James R., and Niessen, Frank R.: Evaluation of a VTOL Flight-Director Concept During Constant-Speed Instrument Approaches. NASA TN D-5860, June 1970.
2. Garren, John F., Jr., Kelly, James R., Sommer, Robert W., and DiCarlo, Daniel J.: Flight Investigation of VTOL Control and Display Concept for Performing Decelerating Approaches to an Instrument Hover. NASA TN D-6108, February 1971.
3. Kelly, James R., Niessen, Frank R., Thibodeaux, Jerry J., Yenni, Kenneth R., and Garren, John F., Jr.: Flight Investigation of Manual and Automatic VTOL Decelerating Instrument Approaches and Landings. NASA TN D-7524, July 1974.
4. Madigan, Ronald J.: Flight Test Experiments to Evaluate Aided-Inertial System Performance for Terminal Guidance. J. Inst. Nav., Vol. 17, No. 1, Spring 1970, pp. 83-91.
5. Anon.: V/STOL Inertial Navigation With Radar Update Capability. IBM No. 69-NC7-027 (Contract No. NAS 12-610, IBM Corp., August 1969. (Available as NASA CR-86234.)
6. Schultz, Donald G., and Melsa, James L.: State Functions and Linear Control Systems. McGraw-Hill Book Co., Inc., c. 1967, pp. 287-295.

TABLE I. DISPLAY INDICATOR SENSITIVITIES

Pitch and roll flight director needles	
Full-scale deflection . . . . .	$\pm 2.0$ cm ( $\pm 0.8$ in.)
Full-scale values for:	
Attitude . . . . .	$\pm 0.35$ rad
Velocity . . . . .	$\pm 10.7$ m/sec ( $\pm 35$ ft/sec)
Position . . . . .	$\pm 85.5$ m ( $\pm 280$ ft)
Power flight director needle	
Full-scale deflection . . . . .	$\pm 1.3$ cm ( $\pm 0.5$ in.)
Full-scale values for:	
Velocity . . . . .	$\pm 5.2$ m/sec ( $\pm 17$ ft/sec)
Position . . . . .	$\pm 30.5$ m ( $\pm 100$ ft)
Glide-slope deviation needle	
Full-scale deflection . . . . .	$\pm 1.8$ cm ( $\pm 0.7$ in.)
Full-scale value for position . . . . .	$\pm 30.5$ m ( $\pm 100$ ft)
Lateral deviation needle	
Full-scale deflection . . . . .	$\pm 1.4$ cm ( $\pm 0.55$ in.)
Full-scale value for position . . . . .	$\pm 45.7$ m ( $\pm 150$ ft)
Rising runway needle	
Full-scale deflection . . . . .	$\pm 1.4$ cm ( $\pm 0.55$ in.)
Full-scale value for position . . . . .	$\pm 30.5$ m ( $\pm 100$ ft)
Radar altimeter	
Instrument diameter . . . . .	7.6 cm (3.0 in.)
Needle deflection from 0 to 30.5 m (100 ft) . . . . .	110 deg
Needle deflection from 30.5 m (100 ft) to 366 m (1200 ft) . . . . .	140 deg
Moving-map sensitivity	
Distance from touchdown less than 610 m (2000 ft) . . . . .	12 m/cm (100 ft/in.)
Distance from touchdown between 610 m (2000 ft) and 2440 m (8000 ft) . . . . .	36 m/cm (300 ft/in.)
Distance from touchdown greater than 2440 m (8000 ft) . . . . .	480 m/cm (4000 ft/in.)

TABLE II. TRANSFER FUNCTION RELATIONSHIPS FOR  
COMPLEMENTARY FILTERING

Input	Output for —	
	$\ddot{x}$	$\dot{x}$
$\ddot{x}$	$\frac{s + k_1}{s^2 + k_1 s + k_2}$	$\frac{1}{s^2 + k_1 s + k_2}$
$\dot{x}$	$\frac{k_2 s}{s^2 + k_1 s + k_2}$	$\frac{sk_1 + k_2}{s^2 + k_1 s + k_2}$

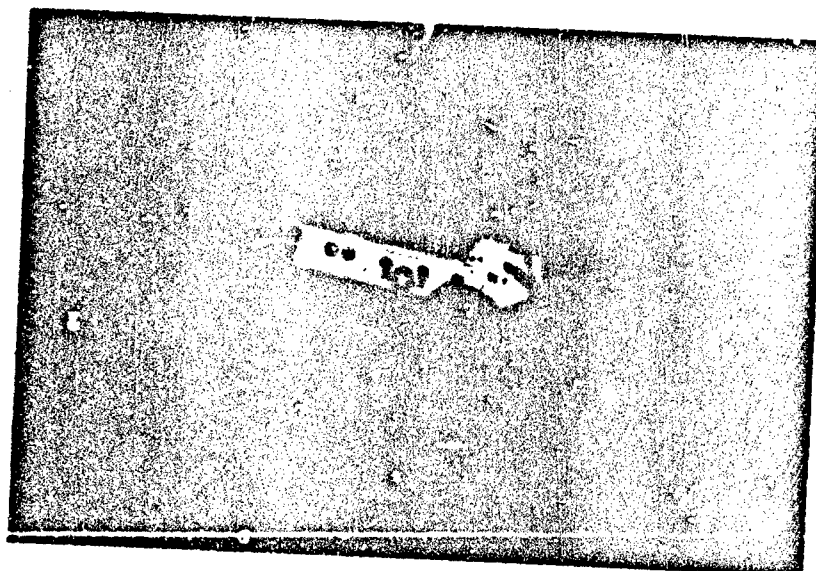


Figure 1. Research helicopter.

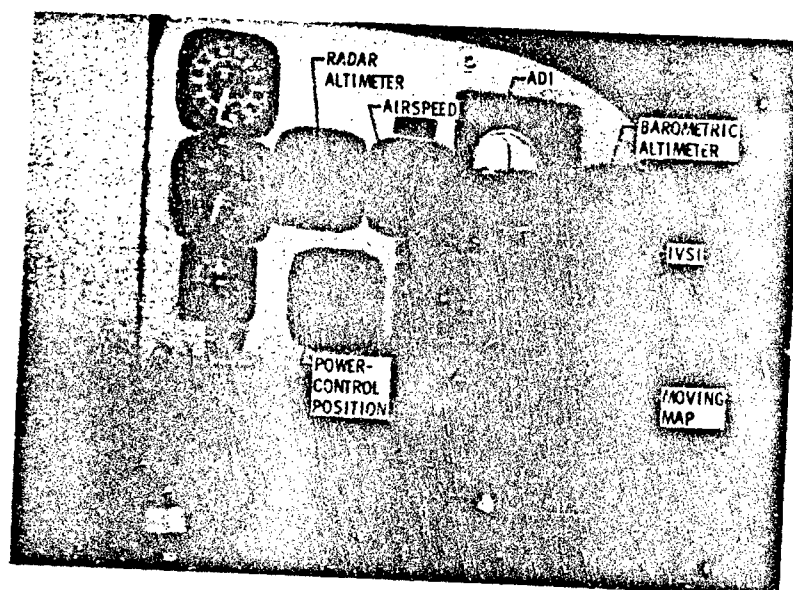


Figure 2. Evaluation pilot's panel.

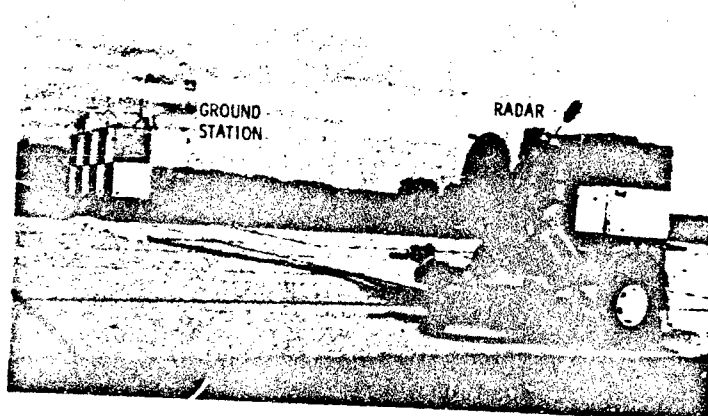


Figure 3. Precision-tracking radar facility.



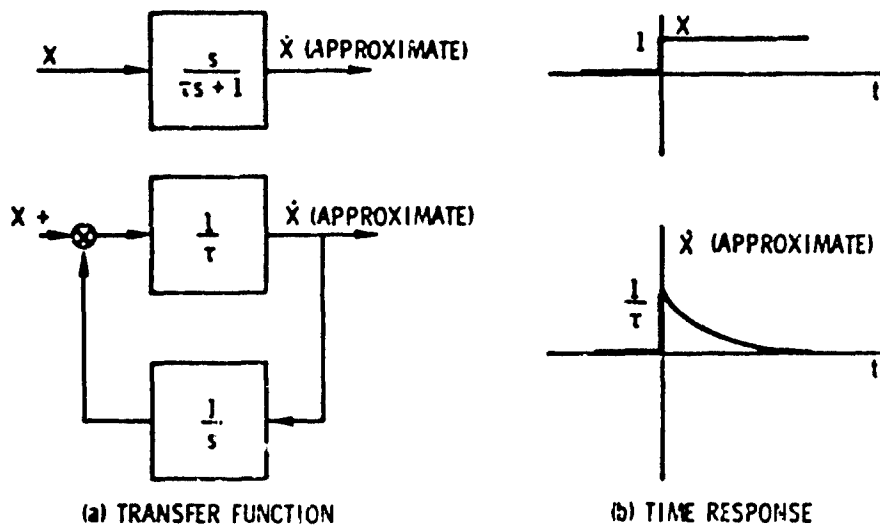


Figure 4. Transfer function and time response for approximate differentiation.

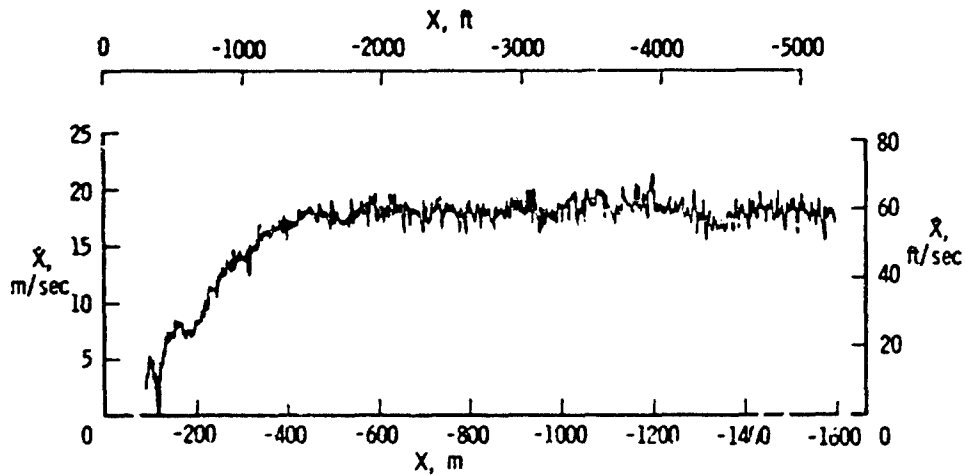


Figure 5. Approximate differentiation of a precision radar signal,  $\tau = 0.5$  sec.

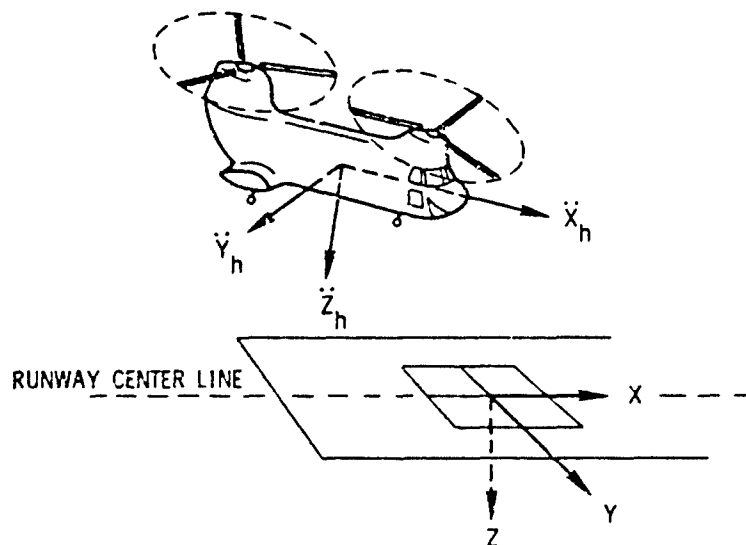


Figure 6. Aircraft and runway reference coordinate frames.

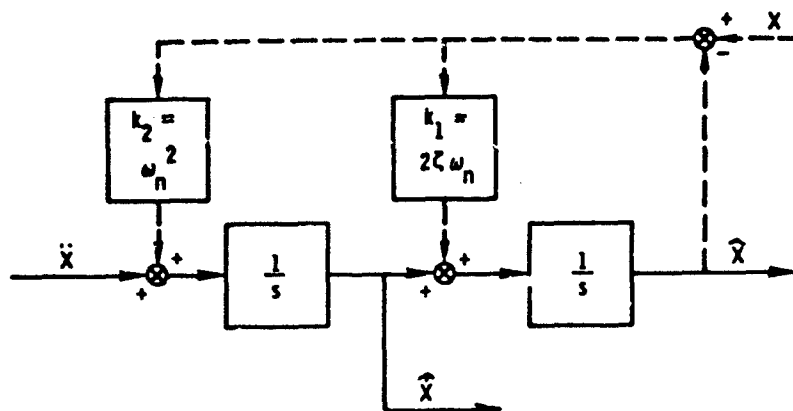


Figure 7. Complementary filter.

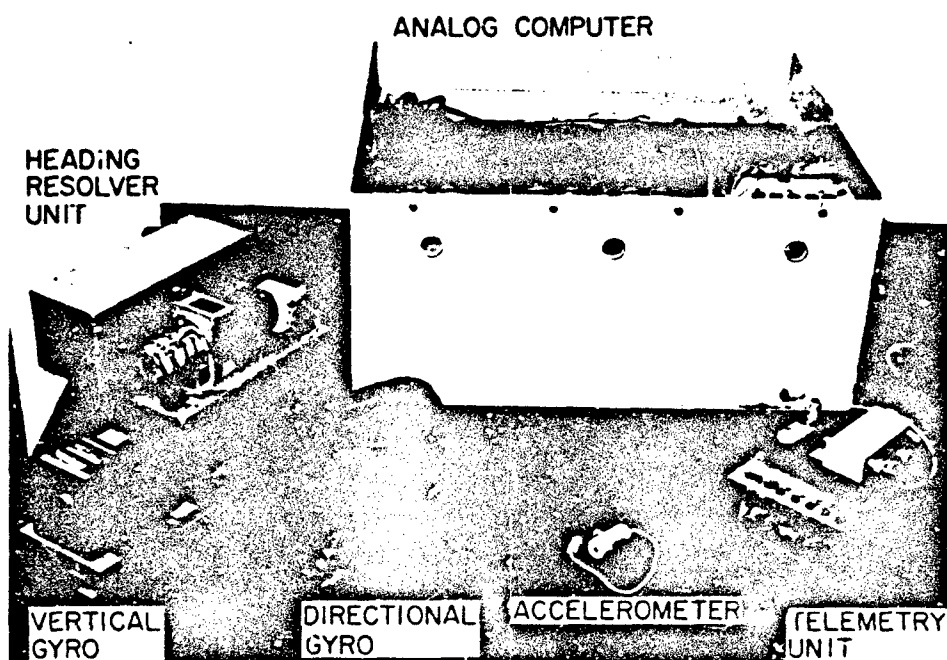


Figure 8. Complementary filtering navigation system equipment.

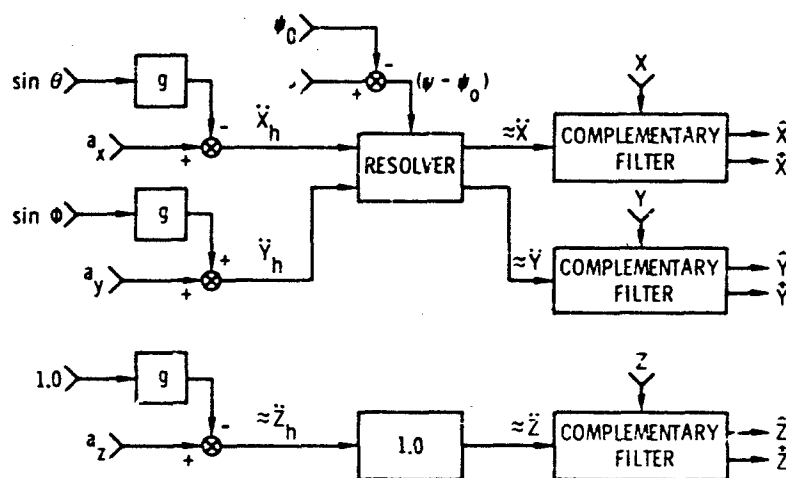
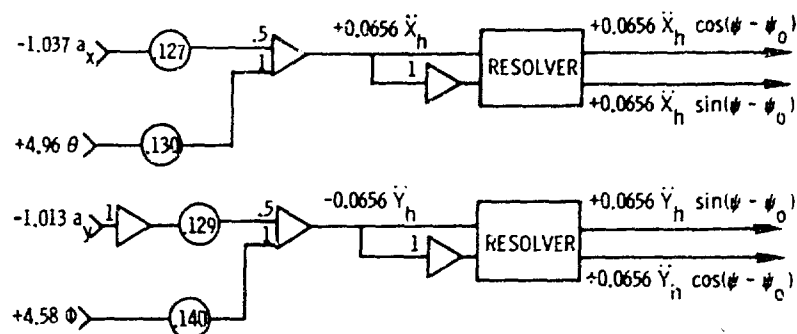
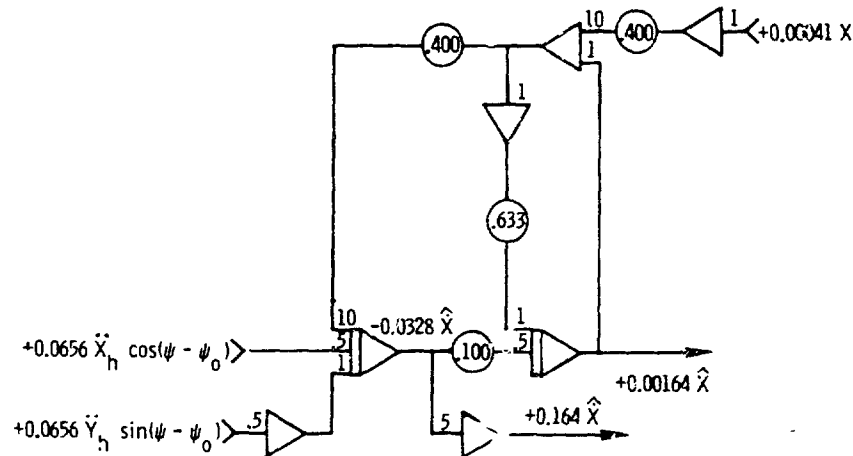


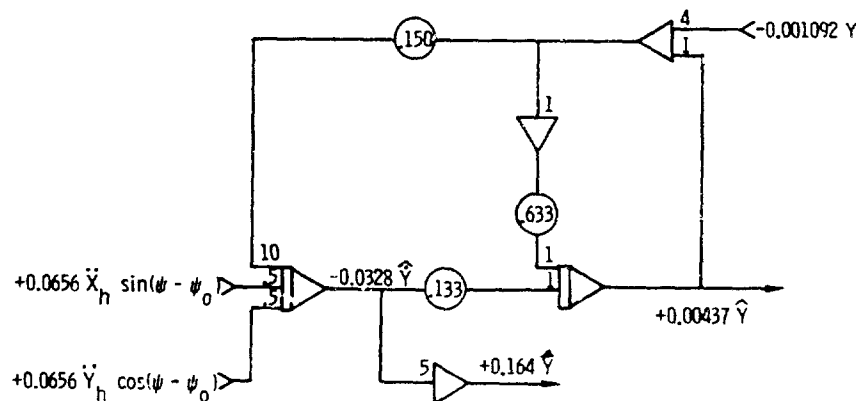
Figure 9. Complementary filtering navigation system computations.



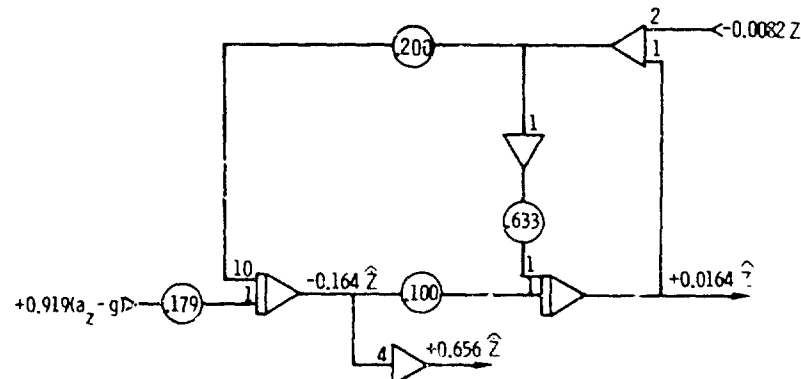
(a) Gravity correction and heading resolver.



(b) Complementary filter for X-axis.



(c) Complementary filter for Y-axis.



(d) Complementary filter for Z-axis.

Figure 10. Analog computer schematic for complementary filtering system. Where a signal value is expressed, the number preceding the symbol indicates the scale factor, in volts per SI Unit.

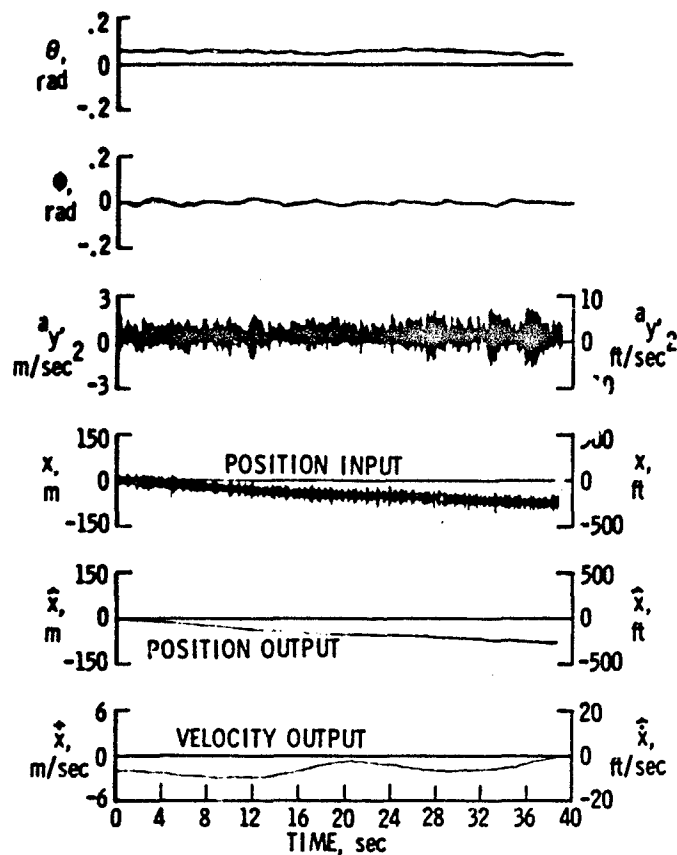


Figure 11. Complementary filtering system input and output signal noise characteristics, X. (Note that  $a_x$  was not recorded.)

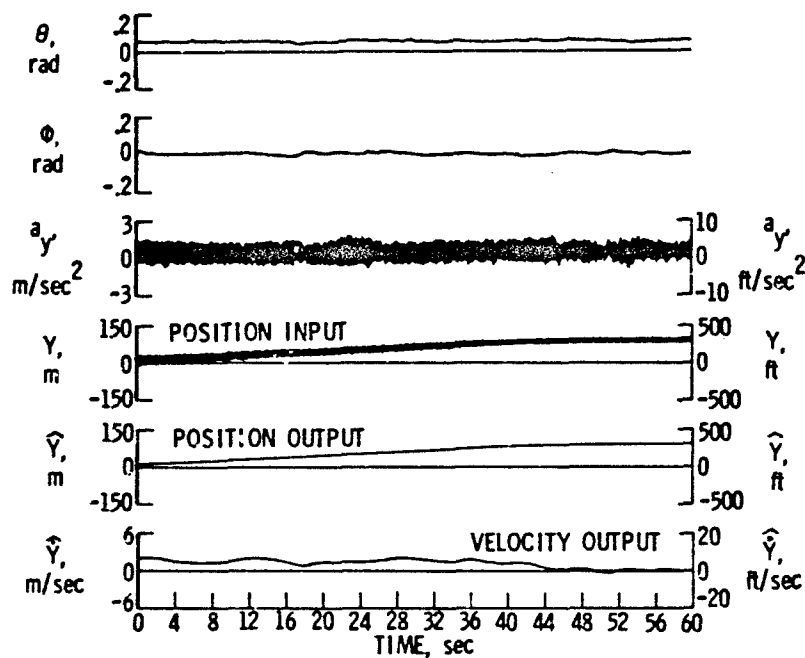


Figure 12. Complementary filtering system input and output signal noise characteristics, Y. (Note that  $a_x$  was not recorded.)

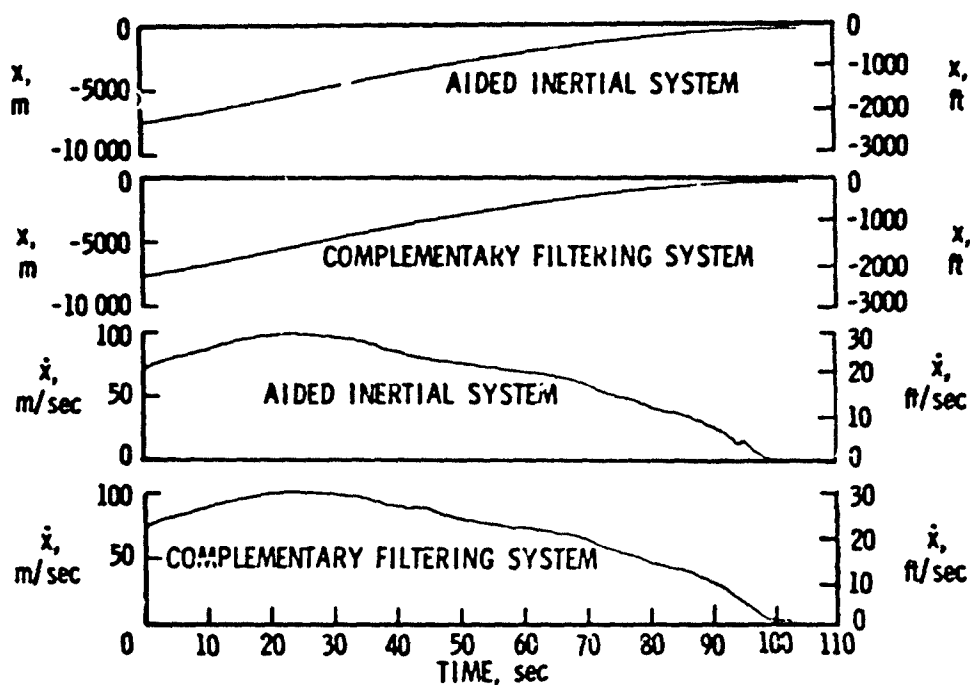


Figure 13. Comparison of complementary filtering system and an aided inertial navigation system. Decelerating approach.

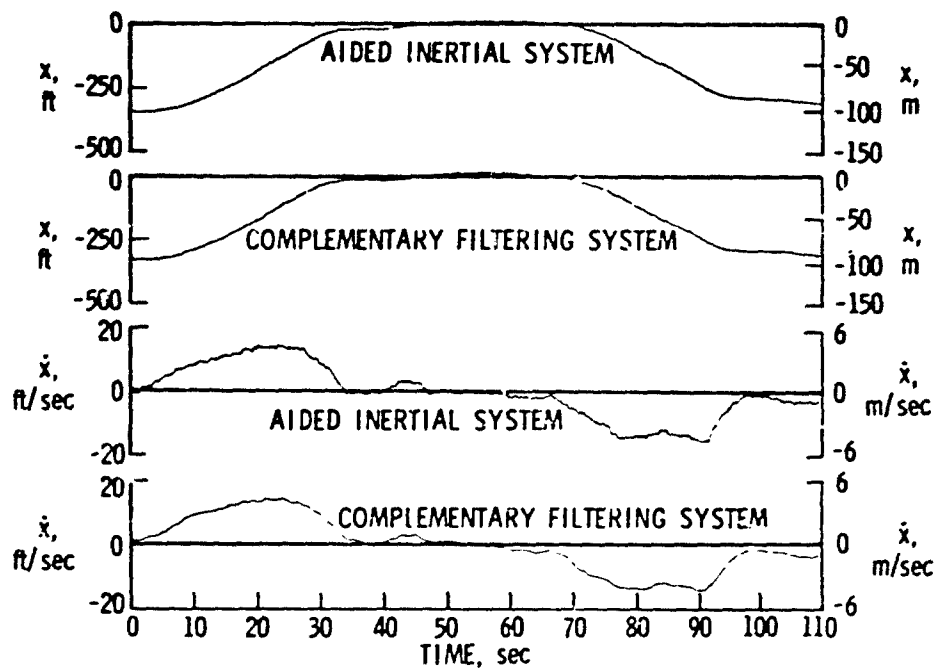


Figure 14. Comparison of complementary filtering system and an aided inertial navigation system. Hovering flight.

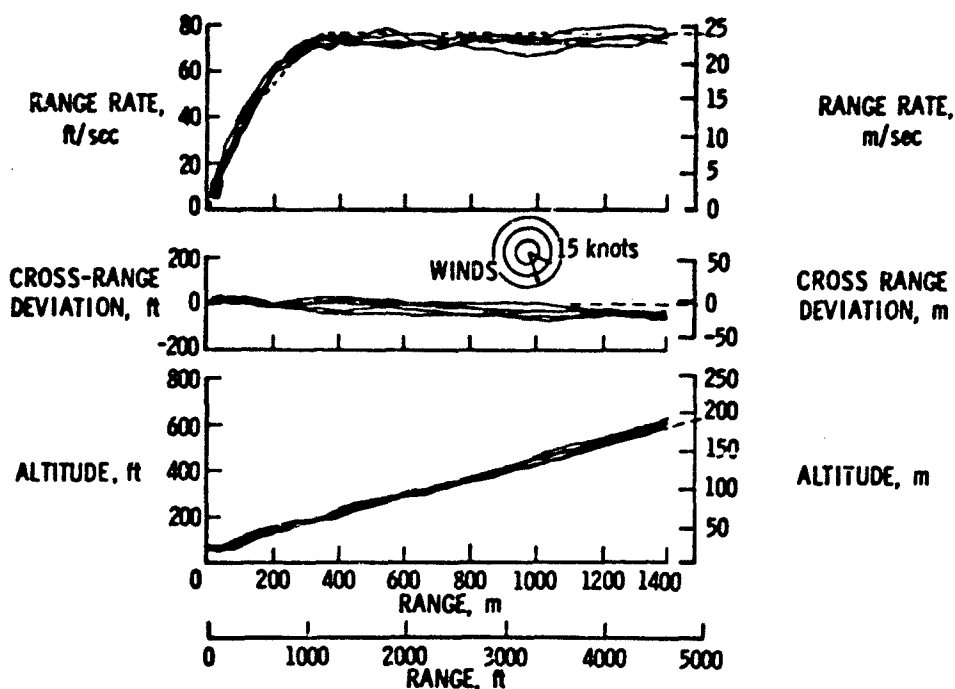


Figure 15. Tracking performance for manual decelerating approaches along a 6° glide path. Dashed lines indicate desired track.

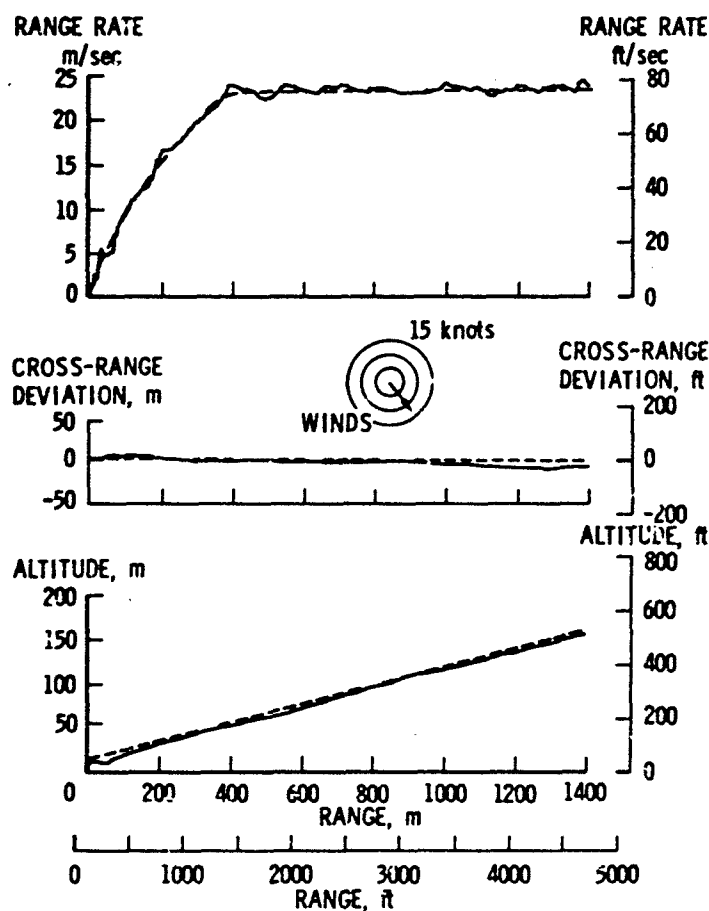


Figure 16. Tracking performance for automatic decelerating approaches along a 6° glide path. Dashed lines indicate desired track.

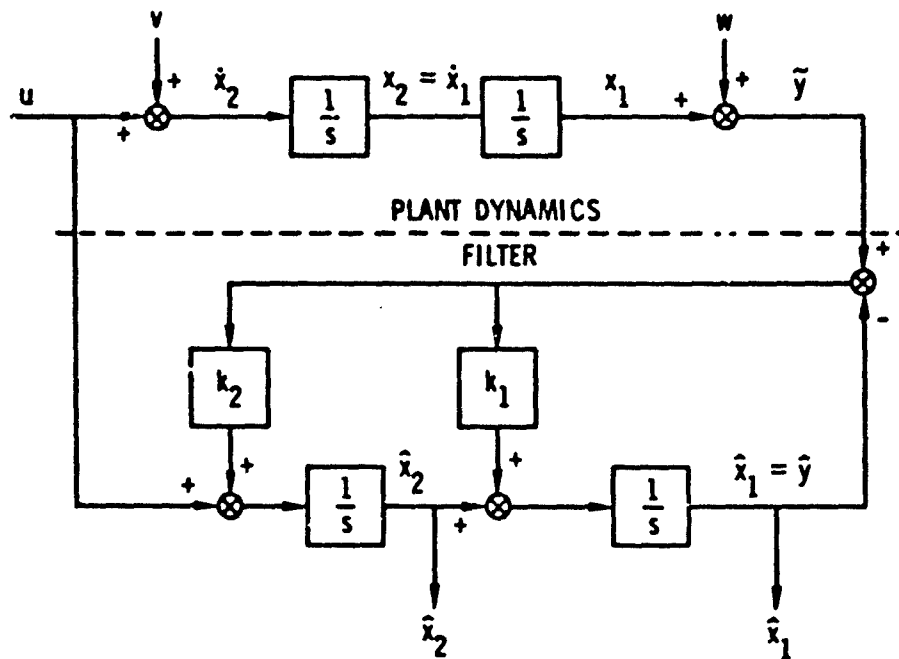


Figure 17. State variable representation of the complementary filtering estimation problem.

# SENSORS AND FILTERING TECHNIQUES FOR FLIGHT TESTING THE VAK 191 AND VFW 614 AIRCRAFT

By  
Dr. Werner E. Seibold  
VFW-Fokker GmbH  
28 Bremen 1, Hünefeldstr. 1-5

## 1.0 SUMMARY

The flow of the flight test data of the VFW 614 (Fig 1-1 and VAK 191B (Fig 1-2) Aircraft from the sensor through the data acquisition, selection and preprocessing process is described in general. An overview over the sensors included in the VFW 614 is given. Two important sensors for Take Off and Landing performance are described. The data smoothing and filtering techniques are discussed whereby special emphasis is given to a new simple and powerful digital filter, the Si or "Riedel filter".

### List of Symbols

$f_1$  input or raw data stream (time history)  
 $f_2$  output or smoothed data stream (time history)  
 $t$  current time  
 $t_0$  centre-time of integration interval  
 $T$  length of integration interval  
 $W$  frequency of weight function (Si-filter)

## 2.0 INTRODUCTION

### 2.1 GENERAL REMARKS

The methods and techniques described in this paper have been developed to solve the following two problems:

- Get a VTOL aircraft vertically off the ground and through the transition to normal airborne flight, and
- Get the certification for a commercial aircraft.

Both aims do not ask for high sophisticated methods to get extreme accuracy but they ask for reasonable and cheap methods to get millions of data processed and reduced. Therefore a lot of effort was spent to get a well defined and efficient overall system. The design goal was to present the required results in final graphical form within 24 hours after flight. In case of critical tests such as stall, only two hours were available for the whole process. Both goals could be achieved by the system and method described below. The aircrafts to which these methods are applied are the VFW 614, a short haul commercial aircraft shown in Figure 1-1 and the VAK 191B, an experimental vertical take-off and landing aircraft, shown in Figure 1-2.

### 2.2 The VFW-Fokker Flight Test Data Acquisition and Processing System - An Overview

The overall data flow can be subdivided into the four major steps: (Fig 2-1)

- Data acquisition, recording and/or transmitting (onboard)
- Telemetry reception or tape playback, quick look data formatting and data selection plus digital tape formatting in the telemetry ground station.
- Data preprocessing, reduction and final output formatting in the computation lab.
- Data and result analysis by engineers and scientists. Figure 2-1 shows these steps in a schematic manner.

This picture only shows the flow of the main data. It does not show the flow of support data such as

- o Channel identification
- o Calibration data

which are of utmost importance to get reasonable data out at all. The four steps mentioned above are in more detail described as follows:

Step I. (In order to describe a typical VFW data acquisition system the VAK 191B System diagram (Figure 2-2) shall be used. The FVW 614 is very similar.)

As you can see, it is subdivided into an FM and a PCM system. The PCM system has normally a sample frequency of 40, 50 or 60 cycles. (50 in case of VAK, 40 and 60 in case of VFW 614) and can therefore easily be used for signal frequencies up to 10 Hz. Super-commutation is possible to double the frequency but it was never really used. Higher frequencies up to the same kHz such as flutter and jet engine vibration are handled by the FM system. The basic philosophy was to use the PCM system as far as possible and to use the FM system only as an exception to cover the frequencies mentioned above. The VAK system has 9 data bits per word (10 for VFW 614). In both aircrafts (VAK 191B and VFW 614) more than 450 sensors are installed, out of which 250 can be recorded or transmitted by the corresponding PCM onboard system. In case of the VAK 191B for instance, the FM system provides 10 channels with subcarrier oscillators of the proportional and constant bandwidth type. The resolution is 0.5% for the PCM and 2...3% for the FM system.



**Step II. The Telemetry Ground station which provides for:**

- o Telemetry signal reception and recording
- o Tape playback
- o Data formatting for quick look
- o Data selection and formatting of digital tape
- o Generation and updating of calibration data base (disk)

is equipped as shown in Figure 2-3. The whole station is mobile and it was used in several places where it produced for the flight test crew on-line graphical time histories (generated by means of the 8-channel brush recorders) and on-line data tables where the data are shown in engineering units together with time and event counter information (generated real time by means of the line printer which is driven by the data preprocessing computer which in turn gets the data real time from the data handler).

**Step III.**

The data preprocessing, reduction and final output formatting is done by means of a big general purpose computer (CDC 6500) to which a graphical display and a microfilm recorder are hooked up (Fig 2-4). These two devices plus the standard line printers provide us with the capability to edit and output data in a way directly usable for engineering analysis and reports. Examples of this will be shown later on. The overall functions we have to perform are:

- o Provide the flight test engineering with
  - a) Data readouts in tabular or graphical form which needs no or only very limited editorial work.
  - b) A "plug-in-capability" so that his special (scientific) computer programs can interface easily with the data stream. This means that his program has to have access to the measurement data and in previous steps generated results in whatever sampling rate and engineering units he wants, and in addition he can feed back his own results into the system for final output formatting or further processing.

In both cases the user assumes that general functions such as

- o data storage and retrieval
- o calibration (in the units he wants)
- o smoothing and filtering are performed by the system.

Figure 2-4 shows the various S/W packages and their major modules through which the flight test data can be processed. Especially the very right one shall be mentioned which has all the capabilities for an integrated flight test data reduction process, whereas the other ones are specialized to do specific and very often needed functions with the highest efficiency possible which never can be reached by a generalized system. The generalized system is called Flight Test Monitor (FTMT) or Data Pool alternatively, because it provides

- a) a monitor routine which can be asked by means of user provided control cards to load and execute user or service modules provided by the system in whatever sequence the user wants, and
- b) retrieves the input data required out of a data pool and stores the output data provided back into it. The data pool consists essentially of random access disk files. The user level "addressing" is done by symbolic parameter identifier and the "elapsed test time". The user also specifies the time increment by which he wants to proceed and the engineering units in which the input data has to be delivered or the output data are provided. By means of a transformation table the proper conversion factor can be defined. By this the user can process the data in whatever units he likes to without any harm or restrictions for pre- or postprocessors. A data compression method is used in order to minimize storage requirements and the time needed for input/output operations. A series of test runs with real flight test data was made in order to find the best compression method. A zero order extrapolator was found to be the most efficient one in terms of reduction factor achieved and processing time required. The tests were based on a study of DFVLR Braunschweig. The achievable reduction factor depends very much on the specified amplitude tolerance which in turn defines the final accuracy. In order to get an optimum between efficiency and accuracy the tolerance can be defined for each channel separately.

**Step IV.**

The final analysis and judgment of the results is of course done by the engineers and scientists who, however, can use the Flight Test Monitor mentioned above for further iterations and in order to gain better understanding of their problems. For instance the very last Figure (Figure 4-16) was generated by means of the FTMT running the steps shown in Figure 2-5.

**3.0 SENSORS****3.1 GENERAL OVERVIEW**

Besides a few special sensors, we used fairly normal sensors and transducers for the different measurement problems which are described below for the VFW 614 especially.

- o Rudder and Tail positioning  
Inductive angle sensor ID 36/45 E (was introduced with respect to flutter investigations).
- o All other "position sensors"  
Film potentiometer C10 155
- o Hydraulic pressures  
Pressure sensors with built in amplifier CEC 493 for prototype No. 1. They were replaced due to money reasons by the type Statham PA-822 (5000 psia, 1000 psia).
- o Air pressures for environmental control system:  
CEC 4-325/Statham PA-822. On pressure 15 psi: PL 283TC, P196, P192 TC and P15TC. They are very sensitive with respect to accelerations and can only be used in stationary a/c status.
- o Throughput: for fuel and hydraulic system  
Cux - turbine - flow meter (output signals have to be transformed to DC voltage which is done by a frequency transformer Typ V224 Fa. Braun Stuttgart).

- Temperatures:
    - Resistor thermometers PT 100 (Hereaus, Hanau)
    - Thermo elements CR/AL used for many purposes in
      - o Hydraulic
      - o Fuel
      - o Environmental control subsystems
  - Accelerometers
    - Types: CEC 4-202 and Statham A69 TC
    - Ranges:  $\pm 5$  g,  $\pm 10$  g,  $\pm 25$  g and  $\pm 50$  g
    - Used in: Fuselage, wings, rudders, engine pylon, gear
  - Jet engine sensors
    - Provided by Rolls Royce
    - Pressures: SE 40, SE 42 (SE Laboratories).
    - Temperatures: Pt 100 and thermoelements CR/Al
  - Speed and Altitude (Static and Total Pressure)
    - Nose boom for static and total pressure (self adjusting). Normal (series) pitot sensor and static holes.
    - For better static pressure: Trailing cone (System Douglas) Trailing bomb (System NLR)
- These systems were used depending on the purpose of a specific test.
- Altitude: Transducers: Rosemount, Typ 840E, and for low altitude Type 1241
- speed: Rosemount Type 831 BD and for low speed PM 51C (Statham, up to 150 kts.)
- Forces
    - Strain gauges
  - Attitude
    - Gyros
  - Optical Information
    - TV and other cameras are used to get optical information about stall behaviour, water splash tests, etc.

### 3.2 SPECIAL SENSORS

The two special sensors which shall be described herein are the Nose Camera and the Inertial Gyro Platform. Both were used first of all in order to obtain take-off and landing performance data. The principle of the nose camera is to take pictures of the runway at rather high frequency (5 per second). The known geometrical relationships between either special or normal markings (lights) along the runway on the one hand and their appearance in the pictures taken by the camera on the other hand allow for calculation of the trajectory and attitude of the aircraft. The time distances between sequential pictures allow for calculation of speeds and accelerations. The method is proven and allows for rather high accuracy, however, it is extremely tedious and cumbersome compared to PCM data because film development and data readout requires special devices and lengthy manual processes. Quick look and corresponding go/no-go decisions for specific tests cannot at all be provided by this method. In order to do this and herewith to increase the efficiency of flight testing the VFW 614 especially at remote test bases the Inertial Gyro Platform was installed. It is shown in Figure 3-1 in its general layout. By means of this device all data necessary for the task mentioned above can be acquired and transmitted to the Telemetry Ground Station, for quick look purposes. The platform basically measures accelerations, which by means of analog integrators can be transformed into speed and length (distance) informations. The problem is the accuracy of the acceleration measurements and the integration process which up to now restricts the applicability of the platform to quick look purposes. There is no doubt that further development to sufficient accuracy will increase the efficiency of take-off and landing as well as noise investigation tests considerably. Figure 3-2 shows results of the platform.

### 4.0 SMOOTHING AND FILTERING - PROBLEMS AND TECHNIQUES

The filtering techniques which are described below are based on the PCM data stream rather than on the FM data stream (see Figure 2-2). (Problems like nonlinearities and offsets in sensor or amplifier outputs are not dealt with in this chapter because they are of static nature and corrected by means of data calibration techniques.) We identified in this data stream basically four different types of dynamic "trouble-makers":

- o Spikes
- o Noise
- o Gap in data stream
- o Dynamic components in signals being expected to be stationary

as they are shown in Figure 4-1.

#### 4.1 Methods

One can basically think of two different ways to get rid of these problems:

- A) use of hardware filters
- B) use of software filters

VFW-Fokker did not make any considerable use of hardware filters onboard of the aircrafts due to increased complexity of the board equipment in the first place. In spite of that the philosophy was to sample and record the data at fairly high rates (40-60 Hz) which gives a lot of built-in redundancy because the normal sensors sampled via the PCM system do not have considerably more than .5 to 5 Hz signal frequency. That says in other words that the smoothing and filtering task is done by software during data selection and preprocessing rather than by onboard hardware. We investigated several algorithms to do this filtering with the basic objectives that

- o the effort to implement the algorithm
  - o the effort or cost to make day to day use of it for millions of data
- and

can be covered within aircraft testing time and budget constraints.

The algorithms we investigated within this framework are the following:

- A) Normal averaging - Sum over  $N$  consecutive samples divided by  $N$ , the next sum starts with the first sample not used by the previous one (Step Size  $3N$ ), Number of output samples reduced by factors of  $N$ .  
Expressed in integral form it is:

$$f_2(t) = \frac{1}{T} \int_{t_0 - \frac{1}{2}T}^{t_0 + \frac{1}{2}T} f_1(t) dt ; t_0 = \frac{1}{2}T, \frac{3}{2}T, \frac{5}{2}T, \dots$$

- B) Gliding Average --- As above but the next sum starts with second sample of the previous one, number of output samples = number of inputs samples.  
The formula is:

$$f_2(t) = \frac{1}{T} \int_{t_0 - \frac{1}{2}T}^{t_0 + \frac{1}{2}T} f_1(t) dt ; t_0 = \frac{1}{2}T, \frac{1}{2}T + dt, \frac{1}{2}T + 2dt, \dots$$

This method is well known and in common use because it is very simple and cheap. Its main disadvantage is its poor frequency response.

- C) Si-function -- As B, but the sum is done with weighted samples.  
The weight function is  $Si(x) = \frac{\sin x}{x}$  (proposed by Dr. Riedel)  
The formula is:

$$f_2(t) = \frac{1}{\int_{t_0 - \frac{1}{2}T}^{t_0 + \frac{1}{2}T} \frac{\sin(\omega t)}{\omega t} dt} \int_{t_0 - \frac{1}{2}T}^{t_0 + \frac{1}{2}T} \frac{\sin(\omega t)}{\omega t} \cdot f_1(t) dt ; t_0 = \frac{1}{2}T, \frac{1}{2}T + dt, \frac{1}{2}T + 2dt, \dots$$

This method is very promising because it allows to exactly define the characteristics of the filter in terms of frequency and phase response, which is possible through proper selection of  $\omega$  (upper frequency limit) and  $T$  (integration interval). The longer  $T$  is selected the better the filter characteristics are. In addition the method is - from the programming and execution time point of view - efficient enough to be used for a reasonable amount of data. (For examples see figures 4-2 to 4-8. The phase error which appears on the time histories can be corrected because it depends only on the frequency limit and not on the signal frequency.)

- D) Gliding least square fit method -- For a restricted number of consecutive samples (set) the least square fit method is used. (The first sample of the next set is the second one of the first set.) This method seems to be promising too but  
  - o the filter characteristics are hard to define
  - o the computational effort is far beyond that of the Si-filter.
 (For examples see figures 4-9 to 4-12).

E) In addition to those filters, we used "valve type filters" for several cases such as  
 (a) spike recovery, and (b) exclusion of dynamic components in stationary data.  
 This method is basically the same in both cases which is to delete those data totally or replace them by artificial ones, which exceed certain limits. The only difference between the two methods is, that in case of spike recovery, the limits are derived from the time history of the channel itself, whereas in the second case another channel opens or closes the "software valve." For instance in case of steady data for flight mechanics all data have to be deleted or disregarded when the g-load exceeds  $1 \pm 0.005g$ . This method is under certain circumstances very useful and it is extremely cheap.

#### 4.2 Application

We investigated the Si-function and the gliding least square fit method theoretically to some extent and concluded out of the results that the Si-function is the more promising one. We integrated this method together with the standard average and the gliding average in the integrated data reduction system and used it especially for speed and altitude filtering for the VFW 614. As you may know, the transformation from Indicated Air Speed (IAS) via Calibrated Air Speed (CAS) to True Air Speed (TAS) requires derivatives of speed and altitude which is numerically very difficult when the signal is too noisy. We got good results with a reasonable effort as soon as we turned down the upper frequency limit to less than 1 Hz (Figure 4-14 and 4-15). We used the "software valve" or "separation" method to get steady lift coefficient vs. angle of attack out of stall test for instance. We calculated both valves over the corresponding time but used only those for which the g-load was within specified limits ( $1 \pm 0.005g$ ). The results are shown in the last two slides. (Fig 4-16, Fig 4-17). An even better picture can be achieved by selecting a smaller bandwidth.

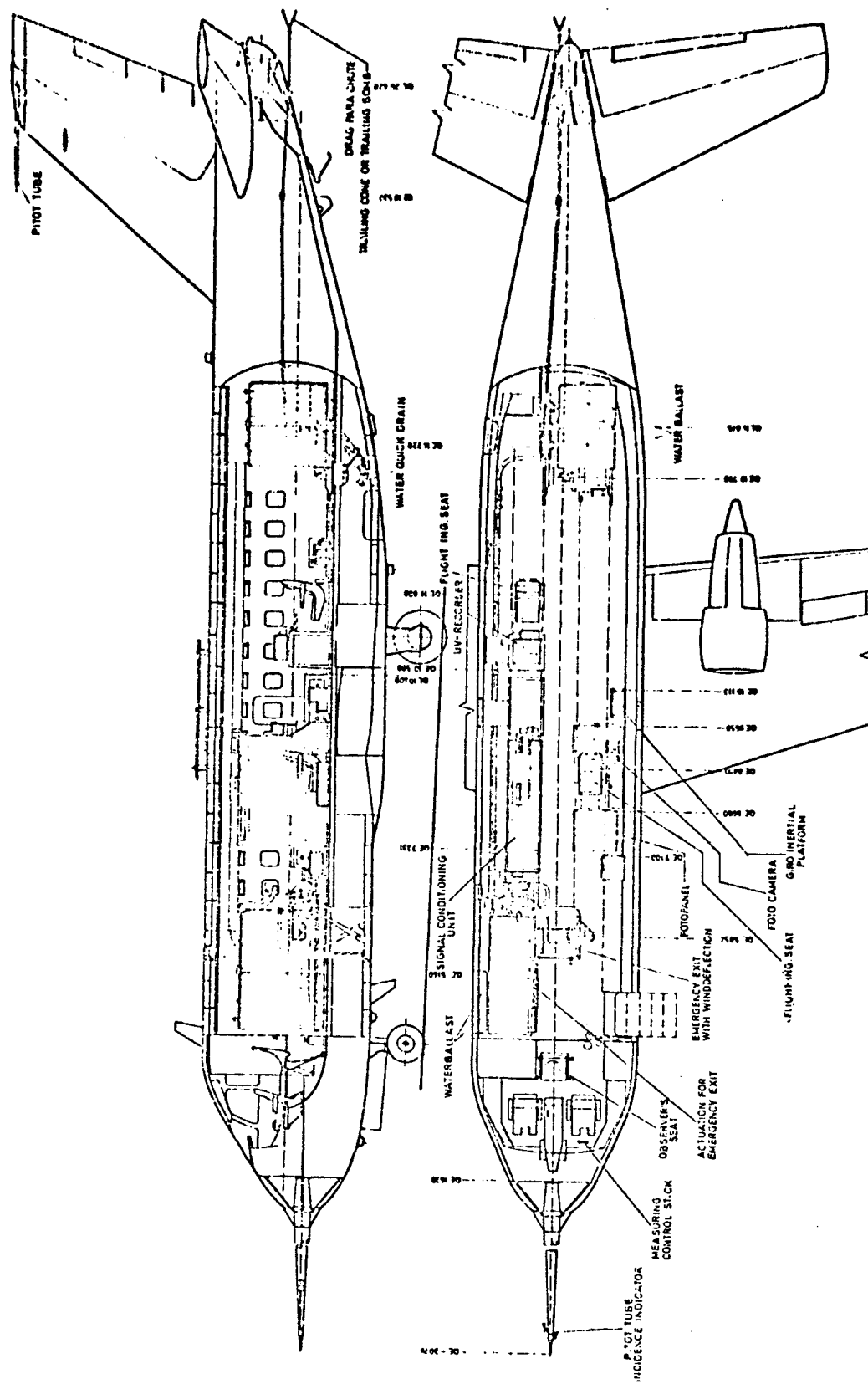


Fig.1-1 VFW 614 Prototype flight test equipment

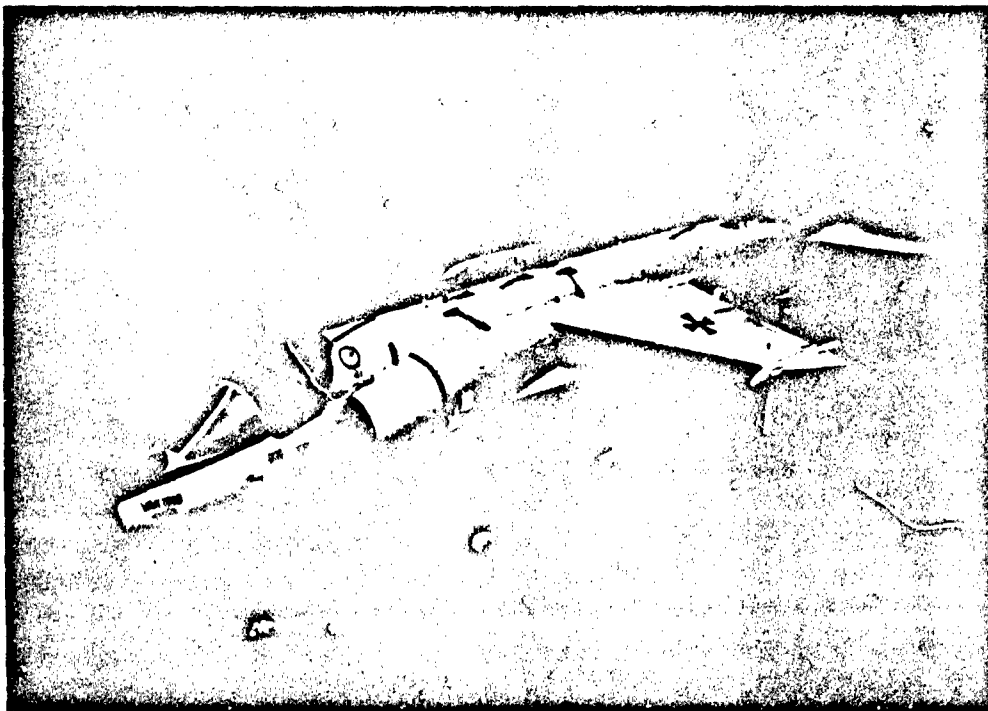


Fig.1-2 VAK 191 B

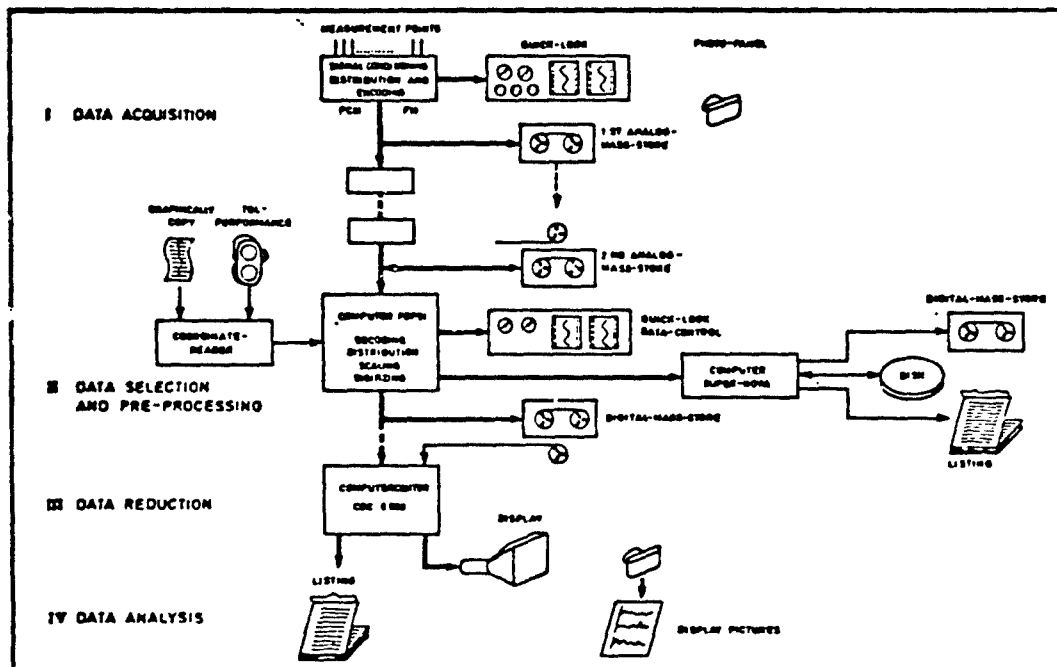


Fig.2-1 Flight test data. Acquisition and processing system

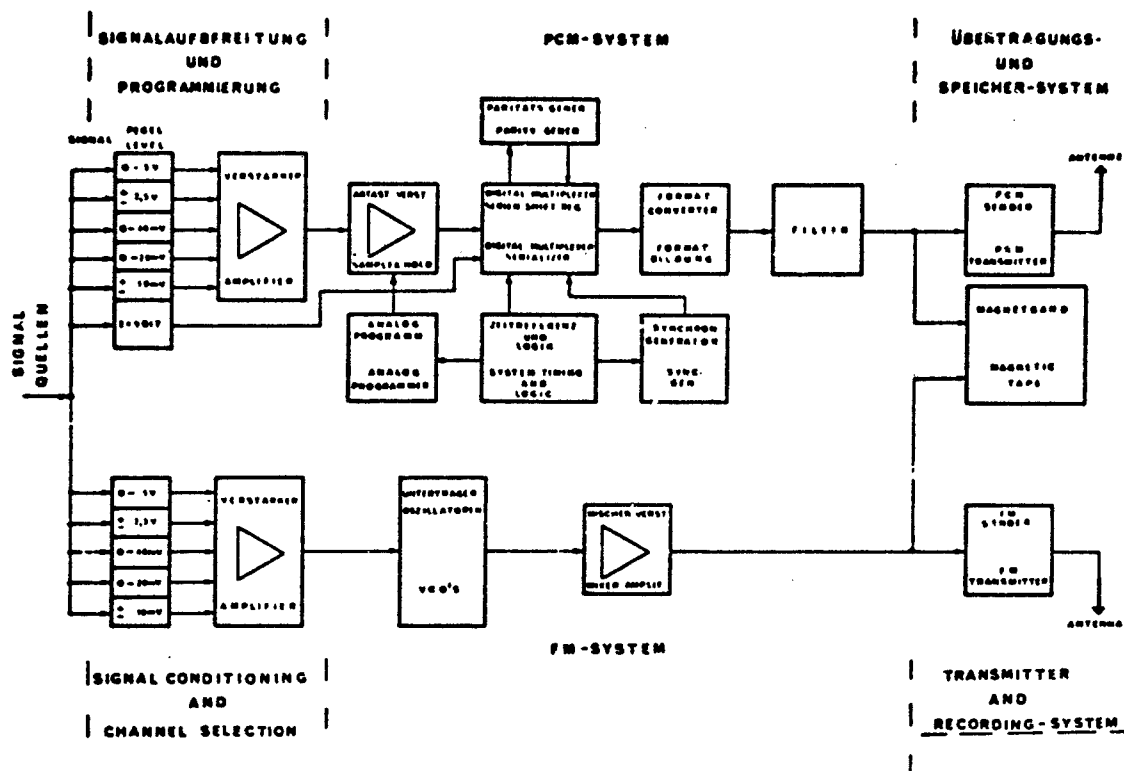


Fig.2-2 VAK 191 B Data acquisition system

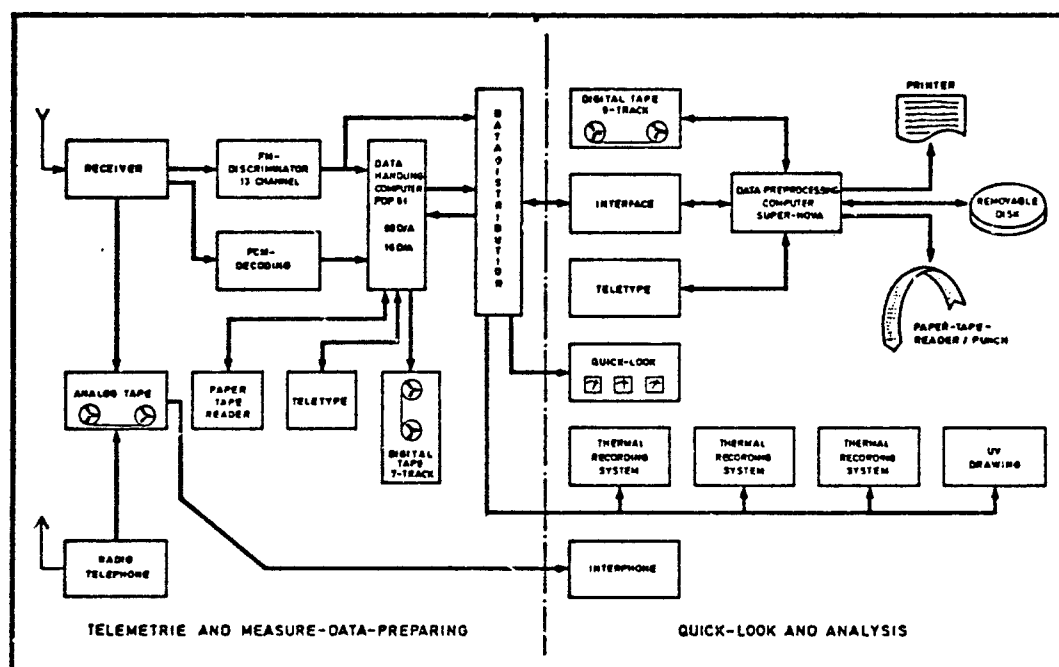


Fig.2-3 Mobile telemetristation

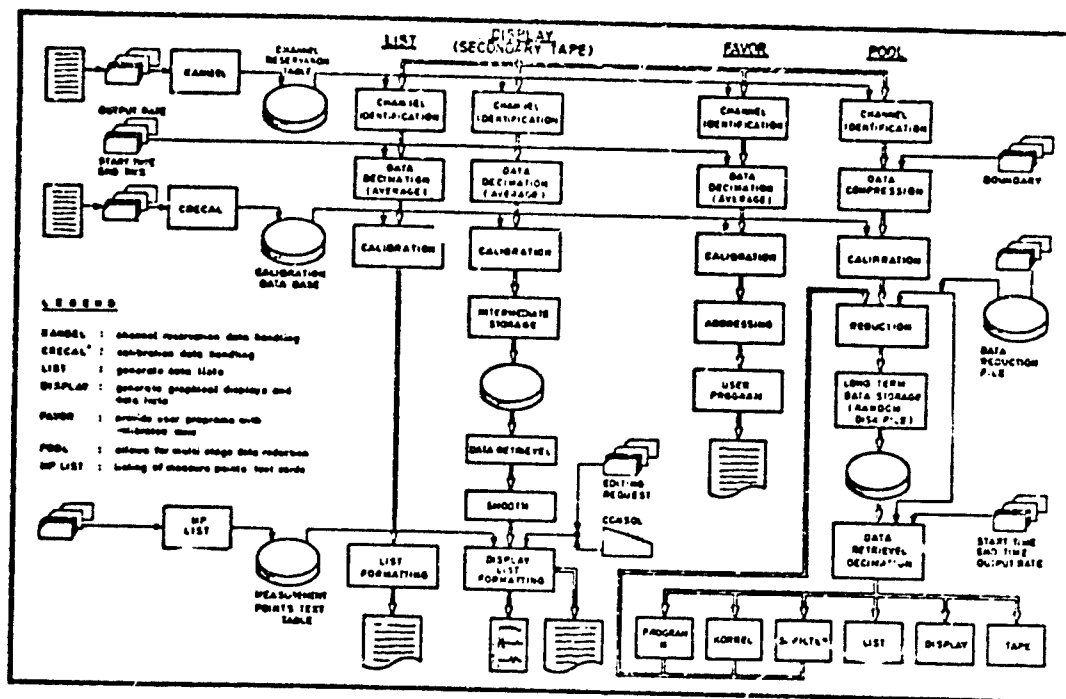


Fig. 2-4 Data preprocessing and reduction system

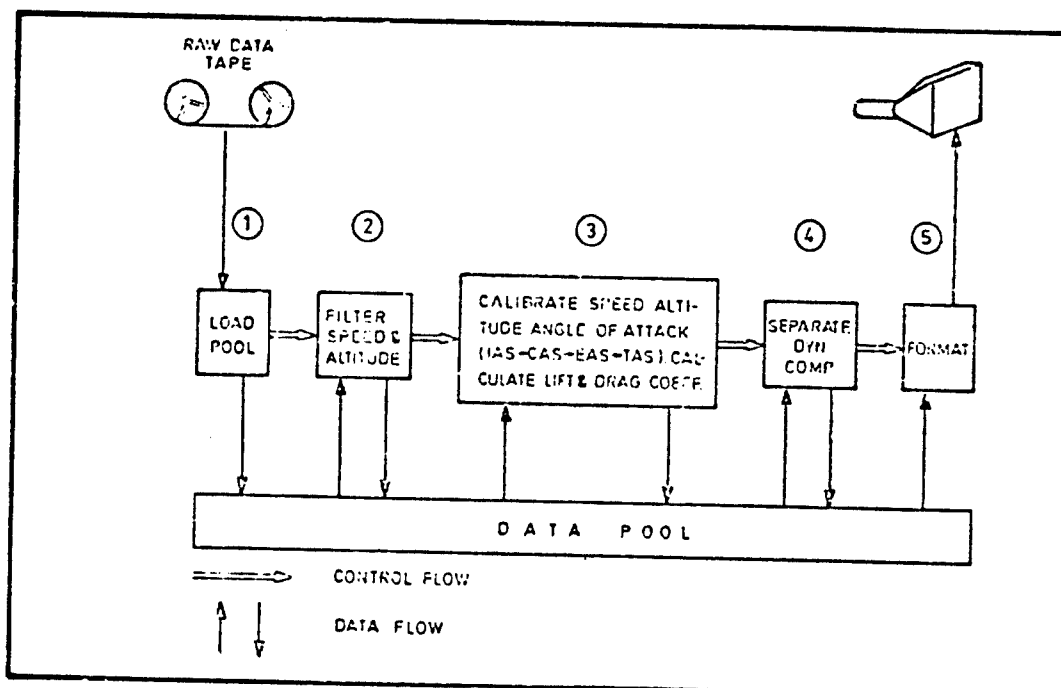


Fig. 2-5 Example for data processing by flight test monitor

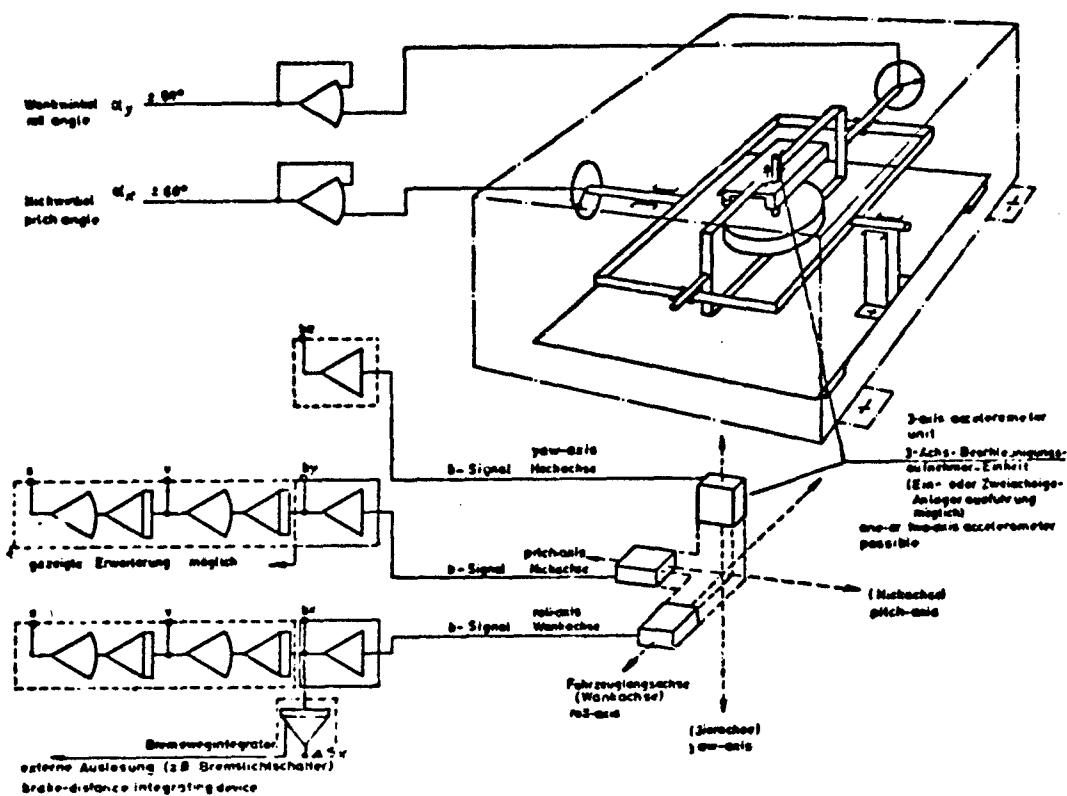


Fig.3-1 Gyro inertial platform

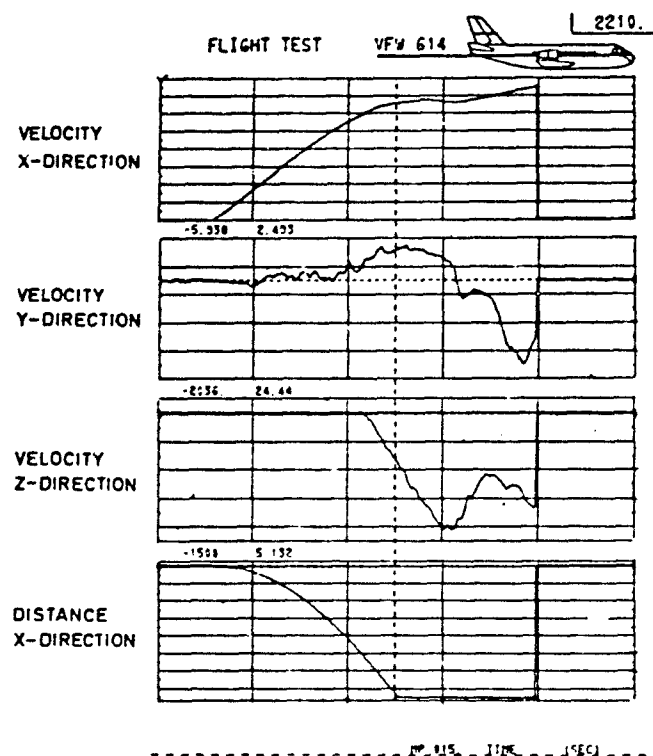


Fig.3-2 Platform results



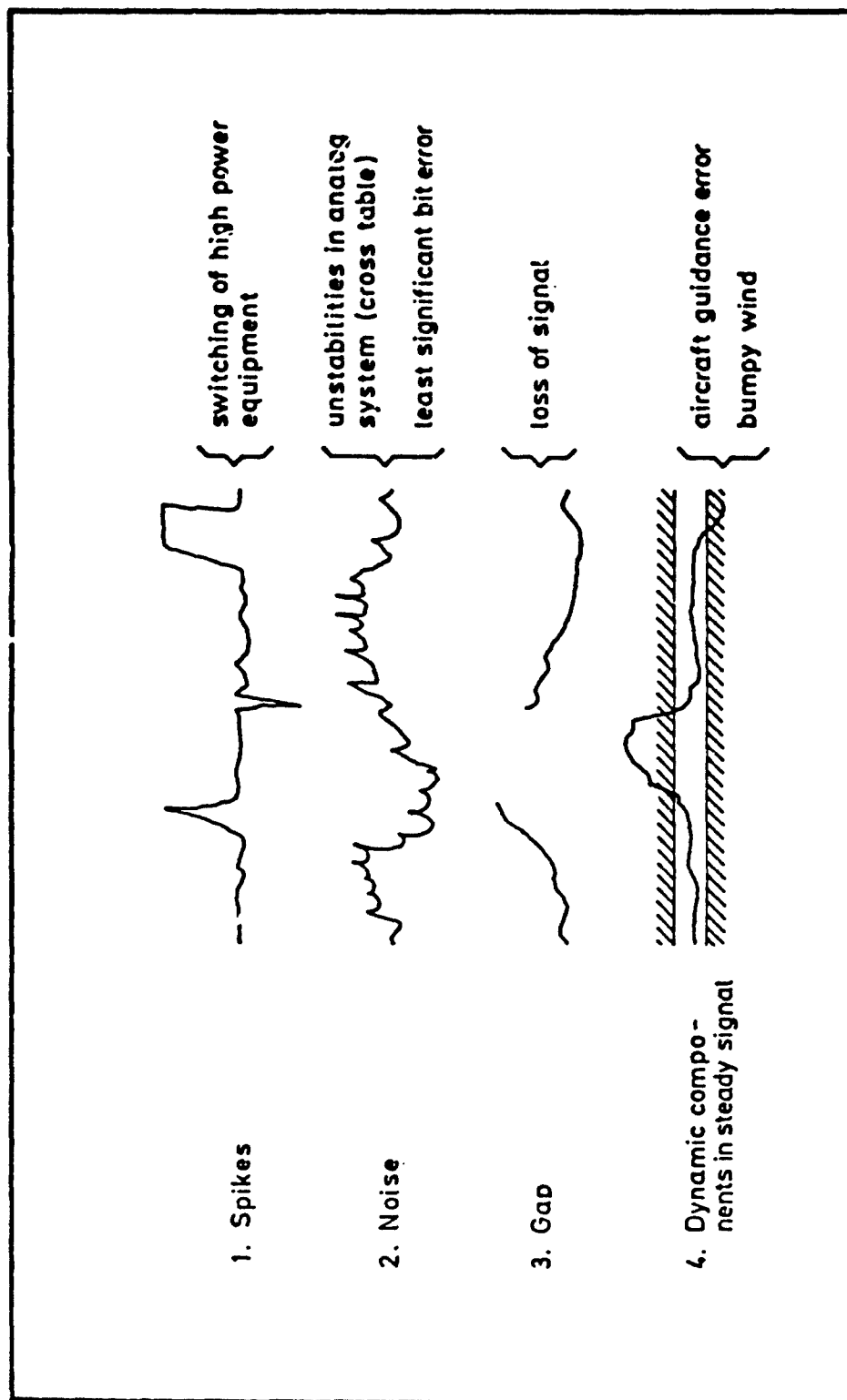


Fig. 4-1 Problem areas in PCM data stream

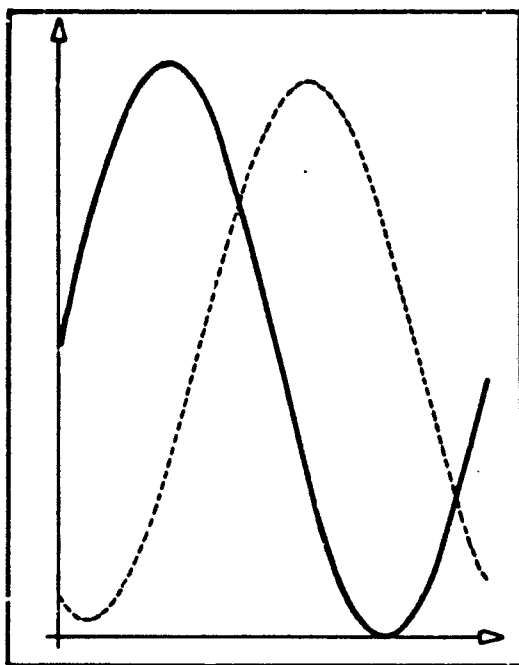


Fig. 4-2

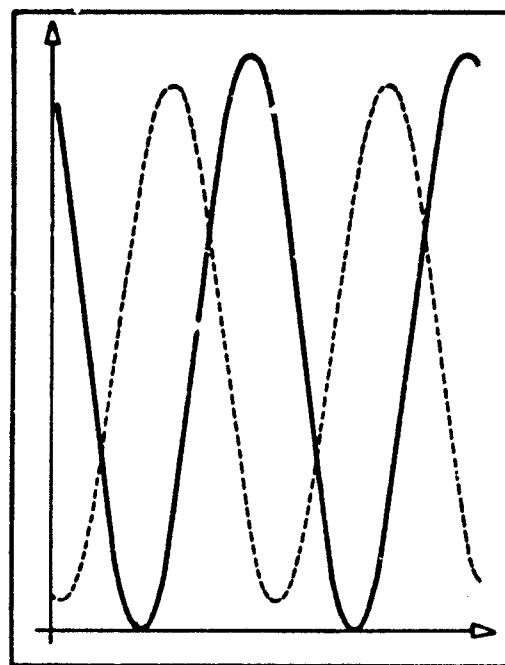
 $F = 1 \text{ Hz}$ 

Fig. 4-3

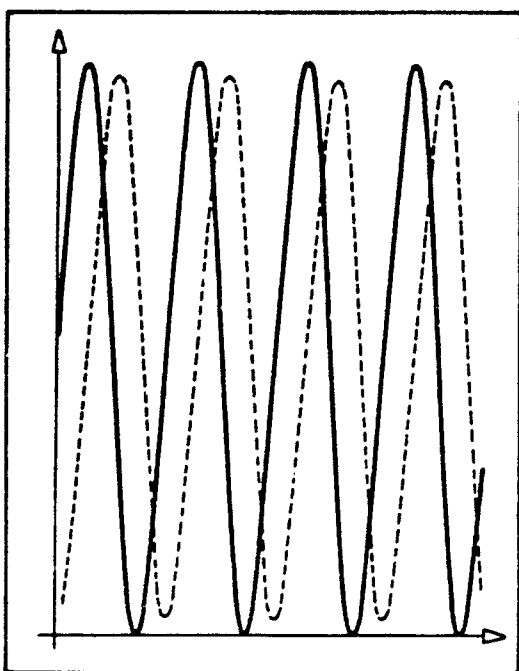
 $F = 2 \text{ Hz}$ 

Fig. 4-4

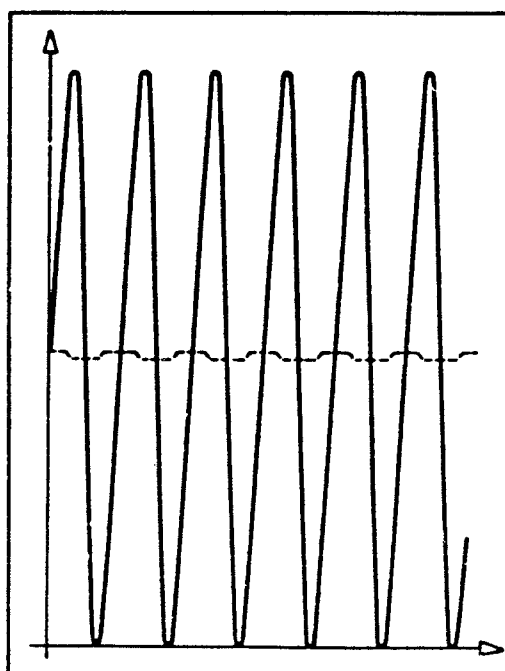
 $F = 4 \text{ Hz}$ 

Fig. 4-5

 $F = 6 \text{ Hz}$ 

## SI-FILTER — TIME HISTORY

UPPER FREQUENCY LIMIT: 5 Hz

NUMBER OF PERIODS : 3 Hz

—— INPUT  
 ---- OUTPUT

Figures 4-2 to 4-5

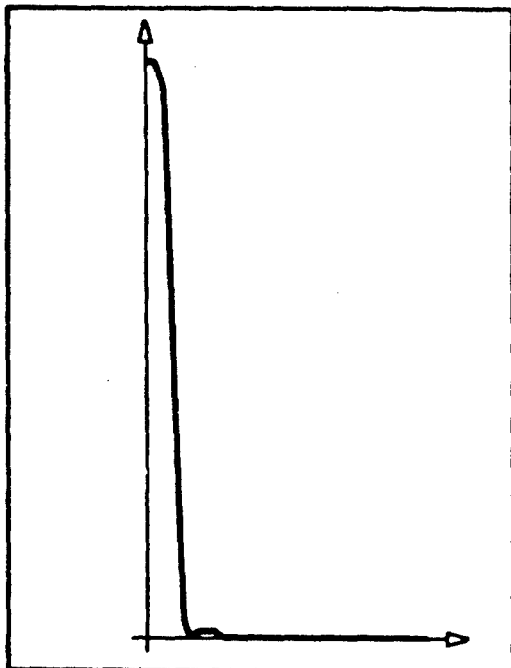


Fig. 4-6  
UPPER FREQUENCY LIMIT 5HZ

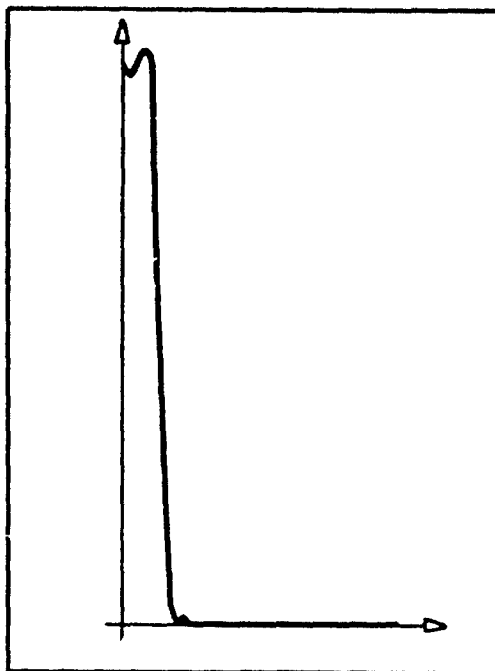


Fig. 4-7  
UPPER FREQUENCY LIMIT 6HZ

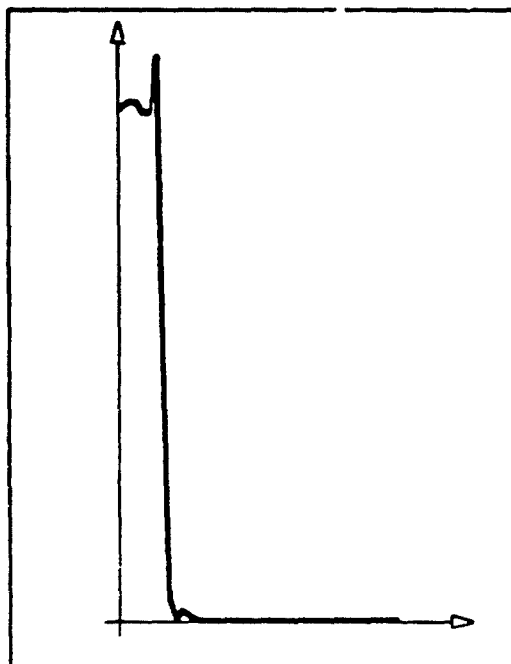


Fig. 4-8  
UPPER FREQUENCY LIMIT 7HZ

# Si-FILTER FREQUENCY RESPONSE

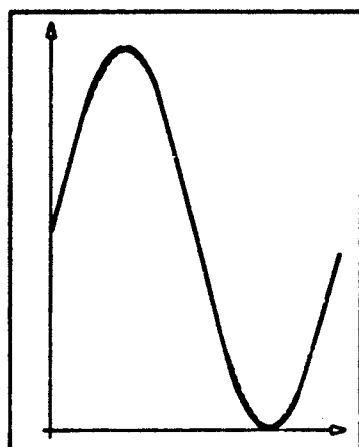


Fig. 4-9

F = 1HZ

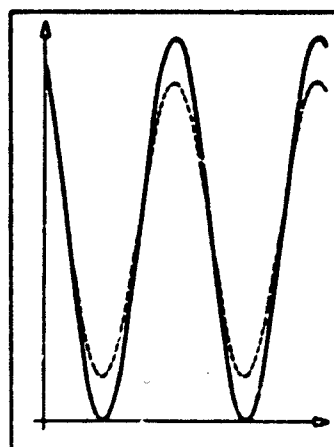


Fig. 4-10

F = 2HZ

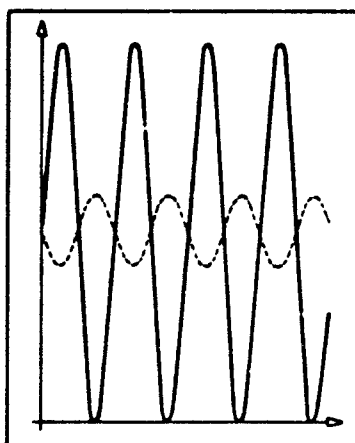


Fig. 4-11

F = 4HZ

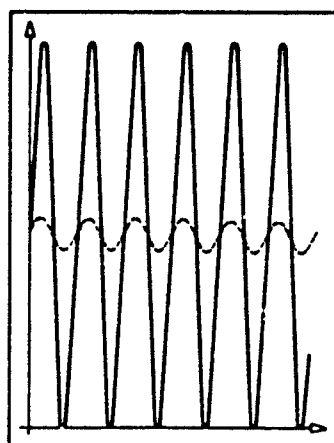


Fig. 4-12

F = 8HZ

## GLIDING LEAST SQUARE FIT

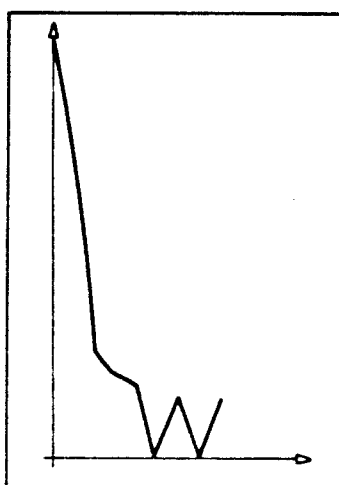
ORDER OF POLYNOMIAL : 2  
NUMBER OF SAMPLES : 30— INPUT  
--- OUTPUT

Fig. 4-13

GLIDING LEAST SQUARE FIT  
FREQUENCY RESPONSES

Figures 4-9 to 4-13

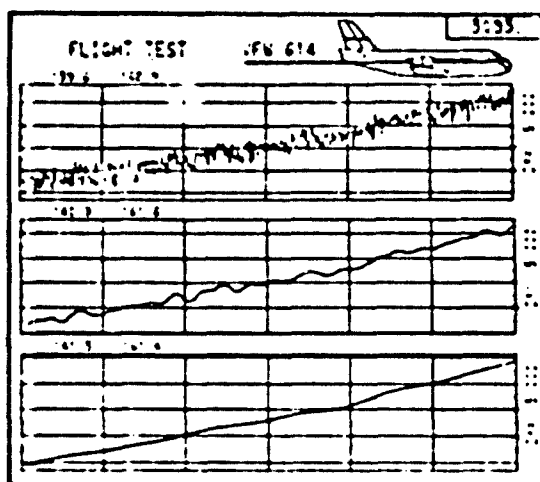


Fig. 4-14 EXAMPLES OF si FILTER APPLIED TO ALTITUDE MEASUREMENT

FREQUENCY LIMIT A.) 1 HZ  
B.) 0,25 HZ  
C.) 0,05 HZ

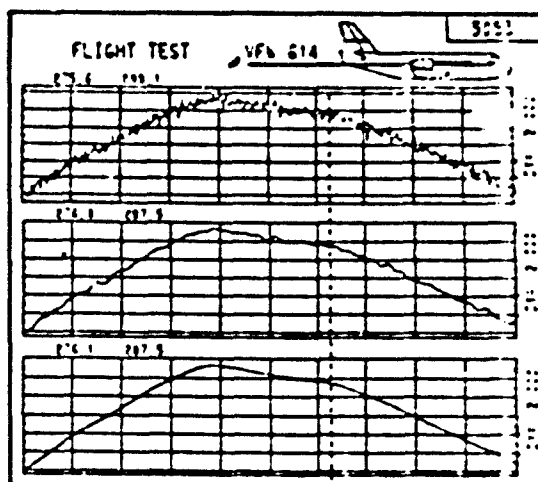


Fig. 4-15 EXAMPLES OF si FILTER APPLIED TO SPEED MEASUREMENT

FREQUENCY LIMIT A.) 1 HZ  
B.) 0,25 HZ  
C.) 0,05 HZ

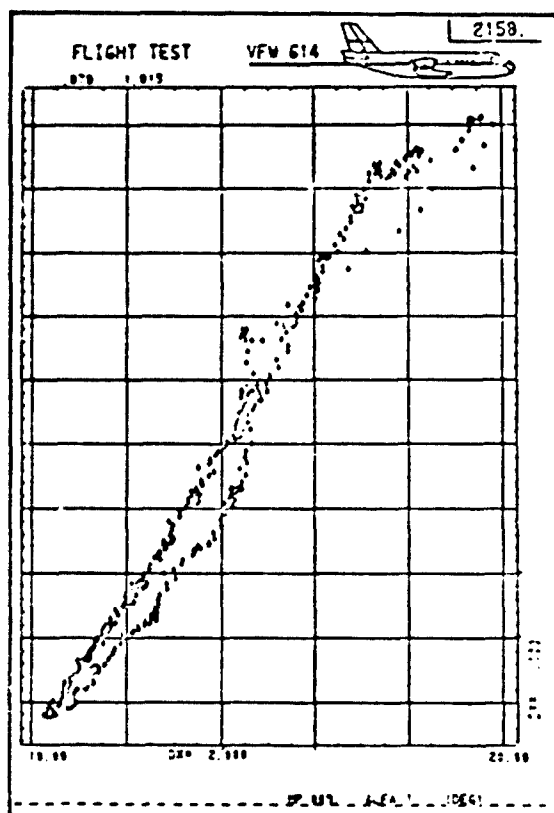


Fig. 4-16 CA VS& WITH DYNAMIC COMPONENTS

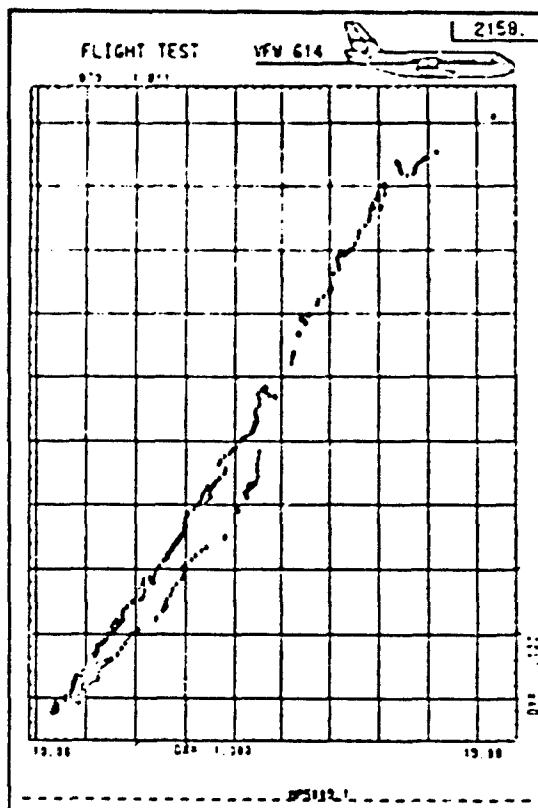


Fig. 4-17 CA VS& DYNAMIC COMPONENTS FILTERED THROUGH "SOFTWARE VALVE"

# DESIGN AND EVALUATION OF A SYMMETRIC FLIGHT-TEST MANOEUVRE FOR THE ESTIMATION OF LONGITUDINAL PERFORMANCE AND STABILITY AND CONTROL CHARACTERISTICS

by

H.W. Kleingeld  
NATIONAL AEROSPACE LABORATORY NLR  
Anthony Fokkerweg 2  
Amsterdam-1017  
The Netherlands

## SUMMARY

Performance and stability and control characteristics of aircraft can be estimated from measurements in one flight test manoeuvre. This requires the manoeuvre to contain quasi steady accelerating parts and non steady oscillating parts. The first element of the manoeuvre provides mainly information about aircraft performance, while the oscillating part yields information about stability and control derivatives.

A moving base simulator has been used to determine the problems which accompany the manual application of the required elevator control input and to teach the pilot to generate the signal without feedback. Results of this evaluation program are given and compared with corresponding results of the actual flight tests.

## 1. INTRODUCTION

The determination of performance or stability and control characteristics from non-stationary flight-tests has been subject of extensive research in the Netherlands. In 1964 a new dimension was added when a method was developed which made it possible to derive longitudinal performance and stability and control data for a large flight envelope from one relatively short manoeuvre (Ref. 1).

Between 1966 and 1968 flight-trials have been made on the DHC Beaver Laboratory aircraft of the Aeronautical Department of the Technological University of Delft to further develop this method for conventional aircraft.

The required characteristics of the above-mentioned manoeuvre and as a consequence the shape of the input signal to the elevator control has been analysed in references 1 and 2.

In the trials different kinds of input signals of various degree of complexity were applied and in the beginning a programmed autopilot was used to generate the correct signals. After much training it was also possible to apply the signals manually with a sufficient degree of repeatability.

In 1970 preparations started to further validate the method on an aircraft equipped with turbo jet propulsion. This type of aircraft was suitable to investigate e.g. compressibility effects and jet engine influence on performance and stability and control characteristics.

The Hawker Siddeley Hunter MK7 laboratory aircraft of the National Aerospace Laboratory in the Netherlands which was available and used for the trials, is a medium high-performance aircraft. It is equipped with special test equipment such as a trailing cone and a nose boom for accurate ambient static pressure measurements and pitot-static tubes in the jet exhaust pipe to enable engine thrust calculation. Four undervang pylons are provided for undervang fuel tanks. During the above-mentioned flight trials one of these positions was taken by an instrument container.

The Hunter project of which the flight trials have been flown between November 1973 and May 1974 can roughly be divided in the following parts:

- Instrumentation of the aircraft
- Preparation and execution of the flight trials
- Processing and analyses of the measured data.

The instrumentation system, which is a further development of the system used in the Beaver trials, is discussed in detail in reference 3.

Preliminary results of the analyses - the flight-path reconstruction in some of the manoeuvres - are given in reference 4.

The preparation and execution of the flight trials form the main part of this paper. In section 2 a qualitative motivation is given for the input signal to the elevator control, which has been used in the trials. Some peculiarities of the aircraft are discussed. In section 3 crew training on a moving base simulator and the execution of the flight program is discussed. In section 4 a summing up of the results of the trials is given. In section 5 some conclusions are presented which can be drawn from this part of the program.

## 2. ELEVATOR CONTROL INPUTS FOR NON-STATIONARY FLIGHT TESTING

### 2.1. General discussion on the shape of the desired manoeuvre

The derivation of performance as well as stability and control characteristics from one non-stationary flight manoeuvre puts different requirements on the information which has to be contained in the measured aircraft responses.

Aircraft performance, such as climb performance and aircraft polars can be derived from measurements taken in quasi-steady accelerated flights. If these measurements differ too much from steady-state conditions a correction has to be made using knowledge of the aircraft aerodynamic model.

Stability and control characteristics can be derived if the aerodynamic model of the aircraft is known. This model can be estimated from measured aircraft responses, provided sufficient information is contained in these responses. As most of the aerodynamic derivatives are related to the short period oscillation, it seems reasonable to assume that oscillations of about the short period frequency in these responses will fulfil the requirement.

If these two types of aircraft responses are combined, aircraft performance and the aerodynamic model can be determined in principle from one manoeuvre whereas the model is then used to correct the performance measurements to steady-state conditions and to calculate longitudinal stability and control derivatives.

## 2.2. Design of a practical elevator control input signal

In preliminary trials on the Hunter, input signals have been considered of various degrees of complexity. It soon became apparent that only very simple input signals could be applied with a reasonable repeatability. The hydraulic control system of the aircraft is very effective and artificial feel is applied independent of airspeed. The resulting control force is thus proportional to control deflection from the trim position. Therefore the forces are relatively high at low speed because of large required control deflections and very low at high speeds. The application of a programmed autopilot could not be considered because no provisions were available in the aircraft.

As a result of these experiences a practical input signal was defined which would generate aircraft responses reasonably close to the requirements of section 2.1 (Fig. 2).

Starting at a low speed in stationary flight, the aircraft was made to accelerate in level flight through the whole speed envelope without pitch oscillations, except every 30 seconds, when 4 block-type oscillations were fed into the elevator control in basically the short period frequency. Between successive series of oscillations the aircraft accelerated steadily. In general 4 to 5 series were contained in one complete manoeuvre. The target "g" levels in the oscillations were set at 0 and +2 g.

## 3. PREPARATION AND EXECUTION OF THE FLIGHT TRIALS

### 3.1. General aspects

From a pilot's point of view a substantial difference exists between stationary and non-stationary flight testing as far as his control actions are concerned.

In the first case the pilot uses his controls to balance the forces and moments on the aircraft. The stabilization of the aircraft on a target speed can be a rather difficult task, especially if height constraints exist. Nevertheless the pilot gets sufficient information from the outside world and his instruments to execute the required task and to check his performance. In most cases ample time is available to stabilize the aircraft and take the measurements.

For non-stationary flight testing definite input signals have to be specified to the pilot. These inputs are then applied to the controls. In most cases a programmed autopilot is not installed in the aircraft. The information from the aircraft response is not available in time to the pilot to estimate the difference with the required response and to take corrective actions. However, with experience he is able to give his opinion on the quality of the manoeuvre and to try and improve his control policy in the following manoeuvres. Training on the simulator and in flight will provide him with this experience which will ensure a reasonable repeatability of the generated input signals.

### 3.2. Use of a moving base simulator

The three degrees of freedom moving base simulator of the Aeronautical Department of the Technological University of Delft has been used extensively for ground training.

The Hunter simulation has been based on available aircraft data, supplemented with subjective opinion of pilots with ample type experience. In the cockpit the original control column and throttle quadrant were replaced by Hunter items. Pitch and roll information was displayed on a "RT" which was flush-mounted in the instrument panel. The visual system of the simulator was used to display a horizon line.

The principal aim of the training sessions was to learn and generate the elevator input signal, given in figure 2.

Preliminary results with all subject pilots showed an overshoot tendency on the elevator time histories (Fig. 3a and 3b). This overshoot tendency could be lessened by training and was eliminated if the rate of elevator deflection was decreased sufficiently (Fig. 3c and 3d). To evaluate the influence of the motion system on the performance, several trials were made without this system. The opinion was that even the limited motion cues which were generated, aided considerably to get the "feel" of the manoeuvres and to restrict the "g" excursions between the limits of 0 and +2 g.

### 3.3. Execution of the flight program

Surprisingly the initial results of the flight trials showed the same overshoot tendency on the elevator time histories as during the ground training (Fig. 4a and 4b). Contrary to the simulator trials hardly any improvement could be obtained with training. Due to the rather violent aircraft motions the control stick could not be stopped in the required position.

To overcome this problem a metal bar was installed in the cockpit (Fig. 5a) which normally slid between the pilot's fingers and the control stick. If the movement of the hand (with the stick) had to be stopped, the pilot pressed the bar firmly between his hand and the control stick (Fig. 5b and 5c). After this device was installed, performance improved considerably although it was never possible to obtain the same regular shape of input signal as in the simulator trials (Fig. 6). The use of buffers to limit control stick movement is not practical because of the change of elevator trim position and deflection with speed.

The amplitude of the control deflections which would result in the  $\pm 1$  g change in normal acceleration could be learned relatively easy and in general the acceleration level remained between 0 and +2 g. It could, however, not always be prevented that some asymmetric motion was induced by the pilot which could not easily be stopped. It can be expected that in trials, which require higher load factors, the flying precision will degrade.

In the initial flight trials some problems were encountered in ending the pitching oscillations after the block signals and the accelerating part of the manoeuvre was not steady enough. After some training this problem was eliminated.

## 4. RESULTS OF THE FLIGHT PROGRAM

When the flight trials were concluded in May 1974 a total number of 19 flights had been made, of which 14 can be further analysed.

The remaining 5 have either been training flights or flights with instrumental mishapening which precluded further utilization. A total of about 50 manoeuvres, flown at altitudes of 10000, 20000 and 30000 ft are further processed at the moment.

### 5. CONCLUSIONS

From the experiences gained in the trials the following conclusions can be drawn:

- An input signal for non-stationary flight testing should be as simple as possible, unless a programmed autopilot is available.
- Training in advance on a moving base simulator can improve performance, but its usefulness should not be overestimated.
- The use of simple aids to guide the pilot's control movements can improve his performance considerably.
- In non-stationary flight testing flying precision will degrade rapidly with an increase of  $g$  load level.

### 6. REFERENCES

1. Gerlach, O.H.      Analyse van een mogelijke methode voor het meten van prestaties en stabiliteits- en besturingseigenschappen van een vliegtuig in niet-stationaire, symmetrische vluchten.  
Technische Hogeschool Delft, Vliegtuigbouwkunde, Rapport VTH-117, 1964 (with English summary).
2. Gerlach, O.H.      The determination of stability derivatives and performance characteristics from dynamic manoeuvres, Delft University of Technology, Department of Aeronautical Engineering, Report VTH-163, 1971.
3. Hoeman, R.J.A.W.    Advanced flight test instrumentation design and calibration, Delft University of Technology, Department of Aeronautical Engineering, Memorandum M-222, 1974.
4. Mulder, J.A.        Estimation of the aircraft state in non-steady flight, Delft University of Technology, Department of Aeronautical Engineering, Memorandum M-221, 1974.





Fig. 1 Hawker Siddeley Hunter MK7

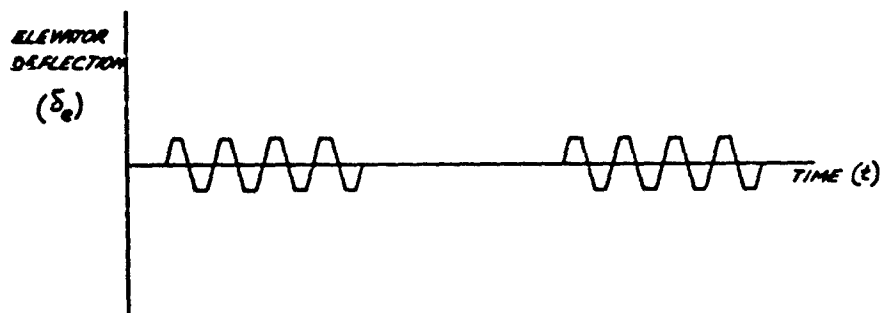


Fig. 2 Diagram of the elevator input signal

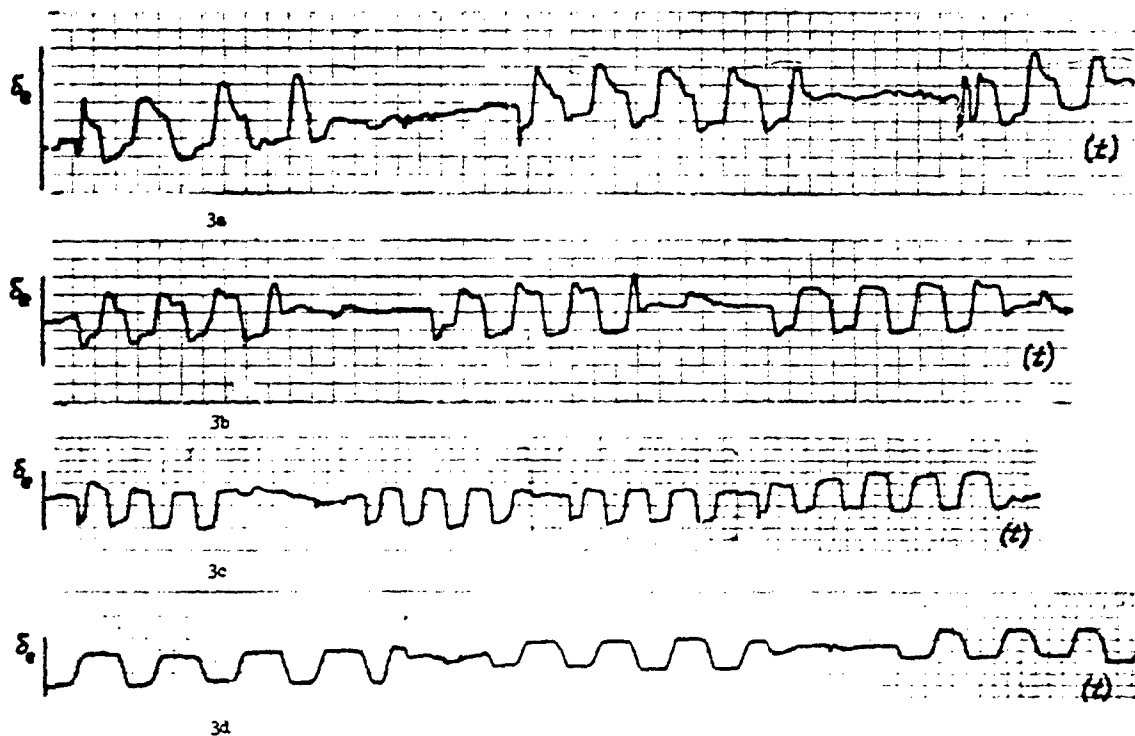
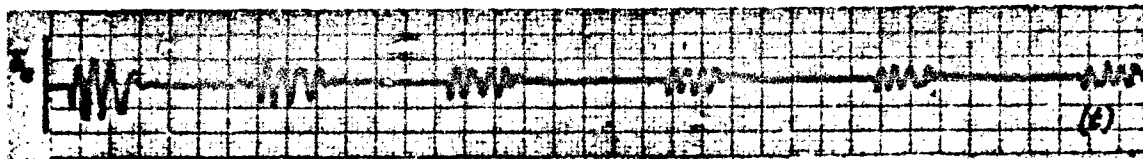
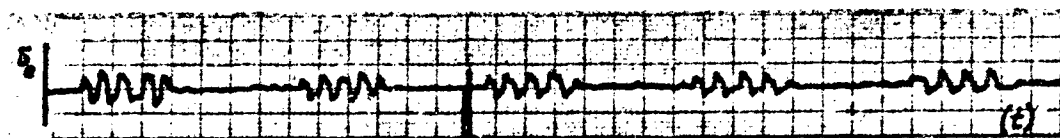


Fig. 3 Recorded elevator time histories in simulator training

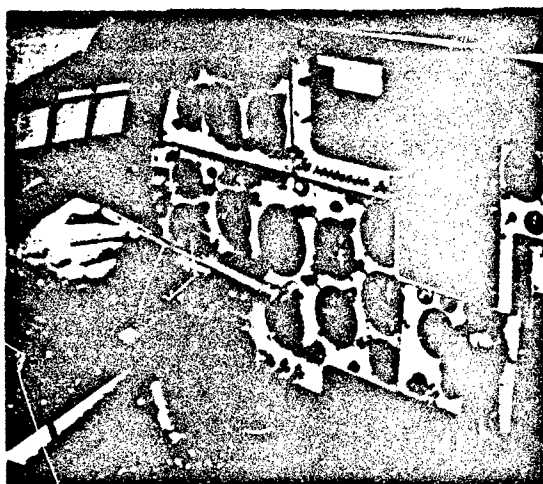


4a

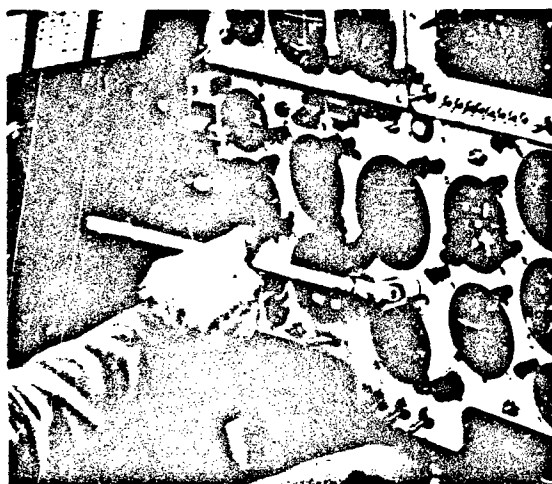


4b

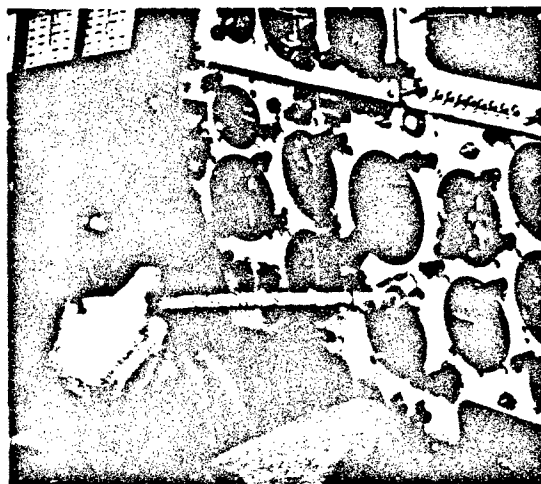
Fig. 4 Measured elevator time histories in flight, before the installation of a bar to control the movement of the hand



5a General view

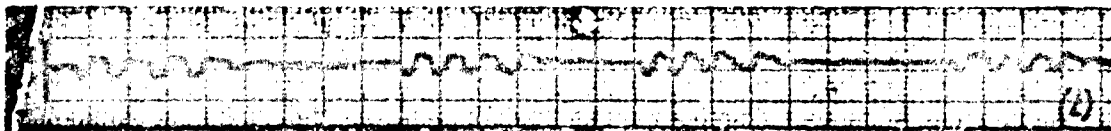


5b Forward control stick position

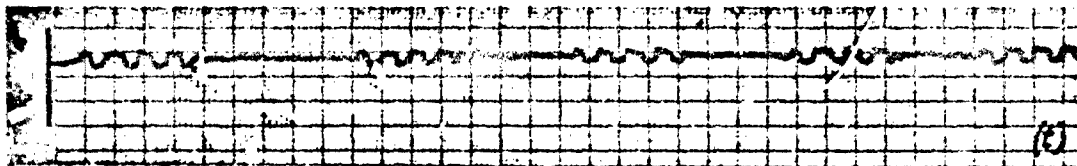


5c Rearward control stick position

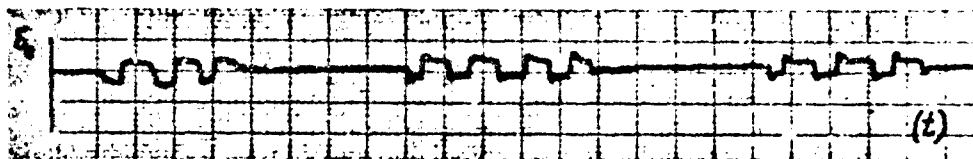
Fig. 5 Bar to control the movement of the hand



6a



6b



6c

Fig. 6 Measured elevator time histories in flight, after the installation of a bar to control the movement of the hand

# DETERMINATION OF STABILITY DERIVATIVES FROM FLIGHT TEST RESULTS

## COMPARISON OF FIVE ANALYTICAL TECHNIQUES

BY

HORST WÜNNENBERG  
HEINZ FRIEDRICH  
ULRICH VON MEIER  
HANS-JOACHIM MUNSER

DORNIER GMBH  
D-799 FRIEDRICHSHAFEN  
POSTFACH 317

### SUMMARY

Five analytical techniques in stability derivatives estimation were compared, in cooperation with the "E-Stelle 61 of the GAF" and with the "DFVLR". The test aircraft, a G 91-T3, was equipped with a sophisticated instrumentation and data acquisition system. The analytical techniques: manual evaluation of special flight maneuvers, time vector method, forced oscillation method, analog matching and regression analysis are compared in relation to the amount of time and equipment for the flight testing, complication of the data reduction and the quality of the results. The accuracy of the data acquisition is the most important problem. Therefore an accurate check of all test data has to be performed before sophisticated evaluation programs are used. As a result it can be summarized that in general several measuring and evaluation techniques should be used in parallel.

### 1. INTRODUCTION

Parameter identification from flight test results is an important and necessary task not only from a research point of view but also for the industrial flight testing. After the begin of the flight testing of a new aircraft the manufacturer has to know very rapidly the actual parameters and derivatives in comparison with the values derived from theory or windtunnel tests. This is necessary to decide whether and what type of modifications of the aircraft or the stability augmentation system have to be made. For the flight testing of the Airforce test departments the problems are similar. Therefore this task was defined in cooperation with the "E-Stelle 61", which is the German Airforce Flight Test Center, and the "DFVLR", the German Aerospace Research Institution.

The aim was to get some practical ideas of the application of 5 different analysing methods, which seemed to be representative for the broad spectrum of the well-known methods and which seemed to be applicable to a more industrial use. Therefore the comparison should include the necessary amount of data acquisition and reduction systems, flight test time, skill of the pilot and the evaluating engineer and last not least the quality of the results.

For the same reasons also manual evaluation techniques without and with computer aid and highly automatic methods for a digital computer use are taken into account. With respect to the aforementioned reasons and the already available practical experience from the Do-31 flight testing we decided to choose the following methods from the manual evaluation techniques:

- evaluation of special maneuvers from analog traces
- time vector method
- forced oscillation method

from the "Output error"-methods

- analog matching

and from the "Equation of motion"-methods

- regression analysis.

## 2. INSTRUMENTATION SYSTEM

As test aircraft a trainer version of the Fiat G-91 was used, fig. 1. The trainer version has the advantage that the flight test engineer could participate at the test flights and could influence the program in the air, if necessary. The aircraft was equipped by a sophisticated instrumentation system which was especially laid out for this task.

As the accuracy of the sensors is one of the most important problems in the field of flight test data analysis, special efforts have been made to get the best possible input data. Therefore for instance two different sensor-systems for angle of attack and sideslip, a Dornier flight log mounted on a sting in front of the aircraft and two additional sensors at the fuselage have been installed. The attitude, rate and acceleration sensors have been mounted on a frame of cast steel, fig. 2. This frame is orthogonal, heatable to compensate temperature effects and at three points rigidly fixed to the structure of the aircraft. The bearings are adjustable to guarantee an exact alignment of the sensor axis to the axis of the aircraft. The whole platform is isolated by damping material and mounted near to the c.g. of the aircraft.

Similar efforts have been made to improve the position signals of the control surfaces. Fig. 3 shows an example of the arrangement for the rudder. To avoid errors by backlash and elasticity the potentiometers have been rigidly mounted as near as possible to the rudder bearings additionally improved by a cog wheel with bias springs.

For the same reasons the range of the sensors has been chosen as small as possible according to the task, fig. 4. You see the range of the different sensor types and the attainable accuracy at the computer input.

Though this instrumentation system is very accurate, there are other errors, which also have to be compensated as well as possible. These are the time or phase errors. They occur due to the fact that the sensor itself has a certain time lag or phase error due to its frequency response and there is an additional time lag resulting from the time intervals during the scanning of the different measuring channels.

Fig. 5 shows, how we have tried to overcome these difficulties in the first step. As the influence of the structure vibrations has to be filtered by low pass filter RC-networks, the time constants of these networks have been chosen together with the known time constants of the sensors so that all signals are related to a reference time. To do this successfully the frequency response of all sensors has to be known. Therefore special test programs for instance for the angle of attack and sideslip sensors had to be carried out. Though these time lag corrections are valid only for the actual flight-mechanical frequencies they considerably improved the results especially of the automatic methods.

Today these corrections are part of a Kalman filter computer program, which shall be used in combination with the regression analysis. Further information will be given in Mr. Friedrich's paper.

The data reduction is done in the usual manner. We use an on-board magnetic tape recorder, which records the data with a frequency of 42 Hz. This tape is digitized, the calibration factors and all the other informations, which are necessary from the flight mechanics point of view, are added. From this basic "computer tape" the special tapes for the different methods are produced.

### 3. MANUAL EVALUATION OF SPECIAL FLIGHT MANEUVERS

This technique is well-known to every flight test engineer, so it needs no large explanations. Only analog traces are necessary for the evaluation. Fig. 6 gives a short summary of the procedures which are necessary for the evaluation of the longitudinal motion. By horizontal flights and steady turns with different load factors the lift coefficient slope over the angle of attack and the horizontal tail efficiency can be evaluated. By repeating this for different c.g. positions the neutral and the maneuver point can be found, which leads to the static stability terms and by this to the value of  $C_{m_0}$ .

In parallel the  $C_{m_0}$  also can be derived from the frequency of the short period oscillation neglecting the damping terms or taking the theoretical values. The combination of the damping derivatives  $C_{m_q} + C_{m_{\dot{\alpha}}}$  are derived from the damping of the short period. In detail the time to half amplitude and the already evaluated  $C_{L_\alpha}$  are used for the determination. The problem of analysing the short period motion is the normally high damping of this mode, so that only very few amplitudes are available for the evaluation. The pilot task is therefore "to feel" the natural frequency and try to excite the aircraft with it by a doublet-elevator input.

The fig. 7 shows the maneuvers and the procedure which have to be done for the evaluation of the lateral coefficients. In this case the problem is a little more complicated as some maneuvers have to be interpreted in parallel. So the pilot has to fly for each point of the interesting flight conditions

- a roll maneuver with a constant ramp aileron input and a load factor of 1 as long as a steady roll rate has built up
- a steady sideslip maneuver
- a Dutch Roll excitation by rudder pulse or doublet inputs.

The last two maneuvers can also be combined. It is important, that during the Dutch Roll oscillation aileron and rudder should be kept exactly zero, which seems to be no easy task for the pilot.

With these maneuvers the procedure of the determination begins with a first approximation of the roll-damping coefficient by neglecting the influence of the sideslip angle  $\beta$ , using the roll acceleration during the ramp input and the stationary relation of roll rate and aileron deflection.

The second step is the interpretation of the Dutch Roll, where the frequency leads directly to  $C_{n_\beta}$  and the damping directly to  $C_{n_r}$ . With this  $C_{n_\beta}$  and the evaluated roll/yaw ratio including the phase angle between  $p$  and  $\beta$   $C_{l_\beta}$  can be determined. With the before calculated  $C_{l_\beta}$  and the aileron effectiveness  $C_{l_\xi}$  a second approximation of the  $C_{l_p}$  is done including the sideslip terms.

Summarizing the experience it can be concluded: With a precise instrumentation system the main parameters can be determined. Though the accuracy of these derivatives is not high, it is a good check for rapid information of the order of magnitude. Also the instrumentation equipment can be checked by this method. The disadvantages are the necessary high skill of the pilot, the large experience of the analyst and the large amount of flying time, which has to be provided for this method.

#### 4. TIME VECTOR METHOD

Another nearly manual technique is the time vector method. Though this method gives even less values than the aforementioned it is of importance mainly as a check instrument for the flight test data. It also leads to the main parameters and therefore should be used if possible to check the results of more sophisticated methods.

This method can be applied to the oscillating modes only, in practice short period and Dutch Roll motion. The required input data are frequency, damping, amplitude ratios and phase relations of the main motion parameters. Fig. 8 shows how these values can be received by an evaluation of the peak values of the oscillating parameters and their temporary position. This procedure was done by a computer program which gives the results by weighting the different parameters according to their deviation and taking the average values by the method of least squares.

As I don't know whether you are all familiar with the time vector philosophy I first shortly repeat the main principles, fig. 9. The phase relation between a parameter and its differentiation is an angle of 90 degrees plus the damping angle  $\epsilon_D$ , and the amplitudes differ by the natural frequency  $\omega_0$ . With these relations an equation of motion can be represented as closed vector diagram, in this simple case of an oscillation with damping an isosceles triangle.

Fig. 10 shows the typical arrangement of the time vector polygons for the Dutch Roll mode. With some experience the derivatives in the form of vector lengths can be reduced from the available input data, though some assumptions have to be made. In this case for instance  $C_{Y\delta}$  corresponds to the theoretical value. The fig. shows the difference of the time vector diagrams calculated with theoretical values and the diagrams which have been constructed with flight test results.

The fig. 11 presents the corresponding relations for the short period mode. In this case we used the results of the next method, the forced oscillation method, which simplified the procedure, as enough amplitudes have been available for the analysis. In this case the assumption has to be made that the elevator effectiveness corresponds to the theoretical value.

Now I should like to demonstrate you shortly, how this checking procedure I mentioned before is working, fig. 12. The first check deals with the phase relations of differentiated parameters, which should be 90 deg. plus  $\epsilon_D$ . The next step checks the amplitude ratios of the derived differentiated parameters, which should be  $\omega_0$ . In the case of this program all derivations of the position angles have been available as measuring data so this check was realistic. The third and fourth check came from the application of the method using the lift equation and the kinematic relation and can easily be understood by the use of the method.

Fig. 13 explains the corresponding check procedure for the lateral motion. In this case, too, the main check is related to the phase relations and the amplitude ratio of differentiated parameters. In addition to that, further checks of the yaw parameter  $\psi$  and its differentiations are possible with the aid of the side force polygon as is indicated on the fig. The results of these checks can then be used to correct either the input informations for this or for other methods.

The possibilities of a parameter identification by means of this method are nevertheless limited as will be shown in the fig. 14. This fig. shows the effects of amplitude and phase errors of the main input data. An amplitude and a phase error of  $\pm 10\%$  was assumed. The latter is corresponding to a time lag of about 0.05 seconds. It can be seen that especially the phase errors lead to large errors of the final results. This fig. is valid for the longitudinal derivatives and the fig. 15 shows the corresponding situation for the lateral derivatives. In this case, too, mainly the phase errors but also frequency errors have an important influence on the evaluated parameters.

Finally, the following can be concluded for this method. It is of importance as a check-instrument and well suitable for the main parameters. The disadvantages are the necessary high accuracy of the test data and the necessary experience of the analyst.

## 5. FORCED OSCILLATION METHOD

Though this method on principle belongs to the manual analysing techniques the main work was done with the aid of a digital computer. For the application of this method a sine-generator has to be installed in the aircraft and fitted to either the elevator or the rudder. In our case we only use the elevator as actuating device as it was simpler to realize. The principles of this method are explained in fig. 16.

The motion parameters which have been excited by the sine-generator, are oscillating with the same frequency but individual amplitude and phase lags. By a Fourier analysis these parameters can be transformed into sine and cosine-parts. If we now put this presentation into the equations of motion and separate into sine and cosine-parts, we get two sets of defining equations. The Fourier coefficients can be evaluated from the traces of the motion parameters by summation formulas instead of the original integrals. To get the necessary sets of equations according to the number of unknowns several frequencies - in practice about ten - have to be provided, whereby the surplus equations are used to improve the results with statistical methods.

As it is possible to do the summation graphically this method requires no computer use, and even in our case, where a computer program was available, a manual check has to be done before the computation, fig. 17. This fig. shows the influence of non-constant periods on the Fourier coefficients. It is therefore necessary to choose only those parts of the traces where the oscillation has reached a stationary state, otherwise the errors become too large.

Of course the latter reduces the practical applicability of this method as a lot of flying time has to be provided regarding also the high numbers of frequencies which additionally have to be stationary. Also the installation of a sine-generator will not always be easily to realize. So this method plays a certain "outsider" role within this comparison.

## 6. ANALOG MATCHING

This technique is the simplest form of the output-error methods. It is wellknown for many years, and in Germany especially the DFVLR has a lot of experience with this method. So within this cooperation the application of this technique was carried out by the DFVLR.

Fig. 18 explains the procedure. From an analog magnetic tape which has been derived from the original "computer tape" the flight test state parameter  $X_{mf}$  and the control parameters  $\Delta F$  are fitted to the computer. Then in the next step the initial reference conditions for the model are computed from the differences of actual values and the computed model values. With these corresponding reference conditions the transients of model and flight test are presented one upon another on a four channel oscillograph, the picture of which can be photographed by a polaroid camera.

With this equipment the operator has to try by iteratively modifying the model parameters to get a good conformity of the model trace with the flight test trace. Fig. 19 shows as an example a comparison before and after the adaption. Though the initial discrepancy between flight and simulation is large, the final fit is relatively good.



The problems of this method are similar to those of the time vector method:

- Only the main parameters can be determined
- There is no unique solution. Each fit can be obtained with several different sets of parameters.
- The success of the method depends highly on the experience of the operator.

Nevertheless it should be mentioned that based on this technique in combination with the philosophy of the manual evaluation method a further improvement seems to be possible. In this case a digital computer program should do the calculations and fitting iterations according to a procedure which should include the flight test maneuver and the way of analysing these maneuvers.

## 7. REGRESSION ANALYSIS

This method is the most sophisticated of this comparison regarding the computing effort, and the simplest concerning the efforts of the flight testing and evaluation. As this technique will be explained in detail by the paper of Mr. Friedrich I only shortly discuss the main principles.

The method belongs to the equation error or equation of motion methods. It is based on the non simplified equations of motion, fig. 20. The coefficients on the left side have to be calculated from the accelerations, mass and moment of inertia terms. Additionally all state and control parameters have to be measured. With these values each observation point, and these are 42 per second, gives a set of equations for all coefficients and derivatives. The large amount of equation sets during a flight phase between two and five minutes is used to improve the results by means of a statistical method, the regression analysis. The mathematical problem is relatively simple as the equations are non-coupled.

The necessary maneuvers are simple but uncomfortable for the pilot, fig. 21. The pilot has to move all control surfaces in a random matter to get all the interesting relations. The fig. shows a typical example for this agitating of the controls.

It is obvious, that this method needs a sophisticated instrumentation system with a very high accuracy, especially no time lag errors should occur. But even other errors of course have a large influence on the results. This can be seen on fig. 22. Here the influence of a c.g. distance correction of the acceleration terms on the evaluated  $C_D$ -value is shown.

Until now the advantages of the method, possible determination of all interesting coefficients and derivatives by only one flight maneuver is connected with a partly bad accuracy of the evaluated results. The check with a simulated flight test showed that in principle it is possible to reach the aim. To get these excellent results in flight, too, high efforts of improving the measuring equipment or the filtering techniques have to be made. We have tried this now by the use of a Kalman filtering technique but the results are not yet available.

## 8. COMPARISON OF THE METHODS

At first a set of determined coefficients and derivatives is compared in relation to the theoretical values. Fig. 23 shows the values for the longitudinal motion. It can be seen that only the regression analysis gives all the interesting values. But if you look on the numbers, some big differences are found. Nevertheless some of them correspond relatively well to the expected ones, f.i.  $C_L$ ,  $C_D$ ,  $C_H$ ,  $C_{D_0}$ ,  $C_{m_0}$  and  $C_{m_1}$ . The other methods show a higher number of "blanks", but the remaining data are relatively good.

Fig. 24 shows the results of the lateral motion derivatives, which gives a similar picture. In this case the results of the regression analysis are much more better than in the longitudinal case, which has encouraged us to continue with this method. The expression "possible" means that this value can easily be computed from the determined moment derivatives. Also in this case the three "manual" methods give less but relatively reasonable results. It is obvious that further improvements of the data acquisition system will also lead to better results for these techniques.

Fig. 25 finally shows the actual comparison of the five evaluation methods due to the criteria which have been mentioned at the beginning of the paper:

#### *Test equipment*

High requirements for a modern PCM data acquisition system are only necessary for the regression analysis, while the other methods can also use available PAM systems. The accuracy of the sensors should be high for nearly all methods but phase lag corrections are extremely necessary for the regression analysis. Only the forced oscillation method needs a sine-generator as additional equipment and also the necessary flight test time is very large so this method is not useful for a routine use in the flight test. On the other hand the necessary flight test time for the regression analysis is very short. Pilot skill has to be high for the manual evaluation techniques, especially if he has to excite exact frequencies.

#### *Evaluation effort*

The necessary computer systems will be available at all flight test centers. The required analysing time is high for the manual methods and of course very low for the automatically working methods. The same can be said regarding to the experience of the analyst. The number of evaluable coefficients and derivatives is limited for the time vector method and the manual evaluation. Forced oscillation and analog matching lead to the main parameters, whereas by the regression analysis, all parameters can be achieved by including performance coefficients. The quality of the coefficients and derivatives is, on the other hand, relatively sufficient for the first methods whereas for the regression analysis it is highly depending on the instrumentation and measuring accuracy.

## 9. CONCLUSION

Though the evaluation of coefficients and derivatives is a hard job and needs a lot of effort, it is an important and a non neglectable task also for an industry flight test program. As preconditions for a successful work in this difficult field we found the following items:

- the main attention should be given to the accuracy of the sensors and the data acquisition
- each set of test data has to be checked before its further use
- the parallel use of at least two different methods is desirable
- A good cooperation of test pilot, flight test engineer and analyst is important
- Large experience of the participating engineers is desirable, too.

Finally the choice of methods which should be applied, depends on the possibilities of the instrumentation system, as the simpler methods need less information than the more sophisticated ones. For an industrial use especially for smaller and simpler aircraft the simpler evaluation techniques therefore still play an important role for the task of parameter identification.

## 10. REFERENCES

- [1] U. von Meier, H. Ruf, H. Friedrich, W. Kohl, A.J. Munser, H. Wönnenberg  
Vergleich von Verfahren zur Durchführung und Auswertung von Flugversuchen zur Bestimmung von Eigenschaften und Leistungen moderner Strahlflugzeuge  
Forschungsbericht aus der Wehrtechnik, BWg-FBWT 73-12, Dezember 1972.
- [2] G. Freysse  
Cours de mécanique du vol de l'avion  
Centre d'essais en vol, No de référence  
E.P.N.E.R. 12, 1968
- [3] K.H. Doetsch  
The time vector method for stability investigations  
ARC R.u.M. 2945, 1953
- [4] K.H. Doetsch  
The time vector method for lateral stability investigations  
REA techn. Rep. 87 200, 1967
- [5] A. Pietraß  
Ermittlung von aerodynamischen Derivativen des Flugzeugs FIAT G 91 T3 aus Flugmessungen durch Variation der Modellparameter am Analogrechner  
DFVLR IB A 10, August 1972
- [6] H. Friedrich  
Determining stability derivatives from flight test results with the aid of regression analysis  
Air Force Systems Command, Wright-Patterson AFB, Ohio,  
Foreign Technology Div., Avail: NTIS CSCL 01/3

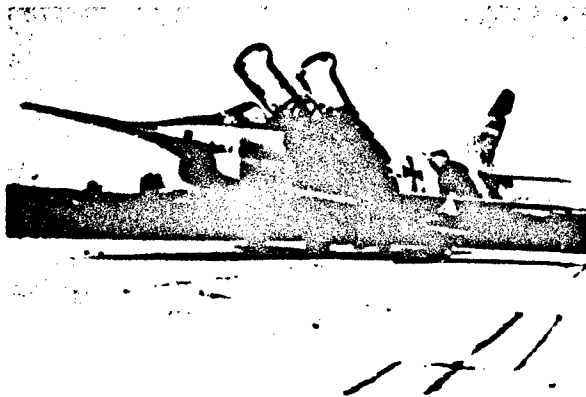


Fig. 1: Test Aircraft Fiat G91 - T3

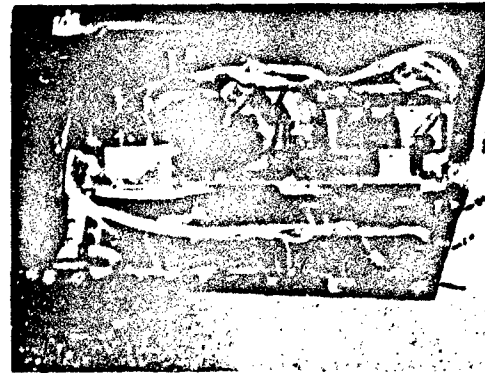


Fig. 2: Test Equipment of the G91 - T3

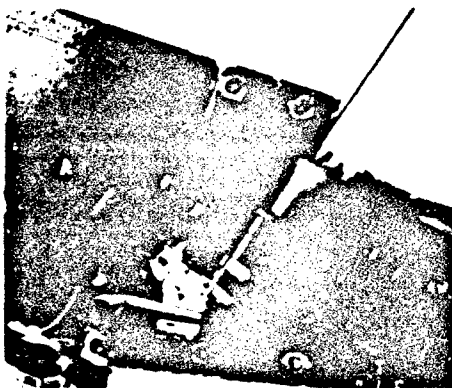


Fig. 3: Position Sensor of the Rudder

Sensor	Dim.	Range	Accuracy
altitude	deg	0 + 300	0,25
angular velocities	deg/sec	$\pm 20 + 40$	$\pm 0,04 + 0,08$
angular accelerations	rad/sec <sup>2</sup>	$\pm 1$	$\pm 0,003$
linear accelerations	g	$\pm 0,3 + 1,5$	$\pm 0,002 + 0,005$
angle of attack	deg	$- 10 + 20$	$\pm 0,2$
angle of sideslip	deg	$\pm 20$	$\pm 0,2$
positions of the control surfaces	deg	$\pm 50$	$\pm 0,1$
anemometric pressures	mb	different	0,5 mb
temperature	centigrad	$- 50 + 60$	$\pm 1$
RPM	%	0 + 100	$\pm 0,1 \%$
fuel flow	l/min	0 + 80	$\pm 5$

Fig. 4: Characteristics of the Instrumentation System

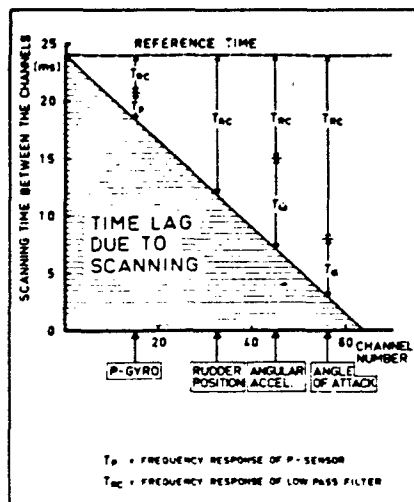


Fig. 5: Example of Time Lag Corrections by RC-Networks

1. HORIZONTAL FLIGHTS WITH DIFFERENT C.G. POSITIONS AND STEADY TURNS WITH DIFFERENT LOAD FACTORS LEAD TO

$$C_L, C_{L_0}, C_{L_1}, C_{m_0}, \text{ NEUTRAL POINT } (C_{m_0})$$

2. FREQUENCY AND DAMPING OF THE SHORT PERIOD OSCILLATION

$$C_{m_0}, C_{m_1} + C_{m_2}$$

Fig. 6: Manoeuvres for Longitudinal Coefficients

1. ROLL MANOEUVRE WITH CONSTANT RAMP INPUT AND  $N = 1$  LEADS TO FIRST APPROX. OF  $C_{\phi 1}$
2. FREQUENCY, DAMPING, ROLL/YAW RATIO AND PHASE ANGLES OF  $\phi$  AND  $\psi$  OF THE DUTCH-ROLL OSCILLATION LEAD TO  $C_{\phi 2}, C_{\psi 2}, C_{\phi}$
3. STEADY SIDE SLIP MANOEUVRES WITH THE BEFORE EVALUATED  $C_{\phi 2}$  AND  $C_{\psi 2}$  LEAD TO  $C_{\phi}, C_{\psi}$
4. SECOND LOOP OF THE ROLL MANOEUVRES INCLUDING  $\psi$  EFFECTS WITH THE BEFORE EVALUATED  $C_{\phi}$  AND  $C_{\psi}$  LEADS TO  $C_{\phi}$

Fig. 7: Manoeuvres and Procedure for Lateral Coefficients

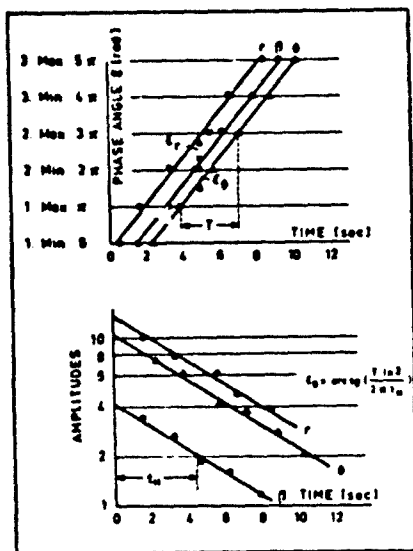


Fig. 8: Evaluation Procedure to get the Basis Data for the Time Vector and Manual Evaluation Method

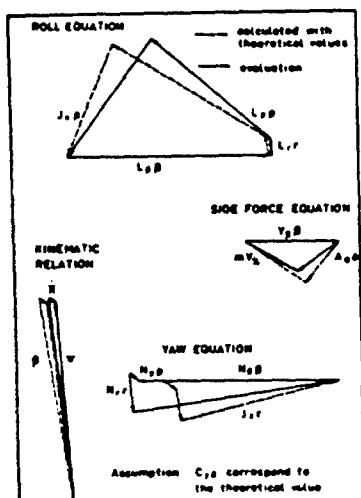


Fig. 10:  
Evaluated Time Vector Polygons  
of the Dutch Roll Oscillation

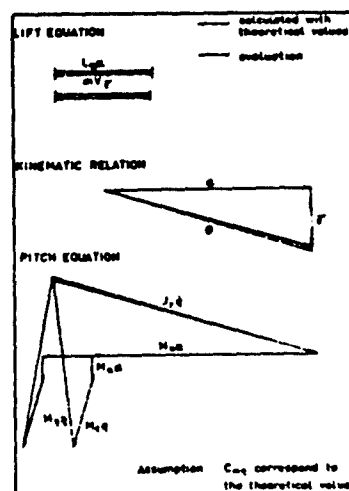


Fig. 11:  
Evaluated Time Vector Polygons of the Short  
Period Oscillation with Periodical Excitation

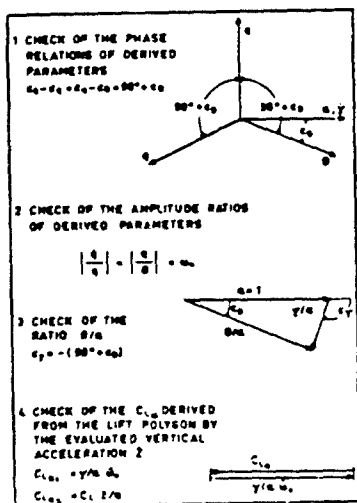


Fig. 12:  
Different Steps of Checks of  
the Evaluated Basis Data for the  
Short Period Oscillation

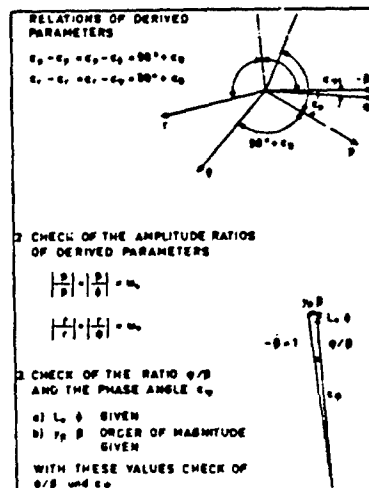


Fig. 13:  
Different Steps of Checks of the Evaluated Basis  
Data for the Dutch Roll Oscillation

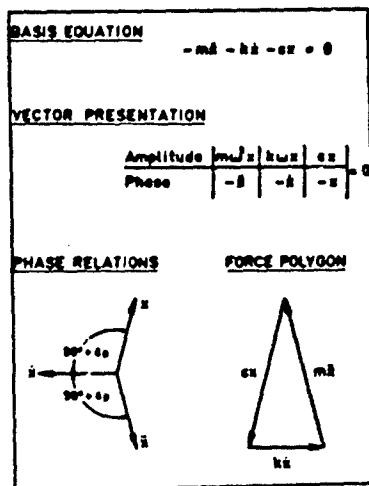


Fig. 9: Basic Principles of the Time Vector Method

10% AMPLITUDE ERROR FOR  $\Delta a_0, \Delta a_1, \Delta a_2, \Delta a_3, \Delta a_4, \Delta a_5$   
 10° PHASE ERROR FOR  $\Delta a_0, \Delta a_1$  ( $\Delta t = 0.05 \text{ sec}$ )

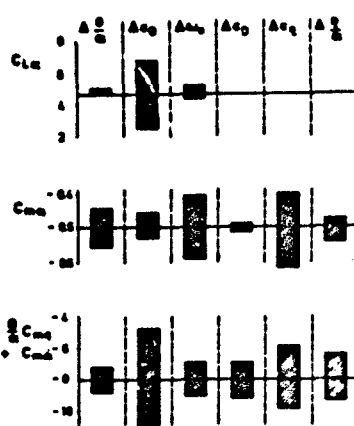


Fig. 14:

Effects of Different Data Errors on the Evaluated Longitudinal Derivatives

10% AMPLITUDE ERROR FOR  $\Delta a_0, \Delta a_1, \Delta a_2, \Delta a_3, \Delta a_4, \Delta a_5$   
 10° PHASE ERROR FOR  $\Delta a_0, \Delta a_1$  ( $\Delta t = 0.05 \text{ sec}$ )

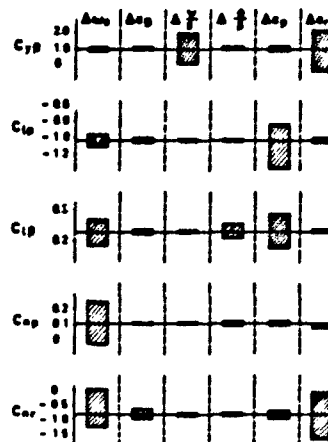


Fig. 15:

Effects of Different Data Errors on the Evaluated Lateral Derivatives

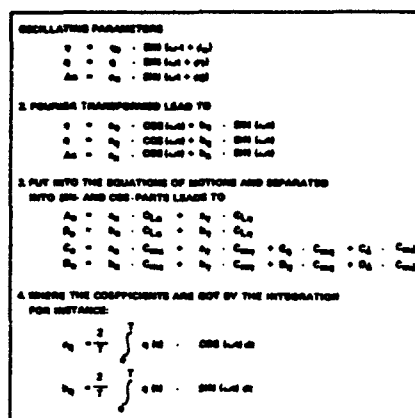


Fig. 16:

Principles of the Forced Oscillation Method

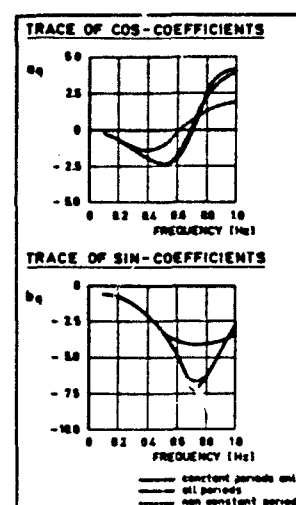


Fig. 17:

Influence of Nonconstant Periods on the Fourier-Coefficients

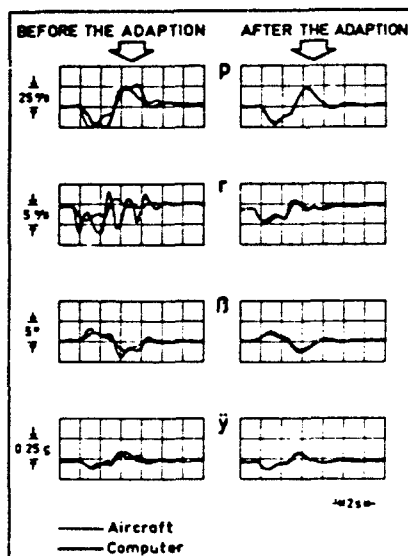


Fig. 19: Comparison of Flight Test and Simulation Data after a Rudder Input

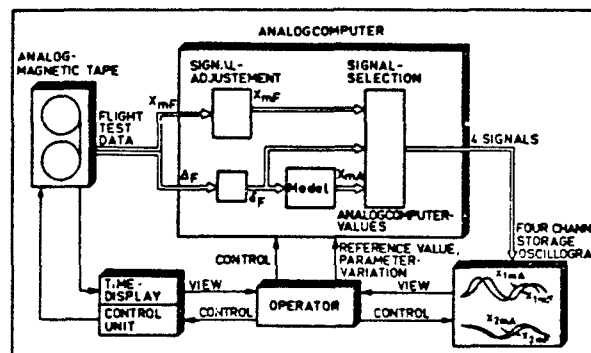


Fig. 18: Procedure of the Manual Adaption of the Model Parameters with the Aid of an Analogcomputer

$$\begin{aligned}
 C_L &= C_{L_0} + C_{L_\alpha} \cdot \alpha + C_{L_\beta} \cdot \beta + C_{L_{\dot{\alpha}}} \cdot \dot{\alpha} + C_{L_{\dot{\beta}}} \cdot \dot{\beta} + C_{L_{\ddot{\alpha}}} \cdot \ddot{\alpha} + C_{L_{\ddot{\beta}}} \cdot \ddot{\beta} \\
 C_D &= C_{D_0} + C_{D_\alpha} \cdot \alpha + C_{D_\beta} \cdot \beta + C_{D_{\dot{\alpha}}} \cdot \dot{\alpha} + C_{D_{\dot{\beta}}} \cdot \dot{\beta} \\
 C_m &= C_{m_0} + C_{m_\alpha} \cdot \alpha + C_{m_\beta} \cdot \beta + C_{m_{\dot{\alpha}}} \cdot \dot{\alpha} + C_{m_{\dot{\beta}}} \cdot \dot{\beta} + C_{m_{\ddot{\alpha}}} \cdot \ddot{\alpha} + C_{m_{\ddot{\beta}}} \cdot \ddot{\beta} \\
 C_Y &= C_{Y_0} + C_{Y_\beta} \cdot \beta + C_{Y_{\dot{\beta}}} \cdot \dot{\beta} + C_{Y_{\ddot{\beta}}} \cdot \ddot{\beta} + C_{Y_p} \cdot p + C_{Y_r} \cdot r \\
 C_l &= C_{l_0} + C_{l_\beta} \cdot \beta + C_{l_{\dot{\beta}}} \cdot \dot{\beta} + C_{l_{\ddot{\beta}}} \cdot \ddot{\beta} + C_{l_p} \cdot p + C_{l_r} \cdot r \\
 C_n &= C_{n_0} + C_{n_\beta} \cdot \beta + C_{n_{\dot{\beta}}} \cdot \dot{\beta} + C_{n_{\ddot{\beta}}} \cdot \ddot{\beta} + C_{n_p} \cdot p + C_{n_r} \cdot r
 \end{aligned}$$

Fig. 20:  
Basic Equations for the Use of the Regression Analysis

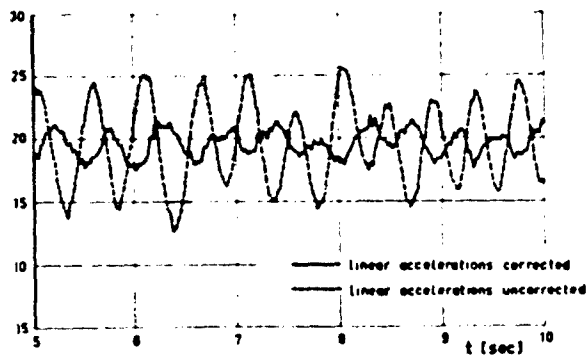


Fig. 22: Influence of a C. C. Distance Correction of the Linear Acceleration Terms on the Evaluated  $C_D$  Values

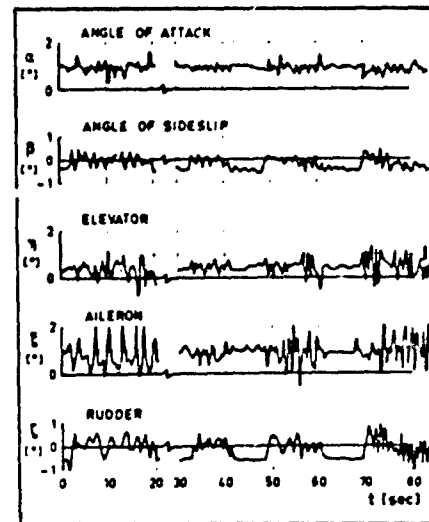


Fig. 21: Typical Inputs for the Regression Analysis

	THEORY	1 ANALOG EVALUATION	2 TIME VECTOR METHOD	3 FORCED OSCILLATION	4 ANALOG BATCHING	5 REGRESSION ANALYSIS
$C_L$	0.13	0.13	-	-	-	0.087
$C_D$	4.88	-4.8	4.88	4.77	4.88	0.188
$C_{L\alpha}$	1.9	-	200	-	-	-394.3
$C_{D\alpha}$	4.2	200	200	200	200	0.23
$C_{L\beta}$	0.48	-0.48	-	0.48	0.27	0.68
$C_D$	0.016	-0.016	-	-	-	0.014
$C_{D\beta}$	0.004	-	-	-	0	0.001
$C_{L\dot{\alpha}}$	0.002	0	-	-	-	0.008
$C_{D\dot{\alpha}}$	-0.00	-0.00	0.01	-0.48	-0.00	0.00
$C_{L\dot{\beta}}$	-2.38	-	-2.3	-	-	42.5
$C_{D\dot{\beta}}$	-0.7	-0.8	-0.7	-0.9	-0.4	-4.01
$C_{L\ddot{\alpha}}$	-0.5	0.5	-	-0.00	-0.5	-0.48

Fig. 23:

Comparison of the Results for the Longitudinal Motion at  $M = 0.8$

	THEORY	1 ANALOG EVALUATION	2 TIME VECTOR METHOD	3 FORCED OSCILLATION	4 ANALOG BATCHING	5 REGRESSION ANALYSIS
$C_L$	-0.23	-	-	-	-1.20	-1.48
$C_D$	0.06	-	200	-	200	-0.23
$C_{L\alpha}$	0.02	200	200	-	200	4.38
$C_{D\alpha}$	0	-	-	-	0.02	-0.08
$C_{L\beta}$	0.16	200	-	-	0.08	0.18
$C_D$	0.34	-0.28	-0.48	-	-	-0.16
$C_{L\dot{\alpha}}$	-2.77	-0.07	-0.07	-	-1.9	-0.47
$C_{D\dot{\alpha}}$	0.00	-	1.27	-	-0.00	0.00
$C_{L\dot{\beta}}$	0.00	-0.20	-	-	-0.00	-0.00
$C_{D\dot{\beta}}$	0.00	-	-	-	-	0.003
$C_L$	0.16	0.28	0.28	-	0.00	0.16
$C_D$	-2.00	-0.00	-0.00	-	-0.10	-0.20
$C_{L\dot{\alpha}}$	-0.00	-0.00	-1.00	-	-0.00	-1.01
$C_{D\dot{\alpha}}$	-0.00	-	-	-	-	-0.00
$C_{L\dot{\beta}}$	-0.17	-0.16	-	-	-0.00	-0.17

Fig. 24: Comparison of the Results for  
Lateral Motion at  $M = 0.45$

	1 ANALOG EVALUATION	2 TIME VECTOR METHOD	3 FORCED OSCILLATION	4 ANALOG BATCHING	5 REGRESSION ANALYSIS
TEST EQUIPMENT	FAIR or POOR	FAIR or POOR	FAIR or POOR	FAIR or POOR	POOR
- Number of test parameters	high	high	high	high	high
- Sensor accuracy	high	high	high	high	high
- Phase lag correction	high	high	high	high	very high
- Additional test equipment	no	no	no	no	no
Flight test time	high	high	very high	high	very short
Post test	high	high	very high	high	low
EVALUATION EFFORT	no	moderate	Digital Comp.	Analog Comp.	Digital Comp.
- computer use	no	high	high	high	high
- calibration time	high	high	high	high	high
- test time of the method	high	high	high	high	low
Number of available test parameters	high	high	high	high	high
Quality of the data	high	high	high	high	highly depending on the equipment

Fig. 25: Comparison of the Methods

# FIVE IDENTIFICATION METHODS APPLIED TO FLIGHT TEST DATA

by Jean-Pierre Choquin

Office National d'Etudes et de Recherches Aéronautiques (ONERA)  
92120 Châtillon (France)

## SUMMARY

The present paper deals with the determination of the parameter of linear multivariable systems using input and output measurements. It is assumed that the physical system, which is to be investigated, can be described by a set of linear differential equations with constant coefficients. These estimations had to be applied to the derivation of active control parameters. Tests of well known methods, such as least squares, modulating functions, conjugate gradients and analog matching, are developed. Some results are proposed to be used as support for the comparison of the different methods.

## CINQ MÉTHODES D'IDENTIFICATION APPLIQUÉES A DES MESURES EN VOL

## RÉSUMÉ

Cette communication a trait à la détermination des paramètres de systèmes linéaires à plusieurs variables à partir des mesures des signaux d'entrée et de sortie de ces systèmes. Le processus physique à étudier est supposé pouvoir être décrit par un ensemble d'équations différentielles linéaires à coefficients constants. Les estimations obtenues sont destinées au calcul de paramètres de contrôle actif. Une comparaison de méthodes connues, telles les moindres carrés, les fonctions modulatrices, les gradients conjugués et l'adaptation analogique, est développée à partir des quelques résultats présentés.

## 1. INTRODUCTION

The problem is to calculate the flight derivatives of aircraft using flight records of the acceleration of the center of gravity, of the angle of attack, of the pitch rate and of the excitation (deflection of elevators or airbrakes).

For each method, the whole measuring time has been used for the evaluation. This way, disturbances and errors in measurements, which are statistically independant from the input signals, can be eliminated.

A theoretical survey is developed in the first part of the paper, then results and comparisons of the methods are exposed.

## 2. SURVEY OF IDENTIFICATION TECHNIQUES

### 2.1. General considerations on system identification

Following Rault [1], we will distinguish three steps in identification :

- characterization : it is a qualitative operation that defines the structure of the system, i.e. type and order of the differential equations which connect inputs and outputs ;

- identification and parameter estimation ;

- checking : it is a necessary step where one checks that the estimated parameters have a physical meaning and that the accuracy of the estimation is good enough.

As only the aerodynamic coefficients of the rigid aircraft intervene in the calculation of gust alleviation laws at this time with the ONERA method, the characterization step is well defined because the differential equations of the motion are well known.

All the data collected in flight on analog tapes have been sampled before being analyzed on a digital computer. The direct current of demodulators, bias, time constants of the different circuits of the analog to digital converting chain have to be looked at very carefully. The problems introduced by noise will be recalled for each method.

### 2.2. Least squares [1]

Let  $y_k$  be an  $(m+1)$  state variable vector and  $x_k = (x_{k1}, \dots, x_{kn})$  an  $(n+1)$  measured variable vector supposed without noise in a first step. Let  $f$  be the function connecting  $y_k$  and  $x_k$  and the unknown parameters vector  $p^T = (p_0, p_1, \dots, p_n)$ . One can write :

$$y_k = f(x_{k1}, p_i) + b_k$$

The least square method consists in minimizing the sum of the squared errors.

$$J = \sum_{k=0}^m (y_k - f(x_{k1}, p_i)_{i=0,n})^2$$

which yields with matrix notation :

$$J = (Y - F(X_k, P))^T (Y - F(X_k, P))$$

To derive the minimum of  $J$ , one writes :

$$\frac{\partial J}{\partial P} = 0$$

$$(1) \quad \frac{\partial F}{\partial P}^T \cdot F(X_k, \hat{P}) = \frac{\partial F}{\partial P} \cdot Y$$



where  $\hat{p}$  is an estimator of  $p$ .

This equation generally cannot be solved because  $F(X_k, p)$  is a non linear function of  $p$ . We will see later that it can be solved by iterative techniques.

Assume now that  $F(X_k, p)$  is a linear function of  $p$ .

$$F(X_k, p) = \Phi p \quad \Phi \text{ is a } (m+1) \text{ matrix}$$

$$\frac{\partial F}{\partial p} = \Phi$$

Equation (1) yields :

$$\Phi^T \Phi \hat{p} = \Phi^T Y \quad \text{thence } \hat{p} = [\Phi^T \Phi]^{-1} \Phi^T Y$$

$$Y = F(X_k, p) + B \quad \text{thence } Y = \Phi p + B$$

$$\hat{p} = [\Phi^T \Phi]^{-1} \Phi^T (\Phi p + B)$$

Let us prove now that  $\hat{p}$  is a non biased solution, i.e. that if  $E(\cdot)$  is the mean operator,  $E(\hat{p}) = p$ . If the coefficients of  $\Phi$  are not correlated with  $B$  and if  $B$  is a zero mean noise and if  $\Phi$  is a deterministic matrix :

$$E(\hat{p}) = E[\Phi^T \Phi]^{-1} \Phi^T (\Phi p + B)$$

$$E(\hat{p}) = [\Phi^T \Phi]^{-1} \Phi^T [\Phi E(p) + E(B)]$$

$$\Rightarrow E(\hat{p}) = [\Phi^T \Phi]^{-1} \Phi^T \Phi p = p$$

We have assumed that the noise occurs only on the output, which is generally true, and that measurement noise and sampling noise built a zero-mean process uncorrelated with the system output.

The second assumption is generally not so obvious, due to the fact that unpredicted inputs generate a non neglectible secondary noise.

It has been supposed that

- $\Phi$  was deterministic,
- $B$  was a zero-mean noise.

As stated in Section 1, all the recorded parameters have been sampled with the measurement noise and also with the noise added by the use of the analog recorder (amplifiers, ...). It follows that  $\Phi$  is not really deterministic.

In the same way,  $B$  is generally not a zero-mean noise. It is possible to avoid this problem by using the weighting least squares method (see figure 2).

Let  $w(t)$  be a zero-mean white noise. We suppose that :

$$b(t) = h(t) * w(t)$$

where  $h(t)$  is a finite order filter.

If the correlation of  $b$  and  $w$  is known, the function can be evaluated. It is then possible to filter the data with  $h^*$  and to apply the least square method to the filtered input and output signals.

But the main problem is the evaluation of  $h$ . Iterative methods have been proposed by Clarke (1967). It is the purpose of the GLS method.

### 2.3. Integrated least squares

Integration helps filtering the noise that appears in the recorded signals. The integrated least square method consists

in applying the least squares method to the integrated equations.

But it is very difficult to define the zero of a measuring device. Instead of measuring  $\Delta(t)$ , one measures  $\Delta(t) + \bar{\Delta}$  where  $\bar{\Delta}$  is in first approximation a constant value.

This method is helpful for high frequency noise but loses its interest when a zero-shift may occur.

### 2.4. Modulating functions

The method consists in expanding the output and input signals in a set of functions. Let  $(\phi_i)_{i=1, n+1}$  be a set of such functions and  $\langle f_i, f_j \rangle$  be the inner product of  $f_i$  and  $f_j$ . One can then write, if  $\Delta$  is one output of the system following a differential equation, the coefficients of which are

$$p_1 \langle \frac{d\Delta}{dt}, \phi_1 \rangle + p_2 \langle \frac{d^2\Delta}{dt^2}, \phi_1 \rangle + \dots + p_m \langle \Delta, \phi_1 \rangle = \langle e, \phi_1 \rangle$$

$$p_1 \langle \frac{d\Delta}{dt}, \phi_2 \rangle + p_2 \langle \frac{d^2\Delta}{dt^2}, \phi_2 \rangle + \dots + p_m \langle \Delta, \phi_2 \rangle = \langle e, \phi_2 \rangle$$

$$p_1 \langle \frac{d\Delta}{dt}, \phi_{nm} \rangle + p_2 \langle \frac{d^2\Delta}{dt^2}, \phi_{nm} \rangle + \dots + p_m \langle \Delta, \phi_{nm} \rangle = \langle e, \phi_{nm} \rangle$$

The choice of the modulating functions eliminates the difficulty of computing the successive derivatives of the signals. For instance :

$$\langle \bar{\Delta}, \phi_1 \rangle = [\bar{\Delta} \cdot \phi_1]_0^T - [\Delta \cdot \phi_1]_0^T + \langle \Delta, \dot{\phi}_1 \rangle$$

If  $\phi_1$  is chosen such that :

$$\phi_1(0) = \phi_1(T) = \dot{\phi}_1(0) = \dot{\phi}_1(T)$$

one gets

$$\langle \bar{\Delta}, \phi_1 \rangle = \langle \Delta, \dot{\phi}_1 \rangle$$

There are no differentiation, which increases the effects of noise, and no integration, which may induce errors on constants. One has only to solve a linear system in  $(p_i)_{i=1, n+1}$ .

Let us note that this method has to be carefully applied because the modulating functions may screen some informations in the signal and generate some others which were not existing.

### 2.5. Conjugate gradients : method of Fletcher and Reeves [2]

The main advantage of the gradient methods is to allow identification of non linear problems by iterative techniques. The way of searching the variables in directions chosen as to accelerate the process changes following the methods. One uses the unit directions of the parameter vectorial space (Gaussian method). Others are using the opposite gradient at the previously determined point of the parameter space (steepest descent).

Let  $J(\bar{x})$  be the non-linear cost function to be minimized. It is a function of  $n$  parameters  $(x_1, x_2, \dots, x_n)$ . Let us assume that  $J(\bar{x})$  and its gradient  $\nabla J(\bar{x})$  are available at each point of the parameter space and that the minimum  $\bar{x}_{min}$  minimizing  $J(\bar{x})$  exists. One can expand  $J(\bar{x})$  in Taylor's expansion in the neighbourhood of  $\bar{x}_{min}$ .

$$J(\bar{x}_{min} + \Delta \bar{x}) = J(\bar{x}_{min}) + \nabla J(\bar{x}_{min})^T \Delta \bar{x} + \frac{1}{2} \Delta \bar{x}^T A \Delta \bar{x} + \text{higher order terms}$$

$$\bar{x}_{min} \text{ minimum } \nabla J(\bar{x}_{min}) = 0 \text{ (necessary condition).}$$

$A$  is the Hessian matrix of  $J$ . It is definite positive and symmetrical if the second derivatives are continuous. In the neighbourhood of  $\bar{x}_{min}$  the gradient is given by:

$$\nabla J(\bar{x}) = A(\bar{x} - \bar{x}_{min})$$

The variation  $J(\bar{x}_{min} + \Delta \bar{x}) - J(\bar{x}_{min})$  is maximized when its derivation is equal to zero:

$$0 = \nabla J(\bar{x}) + A \Delta \bar{x}$$

where  $\bar{x}_i$  is an approximation of  $\bar{x}_{min}$

$$\Delta \bar{x} = -A^{-1} \nabla J(\bar{x}_i)$$

The step of iteration is then defined by:

$$\bar{x}_{i+1} = \bar{x}_i + \Delta \bar{x} = \bar{x}_i - A^{-1} \nabla J(\bar{x}_i)$$

The most difficult problem is the evaluations of  $A^{-1}$ , i.e.  $A$ , because the evaluation of the second derivatives cannot be accurate enough. Indirect methods have been proposed (Shah, Buehler and Kempthorne (1961), Powell (1962)) that use geometric properties of surfaces.

The modification of Fletcher and Powell (1963) of Davidon's procedure (1959) proposes (see ref. 2):

$$\bar{x}_{i+1} = \bar{x}_i + \alpha_i \bar{d}_i$$

with

$$\bar{d}_i = -H_i \nabla J(\bar{x}_i)$$

and  $\alpha_i$  calculated as to minimize  $J(\bar{x}_{i+1})$ .

$H_0, H_1, \dots, H_n$  is a sequence of definite positive matrix.  $H_0$  is generally chosen equal to the unit matrix. This sequence is so built as to modify  $H_i$  at each step of iteration so as the series converges towards  $A^{-1}$  when  $\bar{x}_i$  nears  $\bar{x}_{min}$  (see ref. 5).

$$H_{i+1} = H_i + \frac{\bar{d}_i \bar{d}_i^T}{\bar{d}_i^T A \bar{d}_i} - \frac{H_i \bar{r}_i \bar{r}_i^T H_i}{\bar{r}_i^T H_i \bar{r}_i}$$

with

$$\bar{r}_i = \nabla J(\bar{x}_{i+1}) - \nabla J(\bar{x}_i)$$

The fastest convergence is offered by the steepest descent method but it becomes less accurate in the neighbourhood of the minimum. The use of conjugate directions  $\bar{d}_i$  is generally preferred because it takes into account the local behaviour of the function.

The idea of Fletcher and Reeves was to look for  $\bar{d}_i$  as a linear combination of the opposite gradient at the considered point  $\bar{x}_i$  and the previously determined directions  $\bar{d}_0, \bar{d}_1, \dots, \bar{d}_{i-1}$  so as to fit the orthogonality condition.

$$\bar{d}_i^T A \bar{d}_j = 0; \forall i > j$$

Many coefficients are equal to zero. It comes:

$$\bar{d}_i = -\nabla J(\bar{x}_i) + \beta_{i-1} \bar{d}_{i-1}$$

with

$$\beta_{i-1} = \frac{\|\nabla J(\bar{x}_i)\|^2}{\|\nabla J(\bar{x}_{i-1})\|^2}$$

This yields the final algorithm:

$$\bar{x}_0 \text{ chosen } \bar{d}_0 = -\nabla J(\bar{x}_0)$$

$$\bar{x}_{i+1} = \bar{x}_i + \alpha_i \bar{d}_i$$

position of the minimum of  $J(\bar{x})$  on the line passing by  $\bar{x}_i$  in the direction  $\bar{d}_i$ .

$\Rightarrow \alpha_i$  by minimisation of  $J(\bar{x}_{i+1})$

$$\beta_i = \frac{\|\nabla J(\bar{x}_{i+1})\|^2}{\|\nabla J(\bar{x}_i)\|^2}$$

$$\bar{d}_{i+1} = -\nabla J(\bar{x}_{i+1}) + \beta_i \bar{d}_i$$

until  $\alpha_i \neq 0$

#### Application to non quadratic problems

The convergence depends much on the conjugaison of the generated directions. This conjugaison can be destroyed by non quadratic terms in the cost function and this difficulty is combined with the inaccuracy of the minimization of  $J$  along the last direction.

A partially conjugate gradients method (see ref. 6) can be applied to decrease the length of conjugate gradients cycles for the purpose of minimizing the degradation of conjugaison of the successive directions.

#### 2.6. Analog matching

This method makes it possible to get rapidly good estimations of the parameters and to introduce them as initial values in an iterative method. To avoid the importance of the operator estimation, an adaptative control of the coefficients has been derived (see ref. 3 and 4).

One must remember that all the terms of the equation have not the same weight. It is then recommended to evaluate, with known estimations of the parameters (for instance, wind tunnel values) the frequency bandwidth where the system offers the best sensitivity to a given variable. This can be studied in amplitude Bode's diagram for instance, as shown later.

Let  $J(\bar{x})$  be a cost function. We want it to be always decreasing with time. Its derivative with time has then to be non positive

$$\nabla J(\bar{x})^T \frac{\partial \bar{x}}{\partial t} \leq 0.$$

This is always verified when we choose the law of variations of  $\bar{x}$  with time:

$$\frac{\partial \bar{x}}{\partial t} = -\nabla J(\bar{x}),$$

For non-linear problems it becomes very difficult and very expensive also to develop the analog system because of the rapidly increasing number of good multipliers which are required.

### 3. RESULTS AND COMPARISONS OF THE DIFFERENT METHODS

#### 3.1. Formulation of the problem

Let us recall the formulation of the equations of the longitudinal motion of a rigid aircraft which is used in the different methods. Let  $\ddot{x}$  be the acceleration of the center of gravity  $q$  the pitch rate,  $\alpha$  the angle of attack and  $\delta q_e$  the excitation. It comes:

$$\begin{cases} \ddot{x} = k_a \alpha + k_{q_e} \delta q_e \\ \dot{\theta} = -k_a \alpha - k_{q_e} \delta q_e - k_q \dot{\theta} \end{cases}$$

All the results are compared on figure 7 and time histories are drawn on figure 8 and 9 and compared with the measured functions.

#### 3.2. Some indications on the different methods

##### a) Modulating functions

This method has been tested with the following set of functions:

$$\phi_i\left(\frac{t}{T}\right) = \sqrt{1 - \left(\frac{t}{T}\right)^2} \cdot \mu_i\left(\frac{t}{T}\right)$$

with

$$\begin{cases} \mu_i(x) = \frac{\sin((i+1)\varphi)}{\sin \varphi} & \text{Tchebyshev's polynomials of} \\ x = \cos \varphi & \text{second kind and of order } n. \end{cases}$$

They have been chosen because of the simplicity of the integration by the Gaussian method,

$$\int_{-1}^1 f(x) \sqrt{1-x^2} dx = \sum_{i=1}^N \bar{\omega}_i f(x_i) + R_N$$

where the  $\bar{\omega}_i$  are the weights and  $x_i$  the abscissas of the Gaussian points. And:

$$\begin{cases} x_i = \cos\left(\frac{i\pi}{N+1}\right) \\ \bar{\omega}_i = \frac{\pi}{N+1} \sin^2\left(\frac{i\pi}{N+1}\right) \end{cases}$$

The number of functions has been chosen equal to the number of unknown parameters in order to study the specific properties of this method.

##### b) Analog matching

We shall detail here what has been done on the analog diagram of figure 3 and 4. Let us consider the lift equation of the rigid aircraft

$$\ddot{x} = k_a \alpha + k_{q_e} \delta q_e$$

Let  $\mathcal{E}$  be the error and  $J = \mathcal{E}^2$  the cost function:

$$J = \mathcal{E}^2 = (k_a \alpha + k_{q_e} \delta q_e - \ddot{x})^2$$

$$\frac{dJ}{dt} = 2\mathcal{E} \frac{d\mathcal{E}}{dt} = 2\mathcal{E} \left( \frac{\partial \mathcal{E}}{\partial k_a} \frac{dk_a}{dt} + \frac{\partial \mathcal{E}}{\partial k_{q_e}} \frac{dk_{q_e}}{dt} \right)$$

$$\frac{dJ}{dt} \leq 0 \Rightarrow$$

$$\left( \mathcal{E} \frac{\partial \mathcal{E}}{\partial k_a} \right) \frac{dk_a}{dt} + \left( \mathcal{E} \frac{\partial \mathcal{E}}{\partial k_{q_e}} \right) \frac{dk_{q_e}}{dt} \leq 0$$

This is always obtained by:

$$\begin{cases} \frac{dk_a}{dt} = -\mathcal{E} \frac{\partial \mathcal{E}}{\partial k_a} \\ \frac{dk_{q_e}}{dt} = -\mathcal{E} \frac{\partial \mathcal{E}}{\partial k_{q_e}} \end{cases}$$

To illustrate the note explained in Section 2.6 on the frequency range of the input signals, we can look at figure 6. It should be noted that the  $q$ -parameter is always much smaller than the others. This explains the difficulty encountered for the estimation of this parameter.

This analog method has also been tested with an analog simulation program CSMP-IBM. Some results are shown on figure 10.

##### c) Conjugate gradients

Nothing to explain especially out of the minimization of  $J(\vec{x}_i)$  on the line passing by  $\vec{x}_i$  in the direction  $\vec{d}_i$  for  $J$  quadratic (see ref. 5). Let  $y(\alpha)$  be defined by:

$$y(\alpha) = J(\vec{x}_i + \alpha \vec{d}_i)$$

$$y'(\alpha) = \vec{d}_i^T \cdot \vec{\nabla} J(\vec{x}_i + \alpha \vec{d}_i)$$

Let us note that

$$y(0) = J(\vec{x}_i)$$

$$y'(0) = \vec{d}_i^T \cdot \vec{\nabla} J(\vec{x}_i)$$

Let  $\alpha_m$  be the value of  $\alpha$  minimizing  $J(\vec{x}_i + \alpha \vec{d}_i)$ ; Fletcher and Powell propose,  $J_m$  being an estimate of the minimum:

$$h = \frac{2}{y'(0)} (J_m - J(\vec{x}_i))$$

$$\begin{cases} h = h & \text{if } 0 < h < \frac{1}{\|\vec{d}_i\|} \\ h = \frac{1}{\|\vec{d}_i\|} & \text{otherwise} \end{cases}$$

$y'$  is examined at the points  $\alpha \approx 0, h, 2h, \dots, a, \dots, b$  where  $\alpha$  is doubled each time and where  $b$  is the first of these values at which either  $y'$  is non-negative or  $y$  has not decreased. Then a cubic interpolation given by Davidson is used

$$\bar{y} = 3 \frac{y(a) - y(b)}{b - a} + y'(a) + y'(b)$$

$$w = (\bar{y}^2 - y'(a) \cdot y'(b))^{1/2}$$

The estimate  $\alpha_e$  of  $\alpha_m$  is:

$$\alpha_e = b - \left( \frac{y'(b) + w - \bar{y}}{y'(b) - y'(a) + 2w} \right) (b - a)$$

If neither  $y'(a)$  nor  $y'(b)$  is less than  $y'(\alpha_e)$ , then  $\alpha_e$  is accepted as the estimate of  $\alpha_m$ . Otherwise, according whether  $y'(\alpha_e)$  is positive or negative, the interpolation is repeated over the intervals  $[a, \alpha_e]$  or  $[\alpha_e, b]$  respectively.

### 3.3. Comparisons of the different methods and general considerations on errors

The least squares method can lead to very important errors when used with too many noise-affected signals or too short samples. These samples have to be long enough to allow the assumption that the noise is a zero-mean process and to be short enough so as we are able to assume that the time-dependent parameters are constant.

For the pitch equation, one has to differentiate the measured signal  $\hat{\theta}$  to get the pitch acceleration, and the effects of noise are increased. The integrated least squares have been used to avoid this problem but they need a good knowledge of the initial conditions. Otherwise, one can get a good identity of the measured signal and the calculated signal, but with coefficients which have no physical signification. More important errors on the values of parameters have been noted for integrated least squares than for ordinary least squares.

Filtering eliminates part of the information in the useful signal so that the parameter space is modified. The elimination of a high frequency noise by parallel filtering will unsensitize terms of the highest degree of the transfer function, and slows down their identification.

The modulating functions method avoids the determination of the initial conditions but have to be adapted to each sort of excitation (step, random signals, ...) to keep all informations contained in the signal, without introducing perturbations.

The method which seems to be the best fitted to the problem is the conjugate gradients method because it allows one to build very stressing cost functions, either linear or not, and it converges rapidly enough. But the disturbances generated by noise always exist because noise modify the equi-cost surfaces of the parameter space. The method converges then towards a new minimum as shown on figure 11.

The embarrassing noise for identification is made up by the secondary inputs of the system (gust for instance) which appear at the output as a correlated noise. It is then possible to modify the model so that it becomes adapted to the system.

But noise is not the only cause of error that influences the identification. One may consider two other causes:

- errors due to the assumption of linearity,
- errors due to the approximation of a continuous system by a discrete system.

These errors have an impact on:

- characterization step for the first case,
- sampling rate, the choice of which is difficult. One has to respect the Shannon condition, but the cut-off frequency of a signal is often not derived, and the highest sampling rate compatible with the measurement system is used.

But the requirements which one wants to have on the qualities of a model depend on what one looks for. It should be noted that parameters which are well excited by the input signal can be well identified whatever the method may be.

There are inputs which are called "sphericizing" (cf. ref. 1) that divide the information amongst all parameters and "sensitizing" inputs which focus it onto a given parameter.

As Rault (see ref. 1), we will state that there is more to win with the determination of "sensitizing" input signals than with the amelioration of identification methods. A low noise on a little significant trial can bring a much more important error than a noise with a high amplitude applied on a very significant test.

### 4. CONCLUSION

Identification is an unavoidable step in the conception of CCV systems. The experience collected by using these well known methods incites us on the one hand to investigate possible new methods and on the other hand to extend identification to flexible structures with a view to apply to them mode control processes.

### REFERENCES

- 1 - RICHALET, RAULT et POULIQUEN - Identification des processus par la méthode du modèle. Théorie des systèmes vol. 4, Gordon & Breach (1973).
- 2 - FLETCHER R. and REEVES C.M. - Function minimization by conjugate gradients. The computer Journal, vol. 7 (1964), p. 149-154.
- 3 - ROBERT M., MARCHETTI - Extraction of aerodynamic derivatives from flight data using an analog regression technique. Journal of Aircraft, vol. 5 (1968) n° 1, p. 22-26.
- 4 - KOEHLER R. - Bestimmung von Derivativen der Längsbewegung eines Flugzeuges aus Flugmessdaten durch ein Modell mit automatischen Parametereinstellung. DFVLR Brunswick DLR - FB - 73-13 (1973).
- 5 - FLETCHER R. and POWELL M.J.D. - A rapidly convergent descent method for minimization. The computer Journal, vol. 6 (1973), p. 613.
- 6 - BERTSEKAS D.P. - Partial conjugate gradient methods for a class of optimal control problems. IEEE Transactions of Automatic Control vol. AC-19 (1974), n° 3, p. 209-217.
- 7 - HESTENES M.R. and STIEFEL E. - Methods of conjugate gradients for solving linear systems. J. Res. N.B.S. vol. 49 (1952), p. 409.

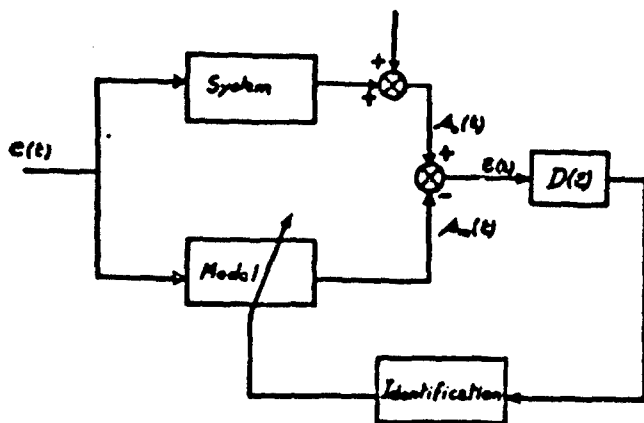


Fig. 1 - Diagram identification procedure.

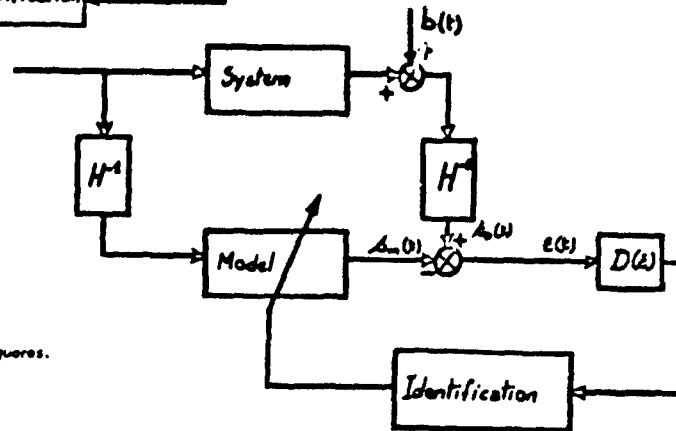


Fig. 2 - Diagram of the weighting least squares.

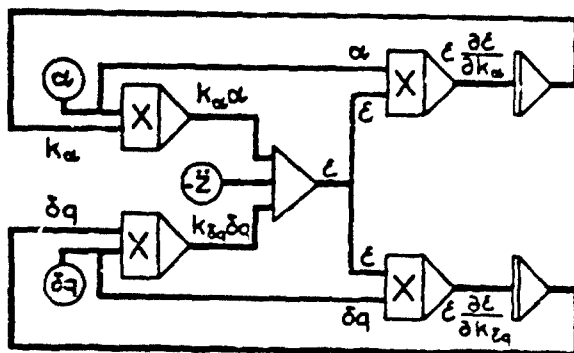


Fig. 3 - Automatic analog matching diagram for the lift equation.

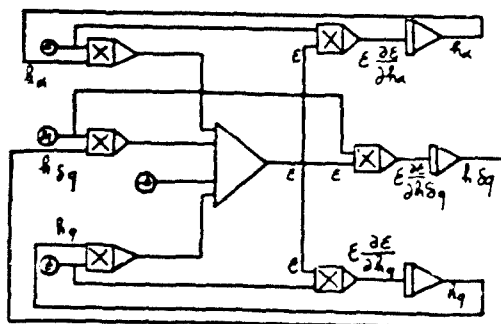


Fig. 4 - Automatic analog matching diagram for the pitch equation.

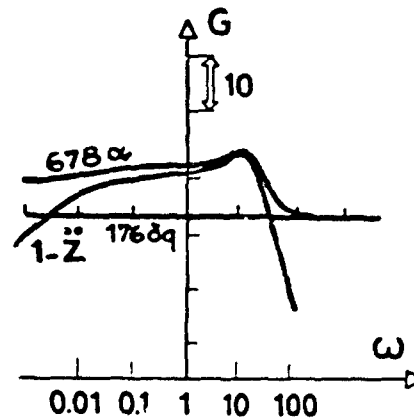


Fig. 5 - Amplitude Bode's diagram for the lift-equation.

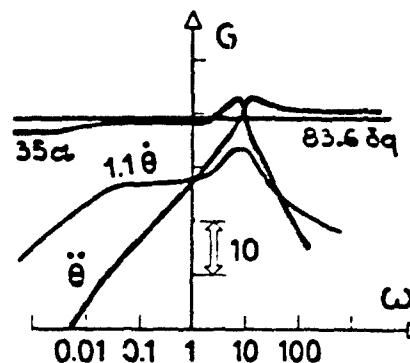


Fig. 6 - Amplitude Bode's diagram for the pitch-equation.

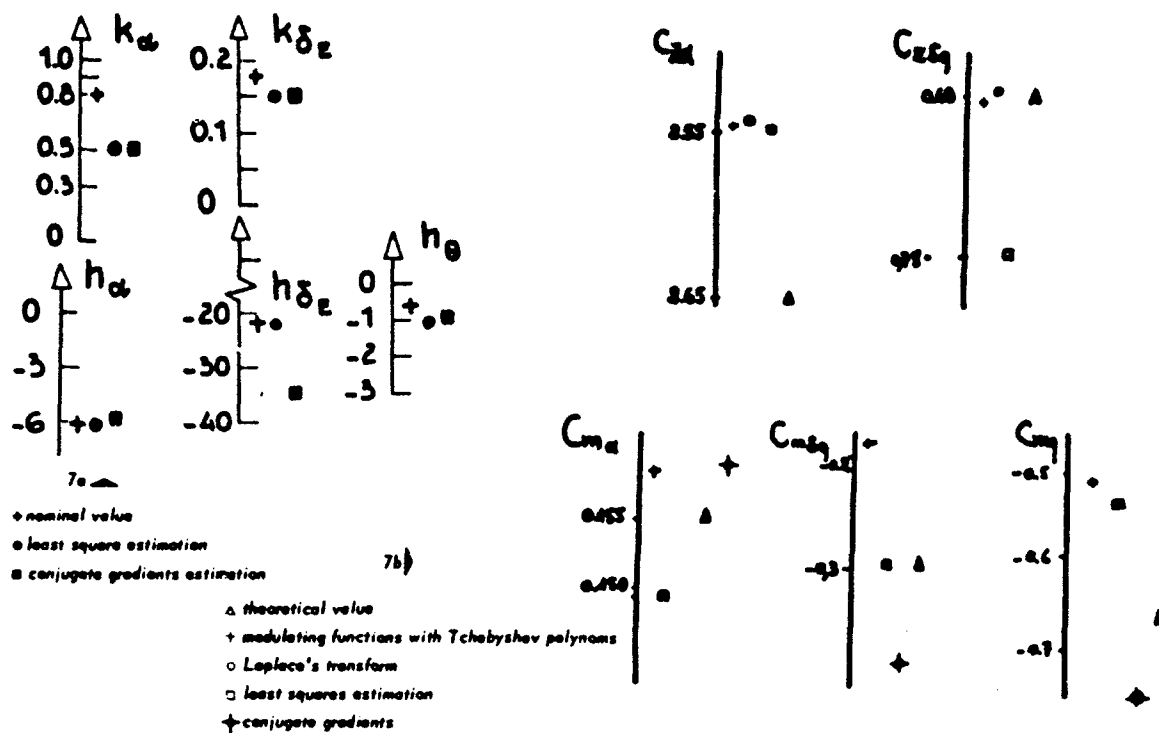
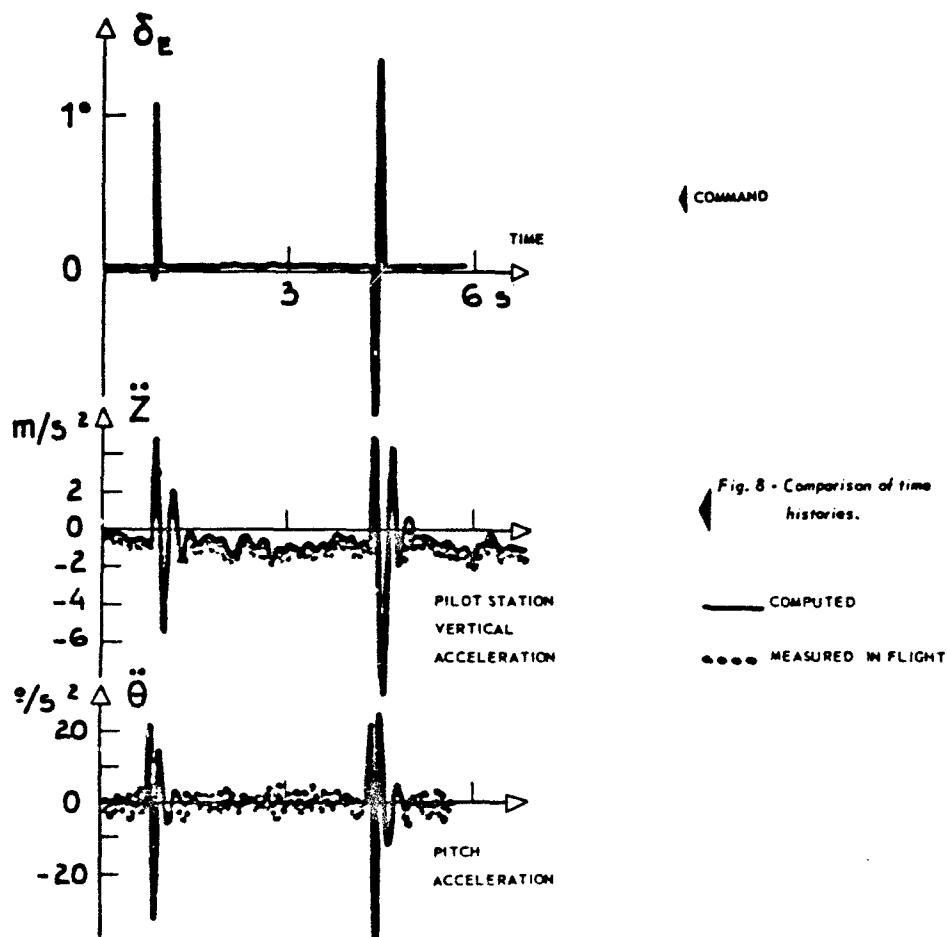


Fig. 7 - Estimation of the aerodynamic derivatives of the rigid aircraft - Subsonic regime.



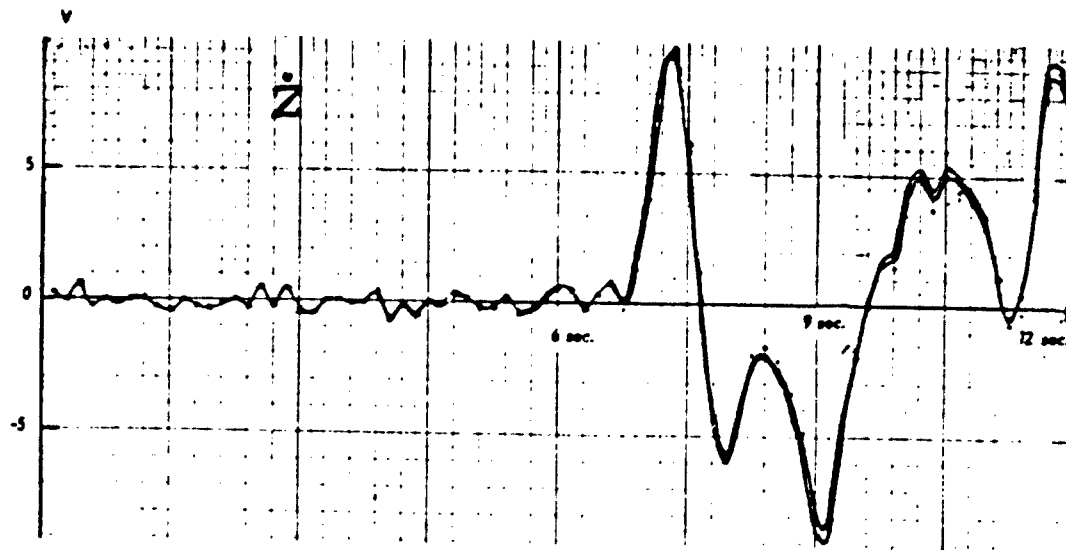


Fig. 9 - Time histories - Modulating functions method.

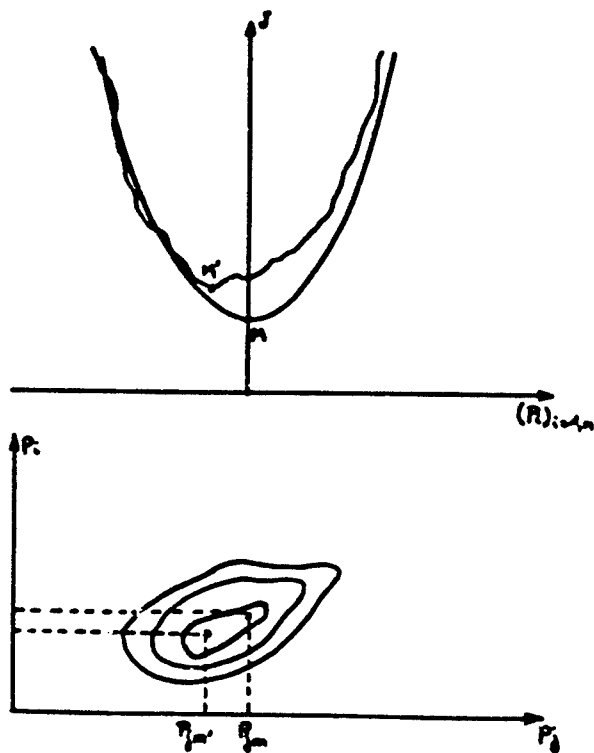
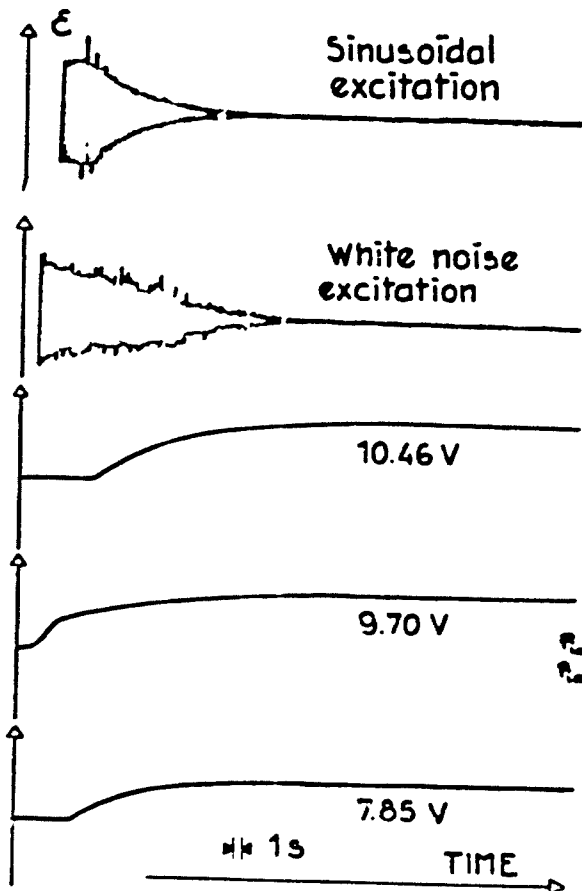


Fig. 11 - Same effects of noise on the estimation of the minimum of the cost function.

Fig. 10 - Analog matching results.

## STATUS OF INPUT DESIGN FOR AIRCRAFT PARAMETER IDENTIFICATION

by

R.K. Mehra  
Harvard University  
Cambridge, Massachusetts, USA

and

N. K. Gupta  
Systems Control, Inc.  
Palo Alto, California, USA

ABSTRACT

This paper presents some recent results on the design of aircraft inputs (i.e. elevator, rudder and aileron deflection time histories) to identify aircraft stability and control derivatives from flight test data. The problem is first reduced to an optimization problem with differential and integral constraints. The criteria used are either expressed in terms of the Cramer-Rao lower bound on the covariance matrix of the parameter estimates or in terms of the maximum prediction error variance. Both time-domain and frequency domain synthesis procedures are discussed. Numerical results are given for linearized longitudinal and lateral dynamics of C-8 and Jet Star aircrafts and comparison with doublet type inputs are made. Outstanding problems and areas for further research are also discussed.

1. Introduction and Background

The determination of aircraft stability and control derivatives involves three interrelated problems of input design, instrumentation and derivate extraction. The importance of choosing appropriate inputs (i.e., control surface deflections) for exciting specific modes of an aircraft or executing specific maneuvers during flight testing has been recognized for a long time, but a systematic attempt has only been made recently [7]. Several considerations which enter into the selection of inputs for an aircraft are:

1. Pilot Acceptability - The inputs should be capable of being implemented easily by a pilot and the resulting response of the aircraft should not endanger pilot safety.
2. Parameter Sensitivity - The measured response of the aircraft should be sensitive to the parameters that are being identified. This is necessary for obtaining good estimates of the parameters from the flight test data during the inverse computation or the identification process.
3. Instrumentation Limitations - The dynamic range of the instruments and their signal-to-noise characteristics impose limitations on the types and magnitudes of aircraft maneuvers. The relationship between input design and instrumentation specification has been emphasized in Ref. [2].
4. Derivative Extraction Method - In the past, the choice of control inputs has often been dictated by the desire to use a particular method for derivative extraction. For example, sinusoidal inputs were used initially to obtain the transfer function of an aircraft at specified frequencies[3]. However, it was soon realized that this was very expensive in terms of the total flight test time required to obtain the aircraft stability and control derivatives. [3] Next, the step and the doublet type of inputs were used and specialized methods such as Prony's Method[4] and the Time Vector Method[5] were devised to extract derivatives. With the more powerful digital techniques available today such as the Newton-Raphson[6, 35] and the Maximum Likelihood Methods[7], arbitrary inputs can be handled and it is no longer necessary to limit the inputs for the success of the derivative extraction method.
5. Modeling Assumptions - The six-degree-of-freedom equations of motion and the nonlinear aerodynamic model for an aircraft contain a large number of parameters (over 200). The simultaneous estimation of all these parameters from a single maneuver is not attempted since this would lead to nonuniqueness and identifiability problems. Generally, linearized decoupled equations of motion are used for the extraction of longitudinal and lateral stability and control derivatives. The inputs selected for exciting these modes should be such that the assumptions of linearity and decoupling are not violated. The inputs currently in use are mostly of the doublet type. The resulting aircraft response in an impulse-type of response about a given trim condition. Generally no attempt is made to optimize the frequency, the shape, or the timing of the impulses in order to make the aircraft response sensitive to the parameters that are being identified.
6. Use of Stability and Control Derivatives - The accuracy requirements for stability and control derivatives are dictated by their final use in response prediction, control system design, wind tunnel correlations, etc. The relative importance of the parameters may vary from one use to the other, thus changing the requirements for parameter accuracies. It is desirable to select those inputs that are optimal with respect to different criteria rather than just one criterion function. The importance of these considerations will be brought out in the next section where different criteria would be examined.

\* The research reported in this paper was made possible through support extended to Systems Control, Inc. by NASA under Contract NAS 4-2068 and to the Division of Engineering and Applied Physics, Harvard University, by the U.S. Office of Naval Research under the Joint Services Electronics Program under Contract N00014-67-A-0298-0006.



We now give a brief historical account of input design for aircraft parameter identification. The first systematic attempt seems to be that of Gerlach [8, 9], who using intuitive arguments selected inputs for damped second order systems. Gerlach's analysis is based on the frequency transfer function of the system and its sensitivity to frequency and to the parameter values. For identifying three parameters of the system Gerlach selects two frequencies in the ratio of 1:3 bracketing the natural frequency of the system. No attempt is made to allocate energy optimally between the two frequencies, but a low pass (sin vt/vt) filter is used to eliminate high frequencies from the input signal. These inputs were used by Gerlach [9] in nonsteady flight testing. A comparison of these inputs with the optimal inputs discussed in section 5 reveals the soundness of Gerlach's intuitive arguments.

Our interest in input design started with some simulation experience with X-22 data [7] where a multistep elevator input was found to give an order of magnitude better estimates of the parameters than a single step input. A mathematical statement of the problem starting initially with a scalar parameter showed that the input design problem could be formulated as a linear quadratic control problem of the maximization type [1]. The solutions to this problem were found to be related to the Sturm-Liouville problem and to the eigenvalue problem for Fredholm Integral equations [1]. The extension to multiparameter problem turned out to be much more complicated than originally expected since a large number of criteria based on different norms of the Fisher Information Matrix<sup>+</sup> can be used. Only the simple and weighted traces of the information matrix could be handled by straightforward extensions and their applicability to aircraft parameter identification was discussed in Ref. [10], where the importance of choosing the weighting matrix properly was emphasized. The trace of the Cramer-Rao lower bound was used by Mahi [11], Goodwin [12] and Reid [13], but only locally optimal numerical results were obtained using gradient-type methods. A more satisfactory approach to the problem was needed and a first hint of such an approach came from Viort [14] and Mehra [15], who formulated the input design problem in the frequency domain and used the important work of Kiefer and Wolfowitz [16, 17, 18] in statistical experimental design. This approach has now been extended to time-domain input design for a large class of systems [19, 20] and will be the subject of subsequent sections of this paper. Recently, Chen [21] has given a formulation of the input design problem as a time-optimal control problem, but the optimal solution to this problem suffers from the same numerical difficulties as faced earlier by Mahi [12] and Goodwin [13]. An approximate solution given by Chen [21] using Walsh function expansions lacks optimality properties.

We digress at this point to present basic ideas of the Kiefer-Wolfowitz [16, 17, 18] approach to experimental design in regression problems. In the sequel, we will show how these results extend to the design of inputs for dynamic systems, both in frequency and time-domain. Consider the problem of choosing values of the independent variables  $x$  from a given set  $X$ , in fitting a regression model between  $y$  and  $x$  of the following type

$$y = f^T(x)\theta + v \quad (1)$$

where  $f(x)$  is an  $m \times 1$  vector of regression functions (e.g.,  $x, x^2, x^3, \dots$ , in polynomial regression),  $\theta$  is an  $m \times 1$  vector of unknown regression coefficients and  $v$  is a random error with zero mean and variance  $\sigma^2$ . The covariance matrix of the least squares estimator  $\hat{\theta}$  is  $M^{-1}$  where  $M$ , the information matrix, is given by

$$M = \frac{1}{\sigma^2} \int_X f(x)f^T(x)\xi(dx) \quad (2)$$

and  $\xi(dx)$  is a probability measure defined over the set  $X$ . If  $N$  values of  $x$  are used in regression, then  $N\xi(dx)$  represents the fraction of measurements made between  $x$  and  $x + dx$ . Kiefer and Wolfowitz [17] show that the probability measure  $\xi(dx)$  can be chosen to be purely discrete, i.e., nonzero for a finite number of  $x$  values. In other words, the optimal design can be chosen to be of the form

$$\xi^*(x) = \{\xi_1, x_1; \xi_2, x_2; \dots; \xi_k, x_k; \sum_{i=1}^k \xi_i = 1\}$$

which concentrates  $N\xi_1$  measurements at  $x_1$ ,  $N\xi_2$  at  $x_2$  and so on. Furthermore, the optimal design  $\xi^*(x)$  is such that if it minimizes  $|M^{-1}|$ , then it also minimizes the maximum response prediction error variance, viz.

$$\max_{x \in X} \{f^T(x)M^{-1}(\xi)f(x)\}.$$

The quantity in brackets can be easily seen to be the variance of  $\hat{y} = f^T(x)\hat{\theta}$  for a given  $x$ . Karlin and Studden [22] give a game-theoretic interpretation of these results and Fedorov [23] discusses a number of interesting examples and applications.

The organization of this paper is as follows. In section 2, we formulate the input design problem mathematically and discuss several criteria for optimization. The solution procedures are described in section 3 and analytical examples are discussed in section 4. Numerical results are discussed in section 5. The last two sections (6 and 7) are devoted to the discussion of outstanding problems and conclusions.

<sup>+</sup>The inverse of the Fisher Information Matrix is the Cramer-Rao lower bound on the covariance of an unbiased estimator of the parameters.

## 2. Statement of the Problem

Consider the linearized equations of motion of an aircraft in state vector form

$$\frac{d}{dt} \mathbf{x}(t) = \mathbf{F}\mathbf{x}(t) + \mathbf{G}\mathbf{u}(t) \quad (3)$$

$$\mathbf{y}(t) = \mathbf{H}\mathbf{x}(t) + \mathbf{v}(t), \quad 0 \leq t \leq T \quad (4)$$

$$\mathbf{x}(0) = \mathbf{0}$$

where  $\mathbf{x}(t)$  is  $n \times 1$  state vector of position and velocity variables (both linear and angular),  $\mathbf{u}(t)$  is  $p \times 1$  vector of input variables (elevator, rudder, ailerons, etc.),  $\mathbf{y}(t)$  is  $p \times 1$  vector of output measurements (angles, velocities, and accelerations, etc.) and  $\mathbf{v}(t)$  is a  $p \times 1$  vector of random measurement errors. The matrices  $\mathbf{F}$ ,  $\mathbf{G}$  and  $\mathbf{H}$  contain stability and control derivatives and all other unknown parameters. The errors  $\mathbf{v}(t)$  are assumed to be gaussian and white viz

$$\mathbf{E}[\mathbf{v}(t)] = \mathbf{0}, \quad \mathbf{E}[\mathbf{v}(t)\mathbf{v}^T(\tau)] = \mathbf{R}\delta_{t,\tau}$$

The unknown but constant parameters in  $\mathbf{F}$ ,  $\mathbf{G}$ ,  $\mathbf{H}$  and  $\mathbf{R}$  are denoted by  $\theta$  ( $n \times 1$  vector). We estimate  $\theta$  from the knowledge of  $\{\mathbf{y}(t), \mathbf{u}(t), 0 \leq t \leq T\}$  using an unbiased efficient estimator  $\hat{\theta}$  with covariance  $\mathbf{M}^{-1}$ , where  $\mathbf{M}$  is the Fisher information matrix [23]. It is required to select a design for input  $\mathbf{u}(t) \in \Omega_u$  such that a suitable criterion function related to the objectives of the identification experiment is optimized.

### 2.1 Input Design Criteria

Aircraft estimation is done for one or more of the following objectives: (a) accurate determination of stability and control derivatives for wind-tunnel correlations and for use in simulators, (b) response prediction, (c) flight control system design, (d) handling qualities and aircraft certification.

Very often, the results of an identification experiment are used for all of the above objectives, but for input design purposes, a single criterion is to be chosen. Since control system design and handling qualities involve further considerations, we would mainly be concerned here with criteria (a) and (b) which will be called, respectively, the Parameter Space and Prediction Error criteria. It will be shown that one may obtain designs that are simultaneously optimal for these two criteria.

#### Parameter Space Criteria

The goodness of parameter estimates is most conveniently expressed in terms of the bias and the covariance properties of the estimates. For input design purposes, one assumes that an unbiased and efficient (e.g. maximum likelihood [7]) estimator is used so that the optimal input design can be carried out independent of the estimator used. This leads to a great simplification since the minimum variance given by the Cramer-Rao lower bound can be easily computed in a number of estimation problems, even though the exact covariance matrix of a particular estimator is very difficult to obtain.

Most of the work in input design is based on the assumption of an a priori estimate  $\theta_0$  for the parameters  $\theta$ . In aircraft input design, such an estimate is available from wind-tunnel tests. The Cramer-Rao lower bound,  $\mathbf{M}^{-1}$ , for the covariance of an unbiased estimator  $\hat{\theta}$  is given as

$$\mathbf{M} = \mathbf{E}_Y \left( \frac{\partial \log p(\mathbf{Y}, \theta)}{\partial \theta} \right) \left( \frac{\partial \log p(\mathbf{Y}, \theta)}{\partial \theta} \right)^T \quad (5)$$

where  $\mathbf{Y}$  denotes the set of observations  $\{\mathbf{y}(t), 0 \leq t \leq T\}$  and the expectation in (5) is taken over the sample space  $\Omega_Y$  of observations<sup>\*</sup>. An expression for  $\mathbf{M}$  will be derived in the next section, but consider first various scalar measures of performance based on  $\mathbf{M}$  and  $\mathbf{M}^{-1}$ .

(i) A-optimality:  $\text{Min}_{\Omega_u} \text{Tr}(\mathbf{M}^{-1})$ , i.e., minimize the average variance of the parameters.

(ii) E-optimality:  $\text{Min}_{\Omega_u} \lambda_{\max}(\mathbf{M}^{-1})$  where  $\lambda_{\max}$  is the maximum eigenvalue of  $\mathbf{M}^{-1}$ .

(iii) D-optimality: Minimize the determinant or the generalized variance  $|\mathbf{M}^{-1}|$ . This is equivalent to minimizing the volume of the uncertainty ellipsoids since

$$|\mathbf{M}^{-1}|^{1/2} = \frac{1}{(2\pi)^{m/2}} \int_{-\infty}^{\infty} \dots \int_{-\infty}^{\infty} \exp \left\{ -\frac{1}{2} \|\theta - \hat{\theta}\|_{\mathbf{M}^{-1}}^2 \right\} d\theta_1 \dots d\theta_m \quad (6)$$

Also,  $\log |\mathbf{M}^{-1}|$  is related to the mutual information between  $\theta$  and  $\mathbf{Y}$ , as shown by Arimoto and Kimura [25].

<sup>\*</sup> If the a priori estimate  $\theta_0$  is regarded as random with a priori probability distribution, Eq. (5) would also involve expectations with respect to this probability distribution. For details, see Ref. [24].

An important advantage of D-optimality is that it is invariant under scale changes in the parameters and linear transformations of the output [15], whereas A-optimality and E-optimality are affected by these transformations. Another advantage of D-optimality, to be shown later, is that it implies, Q-optimality, a prediction error criterion discussed below. Figure 1 shows the above criterion in two dimensions.

It is possible to imbed criteria (i)-(iii) in a more general measure of matrix norm used by Miller and Weber [26].

$$m_s = [1/m \operatorname{Tr} M^s]^{1/s}, \quad s \leq 0 \quad (7)$$

It can be shown that

$$\lim_{s \rightarrow 0} m_s = |M|^{1/m} \quad (8)$$

$$m_{-1} = m / \operatorname{Tr} M^{-1} \quad (9)$$

$$\lim_{s \rightarrow -\infty} m_s = \lambda_{\min}(M) \quad (10)$$

$$m_{s_1} \geq m_{s_2} \quad \text{if} \quad s_1 \geq s_2 \quad (11)$$

**Remark:** Aoki and Staley [27], Mehra [1], Mahi and Napjus [28], and many other authors have used  $\operatorname{Tr}(M)$  or  $\operatorname{Tr}(M^{-1})$  as a criterion. This criterion leads to a quadratic optimization problem which is easy to solve. But it can result in a singular  $M$  and should be used only to obtain start-up inputs for optimizing with respect to one of the above criteria.

**Information Matrix:** In this section, we derive an expression for the Fisher Information Matrix  $M$  using Eq. (5). The log-likelihood function for the system (3)-(4) is

$$L(\theta, R) = -\frac{1}{2} \int_0^T (y(t) - H(\theta)x(t, \theta))^T R^{-1} (y(t) - H(\theta)x(t, \theta)) dt - \frac{T}{2} \log |R| + \text{constant} \quad (12)$$

Taking partial derivatives with respect to elements of  $\theta$  and  $R$ ,

$$\frac{\partial L}{\partial \theta_j} = - \int_0^T (y(t) - H(\theta)x(t, \theta))^T R^{-1} \left( \frac{\partial H}{\partial \theta_j} x(t, \theta) + H(\theta) \frac{\partial x(t, \theta)}{\partial \theta_j} \right) dt \quad (13)$$

$$M_{ij} = E \left( \frac{\partial^2 L}{\partial \theta_i \partial \theta_j} \right) = \int_0^T \left( \frac{\partial H}{\partial \theta_i} x(t, \theta) + H(\theta) \frac{\partial x(t, \theta)}{\partial \theta_i} \right)^T R^{-1} \left( \frac{\partial H}{\partial \theta_j} x(t, \theta) + H(\theta) \frac{\partial x(t, \theta)}{\partial \theta_j} \right) dt \quad (14)$$

$$\frac{\partial^2 L}{\partial R_{kl} \partial \theta_j} = \int_0^T (y(t) - H(\theta)x(t, \theta))^T R^{-1} \frac{\partial R}{\partial R_{kl}} R^{-1} \left( \frac{\partial H}{\partial \theta_j} x(t, \theta) + H(\theta) \frac{\partial x(t, \theta)}{\partial \theta_j} \right) dt \quad (15)$$

$$\text{or} \quad E \left( \frac{\partial^2 L}{\partial R_{kl} \partial \theta_j} \right) = 0 \quad (16)$$

Thus the information matrix for  $\theta$  and  $R$  may be written as

$$M = \begin{bmatrix} M_{\theta\theta} & 0 \\ 0 & M_{RR} \end{bmatrix} \quad (17)$$

where the  $i, j$ th element of  $M_{\theta\theta}$  is given by Eq. (14) and  $M_{RR}$  does not depend on the input  $u(t)$ . Therefore, from now on, we will denote  $M_{\theta\theta}$  by  $M$  and remove  $M_{RR}$  from further consideration.

The sensitivity function equations are easily obtained from Eq. (3) and (4) as

$$\frac{d}{dt} \left( \frac{\partial x(t)}{\partial \theta_i} \right) = F \frac{\partial x(t)}{\partial \theta_i} + \frac{\partial F}{\partial \theta_i} x(t) + \frac{\partial G}{\partial \theta_i} u(t) \quad (18)$$

$$\frac{\partial x(0)}{\partial \theta} = 0 \quad (19)$$

### Prediction Error Criterion

Let us assume that after the maximum likelihood parameter estimate  $\hat{\theta}$  has been obtained, it is required to predict the response of the aircraft to a given input  $\{u_p(t), 0 \leq t \leq T\}$ . Using the equations of motion with  $\hat{\theta}$ , we obtain the maximum likelihood prediction as

$$\hat{y}(t, u_p, \hat{\theta}) = Hx(t, u_p, \hat{\theta}) \quad (20)$$

The prediction error

$$e(t, u_p) = y(t, u_p, \theta) - \hat{y}(t, u_p, \hat{\theta}) = H(\theta)x(t, u_p, \theta) - H(\hat{\theta})\hat{x}(t, u_p, \hat{\theta}) + v(t) \quad (21)$$

Expanding  $H(\theta)$  and  $x(t, u_p, \theta)$  to first order around  $\hat{\theta}$  and neglecting higher order terms in  $(\theta - \hat{\theta})$ , we get

$$e(t, u_p) = \frac{\partial}{\partial \theta} \{H(\theta)x(t, u_p, \theta)\}_{\theta=\hat{\theta}} (\theta - \hat{\theta}) + v(t) \quad (22)$$

The covariance of prediction error is, therefore,

$$E\{e(t, u_p)e^T(t, u_p)\} = \frac{\partial}{\partial \theta} \{H(\theta)x(t, u_p, \theta)\}_{\theta=\hat{\theta}} M(u)^{-1} \frac{\partial}{\partial \theta} \{H(\theta)x(t, u_p, \theta)\}_{\theta=\hat{\theta}}^T + R \quad (23)$$

Denote by

$$J(u, u_p) = \int_0^T E\{e^T(t, u_p)R^{-1}e(t, u_p)\}dt, \text{ the normalized total mean square prediction}$$

error for input  $\{u_p(t), 0 \leq t \leq T\}$ .

Using Eq. (23)

$$J(u, u_p) = \text{Tr}\{M^{-1}(u)M(u_p)\} + T \quad (24)$$

Notice  $u$  is the design input employed during parameter estimation and  $u_p$  is the input used for response evaluation. We now define the input design criterion as a minimax criterion in which  $u \in \Omega_u$  is chosen to minimize the maximum prediction error i.e.

$$\hat{J}(u) = \max_{u_p \in \Omega_{u_p}} J(u, u_p) \quad (25)$$

It is clear that for input design purposes only the quantity  $\text{Tr}\{M^{-1}(u)M(u_p)\}$  is important. In the next section, we show that the prediction error criterion (also called G-optimality) and the determinant criterion (D-optimality) lead to similar input designs.

### 3. Optimal Input Designs

In this section, three methods for input design are considered. The first method produces non-randomized or deterministic time-domain inputs maximizing locally a norm  $m_g$  (see Eq. (7)-(11)) of the information matrix  $M$ . The second method considers a larger class of inputs viz. randomized or stochastic time-domain inputs and produces globally optimal inputs with respect to the above criteria. The third technique synthesizes frequency domain inputs for the stationary case and is computationally much more efficient than the time-domain techniques.

We first express the information matrix  $M$  (Eq. 14) in terms of  $u(t)$  alone using Eqs. (3), (18), and (19). It is convenient to use the transition matrix  $\Phi(t, \tau)$  defined as

$$\frac{d}{dt} \Phi(t, \tau) = F \Phi(t, \tau) \quad (26)$$

$$\Phi(\tau, \tau) = I \quad (27)$$

$$\text{Then } x(t) = \int_0^T \Phi(t, \tau) G u(\tau) d\tau \quad (28)$$

$$\frac{\partial x(t)}{\partial \theta_1} = \int_0^T \left[ \frac{\partial \Phi}{\partial \theta_1}(t, \tau) G u(\tau) + \Phi(t, \tau) \frac{\partial G}{\partial \theta_1} u(\tau) \right] d\tau = \int_0^T A_1(t, \tau) u(\tau) d\tau \quad (29)$$

Thus

$$M_{ij} = \int_0^T \left[ \left( \int_0^t u^T(\tau) \left( \frac{\partial H}{\partial \theta_i} \Phi(t, \tau) G + H A_i(t, \tau) \right) H^{-1} \left[ \int_0^t \left( \frac{\partial H}{\partial \theta_j} \Phi(t, s) G + H A_j(t, s) \right) u(s) ds \right] d\tau \right) \right] dt \quad (30)$$

Eq. (30) may be simplified to

$$M_{ij} = \int_0^T \int_0^T u^T(\tau) W_{ij}(\tau, s) u(s) d\tau ds \quad (31)$$

where  $W_{ij}(\tau, s) = \int_0^T \left[ \frac{\partial H}{\partial \theta_i} \Phi(t, \tau) G + H A_i(t, \tau) \right]^T H^{-1} \left[ \frac{\partial H}{\partial \theta_j} \Phi(t, s) G + H A_j(t, s) \right] dt$  (32)  
(qxq matrix)  $\max(\tau, s)$

In the sequel, we will be concerned with the eigenvalues and eigenfunctions of kernels related to  $W_{ij}(\tau, s)$ . In particular, we would consider the kernel

$$N(\tau, s) = \sum_{i,j=1}^m p_{ij}^{k-1} W_{ij}(\tau, s) \quad (33)$$

(qxq matrix)  $i, j=1$

where  $p_{ij}^{k-1}$  denotes the  $(i, j)$ th element of the matrix  $M^{k-1}$  and  $k$  is a nonpositive integer ( $k \leq 0$ ). The eigenfunctions (qx1) and eigenvalues of  $N(\tau, s)$  are defined by the Fredholm integral equation,

$$\int_0^T N(\tau, s) \pi_i(\tau) d\tau = \xi_i \pi_i(s), \quad i=1, 2, \dots \quad (34)$$

The kernel  $N(\tau, s)$  is symmetric since

$$N^T(s, \tau) = \sum_{i,j=1}^m p_{ij}^{k-1} W_{ij}^T(s, \tau) = \sum_{i,j=1}^m p_{ji}^{k-1} W_{ji}(\tau, s) = N(\tau, s) \quad (35)$$

Thus all the eigenvalues  $\xi_1, \xi_2, \dots$  of Eq. (34) are real and the corresponding normalized eigenfunctions  $\pi_1, \pi_2, \dots$  are an orthogonal and complete set. We may thus expand any function  $u(t)$  in terms of the above eigenfunctions as

$$u(t) = \sum_{i=1}^{\infty} \alpha_i \pi_i(t) \quad (36)$$

where

$$\alpha_i = \langle u(t), \pi_i(t) \rangle = \int_0^T u^T(t) \pi_i(t) dt$$

and

$$\sum_{i=1}^{\infty} \alpha_i^2 = 1 \quad (37)$$

LEMMA 1: The maximum eigenvalue  $\xi_{\max}$  of the homogeneous Fredholm integral equation

$$\int_0^T \left[ \sum_{i,j=1}^m p_{ij}^{k-1} W_{ij}(\tau, s) \right] \pi(\tau) d\tau = \xi_{\max} \pi(s) \quad (38)$$

subject to

$$\int_0^T \pi^T(t) \pi(t) dt = 1 \quad (39)$$

satisfies the inequality

$$\xi_{\max} \geq \text{Tr}[M^k] \quad (40)$$

Proof: Consider

$$\text{Tr}[M^k] = \text{Tr}[M^{k-1} M] = \sum_{i,j=1}^m p_{ij}^{k-1} M_{ij} = \int_0^T \int_0^T \text{Tr} \left( \sum_{i,j=1}^m p_{ij}^{k-1} W_{ij}(\tau, s) \right) u(\tau) u^T(s) d\tau ds$$

Using Eqs. (36) and (37)

$$\text{Tr}[M^k] = \text{Tr} \int_0^T \int_0^T \sum_{k,l=1}^m \sum_{i,j=1}^m p_{ij}^{k-1} w_{ij}(\tau, s) w_k(\tau) w_l^T(s) \alpha_k \alpha_l d\tau ds = \sum_{k=1}^m \alpha_k^2 \xi_k \leq \xi_{\max} \quad (\text{From Eq. (37)})$$

The equality is attained when  $u(s) = w(s)$ , the eigenfunction corresponding to  $\xi_{\max}$ .

We now prove the main theorem for the design of time-domain nonrandomized inputs.

### 3.1 Time Domain Nonrandomized Inputs:

**Theorem 1:** A set of necessary conditions for an input  $\{u^*(t), t \in [0, T]\}$  to maximize  $m_k$ ,  $k \leq 0$  locally subject to the constraint  $\int_0^T u(t)u(t)dt \leq 1$  are

$$(i) \int_0^T u^*(t)u^*(t)dt = 1 \quad (41)$$

(ii)  $u^*(.)$  minimizes the maximum eigenvalue  $\xi_{\max}$  of the nonlinear homogenous Fredholm integral equation

$$\int_0^T M(\tau, s; u)u(\tau)d\tau = \xi u(s) \quad (42)$$

where  $M(\tau, s; u) = \sum_{i,j=1}^m p_{ij}^{k-1}(u)w_{ij}(\tau, s)$  is a symmetric kernel and  $p_{ij}^{k-1}$  is the  $(i, j)$ th element of  $M^{k-1}$

$$(iii) \xi_{\max}(M(\tau, s; u^*)) = \text{Tr}[M^k(u^*)] \quad (43)$$

(iv)  $u^*(.)$  is an eigenfunction of Eq. (42) corresponding to  $\xi_{\max}$ .

**Proof:** (i) follows easily from the fact that  $M$  is scaled by  $\alpha$  when the norm of  $u$  is scaled by  $\alpha$ . Thus the maximum  $m_k$  is attained for maximum norm of  $u(.)$  i.e. Eq. (41).

We now define the Lagrangian function

$$L(u, \lambda) = m_k(u) - \lambda \left[ \int_0^T u^T(t)u(t)dt - 1 \right] \quad (44)$$

where  $\lambda > 0$  is an unknown scalar Lagrange multiplier. A set of necessary conditions for  $u^*$  to be a local maximum are that  $L(u, \lambda)$  be stationary at  $u^*$  and  $L(u^*, \lambda)$  be minimized with respect to  $\lambda$ .

We use a calculus of variations approach to derive the stationarity condition for  $L(u, \lambda)$ . Consider an admissible variation  $\delta u$  in  $u$  and define the change in  $L$  to first order in  $\delta u$  as,

$$\delta L = L(u + \delta u, \lambda) - L(u, \lambda) = \frac{1}{k-1} \text{tr}[M^k(u + \delta u) - M^k(u)] - 2\lambda \int_0^T u^T(t)\delta u(t)dt \quad (45)$$

Now to first order in  $\delta u$ ,

$$\begin{aligned} M_{ij}(u + \delta u) &= \text{Tr} \int_0^T \int_0^T w_{ij}(\tau, s) [u(\tau)u^T(s) + u(\tau)\delta u^T(s) + \delta u(\tau)u^T(s) + \delta u(\tau)\delta u^T(s)] d\tau ds \\ &= M_{ij}(u) + \int_0^T [D_{ij}(\tau) + D_{ji}(\tau)] \delta u(\tau) d\tau \end{aligned} \quad (46)$$

where

$$D_{ij}(\tau) = \int_0^T u^T(s)w_{ij}(\tau, s)ds \quad (47)$$

$$D_{ji}(\tau) = \int_0^T u^T(s)w_{ji}(\tau, s)ds = \int_0^T u^T(s)w_{ij}^T(s, \tau)ds \quad (48)$$

Define an  $m \times m$  matrix  $\delta W$  with elements

$$(\delta W)_{ij} = \int_0^T [D_{ij}(\tau) + D_{ji}(\tau)] \delta u(\tau) d\tau \quad (49)$$

$$\text{Then } M(u + \delta u) = M(u) + \delta W \quad (50)$$

$$\text{tr}[M^k(u + \delta u) - M^k(u)] = k \text{tr}[M^{k-1} \delta W] \quad (51)$$

From Eq. (45),

$$\delta L = \frac{1}{m_k^{k-1}} \text{tr}(M^{k-1} \delta W) - 2\lambda \int_0^T u^T(\tau) \delta u(\tau) d\tau = 2 \int_0^T \left\{ \frac{1}{m_k^{k-1}} \sum_{i,j=1}^m p_{ij}^{k-1} D_{ij}(\tau) - \lambda u^T(\tau) \right\} \delta u(\tau) d\tau \quad (52)$$

For optimality  $\delta L$  should be zero for all admissible variations  $\delta u$  from the optimum  $u^*$ , which implies

$$\sum_{i,j=1}^m p_{ij}^{k-1} D_{ij}(\tau) = m_k^{k-1} \lambda u^T(\tau), \quad \forall \tau \in [0, T] \quad (53)$$

Substituting for  $D_{ij}(\tau)$  from Eq. (47)

$$\int_0^T u^T(s) \sum_{i,j=1}^m p_{ij}^{k-1} W_{ij}(\tau, s) ds = m_k^{k-1} \lambda u^T(\tau)$$

or

$$\int_0^T \sum_{i,j=1}^m p_{ij}^{k-1} W_{ij}(s, \tau) u^*(s) ds = m_k^{k-1} \lambda u^*(\tau) \quad (54)$$

which is the same as Eq. (42) with

$$\xi = m_k^{k-1} \lambda \quad (55)$$

Now we maximize  $L(u^*, \lambda)$  over  $\lambda$ . To evaluate  $\lambda$ , premultiply Eq. (54) on both sides by  $u^{*T}(\tau)$  and integrate over  $\tau$  from 0 to  $T$ . This gives, using Eq. (41)

$$\lambda = \frac{1}{m_k^{k-1}} \text{tr}(M^k) \quad (56)$$

or

$$L(u^*, \lambda) = \lambda \quad (57)$$

We thus choose the smallest  $\lambda$  that satisfies Eq. (54). Since, in this case,  $\xi = m_k^{k-1} \lambda$  and  $k < 0$ , this implies choosing the maximum eigenvalue  $\xi_{\max}$  for determining  $u^*$ . Also  $\xi_{\max} = \text{tr}(M^k)$  which from Lemma 1 is the smallest value of  $\xi_{\max}$ . From this, theorem 1 follows immediately.

**Remark:** Consider the prediction error criterion  $J(u, u_p) = \text{Tr}(M^{-1}(u)M(u_p))$ , which is maximized with respect to  $u_p$ , and minimized with respect to  $u$  both being constrained to be of unit norm. It is easily seen that

$$J(u, u_p) = \sum_{i,j=1}^m p_{ij}(u) M_{ij}(u_p) = \int_0^T \int_0^T u_p^T(\tau) N_o(u, \tau, s) u_p(s) d\tau ds \quad (58)$$

$$\text{where } N_o(u, \tau, s) = \sum_{i,j=1}^m p_{ij}(u) W_{ij}(\tau, s)$$

$$\text{Thus, } \max_{\|u_p\|=1} J(u, u_p) = \xi_{\max}(N_o(u, \tau, s)) \quad (59)$$

The optimal input  $u(\cdot)$  minimizing  $\xi_{\max}(N_o)$  is, therefore, the same as the input  $u^*(\cdot)$  maximizing  $m_o = |M(u)|^{1/m}$ . Thus the, G-optimal and D-optimal inputs are the same. Furthermore,

$$\xi_{\max}(N_o(u^*, \tau, s)) = \text{Tr}[I] = m$$

**Algorithm 1:** The input  $u^*(t)$  maximizing  $|M(u)|$  may be computed as follows.

(a) Start with any input  $u_o$  such that  $M(u_o)$  is nonsingular. Let  $k=0$ .

(b) Compute  $N(u_k, \tau, s) = \sum_{i,j=1}^m p_{ij}(u_k) W_{ij}(\tau, s)$ , and find its maximum eigenvalue - eigenvector (normalized)

pair  $(\xi_{\max}^k, \pi_{\max}^k)$  such that  $\langle u_k, \pi_{\max}^k \rangle \geq 0$ . A method for computing  $(\xi_{\max}^k, \pi_{\max}^k)$  using Riccati Equation is given in Ref. [1].

(c) If  $\xi_{\max} = m$ , stop. Otherwise go to (d).

(d) Let  $u_{k+1} = [(1-\beta)u_k + \beta \pi_{\max}^k] / \|\pi_{k+1}\|$  (60)

Choose  $\beta$  by a one-dimensional search to maximize  $|M(u_{k+1})|$  or any other  $\beta \in (0; 1]$  to ensure that  $|M(u_{k+1})| \geq |M(u_k)|$ . This can always be done away from the optimum since

$$\frac{\partial}{\partial \beta} \log |M(u_{k+1})|_{\beta=0} = 2(\xi_{\max}^k - \alpha) \langle u_k, \tau_{\max}^k \rangle \quad (61)$$

(a) Go back to (b).

In general, if the  $\beta_k$ -sequence is such that  $\sum_{k=0}^{\infty} \beta_k = \infty$  and  $\lim_{k \rightarrow \infty} \beta_k = 0$ , the above iteration would converge to a local maximum of  $|M(u)|$ .

### 3.2 Time Domain Randomized Inputs

If the identification experiment is repeated several times, we may do better by changing inputs according to some probability law. The design problem, then, is to choose the probability distribution function,  $f(u)$  so as to maximize the randomized information matrix

$$M(f) = \int_{\Omega_u} M(u) f(du) \quad (62)$$

It is shown in Ref. [19] that only discrete distribution functions with at most  $n_u = m(m+1)/2$  points need be considered so that

$$M(f) = \sum_{i=1}^{n_u} M(u_i) f_i, \quad \sum_{i=1}^{n_u} f_i = 1$$

An input design consists of  $\{f_i, u_i, i=1, n_u\}$

Since  $M(f)$  is linear in  $f_i$ 's, the determinant  $|M(f)|$  will be a concave function of  $f_i$ 's. Thus the Kuhn-Tucker theorem gives necessary and sufficient conditions for a global maximum. The following result is proved in Ref. [19].

**Theorem 2:** The following are equivalent

(i)  $f^*$  maximizes  $|M(f)|$

(ii)  $f^*$  minimizes  $\max_{u \in \Omega_u} \text{Tr}(M^{-1}(f)M(u_p))$

(iii)  $\max_{u \in \Omega_u} \text{Tr}(M^{-1}(f^*)M(u_p)) = n$  (63)

All designs satisfying (i) - (iii) and their linear combinations have the same information matrix  $M(f^*)$ .

**Remarks:** In general  $|M(f^*)| \geq |M(u^*)|$ , with equality in those cases where  $f^*$  consists of only one point i.e.  $f^*(u^*) = 1$ . Thus, Randomized inputs may be used to obtain lower bounds and approximations to  $u^*$ .

### 3.3 Frequency-Domain Synthesis of Optimal Inputs

If the system described by Eqs. (3)-(4) is (i) stable and time-invariant, (ii) data length  $T$  is large\* and (iii) the noise processes are stationary, one may compute the optimal inputs much more efficiently by using frequency-domain techniques. The basic simplifications comes from three facts: a) The Fourier transformation is an orthogonalizing transformation in the sense that the Fourier series components of a stationary process are orthogonal to each other. Alternatively, the Fourier transformation diagonalizes the covariance matrix of a stationary process. b) The set of all stationary inputs is characterized by the  $q \times q$  spectral density matrix  $S_{uu}(\omega)$  with the frequency variable  $\omega \in (-\infty, \infty)$ . This should be contrasted with the time domain representation of  $U$  as a vector in  $\Omega_u \subset \mathbb{R}^{nq}$ . c) The optimal input can be chosen to be nonrandomized or deterministic in the stationary case (see Theorem 4).

We now state the relevant results for frequency domain synthesis of optimal inputs. For proofs of these results, see Refs. [15, 29].

**THEOREM 3:** The asymptotic per sample Fisher information matrix (MCM) for parameter set  $\theta$  of the system (3)-(4) has the elements

$$\lim_{T \rightarrow \infty} \frac{1}{T} M_{ij} = \bar{M}_{ij} = \text{Re} \frac{1}{2\pi} \int_{-\infty}^{\infty} \text{Tr}(B_{ij}(\omega) dF_{uu}(\omega)) \quad (64)$$

where  $\text{Re}$  denotes real part,  $F_{uu}(\omega)$  is the spectral distribution function of  $u(t)$  and

\* In practice, it has been found that data lengths more than three times the largest time-period are adequate for using the frequency domain method. (See Section 5.1.2.)



$$B_{ij}(\omega) = \frac{\partial T^*(\omega)}{\partial \theta_i} S_{vv}^{-1} \frac{\partial T(\omega)}{\partial \theta_j}$$

(\* denotes complex conjugate and transpose)

$$T(\omega) = H(\omega I - \Phi)^{-1} G \quad (66)$$

$S_{vv}(\omega)$  is the spectral density of measurement noise  $v(t)$ .

**THEOREM 4:** (i) The information matrix  $\bar{M}$  is a real, symmetric, nonnegative definite matrix.

(ii) The set of information matrices  $\bar{M}$  corresponding to all normalized designs (i.e.,

$$1/2\pi \int_{-\infty}^{\infty} \text{Tr } dF_{uu}(\omega) = 1) \text{ is convex and closed.}$$

(iii) For any normalized input design  $F_1$  with mixed spectrum, another design  $F_2$  with a purely point spectrum of less than  $[n(n+1)/2+1]$  points can be found such that  $\bar{M}(F_1) = \bar{M}(F_2)$ .

**Comment:** 1) Notice that in the frequency domain, the role of the probability measure  $f$  is played by the spectral density function. Part (iii) of Theorem 4 implies that a suitably chosen deterministic input will provide as much information as a stochastic input in the stationary case. We will therefore restrict the search for an optimal input to that containing a finite number of frequencies.

**D-optimal design in frequency domain:** We now maximize  $|\bar{M}|$  with respect to  $(F_{uu}(\omega), \omega \in (-\infty, \infty))$  subject to the constraint

$$\frac{1}{2\pi} \text{Tr} \int_{-\infty}^{\infty} dF_{uu}(\omega) \leq 1 \quad (67)$$

The optimal input spectrum  $\hat{F}_{uu}$  will be shown to have the following characteristics.

**THEOREM 5:** For the optimal input spectrum

$$\frac{1}{2\pi} \text{Tr} \int_{-\infty}^{\infty} d\hat{F}_{uu}(\omega) = 1$$

and the following are equivalent

- (i)  $\hat{F}_{uu}$  maximizes  $|\bar{M}|$   
 (ii)  $\hat{F}_{uu}$  minimizes  $\max_{\omega} \lambda_{\max} \left[ \text{Re} \sum_{i,j=1}^n \bar{p}_{ij}(\hat{F}_{uu}) B_{ij}(\omega) \right]$

where  $\bar{p}_{ij}$  is the  $(i,j)$ th element of  $\bar{M}^{-1}$  and  $\lambda_{\max}$  is the maximum eigenvalue of  $qxq$  matrix inside the parentheses.

$$(iii) \max_{\omega} \lambda_{\max} \left[ \text{Re} \sum_{i,j=1}^n \bar{p}_{ij}(\hat{F}_{uu}) B_{ij}(\omega) \right] = n \quad (68)$$

The information matrices of all normalized designs satisfying conditions (i)-(iii) are identical and any linear combination of these designs also satisfy (i)-(iii).

**Algorithm 2:** (a) Start with any design  $F_0$  such that  $\bar{M}(F_0)$  is nonsingular. Let  $k = 0$ .

$$(b) \text{ Compute } D_k = \text{Re} \sum_{i,j=1}^n \bar{p}_{ij}(F_k) B_{ij}(\omega)$$

and find its maximum eigenvalue  $\lambda_{\max}^k(\omega)$ . Find  $\omega_k \in (-\infty, \infty)^*$  by a one dimensional search so that

$$\lambda_{\max}^k(\omega_k) \geq \lambda_{\max}^k(\omega) \quad (69)$$

Also compute the eigenvector  $\nu_{\max}^k$ .

$$(c) \text{ If } \lambda_{\max}^k(\omega_k) = n \quad (70)$$

stop. Otherwise proceed to (d).

\* In most of the practical problems the search for  $\omega_k$  can be confined to a set of reasonable frequency values, e.g.  $[-\omega_m, \omega_m]$ .

(d) Update the design as follows:

$$F_{k+1} = (1 - \alpha_k) F_k + \alpha_k F(\omega_k) \quad (71)$$

where  $F(\omega_k)$  is a design with a single point at  $\omega = \omega_k$  of size  $\psi_{\max}^k (\psi_{\max}^k)^T$ . Choose  $0 < \alpha_k \leq 1$  either by a one-dimensional search or any sequence such that

$$|N^{k+1}| \geq |N^k|, \quad \sum_{k=0}^{\infty} \alpha_k = \infty, \quad \lim_{k \rightarrow \infty} \alpha_k = 0 \quad (72)$$

(e) Go back to (b).

**Remarks:** 1) A comparison of the above algorithm with the corresponding time-domain algorithm 1 reveals its appealing computational simplicity. In the single-input case, the search for the computational simplicity. In the single-input case, the search for the maximum in step b) is a one-dimensional search over the range  $[-\omega_m, \omega_m]$ . In the multi-input case, eigenvalues and eigenvectors of only a  $q \times q$  matrix have to be computed. The time-domain approach, on the other hand, requires computation of eigenvectors and eigenvalues of  $N_q \times N_q$  matrices.

2) The D-optimal frequency domain synthesis problem has a simple game-theoretic interpretation. The nature (maximizer) picks the frequency  $\omega$  and eigenvector direction  $\psi_{\max}$  and the designer picks the input spectrum. The payoff function is a scalar norm of the transfer function covariance matrix.

3) It is not necessary to use sinusoidal inputs to achieve the desired spectrum. Van der Bos [30] shows how a desired spectrum may be achieved using binary valued periodic inputs and Papoulis [31] shows how it may be obtained using the Arcsine law.

#### 4. Analytical Examples

In this section, we discuss a few selected analytical examples to indicate the general nature of the results.

##### 4.1 First Order Systems with Unknown Gain ([32], [1])

Consider a scalar system

$$\dot{x}(t) = -x(t) + \theta u(t) \quad (73)$$

with measurements

$$y(t) = x(t) + v(t) \quad t \in [0, T] \quad (74)$$

where  $v(t)$  is stationary exponentially correlated noise

$$E[v(t)v(\tau)] = ce^{-a|t-\tau|} \quad (75)$$

Using results from Section 3, the optimal input for estimating  $\theta$  is:

$$u^*(t) = A \sin(\omega t + \phi) \quad (76)$$

where

$$\phi = \tan^{-1} \omega \quad (77)$$

and  $\omega$  is a root of the transcendental equation

$$\tan(\omega T + \phi) = \omega/a \quad (78)$$

The frequency  $\omega$  is chosen to maximize the eigenvalue  $\lambda$  of the Fredholm Eq. (42), which can be shown to be

$$\lambda = \frac{1}{2ac} \left[ 1 + \frac{a^2 - 1}{1 + \omega^2} \right] \quad (79)$$

It can be seen that for wide-band noise ( $a^2 > 1$ ), the maximum of  $\lambda$  is attained by the smallest  $\omega$  that satisfies (78). On the other hand, if the noise is narrow band ( $a^2 < 1$ ), the maximum of  $\lambda$  is achieved for the highest possible frequency  $\omega$ . Thus the system is excited at those frequencies where highest signal to noise ratio at the output is obtained.

##### 4.2 Second Order System with Unknown Frequency [20]

$$\ddot{x} + \dot{x} + x = u \quad (80)$$

$$y = x + v \quad (81)$$

Assume  $\theta \geq 1/4$  so that the system is oscillatory. Using results of Theorems 4 and 5, it can be shown that the optimal input for the asymptotic or steady state case is a sinusoid at frequency  $\omega^*$  where

$$\omega = \begin{cases} \theta - 1/2, & \theta > 1/2 & \text{(Low damping)} \\ 0, & 1/4 \leq \theta \leq 1/2 & \text{(High damping)} \end{cases} \quad (82)$$

### 5. Numerical Results

This section presents optimal elevator input to identify parameters in the short period mode and the rudder and aileron inputs to estimate stability and control derivatives in the lateral motions of the aircraft. The input signals are designed for the planned flight test duration, using available instruments and their accuracies and the best a priori estimates of unknown parameter values. Both time domain and frequencies domain techniques are used.

Aircraft motions are simulated to evaluate the optimal inputs relative to conventional inputs and are tested under a variety of off-design parameter values. The accelerations and velocities are also determined to ensure that the inputs are safe and implementable.

#### 5.1 Longitudinal Systems

The longitudinal perturbation motions of a Buffalo C-8 aircraft about a steady trim condition obey the following differential equations (units: meters, deg, sec).

$$\frac{d}{dt} \begin{bmatrix} u \\ \theta \\ q \\ \alpha \end{bmatrix} = \begin{bmatrix} -.02 & -.171 & .001 & .179 \\ 0 & 0 & 1 & 0 \\ .0984 & 0 & \underline{-1.588} & \underline{-.562} \\ -.131 & 0 & 1 & \underline{-.737} \end{bmatrix} \begin{bmatrix} u \\ \theta \\ q \\ \alpha \end{bmatrix} + \begin{bmatrix} 0.0 \\ 0.0 \\ \underline{-1.66} \\ \underline{.005} \end{bmatrix} \delta_s \quad (83)$$

where

$u$  is forward speed,

$\theta$  is pitch angle,

$q$  is pitch rate,

$\alpha$  is angle-of-attack, and

$\delta_s$  is stabilator deflection.

The poles of this system are at

$$\omega_{sp} = -1.6 \pm .62j \text{ (short period mode) and } \omega_{ph} = -.0151 \pm .088j \text{ (phugoid mode)}$$

The first pair of complex roots corresponds to the fast, highly damped, short period mode and the second to the slow, weakly damped, phugoid mode.

It is assumed that there are five unknown parameters, all in the short period mode (underlined). It is well known that the two state (pitch rate and angle-of-attack) model of an aircraft is a good representation of the short period motion. This approximation is used to compute the optimal elevator deflection time history. The equations of motion become

$$\begin{bmatrix} \dot{q} \\ \dot{\alpha} \end{bmatrix} = \begin{bmatrix} \underline{-1.588} & \underline{-.562} \\ 1 & \underline{-.737} \end{bmatrix} \begin{bmatrix} q \\ \alpha \end{bmatrix} + \begin{bmatrix} \underline{-1.66} \\ \underline{.005} \end{bmatrix} \delta_s \quad (84)$$

The noisy measurements of  $q$  and  $\alpha$  are

$$\begin{bmatrix} y_1 \\ y_2 \end{bmatrix} = \begin{bmatrix} 1 & 0 \\ 0 & 1 \end{bmatrix} \begin{bmatrix} q \\ \alpha \end{bmatrix} + \begin{bmatrix} v_q \\ v_\alpha \end{bmatrix} \quad (85)$$

The measurement noise is assumed white. The root mean square errors in the measurements of  $q$  and  $\alpha$  are .70 deg sec<sup>-1</sup> and 1.0 deg, respectively, and the sampling rate is 25 per second.

##### 5.1.1 Time Domain Optimal Inputs

A doublet input, is used, conventionally, to identify the above five parameters. Starting from this doublet, the input design program is used to determine the optimal input for a 6 sec long experiment with 100 deg<sup>2</sup> sec total input energy. The performance index is the trace of the dispersion matrix. The input at the end of each iteration step is shown in Figure 2. Fairly good convergence is obtained in three steps. Table 1 shows the standard deviation in parameter estimates for each of these

inputs.\* Also shown is the value of  $\delta$  which determines the component of new input added to the old input (see Section 3, Algorithm 1).  $\delta$  was taken to be one if the decrease in  $\text{Tr}(D)$ ,  $D=M^{-1}$  was more than 50%. It is clear from Table 1 that the optimal input gives much better parameter estimates (e.g., smaller standard deviations) than the conventional doublet input.

#### Approximation to Optimal Input

The optimal input of Figure 2 is approximated by a sequence of four steps with the same total energy. The approximated input is shown by the broken line in Figure 3. This input is used on the two state, short period approximation of the longitudinal equations of motion (Equation (84)). Table 2 compares parameter dispersions resulting from the optimal and the approximated (suboptimal) inputs. Some parameters have better estimates while other have poorer estimates, with the average variance increasing by about 13%.

Off-Design Parameter Values: Since the input design is based on some a priori parameter values (e.g. wind tunnel values) it is important to study the effect of using these inputs for difference true parameter values. When all five parameters in the short period model are increased by 50% of their initial values, the result is a system with a natural frequency of 1.86 rad/sec and a damping ratio of .94. It is more difficult to identify parameters of this system with the same input energy because of increased damping. Table 3 shows standard deviations of parameter estimates when the approximated input is used on this system with off-design parameter values. There is an increase in estimation errors from design conditions, but the approximated optimal input is still much better than the doublet. Next, the parameters of the system are halved, reducing the natural frequency to .76 rad/sec and the damping ratio to .77. The parameters in this system are easier to identify, but still the approximated input compares favorably with the conventional doublet input.

#### Fourth Order Model

The approximation to optimal inputs, obtained using the two state approximation, is simulated on the four state longitudinal equations of motion (Equation (83)), with measurements of  $q$  and  $\alpha$  only. The measurement error and the sampling rate are the same as before. Table 4 is a comparison of the standard deviations on estimates of  $C_{\dot{q}}$ ,  $C_{\dot{\alpha}}$ ,  $C_{\delta}$ ,  $C_{Z_{\alpha}}$ , and  $C_{Z_{\delta}}$  with the assumption that

the remaining parameters in the system are known. The estimates predicted by the four state model are slightly better than the estimates predicted by the two state model. This is because there is an additional excitation of the short period mode from variations in forward speed.

#### Aircraft Response to Optimal and Conventional Inputs

It is necessary that the optimal inputs, designed for identification, neither produce excessive accelerations for pilot and airframe safety nor involve large excursions in aircraft states for the linearization assumptions to hold. The optimal elevator input of Figure 2 is used with the aircraft model to determine the acceleration and state time histories. The variations of pitch rate, angle-of-attack, vertical acceleration and pitch acceleration are shown in Figures 4a-4d. The peak accelerations for the optimal input and the doublet are comparable. However, when the optimal input is applied larger accelerations persist for a longer period of time. The optimal input results in about the same pitch rate as the doublet but a higher variation in angle-of-attack. The pitch rate, angle-of-attack and accelerations are however reasonable so that the optimal elevator input is implementable.

#### 5.1.2 Frequency Domain Optimal Inputs

As mentioned in section 3, the frequency domain synthesis is computationally much more efficient and produces globally optimal results in the stationary case. Its applicability to short time periods is examined here. Furthermore, it provides a very good starting input for time-domain synthesis.

Optimal elevator input spectrum is determined to identify five parameters,  $Z_{\alpha}$ ,  $M_{\alpha}$ ,  $M_{\dot{q}}$ ,  $Z_{\delta}$  and  $M_{\delta}$  in the short period, mode of the C-8 aircraft. The equations of motions and the set of available measurement for this aircraft are as given below. Two criteria of optimality are used viz: (a) (a)  $\text{Min } |D|$  and (b)  $\text{Min } \text{Tr}(D)$ , where  $D=M^{-1}$ . Now since there are five parameters and two outputs, the minimum number of frequencies for a nondegenerate design is two and the maximum number of frequencies required in an optimal design is  $\frac{5 \times 6}{2}$ , i.e. fifteen (see Theorem 4).

To minimize the determinant of the dispersion matrix, the initial input is selected to have two frequencies at 0 cps and at .125 cps with equal power. Figure 5 shows the spectrum of the elevator deflection input after each iteration. Notice that during some iteration steps, the program puts more power at already chosen frequencies. After eight iterations, the change in the determinant of the dispersion matrix is less than .1% from the previous step. There is a total of seven frequencies

\* The standard deviation format of Table 1 is used through. These quantities are the square roots of the diagonal elements of the Cramer-Rao lower bound and represent the lowest possible value of the parameter estimate standard deviations which can be attained using an unbiased and efficient parameter identification procedure. These lower bounds rather than parameter estimates based on individual runs are a meaningful comparison of different inputs, a better input giving a smaller lower bound. The nominal parameter values are given for reference. Computation of actual parameter variances requires monte carlo runs and is found to agree closely with the lower bounds as shown in Ref. [10].

in the final input spectrum.

This input has interesting characteristics. The spectrum is divided into two parts: A low frequency input to identify gains and a high frequency input to identify natural frequency and damping, etc. The higher frequency input occurs around the natural frequency, which is reasonable. Table 5 shows the standard deviations (lower bound) on parameter estimates for an average 12 sec long experiment when the system is in steady state and the energy in input is 200 deg<sup>2</sup> sec. Also shown are the trace and determinant of the information matrix and the trace of the dispersion matrix. Next, the frequencies close to each other are lumped and ones with negligible power are dropped to get the spectrum of Figure 6. The standard deviations on parameter estimates for this simplified design in steady state for the same experiment duration and input energy are also shown in Table 5. There has been an improvement in the determinant of M and trace of D, showing the value of the simplification.

The frequency domain inputs are designed with the assumption of steady state. If the flight testing time is short, the aircraft does not reach a steady state. To find the true information matrix for a 12 sec long test starting from zero initial conditions, a time domain input based on the frequency spectrum and same average power is generated and is shown in Figure 7. This time domain input is not unique since the initial phase relationship between the sinusoidal inputs is arbitrary. Table 5 gives the parameter standard deviations and trace and determinant of information and dispersion matrices when initial phases are chosen at random. The parameter standard deviations deteriorate by 5% to 15%. A better result could be obtained by optimizing the initial phases.

Equivalent results with Tr(D) as the criterion are given in Ref. [20]. The difference in input spectrum is very small.

#### Effect of Data Length

If the system starts from zero initial conditions, the performance of an input of finite length is poorer than predicted on the assumption of steady state. To determine the duration of the experiment when this approximation becomes serious, time traces of elevator deflections 4 to 12 sec long are obtained based on the simplified spectrum of the Tr(D) criterion. Each of these inputs is used with the state and measurement equations and the resulting information and dispersion matrices are determined. Table 6 gives the ratio of standard deviations of parameter estimates for these finite inputs (with the system starting from zero initial conditions) to the standard deviations in steady state (for the same average input power and experiment duration). Trace and determinant of the information and dispersion matrices are also compared using simulated data. The asymptotic value of these ratios for long experiments is one. For experiments shorter than 8 sec, the deterioration is serious. The inputs are good for experiments longer than 10 sec. This corresponds to above two cycles of the natural short period mode.

#### Aircraft Response to the Frequency Domain Optimal Inputs

The root-mean-square (RMS) state deviations are computed for the frequency domain inputs. For an average input power of 16.67 deg<sup>2</sup>, the RMS state values are shown in Table 7.

#### 5.1.3 Comparison of Frequency Domain Inputs with Conventional and Optimal Time Domain Inputs

Table 8 shows a comparison of standard deviations on parameter estimates for the frequency domain input, the optimal time domain input, and the doublet. The steady state frequency domain value is a lower limit on Tr(D) for an input with 100 deg<sup>2</sup> sec input energy in a 6 sec long flight test. The time domain input is optimized for a 6 sec long experiment and gives 50% better result than the time trace from the frequency domain input. Nevertheless, the input resulting from the frequency domain approach is superior to a doublet. As mentioned earlier, this would be an excellent first pass at the optimal input and is useful for starting the time domain program.

#### 5.2 Inputs for the Lateral System

The equations of motion for lateral motions of one version of a Jet Star flying at 573.7 meters/sec. at 6,096 meters are [33] (all in units of deg, sec.)

$$\frac{d}{dt} \begin{bmatrix} \beta \\ \gamma \\ p \\ r \end{bmatrix} = \begin{bmatrix} -.119 & .0565 & 0 & -1 \\ 0 & 0 & 1 & 0 \\ -.443 & 0 & -.935 & .124 \\ .299 & 0 & -.119 & -.178 \end{bmatrix} \begin{bmatrix} \beta \\ \gamma \\ p \\ r \end{bmatrix} + \begin{bmatrix} 0 & .0289 \\ 0 & 0 \\ 2.88 & 1.40 \\ 0.0 & -1.55 \end{bmatrix} \begin{bmatrix} \delta_a \\ \delta_r \end{bmatrix} \quad (86)$$

where  $\beta$  is sideslip angle,  $\gamma$  is roll angle, and  $p$  and  $r$  are roll and yaw rates, respectively. Aileron and rudder are two control inputs. Noisy measurements of the four states  $\beta$ ,  $\gamma$ ,  $p$  and  $r$  are available.

The noise in measurements is white and Gaussian with root-mean-square values of 1 deg ( $\beta$ ), .5 deg ( $\gamma$ ), .71 deg sec<sup>-1</sup> ( $p$ ) and .71 deg sec<sup>-1</sup> ( $r$ ).

The sampling rate is 25 per second. The poles of the system are at

$$-.0511 \pm 1.78 j \text{ (Dutch roll)}, -1.12 \text{ (Roll)} \text{ and } -.00667 \text{ (Spiral)}$$

The inputs are designed to identify the parameters which predominantly affect the Dutch-roll mode (underlined in Eq. (86)).

### 5.2.1 Rudder Input (Time-Domain)

The optimal rudder input to minimize the sum of variances of the five parameters is determined and is shown in Figure 8. The duration of the simulated test is 8 sec. and the input energy is 100 deg<sup>2</sup>-sec. The comparison of standard deviations on parameters resulting from the optimal input and the doublet is given in Table 4. The optimal input results in better parameter estimates than the doublet, based on comparing the standard deviations.

### Simultaneous Rudder and Aileron Inputs

New simultaneous rudder and aileron inputs are designed to identify lateral parameters. The inputs with combined energy of 100 deg<sup>2</sup>-sec are shown in Figure 9. The aileron input amplitude is very small. The estimates resulting from this simultaneous input are presented in Table 9. There is a very small improvement over the single rudder input case, as would be expected since the rudder input is much more effective in estimating these five parameters than the aileron input. Larger aileron deflections can be obtained by placing separate energy constraints on the aileron and the rudder.

### 5.2.2 Frequency Domain Lateral Inputs

The lateral system of Section 4.3 with unknown  $C_{y\beta}$ ,  $C_{l\beta}$ ,  $C_{n\beta}$ ,  $C_{nr}$  and  $C_{n\delta_r}$  is used as the example to determine the optimal rudder input spectrum to minimize the trace of the dispersion matrix. The optimum input spectrum has two frequencies: at 0 cps with 12% of total input power and at .285 cps with 88% of input power. The second frequency is very close to the natural frequency of the Dutch-roll mode. Since the Dutch-roll mode for this aircraft has low damping, this input would produce large state excursions in steady state. This occurs because there are no constraints on the state variables.

Table 10 shows a comparison of standard deviations for this frequency domain input and the time domain input for an 8 sec long simulated flight test. Because of low damping, the system is far from steady state for the duration of the experiment. Standard deviations on parameter estimates predicted on the assumption of steady state are too optimistic.

### 5.3 Considerations of Primary/Secondary Derivatives

In many aircraft identification problems of interest, it is necessary to obtain accurate estimate of only a subset of all unknown parameters. The parameters whose estimates are required are called primary and the remaining unknown parameters are called secondary. There is no direct incentive to obtain good estimates of the secondary parameters. The inputs should be designed such that the secondary parameters are estimated only to the extent that they keep reduce uncertainty in primary parameters resulting from errors in secondary parameters. The input design technique presented previously can be used to determine control signals to identify only the primary parameter.

The Buffalo C-8 aircraft, whose equations of motion are given in Eq. (83) is used as an example. It is assumed that the input is to be designed to provide the best estimate of  $C_{mq}$ , while in addition to  $C_{mq}$  four other parameters,  $C_{za}$ ,  $C_{na}$ ,  $C_{z\delta_a}$ , and  $C_{n\delta_a}$  are also unknown. The starting input is the optimal input when all parameters are equally important. The input after one iteration is shown in Figure 10. It looks quite similar to the input when all parameters are weighted equally. The standard deviations of parameter estimates for these two inputs are compared in Table 11. The standard deviations of  $C_{mq}$  and  $C_{n\delta_a}$  decrease by about 3% while those of other parameters increase. This shows that to get a good estimate of  $C_{mq}$  it is necessary to have a good estimate of  $C_{n\delta_a}$  also. Since  $C_{mq}$  is an important parameter in the system, even when all the parameters are to be identified, good estimate of  $C_{mq}$  is obtained. The considerations of primary and secondary parameters may be more useful when the two sets of parameters affect different modes.

## 6. Outstanding Problems in Input Design for Stability and Control Testing

### 6.1 Nonlinear Dynamics and Aerodynamics

The input design technique presented in Section 3 uses linear perturbation equations of motion about a trim condition. Substantial nonlinear aerodynamic effects are present, however, in the high angle-of-attack flight regime for a conventional aircraft and in the transition regime for a vertical take-off and landing aircraft. In addition, large angular motions, encountered in certain maneuvers, introduce nonlinear dynamical effects. In such circumstances, a perturbation model is inadequate and the complete nonlinear model must be considered for input design.

An initial attempt at input design for the high angle-of-attack regime was made by Hall, Gupta, and Smith [34]. Considerable further work is required before a practical technique is developed. A general theoretical approach for solving this problem is given in Ref. [19]. It would probably be more fruitful to restrict the class of inputs in such a way that the resulting input design is simplified. For example, the input may be represented as a finite sum of harmonic or Walsh functions.

## 6.2 Hard Constraint on Control Input

There are often constraints on the maximum input amplitude either because of mechanical limits on stick or control surface deflection or the assumption of linear control effectiveness. These constraints can be satisfied by scaling down the input energy. This technique, however, does not make full use of the available input amplitude. The criterion function (e.g. weighted trace or determinant of the dispersion matrix) must be minimized directly under the constraint.

$$|u_i(t)| \leq a_i \quad i=1,2, \dots, q$$

for each of the  $q$  inputs. The optimal inputs are of the bang-bang type and may be calculated using Algorithm 1 by solving a quadratic programming problem during each iteration [19].

## 6.3 Input Design in the Presence of Wind Gusts

Often there may be wind gusts or turbulence present during the flight test. These gusts have two major effects on parameter estimation. First, they cause additional excitation of the aircraft which enhances parameter identification accuracy. Second, wind gust produce uncertainties in state estimates thus reducing the accuracy with which the parameter can be determined. Analytically the effect of the process noise on optimal input can be taken into account with some additional terms as shown in Refs. [19, 29].

## 6.4 State Constraints

Quadratic state constraints of the type  $\int_0^T x^T(t) A x dt \leq c$  can be handled via control transformations as shown in Ref. [24]. It may be important to incorporate these constraints in aircraft input design if excessive velocities or accelerations are produced by unconstrained designs.

## 7. Conclusions

A comprehensive account of input design theory and results for estimating aircraft stability and control derivatives is provided in this paper. It is shown by numerical examples how optimally designed inputs provide smaller variances on the parameter estimates as compared to conventional inputs. Both time-domain and frequency domain synthesis techniques for computing deterministic as well as stochastic inputs are presented and their applicability to the aircraft problem is discussed. It would seem that the next logical step would be to use these inputs during flight tests in order to verify the theoretical results presented in this paper.

## References

1. R. K. Mehra, "Optimal Inputs for Linear System Identification," IEEE Transactions on Automatic Control, June 1974. (Also, JACC, 1972.)
2. J. Sorenson, "Analysis of Instrumentation Error Effects on the Identification Accuracy of Aircraft Parameters," Contract NAS 1-10791, May 1972.
3. C. L. Muzzev and E. A. Kidd, "Measurement and Interpretation of Flight Test Data for Dynamic Stability and Control," Chapter 11, AGARD Flight Test Manual, Pergamon Press, 1959.
4. H. Greenberg, "A Survey of Methods for Determining Stability Parameters of an Airplane from Dynamic Flight Measurements," NASA TN 2340, April 1951.
5. C. H. Wolocowicz, "Considerations in the Deterministic of Stability and Control Derivatives and Dynamic Characteristics from Flight Data," AGARD Report 549, Part I.
6. G. C. Goodwin, "Application of Curvature Methods to Parameter and State Estimation," Proc. IEEE, Vol. 16, No. 6, June 1969.
7. R. K. Mehra, et al., "Maximum Likelihood Identification of Aircraft Stability and Control Derivatives," Journal of Aircraft, February 1974.
8. P. H. Gerlach, "Analyse van een mogelijke methode voor het meten van prestaties en stabiliteits- en besturingseigenschappen van een vliegtuig in niet-stationaire, symmetrische vluchten" (In Dutch with summary in English), Delft University of Technology, Department of Aeronautical Engineering, Report UTH-117, Delft, 1964.
9. O. H. Gerlach, "The Determination of Stability Derivatives and Performance Characteristics from Dynamic Maneuvers," 38th AGARD Flight Mechanics Panel, Toulouse, France, 1971.
10. R. K. Mehra and D. E. Stepner, "Optimal Inputs for Aircraft Parameter Identification," International Conference on Systems and Control, Coimbatore, India, August 1973.
11. N. E. Nahi and D. E. Wallis, Jr., "Optimal Inputs for Parameter Estimation in Dynamic Systems with White Noise Observation Noise," Preprints, Joint Automatic Control Conference, Boulder, Colorado, August 1969.
12. G. C. Goodwin, "Optimal Input Signals for Nonlinear System Identification," Proc. IEE, 118, 7, 922-926, 1971.
13. D. B. Reid, "Optimal Inputs for System Identification," Stanford University, Report No. SUDAAR 440, May 1972.

14. B. Viort, "D-Optimal Designs for Dynamic Models; Part I, Theory: Part II. Applications," TR 314, 316, Department of Statistics, University of Wisconsin, October, November 1972.
15. R. K. Mehra, "Frequency-Domain Synthesis of Optimal Inputs for Linear System Parameter Estimation," TR 643, Division of Engineering and Applied Physics, Harvard University, July 1973.
16. J. Kiefer, "Optimum Experimental Designs," J. Roy Statistics, Soc., Ser. B, Vol. 21, pp. 273-319, 1959.
17. J. Kiefer, and J. Wolfowitz, "The Equivalence of Two Extremum Problems," Canadian Journal of Math., 12, pp. 363-366, 1960.
18. J. Kiefer, "Optimum Experimental Designs V with Applications to Systematic and Rotable Designs," Proc. Fourth Berkeley Symposium Math. Statistics Problem 1, pp. 381-403, 1960.
19. R. K. Mehra, "Synthesis of Optimal Inputs for Multiinput Multioutput (MIMO) Systems with Process Noise; Part II: Time Domain Synthesis", TR 649, Division of Engineering and Applied Physics, Harvard University, February 1974. (Also 1974 Decision and Control Conference, Phoenix, Arizona.)
20. M. K. Gupta, W. E. Hall, Jr., "Input Design for Identification of Aircraft Stability and Control Coefficients," Technical Report, Systems Control, Inc., Palo Alto, California, March 1974.
21. R. T. M. Chen, "Input Design for Parameter Identification - Part I: A New Formulation and a Practical Problem," Preprints 1974 Joint Automatic Control Conference, Austin, Texas, June 1974.
22. S. Karlin and W. Studden, "Optimal Inputs for Nonlinear Process Parameter Estimation," IEEE T-Aero. and Elec. Systems, Vol. AES-10, No. 3, May 1974.
23. V. V. Fedorov, Theory of Optimal Experiments, Academic Press, 1972 (Russian Translation).
24. R. K. Mehra, "Optimal Input Signals for Parameter Estimation in Dynamic Systems -- Survey and New Results", IEEE Transactions on Automatic Control, December 1974.
25. S. Arimoto and H. Kimura, "Optimum Input Test Signals for System Identification -- An Introduction-Theoretical Approach," Int. J. System Sci., 1, 3, 279-290, 1971.
26. P. C. Muller and H. I. Weber, "Analysis and Optimization of Certain Qualities of Controllability and Observability for Linear Dynamical Systems," Automatica, Vol. 8, pp. 237-246, 1972.
27. M. Aoki and R. M. Staley, "On Input Signal Synthesis in Parameter Identification," Automatica, 6, 431, 1970.
28. N. E. Nahi and G. A. Napjus, "Design of Optimal Probing Signals for Vector Parameter Estimation," Preprints, IEEE Decision and Control Conference, Miami, Florida, December 1971.
29. R. K. Mehra, "Synthesis of Optimal Inputs for Multiinput Multioutput (MIMO) Systems with Process Noise; Part I: Frequency Domain Synthesis, TR 649, Division of Engineering and Applied Physics, Harvard University, February 1974. (Also 1974 Decision and Control Conference, Phoenix, Arizona.)
30. A. Van den Bos, "Construction of Binary Multifrequency Test Signals," IFAC Symposium on Identification, Prague, 1967.
31. A. Papoulis, "Probability, Random Variables and Stochastic Processes," McGraw Hill, pp. 483, 1965.
32. V. S. Levadi, "Design of Input Signals for Parameter Estimation," IEEE Transactions on Automatic Control, Vol. AC-11, pp. 205-211, April 1966.
33. R. K. Hetley and W. F. Jewel, "Aircraft Handling Quantities Data," STI Technical Report, 1004-1, May 1974.
34. W. E. Hall, N. K. Gupta, and R. Smith, "Identification of Aircraft Stability and Control Coefficients for the High Angle-of Attack Regime", SCI Technical Report to the Office of Naval Research under Contract No N00014-72-C-0328, No. 2, March 1974.
35. Taylor, et. al., "A Comparison of Newton-Raphson and Other Methods for Determining Stability Derivatives from Flight Data," Third Technical Workshop on Dynamic Stability Problems, NASA Ames Research Center, 1968.



Table 1. Standard Deviations of Parameter Estimates for Inputs at the End of Each Iteration

Length of Simulated Flight Test = 6 sec.  
Total Input Energy = 100 deg<sup>2</sup>/sec.

Iteration	Standard Deviations					Tr(D)	P
	$C_{\delta_a}$	$C_{\delta_r}$	$C_{\delta_b}$	$C_{\delta_p}$	$C_{\delta_q}$		
Iteration 0 (Doublet)	219	.362	126	.0970	.0957	100	
Iteration 1	206	.0703	.0629	.193	.0432	150	1.0
Iteration 2	113	.0729	.0595	.0620	.0421	.0272	.61
Iteration 3	113	.0676	.0561	.0672	.0400	.0264	.61
Parameter Value	-1.560	-.562	-.717	-1.66	0.0		

[All in units of deg./sec.]

Table 2. Comparison of Optimal and Approximated Inputs

Duration of Simulated Flight Test = 6 sec.  
Total Input Energy = 100 deg<sup>2</sup>/sec.

	Standard Deviations					Tr(D)
	$C_{\delta_a}$	$C_{\delta_r}$	$C_{\delta_b}$	$C_{\delta_p}$	$C_{\delta_q}$	
Optimal Input	.115	.0676	.0561	.0672	.0400	.0264
Approximated Input	.126	.0690	.0497	.0807	.0101	.0299
Parameter Value	-1.560	-.562	-.717	-1.66	0.0	

[All in units of deg./sec.]

Table 3. Approximated Input Under Design and Off-Design Conditions

Length of Simulation = 6 sec.  
Total Input Energy = 100 deg<sup>2</sup>/sec.

Parameters	Pitch Frequency	Yawing Rate	Input	Standard Deviations					Tr(D)
				$C_{\delta_a}$	$C_{\delta_r}$	$C_{\delta_b}$	$C_{\delta_p}$	$C_{\delta_q}$	
Nominal	1.13	.07	Approximated	.126	.0690	.0497	.0807	.0101	.0299
			Doublet	.219	.362	.126	.0970	.0957	.100
All Parameters 10% Change	1.06	.06	Approximated	.126	.0690	.0497	.0807	.0101	.0299
			Doublet	.219	.362	.126	.0970	.0957	.100
All Parameters 1% Change	.99	.07	Approximated	.0656	.0250	.0269	.0170	.0200	.0071
			Doublet	.126	.362	.126	.0970	.0957	.100

Table 5. Errors in Parameter Estimates Using |D| as the Optimality Criterion

Duration of Simulated Flight Test = 12 sec.  
Total Input Energy = 200 deg<sup>2</sup>/sec.

Input	Standard Deviations					Tr(D)	P	Tr(D)
	$C_{\delta_a}$	$C_{\delta_r}$	$C_{\delta_b}$	$C_{\delta_p}$	$C_{\delta_q}$			
Frequency Domain Input	.0015	.0017	.0010	.0071	.0200	$1.29 \times 10^{-5}$	$2.07 \times 10^{-5}$	.0190
Steady State Value								
Uniquely Freq. Domain Input	.0010	.0015	.0010	.0060	.0200	$1.20 \times 10^{-5}$	$2.00 \times 10^{-5}$	.0150
Steady State Value								
Time Domain Input Freq. Spectrum	.0010	.0010	.0010	.0060	.0200	$1.10 \times 10^{-5}$	$1.21 \times 10^{-5}$	.0100
Steady State Value								
Parameter Value	-1.560	-.562	-.717	-1.66	0.0			

[All in units of deg./sec.]

Table 7. RMS State Deviations for Frequency Domain Inputs (Simulation)

Criterion	Pitch Rate	Angle-of-Attack
D	3.19 deg/sec	2.95 deg
Tr(D)	3.05 deg/sec	2.52 deg

Table 9. Parameter Estimate Standard Deviations for Different Lateral Inputs

Duration of Simulated Flight Test = 6 sec.  
Total Input Energy = 100 deg<sup>2</sup>/sec.

Input	Standard Deviations					Tr(D)
	$C_{\delta_a}$	$C_{\delta_r}$	$C_{\delta_b}$	$C_{\delta_p}$	$C_{\delta_q}$	
Steady State Doublet	.219	.362	.126	.0970	.0957	.100
Optimal Frequency Domain Input	.115	.0676	.0561	.0672	.0400	.0264
Optimal Frequency Domain Input	.115	.0676	.0561	.0672	.0400	.0264
Parameter Value	-1.560	-.562	-.717	-1.66	0.0	

[All in units of deg./sec.]

Table 4. Comparison of Standard Deviations on Parameter Estimates Predicted by Two State and Four Models

Length of Simulation = 6 sec.  
Total Input Energy = 100 deg<sup>2</sup>/sec.

Model	Standard Deviations					Tr(D)
	$C_{\delta_a}$	$C_{\delta_r}$	$C_{\delta_b}$	$C_{\delta_p}$	$C_{\delta_q}$	
Four State	.115	.0676	.0561	.0672	.0400	.0264
Two State	.113	.0676	.0561	.0672	.0400	.0264
Parameter Value	-1.560	-.562	-.717	-1.66	0.0	

[All in units of deg./sec.]

Table 6. Ratio of Parameter Estimates Standard Deviation for Short Experiments to Steady State Experiments

Length of Simulated Flight Test	Standard Deviations for Short Experiments					Tr(D) Ratio	P Ratio	Tr(D) Ratio
	$C_{\delta_a}$	$C_{\delta_r}$	$C_{\delta_b}$	$C_{\delta_p}$	$C_{\delta_q}$			
6 sec	2.0	0.0	1.7	2.0	.93	.70	.91	0.3
8 sec	1.4	1.1	1.4	1.3	1.3	.70	.87	1.0
10 sec	1.4	1.2	1.06	1.3	1.99	1.00	1.1	1.0
12 sec	1.1	1.01	1.0	1.1	1.01	1.00	1.2	1.0
14 sec	1.00	1.01	1.01	1.07	1.0	1.00	1.15	1.1
Infinity	1.0	1.0	1.0	1.0	1.0	1.0	1.0	1.0

Table 8. Comparison of Time Domain and Frequency Domain Approach (Tr(D) Criterion)

Duration of Simulated Flight Test = 6 sec.  
Total Input Energy = 100 deg<sup>2</sup>/sec.

Input	Standard Deviations					Tr(D)
	$C_{\delta_a}$	$C_{\delta_r}$	$C_{\delta_b}$	$C_{\delta_p}$	$C_{\delta_q}$	
Steady State Frequency Domain	.102	.0401	.0090	.0620	.0161	.0011
Steady State Time Domain	.100	.0419	.0794	.0601	.0400	.0000
Optimal Time Domain	.113	.0676	.0561	.0672	.0400	.0264
Doublet	.219	.362	.126	.0970	.0957	.100
Parameter Value	-1.560	-.562	-.717	-1.66	0.0	

Table 10. Comparison of Frequency Domain and Time Domain Optimal Lateral Inputs

Duration of Simulated Flight Test = 6 sec.  
Total Input Energy = 100 deg<sup>2</sup>/sec.

Input	Standard Deviations					Tr(D)
	$C_{\delta_a}$	$C_{\delta_r}$	$C_{\delta_b}$	$C_{\delta_p}$	$C_{\delta_q}$	
Frequency Domain Optimal Input	.0015	.0017	.0010	.0071	.0200	.0000
Time Domain Optimal Input	.0010	.0015	.0010	.0060	.0200	.0000
Optimal Time Domain	.0010	.0010	.0010	.0060	.0200	.0000
Parameter Value	-1.560	-.562	-.717	-1.66	0.0	

[All in units of deg./sec.]

\*Values shown in Tr(D) cannot be achieved starting from zero initial conditions

Table 11. Comparison of Standard Deviations on Parameter Estimates with All Parameters Equally Important vs.  $C_{m\dot{\theta}_q}$  Primary

Length of Simulated Flight Test = 6 sec.  
Total Input Energy = 100 deg<sup>2</sup>/sec.

	Standard Deviations					Tr(D)
	$C_{m\dot{\theta}_q}$	$C_{m\ddot{\theta}_q}$	$C_{\dot{\theta}_q}$	$C_{\ddot{\theta}_q}$	$C_{\theta_q}$	
Parameters Equally Important	.113	.0676	.0941	.0672	.0400	.0264
$C_{m\dot{\theta}_q}$ Primary	.110	.0747	.0615	.0651	.0415	.0275
Parameter Values	-1.500	-.562	-.737	-1.46	0.0	

(All in units of deg./sec.)

Fig. 2. Input at the End of Each Iteration

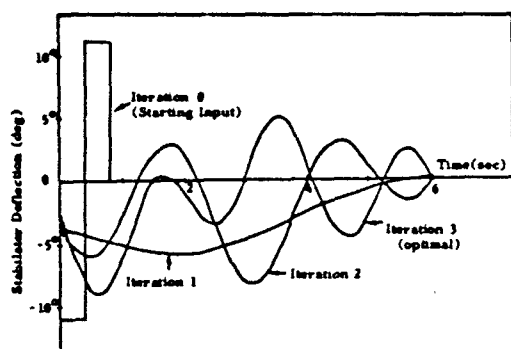


Fig. 4a. Comparison of Pitch Rates for Doublet and Optimal Control (Simulation)

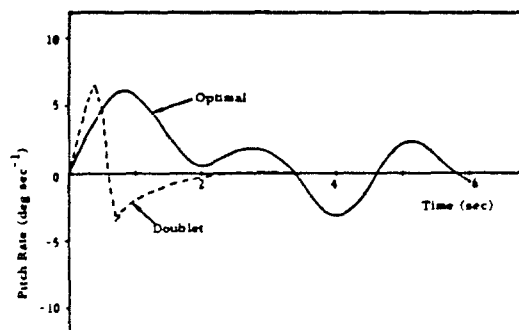


Fig. 1. Uncertainty Ellipsoid in Two-Dimensions

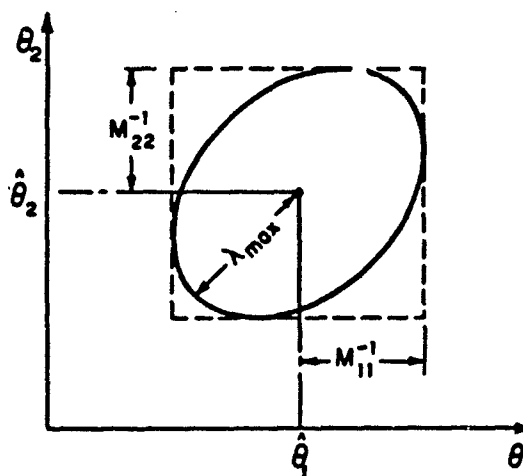


Fig. 3. Optimal and Approximated Elevator Inputs

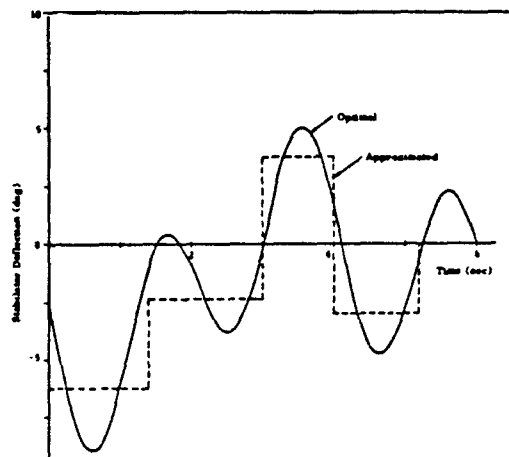


Fig. 4b. Comparison of Angle-of-Attack Variation for Doublet and Optimal Input (Simulation)

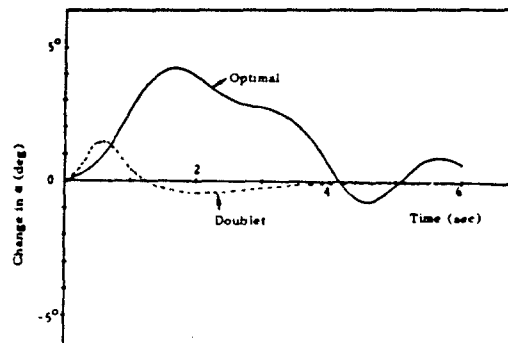


Fig. 4c. Comparison of Vertical Acceleration and Optimal Input (Simulation)

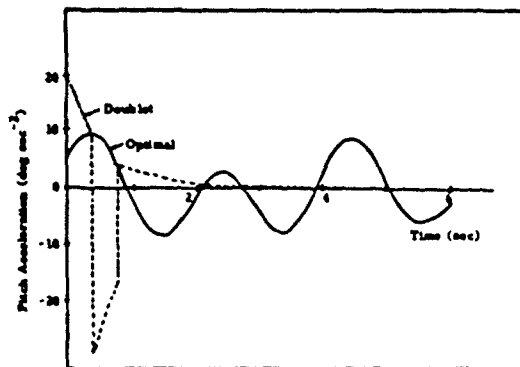


Fig. 4d. Comparison of Pitch Acceleration for Doublet and Optimal Input (Simulation)

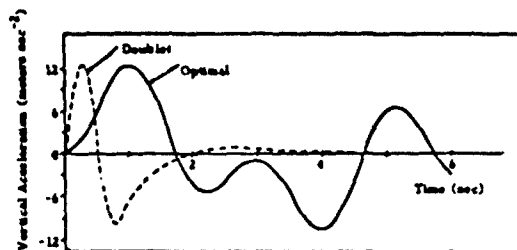


Fig. 5. Steps in the Computation of Optimal Input ( $\min |D|$ ) to Identify Parameters in the Short Period Mode of a C-8 Aircraft

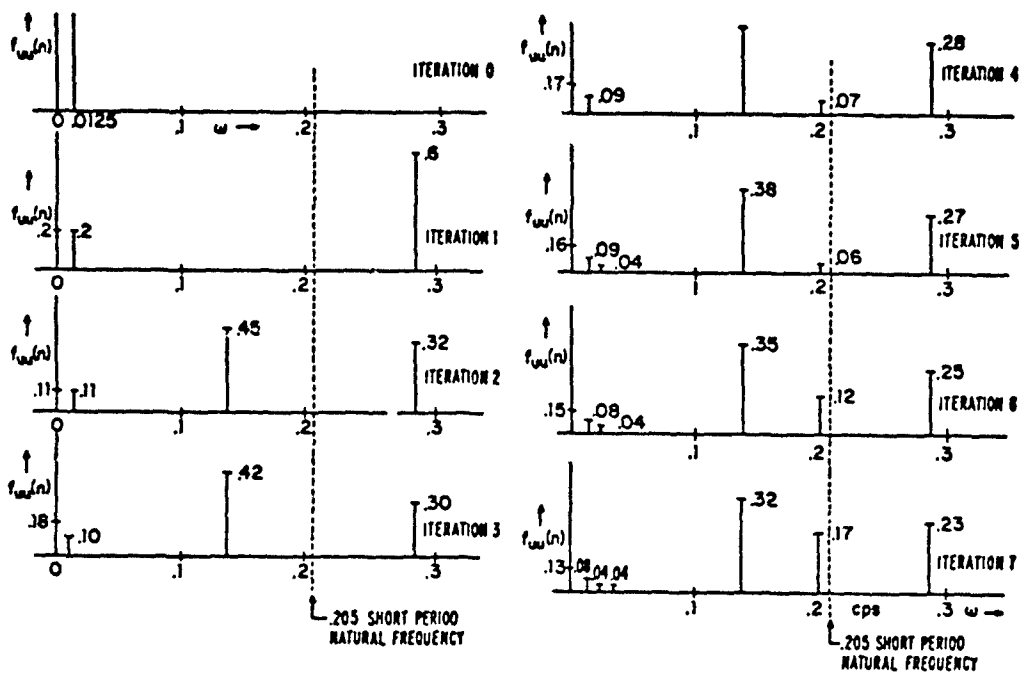


Fig. 6. Simplified Input Spectrum to Minimize  $|D|$

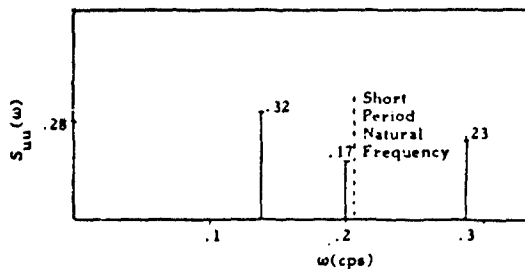


Fig. 7. Elevator Deflection Time History Based on Spectrum of Fig. 6 ( $\min |D|$ )

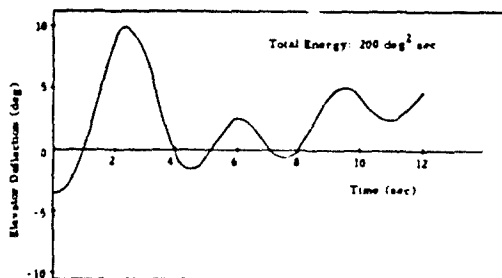


Fig. 8. Optimal Rudder Input to Identify Five Parameters in the Lateral Motion of an Aircraft

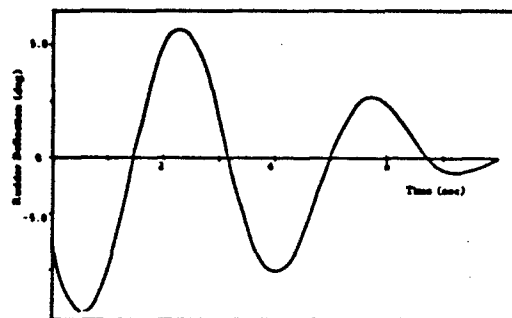


Fig. 9. Simultaneous Rudder and Aileron to Identify Five Lateral Parameters

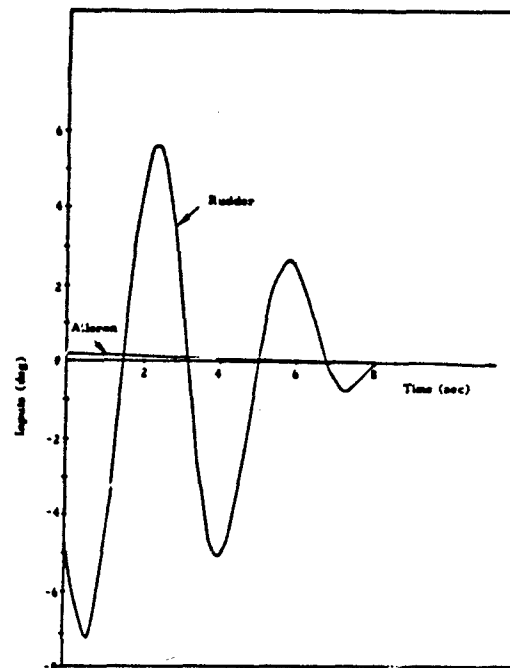
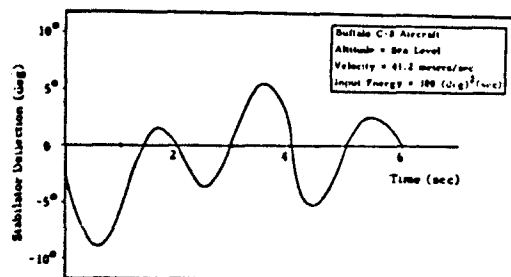


Fig. 10. Optimal Elevator Deflection ( $C_{m\dot{q}}$  Only Primary Derivatives)



# INPUT DESIGN FOR AIRCRAFT PARAMETER IDENTIFICATION: USING TIME-OPTIMAL CONTROL FORMULATION\*

By

Robert T.N. Chen  
Principal Engineer  
Flight Research Department  
Calspan Corporation  
Buffalo, New York

## ABSTRACT

This paper presents a new formulation and a practical and useful solution to the input design for identification of aircraft stability and control parameters. The new formulation directly addresses the following question: for a given measurement system and with prescribed constraints on the input and output magnitudes, what should the input functions be and for how long should the data record be taken to enable identification of system parameters to specified accuracy? Time optimal control theory is used in the formulation of this important problem. Necessary conditions and the structure of the optimal control input are discussed. By using Walsh functions and calculating the Cramer-Rao lower bounds recursively, a practical and useful design procedure is then presented. Application of the new approach are then made to the design of flight test inputs for identification of stability and control parameters of several types of aircraft.

## 1.0 INTRODUCTION

In gathering flight test data using the available measurement system for identification of aircraft stability and control parameters, there are two important questions to be answered: (i) what should the input function be so that the aircraft may be properly excited, and (ii) for how long should the data record be taken to enable identification of the parameters to a desired level of accuracy?

In the past, the input design problem has been formulated to address only the first question by specifying a priori the length of the data record to be taken. The input design problem formulated in this way becomes, as it is now well known, a typical fixed-time-interval optimal control problem for which an "optimal" input function within the specified time interval is to be obtained by maximizing some function of Fisher's information matrix<sup>1-6</sup> or minimizing some function of the error covariance matrix<sup>7,8</sup> as the index of performance. When the number of parameters to be identified is more than one (as is usually the case in practice) the use of a proper index of performance for the fixed-time-interval optimal input design becomes less obvious; weighting factors must now be introduced to produce a compromise for the relative accuracy requirement of the parameters to be identified. Indeed, the choice of a suitable index of performance has been and still is a debated issue.<sup>5,7,9</sup>

More importantly, with the fixed-time-interval input design formulation, the important second question mentioned earlier cannot be effectively answered, because the time interval for optimization is fixed a priori and the parameter accuracy achievable, which is the end product of real interest, is not directly considered in the input design.

To overcome the above inherent difficulties with the existing formulation based on fixed-time-interval optimization, the problem has recently been formulated as a time-optimal control problem addressing the above two questions directly and simultaneously. (11) In aircraft flight test applications, for example, this new formulation can mean less flight time for data gathering and less time and money required for processing the flight test data and identifying the stability and control parameters. Furthermore, with this new formulation, a meaningful trade-off study can be performed, as illustrated in this paper, to assist preflight planning concerning requirements of instrumentation accuracy, type and redundancy, and permissible control authority for test inputs, etc.

The remainder of the paper is organized as follows: Section 2 presents the new formulation and discusses the necessary conditions and the control structure for the optimal input. Section 3 presents a practical and useful design procedure using Walsh functions and converting the calculation of the Cramer-Rao lower bounds from a "batch process" into a recursive process. Applications of this approach to the design of input for identification of stability and control derivatives of several types of aircraft are given in Section 4.

## 2.0 TIME-OPTIMAL INPUT DESIGN FORMULATION

Consider the following nonlinear dynamic system and associated measurement system:

$$\dot{x} = f(x, p, u), \quad x(0) = x_0 \quad (1)$$

$$y = h(x, p, u) + v(t) \quad (2)$$

\*This work was supported partially by Calspan internal research and partially by Contract No. N00019-73-C-0504.

where  $x$  is the state vector (n-vector);  $p$  is the unknown parameter vector (q-vector);  $u$  is the input vector (r-vector);  $y$  is the output vector (m-vector); and  $w$ , an m-vector, is Gaussian white noise with zero mean and covariance function,

$$E \{ w(t) w^T(\tau) \} = R \delta(t - \tau) \quad (3)$$

with  $R$  being a diagonal constant matrix. Fisher's information matrix  $M$  is given by

$$M = \int_0^{t_f} \left[ \frac{\partial h}{\partial x} \frac{\partial x}{\partial x_0} \mid \frac{\partial h}{\partial p} + \frac{\partial h}{\partial x} \frac{\partial x}{\partial p} \right]^T R^{-1} \left[ \frac{\partial h}{\partial x} \frac{\partial x}{\partial x_0} \mid \frac{\partial h}{\partial p} + \frac{\partial h}{\partial x} \frac{\partial x}{\partial p} \right] dt \quad (4)$$

Define the matrix  $C$  to be

$$C = M^{-1} \triangleq \{ C_{ij} \} \quad (5)$$

Then the diagonal terms of the matrix  $C$  are the Cramer-Rao lower bounds, which are the theoretical lower bounds of the variances of any unbiased estimates of the initial state  $x_0$  and the parameter vector  $p$ .<sup>14</sup> The identifiability of these parameters is equivalent to the invertability of the matrix  $M$ .<sup>4</sup> Thus, if these parameters are assumed to be identifiable, then  $C$  and  $M$  are positive definite symmetrical matrices.

In Eq. (4), the sensitivity functions  $\frac{\partial x}{\partial x_0}$  and  $\frac{\partial x}{\partial p}$  are integrated using the following sensitivity equations:

$$\frac{d}{dt} \left( \frac{\partial x}{\partial x_0} \right) = \left( \frac{\partial f}{\partial x} \right) \left( \frac{\partial x}{\partial x_0} \right), \quad \frac{\partial x}{\partial x_0} (0) = I_n \quad (6)$$

$$\frac{d}{dt} \left( \frac{\partial x}{\partial p} \right) = \left( \frac{\partial f}{\partial x} \right) \left( \frac{\partial x}{\partial p} \right) + \frac{\partial f}{\partial p}, \quad \frac{\partial x}{\partial p} (0) = 0 \quad (7)$$

along with Eq. (1). The physical constants on the input and the state are

$$|u(t)| \leq U \quad (8)$$

$$|x(t)| \leq X \quad (9)$$

where  $U$  and  $X$  are constant vectors. Notice that the constraint, Eq. (9), is required for the equation of motion, Eq. (1), to remain valid and/or to keep the output  $y$  within the limits of the sensors.

The problem of designing optimal inputs for parameter identification is now formulated as follows: find the optimal control  $u^*(t)$  that minimizes the final time  $t_f$ , i.e.:

$$J = \int_0^{t_f} dt \quad (10)$$

subject to the constraints, Eq. (1), (2), (8) given earlier\* and Eq. (11) below:

$$0 < C_{ii} \leq \sigma_i^2, \quad i = 1, 2, 3, \dots, n+q \quad (11)$$

where  $\sigma_i$  are given positive constants signifying maximum standard deviation allowable for the identification of initial state variables  $x_0$  and the unknown parameters  $p$  using an efficient estimator (i.e. an unbiased minimum variance estimator).

The time-optimal control problem formulated above belongs to a special class of time-optimal intercept problem, in which the target set is stationary.<sup>15</sup> To see this, consider Eq. (4) and (5). Let the integrand in Eq. (4) be denoted by  $S^T Q^{-1} S$ , i.e.:

$$S \triangleq \left[ \frac{\partial h}{\partial x} \frac{\partial x}{\partial x_0} \mid \frac{\partial h}{\partial p} + \frac{\partial h}{\partial x} \frac{\partial x}{\partial p} \right] \quad (12)$$

Then a differentiation of Eq. (4) and (5) yields the following nonlinear matrix differential equation

$$\dot{C} = -CS^T R^{-1} SC \quad (13)$$

which, together with the dynamic system, Eq. (1) and (2), and the sensitivity system, Eq. (6) and (7), governs the time-evolution of the error covariance matrix  $C$ . Notice that since the parameters  $x_0$  and  $p$  are assumed to be identifiable,  $C$  is symmetrical and positive definite at each time instant. Thus, there are a total of only  $\frac{1}{2}(n+q)(n+q+1)$  state variables of interest in Eq. (13).

\*State variable constraints Eq. (9) will be discussed later.

The initial condition  $C(0)$  is the covariance matrix associated with the nominal values of  $X_0$  and  $p$  used in the input design\* (the first iteration in the sequential improvement implied in the input design for parameter identification). This is a Bayesian interpretation; and the matrix  $M$  in Eq. (4) is to be considered as added information. For the non-Bayesian case,  $C_0 \rightarrow \infty$ , and a large positive number, say  $10^{18}$ , may be used for the diagonal terms of  $C(0)$ , with zeros for the off-diagonal terms. Now, the constraints, Eq. (11), thus form a "stationary target set", which is an  $(n+q)$  dimensional rectangular region  $R_y$  composed of

$$\sigma_i \leq C_{ii}(t_f)^{\frac{1}{2}} > 0, \quad i = 1, 2, \dots, n+q \quad (14)$$

For example, for  $n+q=2$ , the region  $R_y$  is a rectangle as shown in Figure 1.

The problem formulated at the beginning of this section is seen to have been converted into the following time-optimal control to a stationary target set. Find the control  $u^*(t)$ , which controls the system of order  $\frac{1}{2}(q+3n)(n+q+1)$  composed of

- |                                     |   |                                     |
|-------------------------------------|---|-------------------------------------|
| (a) original dynamic system (1)     | - | $n$ equations                       |
| (b) sensitivity system (6) and (7)  | - | $n(n+q)$ equations                  |
| (c) error covariance equations (13) | - | $\frac{1}{2}(n+q)(n+q+1)$ equations |

to the target set, Eq. (14), in minimum time subject to the inequality constraints of the control variable, Eq. (8).

It is useful to give a geometrical interpretation of this problem parallel to that for the time-optimal intercept problem.<sup>15</sup> Let  $R_y^*$  be the augmented state space of dimension  $\frac{1}{2}(q+3n)(n+q+1)$  which corresponds to the target set  $R_y$  defined by (14). Let  $X_{t_i}$  be the reachable augmented state space at time  $t_i$  using the control  $u(t)$  within the constraints, Eq. (8); and let  $Y_{t_i}$  be the corresponding reachable spaces in the target space. Figures 1 and 2 show a geometrical interpretation of the time-optimal solution for a two-parameter case (i.e.,  $n+q=2$ ).

From Figure 1, it is seen that since  $C_{ii}$  are monotonically decreasing with time as is evident from Eq. (4), (5), or (13), the time-optimal control will occur at the boundary of the target region  $R_y$ . From these observations, consideration may therefore be given to replacing the inequality constraints of Eq. (14) with the equality constraint

$$C_{ii}(t_f) = \sigma_i^2 \quad (15)$$

one at a time and test the conditions

$$C_{jj}(t_f) \leq \sigma_j^2 \quad (16)$$

for all  $j \neq i$ . By using this procedure for all  $i = 1, 2, \dots, n+q$ , candidate solutions and hence the time-optimal control may be obtained.

#### Necessary Conditions for Optimal Control

We now discuss the necessary conditions. Let the augmented system of order  $\frac{1}{2}(q+3n)(n+q+1)$  discussed above be described by

$$\dot{\hat{x}} = \hat{f}(\hat{x}, u), \quad \hat{x}(0) = \hat{x}_0 \quad (17)$$

where

$$\hat{x} = (c^T, S_{x_0}^T, S_p^T, x^T)^T \quad (18)$$

with  $c$  being the  $\frac{1}{2}(n+q)(n+q+1)$ -vector, which is composed of the upper triangular elements of the matrix  $C$ , i.e.

$$c = (c_{11}, c_{12}, c_{13}, \dots, c_{1n+q}; c_{22}, c_{23}, \dots)^T$$

$$S_{x_0} = (S_1^T, S_2^T, \dots, S_n^T)^T \quad (19)$$

$$\frac{\partial x}{\partial x_0} \triangleq [S_1, S_2, \dots, S_n] \quad (20)$$

\*The input design problem discussed here assumes that there exists some a priori knowledge of the parameter values either from other independent sources or from identification using non-optimal inputs. Sequential improvement is implied here.

$$S_p = (S_{n+1}^T, S_{n+2}^T, \dots, S_{n+q}^T)^T \quad (21)$$

$$\frac{\partial x}{\partial p} = [S_{n+1}, S_{n+2}, \dots, S_{n+q}] \quad (22)$$

The Hamiltonian is

$$H = 1 + \lambda^T \hat{f} \quad (23)$$

Beginning with  $i = 1$  in Eq. (15), the necessary conditions are<sup>16</sup>

$$\dot{\hat{x}} = \hat{f}(\hat{x}, u), \quad \hat{x}(0) = \hat{x}_0 \quad \text{given} \quad (24)$$

$$\dot{\lambda} = -\lambda^T \hat{f}_x, \quad C_{11}(t_f) = \sigma_1^2, \quad \lambda_2(t_f) = \lambda_3(t_f) = \dots = 0 \quad (25)$$

$$0 = \lambda^T \hat{f}_u, \quad (\lambda^T - \text{optimality conditions for control input } u(t)) \quad (26)$$

$$-1 = (\lambda^T \hat{f})_{t=t_f}, \quad (\text{for } t_f) \quad (27)$$

Now, for  $i = 2$ , all the equations are the same as listed above, but the boundary conditions for  $\lambda(t_f)$  become

$$C_{22}(t_f) = \sigma_2^2, \quad \lambda_1(t_f) = \lambda_3(t_f) = \lambda_4(t_f) = \dots = 0$$

where

$$\lambda = (\lambda_1, \lambda_2, \dots, \lambda_{\frac{1}{2}(q+3n)(n+q+1)})^T$$

For  $i = 3, 4, \dots, n+q$ , similar results follow.

#### Optimal Control Structure

In many practical situations, the control  $u(t)$  enters into the dynamic system, Eq. (1), in a linear fashion, e.g.

$$f(x, p, u) = f_1(x, p) + B(x)u, \quad (28)$$

and  $\partial h / \partial x$  and  $\partial h / \partial p$  are independent of  $u$ .

In this case, Eq. (17) becomes

$$\hat{f}(\hat{x}, u) = \hat{f}_1(\hat{x}) + \hat{B}(\hat{x})u \quad (29)$$

and the conditions for the time-optimal control, Eq. (26) become

$$u^* = -U \operatorname{sgn} \{ \hat{B}^T(\hat{x}) \lambda \} \quad (30)$$

where  $\operatorname{sgn} \{x\} = 1$  if  $x > 0$   
 $= -1$  if  $x < 0$

which indicates that the optimal control is bang-bang.

The above necessary conditions may be extended to the case when the constraints on the state variables of Eq. (9) are considered; an approach such as that described in Reference 16 (page 117) may be employed. We will not repeat it here.

As shown previously in the simple illustrative example<sup>11</sup>, the necessary conditions, Eq. (24) - (27), are fairly complicated. Computer implementations for the solution of this type of problem are rather involved as discussed in many standard texts (e.g., Reference 15). Because of budgetary limitation, no attempts have been made to try to implement a time-optimal control algorithm, based on the above necessary conditions, on a computer (although we strongly recommend it be done). Instead, use has been made of the structure of the optimal input in developing a practical and economical search routine for input design as discussed in the next section.



### 3.0 A SUBOPTIMAL INPUT DESIGN USING WALSH FUNCTIONS

A practically useful suboptimal solution to the time-optimal control formulation for the input design problem is presented in this section. The solution is obtained by using an efficient direct search procedure which makes use of the bang-bang structure of the optimal input discussed in the preceding section and calculates the error covariance matrix in a recursive manner.

First, the error covariance matrix calculated in the "batch process" of Eq. (5) was converted into a recursive algorithm. This operation makes it possible to determine the length of the data record required to meet the desired level of parameter identification accuracy. It also permits various suboptimal input design schemes to be devised using the time rate of change of the error variance.

Secondly, to help determine the proper switching time in the bang-bang structure of the optimal input, the Walsh functions were selected as a candidate family of functions from which to choose the suboptimal control input. Aside from the bang-bang structure of the Walsh functions, they are easy to implement and their orthogonal characteristics are very desirable for use in multi-input systems.

#### Recursive Calculation of the Error Covariance Matrix

For digital computation with integration step size  $\Delta t$ , the error covariance matrix of Eq. (5) may be calculated using

$$C_K = \left\{ \sum_{i=0}^K [S_i^T R_i^{-1} S_i] \right\}^{-1} \quad (31)$$

where  $R_i = \frac{1}{\Delta t} R$ , and  $S_i \triangleq \left. \frac{\partial x}{\partial \theta} \right|_{t_i, \Delta t}$  is the solution of the dynamic system, Eq. (1), (2), and the sensitivity system, Eq. (6) and (7), at  $t = i \Delta t$ .

Using the Matrix Inversion Lemma<sup>12, 17</sup>, Eq. (31) may be converted into the following desired recursive relationship.

$$C_{K+1} = C_K - C_K S_{K+1}^T \left[ S_{K+1} C_K S_{K+1}^T + R_i \right]^{-1} S_{K+1} C_K \quad (32)$$

This relationship will be used in conjunction with the use of Walsh functions to design a suboptimal input.

#### Walsh Function Generation

The Walsh functions, which assume the values of +1 or -1 in an alternative manner, are a complete set of orthonormal basis functions over some interval, say (0,T). Extensive discussions on the generation of Walsh functions have been given by Walsh<sup>18</sup>, Harmuth<sup>19</sup>, and Swick<sup>13</sup>. A sample set of Walsh functions  $Wal(i, t), i=0, 1, \dots, 7$  is shown in Figure 3.

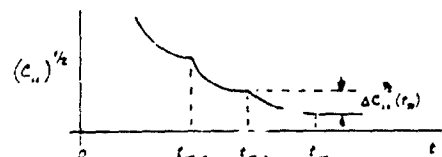
Using symmetric and skew-symmetric properties of the Walsh functions, Swick<sup>13</sup> has developed a systematic way of independently generating each individual Walsh function. His procedure was implemented on a computer to independently generate any one Walsh function with index  $i$  from a set (0, 1, 2, ..., 31) for suboptimal input design applications. To call for a specific Walsh function, it is necessary only to specify three parameters in this computer routine: (a) orthogonal interval, (b) the Walsh function index, and (c) the amplitude.

#### Computational Steps for Suboptimal Input Design

The direct-search input design procedure uses the following basic computational steps in each design stage:

- Step 1 Select a large time interval T (second), beyond which all computation will stop.
- Step 2 Begin with a  $Wal(i, t)$  with  $i = N$ , sufficiently large so that the system response will be small and well within the constraints on the magnitude of the state variables (if imposed).
- Step 3 Calculate the error covariance matrix  $C$  recursively by Eq. (32).
- Step 4 At each computing point  $t_k = k \Delta t$ , test to see if
 
$$(C_{jj})^{\frac{1}{2}} \leq \sigma_j \quad \forall_j$$

where  $\sigma_j$  are the parameter-accuracy specifications. If yes, record  $t_f$ . Let  $i = i - 1$  and go to Step 2. If no, continue.
- Step 5 At each switching instant  $t_n$  compute  $\Delta C_{ii}^{\frac{1}{2}}(t_n) = C_{ii}^{\frac{1}{2}}(t_n) - C_{ii}^{\frac{1}{2}}(t_{n-1})$ ,  $\forall i$



\*The initial conditions were discussed previously. For non-Bayesian case, the initial condition may also be taken at the value when the full rank of Eq. (31) is reached.

and test the effectiveness of the previous switching\*

$$\Delta(C_{ii}) \leq C\sigma_i, \forall i$$

where  $C \ll 1$ , is a positive number, e.g. 0.05. If yes, continue; if no, set  $i = i - 1$  (or reducing the switching frequency by a factor of 2) and go the Step 2.

- Step 6 The results of the preceding steps will be a subset of Walsh functions  $\text{Wal}(i, T)$  which meets the parameter-accuracy specification with corresponding final time  $t_f$ ; and the suboptimal input is the one with the smallest  $t_f$ , if the constraints on the magnitude of the state variables are not imposed. If these constraints are imposed, the suboptimal input of interest will be that with the smallest  $t_f$  among those that satisfy the state magnitude constraints.

For multi-input cases (i.e.,  $u(t)$  is a r-vector), the preceding procedure is the same with the exception that Step 2 is now replaced by a set of r numbers, i.e.

$$i = N, N-1, \dots, N-r+1$$

for each corresponding control input.

It should be noted that the above basic computational steps are for each design stage, which yields a single desirable Walsh function. Should a multi-stage design be required, the basic steps listed above may be used repeatedly. When the number of parameters to be identified is large and the accuracy specification for the parameter identification is high, it may not be possible to complete the design in a single stage; in this case, a multi-stage design will be required to complete the design as will be illustrated in the next section. If it is impossible to complete the design in a single stage, the accuracy requirements corresponding to the group of parameters, which consistently failed the accuracy test (Step 4), may be judiciously relaxed. Complete the first stage design with the relaxed specification and then proceed to the second stage design by restoring the accuracy specification and reducing the value of  $C$  in Step 5. This procedure is permissible, because the error covariance matrix is calculated recursively as shown in Eq. (32). As such, the error covariance matrix calculated at the end of the first stage can be used as the initial condition for the second stage design and so on. The following figure illustrates the case in which the design is completed in two stages.

First stage input design



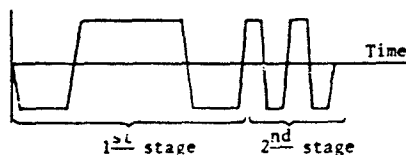
First stage design using some relaxed specification.

Second stage input design



Second stage design using the result of 1st stage design and original specification.

Combined suboptimal input



Unlike a single stage design in which the above procedure yields a unique design, a multi-stage design will in general result in nonunique design; and the final selection of a suitable multi-stage design could, for instance, be determined from the ease with which the flight test implementation may be achieved.

#### 4.0 APPLICATIONS

The suboptimal input design scheme described in the previous section was applied to several examples described below.

##### 4.1 An Illustrative Example (Comparison with Goodwin's Optimal Input<sup>7</sup>)

As an illustrative example, consider the following first order system previously studied by Goodwin<sup>7</sup>.

$$\dot{x} = ax + bu, \quad x(0) = 0, \quad |u| \leq 1$$

$$y = x + v$$

\*Inclusion of a test for correlation coefficient's has recently been suggested by J.V. Labacqz.

where the measurement noise  $v(t)$  is white, Gaussian with  $E\{v(t)\} = 0$  and  $E\{v(t)v(\tau)\} = \delta(t-\tau)$ . The parameters  $a$  and  $b$ , to be identified, are known to have nominal values of  $-1$ , and  $1$  respectively. Goodwin's input function obtained by minimizing the trace of the error covariance matrix  $C$  with a fixed time interval of 10 seconds is shown in Table I. For an integration step-size  $\Delta t = 0.05$  second, the  $\sigma_i$  and  $\text{tr} C$  are also shown in the table. Using these  $\sigma_i$  as the parameter-accuracy specification, the results of applying the suboptimal input design scheme discussed in Section 3 are shown in the last column. The design was completed in a single stage. It is seen that the results are somewhat better than Goodwin's.

In an attempt to see the difference in effectiveness between the two input functions geometrically, the propagation of  $\sigma_i$  as illustrated earlier in Figure 1 was plotted on Figure 4 for the two input functions together with some input function, generated by perturbing slightly the switching times. The difference in the effectiveness is readily seen from this figure. Recall that Goodwin used the fixed-time-interval of 10 seconds and the performance index is the trace of  $C$  matrix, which is a circle in the  $\sigma_a - \sigma_b$  plane with origin at  $\sigma_a = \sigma_b = 0$  in this case (if a weighted trace of  $C$  had been used, it would have been an ellipse instead). The input is seen to generate the  $\sigma_i$  trajectory to touch a smallest circle in  $\sigma_a - \sigma_b$  plane in 10 seconds; and as a result of this formulation, the desired accuracy may not be achieved. On the other hand, we used here the least time to touch the accuracy target as the criterion, and the resulting input guaranteed that the desired accuracy was obtained.

#### 4.2 Input Design to Identify Aircraft Longitudinal Short-Period Parameters

Consider the identification of the stability and control derivatives for the longitudinal short-period equations of motion of a conventional aircraft.<sup>6</sup> The equations of motion and the measurements are given by:

$$\begin{pmatrix} \dot{q} \\ \dot{\alpha} \end{pmatrix} = \begin{pmatrix} M'_q & M'_\alpha \\ 1 & Z_\alpha \end{pmatrix} \begin{pmatrix} q \\ \alpha \end{pmatrix} + \begin{pmatrix} M'_{\delta_c} \\ Z_{\delta_c} \end{pmatrix} \delta_c$$

$$y = \begin{pmatrix} y_1 \\ y_2 \end{pmatrix} = \begin{pmatrix} q \\ \alpha \end{pmatrix} + \begin{pmatrix} v_1 \\ v_2 \end{pmatrix}$$

Assume that the measurement noise vector  $v = (v_1, v_2)^T$  is independent, Gaussian white noise with zero mean and covariance function

$$E\{v(t)v^T(\tau)\} = \begin{bmatrix} 0.02 & 0 \\ 0 & 0.04 \end{bmatrix} \delta(t-\tau)$$

and that the nominal values of the derivatives are assumed to be

$$\begin{aligned} M'_q &= -1.588 & Z_\alpha &= -0.737 \\ M'_\alpha &= -0.562 & Z_{\delta_c} &= -0.005 \\ M'_{\delta_c} &= -1.66 \end{aligned}$$

Using a fixed-time interval  $t_f = 4$  sec, and using the input energy constraint,

$$\int_0^4 u^2(t) dt = 310,$$

a maximization of the  $\text{tr} M$  leads to the results<sup>6</sup> shown in the "optimal input" of Table II. For the sake of facilitating a direct comparison with the result obtained earlier in Reference 6, it was assumed that the level of accuracy desired was the same as that produced from that input. The control excursion permissible is limited to only  $\pm 8.792$  degrees (for which the energy is less than 310 for 4 seconds with bang-bang input structure). The next column in Table II shows the suboptimal input design results. To achieve or exceed the basic specification, it requires only 3.96 seconds of data record with less input energy than that for the "optimal input" of Reference 6 as shown in the third column. Note that, although the accuracy ( $\sigma$ ) of  $M_\alpha$  just achieves the specification, the remaining four parameters considerably exceed the accuracy specification. Furthermore, as shown in Figure 5, the control excursion is smaller and the aircraft motion is smaller for the suboptimal input, which is also easier to implement in flight testing. The last column in Table II shows the results for meeting a 25% more accurate criterion than the basic specification. In this example, the design was again completed in a single stage.

#### 4.3 X-22A Aircraft Application

The suboptimal input design scheme was also used to design control surface inputs for the identification of the X-22A aircraft longitudinal stability and control parameters at certain fixed operating points. The data used for the input design are shown in Table III. The results for the basic design are shown in Table IV. Because the desired level of accuracy was not very high in this example ( $\sigma_i$  desired ranged from 10 to 20% of their parameter values) the design was again carried out in a single stage as was done in the previous two examples. It is interesting to point out that the "characteristic" switching frequency of the input was 1.12 rad/sec, which lay in the frequency range of the short period, 2.19 rad/sec, and the phugoid, 0.27 rad/sec of the aircraft as calculated using the parameter values used for the input design.

Computer runs were also made to assess the effects of changes of control excursions and the measurement noise level. The design results are shown in the last two columns of Table IV, designated as cases 2 and 3, respectively. By comparing these two cases with Case 1, it is seen that an increase in the control authority increases the switching frequency and shortens the data length. A decrease in the measurement noise level by a factor of 2 (a factor of 4 for R) results in a variable switching frequency and as might be expected, shortens the data length required to meet the same desired level of accuracy.

#### 4.4 Application to a Medium Transport Aircraft

The purpose of this application was to design an elevator input function for the identification of eight longitudinal stability and control derivatives of a medium transport aircraft to within 10% accuracy (in terms of  $\sigma$ ) for all the eight derivatives shown in Table V. In this case the design was completed in two stages, because the level of accuracy desired for all the parameters was relatively high. In the initial attempts to complete the design in a single stage, it was observed that the parameter  $Z_{\dot{\delta}_r}$  consistently failed its accuracy test, and hence the necessity for multi-stage design became apparent. As shown in Table V, the first stage design was accomplished by relaxing the accuracy for  $Z_{\dot{\delta}_r}$  from 10% to 20%. The length of the data record required to meet this relaxed specification was 12.05 seconds.

The 2nd stage design was performed by restoring the accuracy for  $Z_{\dot{\delta}_r}$  back to 10% and reducing the value of  $\epsilon$  in Step 5 from 0.01 to 0.001. Also, in an attempt to reduce  $t_s$ , the time duration required to meet the specification, permissible control authority was doubled from  $\pm 1.5^\circ$  to  $\pm 3^\circ$ . Figure 6 shows the responses of the aircraft to the combined suboptimal input. It is interesting to note that the two characteristic frequencies of the designed input again lie between the short period and phugoid frequencies of the aircraft.

#### 4.5 Application to a Large Aircraft

The objective of this application was to design a better flight test rudder input for identification of the lateral-directional stability derivatives and rudder control derivatives of a large aircraft to within a desired level of accuracy. The data used in the input design are shown below. They include the equations of motion, initial parameter estimate and the desired accuracy of the parameter identification, estimated error of the response variables measured, and the permissible control excursion.

##### (a) Equations of Motion

$$\frac{d}{dt} \begin{bmatrix} p \\ \phi \\ r \\ \beta \\ \delta_r \end{bmatrix} = \begin{bmatrix} L'_p & 0 & L'_r & L'_\beta & L'_{\dot{\delta}_r} \\ 1 & 0 & 0 & 0 & 0 \\ N'_p & 0 & N'_r & N'_\beta & N'_{\dot{\delta}_r} \\ \frac{Y_p}{V_0} + a_0 & \frac{g}{V_0} & \frac{Y_r}{V_0} - 1 & \frac{Y_\beta}{V_0} & \frac{Y_{\dot{\delta}_r}}{V_0} \\ 0 & 0 & 0 & 0 & -1 \end{bmatrix} \begin{bmatrix} p \\ \phi \\ r \\ \beta \\ \delta_r \end{bmatrix} + \begin{bmatrix} 0 \\ 0 \\ 0 \\ 0 \\ 10 \end{bmatrix} \delta_{rp}$$

##### (b) Initial Parameters Estimate and Desired Accuracy

##### (c) Estimate Measurement Error

Para.	Actual Para. Values	Initial Para. Est. Value	Desired Accuracy ( $\sigma$ )	Unit	Meas. Variables	Unit	Error ( $\sigma$ )
$L_p$	-1.719	-1.375	0.138	sec <sup>-1</sup>	$p$	deg/sec	0.02
$L_r$	1.164	1.397	0.419	sec <sup>-1</sup>	$\phi$	deg	0.02
$L_\beta$	-31.49	-25.192	7.558	sec <sup>-1</sup>	$r$	deg/sec	0.02
$L_{\dot{\delta}_r}$	0.443	0.354	0.106	sec <sup>-1</sup>	$\beta$	deg	0.03
$N_p$	-0.0078	-0.006	0.003	sec <sup>-1</sup>	$\delta_r$	deg	0.007
$N_r$	-0.3	-0.360	0.036	sec <sup>-1</sup>			
$N_\beta$	3.686	2.949	0.295	sec <sup>-1</sup>			
$N_{\dot{\delta}_r}$	-0.679	-0.815	0.082	sec <sup>-1</sup>			
$(Y_p/V_0) + a_0$	0.0194	0.023	0.006	--	(d) Permissible Control Excursion		
$(Y_r/V_0) - 1$	-0.9939	-1.193	0.238	--			
$Y_\beta/V_0$	-0.161	-0.138	0.041	sec <sup>-1</sup>			
$Y_{\dot{\delta}_r}/V_0$	0.0135	0.010	0.005	sec <sup>-1</sup>			
					$ \delta_{rp} $	$\leq$	1 inch
					$(\delta_{rp})_{max}$	$=$	3.25 inch

As can be seen in these data, the initial parameter values used for the input design are not the actual values; they are about 20% off the actual. The desired accuracy specifications as expressed in terms of  $\sigma$  are approximately 10 to 30% of the initial parameter values. The designed input is shown in Table VI in which the effectiveness of the suboptimal input is compared with that of the conventional rudder doublet (with its "frequency" approximately equal to the Dutch roll frequency). Significant improvement of the designed input over the conventional input is clearly shown.

Table VII shows the sensitivity of the designed input with the variation in the control excursion (or authority) permissible and the level of the measurement noise. Note that as the control authority enlarges, the "switching frequency" increases and, of course, the time to meet the identification accuracy specification  $t_s$  is shortened. Increasing the measurement noise level slows down the switching frequency and increases  $t_s$ .

An alternate set of initial parameter estimates, desired accuracy, and measurement noise (significantly higher than that previously used) as shown below was also tried for rudder input design. The initial parameter estimate was obtained from actual identification of the parameters from computer generated data using a doublet input and including simulated process and measurement noises. This exercise was designed to simulate the case in which the initial parameter value used for the input design was obtained from a non-optimal input.

(b) Initial Parameter Estimate and Desired Accuracy (c) Estimated Measurement Error

Para.	Actual Para. Values	Initial Para. Est. Value	Desired Accuracy	Unit	Measured Variables	Unit	Error
$L_p$	- 1.719	- 1.31	0.131	sec <sup>-1</sup>	$\rho$	deg/sec	0.2
$L_r$	1.164	3.87	0.774	sec <sup>-1</sup>	$\phi$	deg	0.08
$L_{\delta_r}$	-31.49	-28	3.6	sec <sup>-1</sup>	$r$	deg/sec	0.04
$L_{\delta_p}$	0.443	1.17	0.234	sec <sup>-1</sup>	$\beta$	deg	0.04
$N_p$	- 0.0078	- 0.0304	0.00608	sec <sup>-1</sup>	$\delta_r$	deg	0.007
$N_r$	- 0.3	- 0.444	0.0444	sec <sup>-1</sup>			
$N_{\delta_r}$	3.686	3.45	0.345	sec <sup>-1</sup>			
$N_{\delta_p}$	- 0.679	- 0.7	0.7	sec <sup>-1</sup>			
$(Y_p/V_0) \cdot \alpha_0$	0.0194	0.0204	0.0041	--			
$(Y_r/V_0) - 1$	- 0.9930	- 0.9886	0.1977	--			
$Y_{\delta_r}/V_0$	- 0.161	- 0.163	0.0326	sec <sup>-1</sup>			
$Y_{\delta_p}/V_0$	0.0135	0.0128	0.0026	sec <sup>-1</sup>			

The results of the input design are shown in Table VIII. In this case, a two-stage design was required to meet the specification. The first stage design was performed by relaxing the specifications of  $N_p$ ,  $Y_{\delta_r}/V_0$ , and  $Y_{\delta_p}/V_0$  as indicated in the table. The designed input is again significantly better than the conventional rudder doublet input. Aircraft responses to the suboptimal input were only slightly larger than those to the conventional rudder doublet and were within the permitted ranges.

## 5.0 CONCLUSIONS

The following conclusions are evident from the development given in the preceding sections:

- (i) The time-optimal control formulation proposed in this paper provides a direct answer to the question of the length of data record and the corresponding control input required to meet the parameter-accuracy specification. This formulation is equally applicable to linear and nonlinear flight regimes.
- (ii) This new formulation removes the inherent difficulty associated with the selection of a suitable index of performance for the fixed time-interval formulation of input design in the identification of aircraft parameters.
- (iii) This new formulation can mean less flight time for data gathering and less time and money for data processing. It also permits a meaningful trade-off study of requirements for instrumentation accuracy and permissible control surface excursions.
- (iv) The recursive computation of the error covariance matrix is a useful tool to determine from the existing data record the adequacy and the length of the data record required to meet the desired level of accuracy of the parameter identification. It also permits various suboptimal input designs schemes to be devised using the time rate of change of the error variances.
- (v) The suboptimal input design scheme proposed in this paper has been shown to give better results than have been obtained heretofore using the fixed time-interval formulations. It gives an input function which is effective and easy to implement for flight testing.

## REFERENCES

1. Nahi, N.E. and D.E. Wallis, Jr.: "Optimal Control for Information Maximization in Least-Square Parameter Estimation." SAMSO-TR-68-177, January 1968.
2. Nahi, N.E. and D.E. Wallis, Jr.: "Optimal Inputs for Parameter Estimation in Dynamic Systems with White Observation Noise." Preprint of 1969 JACC, pp. 506-516, 1969.
3. Aoki, M. and R.M. Staley: "On Input Signal Synthesis in Parameter Identification." Automatics, Vol. 6, pp. 431-440, 1970.
4. Chen, R.T.N., et al: "Development of Advanced Techniques for the Identification of V/STOL Aircraft Stability and Control Parameters." Calspan Report No. BM-2820-F-1, August 1971.
5. Nahi, N.E. and G.A. Napjus: "Design of Optimal Probing Signals for Vector Parameter Estimation." Paper presented at 1971 IEEE Conference on Decision and Control.

6. Mehra, R.K.: "Optimal Inputs for Linear System Identification." Proc. JACC 1972, pp. 811-820, August 1972.
7. Goodwin, G.C.: "Input Synthesis for Minimum Covariance State and Parameter Estimation." Electronic Letters, Volume 5, No. 21, 16 October 1969.
8. Goodwin, G.C.: "Optimal Input Signals for Nonlinear-System Identification." Proc. IEEE, Vol. 118, No. 7, pp 922-926, July 1971.
9. Tse, E.: "Information Matrix and Local Identifiability of Parameters" Proc. JACC pp. 611-619, 1973
10. Chen, R.T.N.: "Toward a Better Physical Understanding of Input Design for Parameter Identification." Calspan X-22A TM No. 44, October 10, 1972.
11. Chen, R.T.N.: "Input Design for Parameter Identification--Part I: A New Formulation and a Practical Solution." Proc. JACC pp. 398-408. June 1974.
12. Ho, Y.C.: "On the Stochastic Approximation Method and Optimal Filtering Theory." Journal of Mathematical Analysis and Application, Vol. 6, 1963, pp. 152-154.
13. Swick, D.A.: "Walsh Function Generation." IEEE Transactions IT-15, p. 167, 1969.
14. Nahi, N.E.: "Estimation Theory and Application." John Wiley, 1969.
15. Athans, M. and P.L. Falb: "Optimal Control - An Introduction to the Theory and its Applications." McGraw-Hill, 1966.
16. Bryson, A.E., Jr. and Y.C. Ho: "Applied Optimal Control." Blaisdell Publishing Co., 1969.
17. Chen, R.T.N.: "A Recurrence Relationship for Parameter Estimation Via Method of Quasi-Linearization and its Connection with Kalman Filtering." Journal of AIAA, pp. 1696-1698, September 1970.
18. Walsh, J.L.: "A Closed Set of Normal Orthogonal Functions." American Journal of Mathematics, Vol. 45, pp. 5-24, 1923.
19. Harmuth, H.F.: "A Generalized Concept of Frequency and Some Applications." IEEE Transactions I.T., Vol. 14, pp. 275-382, May 1968.

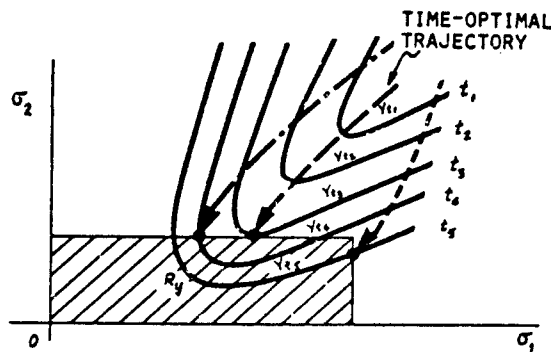


Figure 1 Target Set and Time-Optimal Trajectory

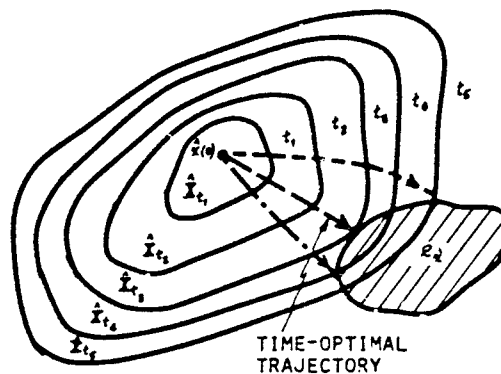


Figure 2 Augmented State Space and Time-Optimal Trajectory

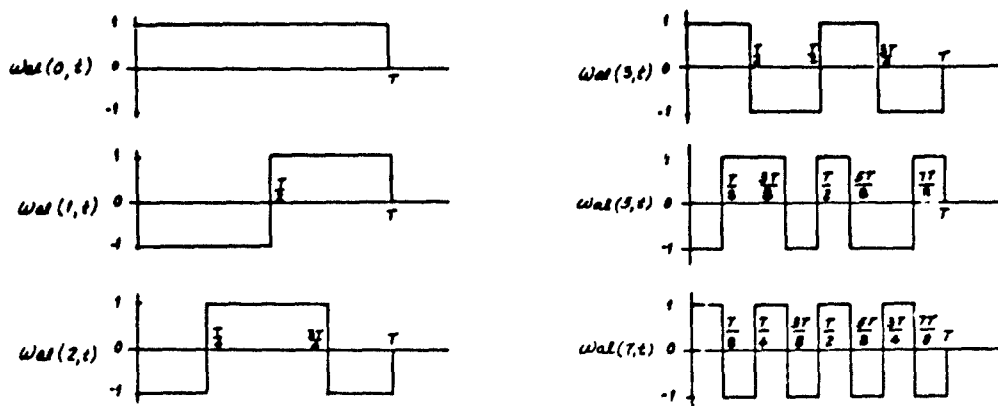


Figure 3 A Sample Set of Walsh Functions

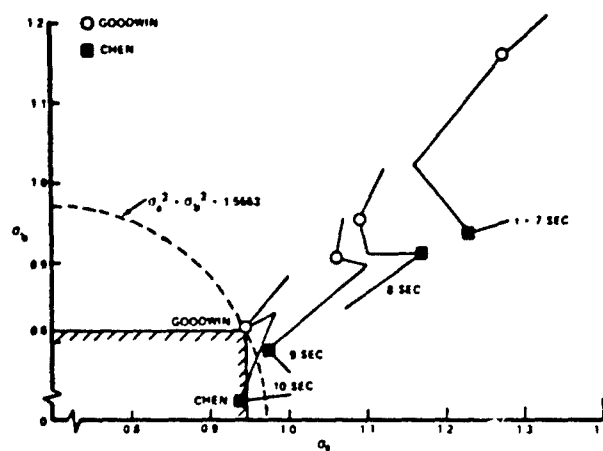
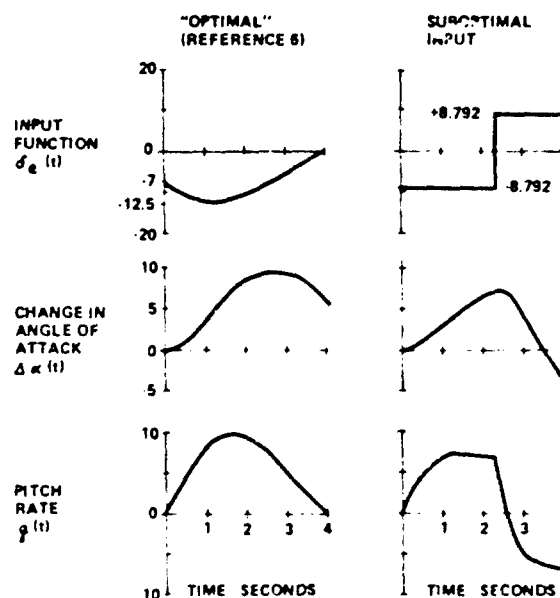
Figure 4 Comparison of Two Different Inputs on  $\sigma_2$  Plane

Figure 5 Aircraft Response Comparison

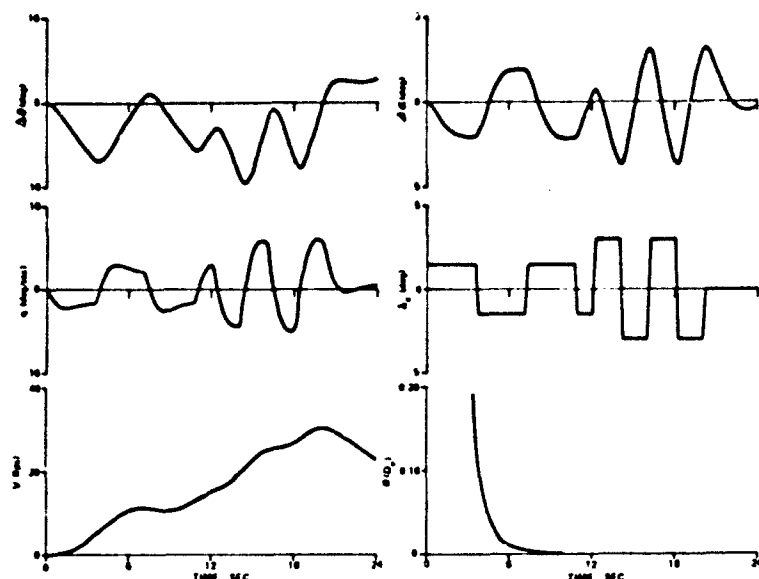


Figure 6 Aircraft Responses to Designed Input

Table I  
Length of Data Record to Achieve or Exceed  
Parameter-Accuracy Specification  
( $\Delta t = 0.05$  sec)

CASES PARAMETERS	"OPTIMAL INPUT" (REF. 7)	SUBOPTIMAL INPUT AS LEAST AS GOOD AS "OPTIMAL INPUT"
INPUT FUNCTION		
$(\sigma_i)_{\min}$ (a)	0.94453	0.94271
$(\sigma_i)_{\min}$ (b)	0.81437	0.75305
$\sum_{i=1}^2 (\sigma_i)^2_{\min}$	1.5553	1.4558
$t_f$ (SEC)	10	9.45
INPUT ENERGY	BASIC	SMALLER THAN BASIC

Table II  
Length of Data Record to Achieve or Exceed  
Parameter-Accuracy Specification  
( $\Delta t = 0.02$  sec)

CASES PARAMETERS	"OPTIMAL INPUT" (REF. 6)	SUBOPTIMAL INPLY AT LEAST AS GOOD AS "OPTIMAL" INPUT	SUBOPTIMAL INPUT AT LEAST 25% BETTER THAN "OPTIMAL INPUT"
INPUT FUNCTION $\delta_e(t)$			
$\sigma_1$	0.16957	0.12144	0.12022 (0.12720)*
$\sigma_2$	0.06605	0.06598	0.04817 (0.04954)
$(\sigma_i)_{\min}$	0.09601	0.07187	0.07159 (0.07201)
$\sigma_{\Sigma}$	0.03684	0.03233	0.02396 (0.02763)
$\sigma_{\delta e}$	0.02564	0.02085	0.01830 (0.01923)
$\sum_{i=1}^2 (\sigma_i)^2_{\min}$	0.04435	0.02575	0.02280
$t_f$ (SEC)	4	3.96	4.86
INPUT ENERGY	BASIC	SMALLER THAN BASIC	NOT APPLICABLE

\*Numbers in parentheses are for 75% of the quantities in the second column



Table III  
X-22A Aircraft Data for Input Design

## (a) EQUATIONS OF MOTION

$$\frac{d}{dt} \begin{bmatrix} \Delta u \\ \Delta w \\ q \\ \Delta \theta \end{bmatrix} = \begin{bmatrix} X_u & X_w & -w_0 & X_\theta - g \\ Z_u & Z_w & u_0 & Z_\theta \\ M_u & M_w & M_q & M_\theta \\ 0 & 0 & 1 & 0 \end{bmatrix} \begin{bmatrix} \Delta u \\ \Delta w \\ q \\ \Delta \theta \end{bmatrix} + \begin{bmatrix} X_{\delta_{ES}} \\ Z_{\delta_{ES}} \\ M_{\delta_{ES}} \\ 0 \end{bmatrix} \delta_{ES}$$

## (b) INITIAL PARAMETER ESTIMATES AND DESIRED PARAMETER IDENTIFICATION ACCURACY AT DUCT ANGLE OF 15°

PARAMETERS	ACCURACY DESIRED		EST. PARA. VALUE FOR INPUT DESIGN
	UNIT	(σ)	
$M_u$	rad/sec <sup>2</sup> /ft/s	0.0005	-0.0058
$M_w$	rad/sec <sup>2</sup> /ft/s	0.0005	-0.0073
$M_q$	1/sec	0.10	-1.73
$M_\theta$	1/sec <sup>2</sup>	0.50	-3.49
$M_{\delta_{ES}}$	rad/sec <sup>2</sup> /in	0.03	.29
$X_u$	1/sec	0.05	-0.10
$X_w$	1/sec	0.01	0.065
$X_\theta$	ft/sec <sup>2</sup> /rad	2.00	-2.85
$X_{\delta_{ES}}$	ft/sec <sup>2</sup> /in	0.10	0.24
$Z_u$	1/sec	0.20	-0.50
$Z_w$	1/sec	0.02	-0.50
$Z_\theta$	ft/sec <sup>2</sup> /rad	6.00	32.4
$Z_{\delta_{ES}}$	ft/sec <sup>2</sup> /in	0.50	-2.70

## (c) MEASUREMENT NOISE

$$\begin{aligned} \sigma_u &= 1.0 \text{ ft/sec} \\ \sigma_w &= 0.25 \text{ ft/sec} \\ \sigma_\theta &= 0.15 \text{ deg} \\ \sigma_q &= 0.10 \text{ deg/sec} \end{aligned}$$

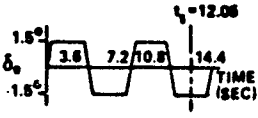
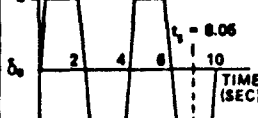
## (d) PERMISSIBLE CONTROL EXCURSION

$$|\delta_{ES}| \leq 1.5''$$

Table IV  
Length of Data Record to Achieve or Exceed  
Parameter-Accuracy Specification  
X-22A Aircraft Application  
(Δt = 0.05 sec)

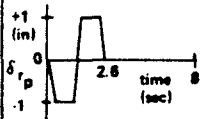
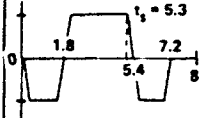
CASES PARAMETERS		1. BASIC DESIGN	2. EFFECT OF CONTROL EXCURSION PERMISSIBLE	3. EFFECT OF MEASUREMENT NOISE LEVEL (R = R <sub>0</sub> /4)
DESIRED σ		MIN σ ACHIEVABLE	MIN σ ACHIEVABLE	MIN σ ACHIEVABLE
$X_u$	0.05	0.00844	0.00905	0.01586
$X_w$	0.01	0.0099	0.00991	0.00994
$X_\theta$	2.00	1.33979	1.53180	1.58813
$X_{\delta_{ES}}$	0.10	0.09921	0.05105	0.06006
$Z_u$	0.20	0.01546	0.01328	0.02869
$Z_w$	0.02	0.01118	0.00979	0.01479
$Z_\theta$	6.00	1.69482	1.68376	2.76175
$Z_{\delta_{ES}}$	0.50	0.05169	0.32467	0.02453
$M_u$	0.0005	0.00030	0.00025	0.00036
$M_w$	0.0005	0.00017	0.00015	0.00015
$M_q$	0.10	0.00747	0.00525	0.00364
$M_\theta$	0.50	0.03038	0.02775	0.03213
$M_{\delta_{ES}}$	0.03	0.00060	0.00050	0.00034

Table V  
Elevator Input Design for  
a Medium Transport Aircraft  
(Two-Stage Design)

CASE PARAMETERS			FIRST STAGE DESIGN	SECOND STAGE DESIGN
				
	PARA. VALUE FOR DESIGN	DESIRED $\sigma$ (10% PARA. VALUE)	MIN. $\sigma$ ACHIEVABLE @ END OF 1st STAGE	MIN. $\sigma$ ACHIEVABLE @ END OF 2nd STAGE
$D_y$	-0.0313	0.00313	0.00121	0.00107
$D_z$	0.3175	0.03175	0.01338	0.00983
$M_y$	0.008	0.0008	0.0006	0.00038
$M_z$	-0.944	0.0944	0.02055	0.00843
$N_y$	-1.185	0.1185	0.01357	0.00816
$N_z$	-2.648	0.2648	0.02009	0.00735
$Z_y$	-1.038	0.1038	0.00957	0.00553
$Z_z$	-0.06	0.006* (0.012)	0.01190	0.00599
$\Sigma \sigma_i^2$			0.00142	0.000356

\*.006 INITIALLY, THEN RELAXED TO .012 FOR FIRST STAGE DESIGN.

Table VI  
Comparison of Conventional and Suboptimal Rudder  
Input for Parameter Identification\*

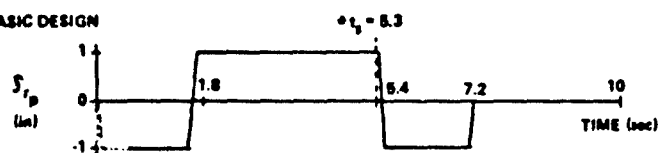
PARAMETERS	ACTUAL PARAMETERS VALUE	INITIAL PARAMETERS VALUE USED IN INPUT DESIGN	BEST ACCURACY ACHIEVABLE ( $\sigma$ ) FOR 8 sec DATA	
			CONVENTIONAL RUDDER DOUBLET	SUBOPTIMAL INPUT
				
$L_p$	-1.719	-1.375	0.0689	0.0325
$L_r$	1.184	1.397	0.3573	0.1982
$L_\beta$	-31.49	-25.192	0.6518	0.3557
$L_{\delta_r}$	0.443	0.354	0.0101	0.0109
$N_p$	-0.007802	-0.006	0.0088	0.0041
$N_r$	-0.3	-0.360	0.0447	0.0247
$N_\beta$	3.685	2.949	0.0840	0.0459
$N_{\delta_r}$	-0.679	-0.815	0.0029	0.0025
$(Y_p/Y_0) + \alpha_0$	0.01945	0.023	0.0030	0.0013
$(Y_r/Y_0) - 1$	-0.9939	-1.193	0.0203	0.0098
$Y_\beta/Y_0$	-0.1727	-0.138	0.0308	0.0204
$Y_{\delta_r}/Y_0$	0.01281	0.010	0.0064	0.0035
$\Sigma \sigma_i^2$	-	-	0.5680	0.1703

\*MEASUREMENT ERRORS,  $H = \text{DIAG. } [(0.02)^2, (0.02)^2, (0.02)^2, (0.03)^2, (0.007)^2]$

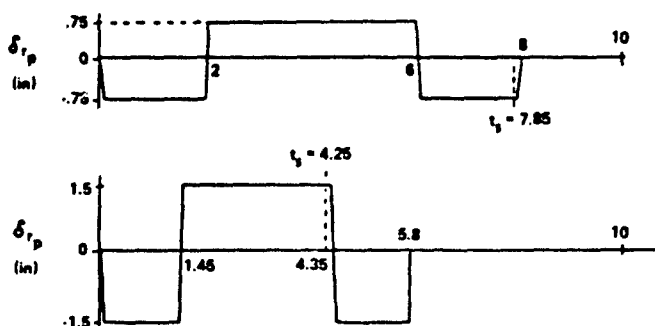
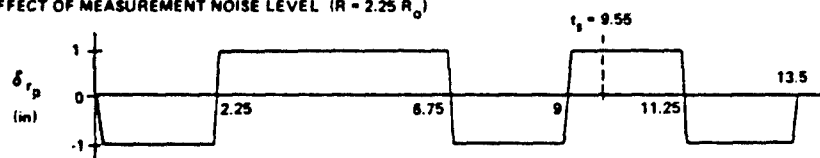
Table VII  
Rudder Input Sensitivity

- INITIAL PARAMETER ESTIMATE: 20% OFF ACTUAL VALUE
- MEASUREMENT ERRORS,  $R_0 = \text{DIAG. } [(0.02)^2, (0.02)^2, (0.02)^2, (0.03)^2]$

## A. BASIC DESIGN

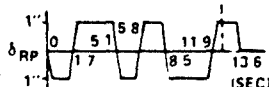
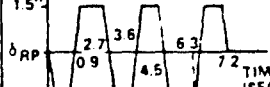


## B. EFFECT OF CONTROL EXCURSION PERMISSIBLE

C. EFFECT OF MEASUREMENT NOISE LEVEL ( $R = 2.25 R_0$ )

\*  $t_p$  : TIME REQUIRED TO MEET THE SPECIFICATION OF PARAMETER IDENTIFICATION ACCURACY.

Table VIII  
Rudder Input for a Large Aircraft  
(Two-Stage Design, Alternate Specification)

CASE PARAMETERS		FIRST STAGE 	SECOND STAGE 
		MIN. $\sigma$ ACHIEVABLE @ END OF 1st STAGE	MIN. $\sigma$ ACHIEVABLE @ END OF 2nd STAGE
$L_p$	0.131	0.04241	0.03481
$L_r$	0.774	0.25578	0.18292
$L_z$	5.6	0.43148	0.34871
$L_{A_r}$	0.234	0.02870	0.01901
$N_p$	0.00608*	0.00541	0.00445
$N_r$	0.0444	0.03281	0.02351
$N_z$	0.345	0.05644	0.04525
$N_{A_r}$	0.07	0.00497	0.00323
$\frac{Y_p}{V_0} + 1$	0.0041*	0.00209	0.00174
$\frac{Y_r}{V_0} - 1$	0.1977	0.01399	0.01055
$\frac{Y_z}{V_0}$	0.0326	0.02393	0.01877
$\frac{Y_{A_r}}{V_0}$	0.0026*	0.00382	0.00255
$\Delta \sigma^2$		0.2593	0.15973

\* INITIAL VALUE, THEN RELAXED FOR FIRST STAGE DESIGN

## DETERMINATION OF AERODYNAMIC DERIVATIVES FROM TRANSIENT RESPONSES IN MANOEUVRING FLIGHT

by

A. Jean Ross  
 Royal Aircraft Establishment  
 Farnborough, England

## SUMMARY

The paper describes some of the work done on aircraft parameter identification at RAE Farnborough, at the Cranfield Institute of Technology under UK Government sponsorship, and at the British Aircraft Corporation (Warton Division).

The RAE computer programs are based on the method of differential corrections, and the lateral program is being applied to the analysis of Dutch roll oscillations of aircraft performing high-g manoeuvres, to obtain aerodynamic derivatives up to angles of attack near the onset of wing rock.

The CIT computer program includes four progressively more complicated estimation methods, and results are presented for the longitudinal response of the slender wing research aircraft (HP 115). Non-linear aerodynamics are shown to have significant effects at the higher angles of attack.

The BAC computer program uses a type of hill-climbing technique, and has been used to obtain derivatives from lateral responses, both rapid rolls and wing rock.

## 1. INTRODUCTION

The art of obtaining aerodynamic derivatives from flight records has been studied and practiced in the UK using various methods in the past (time vector, Shinbrot, analogue matching etc.), but application of optimisation techniques has only received serious attention comparatively recently. Computer programs using such digital methods, which have been successfully implemented at the Royal Aircraft Establishment, Cranfield Institute of Technology and British Aircraft Corporation (Warton Division), are briefly described in this paper and some of the results pertaining to aircraft flying at high angles of attack are presented.

The need for analysis methods which could be used for nonlinear equations of motion became apparent in Aerodynamics Department, RAE in 1968, when free-flight model tests of slender aircraft under lifting conditions exhibited strong coupling between longitudinal and lateral responses. Digital computer programs originally developed for trajectory and response analysis of rockets, based on the Newton-Raphson technique, were successfully adapted<sup>1</sup> to the transient equations of motion with five degrees of freedom, and the same basic analysis method is now being used<sup>2</sup> for the analysis of responses of full-scale aircraft (section 2). In parallel, Avionics Department at RAE developed an optimisation method<sup>3</sup>, based on a hill-climbing technique, for use on a hybrid computer, but the computer time required for convergence has proved rather lengthy, and so the method is not being used extensively.

More basic research into the development and use of computer techniques for parameter identification is being done by Dr. Klein<sup>4</sup> at CIT, under research contract with the Procurement Executive of the Ministry of Defence, in close collaboration with Aerodynamics Department at RAE. The analysis methods included in the current program are described in section 3, and are extensions of the Newton-Raphson technique, yielding and making more use of statistical information than the current RAE programs.

The aim of the Flight Test and Aerodynamics Departments at BAC (Warton) has been to obtain, in collaboration with their Mathematics Division, a computer program<sup>5</sup> which can be used on a routine basis to analyse flight records almost 'on-line' (section 3). The optimisation technique used is similar to hill-climbing, and thus differs from the method used at RAE and CIT, but as yet there has not been opportunity to compare the results obtained with the three programs.

Each team has experience of analysing the classic types of responses, longitudinal short-period, and lateral Dutch roll oscillations, and each has been applying the methods to responses which cannot be analysed using linear techniques, in particular to lateral responses for various aircraft at high angle of attack and high subsonic Mach number. Results for two aircraft are presented in the descriptions of the work at RAE and BAC (sections 2 and 4) and the latter also includes analysis of rapid-roll manoeuvres. The variation of some of the derivatives with angle of attack is presented, and compared with tunnel and estimated values where available. For both aircraft considered, the trends indicate that the Dutch-roll oscillation becomes dynamically unstable as angle of attack is increased, so that the uncommanded wing-rock oscillation can be identified with a negatively damped Dutch-roll type of motion.

The example chosen<sup>6</sup> from the analysis done at CIT (section 3.3) is the highly-damped, nonlinear longitudinal response to elevator pulse of the HP 115 slender-wing research aircraft throughout its angle of attack range. In this case, the response measurements had not yielded any quantitative aerodynamic data using analysis techniques available when the measurements were obtained<sup>7</sup>. The effects of second-order aerodynamic derivatives are shown to be significant in obtaining a good fit to the response data, but their values cannot be derived from the responses available for analysis.

The fourth parts of each of sections 2, 3 and 4 describe briefly the possible future development of the three computer programs, and the types of problem likely to be studied.

## 2. WORK AT THE ROYAL AIRCRAFT ESTABLISHMENT

## 2.1 Description of analysis method

The computer programs currently in use in Aerodynamics Department, RAE, were developed<sup>1</sup> for the analysis of the coupled longitudinal and lateral oscillations of free-flight models of aircraft. A digital method of analysis became necessary when models were flown at non-zero lift (on a barrel-roll trajectory), as the disturbances applied by small pulse rockets caused significant response in the longitudinal short-period mode when attempting to excite the lateral Dutch-roll oscillation. The aerodynamic derivatives were obtained successfully<sup>2</sup>, using a Newton-Raphson technique to give an iterative optimisation procedure. The same basic computer program has been adapted<sup>2</sup> for a analysis of responses of full-scale aircraft, one for longitudinal motion, and one for lateral motion in the presence of longitudinal disturbances. The programs have also been made more versatile than the original, as the parameters to be identified may now be specified in the data, without changing the program.

The cost function is the sum of the squares of the weighted differences between the computed instrument readings and the actual recorded readings, and the unknown parameters are the aerodynamic derivatives, the initial conditions, and the instrument offset errors. The corrections required for the updating of the parameters at each iteration are obtained from the partial derivatives of the equations of motion with respect to the parameters. Statistically the simplest output error method is used, with no process noise assumed, and *a priori* values are not set for the parameters. The relative weightings<sup>3</sup> applied to the instrument readings are usually chosen according to the magnitudes of the responses.

The equations of motion are those for the perturbations in the response variables about a trim state, which need not be steady level flight, and at present only linear aerodynamic derivatives are included. In the program for the analysis of lateral responses, the measured angle of attack and rate of pitch are used as known disturbance inputs. For example, the sideforce equation is written as

$$\dot{v}' = y_v v' + y_{p'} p' + y_{r'} r' + y_{\xi'} \xi' + y_{\zeta'} \zeta' - V(r' + r_e) + w(p' + p_e) + g a_{ye} + g \cos \theta_e \sin \phi,$$

where  $'$  denotes the perturbation from the trim state, denoted by the suffix 'e'. The steady trim value  $a_{ye}$  is included to allow the total measured angle of attack ( $w = V \sin \alpha$ ) to be used in the  $p w$  term, and the total computed angle of bank in the gravity term.

The computed instrument readings are obtained from the steady state and the perturbations, e.g. the sideslip vane angle at  $x_3, z_3$  relative to the centre of gravity is given by

$$\beta^0 = \frac{180}{\pi} \left\{ v' + v_e + x_3(r' + r_e) - z_3(p' + p_e) \right\} / V + E\beta,$$

where  $E\beta$  is the offset error of the vane.

The complete sets of equations for the longitudinal and lateral programs are given in Ref.2.

## 2.2 Application of programs

The longitudinal and lateral derivatives of the Hunter Mk.12 aircraft in l-g flight are currently being determined, to give data needed for the next phases of the research programme on manoeuvre-demand systems. The opportunity is being taken to compare results from the responses due to the usual control inputs to excite short-period and Dutch roll oscillations (elevator doublet and rudder pulse respectively), and from responses due to sequences of arbitrary control inputs.

The lateral program is also being used in the study of the wing-rock phenomenon<sup>4</sup>, as it appeared from theoretical estimates that, for the Gnat Trainer aircraft, the Dutch roll becomes unstable at high angles of attack and high subsonic Mach number. A flight test programme is almost complete, in which ranges of Mach number at three different heights are covered, throughout the angle of attack range from l-g flight up to and including the onset of wing-rock. The test procedure for the pilot is, at given Mach number and initial height, to

- (i) increase angle of attack, in a diving banked turn until buffet and subsequently wing-rock occurs,
- (ii) decrease angle of attack to well below buffet, and excite Dutch roll oscillation with a rudder pulse,
- (iii) increase angle of attack to near buffet onset, and excite Dutch roll oscillation,
- (iv) increase angle of attack further, and if possible, excite Dutch roll oscillation in buffet,
- (v) increase angle of attack until onset of wing-rock.

At each test point, (i) to (v), the pilot aims to maintain constant angle of attack and Mach number, although this condition is very difficult to achieve at the higher angles.

<sup>4</sup> 'Wing-rock' is used in the sense of an uncommanded lateral oscillation of either diverging or steady amplitude.

The analysis began with the responses obtained at the lower angles of attack, and then proceeded to selected responses at the higher angles of attack, chosen on the basis of small variations in  $\alpha$  and  $M$ . At present, the wing-rock responses are being analysed using the equations of motion with linear derivatives, and so divergent and steady amplitude oscillations are treated in separate portions.

Definition of the steady state has caused difficulty, as the offset errors of the rate gyros appear to vary with flight condition, and bank angle cannot be recorded with the instrumentation available. The equations for a steady co-ordinated turn have been used to evaluate  $p_e, q_e, r_e, \theta_e, \phi_e$ , assuming that zero errors in recorded angle of attack and normal acceleration are negligible.

### 2.3 Results for Dutch roll analysis (Gnat aircraft)

An example of the measured and computed Dutch roll responses obtained at low angle of attack is shown in Fig. 1, together with the aileron input and angle of attack variation. Corresponding results at higher angle of attack for a Dutch roll in buffet, Fig. 2, indicate that the fit obtained is not so close, but is acceptable.

The preliminary results for some of the derivatives are shown in Fig. 3, up to angles of attack just below the onset of wing-rock, and covering the Mach number range 0.72 to 0.82. The derivatives  $C_{l_r}$  and  $C_{n_p}$  were not determined, but kept constant at their estimated values. It may be seen that the values of  $C_{n_\delta}$  are close to the tunnel results, and maintain a near-constant level. The computed values of  $C_{l_\delta}$  are generally larger in magnitude than the tunnel results, but may indicate a loss in  $C_{l_\delta}$  at the higher angles of attack. The damping-in-roll derivative,  $C_{l_p}$ , has greater scatter than the derivatives due to sideslip, but the mean level is at a lower magnitude than the estimated variation. It does not appear possible to determine the damping-in-yaw derivative,  $C_{n_r} - C_{n_\delta}$ , as two distinct levels are indicated (with large expected errors) at the higher angles of attack. Currently, some of the responses are being tested to see if  $C_{n_p}$  can be determined instead, as theoretical work has indicated that  $C_{n_p}$  may have a greater influence on the overall damping of the lateral oscillation than  $C_{n_r} - C_{n_\delta}$ .

### 2.4 Future work

The analysis of wing-rock oscillations is continuing, the aim being to establish the adequacy or otherwise of linear aerodynamics to define the transient flight behaviour.

In addition a projected research programme on a transport aircraft calls for the identification of aerodynamic derivatives, and so preliminary consideration is being given to the representation and analysis of a large flexible aircraft for which the rigid-body and bending modes may interact significantly.

## 3. WORK AT CRANFIELD INSTITUTE OF TECHNOLOGY

### 3.1 Description of analysis methods

The research on aircraft parameter identification at Cranfield Institute of Technology is supported by MOD(PE) contract, and has been directed towards analysis of responses expected to be difficult, for example, heavily damped oscillations, rapid rolling, and nonlinear problems. Some of the work has been reported elsewhere, and the following description is taken mainly from Ref. 4.

The computer program developed incorporates four methods of estimating the parameters, and is applicable to linear and nonlinear problems. The four methods are summarised in Table 1, which illustrates the progressively more complicated cost functions and updating used. The equation error method is only used as a start-up procedure for the output error methods if initial guesses for the parameters are not otherwise available.

The weighted least squares method provides unbiased estimates of the unknown parameters provided that the mathematical model of the motion is correct and there is no noise on the measured inputs. The weighting matrix,  $W_1$ , applied to the instrument readings is kept constant throughout the iterations.

The maximum likelihood method assumes that the error distribution of instrument readings is known, and in practice is taken to be Gaussian. The weighting matrix  $W_1$  is updated iteratively as the inverse of the covariance matrix of the measurement noise,  $W_1 = R_1^{-1}$ . This method usually requires more iterations and better starting estimates than for weighted least squares, and so it is useful to have both methods in the same computer program, with control switched as the iteration proceeds.

In the Bayesian method of estimation, the unknown parameters are treated as random variables. If Gaussian distributions are assumed, then the weighting applied to the parameter corrections is obtained from the covariance matrix of the *a priori* known parameters. Again, it is profitable to progress from maximum likelihood to Bayesian methods.

The nonlinear problems are covered by the same computing algorithm used for the linear equations of motion, by introducing the augmented input vector, which includes the nonlinear terms with the input variables. The basic program contains the linear aerodynamic derivatives, either for longitudinal or lateral responses, and a separate subroutine is prepared for each nonlinear problem considered.

The instrumentation assumed consists of the usual accelerometers, rate gyros and incidence probes, corrected for transducer positions and the responses to be fitted are selected according to the actual flight instrumentation.

The scheme has been implemented at CIT on a small computer using an intermediate level interpretative language which was designed specifically for experimental data analysis applications, as described by its originator in Ref.10. The language offers considerable operational flexibility, enabling acquisition, scaling, transformation and processing of data to take place without intermediate storage, and allowing 'hands on' control even, under some circumstances, during program execution. The consequences of this last feature are that wayward runs can often be 'rescued' without the need for restarting the entire process, and that the general program can be incorporated, without modification, into a special purpose program to enable data to be input and output in a user-oriented format. The disadvantage of the language is the relative slowness of execution due to its interpretative nature. FORTRAN versions of the program are to be prepared, for general use on other computers.

### 3.2 Application of programs

The longitudinal responses obtained on the Bassett variable stability aircraft<sup>11</sup> for 'extreme' characteristics have been analysed, altering the derivatives  $C_{m\dot{\alpha}}$ ,  $C_{m\dot{\delta}}$  and  $C_{m\dot{q}}$  to give negative static margin, and low and high values of damping. In all cases the fit between measured and computed responses is satisfactory, and the derivatives obtained with acceptable accuracy. The lateral responses were used to study the effects of making large changes in individual derivatives. The results showed that changes in mode characteristics and no appropriate changes in control input resulted in strong correlation between parameter estimates, causing decreased identifiability for some parameters.

The MS760 Paris aircraft has also been used for parameter identification studies, both for longitudinal and lateral responses, and a study was made of different input forms. Simulated rapid rolling responses (using North American F-100 data) have been analysed, fitting the lateral responses in the presence of 'measured' longitudinal responses. The results of these three computational experiments are reported in Ref.4.

The computer program has also been used to analyse<sup>6</sup> the highly-damped longitudinal response of the HP 115 slender-wing research aircraft throughout its angle of attack range. Although strictly this example is not in the category of 'manoeuvring flight' (the tests being carried out at nominally 1-g conditions), the large angles of attack achieved make it non-standard as regards usual identification problems, and so the results are included in this Report (section 3.3).

As expected in a research programme which is deliberately aimed at difficult cases, a number of problems have arisen, some of which have yet to be solved (section 3.4). The problems of including non-linearities in the mathematical model has been overcome, from a computational point of view, by considering the nonlinear terms to be additional inputs to the system, as mentioned previously. The problem of modelling a complicated system raises the fundamental question of how complex the model should be, the best relationship between complexity and measurement information not being clear. If too many unknown parameters are sought for a limited amount of data then a reduced reliability of evaluated parameters can be expected, or attempts to identify all parameters might fail. Allied with this uncertainty is the choice of input form, which is being studied as opportunity arises. Divergence only occurs rarely, due to the progressive nature of the fitting process; however, difficulty arises in deciding whether the estimated values of the parameters are meaningful, and whether the optimum set of parameters have been chosen for analysis. Criteria for assessment are being tested, but no recommendations are possible as yet.

### 3.3 Results for longitudinal response analysis (HP 115 aircraft)

The experimental data has been taken from flight measurements of the longitudinal short-period oscillation of a slender-wing research aircraft, excited from straight and level steady flight by elevator deflections, at different airspeeds between 70 and 160 kn. The resulting airspeed changes during the transient motion were negligible. The response variables analysed were rate of pitch and normal acceleration, with elevator angle as the control input. The angle of attack measurements were found to be suspect, due probably to vane stiction, and so were not included in the analysis.

On the basis of wind-tunnel tests and preliminary flight measurements, the normal force and pitching moment were assumed to have derivatives with respect to  $\alpha$ ,  $q$ ,  $\dot{\eta}$ ,  $\dot{\eta}^2$ ,  $q\dot{\eta}$  and  $\dot{\eta}\alpha$ . It was found that, at the lower angles of attack, a good fit could be obtained using zero values for all the second order derivatives, and for  $C_{z\dot{\eta}}$  and  $C_{m\dot{\eta}}$  (Fig.4). For most responses,  $C_{zq}$  and  $C_{m\dot{q}}$  had to be fixed at values measured in the wind-tunnel and in steady flight respectively. The values of the parameters were compared with those obtained from (i) application of the maximum likelihood technique in the frequency domain, and (ii) the nonlinear model, with *a priori* values assigned to the analysed derivatives. The three sets of values agreed well, usually within the indicated errors, but the fit obtained for the normal acceleration was significantly better with the nonlinear model.

At high angles of attack, the linear model was found to be inadequate, the mismatch in normal acceleration being observable in Fig.5. The introduction of the nonlinear terms reduces this error, and the resulting autocovariance function is quite close to that of white noise (see Fig.5). The use of the nonlinear model also had a significant effect on the damping-in-pitch derivative,  $C_{m\dot{q}} + C_{m\dot{\alpha}}$ , which was strongly correlated with  $C_{m\dot{\alpha}}$  for the linear model. The remaining derivatives did not differ significantly from those derived with the linear model.

The resulting variation of the estimated derivatives with angle of attack is shown in Figs. 7a and b, together with results from wind-tunnel and steady flight tests where available. The trends of  $C_{m\alpha}$  and  $C_{m\eta}$  with increasing angle of attack agree well with the tunnel results<sup>12</sup>, although the general level of  $C_{m\eta}$  is closer to the results from steady-state flight tests. At the higher angles of attack the values of  $C_{z\alpha}$  and  $C_{m\alpha} + C_{m\eta}$  depart slightly from the tunnel results (those for damping-in-pitch derivative being taken from a slender-wing model of similar planform).

Comparisons were also made between results obtained from responses due to different types of elevator input: stick-forward pulse and square pulse, and stick-back sharp pulse. The latter was not so effective in exciting good responses for analysis, one set of parameters demonstrating this being the average values of the partial derivatives,  $\partial q/\partial C_{m\alpha}$ ,  $\partial n_z/\partial C_{m\alpha}$  etc., which were numerically smaller. The responses with effective inputs were analysed, using the nonlinear model to give results for  $C_{z\eta}$ ,  $C_{m\eta}$  and  $C_{m\dot{\eta}}$ , shown in Fig. 7b. Preliminary examination of the flight records had indicated the possible presence of lift and moment due to rate of application of elevator control, and the degree of consistency throughout the angle of attack range seems to substantiate the existence of significantly large values of  $C_{z\eta}$  and  $C_{m\eta}$  for slender aircraft with trailing edge controls.

### 3.4 Future work

It is envisaged that the tests currently being flown using the Folland Gnat aircraft in the RAE wing-rock investigation will be analysed at Cranfield, to supplement the parameter identification results being obtained at the RAE (section 2). In parallel with this work, the theoretical background and computational implementation of methods to analyse flight responses containing inputs from atmospheric turbulence are being studied, and further nonlinear responses, in particular helicopter data, are to be analysed.

## 4. WORK AT BRITISH AIRCRAFT CORPORATION (WARTON)

### 4.1 Description of analysis method

The Flight Test and Aerodynamics Departments at BAC (Warton) have used various methods in the analysis of flight records of military aircraft, for example, Lightning, TSR2, Jaguar<sup>13,14</sup>, to obtain both performance and handling parameters, and aerodynamic derivatives. Experience is now being gained in using a digital computer program<sup>5</sup> based on a least-squares technique, to obtain aerodynamic derivatives needed to establish handling boundaries for flight clearance.

The error between measured and computed response time histories is expressed as a sum of squares and to this is added a similar term for the *a priori* weighting to give the cost function

$$J = \sum_{i=1}^{N_z} \sum_{j=1}^{N_t} \left( \frac{z_{ij} - \hat{z}_{ij}}{\sigma_j} \right)^2 + KN_c \sum_{i=1}^{N_c} \left( \frac{c_i - c_{oi}}{u_i} \right)^2.$$

The  $N_z$  responses  $\hat{z}_{ij}$  measured at  $N_t$  time points are matched to the computed response  $z_{ij}$ . The usual number of responses is five, namely sideslip, roll rate, pitch rate, yaw rate and normal acceleration factor.  $\sigma_j$  is the standard deviation of the noise assumed on response 'j', and is usually chosen to be the accuracy to which the appropriate instrumentation can measure, although the value may subsequently be updated (but not automatically) on the basis of results obtained.

A total of  $N_c$  derivatives are variable, and are to be found,  $c_i$  being the current value of the  $i$ th derivative, and  $c_{oi}$  being its *a priori* value.  $u_i$  is the 'uncertainty' of variable 'i', and represents the confidence level of the value  $c_{oi}$ , i.e. it is believed that the correct value of  $c_i$  lies in the region  $c_{oi} \pm u_i$ . The values of  $u_i$  have usually to be chosen on past experience.

The scaling factor  $K$  affects the relative weightings between the response part of the cost function and the *a priori* part.  $K$  is normally set to unity, although sometimes a value of zero is used to obtain the best possible fit, ignoring *a priori* values.

The cost function is minimised using Powell's method<sup>15</sup> for minimising a sum of squares without calculating derivatives, and so differs from the techniques used in the RAE and CIT programs. The variation of responses with the derivatives is obtained by a purely numerical process.

The mathematical model of the equations of motion contains the five degrees of freedom  $\alpha$ ,  $\beta$ ,  $p$ ,  $q$ ,  $r$ , in terms of their increments  $\Delta\alpha$  etc. from the initial trimmed state. The aerodynamic forces and moments are expressed as the usual derivatives, together with second order derivatives with respect to angle of attack, and control deflections. Also included are engine gyroscopic contributions. The attitude of the aircraft is represented by the direction cosines of the body-fixed axis system relative to earth. The computed instrument readings for  $\alpha$ ,  $\beta$  and  $a_z$  are corrected for transducer positions relative to the cg.



## 4.2 Application of the program

The aim is to process and analyse flight data in parallel with the flight-test programme, and so the analysis program has been made compatible with other computer programs and data stores, to give acceptable turn-round times between flight experiment and the obtaining of analysed results. The flight data is taken from the computer file storing all the relevant flight test runs, and the initial estimates of the derivatives are interpolated from the data in the derivative file store. These latter may be overwritten by either arithmetic or algebraic values obtained from other sources.

Results have been obtained from responses due to stick jerks and slow rudder doublets in level flight, (exciting the longitudinal short period and lateral Dutch roll oscillations respectively), from Dutch rolls excited during high-g turns, and from rapid roll responses, again at high-g. The latter manoeuvre is defined by the control sequence: elevator to give required g-level in turn, then step input to aileron (or roll control), with elevator and rudder held nominally constant. No attempt has been made to modify these standard test techniques, as they usually yield sufficient information for flight clearance. Instead, the advantage of the present analysis method is the ability to use more of the flight records so obtained, in terms of including transient motion due to control inputs exciting the response, without recourse to handmatching. To date, over 200 rapid roll responses have been matched, half of them requiring little effort from the analysts, but 20% requiring considerable effort to achieve a good match. In addition, about 60 responses at high angle of attack, mainly wing rock, have been considered. 15% of these had to be abandoned, due to limitations in the present mathematical model which only includes linear variation of the lateral derivatives with angle of attack, and the remaining responses required some effort to analyse.

The responses in rapid rolling have been used to obtain derivatives at relatively high angles of attack, including the derivative  $C_{n_p}$ , yawing moment due to rate of roll, and to obtain significant cross-coupling derivatives. The need to establish quickly the trends of derivatives with increasing angle of attack and Mach number, in order to define the conditions for the next flight test in the series, has been the main impetus in developing the present computer program.

Most of the problems encountered in using the program have been related to the experiments at high angles of attack. Originally the computer program required analysis to start from a trimmed state, but has now been modified to allow for initial accelerations, so that more flight records may be analysed. The datum shifts (zero errors) on the instrumentation are currently estimated from flight records taken during trimmed flight, which may lead to some uncertainty. As in the work at RAE, it is not easy to obtain records of wing-rock for relatively steady values of angle of attack and Mach number, so that the choice of time histories to be analysed needs to be made by an experienced flight analyst. In fact, there is general agreement among research workers in the United Kingdom that an important factor in making efficient use of the analysis programs such as those described in this Report is the active collaboration of both Flight Test and Flight Dynamics teams, to monitor the work being done. Experience is being gained in interpreting the various error parameters available from the computer output, in particular the sensitivities of response variables to the parameters, and the errors in the responses.

## 4.3 Results for rapid rolling and wing-rock (combat aircraft)

The RAC results presented here were obtained from matching the lateral responses of a fighter-strike aircraft, at high angles of attack.

The aircraft exhibits wing-rock and a departure termed 'yaw off' by the pilots, but both characteristics have been shown to be identified with dynamic instability of the Dutch roll oscillation, that is, loss of damping. Some rapid roll responses were also analysed, and a sample of the results are presented here. Figs. 8 and 9 show the measured and computed responses obtained in rapid rolls and wing-rock respectively, and variations of the derivatives with angle of attack are given in Fig. 10. Some estimates of the derivatives have also been made, based on tunnel tests and trends in the calculated Dutch roll characteristics, and are shown for comparison. In this analysis of the flight data, the derivatives due to rate of yaw were kept constant at their *a priori* values.

The yawing moment due to sideslip becomes negative at the higher angles of attack, but the rolling moment,  $C_{l_p}$ , is sufficiently large and negative to maintain the Dutch roll mode as an oscillation. The trends of the derivatives due to rate of roll with increasing angle of attack both have adverse effects on Dutch roll damping, the rolling moment decaying towards zero, and the yawing moment becoming significantly negative. The decay in  $C_{l_p}$  had been anticipated in the estimate, but the marked variation of  $C_{n_p}$  was unexpected.

Analysis of flight records of other configurations of the aircraft has shown that the rolling moment due to sideslip is highly dependent on the type of store load, although the other derivatives were not so sensitive. (With stores,  $C_{n_\beta}$  is of course less positive.)

## 4.4 Future work

The computer program is currently being streamlined further for use on a routine basis, and a study is being made of the effects of choice of confidence limits in the *a priori* values of derivatives in order to obtain a simplified guide. The use of the correlation matrix to decide on parameters to include in the analysis is also to be investigated.

Possible extensions to the program are to account for variations in forward speed (six degrees of freedom), and to include further nonlinear aerodynamics, probably by combining linear increments with given forms of variation with angles of attack and sideslip.

## 5. CONCLUSIONS

The digital computer program developed in three centres in the UK are showing themselves to be capable of identifying the aerodynamic derivatives from responses obtained in manoeuvres at high angle of attack, although care and judgement are needed in assessing the results.

At RAE and CIT the available computer programs are proving to be valuable tools in the research work on wing-rock, the flight measurements of responses being used to obtain values of derivatives which can help identify the basic aerodynamics of the phenomenon. The Cranfield program has also been applied successfully to the analysis of longitudinal responses due to nonlinear aerodynamic forces and moments.

In an aircraft firm, such as BAC, the emphasis must be on having methods of analysis which give quick and reasonably accurate results for aerodynamic derivatives, to be used as background information in the assessment of flying qualities of an aircraft in its various configurations and throughout its flight envelopes. Application of the analysis program to measurements at the extremes of the flight envelope has given aerodynamic derivative data which is currently not available from wind-tunnel tests.

### Acknowledgments

The work at BAC (Warton) has been described with their permission, and acknowledgments are specially due to Messrs. T.B. Saunders and D. Booker for their willing co-operation and help in supplying the material. Dr. Klein is also to be thanked for his help and advice in preparing the description of his work.

Table 1

SUMMARY OF METHODS USED AT CIT

Method	Cost function	Estimate of parameters, $\gamma$
Equation error:		
Regression analysis	$\frac{1}{2} \sum_{i=1}^N   \dot{x}_{E_i} - \dot{x}_i  ^2 W_i$	$\gamma = \left( \sum_{i=1}^N X_i X_i^T \right)^{-1} \sum_{i=1}^N X_i \dot{x}_{E_i}$
Output error:		$\Delta \gamma =$
Weighted least squares	$\frac{1}{2} \sum_{i=1}^N   z_i - y_i  ^2 W_i$	$\left( \sum_{i=1}^N H_i^T W_i H_i \right)^{-1} \sum_{i=1}^N H_i^T W_i (z_i - y_i)$
Maximum likelihood	$\frac{1}{2} \sum_{i=1}^N   z_i - y_i  ^2 R_i^{-1} + \frac{N}{2} \ln  R_i $	$\left( \sum_{i=1}^N H_i^T R_i^{-1} H_i \right)^{-1} \sum_{i=1}^N H_i^T R_i^{-1} (z_i - y_i)$
Bayesian	$\frac{1}{2} \sum_{i=1}^N   z_i - y_i  ^2 R_i^{-1}$ $+ \frac{1}{2}   \gamma - \gamma_0  ^2 R_2^{-1} + \frac{N}{2} \ln  R_i $	$\left( \sum_{i=1}^N H_i^T R_i^{-1} H_i + R_2^{-1} \right)^{-1} \times$ $\left\{ \sum_{i=1}^N H_i^T R_i^{-1} (z_i - y_i) - R_2^{-1} (\gamma - \gamma_0) \right\}$

### Definitions:

$H_i$  = gradient matrix  
 $N$  = number of data points

$R_1$  = covariance matrix of measurement noise,  $R_1 = \frac{1}{N} \sum_{i=1}^N (z_i - \hat{y}_i)(z_i - \hat{y}_i)^T$

$R_2$  = covariance matrix of *a priori* known parameters,  $R_2 = E\{(\gamma - \gamma_0)(\gamma - \gamma_0)^T\}$

$W_i$  = weighting matrix  
 $X_i$  = matrix of measured state and input variables  
 $\dot{x}_i$  = state vector  
 $y_i$  = output vector  
 $z_i$  = measurement vector

$\gamma$  = parameter vector  
 $E\{\}$  = expected value,  $\gamma_0 = E\{\gamma\}$

## SYMBOLS (not defined in text)

$a_y, a_z$	acceleration factors in $y$ and $z$ directions, respectively	$\alpha$	angle of attack, rad
$C_l$ etc.	non-dimensional aerodynamic derivative	$\beta$	angle of sideslip, rad
$g$	acceleration due to gravity, $m/s^2$	$\zeta, \eta, \zeta$	deflection of aileron, elevator and rudder, respectively
$p, q, r$	angular rate of roll, pitch and yaw respectively, rad/s	$\theta$	angle of pitch
$v, w$	velocity components in $y$ and $z$ directions respectively, m/s	$\phi$	angle of bank
$V$	forward speed, m/s		
$x, y, z$	body-axis system		
$y_v$ etc.	dimensional aerodynamic derivatives, divided by aircraft mass		

## REFERENCES

No.	Author	Title, etc.
1	A.P. Waterfall	"A technique for the automatic, digital analysis of flight dynamic response data." RAE Technical Report 70228 (1970) (ARC R & M 3699)
2	A. Jean Ross G.W. Foster	"Fortran programs for the analysis of transient longitudinal and lateral responses of aircraft." RAE Technical Report to be published.
3	D. Fry G.T. Shanks	"The identification of the Hunter Mk.12 aerodynamic derivatives using an automatic model-matching technique." RAE Technical Report 72103 (1972)
4	V. Klein	"Parameter identification applied to aircraft." Cranfield Institute of Technology, CIT-PI-73-018 (1973)
5	K.G. Moore	"Extraction of aerodynamic derivatives by matching flight data. Part II Computer program description." British Aircraft Corporation Ltd., Program STOB27A, (1974)
6	V. Klein	"Longitudinal aerodynamic derivatives of a slender delta-wing research aircraft extracted from flight data." Cranfield Institute of Technology, to be published.
7	P.L. Bisgood	"Results of flight tests on a slender-wing low-speed research aircraft (HP 115)." AGARD Report 535 (1966)
8	A. Jean Ross G.F. Edwards A.P. Waterfall	"The dynamic stability derivatives of a slender wing at zero and moderate lift; a comparison of theory with free-flight model tests, $M = 0.8$ to $2.0$ ." RAE Technical Report 73097 (1973)
9	H.H.B.M. Thomas A. Jean Ross	"The role of theoretical studies of flight dynamics in relation to flight testing." Paper 22 of AGARD Conference Proceedings No.119 on Stability and Control (1972)
10	D.A. Williams	"CALC: an intermediate level interpretive language for processing experimental records using a small general purpose digital computer." Cranfield Institute of Technology, COA-DA-002 (1973)
11	C.A. Martin	"Variable stability installation in Bassett Aircraft XS-743." Cranfield Institute of Technology, COA-DA-014 (1973)
12	P.B. Engler G.F. Moss	"Low-speed wind-tunnel tests on a 1/8th scale model of Handley-Page HP 115." ARC R & M 3486 (1965)
13	B.R.A. Burns	"Experience with Shinbrot's method of transient response." AGARD Report 549 - Part II (1966)
14	B.R.A. Burns	"Stability and control test methods used on the Lightning and TSR2." British Aircraft Corporation, Report Ac 244 (1965)
15	M.J.D. Powell	"A method of minimising a sum of squares of nonlinear functions without calculating derivatives." Computer Journal, Vol.7, No.4, p.303.

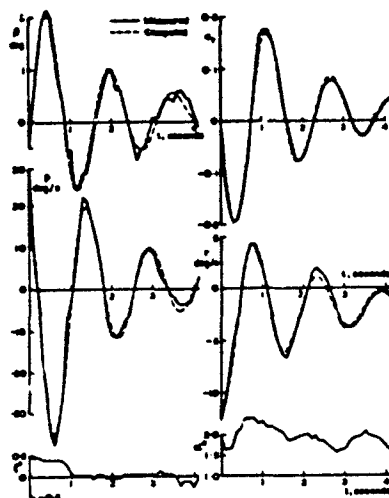


FIG. 1 DUTCH ROLL AT LOW ANGLE OF ATTACK, GNAT AIRCRAFT

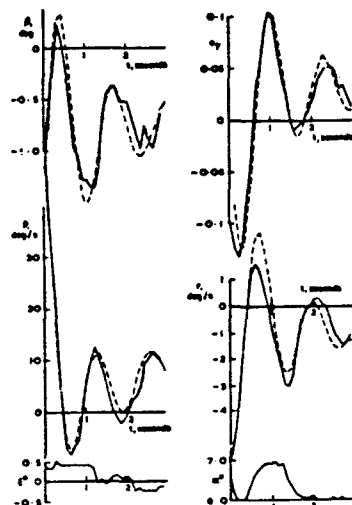


FIG. 2 DUTCH ROLL IN BUFFET, GNAT AIRCRAFT

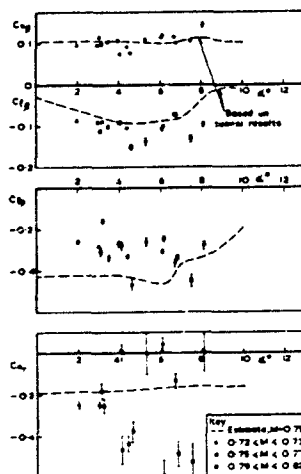
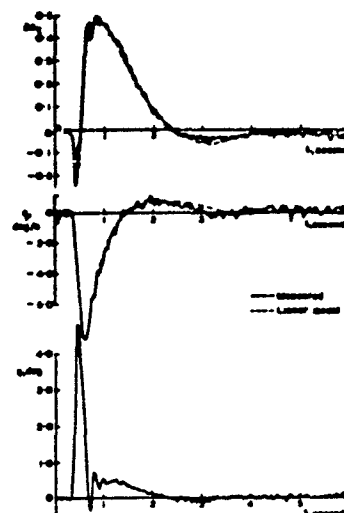
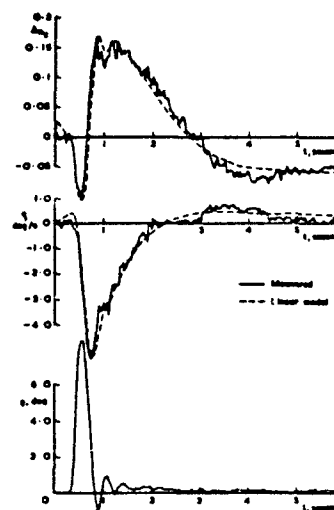
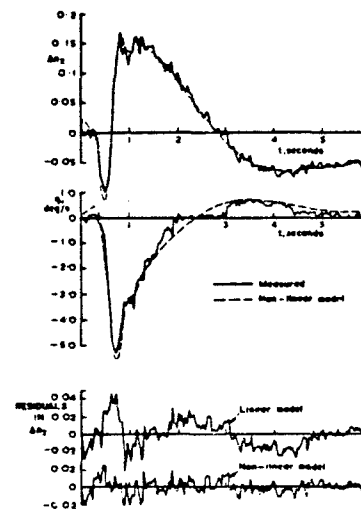


FIG. 3 AERODYNAMIC DERIVATIVES, GNAT AIRCRAFT

FIG. 4 LONGITUDINAL RESPONSE,  $\alpha = 7.2$ , LINEAR MODEL, HP 115 AIRCRAFTFIG. 5 LONGITUDINAL RESPONSE,  $\alpha = 20.3^\circ$ , LINEAR MODELFIG. 6 LONGITUDINAL RESPONSE,  $\alpha = 20.3^\circ$  NON-LINEAR MODEL, HP 115 AIRCRAFT

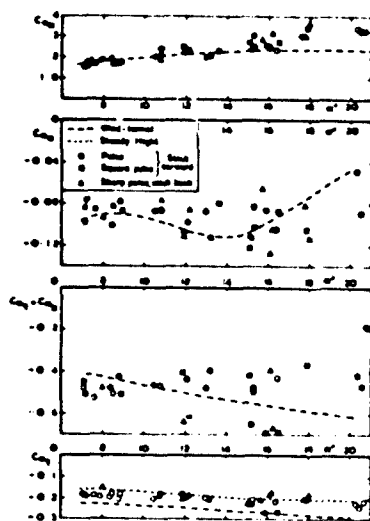
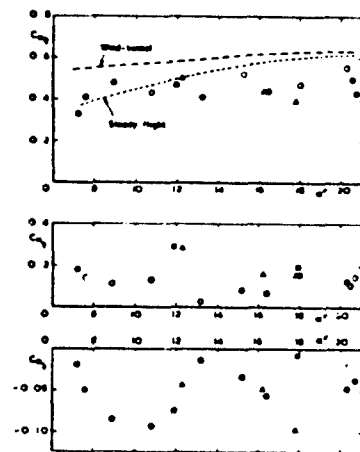
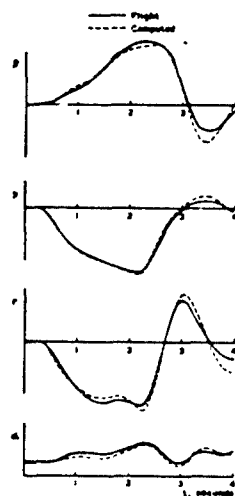
FIG. 7a AERODYNAMIC DERIVATIVES,  
HP 115 AIRCRAFTFIG. 7b AERODYNAMIC DERIVATIVES, CONT.,  
HP 115 AIRCRAFT

FIG. 8 RAPID ROLL OF COMBAT AIRCRAFT

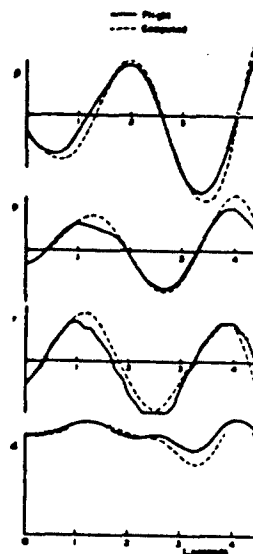
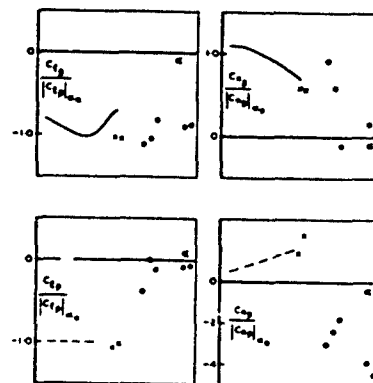


FIG. 9 WING ROCK OF COMBAT AIRCRAFT



Derivative analysis {  $\bullet$  Rapid roll  
 $\bullet$  Wing rock  
 Wind tunnel  $\bullet$  Flight  
 Estimate  $\bullet$  Estimate  
 Note: Derivatives divided by values estimated  
 for low angle of attack

FIG. 10 DERIVATIVES FOR COMBAT AIRCRAFT

## ADVANCEMENT IN PARAMETER IDENTIFICATION AND AIRCRAFT FLIGHT TESTING

Roger A. Burton  
Systems Analyst Specialist  
Flight Test Division  
Naval Air Test Center  
Patuxent River, Maryland 20670  
USA

## SUMMARY

This paper presents results from an ongoing program at the Naval Air Test Center to develop parameter identification technology with specific emphasis placed on studies conducted in parameter identifiability and "optimal" control inputs for parameter estimation. Navy applications for parameter identification technology are discussed with specific areas in aircraft stability and control testing outlined. Specific criteria required for defining optimal control inputs and establishing parameter identifiability are discussed. Parameter identification results from the analysis of flight test data are presented which establish the need for considering input design in planning tests for extracting aerodynamic coefficients from flight test data. Parameter identifiability results for specific control inputs used are presented. In cases where identifiability problems are shown to exist the use of a rank deficient solution to improve parameter identifiability is demonstrated.

## SYMBOLS

$a_z$	acceleration in Z axis
$a_y$	lateral acceleration
$g$	acceleration due to gravity
$l_a$	distance from center of gravity to angle of attack vane
$l_\beta$	distance from center of gravity to sideslip vane
$K_d$	Dutch roll root residue
$K_{ss}$	steady state gain
$K_\phi$	root locus gain for the roll rate to aileron transfer function
$K_\alpha$	angle of attack vane scale factor
$K_\beta$	sideslip vane scale factor
$M$	pitching moment
$M(\cdot)$	pitching moment derivative
$N$	yawing moment
$N(\cdot)$	yawing moment derivative
$N_y^x$	transfer function numerator polynomial for the x to y transfer function
$n_z$	normal acceleration
$n$	random white noise
$L$	rolling moment
$L(\cdot)$	rolling moment derivative
$p$	roll rate
$q$	pitch rate
$R$	measurement noise covariance matrix
$r$	yaw rate
$s$	laplace operator
$T$	transpose
$J$	cost function

$u$	longitudinal airspeed
$u_0$	longitudinal trim airspeed
$v$	eigenvector
$X$	longitudinal force
$X()$	longitudinal force derivative
$Y$	side force
$Y()$	side force derivative
$Z$	vertical force
$Z()$	vertical force derivative
$\alpha$	angle of attack
$\alpha_g$	gust angle of attack
$\beta$	sideslip angle
$\beta_g$	gust sideslip angle
$\Delta$	characteristic equation
$\delta a$	aileron position
$\delta e$	elevator position
$\delta R$	rudder position
$\zeta$	damping ratio
$\theta$	pitch angle
$\lambda$	eigenvalue
$\sigma_x$	standard deviation of the x calculated response with respect to the x measured response
$\tau_R$	roll mode time constant
$\tau_S$	spiral mode time constant
$\phi$	roll angle
$\omega_c$	gust break frequency
$\omega_n$	natural frequency

Subscripts

$i$	index
$m$	measured
$sp$	short period

## INTRODUCTION

The Naval Air Test Center (NATC) is conducting a research program to develop airframe parameter identification technology for use in flight testing Navy aircraft. This program was initiated in 1971 between the Naval Air Systems Command (NAVAIR) and NATC. During this same time period the Office of Naval Research (ONR) issued a contract to Systems Control, Inc. (SCI) to advance the state-of-the-art in parameter identification methods. In 1973 a concentrated effort was conducted by the Navy to continue the development of this new technology by forming a joint program between NATC, NAVAIR, ONR and SCI. This paper will present the results of this joint program to date including a discussion of Navy applications for parameter identification and flight test results.

## BACKGROUND

Many flight test applications of airframe parameter identification techniques have surfaced in recent years as the technology in this field has continuously increased. For example, the determination of the compliance of an aircraft's flying qualities with

the requirements of military specification MIL-F-8785B (reference (1)) has long been a costly, time consuming facet of aircraft flight testing. However, it now appears possible that a considerable portion of the flight test program can be eliminated through use of airframe parameter identification. This recent technology would be employed to extract the aircraft stability and control derivatives from data obtained through a limited number of flight tests. These derivatives in turn, would be used to verify the aircraft's compliance with the military specification requirements. In addition, the steady growth in the complexities of these aircraft specification requirements and automatic landing systems have changed the complexion of the requirements set upon the flight test community for data accuracy and evaluation techniques. These new requirements for improved data accuracy and more complicated evaluation techniques can be fulfilled by using this new airframe identification technology. Thus the desire to reduce the amount of flight time spent on specification testing and the increased complexity of aircraft systems and specification requirements has prompted the development of airframe parameter identification technology at NATC.

#### SCOPE OF INVESTIGATION

During the parameter identification program at NATC beginning in 1971, both classical and advanced airframe parameter identification methods have been studied. This approach was taken in order to develop a wide spectrum of experience in parameter estimation theory and applications. Classical methods that were programmed during this period are analog matching, least squares, z-transform, Fourier transform, and Newton-Raphson. (Results from these earlier programs are published in references 2 and 3.) The advanced statistical method that has been programmed is the maximum likelihood approach to parameter identification. This later effort is the topic of this paper with emphasis placed on parameter identifiability studies conducted. The major efforts in this area have been in establishing criteria for the determination of "optimal" inputs for parameter estimation and identifiability of system parameters.

A flight test program was conducted in support of the development of the maximum likelihood parameter identification algorithm. The purpose of this flight test program was to gather data to exercise the parameter identification algorithms programmed and to determine the proper data gathering procedures. This later task is the major effort in this program and its objective is to determine the effects of control system inputs on parameter identification estimates. The determination of the proper data gathering procedures is basically an experimental study to solve the parameter identifiability problem by determining an "optimal" control input that will result in the "best" parameter estimates. The types of control inputs that are being used to generate data in the longitudinal axis are pulse, step, doublet, sine wave, variable frequency sine wave, and random. Aileron pulse, aileron step, aileron doublet, rudder doublet, aileron-rudder doublet, aileron sine wave, rudder sine wave, and aileron-rudder sine wave inputs are being used to excite the airplane motion in the lateral-directional axes. The F-14A airplane BuNo 157987 was the flying test bed for this program and during the period May 1974 to September 1974 eight flights were flown to obtain flight test data. During these flights, 196 maneuvers (inputs) were performed to collect data for the input design experiments. Tests were conducted in the cruise and power approach configurations at flight conditions of approximately 0.6 Mach at 15,000 and 30,000 feet altitude.

#### FLIGHT TEST APPLICATIONS

Navy applications for airframe parameter identification technology include stability and control testing, system simulation, establishment of a data base for operational flight trainers, and the determination of aircraft frequency response for evaluation of automatic carrier landing systems. The basic procedure used is to first estimate the aircraft parameters of interest over the required flight envelope. These estimated parameters are then used to determine aircraft stability and control characteristics, operational flight trainer data base, or frequency response. The following section will be limited to a discussion of the Navy applications of parameter identification to aircraft stability and control testing.

##### Flying Qualities Specification Compliance

The new flying qualities specification (reference 1) has many new parametric requirements which require the use of an advanced airframe parameter identification technique for determination of specification compliance. In the longitudinal axis the new requirements of interest are short period damping ( $\zeta_{sp}$ ), frequency ( $\omega_{nsp}$ ) and acceleration sensitivity ( $\frac{n_z}{\alpha}$ ). The requirements for ( $\frac{n_z}{\alpha}$ ) are given in graphical form in figure 1.

There are several flight test procedures which have been proposed for determining ( $\frac{n_z}{\alpha}$ ) including short period free response to a doublet input, wind up turns, steady pull ups, and frequency response to sinusoidal inputs. A mathematical expression for ( $\frac{n_z}{\alpha}$ ) steady state is given by:

$$\left. \frac{n_z}{\alpha} \right|_{ss} = \frac{-u_0}{g} \left[ \frac{-M_\alpha + M\delta_e Z_\alpha}{Z\delta_e} \right] \quad (1)$$



The primary difference in these test procedures for determining  $(\frac{n_z}{a})$  is the tail lift term  $Z_{\delta_e}$ . The short period free response to a doublet does not consider this term (the value obtained for  $(\frac{n_z}{a})$  is for the untrimmed lift curve slope). The windup turn and steady pull-up maneuvers give the value for  $(\frac{n_z}{a})$  under steady state (low frequency conditions) assuming that pitch rate effects on  $Z_{\delta_e}$  are small. The correct value for  $(\frac{n_z}{a})$  will be obtained from sinusoidal inputs in that this value contains the tail lift term at the frequency at which the airplane normally responds to control inputs. This correct value of  $(\frac{n_z}{a})$  can be determined using estimated aircraft stability and control derivatives to calculate the transfer function parameters of the pitch rate to elevator  $(\frac{\dot{\theta}}{\delta_e})$  and angle of attack to elevator  $(\frac{\alpha}{\delta_e})$  transfer functions.

$$\frac{\dot{\theta}}{\delta_e}(s) = \frac{S N_{\delta_e}^{\theta}}{\Delta} \quad (2)$$

$$\frac{\alpha}{\delta_e}(s) = \frac{N_{\delta_e}^{\alpha}}{\Delta} \quad (3)$$

where  $N_{\delta_e}^{\theta}$ ,  $N_{\delta_e}^{\alpha}$  are the transfer function numerator polynomials and  $\Delta$  is the characteristic equation of the system. An analytical expression for  $(\frac{n_z}{a})$  can be formed using the linear relationship for normal acceleration

$$n_z = \frac{u_0}{g} (\dot{\theta} - \dot{\alpha}) \quad (4)$$

and equations (2) and (3).

$$\frac{n_z}{a}(s) = \frac{u_0}{g} \left[ \frac{S (N_{\delta_e}^{\theta} - N_{\delta_e}^{\alpha})}{N_{\delta_e}^{\alpha}} \right] \quad (5)$$

The normal acceleration sensitivity  $(\frac{n_z}{a})$  is calculated from equation (5) by substituting  $j\omega$  for  $s$  and evaluating the expression at the short period frequency ( $\omega_{nsp}$ ).

Another new longitudinal requirement of MIL-F-8785B is the specification of a maximum value of damping ratio ( $\zeta$ ) now specified for the short period mode. In general, classical hand measurement techniques are not successful in accurately predicting the damping ratio for heavily damped systems which characterize modern Navy aircraft with a stability augmentation mode engaged. Thus airframe parameter identification techniques can be used to fulfill this new data requirement, since the damping ratio can be expressed as a combination of stability derivatives. Thus in the longitudinal axis if the transfer function parameters or stability derivatives can be estimated, the specification requirements that can be determined are  $\omega_{nsp}$ ,  $(\frac{n_z}{a})$ ,  $\zeta_{sp}$ ,  $\omega_{np}$  and  $\zeta_p$ .

In the lateral-directional axis, MIL-F-8785B sets new requirements for Dutch roll damping ( $\zeta_d$ ) and frequency ( $\omega_{nd}$ ), spiral mode ( $1/t_s$ ), roll mode ( $1/t_r$ ), and roll rate specifications. In addition to the updated military specification requirements in the lateral-directional axes, there are also new parametric requirements in the detail specifications for the S-3A (reference 4) and F-14A (reference 5) airplanes. These new requirements are in the form of the Dutch roll coupling parameter ( $\omega_{n\phi}$ ) and the Dutch

roll excitation parameter ( $\frac{K_d}{K_{ss}}$ ). These new specification requirements in the lateral-directional axes are difficult to determine accurately because the effects of the spiral, roll and Dutch roll modes cannot be easily separated using conventional techniques. However, these new lateral-directional requirements can easily be determined if the roll rate to aileron transfer function is calculated using estimated stability and control derivatives.

$$\frac{P_a(s)}{s_a} = \frac{K_d \left( \frac{s^2}{\omega_{n\phi}^2} + \frac{2\zeta_\phi}{\omega_{n\phi}} s + 1 \right)}{(\tau_s s + 1)(\tau_R s + 1) \left( \frac{s^2}{\omega_{nd}^2} + \frac{2\zeta_d}{\omega_{nd}} s + 1 \right)} \quad (6)$$

The specification requirements which can be determined from the matched transfer function parameters are  $\omega_{nd}$ ,  $\zeta_d$ ,  $\tau_s$ ,  $\tau_R$ ,  $\omega_{n\phi}$  and  $K_d$ . In order to determine  $K_d$  from this data, the matched transfer function poles and zeros are plotted on an S-plane as shown in figure 2.

The term  $K_d$  is then determined as the residue measured from the Dutch roll pole and is given by:

$$\frac{K_{Dutch}}{Residue} = \frac{a b}{e \omega_{nd} \omega_d} \quad (7)$$

The term  $K_{ss}$  is the steady state residue and is measured from the origin, assuming that  $1/\tau_s = 0$ .

$$\frac{K_{ss}}{Residue} = \frac{\omega_{n\phi}^2 \tau_R}{\omega_{nd}^2} \quad (8)$$

Thus  $K_d/K_{ss}$  is determined as the ratio of equations (7) and (8).

#### STATUS OF NAVY PARAMETER IDENTIFICATION CAPABILITY

Successful completion of the joint program among NATC, NAVAIR, ONR and SCI has resulted in the development of an advanced state-of-the-art maximum likelihood identification computer program called SCIDNT. This computer program was implemented on the NATC Real Time Data Processing System (RTPS) in August, 1974 and has subsequently been successfully used to identify aircraft stability and control parameters from flight test data. This identification algorithm is programmed in a general format to provide the capability for identifying linear and nonlinear aircraft models and easily modifying the equations of motion and instrumentation equations. SCIDNT contains many advanced features which enable it to more readily handle the flight test data analysis problem. These capabilities and options of SCIDNT are outlined in Table I. In its present form SCIDNT can determine the stability and control derivatives for the linearized, uncoupled longitudinal and lateral aircraft equations of motion in the presence of wind gusts and measurement errors. These equations of motion and measurement equations are presented below:

##### Longitudinal Equations of Motion:

$$\dot{\alpha} = Z_\alpha(\alpha + \alpha_g) + Z_u u + Z_q q - \frac{g}{u_0} \sin \theta_0 + Z_{\delta_e} \delta_e \quad (9)$$

$$\dot{u} = X_u(\alpha + \alpha_g) + X_u u + X_q q - g \cos \theta_0 + X_{\delta_e} \delta_e \quad (10)$$

$$\dot{q} = M_\alpha(\alpha + \alpha_g) + M_u u + M_q q + M_{\delta_e} \delta_e \quad (11)$$

$$\dot{\theta} = q \quad (12)$$

$$\dot{\alpha}_g = -\omega_c \alpha_g + n_6 \quad (13)$$

##### Longitudinal Measurement Equations:

$$\alpha_m = K_\alpha (\alpha + \alpha_g) + \frac{Z_\alpha K_\alpha}{u_0} q + n_1 \quad (14)$$

$$u_m = u + n_2 \quad (15)$$

$$q_m = q + n_3 \quad (16)$$

$$\theta_m = \theta + n_4 \quad (17)$$

$$a_{z_m} = u_0 (Z_\alpha(\alpha + \alpha_g) + Z_{\delta_e} \delta_e) + n_5 \quad (18)$$

#### Lateral Equations of Motion:

$$\dot{p} = L_p p = L_{Tr} + L_{\beta} (\beta + \beta_g) + L_{\delta_a} \delta_a + L_{\delta_R} \delta_R \quad (19)$$

$$\dot{r} = N_p p = N_{Tr} + N_{\beta} (\beta + \beta_g) + N_{\delta_a} \delta_a + N_{\delta_R} \delta_R \quad (20)$$

$$\dot{\beta} = \sin \alpha_0 p - \cos \alpha_0 r + Y_{\beta} (\beta + \beta_g) + \frac{g}{u_0} \cos \theta_0 + Y_{\delta_a} \delta_a + Y_{\delta_R} \delta_R \quad (21)$$

$$\dot{\phi} = p + \tan \theta_0 \quad (22)$$

$$\dot{\beta} = -\omega_c \beta_g + n_6 \quad (23)$$

#### Lateral Measurement Equations:

$$p_m = p + n_1 \quad (24)$$

$$r_m = r + n_2 \quad (25)$$

$$\beta_m = K_{\beta} (\beta + \beta_g) + \frac{L_{\beta} K_{\beta}}{u_0} r + n_3 \quad (26)$$

$$\phi_m = \phi + n_4 \quad (27)$$

$$a_{ym} = u_0 (Y_{\beta} (\beta + \beta_g) + Y_{\delta_a} \delta_a + Y_{\delta_R} \delta_R) + n_5 \quad (28)$$

One of the more important data analysis problems that is addressed in SCIDNT is the identifiability problem associated with accurately extracting stability and control derivatives from flight test data. This identifiability problem is related to the degree of excitation of the modes of a system by a particular input and the corresponding ability to identify the parameters of the system (reference 6). In other words, in order to identify a mode (or parameters) of a system that particular mode must be excited by the input. This parameter identifiability problem also relates to whether a parameter can be identified by itself or whether it is identifiable only as part of a linear combination of several parameters (reference 6). Parameter identifiability problems usually manifest themselves in the identification procedure as either physically nonrealizable parameter estimates, large parameter error covariances, or problems in inverting the information matrix. SCIDNT uses three different approaches to alleviate parameter identifiability problems:

- a. Parameters may be fixed or constrained to be within certain bounds.
- b. A priori weighing may be placed on parameters estimates.
- c. A rank deficient solution may be used to compute the inverse of the information matrix.

These three techniques can be used separately or in conjunction with each other in SCIDNT to alleviate the parameter identifiability problems. Parameter fixing or constraining and a priori weighing are subjective techniques and their use is well documented in the literature. Since these two techniques require a high degree of operator skill for successful implementation, a more generalized method (automatic or black box procedure) is desirable for use by the practicing flight test engineer. The technique implemented in SCIDNT to solve this problem is the use of a rank deficient solution to handle the numerical problems (identifiability problems) associated with inverting the information matrix and obtaining accurate parameter estimates and error covariances. These numerical problems can be related to the spread in the eigenvalues of the information matrix (reference 6). For example, neglecting computer round-off and other computational errors, a perfect dependency among parameters would result in a zero eigenvalue and a subsequent difficulty in inverting the information matrix. Thus for this case, a rank deficient solution can be used in SCIDNT to calculate the inverse of the information matrix. In actual analysis of flight test data, computational errors restrict the existence of an actual zero eigenvalue and thus the spread between the smallest and largest eigenvalues will be many orders of magnitude with the smallest eigenvalue being non-zero. When the spread in the eigenvalues is large, the smaller eigenvalues can be related to singular directions in parameter space and indicate parameters or combinations of parameters which cannot be identified. It has been demonstrated by using the rank deficient solution option of SCIDNT that numerical convergence can be achieved (with reasonable parameter estimates) in cases where previous computer runs did not converge. The utilization of the rank deficient analysis in SCIDNT will be discussed in the Flight Test Results Sections.

#### FLIGHT TEST RESULTS

This section presents representative data from the input design experiments to demonstrate the feasibility of using an "optimal" control input to improve parameter identifiability. The criteria used to quantitatively establish improvement in parameter identifiability were comparisons of:

- a. Stability and control derivative estimates.
- b. Standard deviation of parameter estimate error (confidence bounds).
- c. Eigenvalue spread of the information matrix.
- d. Parameter step size (convergence characteristics).
- e. Cost function variation.
- f. Standard deviation of the computed time history with respect to the measured response ( $\sigma_x$ ).
- g. Estimates of transfer function parameters (stability and control specification requirements) computed from parameter estimates.
- h. Aircraft response prediction.

Normally the "true value" of the parameters (stability and control derivatives) is not known; however a priori knowledge of the values of the transfer function parameters (damping, frequency and time constants) does exist based on classical hand measurement techniques. Thus comparisons between the transfer function parameters based on classical hand measurement techniques and those computed from SCIDNT parameter estimates will indicate the relative accuracy of the estimated stability and control derivatives.

#### Longitudinal Parameter Identifiability

The longitudinal analysis was conducted using the short period approximation to the longitudinal dynamics of the airplane. This was accomplished by setting the derivatives  $X_a$ ,  $X_u$ ,  $X_q$ ,  $X_{\dot{\delta}_e}$ ,  $M_u$ , and  $Z_u$  in equations 9, 10, and 11 equal to zero. The process noise option was not used in this case and pitch rate corrections to angle of attack were not made. A time history match for the response to a doublet input is presented in figure 3. This comparison of time histories shows only a fair match between the flight test data and computed response from SCIDNT and in practice would not be acceptable for use in satisfying flight test data requirements. The estimated stability and control derivatives for this run are presented in Table II. The matched response for a sine wave input is presented in figure 4. The estimated stability and control derivatives for this run are presented in Table III. A comparison between figures 3 and 4 shows that the time history match for the sine wave input is considerably better than that achieved using the doublet input. Referring to Table II, it is seen that the term  $Z_{\dot{\delta}_e}$  did not converge using a doublet input (high standard deviation and large parameter step size) whereas in Table III  $Z_{\dot{\delta}_e}$  did converge for the response generated using a sine wave input. In fact, comparisons of Tables II and III show that for all but one parameter the standard deviation of the estimate error and the parameter step size decreased when going from a doublet to a sine wave input. Corresponding decreases in the cost function variation and the standard deviation of the computed time history with respect to the measured response ( $\sigma_x$ ) were also observed; however, the eigenvalue spread of the information matrix was larger for the sine wave input than it was for the doublet input. Thus for this case using a more complicated input did not decrease the eigenvalue spread; however, an improvement in parameter identifiability was observed using the sine wave input as indicated by the variation in the other criteria used for this analysis. This improvement in parameter identifiability and the accuracy of the estimated parameters is also indicated by the comparison of short period damping, frequency and normal acceleration sensitivity ( $n_z/\alpha$ ) presented in Table IV for classical analysis and identification results. The classical analysis results were computed using hand measurement techniques for damping (peak to peak method), frequency (measured period of oscillation) and ( $n_z/\alpha$ ) (ratio of the envelope of the  $n_z$  and  $\alpha$  responses to a sine wave input at the short period frequency). As shown, both the doublet and sine wave results represent reasonable estimates of these parameters; however, in all cases the results from the sine wave input are closer to the classical analysis values. Since a reasonable amount of confidence is placed on the classical results for this case, this comparison indicates that the use of a sine wave input as compared to a doublet input does improve the identifiability and thus the accuracy of the longitudinal stability and control derivative estimates. It should be emphasized that these results are only a small sample from the total longitudinal data being analyzed and that one cannot conclude from these limited results that a elevator sine wave as compared to a elevator doublet is a better input for parameter estimation.

Another criteria often used to demonstrate the accuracy of estimated stability and control derivatives is aircraft response prediction. This technique is illustrated in figure 5. In this case a doublet input (input 1) was used to excite the aircraft response at one flight condition and then SCIDNT was used to identify the stability and control derivatives. A second input (sine wave) was then used to excite the airplane at the same flight condition. The identified model from the doublet input was then used in conjunction with the sine wave input to determine if the identified model would predict the aircraft response for the different input. The results from these tests are presented in figure 6. As shown, the identified model was successful in predicting the aircraft response giving a good indication of the accuracy of the identified stability and control derivatives.

### Lateral-Directional Parameter Identifiability

The lateral-directional parameter identifiability study was conducted using equations 19 through 28. The process noise option of SCIDNT was not used during this analysis and yaw rate corrections to sideslip angle were not made ( $K_g=0$ ). Parameters were estimated in three distinct steps using six iterations of the computer program. Initially least squares start up values were used and the  $N$  and  $Y$  derivatives were estimated holding the  $L$  derivatives constant. Next the  $L$  derivatives were estimated holding the  $N$  and  $Y$  derivatives from Step (1) constant. The final step in the procedure was to fine tune the parameter estimates by estimating all of the derivatives ( $N, Y, L$ ) at once using as start up values the results from Steps (1) and (2). Typical results for rudder doublet, aileron-rudder doublets and aileron-rudder sine waves are presented in Tables V through IX and a time history match for an aileron-rudder doublet is presented in figure 7. The parameter estimates for these maneuvers (Table V) show that the aileron rudder doublet and sine wave inputs gave reasonable estimates of the stability and control derivatives whereas the rudder input resulted in estimates that for some parameters were of the wrong sign ( $N_g, L_r$ ). In addition, the estimates for the rudder input case are several orders of magnitude different than those observed from the aileron-rudder inputs. Comparison of the parameter step sizes (Table VI) and standard deviations (Table VII) shows that SCIDNT had better convergence properties and lower standard deviations for the aileron-rudder inputs as compared to the rudder only doublet. A comparison of the eigenvalue separation and the standard deviations of the time history fits resulting from these three inputs are presented in Table VIII. As shown, the aileron-rudder doublet resulted in the lowest eigenvalue separation and the best overall time history matches. All three inputs resulted in reasonable estimates of aircraft Dutch roll frequency and damping characteristics as compared to classical analysis results; however, the rudder doublet input did not give good estimates of roll and spiral mode time constants. These comparisons indicate that by using a combination aileron-rudder input parameter identifiability is improved over that obtained using rudder only inputs (similar results were obtained using aileron only inputs). This improvement in parameter identifiability was obtained not only for the rolling derivatives (rudder only inputs primarily excite the yaw and side force derivatives) but for the yaw and side force derivatives as well. This can be attributed in part to the ability to obtain better estimates of the coupling derivatives (due to better excitation of aircraft response) which in turn result in better estimates of the non-coupling derivatives. These examples clearly demonstrate from a practical viewpoint that the accuracy of parameter estimates and the ability to identify aircraft parameters is input dependent. The data presented here for the lateral-directional parameter identifiability study is limited in scope and does not represent a complete data base at this time for specifying the "optimal" control input. However, a case has been made for the need to consider the parameter identifiability/input design problem in planning flight tests. In fact, many factors have been observed during these tests which will lead to the establishment of criteria for "optimal" control inputs. Such factors as input frequency, input energy and amplitude of aircraft response have been observed to have a significant influence on parameter identifiability as well as the type of input used. These factors are currently being investigated as well as those discussed in items a through g of this section to establish the criteria for determining the "optimal" input.

Advanced concepts which give a more concise description of the total information about all parameters in the system are also under consideration. For example the information matrix ( $M$ ) or dispersion matrix ( $M^{-1}$ ) could be used to determine the identifiability of system parameter from a given set of flight data (reference 7). The dispersion matrix represents a lower bound on parameter error covariances and thus the trace of this matrix would give the sum of the parameter error covariances. Small values of the trace would indicate a good set of data whereas large values would indicate identifiability problems. The determinate of the dispersion matrix could also be used for this purpose, since its value would represent the product of the covariances in the principle directions in parameter space.

#### Rank Deficient Solution

In cases where parameter identifiability problems are observed the rank deficient solution of SCIDNT can be used to improve parameter estimates and algorithm convergence characteristics. The estimation results from the analysis of the rudder doublet input data presented in Tables V through IX show that a parameter identifiability problem exists for this set of data. Parameter estimates for this input were characterized by incorrect signs, large parameter step sizes, and large parameter error standard deviations. This parameter identifiability problem was solved in the past by a priori weighting and fixing parameters; however, by using the rank deficient solution it is no longer necessary to subjectively weight and fix various parameters but instead the rank deficient solution fixes combinations of parameters corresponding to nearly zero eigenvalues. Each of these small eigenvalues represent a singular direction in parameter space and a combination of parameters that cannot be uniquely identified. The implementation of the rank deficient solution can be illustrated by considering the  $n \times n$  information matrix ( $M$ ) in terms of its eigenvalues and eigenvectors (reference 6).

$$M = \sum_{i=1}^n \lambda_i V_i V_i^T \quad (29)$$

where  $\lambda$  and  $V$  represent the eigenvalues and eigenvectors, respectively. The inverse of

the information matrix is given by:

$$M^{-1} = \sum_{i=1}^n \frac{1}{\lambda_i} V_i V_i^T \quad (30)$$

The parameter step ( $\Delta\theta$ ) in the numerical optimization procedure is:

$$\Delta\theta = M^{-1} \left( \frac{\partial J}{\partial \theta} \right)^T \quad (31)$$

where  $\theta$  represents the vector of parameters to be identified. The rank deficient solution in concept neglects any eigenvalues below a predetermined threshold  $k$  in computing the inverse of the information matrix.

$$M^{-1} = \sum_{i=1}^{n-k} \frac{1}{\lambda_i} V_i V_i^T \quad (32)$$

where the relationship for the cutoff threshold is given by:

$$\lambda_i < k \lambda_{\text{MAX}} \quad (33)$$

Thus all eigenvalues less than  $k \lambda_{\text{MAX}}$  would be discarded. In the example given in equation (32)  $k$  of the  $n$  eigenvalues would be discarded in computing the inverse of the information matrix. The practical limitations of utilizing the rank deficient solution are that the parameter step sizes will be small (slow convergence) and good start up values are required.

Thus in trying to improve the identifiability of the rudder doublet data the eigenvalue threshold was set to  $k = 10^{-4}$ . The results from this rank deficient solution are compared with the previous rudder doublet data in Table X. As shown, improvements in parameter identifiability were obtained as indicated by more realistic parameter estimates ( $N_{\delta}$  and  $L_r$  now have the correct sign) and reduced parameter estimate error standard deviations and step sizes. Time history matches were considered good for this case and were better than those achieved for sideslip and lateral acceleration without the rank deficient solution. This example illustrates that the rank deficient solution can be successfully used to correct parameter identifiability problems and represents an advancement in the state-of-the-art when compared to previous methods for improving identification algorithm convergence characteristics.

#### CONCLUDING REMARKS

The parameter identifiability investigations conducted have established the need for considering input design in planning tests for extracting aerodynamic coefficients from flight test data. Using an elevator sine wave input to generate aircraft responses in the longitudinal axis improved parameter identifiability as compared to using a more simple elevator doublet input. Lateral-directional tests using aileron pulses, rudder doublets, aileron-rudder doublets and aileron-rudder sine wave inputs showed that the combination aileron-rudder inputs resulted in improved parameter identifiability. Parameter identifiability is the interaction of many criteria and cannot for example be stated simply in terms of eigenvalue separation. The information content in a set of data containing the system parameters is affected by input type, input frequency, input energy and amplitude of aircraft response. These factors have been observed to influence parameter identifiability criteria such as eigenvalue spread, parameter error standard deviation, parameter convergence, time history matches, cost function variation, and accuracy of estimates. In cases where parameter identifiability problems exist a rank deficient solution can be used to improve the quality of parameter estimates.

The results from the current program in parameter identifiability will be used in a research effort in 1975-76 to develop a real time data quality analysis algorithm for on-line verification of parameter identifiability. Additional research programs that will be conducted during this time frame include development of input design and model structure determination algorithms, implementation of SCIDNT nonlinear analysis capability, and the implementation of a helicopter analysis program.

#### REFERENCES

1. Military Specification MIL-F-8785B(ASG), Flying Qualities of Piloted Airplanes, 7 August 1969.
2. Burton, R. A. and McCue, J.J., NATC Technical Report FT-28R-73, Development of Flight Test Technology - Transfer Function Approach to Airframe Parameter Identification Using an Analog Computer, 28 June 1973.
3. Burton, R. A. and May, W.D., NATC Technical Report FT-77R-73, First Interim Report - Development of Digital Airframe Parameter Identification Technology, 21 January 1974.
4. Detail Specification for the Model S-3A Aircraft Weapon System SD-562-1 of 27 June 1969.
5. Detail Specification for Advanced Carrier Based Fighter Aircraft Weapon System, Model F-14A Airplane, SD-561-1 of 10 January 1969.

6. Stepner, D.E. and Mehra, R.K., NASA Contractor Report CR-2200, Maximum Likelihood Identification and Optimal Input Design for Identifying Aircraft Stability and Control Derivatives, March 1973.
7. Hall, W.E., Gupta, N.K. and Smith, R.G., Systems Control, Inc., Engineering Report - Identification of Aircraft Stability and Control Coefficients for the High Angle-of-Attack Regime - Technical Report No. 2, March, 1974.

TABLE I  
SCIDNT Capabilities and Options

NUMBER	DESCRIPTION
1.	Any parameter may be fixed or constrained to be within certain bounds.
2.	A priori weighting may be placed on parameter estimates.
3.	Standard deviations of parameter estimation errors are computed.
4.	Biases and random noise errors in instruments are computed.
5.	Process noise may be included and its magnitude and break frequency identified.
6.	Process noise effects may be included but not identified.
7.	Measurements from failed instruments may be deleted.
8.	States may be deleted which do not significantly enter the aircraft modes of the particular data record considered.
9.	Rank deficient solution may be used to compute the inverse of the information matrix.

TABLE II  
SCIDNT Estimates of Longitudinal Short Period Stability and Control Derivatives Using a Doublet Input

Derivatives	$Z_a$	$M_a$	$M_q$	$Z_{\delta_e}$	$M_{\delta_e}$
Estimate	-0.553	-2.076	-0.670	-0.035	-4.621
Standard Deviation	0.0038	0.0082	0.0071	0.0055	0.023
Parameter Step Size	0.0045	0.012	0.004	0.018	-0.016
Eigenvalue Spread	$0.609 \times 10^2$				
Cost Function Value	$-2.84 \times 10^3$				
Time History Matches	$\sigma_a = .00276$ $\sigma_\theta = .0102$ $\sigma_q = .0086$ $\sigma_{a_z} = 2.95$				

TABLE III  
SCIDNT Estimates of Longitudinal Short Period Stability Using a Sine Wave Input

Derivatives	$Z_a$	$M_a$	$M_q$	$Z_{\delta_e}$	$M_{\delta_e}$
Estimate	-0.501	-2.13	-0.711	-0.167	-5.075
Standard Deviation	0.0028	0.0068	0.0064	0.006	0.021
Parameter Step Size	0.002	0.006	0.003	0.008	-0.023
Eigenvalue	$0.225 \times 10^3$				
Cost Function Variation	$-2.80 \times 10^3$				
Time History Matches	$\sigma_a = .0060$ $\sigma_\theta = .0100$ $\sigma_q = .0046$ $\sigma_{a_z} = 2.56$				

TABLE IV  
Comparison of Longitudinal  
Short Period Characteristics

Description	Damping Ratio ( $\zeta_{sp}$ )	Frequency ( $\omega_{nsp}$ ) (rad/sec)	$\frac{n_z}{a}$ (g/rad)
Classical	0.31	1.58	10.3
SCIDNT-Douplet	0.42	1.599	11.62
SCIDNT-SINE	0.384	1.592	10.06

TABLE V  
Lateral-Directional Parameter Estimates

Parameter	Input		
	Rudder (1) Douplet	Aileron (1) Rudder Douplet	Aileron (1) Rudder Sine
$L_p$	-7.799	-2.402	-2.612
$L_r$	-3.126	1.474	2.292
$L_\beta$	-25.29	-8.352	-7.789
$N_p$	-3.381	-0.0270	-0.0225
$N_r$	-3.450	-0.632	-0.459
$N_\beta$	-7.929	2.12	1.969
$Y_\beta$	-0.0876	-0.0813	-0.0832
$L_{\delta_a}$	9.57 <sup>c</sup>	11.34	10.189
$N_{\delta_a}$	0.24 <sup>c</sup>	0.24 <sup>c</sup>	0.24 <sup>c</sup>
$Y_{\delta_a}$	0 <sup>c</sup>	0 <sup>c</sup>	0 <sup>c</sup>
$L_{\delta_R}$	-2.954	-2.476	-4.738
$N_{\delta_R}$	.785	1.816	1.614
$Y_{\delta_R}$	-0.0267 <sup>c</sup>	-0.0267 <sup>c</sup>	-0.0267 <sup>c</sup>

Note: (1) The superscript c indicates that the parameter was held constant during the estimation procedure.



TABLE VI  
Lateral-Directional Parameter Step Size

Parameter	Input		
	Rudder Doublet	Aileron Rudder Doublet	Aileron Rudder Sine
$L_p$	-0.128	-0.0145	0.135
$L_r$	-1.048	-0.0384	0.0539
$L_\beta$	-2.204	-0.0365	0.637
$N_p$	4.586	-0.0022	-0.00038
$N_r$	3.662	0.0142	-0.00057
$N_\beta$	13.32	-0.0026	0.00821
$Y_\beta$	-0.0016	-0.000063	0.00131
$L_{\delta_a}$	-	0.0662	-0.561
$N_{\delta_a}$	-	-	-
$Y_{\delta_a}$	-	-	-
$L_{\delta_R}$	-0.541	0.0363	-0.178
$N_{\delta_R}$	0.731	-0.0129	0.0409
$Y_{\delta_R}$	-	-	-

TABLE VII  
Lateral-Direction Parameter Error  
Standard Deviation

Parameter	Input		
	Rudder Doublet	Aileron Rudder Doublet	Aileron Rudder Sine
$L_p$	7.978	0.0657	0.116
$L_r$	7.145	0.1056	0.111
$L_\beta$	24.14	0.193	0.319
$N_p$	2.596	0.0064	0.0042
$N_r$	2.326	0.0097	0.00467
$N_\beta$	7.851	0.0194	0.0134
$Y_\beta$	0.00103	0.0011	0.00062
$L_{\delta_a}$	-	0.269	0.410
$N_{\delta_a}$	-	-	-
$Y_{\delta_a}$	-	-	-
$L_{\delta_R}$	1.749	0.0729	0.154
$N_{\delta_R}$	0.568	0.0179	0.0163
$Y_{\delta_R}$	-	-	-

TABLE VIII  
Additional Lateral-Directional Parameter  
Identifiability Characteristics

Parameter	Input		
	Rudder <sup>(1)</sup> Doublet	Aileron <sup>(2)</sup> Rudder Doublet	Aileron <sup>(2)</sup> Rudder Sine
Eigenvalue Separation	$-0.121 \times 10^7$	$0.107 \times 10^6$	$0.140 \times 10^7$
Cost Function Value	$-0.273 \times 10^4$	$-0.305 \times 10^4$	$-0.513 \times 10^4$
$\sigma_p$	0.0348	0.0301	0.0486
$\sigma_r$	0.0132	0.0177	0.0198
$\sigma_\beta$	0.019	0.0156	0.0163
$\sigma_\phi$	0.0626	0.0204	0.0892
$\sigma_{a_y}$	0.732	0.892	0.616

Note: (1) Smallest eigenvalue is negative.  
(2) All eigenvalues are positive.

TABLE IX  
Lateral-Directional Modal Characteristics

Parameter	Conventional Analysis	Input		
		Rudder Doublet	Aileron Rudder Doublet	Aileron Rudder Sine
$1/\tau_s$	$\approx 0$	-0.124	-0.0188	0.00831
$1/\tau_R$	2.4 to 2.6	10.69	2.48	2.673
$\zeta_d$	0.1	0.171	0.201	0.166
$\omega_{nd}$	1.53	1.54	1.528	1.480

TABLE X  
Parameter Identification Results Using A Rank Deficient Solution  
For Rudder Doublet Data(1)

Derivative	$L_p$	$L_r$	$L_\beta$	$N_p$	$N_r$	$N_\beta$	$Y_\beta$	$L_{\delta_R}$	$N_{\delta_R}$
Estimate	-1.750 (-7.799)	2.412 (-3.126)	-5.869 (-25.29)	-0.026 (-3.381)	-0.540 (-3.450)	2.253 (-7.929)	-0.079 (-0.0876)	-6.451 (-2.954)	1.936 (0.785)
Standard Deviation	0.248 (7.978)	0.186 (7.145)	0.555 (24.14)	0.017 (2.596)	0.019 (2.326)	0.037 (7.851)	0.0007 (0.00103)	0.547 (1.749)	0.034 (0.568)
Parameter Step Size	0.009 (-0.128)	-0.004 (-1.048)	-0.001 (-2.204)	-0.009 (4.586)	-0.004 (3.662)	-0.022 (13.32)	+0.0002 (-0.0016)	-0.003 (0.541)	-0.013 (0.731)
Cost Function Value	-0.228 $\times 10^4$ (-0.273 $\times 10^4$ )								
Time History Matches	$\sigma_p = 0.099$ (0.0348) $\sigma_\phi = 0.139$ (0.0626) $\sigma_{ay} = 0.630$ (0.732) $\sigma_r = 0.0262$ (0.0132) $\sigma_\beta = 0.0089$ (0.019)								

Notes: (1) The values in parenthesis are from Tables V - IX for the rudder doublet results without the rank deficient solution.

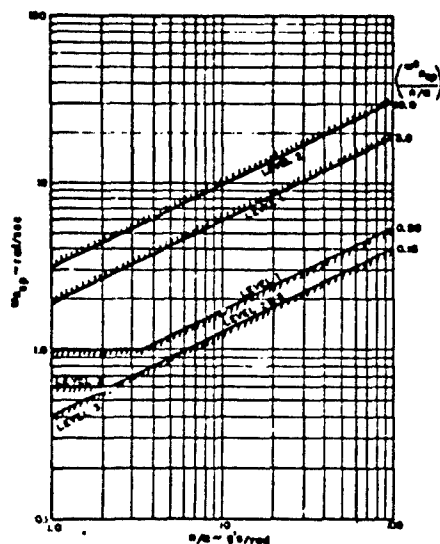


FIGURE 1  
MIL-F-8785B SHORT PERIOD FREQUENCY AND ACCELERATION SENSITIVITY REQUIREMENTS

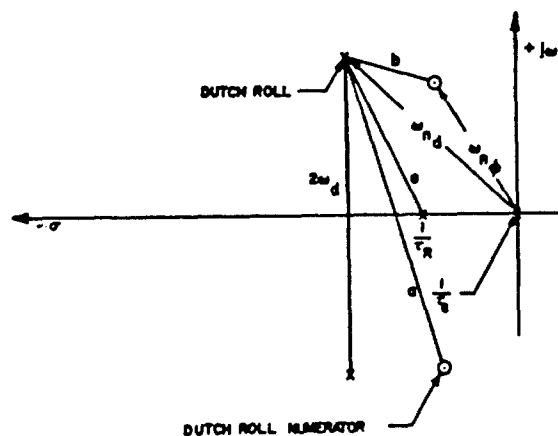


FIGURE 2  
S-PLANE PLOT OF THE ROLL RATE TO AILERON TRANSFER FUNCTION

SYMBOL	DEFINITION
- - -	COMPUTED RESPONSE
+++	FLIGHT DATA

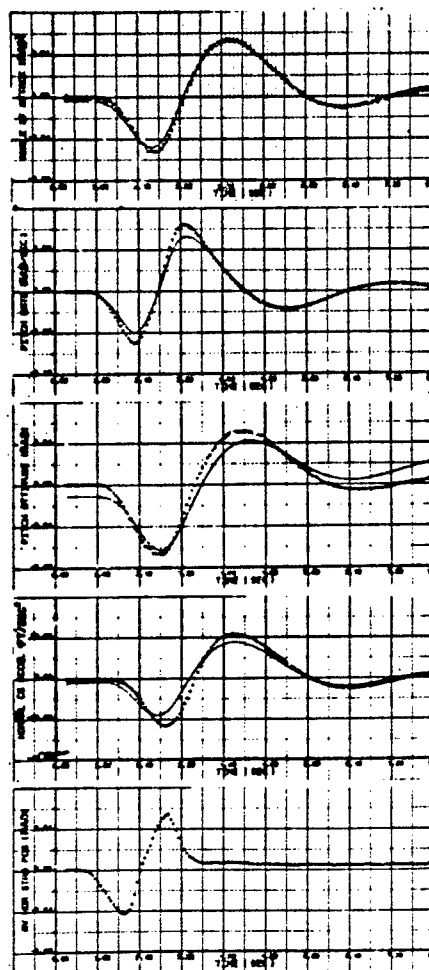


FIGURE 3  
TIME HISTORY MATCH FOR AIRCRAFT RESPONSE  
TO AN ELEVATOR DOUBLET INPUT

SYMBOL	DEFINITION
- - -	COMPUTED RESPONSE
+++	FLIGHT DATA

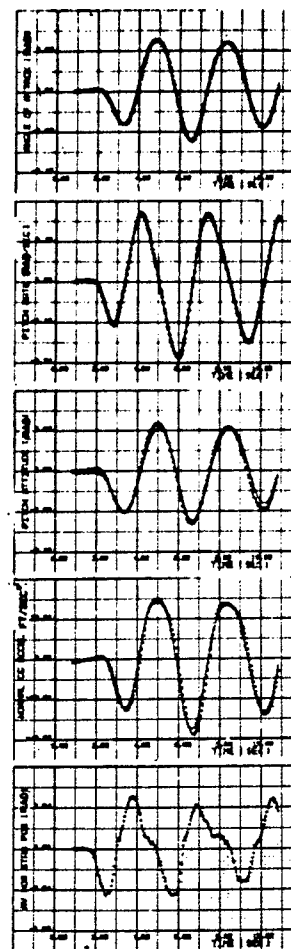


FIGURE 4  
TIME HISTORY MATCH FOR AIRCRAFT RESPONSE  
TO AN ELEVATOR SINE WAVE INPUT

15-16

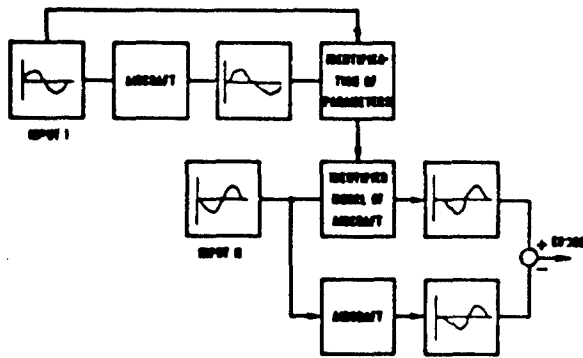


FIGURE 5  
PREDICTION TECHNIQUE FOR DETERMINING  
ACCURACY OF PARAMETER ESTIMATES

SYMBOL  
- - - - -

+ + + +

DEFINITION  
PREDICTED RESPONSE USING  
MODEL DERIVED FROM INPUT 1  
(DOUBLET)

FLIGHT DATA FROM INPUT 2  
(SINE WAVE)

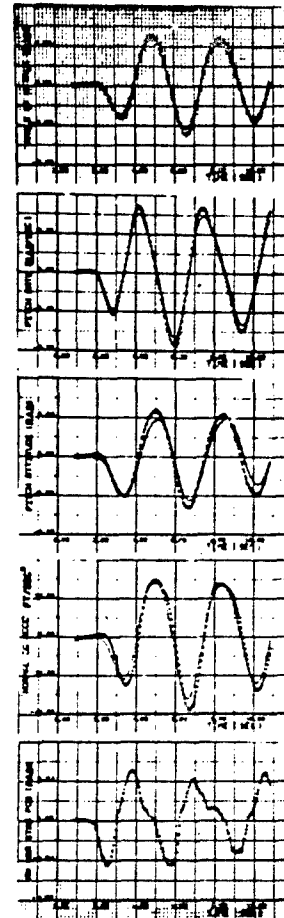


FIGURE 6  
COMPARISON OF MEASURED RESPONSE BASED ON A  
SINE WAVE INPUT AND PREDICTED RESPONSE BASED  
ON ESTIMATED PARAMETERS USING A DOUBLET INPUT

## SYMBOL

---

+++

## DEFINITION

COMPUTED RESPONSE

FLIGHT DATA

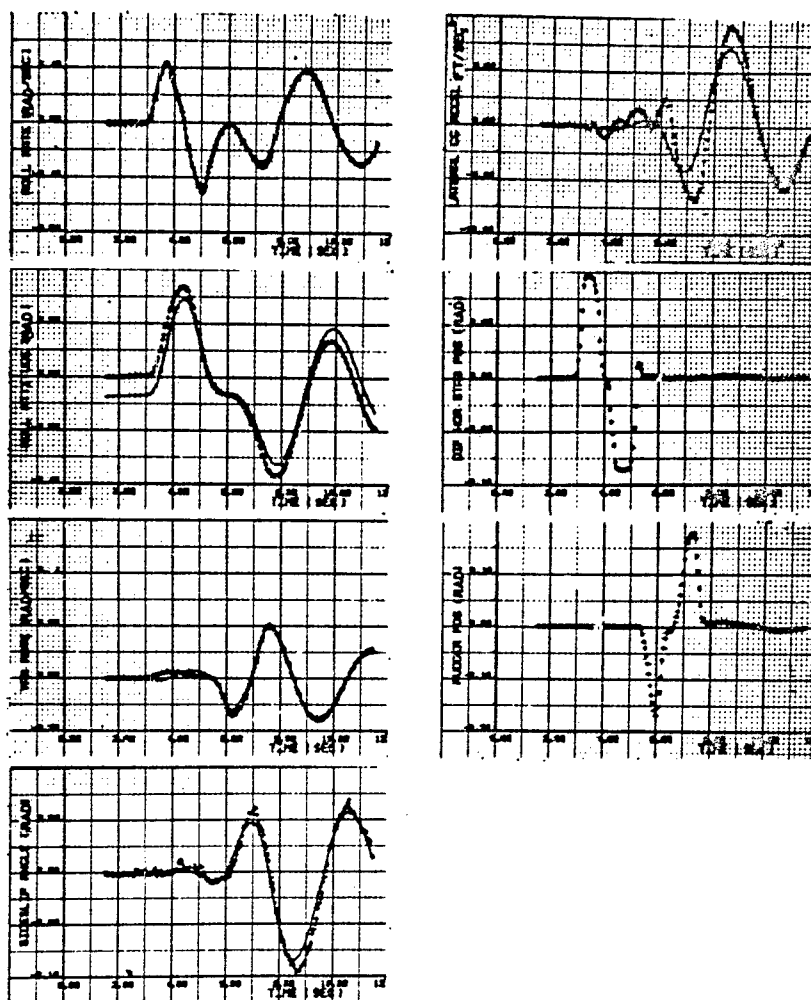


FIGURE 7

TIME HISTORY MATCH FOR AIRCRAFT  
RESPONSE TO AN AILERON-RUDDER  
DOUBLET INPUT

## PRACTICAL ASPECTS OF USING A MAXIMUM LIKELIHOOD ESTIMATOR

Kenneth W. Hiff  
Aerospace Engineer

and

Richard E. Maine  
Aerospace Engineer  
NASA Flight Research Center  
P. O. Box 273  
Edwards, California 93523  
USA

## SUMMARY

It has been known for several years that stability and control derivatives can be obtained from flight data by using nonlinear minimization techniques. The maximum likelihood estimator method (sometimes referred to as the Newton-Raphson method) has been one of the more popular methods for this type of analysis.

Some investigators maintain that although the maximum likelihood estimator method should be adequate in theory, it is not practical for routine use on a large quantity of flight data. This paper discusses the application of a maximum likelihood estimator to flight data and proposes procedures to facilitate routine analysis of a large amount of flight data. Flight data are used to demonstrate the proposed procedures.

Modeling considerations for the system to be identified, including linear aerodynamics, instrumentation, and data time shifts, and aerodynamic biases for the specific types of maneuvers to be analyzed are discussed. Data editing to eliminate common data acquisition problems, and a method of identifying other problems are considered. The need for careful selection of the maneuver or portions of the maneuver to be analyzed is pointed out. Uncertainty levels (analogous to Cramér-Rao bounds) are discussed as a way of recognizing significant new information.

## SYMBOLS

$A$	stability matrix
$a_n$	normal acceleration, g
$a_x$	longitudinal acceleration, g
$a_y$	lateral acceleration, g
$B$	control matrix
$C_{D_{trim}}$	coefficient of drag at trim condition
$C_{L_{trim}}$	coefficient of lift at trim condition
$C_{n_p}$	coefficient of partial derivative of yawing moment with respect to roll rate
$C_{y_\beta}$	coefficient of partial derivative of side force with respect to sideslip angle
$C_{z_\alpha}$	coefficient of partial derivative of "normal" force with respect to angle of attack
$c$	vector of unknown coefficients
$c_0$	vector of <i>a priori</i> estimates of unknown coefficients
$D_1$	weighting matrix for observation vector
$D_2$	weighting matrix for <i>a priori</i> estimate vector
$G$	partition of matrix relating state vector to observation vector

$g$	acceleration due to gravity, m/sec <sup>2</sup> (ft/sec <sup>2</sup> )
$H$	partition of matrix relating control vector to observation vector
$I$	identity matrix
$I_X$	moment of inertia about roll axis, kg-m <sup>2</sup> (slug-ft <sup>2</sup> )
$I_{XZ}$	cross moment of inertia between roll and yaw axis, kg-m <sup>2</sup> (slug-ft <sup>2</sup> )
$I_Y$	moment of inertia about pitch axis, kg-m <sup>2</sup> (slug-ft <sup>2</sup> )
$I_Z$	moment of inertia about yaw axis, kg-m <sup>2</sup> (slug-ft <sup>2</sup> )
$J$	cost functional
$K$	scale weighting factor for <i>a priori</i> weighting matrix
$n$	Gaussian white noise vector
$p$	roll rate, deg/sec or rad/sec
$q$	pitch rate, deg/sec or rad/sec
$R$	acceleration transformation matrix
$r$	yaw rate, deg/sec or rad/sec
$T$	total observation time, sec
$t$	intermediate or incremental time, sec
$u$	control vector
$V$	velocity, m/sec (ft/sec)
$v$	variable bias vector for nonstate measurements
$x$	state vector
$y$	observation vector
$z$	measurement of observation vector
$\alpha$	angle of attack, deg or rad
$\beta$	angle of sideslip, deg or rad
$\delta_a$	aileron deflection, deg or rad
$\delta_e$	elevator deflection, deg or rad
$\delta_r$	rudder deflection, deg or rad
$\theta$	pitch angle, deg or rad
$\phi$	bank or roll angle, deg or rad
$O$	null matrix
Subscript:	
$b$	with respect to body axis
Superscripts:	
$*$	matrix transpose
$\cdot$	derivative with respect to time

## INTRODUCTION

Extraction of stability and control derivatives from flight data has been of interest for many years. In 1966 the NASA Flight Research Center started the development of a nonlinear minimization digital program for the extraction of these derivatives. The maximum likelihood estimator method (sometimes referred to as the Newton-Raphson method, as in refs. 1 and 2) which resulted from that study has been applied to more than 1500



maneuvers from 19 aircraft over the past 8 years. The method was used routinely on most of these maneuvers. This paper discusses the Flight Research Center experience, particularly in derivative extraction in a batch processing mode.

Some investigators maintain that the maximum likelihood estimator method is not practical for routine use on a large quantity of flight data. With certain qualifications, we have found that most of the difficulties have arisen from modeling or data problems. We point out how these difficulties can be isolated and, in some instances, accounted for. Although this paper deals specifically with the digital computer program developed at the Flight Research Center, much of the discussion applies to any maximum likelihood estimator program with essentially the same options.

#### MAXIMUM LIKELIHOOD ESTIMATOR METHOD

The maximum likelihood estimator method is one means of estimating aircraft stability and control derivatives from flight maneuvers.

The equations that are used to describe the aircraft system in the maximum likelihood estimator method are as follows:

$$\left. \begin{aligned} \dot{R}x(t) &= Ax(t) + Bu(t) \\ y(t) &= \begin{bmatrix} -I \\ G \end{bmatrix} x(t) + \begin{bmatrix} 0 \\ H \end{bmatrix} u(t) + \begin{bmatrix} 0 \\ v \end{bmatrix} \\ z(t) &= y(t) + n(t) \end{aligned} \right\} \quad (1)$$

where

$x(t)$	state vector
$u(t)$	control vector
$y(t)$	calculated response vector
$z(t)$	measured response vector
$n(t)$	measured noise vector
$v$	instrument bias vector

and the unknown coefficients of the system appear in the  $A$ ,  $B$ ,  $G$ , and  $H$  matrices and the  $v$  and  $x(0)$  vectors. All the unknown coefficients form a vector  $c$ , thus the unknown stability and control derivatives are contained in the vector  $c$ .

The maximum likelihood estimator method is defined as the minimum of the following cost functional with respect to the vector of unknown coefficients,  $c$ :

$$J = \frac{1}{T} \int_0^T [z(t) - y(t)]^* D_1 [z(t) - y(t)] dt \quad (2)$$

where  $T$  is the total observation time of the maneuver, and  $D_1$  is the inverse of the measurement covariance matrix. The controls are assumed to be known and noiseless.

Independent estimates of the unknown coefficients are often available from wind-tunnel data, previously obtained flight data, or calculated estimates. It is desirable to use this *a priori* information in conjunction with the maximum likelihood estimator so that all the information available is used to obtain the estimates and no change is made in the derivatives from the *a priori* values unless there is sufficient information in the flight data to justify a change. The cost functional is expanded to include a penalty for a departure from the *a priori* values. This is referred to as the modified maximum likelihood estimator method and is implemented by minimizing the following cost functional with respect to the vector of unknown coefficients,  $c$ :

$$J = \frac{1}{T} \int_0^T \left\{ [z(t) - y(t)]^* D_1 [z(t) - y(t)] \right\} dt + (c - c_0)^* K D_2 (c - c_0) \quad (3)$$

where  $c_0$  is the vector of *a priori* estimates of the vector  $c$  and  $K D_2$  is the weighting matrix for the *a priori* information. This cost functional can be derived in the same way as that for the maximum likelihood estimator by using the joint probability  $p(z, c)$  instead of the conditional probability  $p(z/c)$ . A more detailed discussion of the modified maximum likelihood estimator method is presented in references 1 and 2.

#### DESCRIPTION OF NASA FLIGHT RESEARCH CENTER COMPUTER PROGRAM

The NASA Flight Research Center uses a series of three FORTRAN programs to automatically extract stability and control derivatives from flight data using the maximum likelihood estimator method. The first program (SETUP) preconditions the data to be used; the second program (MMLE) contains the maximum likelihood estimator algorithm, as described in references 1 and 2; and the third program (SUMARY) provides a means of displaying and summarizing the results. The function of these programs and the various options we have found to be necessary are described briefly in this section.

The first program, SETUP, automatically determines the flight condition and the necessary startup values from the flight data for use in the second program. The SETUP program punches a startup card deck and creates a file containing the flight time history. Any of these automatic features can be overridden. Only the following

information is absolutely required for a maneuver to be analyzed:

- (1) The start and stop time for each maneuver.
- (2) A digitized file with the pertinent quantities required for each maneuver, including the flight condition.
- (3) The geometric characteristics of the vehicle, including instrument locations.
- (4) A complete set of nondimensional *a priori* derivatives.
- (5) An indication of which controls move independently during each maneuver.

The second program, MMLE, provides estimates of the unknown coefficients of Eqs. (1). These equations are written with respect to arbitrary accelerometer locations. To use the MMLE program, the  $D_1$  and  $D_2$  matrices of Eq. (3) need to be known. Usually the matrices are determined from maneuver data that agree with data based on the mathematical model, and the matrices should remain fixed until some major change in instrumentation occurs. The program has a mode that determines either the  $D_1$  or  $D_2$  matrix, or both. The  $D_1$  matrix (assumed to be diagonal) is determined such that the weighted error on each measurement is approximately unity. This is achieved by letting the algorithm converge to a solution, adjusting the  $D_1$  matrix elements appropriately, and then, with this new  $D_1$  matrix, letting the algorithm converge. This procedure is automatically repeated until the weighted error of each measurement is within some tolerance of unity. Once the  $D_1$  matrix has been determined, the elements of the  $D_2$  matrix can be specified. The  $D_2$  matrix (assumed to be diagonal) is obtained by allowing the algorithm to converge for a fixed  $D_2$  matrix with various values of  $K$  (Eq. (3)). Then plots are provided for each converged estimate as a function of  $K$ . The elements of the  $D_2$  matrix can be adjusted so that all the coefficients start to deviate from the *a priori* estimates at approximately the same value of  $K$ . The  $D_1$  and  $D_2$  matrix determination is discussed in more detail in reference 2.

Three aids are available in the MMLE program with which the input data can be modified either to correct the data or to specify changes to the model being used. These are as follows:

- (1) Any of the input signals can be biased, corrected for instrument position, or multiplied by a constant.
- (2) Extra inputs are allowed for inputting information needed to correct the model.
- (3) Multiple time histories can be analyzed as one case for maneuvers made at approximately the same flight condition.

Three means of identifying data deficiencies or modeling errors are also available. These are discussed in the DATA EDITING section (p. 8).

The third program, SUMMARY, provides plots of the estimated derivatives and uncertainty levels (Cramér-Rao bounds of ref. 2) from the punched card output of the MMLE program. These derivatives are plotted as a function of angle of attack. Various symbols can be used to represent Mach number, configuration, or any other parameter of interest. *A priori* estimates (or any other estimates) can be included on this plot.

#### NASA FLIGHT RESEARCH CENTER EXPERIENCE

The NASA Flight Research Center has been using the maximum likelihood estimator method to extract stability and control derivatives from flight data for 8 years. More than 1500 maneuvers from 19 aircraft have been analyzed. The flight conditions have included Mach numbers up to 5 and altitudes to 30,700 meters (100,000 feet), angles of attack from  $-20^\circ$  to  $40^\circ$ , and elevated normal acceleration maneuvers up to  $4g$ . Virtually all derivative extraction at the NASA Flight Research Center is done with the modified maximum likelihood estimator program discussed in this paper.

The Flight Research Center's experience is summarized in the following table:

Aircraft	Maneuvers analyzed	Maneuvers successfully analyzed	Utilization, percent
X-15	Unknown	<sup>a</sup> 1	---
XB-70	Unknown	<sup>a</sup> 30	---
M2-F2	Unknown	<sup>a</sup> 5	---
HL-10	Unknown	<sup>a</sup> 75	---
M2-F3	155	110	71
X-24A	Unknown	<sup>a</sup> 15	---
F-111A	Unknown	<sup>a</sup> 10	---
CV-990	90	90	100
F-8 (supercritical wing)	320	260	81
YF-12	30	30	100
F-4C	11	10	91
JetStar	265	260	98
F-111A TACT (baseline)	181	150	83
X-24B	103	92	89
F-15 (subscale model)	139	112	81
TACT	192	164	85
PA-30	86	85	99
YF-2B	15	11	73
F-16	33	32	97

<sup>a</sup>Rounded to the nearest 5.

As shown, for the more conventional aircraft, nearly 100 percent of the maneuvers were analyzed successfully. For the experimental aircraft, with which it is more difficult to maintain an exact flight condition, the successful analyses are as low as 70 percent. Overall, 87 percent of the maneuvers were successfully analyzed. Most of the M2-F3 lifting body maneuvers that were not successfully analyzed were those on which unsteady transonic flow occurred. The low utilization percentage for the F-111A airplane is attributed to the lateral-directional motion which occurred during more than half of the longitudinal maneuvers performed at high normal acceleration. The lateral-directional variables were not recorded; therefore, the cross coupling effect on the longitudinal mode could not be corrected for. The F-15 remotely piloted subscale model experienced buffet at angles of attack between  $20^\circ$  and  $35^\circ$ , which accounts for most of the unsuccessfully analyzed maneuvers. For a maneuver of average length, 20 seconds of computer time are required per submittal for a longitudinal maneuver and 40 seconds for a lateral-directional maneuver. In this context, a submittal refers to submitting a maneuver for processing or to resubmitting a maneuver once any desired changes have been made to the data to improve the derivative extraction process.

In general, the maximum likelihood estimator method has been extremely useful in derivative extraction. Most of the resulting fits have been "nearly" perfect, particularly when the percentage of utilization was high. Recently, 86 maneuvers performed during a PA-30 flight, with the airplane in three different configurations, were analyzed in the batch processing mode. The maneuvers were considerably longer than an average maneuver. After the flight, the data were stripped out on a Sanborn recorder and the maneuver times were read off. The raw data was in PCM form in engineering units. The entire derivative extraction process, including the creation of the original data files and the final summary plots of the derivatives for the three PA-30 configurations throughout the angle-of-attack range, required only 12 engineering hours and 1 3/4 hours of CDC 6500 computer time. Eighty-five of the 86 maneuvers were successfully analyzed; therefore, each maneuver required less than 9 minutes of engineering time and approximately 1 1/4 minutes of computer time. These results are typical for maneuvers analyzed under ideal conditions.

For "good" data, such as those for the PA-30 airplane, the average maneuver required fewer than 1.2 submittals per maneuver. For data obtained when the flight condition was difficult to maintain, such as the F-111A elevated normal acceleration maneuvers, 2.3 submittals per maneuver were required. For analysis of extremely marginal maneuvers, when the derivative estimates are important because only one maneuver is available or the estimates are needed before further flight envelope expansion, five or six submittals may be appropriate.

Although the use of the maximum likelihood estimator method has been successful at the NASA Flight Research Center, difficulties have been encountered in 10 percent to 15 percent of the maneuvers analyzed which necessitated more in-depth analysis before good estimates of the stability and control derivatives could be obtained. The next three sections discuss means of improving the quality of the estimates, major error sources, and data editing techniques that we have found to be valuable in using the maximum likelihood estimator method in the batch processing mode.

#### IMPROVING QUALITY OF ESTIMATES

Sometimes no estimates, or only poor estimates, of the unknown coefficients can be obtained. This can result from applying the maximum likelihood estimator carelessly even when the standard model is valid. If certain situations are avoided or identified, the estimation process can proceed routinely.

##### Dependent Variables

One type of poor estimate results from not having a completely independent set of unknown coefficients. This occurs most commonly in determining aerodynamic and instrument biases. If the two sets of biases are not linearly independent, the resulting estimates of these biases are obviously meaningless. Usually this problem has little effect on the estimates of the stability and control derivatives, but it can slow the convergence of the algorithm. When dealing with both aerodynamic and instrument biases, the aerodynamic biases should be permitted to vary for each state being fit and the instrument biases to vary only for the nonstate measurements, such as an accelerometer measurement. This ensures a linearly independent set of biases.

Still other types of linear dependence can occur when a vehicle is operating with the stability augmentation system on and no independent control inputs are made by one or more of the controls being used in the augmentation system. An independent input is always preferable, but if this requirement is not met, it is still possible to obtain useful results. The stability augmentation results in one of the control variables being nearly indistinguishable from the state variable being fed back. This can be overcome by not allowing the derivatives of the control in question to vary. In reality, of course, the control is only "nearly" dependent on the state, because several electrical and mechanical devices are engaged before the state measurement affects the control. Usually this near dependence is enough to result in poor estimates of several of the derivatives.

Another kind of near dependence may occur when two controls, such as an interconnected aileron and spoiler, move together throughout most of the command range. Usually this is best dealt with by using the average deflection of the two controls and estimating one set of control derivatives for the two controls. Sometimes the effect of one of the controls is much larger than that of the other. In this instance, the more effective control should be used for the estimated derivatives, and the derivatives of the other control should be fixed.

When linear independence or near linear dependence has occurred, one method that has been used with some success is *a priori* weighting, with the weighting somewhat higher on the nearly dependent variables than on the independent variables. This approach can sometimes be successful in apportioning the values of the dependent derivatives, particularly when stability augmentation is used. In this instance *a priori* weighting should be done carefully, because meaningless estimates may result.

##### Structural Noise

All aircraft have observable structural modes which usually cause no problem because their frequencies are high compared to the aerodynamic frequencies. Generally, if the structural frequencies are more than a factor of 5 or 10 higher than the highest aerodynamic frequency, they can be neglected unless they interfere with the control position measurements. The estimates of the derivatives usually are unaffected by high-frequency

structural noise. However, if the structural frequency is near the aerodynamic frequency, two approaches can be taken. The structural modes can be treated as known and their effect subtracted from the data before the derivatives are extracted. The second and more difficult approach is to model the structural modes as well as the aerodynamic modes and then estimate the unknown coefficients for all the modes. This would require significant modifications to the maximum likelihood estimator program being discussed.

As noted, significant structural vibration that affects control measurements can cause problems in the application of the maximum likelihood estimator. The power spectra of the control measurement can be determined, and the frequency of the structural vibration can then be identified. A notch digital filter can be used to filter out that structural frequency from the raw data, if it is much higher than the aerodynamic frequencies. It is usually desirable to filter all the measurements with the same filter. It is important to exclude structural vibration from the control measurement, because the maximum likelihood estimator method is based on the assumption of a noiseless control input.

#### Drift

Drift in the states is another possible problem. This drift is caused by small vehicle nonlinearities, which may result from unsteady aerodynamics or a variation of the flight condition. Usually the drift causes no particular problem, since the maneuver need only be shortened to improve the analysis. However, when more than one sharp control input occurs, the drift has a significant adverse effect. This can be seen in figure 1, which compares the measured data for aileron and rudder control inputs with the data computed from the estimated derivatives. As shown, a significant amount of drift occurred before any rudder input was made. The algorithm attempts to match the time history during the rudder input, but is unable to compensate for the drift, resulting in poor rudder derivatives. The problem can be overcome by reinitializing the algorithm before the rudder input occurs, which is referred to as analyzing multiple maneuvers. This results in no significant error in the states at the time of the input. Figure 2 shows the fit obtained from the multiple maneuver analysis. As can be seen, the fit is now excellent, resulting in good rudder derivatives. This procedure can also decrease the time during which negligible motion occurs between pulses. The use of the multiple maneuver approach can also enhance the data analysis by providing only one set of estimates for several maneuvers made at the same flight condition.

#### Uncertainty Levels

Errors in the estimated coefficients can be found by using uncertainty levels. Uncertainty levels are proportional to the approximation of the Cramér-Rao bounds described in reference 2 and are analogous to standard deviations of the estimates. The larger the uncertainty level, the greater the uncertainty. Therefore, by comparing the uncertainty levels for the same coefficient obtained from different maneuvers, one estimate may be found to be more valid than another. By using these levels, additional information about the estimate is obtained. For example, if a coefficient agrees with the *a priori* estimate and has a small uncertainty level, independent information from the maneuver agrees with the *a priori* estimate. If the coefficient has a large uncertainty level, little new information was obtained from the maneuver and the *a priori* estimate is still the best estimate. Sometimes the *a priori* weighting is not sufficient to force the coefficient to the *a priori* value, and there is a good deal of scatter in the estimates. In this instance, the uncertainty levels can show the best estimates, that is, the estimates having the smallest uncertainty levels, and permit an accurate fairing of the data. For example, figure 3(a) shows a large amount of scatter in the  $C_{n_p}$  estimate for three flap settings. Therefore, we can

conclude that little information about  $C_{n_p}$  was obtained from the analysis that yielded these data. If the data of

figure 3(a) are supplemented with the uncertainty levels associated with each data point, as in figure 3(b), it becomes evident that the data with the small uncertainty levels define a consistent trend with angle of attack as is shown by the fairing. It is of interest that the data with the small uncertainty levels were obtained from maneuvers in which all inputs were made with the aileron control. The other data were from maneuvers in which all inputs were made by the rudder control. The aileron and rudder control data are shown separately in figure 4(a). The fairing in the plot of aileron maneuver data is the same fairing as shown in figure 3(b) based on the uncertainty levels. As pointed out previously, the use of multiple maneuver analysis enhances the analysis of data by providing only one estimate of several maneuvers at the same flight condition. Thus, because the rudder data provided poor estimates and the aileron data gave good estimates, it seems reasonable to combine the data for the aileron and rudder inputs made at the same flight condition and use the multiple maneuver approach. The results of this approach are shown in figure 4(b) for the data presented in figure 3(b). The fairing is that shown in figure 3(b) based on the uncertainty level analysis and agrees well with the data obtained from the multiple maneuver analysis. In this instance the uncertainty levels were not needed in the multiple maneuver analysis because all the spurious points disappeared, but this usually cannot be counted on. Therefore, uncertainty levels as well as multiple maneuver analysis can be used to improve the quality of estimated coefficients.

#### MAJOR ERROR SOURCES

In any stability and control flight-test program, difficulties with data or modeling should not be unexpected. Frequently these problems, such as data spikes, can be observed by a cursory look at the initial flight results; however, other less obvious problems should also be expected. Two of the most common major error sources are the improper specification of the instrumentation and data acquisition system and inaccurate modeling. These error sources and the procedures that can be used to determine when errors occur are discussed in this section.

#### Instrumentation and Data Acquisition System

Basic to the accuracy of any instrumentation system is the proper specification of corrections. These corrections for aircraft stability and control analysis must include instrument calibration, accelerometer location correction, and angle-of-attack- and angle-of-sideslip-vane corrections. The instruments must be carefully positioned to avoid measuring structural vibration and undesirable flow effects. As an example, one simple consideration is that the location of some of the instruments has not been properly accounted for. This is

particularly important for vanes and accelerometers. These two corrections can be readily specified in the MMLE program. If corrections are not made to the data for the vane locations, the fit of the data is poor, particularly when angular rates are high. If the accelerometer position is not correctly accounted for, some of the estimated derivatives ( $C_{Y\beta}$  and  $C_{Z\alpha}$ , in particular) will be affected. It usually becomes evident that this correction has not been made by comparing the measured and the computed data.

The resolution and accuracy of the instrumentation must be taken into account. If measurement noise is small, fairly low resolution can be tolerated on any non-control measurement, although the lower the resolution the poorer the estimates. Low resolution of the control measurement can be intolerable, because most motions are derived from control movement. If the control position is not accurately defined on a sampled time history, the predicted motion will not be acceptable. If the predicted motion is incorrect, the estimates of the derivatives, particularly the control derivatives, will be severely degraded. For very low resolution of the control measurement, the movement of the control could be missed completely.

The sample rate chosen for the data can also have a marked effect on the quality of the estimated derivatives. In most aircraft stability and control analyses, the determining factor is the accurate definition of the control motion. Rapid excursions are caused by rapid control inputs, thus dictating the required sample rate. For a low sample rate, the initial motion of the control would be missed and the vehicle could appear to respond before the control motion began. As pointed out, the resulting control time history would result in unacceptable predicted motion, thus degrading the estimated derivatives. For most aircraft, 20 samples per second is acceptable, but 50 samples per second is more desirable. For very slow control motions, less than 20 samples per second might prove to be acceptable.

For considerations other than control motion requirements, a sample rate of 10 samples per cycle has been found to be desirable. In phugoid mode analysis, for example, 10 samples per cycle may result in very low sample rates. It should be noted that the integration routine used in the maximum likelihood estimator method may need to be modified if the sample rates are very low.

Time, or phase, shifts must also be considered. Time shifts can occur when continuous data is sampled sequentially. Particularly where the sample interval is large, the time shift between a measurement sampled at the beginning of the interval and a measurement sampled at the end of the interval becomes significant. Because the maximum likelihood estimator algorithm assumes that all samples occur simultaneously, this would cause errors in the measurement data. Once again this becomes particularly important when the control input is sampled at a significantly different time than one or more of the other measurements. If the instrumentation system cannot otherwise meet the minimum sample rate requirement, this effect can be compensated for in the data before the analysis begins by time shifting the appropriate signals.

A phase shift due to instrumentation filters can cause a similar problem. All filter rolloff frequencies should be kept much higher than the aerodynamic frequencies of interest. If a filter is unavoidable, all the measurements should be filtered with the same filter or a phase shift correction should be applied to the raw data for all the filtered measurements.

#### Modeling Problems

As used here, modeling problems refer to considerations that the analyst must take into account to obtain the best possible estimates. These considerations are viewed with regard to the standard linear model, which assumes that all motion occurs in either the longitudinal or the lateral-directional mode. That is, the standard model is valid for level flight, a steep descent, a steady turn (elevated normal acceleration), or a spiral descent. However, refinement to the standard linear model is sometimes necessary. Modeling problems can be placed in one of the following categories:

- (1) The linear model may no longer adequately approximate the aircraft, but a known nonlinear model is available.
- (2) The aircraft may be subjected to unknown external inputs.
- (3) No known model may exist for some phenomenon affecting the aircraft.

Typical problems for each of these categories will be discussed when meaningful results can be obtained by either modifying the maximum likelihood estimator algorithm or the model itself.

#### Known Linear Model

The simplest type of modeling problems occur when the model is known to be nonlinear but can be modified to be linear with additional known inputs. Mode coupling between the lateral-directional and the longitudinal modes is an example of a nonlinear model of this type. Coupling usually occurs when the vehicle cannot be completely stabilized while stability and control maneuvers are being performed. This occurs frequently during steady turns or high-angle-of-attack maneuvers. If it is assumed that the measurements of the motions in the modes not being analyzed are sufficiently accurate, these measurements can be treated as known. Thus the coupling terms appear as known external inputs to the mode under investigation. The model is once again linear, and the maximum likelihood estimator of Eqs. (2) or (3) can be applied and the additional terms treated as extra controls.

Figure 5 is a time history of a longitudinal maneuver in which significant lateral-directional motions were experienced. The fit of the flight and estimated data is not particularly good because the aircraft was at an extreme angle of attack and was difficult to stabilize in the lateral-directional mode. If the refinements and additions listed in the table on the following page were made to the longitudinal equations of motion, the fit would be that shown in figure 6.

Equation defining -	Refinement or addition
$\dot{\alpha}$	$\frac{1}{\cos \beta} \left[ \frac{g}{V} (\cos \theta \cos \varphi \cos \alpha + \sin \theta \sin \alpha) \right] - \tan \beta (p_b \cos \alpha + r_b \sin \alpha)$
$\dot{q}$	$r_b p_b \frac{I_z - I_x}{I_y} + (r_b^2 - p_b^2) \frac{I_{xz}}{I_y}$
$\dot{\epsilon}$	$-r_b \sin \varphi$

This fit is considered exceptionally good for a high-angle-of-attack maneuver, and the resulting derivatives were in good agreement with derivatives for maneuvers performed at the same flight condition but with little lateral-directional motion.

Another modeling problem occurs when the linear model of the aircraft breaks down and the nonlinear model is known but cannot be put into linear form. An example of this is the need to include the drag polar in the model. The cost functional to be minimized is an extension of Eq. (2). The algorithm is essentially the same as that for the maximum likelihood estimator used to minimize Eq. (2), but the state equations are no longer linear. Figure 7 is a comparison of longitudinal maneuver data that require a nonlinear model and the computed data based on the estimates from the algorithm just discussed. The fit is excellent. The drag polar obtained from this maneuver is compared in figure 8 with wind-tunnel estimates of the drag polar. The agreement is relatively good.

#### Unknown External Disturbances

Modeling problems caused by unknown external disturbances are encountered when an aircraft flies through a wake vortex or in atmospheric turbulence. Figure 9 is a comparison of flight data obtained in atmospheric turbulence with data obtained with the maximum likelihood estimator of Eq. (2). As can be seen, the fit is unacceptable. A maximum likelihood estimator derived by Balakrishnan can be applied to data obtained in atmospheric turbulence if the Dryden model of turbulence is used. The method (ref. 3) estimates the turbulence as a function of time in addition to the unknown coefficients. The data shown in figure 9 were analyzed in reference 4 using Balakrishnan's maximum likelihood estimator. As shown in figure 10, the resulting fit is now virtually perfect.

#### Unknown Model

The third type of model breakdown for which no known model exists cannot generally be handled. Many nonlinear models can be approximated easily by a power series expansion, but this type of analysis yields meaningless results in that the coefficients extracted have little physical meaning. An example of model breakdown, for which even a power series expansion does not approximate the nonlinearity, occurs during aerodynamic separation. Although many causes of aerodynamic separation are known, the time at which the separation occurs and the frequency with which it occurs are random. Thus little can be done to extract meaningful stability and control derivatives unless the separation is mild enough that a known model can adequately approximate the overall resulting motion. Figure 11 shows data obtained in a flight region where aerodynamic separation was known to exist. These data are compared with data computed from the maximum likelihood estimates obtained by using Eq. (2). The fit, although sometimes poor, indicates that the computed data approximate the flight data. Therefore, a fairly good linear approximation was obtained to the data showing aerodynamic separation, and the resulting estimated coefficients agreed well with those obtained where aerodynamic separation was not evident.

#### DATA EDITING

Data editing problems that may be rectified fall into two categories: (1) problems with the measurements, and (2) problems caused by inconsistencies in the model, which may be the result of something as simple as the wrong values of some geometric constants being used. Both types of problems are usually found by looking at the raw data or by using the MMLE or SUMMARY programs to find any inconsistencies. The MMLE program will point out all of these problems, unless a flight condition is incorrectly identified, but will require a computer submittal. Means of identifying data problems can be summarized as follows (parenthetical notations are referred to in the table on page 9):

- Although inspection of raw data plots is always the easiest approach, frequently the problem cannot be detected in this way. (Raw data)

The following features of the MMLE program can be extremely helpful in detecting data problems:

- If the weighted error (value of cost functional) exceeds a given error, a time history of the measured data is printed out. This usually indicates a major problem in the measured data. (MMLE-1)

- The program can be submitted to obtain a plot that compares the computed data based on the startup values with the measured data. (MMLE-2)

- A time history plot comparing the computed data, based on the values of the converged estimated derivatives, with the measured data can be obtained. This feature can frequently be made more useful by increasing the a priori weighting when a converged solution cannot otherwise be obtained. (MMLE-3)

- The SUMMARY program presents all the estimated coefficients as well as the uncertainty levels plus any a priori coefficients that are available. Many types of data problems are indicated by comparing the individual estimates and the corresponding uncertainty levels. (SUMMARY)

Common data or modeling problems are listed in the following table. Means of identifying the problems (keyed to the preceding discussion) are indicated in the order of their effectiveness, based on the amount of effort required.

Problem	To identify origin of problem use -
Data spikes	Raw data, MMLE-1, MMLE-2, MMLE-3
Time dropouts	Raw data, MMLE-1, MMLE-2, MMLE-3
Data dropouts	Raw data, MMLE-1, MMLE-2, MMLE-3
Improper time increment for maneuver	Raw data, MMLE-1, MMLE-2, MMLE-3
Coupling between modes	Raw data, MMLE-3, MMLE-1
Wrong magnitudes or signs on measurements	MMLE-3, MMLE-2, MMLE-1
Data nonlinear	MMLE-3, MMLE-2, MMLE-1
Wrong sample rate	MMLE-3, MMLE-2, MMLE-1
Wrong modes being analyzed	MMLE-1, MMLE-2, MMLE-3
Low resolution on measurements	MMLE-1, MMLE-2, MMLE-3
Noise on controls	MMLE-1, MMLE-2, MMLE-3
Maneuver needs to be shortened	MMLE-1, MMLE-2, MMLE-3
Phase or time shift in signals	MMLE-3
Different frequency and damping on different signals	MMLE-3
Turbulence or wind shear during maneuver	MMLE-3
Needs to be broken into several maneuvers	MMLE-3
Low resolution on controls	MMLE-1, MMLE-2, MMLE-3, SUMMARY
Control derivatives varying but control fixed	MMLE-3, SUMMARY, MMLE-1
Velocity, dynamic pressure, or geometric constant wrong	SUMMARY, MMLE-3
Stability augmentation system on (no independent control motion)	MMLE-3, SUMMARY
Wrong center of gravity or accelerometer position	MMLE-3, SUMMARY
Wrong weighting matrix	MMLE-3, SUMMARY
Wrong flight condition	SUMMARY

#### CONCLUDING REMARKS

A maximum likelihood estimator computer program has been used at the NASA Flight Research Center for the past 8 years to extract stability and control derivatives from flight data. The program, together with two associated programs, has been effective in analyzing 87 percent of the aircraft stability and control maneuvers attempted. More than 1500 maneuvers from 19 different aircraft have been successfully analyzed. For maneuvers analyzed under ideal conditions, each successful analysis required less than 9 minutes of engineering time and 1 1/4 minutes of CDC 6500 computer time per maneuver; fewer than 1.2 submittals per maneuver were needed. Maneuvers that were not successfully analyzed in a routine manner were often salvaged by more extensive analysis.

#### REFERENCES

1. Taylor, Lawrence W., Jr.; and Iliff, Kenneth W.: A Modified Newton-Raphson Method for Determining Stability Derivatives From Flight Data. Computing Methods in Optimization Problems - 2, Lotfi A. Zadeh, Lucien W. Neustadt, and A. V. Balakrishnan, eds., Academic Press, 1969, pp. 353-364.
2. Iliff, Kenneth W.; and Taylor, Lawrence W., Jr.: Determination of Stability Derivatives From Flight Data Using a Newton-Raphson Minimization Technique. NASA TN D-6579, 1972.
3. Balakrishnan, A. V.: Stochastic Differential Systems I - Filtering and Control - A Functional Space Approach. Lecture Notes in Economics and Mathematical Systems, 84, M. Beckman, G. Goos, and H. P. Künzi, eds., Springer-Verlag, 1973.
4. Iliff, K. W.: Identification and Stochastic Control With Application to Flight Control in Turbulence. UCLA-ENG-7340, School of Engineering and Applied Science, Univ. of Calif., Los Angeles, Calif., May 1973.

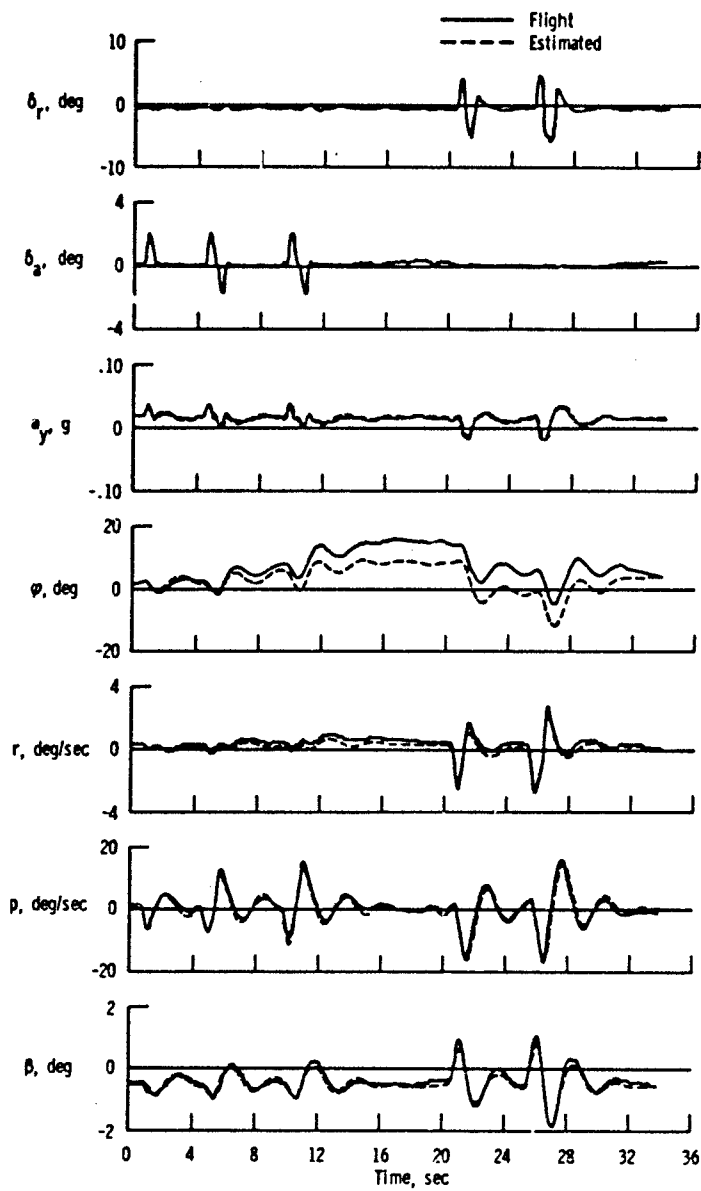


Figure 1. Comparison of flight and estimated data showing significant measurement drift at time of rudder control input.



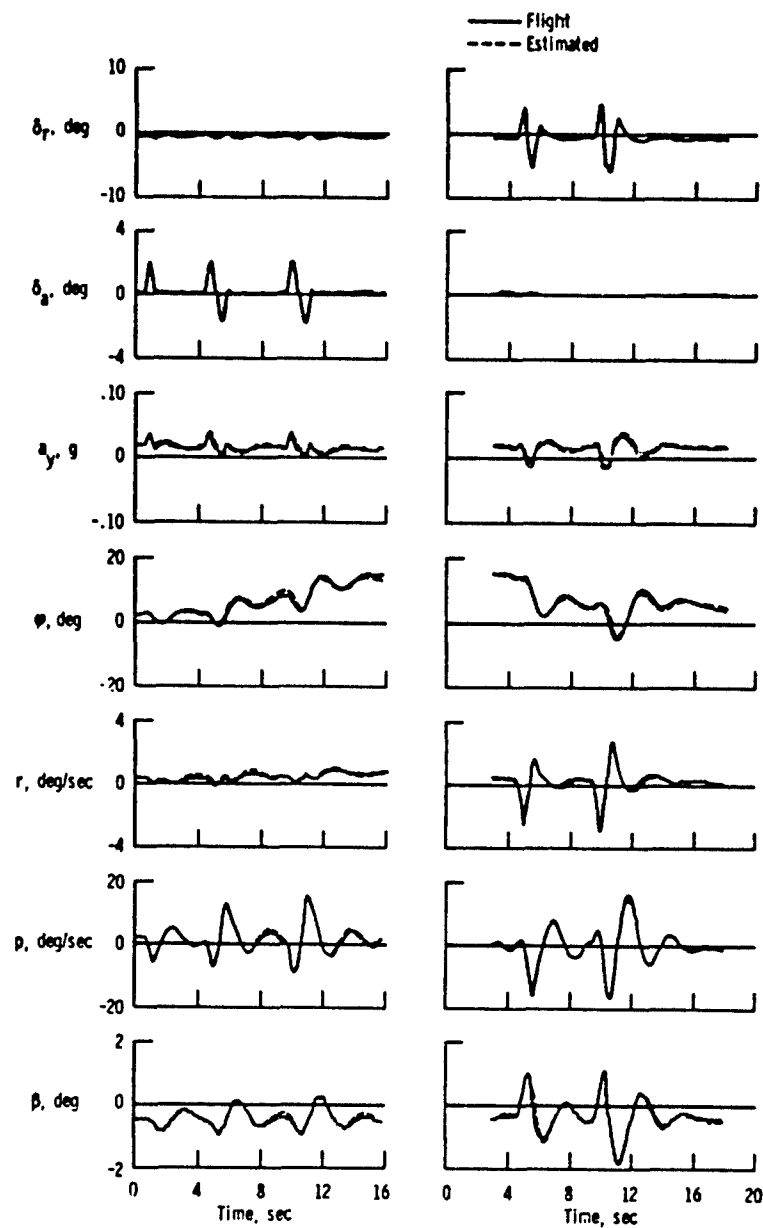


Figure 2. Comparison of flight and estimated data of figure 1 showing the improved fit resulting from multiple maneuver analysis.

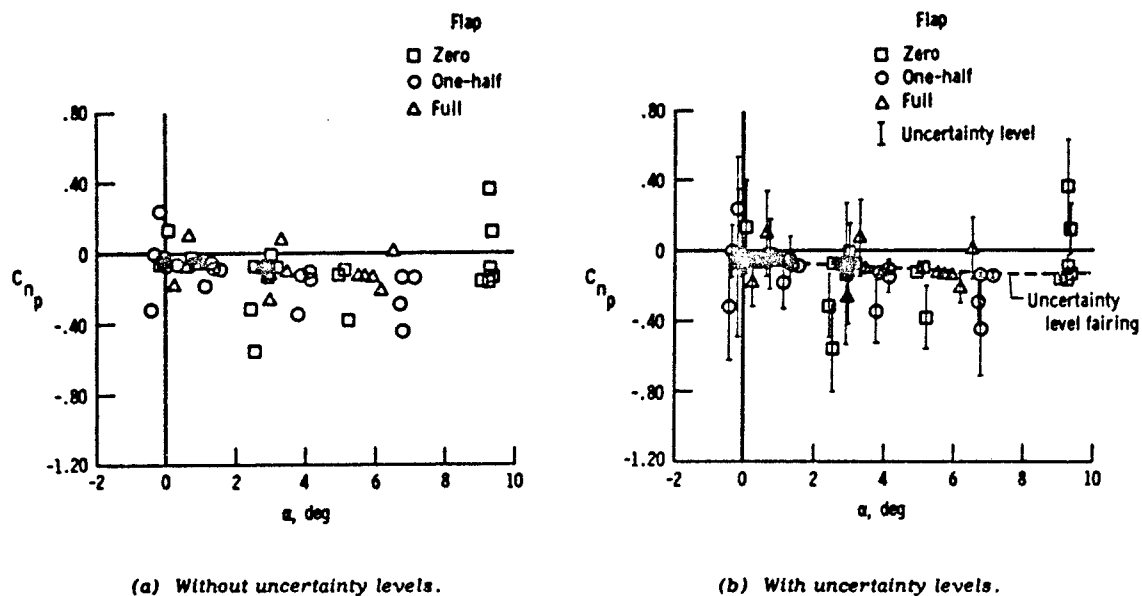


Figure 3. Variation of  $C_{np}$  with angle of attack showing the advantage of using uncertainty levels.

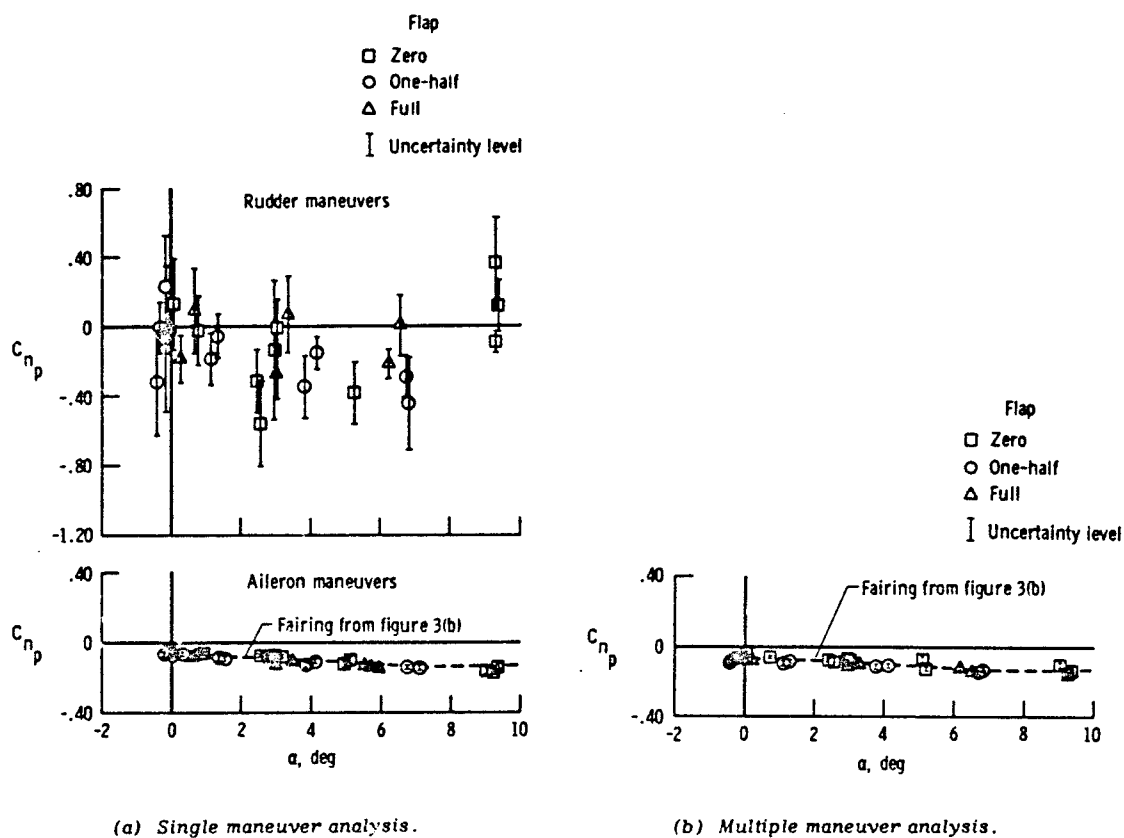


Figure 4. Variation of  $C_{np}$  with angle of attack for single and multiple maneuver analysis.

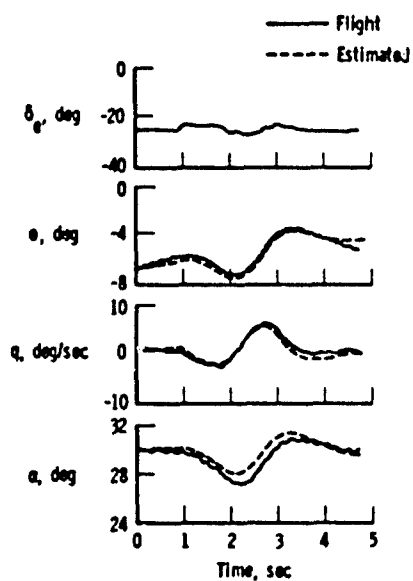


Figure 5. Time history of longitudinal maneuver showing the effect ignoring lateral-directional coupling terms in high-angle-of-attack data.

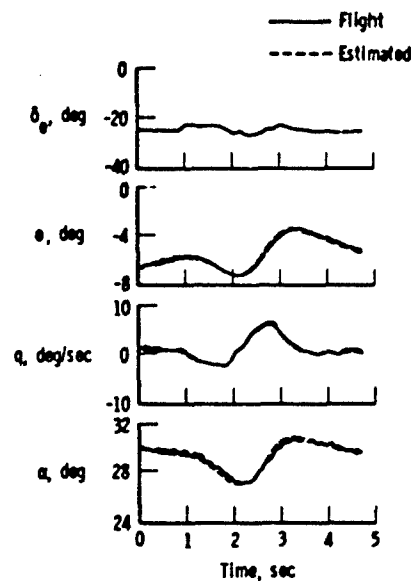


Figure 6. Time history of longitudinal maneuver showing improvement in data of figure 5 after inclusion of lateral-directional coupling terms.

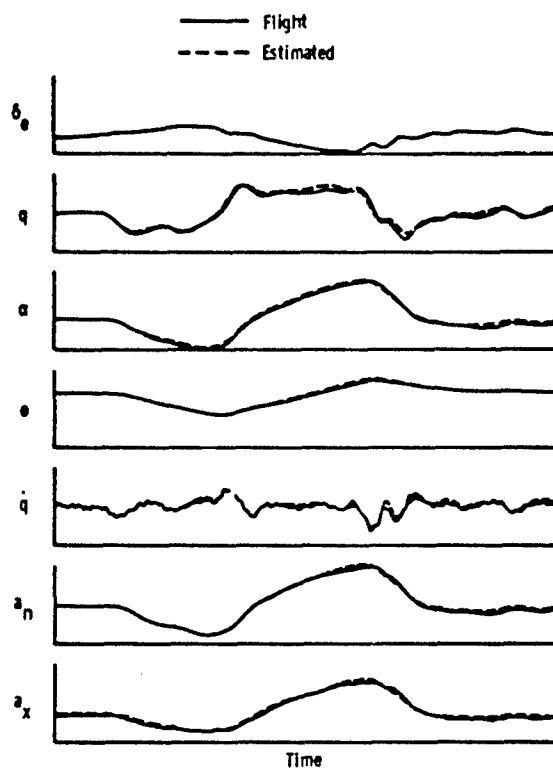


Figure 7. Comparison of flight and estimated data using a nonlinear model.

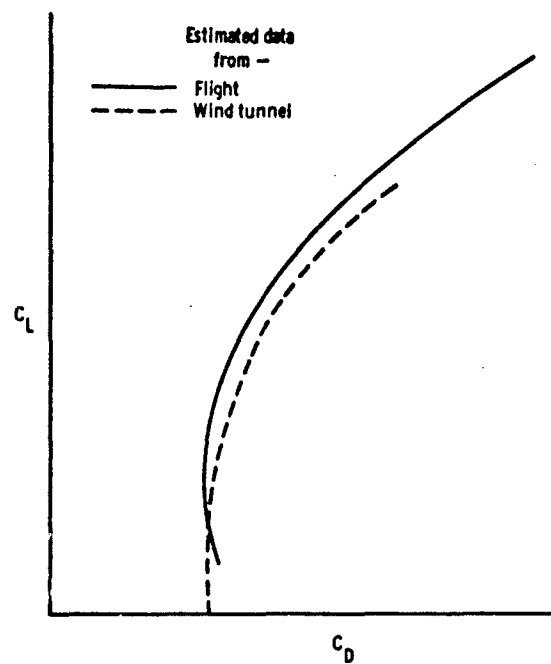


Figure 8. Comparison of drag polars obtained from estimates based on wind-tunnel and flight data.

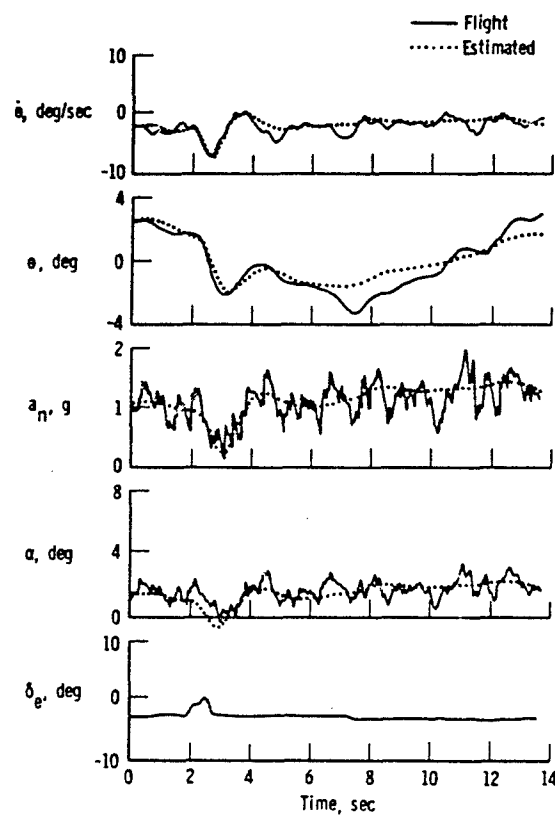


Figure 9. Comparison of flight data obtained in turbulence with estimated data which neglect the effect of turbulence.

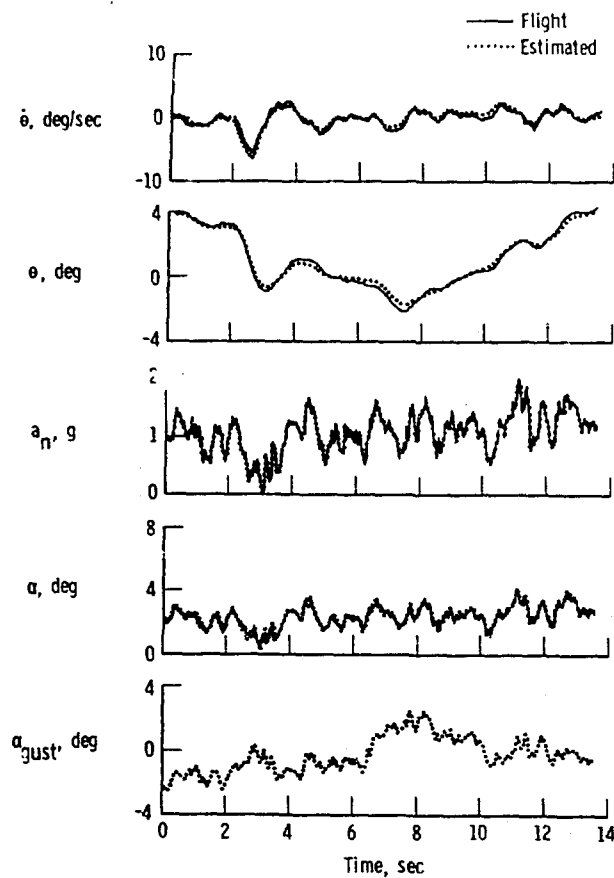


Figure 10. Comparison of flight data obtained in turbulence with estimated data which include the effect of turbulence.

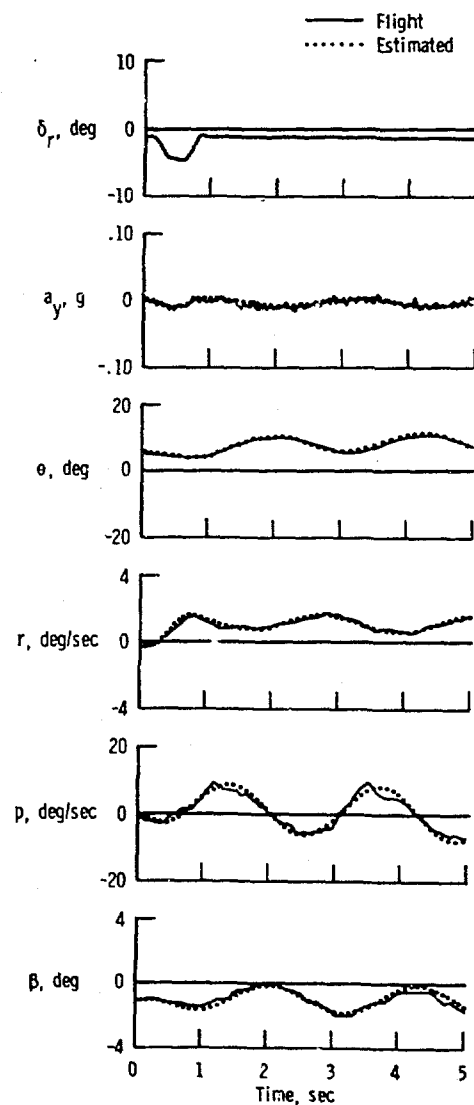


Figure 11. Comparison of flight data obtained in buffet with estimated data which neglect the effects of buffet.

# DETERMINATION OF AIRCRAFT DERIVATIVES BY AUTOMATIC PARAMETER ADJUSTMENT AND FREQUENCY RESPONSE METHODS

M. Marchand  
R. Koehler

Institut für Flugmechanik  
Deutsche Forschungs- und Versuchsanstalt  
für Luft- und Raumfahrt e.V. (DFVLR)  
Braunschweig-Flughafen

## Summary

The paper reviews the experiences at DFVLR Research Center Braunschweig in the estimation of aircraft parameters by means of three identification methods: Frequency response, maximum-likelihood, and model with automatic parameter adjustment. Results using flight test data from the Do-27 and HFB-320 aircraft are presented. The effects of including nonlinear terms and turbulence in the model are also discussed.

Furthermore, the model with automatic parameter adjustment method was used for studying the problems of derivative identification for rotorcraft type vehicles. Preliminary results obtained when evaluating simulated Sikorsky S-61 flight data with various input signals are given.

Finally, some aspects of designing input signals for flight tests are discussed. In this subject, a method is described for the design of short-time signals which allow a good identification of the system parameters and are still easily flown by the pilot.

## 1. Introduction

This paper shall give an insight into the activities of the DFVLR-Institute for Flight Mechanics in the field of system identification of fixed wing aircraft and helicopters. So far, emphasis has been placed on the development and application of the following three methods:

- Frequency response
- Maximum-likelihood with Newton-Raphson iteration
- Model with automatic parameter adjustment.

These solution methods differ primarily in the following major ways:

- Time domain - versus - frequency domain
- Digital evaluation - versus - hybrid evaluation
- Equation error criterion - versus - output error criterion
- Off-line evaluation - versus - on-line evaluation

Having all three methods available, it is therefore possible to obtain the results of an identification by using several different techniques.

The development and application of identification methods described above is only one part of the work which is necessary for a successful parameter determination. The other part consists of a thorough theoretical preparation for actual flight tests. In this respect, the following tasks are required:

- Determination of the correct model structure
- Investigation of the influence and, therefore, the ability to identify the coefficients of the chosen model
- Design of appropriate inputs to the model.

All of these tasks are also being conducted in the DFVLR.

The methods described above are not only applied to fixed wing aircraft but also to helicopters. In order to investigate the problems of parameter identification of unstable helicopters, simulations are being performed at present in which the model structures, test signals and evaluation methods are being investigated. Some of the results obtained will be discussed in more detail in this paper.

Finally, work for optimization of input signals shall be mentioned. Emphasis is placed on such signals which can be simply flown by the pilot. For instance, as will be also described in detail later, sequences of step functions, similar to the binary random functions, are optimized.

## 2. List of Symbols

$a_x, a_z$	longitudinal and vertical accelerations at center of gravity
$C_{x\dot{u}}, C_{z\dot{u}}$	nondimensional longitudinal force and normal-force derivatives
$C_{m\dot{q}}$	nondimensional pitching moment derivative
$F$	frequency response function
$p$	roll rate
$q$	pitch rate
$R$	correlation function
$S$	spectral density function
$u$	longitudinal velocity component
$v$	vertical velocity component
$\alpha$	angle of attack
$\beta$	angle of sideslip
$\gamma$	flight path angle
$\delta$	control deflection
$\delta_a, \delta_e$	aileron and elevator deflections
$\varepsilon$	equation error
$\theta$	pitch attitude
$\theta_c$	lateral control deflection
$\theta_R$	pitch attitude of rotor tip plane
$\sigma$	standard deviation
$\phi$	roll angle
$\phi_R$	roll angle of rotor tip plane
$\omega$	frequency

## 3. Methods for Parameter Identification

### 3.1 Frequency response methods

The method for the determination of the frequency response values has been known for some time and often employed in the past. However, a systematic evaluation of the frequency response values has rarely been performed. It was therefore the aim of our efforts to develop methods and computer programs for the analytic presentation of the transfer functions and the identification of the system parameters from the frequency response values. Figure 1 shows that two ways in which this is possible. In this paper, only the method for determining the equation coefficients for the frequency response method shall be discussed while, thereafter, the transfer functions and their poles and zeros can also be determined (ref. 1).

Basic concepts of the frequency response method are shown in Figure 2. In this method, the frequency responses are first calculated from the flight test data. Figure 3 shows the necessary numerical operations and, in parallel, the corresponding transformations of the equations of motion into the frequency domain. After the transformations, the transformed equations have the same coefficients as the original equations and the corresponding estimated values of the frequency response (e.g.,  $F_{a_2\delta}$ ,  $F_{\alpha\delta}$ ) have taken the place of the time histories of signals (e.g.  $a_z$ ,  $\alpha$ ,  $\delta$ ). Thus, as an example, the simplified Z-equation in the time domain is written

$$a_z(t) = Z_a a(t) + Z_\delta \delta(t) + \dots$$

while, according to Figure 3, it is written in the frequency domain as

$$F_{a_z\delta}(\omega) = Z_a F_{a\delta}(\omega) + Z_\delta + \dots$$

Since the coefficients are the same, we have the possibility to determine these equation coefficients by applying an equation error method on the frequency domain equations. Figure 4 presents such a method. The criterion results from the maximization of the likelihood function of the equation errors. The statistical characteristics of the frequency response errors, which has been treated in former paper, are used to determine the variances of the equation errors (refs. 2 and 3). As estimated values of the unknown coefficients are also required for the calculation of the variances, the method is an iterative one. The method converges very rapidly, so that four iteration steps are sufficient if no a-priori information on the system parameters is used.

Beside the quick convergence, the method has two other advantages which result from the use of correlation technique:

1. The amount of data to be evaluated with the iterative method is essentially lower than the number of measured values. Therefore, little computing time is necessary after the initial correlation calculation (which must be performed only once). In addition, if a greater number of evaluations with different models is to be performed, the initial correlation calculation need not be repeated.
2. Noise which is independent of the input is largely suppressed by the correlation of the signals with the input signal. This leads to a reduction of the systematic errors in the parameters as compared to those obtained when applying the equation-error-method in the time domain.

The essential disadvantages of this method are that it does not provide the initial values of the state variables which are required for a comparison of the model output with the test data, and that, when nonlinear terms in the model are taken into account, the reference values of the state variables and the bias errors of the measurements must be known. Therefore, a state estimation program is additionally required in the case of nonlinear models. This program must estimate the initial values of the state variables and the bias errors of the measurements.

Figure 5 shows a comparison of Do-27 flight data with the model outputs using this solution technique. Results from flight tests with HFB-320 using this solution technique are treated in connection with the maximum-likelihood identification presented in the following section.

### 3.2 Maximum-Likelihood method

For the evaluation of flight tests, a maximum-likelihood method was employed in addition to the frequency response method. This method is known as Newton-Raphson method or method of quasilinearization and needs no further explanation (refs. 4 and 5). In this paper, some results are presented which were obtained using this method. A 12 second portion of a flight test with HFB-320 serves as example. Different mathematical models were investigated including: a linear model, a nonlinear model with a quadratic influence of the angle of attack on the X-force, and a model with turbulence influence included.

Figure 6 shows a comparison of the results between using a linear and a nonlinear model. As the two models used differed only in the  $C_{Xa2} a^2$  term in the X-equation, an essential difference in curve fitting results only at the  $a_X$ -signal. The figure shows, therefore, that a better fitting of the  $a_X$ -curve will be achieved with the quadratic model. This is further confirmation of the fact that the quadratic term of  $a$  must not be neglected in the X-equation as already reported in other papers (refs. 6 and 7).

Figure 7 compares the measured output signals with the outputs obtained using the nonlinear model. For a comparison, it further shows the result of an identification using the previously discussed frequency response method. As the evaluation with the frequency response method was made on the basis of a linear model, the curve fitting in the case of the  $a_X$ -signal is not ideal. Both methods show some deviation during the time history of the angle of attack. This deviation was attributed to turbulence effect.



For this reason, a M-L identification was performed with a model including turbulence. Here, a further improvement of the fitting in the case of the  $a_z$ -signal could be observed, as is shown in Figure 8. In the case of the other signals, no major improvement could be obtained which is probably due to measurement noise. Therefore, it seems reasonable to conclude that an extended model which takes measurement noise as well as turbulence at the angle of attack into account should be used. This corresponds to ref. 8.

Figure 9 presents a comparison of the parameters identified for the HFB-320 aircraft from five sources: windtunnel data, frequency response method solution, and the linear, nonlinear, and nonlinear with turbulence solutions with the M-L method. It should be noted that there is no solution for  $C_{Xa2}$  for the linear models since it is a nonlinear term and that the value of  $C_{Z_{\delta a}}$  varies because the term has little influence in the equations.

### 3.3 Model with automatic parameter adjustment

Figure 10 shows the block diagram of the model with automatic parameter adjustment method. The model has the structure of the equations of motion and provides the equation errors which result from the input and output signals and the estimated model coefficients. The gradient of the parameters to be adjusted is calculated by means of a cost function. The final estimates of the parameters are determined by means of integration. This method is described in ref. 6 in more detail. Figure 11 presents some results using this method with Do-27 aircraft flight data.

It is possible with this method to investigate and to make visible the influence of changes in the model structure. Coefficients which adjust themselves very slowly or not at all to a final value have little influence in the model and can be considered as unessential. Further, a completion of the model, for instance, by means of nonlinear terms, provides better time histories of the coefficients. This can be shown by means of examples of models with and without  $C_{Xa2}$  (Figure 12). Using the linear model, an equation error  $-C_{Xa2} a^2$  appears. The circuitry tries to compensate this error by a continuous variation of the coefficient  $C_{Xa}$ . This becomes evident from the comparison of the time histories for  $C_{Xa}$  of the linear to the nonlinear model.

Owing to the possibility of using a hybrid computer, a further development of the procedure was possible. With this computer, a repetitive playback of the digitally stored measured values becomes possible. Figure 13 shows that extremely short flight times can also be evaluated using this method.

In the non-iterative case it may occur that the adjustment process of the parameters is not yet concluded at the end of the test time, as shown in the center of the figure. In this case the measured data may be fed to the model again in an iterative method as presented at the bottom of the figure. Maneuvers flown at different times can be evaluated using the same technique by placing one immediately after another.

At present, this technique of repetitive calculation is being used for fundamental investigations into identification of helicopter parameters. This is required because the helicopter instability allows only very short test times. An additional difficulty is encountered with the high-frequency rotor dynamics. The work, therefore, has the following objectives:

1. Determine if the reduced so-called quasistationary model (which results from neglecting inertia and damping of the rotor disc in the complete model) is applicable for this solution technique.
2. Determine how readily the required derivatives can be identified.
3. Choose and optimize the appropriate test signals.

Reference 9 reports the first results of these studies.

As an example of an application of the method, a linear model of the Sikorsky S-61 helicopter was simulated and then analyzed. The simulation had six degrees-of-freedom which consisted on four degrees-of-freedom of the fuselage motion and two degrees-of-freedom of the rotor tip plane ( $u, v, \phi, \theta, \phi_R, \theta_R$ ). On the other hand, for this case the analysis was based on neglecting the derivations of  $\dot{\phi}_R$  and  $\dot{\theta}_R$  giving a reduced system of only four degrees-of-freedom ( $u, v, \phi, \theta$ ). Figure 14 shows that the reduced model over a wide frequency domain corresponds very well to the original model. Deviations only occur at high frequencies where the dynamics of the rotor disc plays a significant role.

Figure 15 shows two input signals used for this method and their spectra. As signal 1 shown at the top of the figure contains too little information in the low frequency domain, an additional test with signal 2 shown at the bottom of the figure was conducted. Subsequently, the time histories of both tests were arranged one after another for the evaluation. The evaluation with test signal 1 alone showed poor agreement in the lower frequency domain, whereas the evaluation with both signals showed good agreement as shown in Figure 16. In the case of very high frequencies, deviations from the 6-degrees-of-freedom model were contributed to the rotor dynamics as previously described. On the other hand, the identifications found in this high frequency domain correspond very well to the reduced 4-degrees-of-freedom model presented in Figure 14. In the time history plot, shown in Figure 17, the deficiency of the single input solution is not so evident as in the frequency response plots of Figure 16. This arises because the time histories contain less information on the low-frequency behaviour due to the short test time than the corresponding frequency-response curves. Finally, using both signals, Figure 18 shows that the model could be well identified.

#### 4. Optimization of Input Signals

The results of the helicopter simulation have shown that the quality of the identified model essentially depends on the choice of input signals. Methods for the optimization of input signals have already been published, e.g. in ref. 10. Such methods which provide continuous signals, make great demands on the ability of the pilot to steer exactly the prescribed signal. With respect to the pilot, it is more favorable to optimize a sequence of easily controllable signals, for instance, step functions. A first step in this direction is the use of binary random processes as a signal generator. As such processes have a known performance spectrum, the information contents of the signal can be easily judged and influenced. Such signals were applied with good success in the Do-27 and HFB-320 flight test. However, Figure 15 showed that, in the case of short flight times, signals of this type still do not show an ideal power spectrum curve. The spectrum of the random process cannot be realized within the short time of 20 seconds, therefore, sharp peaks and breaks will result. For this reason a method was developed that optimized the sequence of the step functions for a prescribed total time, length of interval, and step height. The criterion used to make this determination is the approach of the signal spectrum to the spectrum of the corresponding random process. First results are shown in Figure 19 which shows namely two optimized input signals of a time duration of only 7 seconds each. These signals have, in spite of the short test time, a flatter spectrum than the signal used for the helicopter simulation which had a test time duration of 20 seconds. In addition, the signals are built up so simply that they can be easily flown by the pilot after little training. The amplitudes of the first signal shown at the top of Figure 19 are equally large positively and negatively. The disadvantage of this signal is the low value of the power spectrum at low frequencies. This disadvantage, however, can be eliminated by a displacement of the signals as shown in the lower part of Figure 19. Note the improved corresponding power spectrum in the low frequency domain.

Before determining optimal input signals for a flight test according to the described procedure, one has to estimate which frequencies the signals should include. For this, a procedure was developed that uses the Bode plot of the frequency responses. In applying the method, first the magnitude of the frequency responses multiplied by the corresponding equation coefficient is plotted. An example of such a plot is given in Figure 20 which shows the dependency of the terms of the rolling moment equation on the frequency. In the case where forcing is introduced with a definite frequency, only those coefficients which exercise an essential influence at this frequency within the equation can be determined. Further, under other circumstances, only ratios of coefficients can be determined. This occurs, for instance, if the known inertia terms are of no importance and thus the equation has no dominating term with a known coefficient.

Figure 20 contains an example of such a case in the lower frequency domain. Additionally, which parameters can be defined in the different frequency ranges is also shown in this figure.

Using the same procedure as the example above, one produces the corresponding diagrams for all the other equations and input signals. Combining this information, the required frequency domain for the input signal can be found. In addition, the time interval needed for the input signal can also be determined from the upper frequency limit.

Compared to an optimization of signals in the time domain, this method offers a number of practical advantages:

1. Several input signals with good power spectra can be developed independently of the aircraft being tested. The final adjustment of these signals to the test aircraft is then made by varying the time scale without changing the amplitude variation of the signal.
2. The pilot needs to memorize the form (amplitude variation) of the test signals only once even though the test time of the signal is changed from run to run.
3. Owing to the flat spectrum, the signal is suitable even if the actual behaviour of the aircraft deviates from that of the a-priori model.

## 5. Conclusions

Three methods for system identification have been used in the Institute for Flight Mechanics of the DFVLR: the frequency response method, the maximum-likelihood method and the model with automatic parameter adjustment method. The evaluation of flight tests with Do-27 and HFB-320 have demonstrated that model output and flight test data correspond better when the quadratic influence of the angle of attack is taken into account. The inclusion of turbulence at the angle-of-attack signal only partial improves the solution. It appears that, when using signals from vane type instrument, measurement noise as well as turbulence have to be taken into account for a more accurate solution.

The method with automatic parameter adjustment can be employed as an on-line method in the case of measuring times of long duration as well as an iterative method in the case of short measuring times. In the later case, problems of helicopter identification were investigated. In so doing, an identification was performed on a six-degree-of-freedom helicopter simulation using a reduced model with four degrees-of-freedom. It appeared that with suitable input signals good correspondence between this theoretical and identified model could be obtained.

The choice of suitable input signals and/or their optimization is an important supposition for performing a successful system identification. In those cases in which the pilot has to control the inputs, the signals must have a particularly simple form. On the other hand, they shall contain the information required for the parameter determination. Therefore, a method was developed consisting of two steps in which, at first, type and frequency domain of the signal are determined and, subsequently, time history with regard to the desired spectrum is optimized.

In the present paper, all the activities of the DFVLR in the fields of system identification and signal optimization could not be discussed. It is the aim of these efforts, to work with several methods which are independent of each other. In this way, the methods can be adapted to the special conditions of flight tests and the obtained results can be confirmed.

## 6. References

1. Marchand, M. The Identification of Linear Multivariable Systems from Frequency Response Data. 3rd IFAC Symposium on Identification and System Parameter Estimation, The Hague/Delft (1973).
2. Marchand, M. Über den statistischen Fehler von Frequenzgangmessungen bei digitaler Auswertung. DLR FB 69-28 (1969).
3. Koehler, R. Über die statistischen und systematischen Fehler bei der Systemanalyse am Analogrechner mit Hilfe stochastischer Signale. DLR FB 69-19 (1969).
4. Iliff, K.W., Taylor, L.W., Jr. Determination of Stability Derivatives from Flight Data Using a Newton-Raphson Minimization Technique. NASA TN D-6579 (1973).
5. Plaetschke, E. Kennwertermittlung mit Maximum-Likelihood-Verfahren. DFVLR-IB 154-74/20 (1974).
6. Koehler, R. Determination of the Derivatives of Longitudinal Motion of an Aircraft from Flight Data by a Model with Automatic Parameter Adjustment. Translation of DLR-FB 73-13 (1973). RAE Library Translation 1740 (1973); Library Translation ESRC TT-3 (1974).
7. Wingrove, R.C. Estimation of Longitudinal Aerodynamic Coefficients and Comparison with Wind-Tunnel Values. Symposium of Parameter Estimation Techniques and Application in Aircraft Flight Testing, NASA Flight Research Center Edwards (1973).
8. Iliff, K.W. Identification of Aircraft Stability and Control Derivatives in the Presence of Turbulence. Symposium of Parameter Estimation Techniques and Application in Aircraft Flight Testing, NASA Flight Research Center Edwards (1973).
9. Gmelin, B., Kaletka, J., Mix, O. Parameteridentifizierung von Drehflüglern. To be published in Zeitschrift für Flugwissenschaften, Vol. 22, No. 12, December 1974.
10. Stepner, D.E., Mehra, R.K. Maximum-Likelihood-Identification and Optimal Input Design for Identifying Aircraft Stability and Control Derivatives. NASA CR-2200 (1973).

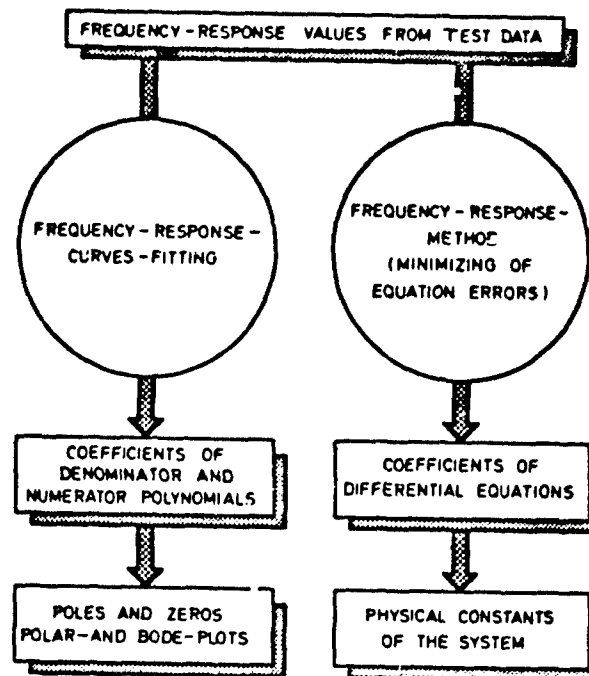


Fig. 1 Parameter identification in the frequency domain

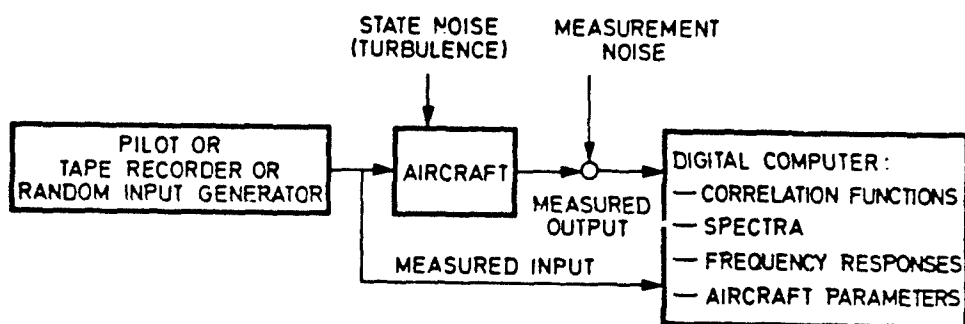


Fig. 2 Basic concept of frequency-response-method for system identification

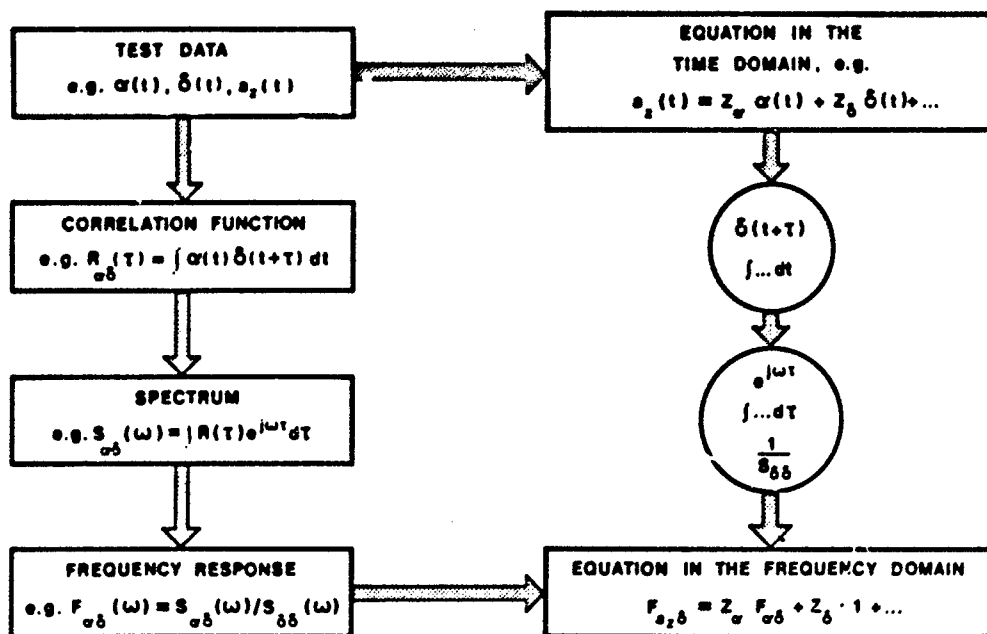


Fig. 3 Transformation of signals and equations into the frequency domain

## KOMPLEX SYSTEM EQUATIONS:

$$\sum_v F_v(\omega_1) p_v = c_1 + jc_2$$

$$\sum_v F_v(\omega_2) p_v = c_3 + jc_4$$

$\begin{matrix} \vdots \\ \vdots \end{matrix} \setminus \begin{matrix} \text{EQU. ERRORS} \\ \text{SYSTEM PARAMETERS} \end{matrix}$   
 FREQUENCY - RESPONSE - VALUES

## MAXIMUM - LIKELIHOOD - CRITERION:

$$\sum_v \frac{\epsilon_v^2}{\sigma_v^2} = \min$$

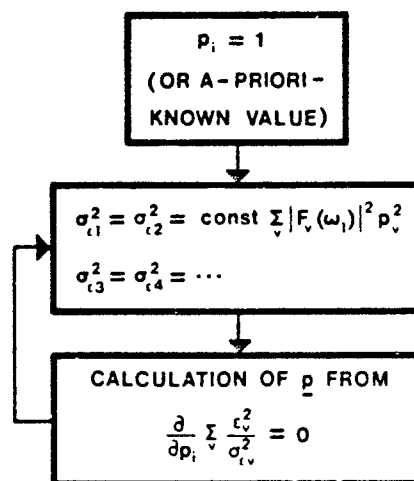


Fig. 4 Parameter estimation method in the frequency domain

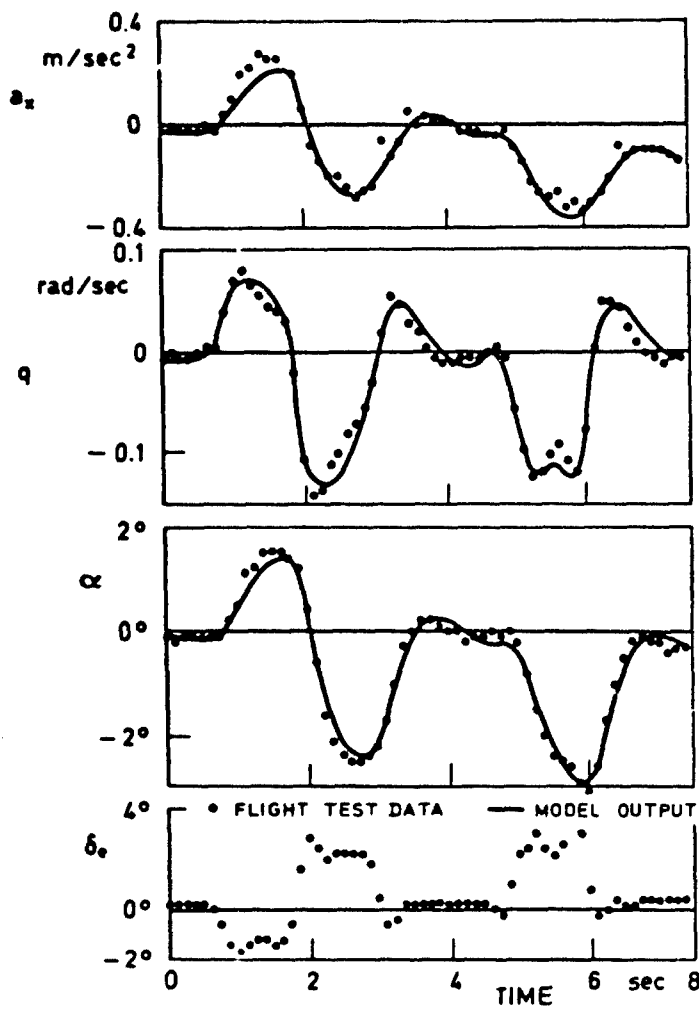


Fig. 5 Results of system identification with frequency-response-method (Do-27 flight test)

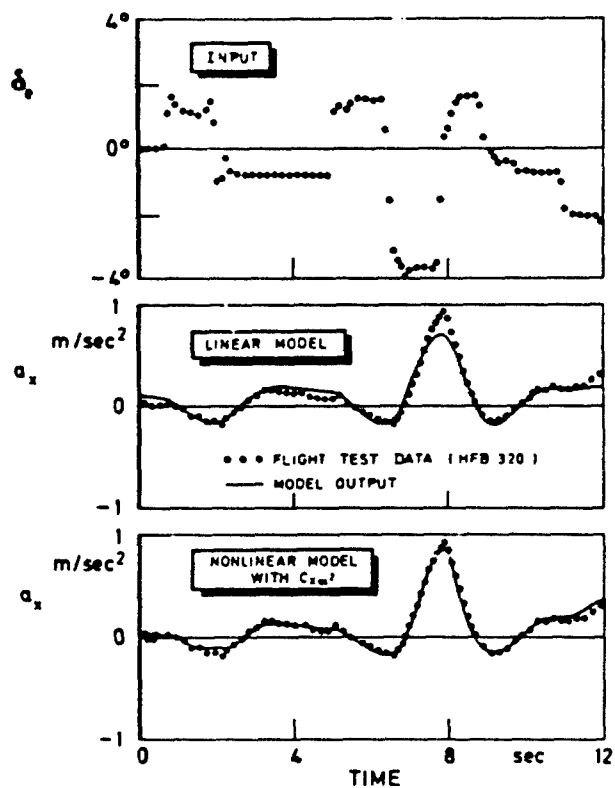


Fig. 6 Effect of  $\alpha^2$  on longitudinal acceleration

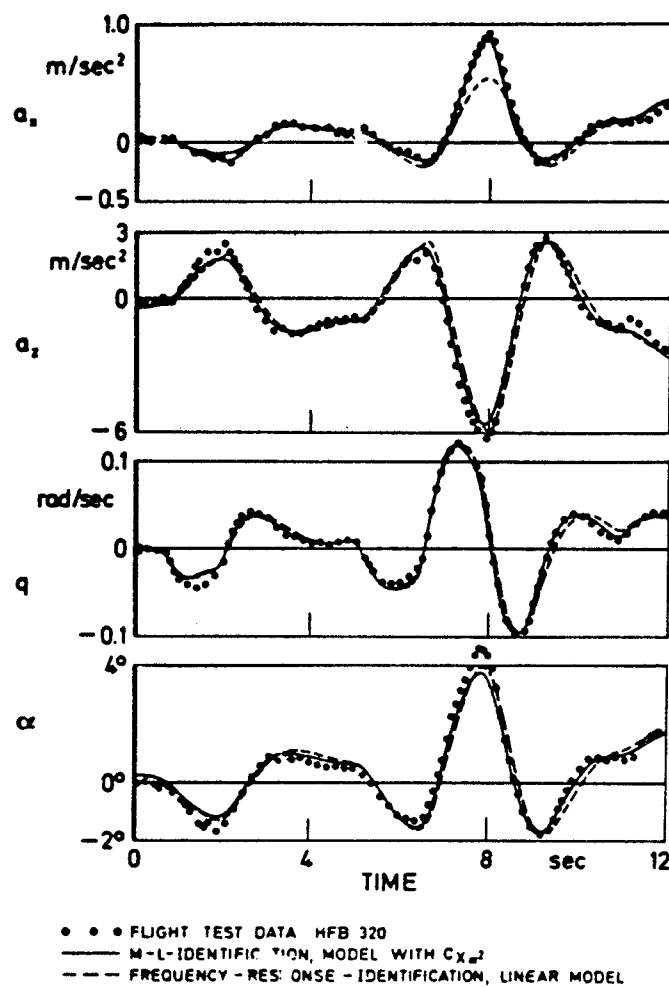


Fig. 7 Identification results (time histories)



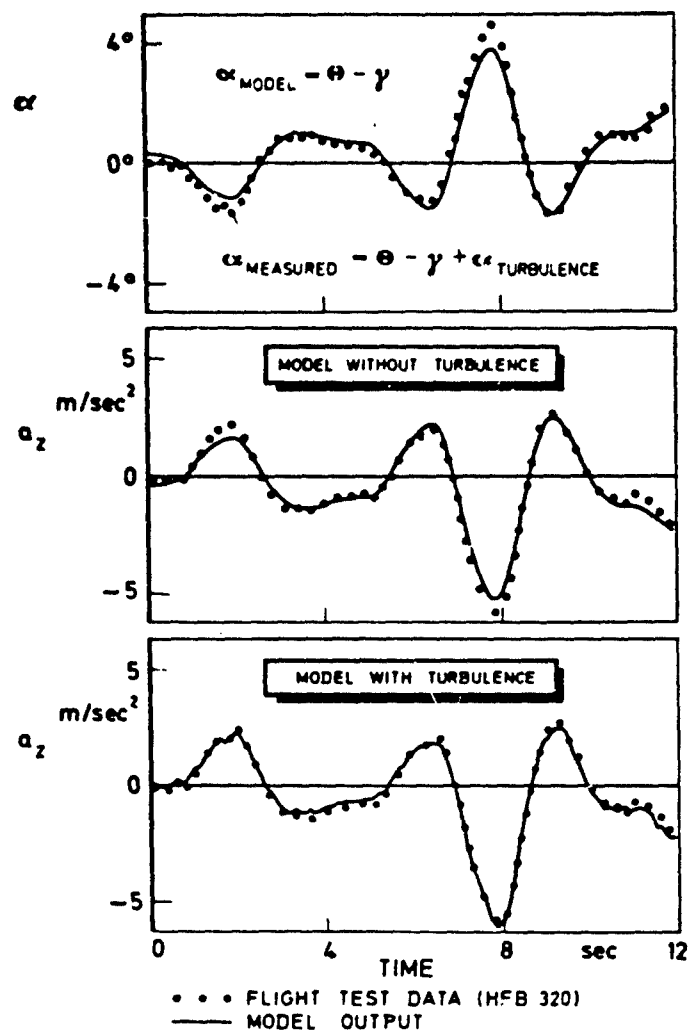


Fig. 8 Effect of turbulence on vertical acceleration

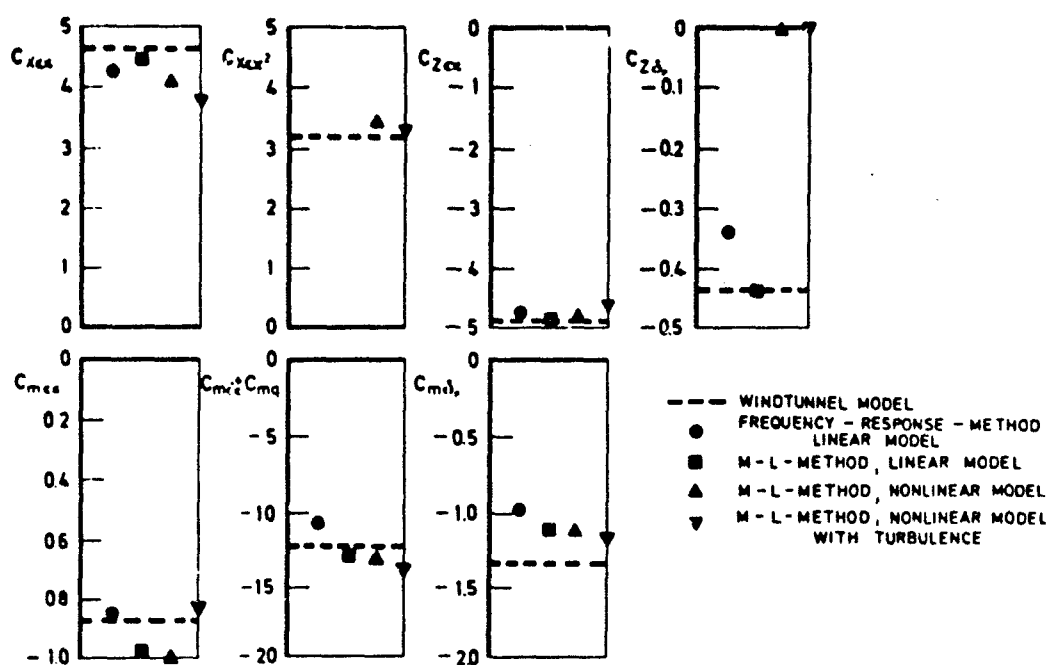


Fig. 9 Identification results of HFB 320 flight tests

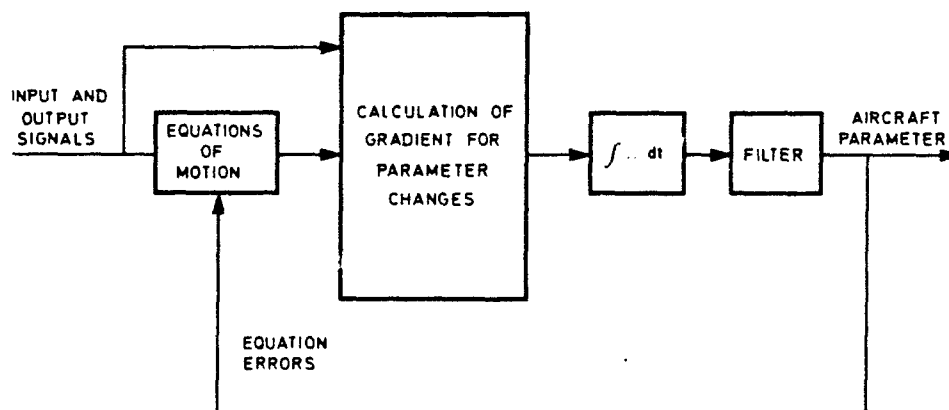


Fig. 10 Basic concept of model with automatic parameter adjustment

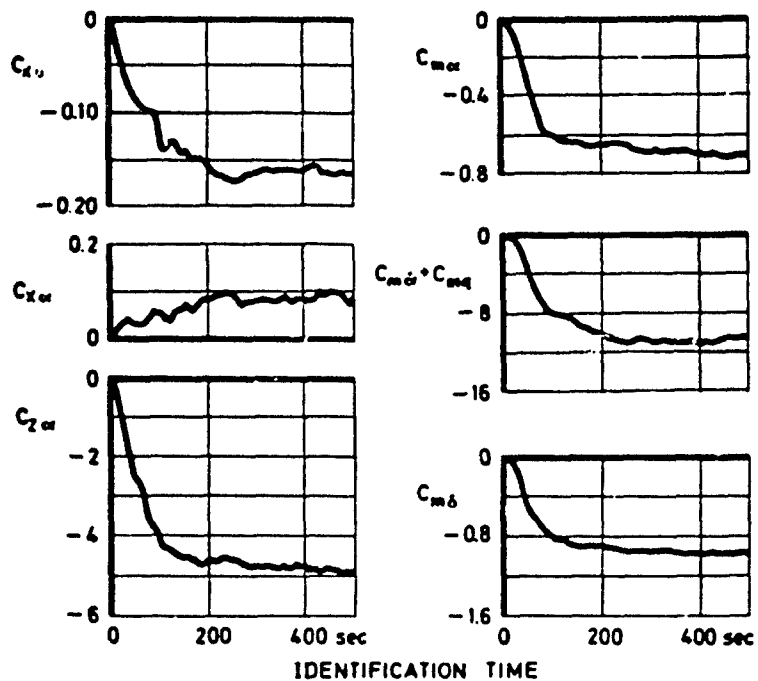


Fig. 11 Results from model with automatic parameter adjustment (evaluation of Do-27 flight test)

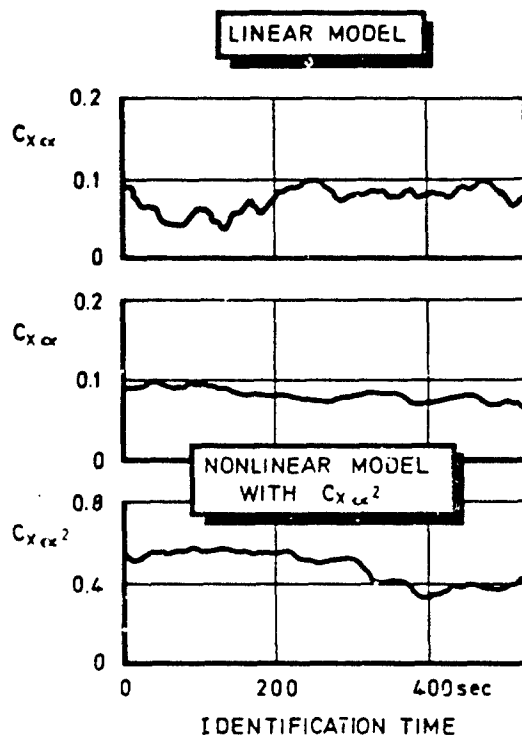


Fig. 12 Influence of nonlinear term  $C_{x\alpha^2}$  on the identification of longitudinal-force derivatives (evaluation of Do-27 flight test)

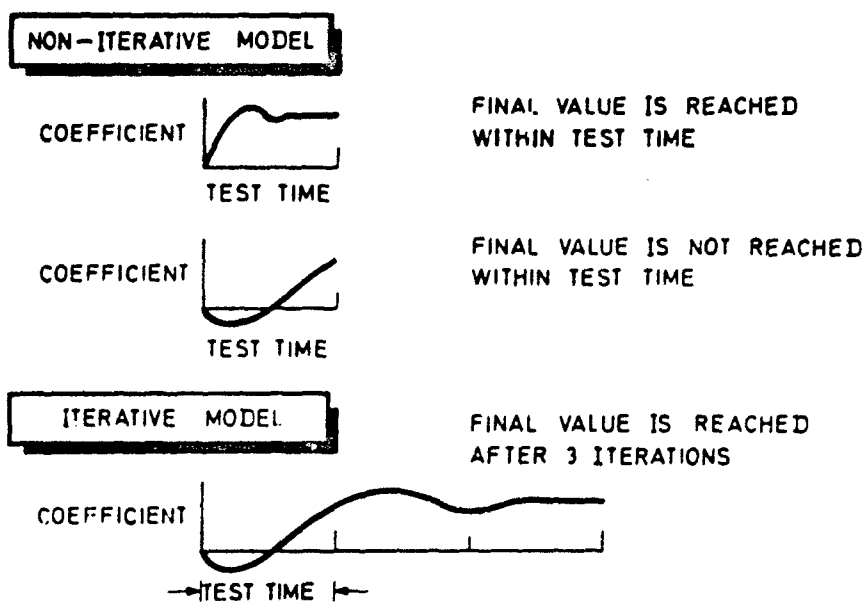


Fig. 13 Iterative model with automatic parameter adjustment

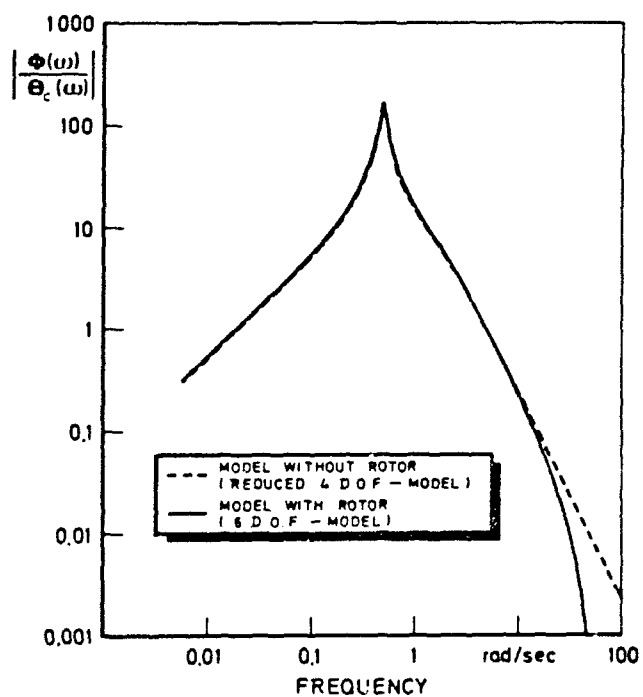


Fig. 14 Frequency response of Sikorsky S-61 rotorcraft model

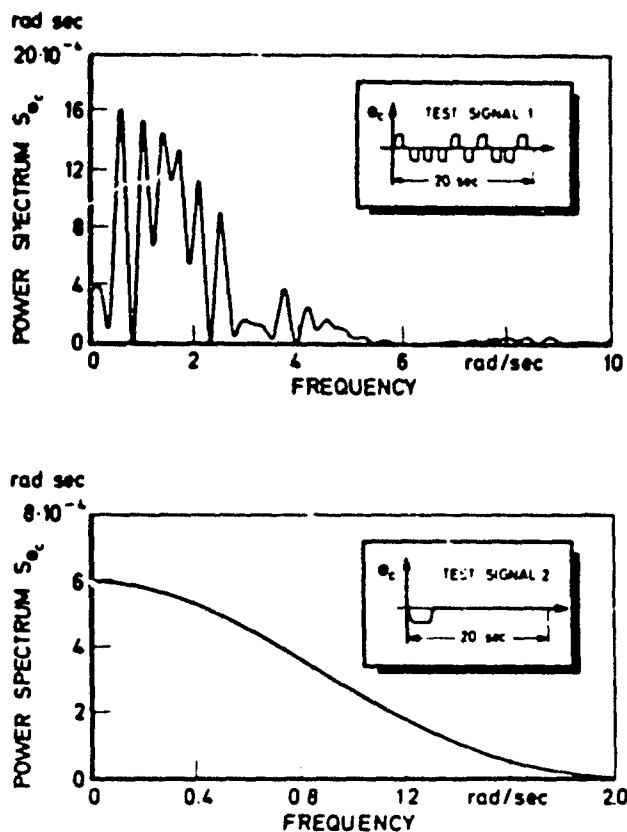


Fig. 15 Time histories and power spectra of two test signals

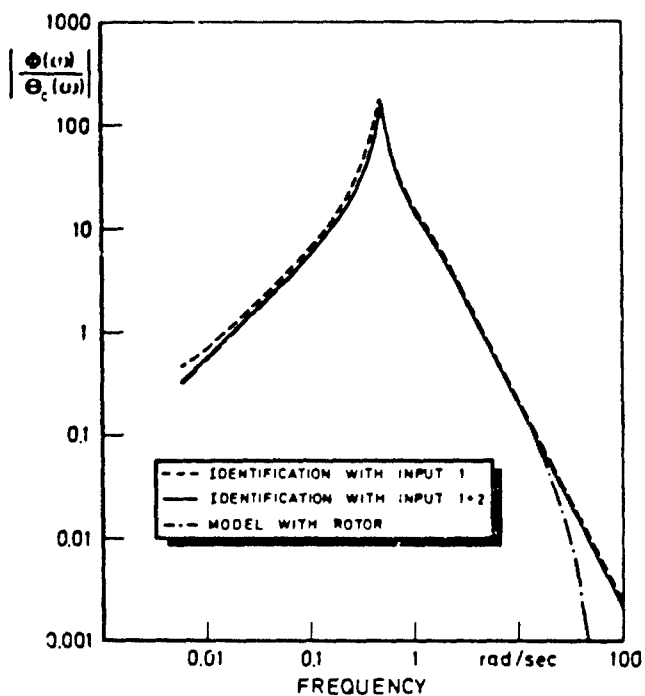


Fig. 16 Influence of test signals on identification results (frequency response)

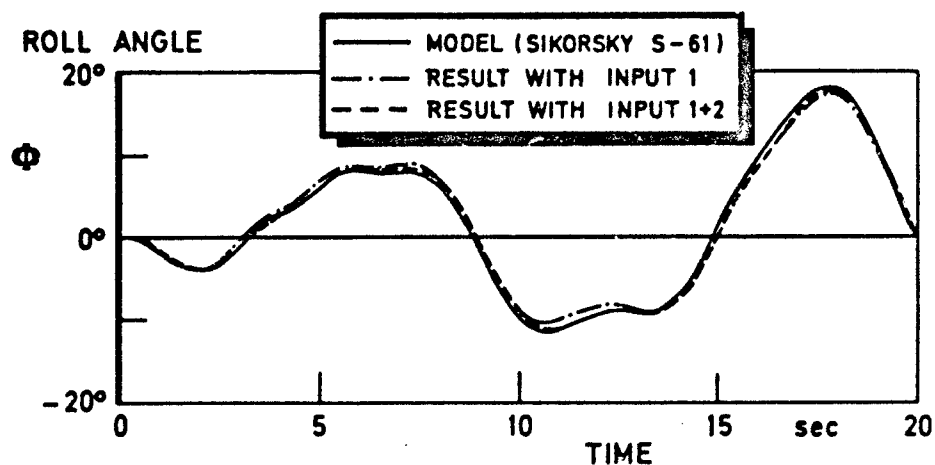


Fig. 17 Example for identification results with different inputs

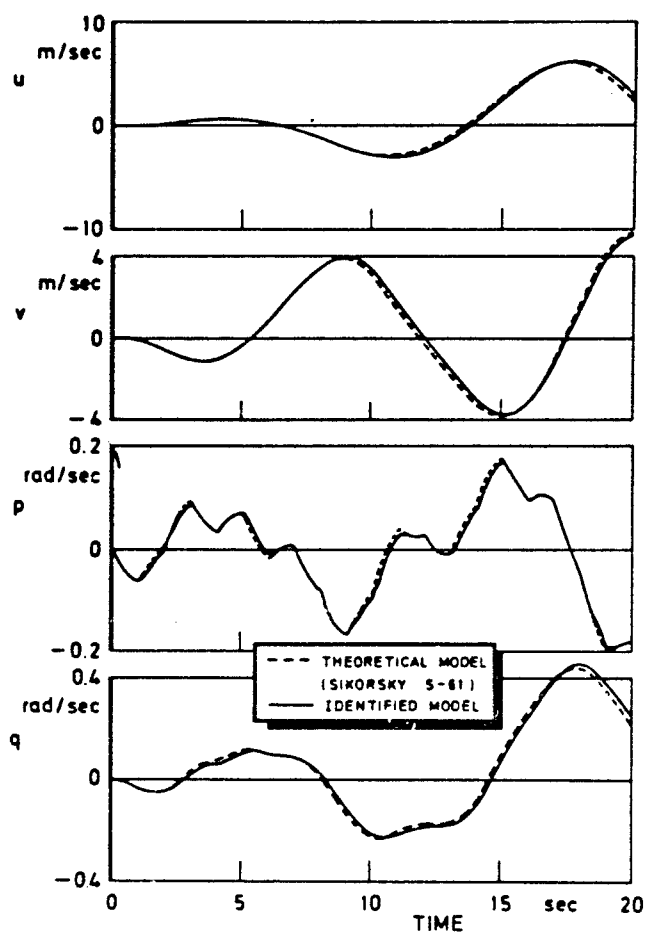


Fig. 18 Identification results from simulated helicopter test data.  
(Simulation: 6-degrees-of-freedom model, identification:  
reduced 4-degrees-of-freedom model)

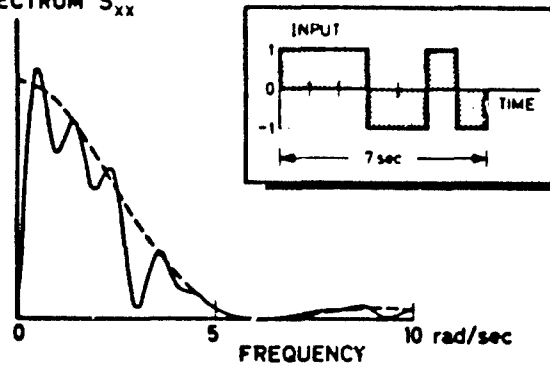
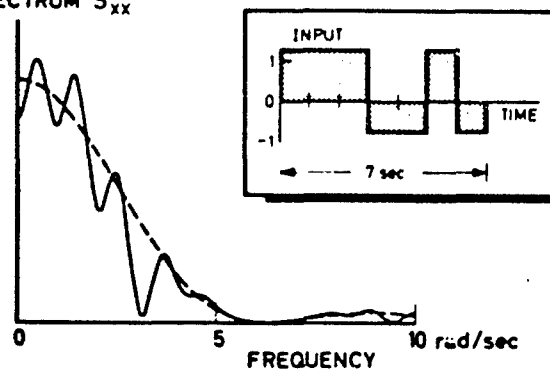
SPECTRUM  $S_{xx}$ 

Fig. 19 Spectrum of random process and short-time input signals

SPECTRUM  $S_{xx}$ 

--- SPECTRUM OF RANDOM PROCESS  
 — SPECTRUM 7-SEC-INPUT

OPTIMUM FREQUENCY RANGES FOR DETERMINATION OF			
$L_p/L_{\delta a}$	$L_p/L_{\delta a}$	$L_p/L_{\delta a}$	$L_{\delta a}$
$L_{\delta a} \delta a$			

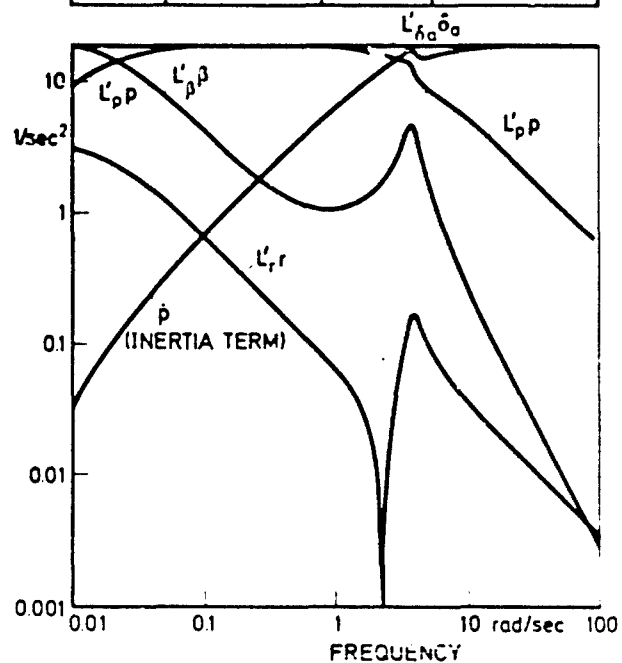


Fig. 20 Bode-plot of rolling moment terms of F-4 aircraft and optimum frequency ranges for the determination of rolling moment derivatives

# A COMPARISON AND EVALUATION OF TWO METHODS OF EXTRACTING STABILITY DERIVATIVES FROM FLIGHT TEST DATA

by

Paul W. Kirsten  
Aerospace Research Engineer  
Air Force Flight Test Center  
Edwards AFB, California, USA

## SUMMARY

Two methods for extracting stability derivatives from flight data are compared. A modified Newton-Raphson minimization technique and a digital-analog (hybrid) matching technique were used to analyze the same data maneuvers obtained from two aircraft. About 55 maneuvers of an F-111E aircraft were analyzed over a Mach number range of 0.3 to 2.0 and an angle of attack range of 3 to 19 degrees. About 15 maneuvers were analyzed for the X-24A lifting body at Mach numbers of 0.8 and 0.9 and an angle of attack range of 4 to 13 degrees. Stability derivatives were extracted from these maneuvers, and the results from the two techniques along with wind tunnel results were compared. The hybrid matching mathematical model contained complete five-degree-of-freedom equations (no velocity derivatives) with variable dynamic pressure, whereas the Newton-Raphson model used uncoupled, three-degree-of-freedom equations with constant dynamic pressure. Both techniques were found to be capable of giving accurate results, but required a fairly extensive knowledge of the method being used. Since the Newton-Raphson technique tends to be less time consuming, it is better suited for processing large quantities of data maneuvers. Hybrid matching is well suited for programs in which a limited amount of data is processed for each flight; or for analyzing maneuvers which are highly coupled or transient in nature; requiring complete five-degree-of-freedom equations.

## LIST OF SYMBOLS

$a_{x_b}$	acceleration along body x-axis (longitudinal)	$p_b$	body axis roll rate
$a_{y_b}$	acceleration along body y-axis (lateral)	$\frac{p_b}{2V_t}$	wingtip helix angle (the helix angle described by a wingtip during a rolling maneuver)
$a_{z_b}$	acceleration along body z-axis (normal)	$q$	dynamic pressure
$b$	reference span	$q_b$	body axis pitch rate
$\bar{c}$	reference length	$r_b$	body axis yaw rate
$c_g$	center of gravity	$S$	reference area
$C_l$	rolling moment coefficient	SAS	stability augmentation system
$C_m$	pitching moment coefficient	$t$	a function of time
$C_{m_0}$	pitching moment coefficient bias	$V_t$	true airspeed
$C_{N_0}$	normal force coefficient	$X_t$	longitudinal force divided by mass
$C_{N_0}$	normal force coefficient bias	$Y$	side force divided by mass and velocity
$C_n$	yawing moment coefficient	$Z$	normal force divided by mass and velocity
$C_y$	side force coefficient	$\Delta$	prefix meaning increment
$D_1$	weighting matrix for measured state parameters	$\alpha$	angle of attack
$D_2$	weighting matrix for <u>a priori</u> estimate vector	$\beta$	sideslip angle
$g$	acceleration due to gravity	$\delta a$	total aileron deflection
$h$	pressure altitude	$\delta c, \delta c_1$	additional control deflection
$I_x$	moment of inertia about the x-body axis	$\delta c_2$	elevator deflection
$I_{xy}$	product of inertia about the x- and y-body axes	$\delta e$	constant control deflection
$I_{xz}$	product of inertia about the x- and z-body axes	$\delta r$	rudder deflection
$I_y$	moment of inertia about the y-body axis	$\theta$	pitch angle
$I_{yz}$	product of inertia about the y- and z-body axes	$\Lambda$	F-111E wing sweep angle
$I_z$	moment of inertia about the z-body axis	$\phi$	bank angle
$J$	cost functional or weighted mean square fit error	Subscripts:	
$L$	rolling moment divided by the moment of inertia about the x-axis	$\delta a, \delta c, \delta c_1, \delta c_2$	partial derivatives
$M$	pitching moment divided by the moment of inertia about the y-axis	$\delta e, \delta r, \delta \theta, p, q, r$	with respect to
$M$	Mach number	$V, \alpha, \beta, \phi, \theta$	subscripted variables
$m$	mass		
$N$	yawing moment divided by the moment of inertia about the z-axis		



## 1.0 Introduction

The importance of aircraft stability and control derivatives in the development and evaluation of a successful aircraft has been recognized for some time. In recent years, highly automated data acquisition systems and advanced derivative extraction techniques have been developed for determining aircraft stability and control derivatives from flight test measurements. These advanced techniques have made possible a more accurate and timely flight test estimation of derivatives than obtainable with previous techniques and have, therefore, made the effort to obtain them more justifiable.

There are three essential elements in the identification of aircraft parameters from flight data:

1. Adequate instrumentation (the right kind of sensors with necessary accuracy) and recording equipment with which to collect the flight data.
2. A proper sequence of flight control inputs (surface deflections) which will excite all the aircraft response modes from which parameters are to be extracted.
3. Algorithms and computer programs to identify the derivatives, their confidence levels, and related effects such as sensor errors and wind gusts.

The last two of these elements are the primary concern of this report. Instrumentation systems will not be discussed in detail. It should be completely understood, however, that the accuracy of the extracted derivatives is a direct function of the accuracy of the instrumentation system used. The accuracy of the weight, balance, and inertia data is equally important of course, as is the measurement of flight conditions (especially dynamic pressure).

Two methods for extracting stability and control derivatives from flight data are compared in this report. A modified Newton-Raphson minimization technique and a digital-analog (hybrid) matching technique were used to analyze the same test maneuvers obtained from two aircraft: an F-111E and an X-24A lifting body.

The main purposes of this study were to (1) compare results from the two methods over a large sampling of similar flight data maneuvers, and (2) to determine the suitability of each program for use on routine stability and control test programs by relatively inexperienced personnel.

This study compared and evaluated two specific existing programs and, not necessarily, the manual matching concept versus the digital Newton-Raphson concept. Improved versions of the Newton-Raphson program used in this study are presently being developed by NASA-FRC and other organizations.

## 2.0 Flight Data Requirements

The flight test parameters that are necessary for the two derivative extraction techniques for the lateral-directional and longitudinal modes are listed in table I.

The requirements for the two techniques are the same except for angle of attack in the lateral-directional mode, dynamic pressure, and coupling between axes. The Newton-Raphson technique uses a constant average  $\alpha$  in its lateral-directional equations in order to keep the computations linear. A variable  $\alpha$  is used in the hybrid matching technique. Dynamic pressure is also considered a constant average value in the Newton-Raphson technique whereas hybrid matching uses the time history of the parameter. Coupling between the longitudinal and lateral-directional axes is accounted for in the Hybrid program and is not accounted for in the Newton-Raphson program.

It is essential that all control parameters be submitted as inputs to the models in both techniques. This includes all control surface deflections such as rudders, ailerons, spoilers, and flaps, reaction control rockets, and any other control input that could have induced motion in the aircraft during the selected time segment.

It is desirable to have time histories of the angular accelerations  $\ddot{p}_b$ ,  $\ddot{r}_b$ , and  $\ddot{q}_b$ . These parameters will add some information in the analysis and may improve the results somewhat. Accurate, high confidence instrumentation for the direct measurement of rotational accelerations has not yet been developed, however, and valid analysis can be made without them.

An accurate set of inertias must be implemented in both techniques. The accuracy of the derivative values are a direct function of how accurately the moments of inertia have been calculated.

Experience has shown that the flight data should be sampled at 50 samples per second for a fighter type aircraft. Lower sampling rates are probably adequate for larger, slower responding aircraft; however, rates below 20 samples per second could produce questionable results due to the inability to accurately define the control surface movement.

TABLE I

Flight Parameter	Newton-Raphson	Hybrid Matching
Lateral-Directional Mode		
Control Parameters	Required Time History	Required Time History
$p_b$	↓	↓
$r_b$		
$\delta$		
$\phi$		
$a_{yb}$		
$a$	Required Constant Average Value	↓
$q_b$		
$\theta$		
$\dot{p}_b$		
$\dot{r}_b$		
	Preferred Time History	Required Constant Average Value Preferred Time History
	↓	↓
Longitudinal Mode		
Control Parameters	Required Time History	Required Time History
$q_b$	↓	↓
$a$		
$\theta$		
$a_{zb}$		
$\dot{q}_b$		
$p_b$	Preferred Time History	Preferred Time History
	Not Used	Required Time History
$r_b$	↓	↓
$\delta$		
$\phi$		
		Constant Average Value

---



---

### Longitudinal Model

---



---

$V_t$ $a_{xb}$	Required time histories in the Newton-Raphson program for an analysis in three-degree-of-freedom in the longitudinal mode. These parameters are not required for a two-degree-of-freedom analysis.
-------------------	----------------------------------------------------------------------------------------------------------------------------------------------------------------------------------------------------

---



---

### Both Modes

---



---

$\eta$  $V_t$  Weight inertias $c_g$ (for $c_g$ corrections to accelerometer data)	Required Constant Average Value  ↓	Required Time History  ↓  Required Constant Average Value
------------------------------------------------------------------------------------------------------	---------------------------------------------	-----------------------------------------------------------------------------

### 3.0 Test Maneuvers

The Newton-Raphson and hybrid matching programs are both capable of analyzing all types of flight test maneuvers or vehicle oscillations, as long as they can be adequately described by the mathematical model of the particular program. Also, both programs can be used to analyze either SAS-off or SAS-on oscillations in the lateral-directional or longitudinal axes. There are, however, considerations to be given to the type of flight test maneuver performed which will lead to the most accurately determined set of stability and control derivatives. These considerations are discussed below.

The type of flight test maneuver used to extract stability and control derivatives is very important. A maneuver which excites all the aircraft response modes and tends to isolate the effects of individual derivatives is highly desirable. A lateral-directional maneuver which has been found to satisfy the above conditions is (figure 2) a sharp rudder input, followed by a control surface fixed (SAS-off) oscillation, and terminated with a sharp aileron input.\* (A similar maneuver is desirable in the longitudinal axis, using longitudinal control surfaces as the forcing functions.) This is the maneuver which was used for all data analyzed in this report. In this type of maneuver, the control derivatives  $C_{l\delta r}$ ,  $C_{n\delta r}$ ,  $C_{y\delta r}$ ,  $C_{l\delta a}$ ,  $C_{n\delta a}$ , and  $C_{y\delta a}$  are most accurately determined at the time of the appropriate sharp control surface input. Sideslip derivatives  $C_{l\beta}$ ,  $C_{n\beta}$ , and  $C_{y\beta}$  and damping derivatives  $C_{l_p}$ ,  $C_{n_p}$ ,  $C_{l_r}$ , and  $C_{n_r}$  are more accurately derived from the free oscillation portion of the maneuver when control surfaces were not influencing vehicle motion. When conditions dictate that this maneuver be performed with augmentation on, the accuracy of the sideslip derivatives may deteriorate somewhat, and the effect of damping derivatives is severely masked by control surface motion.

### 4.0 Analysis Methods and User Comments

#### 4.1 The Hybrid Matching Program

The hybrid matching technique is an extended and improved version of the old analog matching technique which has been used for many years to extract stability derivatives from flight test data (reference 3). The revisions and improvements made to the program provide for a much more accurate estimation of derivatives in significantly less time than the earlier techniques.

---

\* A rudder pulse is performed first since it does not cause a significant angle of attack change on most airplanes. This is important if the derivatives to be identified vary with angle of attack.

In the hybrid program, flight test data is stored directly in the digital computer using magnetic tape. This eliminates the need for tracing flight data curves manually, which results in a considerable savings of time and a completely accurate display of flight data. Flight data are transferred from the digital computer to the analog computer where the equations of motion are solved in a repetitive operation mode (50 times per second). This mode allows the operator to instantaneously see the effect of changing derivatives. The computed response and actual flight response appear simultaneously on an oscilloscope as standing wave time histories. This direct display of flight and computed time histories negates the need for transparent plastic overlays of the flight data, thereby eliminating the considerable amount of parallax and distortion which is associated with using overlays. Stability and control derivatives are then manually varied until the computed solution matches the flight data as closely as possible. Thus, all of the logic in the hybrid matching technique is supplied by the human operator.

The hybrid program has an important feature of uncoupling the equations of motion, which allows the operator to more clearly see the effect of changing individual derivatives and therefore, more rapidly arrive at an initial estimation of the derivatives. Uncoupling the equations of motion is accomplished by using the measured flight time histories of the response parameters  $p_b$ ,  $r_b$ ,  $q_b$ ,  $\alpha$ ,  $\beta$ , and  $\phi$  as well as the control surface time histories in the equations. Equations of motion for both programs are contained in Figure 1. Therefore, the only variables in each equation are the stability and control derivatives. The effect of each derivative is isolated to one equation, which allows the operator to more clearly see the result of changing one particular derivative on the computed response of the vehicle. (There are some interaction effects due to the  $I_{xz}$  terms in the equations. However, since  $I_{xz}$  is usually a relatively small quantity, these effects are insignificant.) In this matter, the roll derivatives  $C_{l\beta}$ ,  $C_{l\delta_a}$ ,  $C_{l\delta_r}$ ,  $C_{lp}$ , and  $C_{lr}$  are obtained by analyzing the  $\dot{p}_b$  equation. The yaw derivatives  $C_{n\beta}$ ,  $C_{n\delta_a}$ ,  $C_{n\delta_r}$ ,  $C_{nr}$  are obtained from the  $\dot{r}_b$  equation. Side force derivatives  $C_{y\beta}$ ,  $C_{y\delta_r}$ , and  $C_{y\delta_a}$  are derived through the solution of the  $\dot{a}_{yb}$  equation. In the longitudinal mode,  $C_{m\alpha}$ ,  $C_{m\delta_e}$ , and  $C_{mq}$  are obtained from the  $\dot{q}_b$  equation and  $C_{N\alpha}$  and  $C_{N\delta_e}$  from the  $\dot{a}_{zb}$  equation.

After the best comparison between computed results and flight values is obtained in the uncoupled mode, the computer model is switched to the coupled mode and refinement of the match of the computed solution to flight values is performed (if necessary). In the fully coupled lateral-directional mode, the  $p_b$ ,  $r_b$ ,  $\beta$ , and  $\phi$  terms in the  $\dot{p}_b$ ,  $\dot{r}_b$ , and  $\dot{\beta}$  equations are computed solutions rather than flight values. The pitch rate and angle of attack terms in these equations remain flight data. In the coupled longitudinal mode, the  $q_b$  and  $\alpha$  terms in the  $\dot{q}_b$ ,  $\dot{\alpha}$ , and  $\dot{a}_{zt}$  equations are computed solutions. The lateral-directional terms,  $p_b$ ,  $r_b$ ,  $\beta$ , and  $\phi$  remain flight values.

#### 4.2 The Modified Newton-Raphson Technique

The modified Newton-Raphson technique used for extracting stability and control derivatives by the AFFTC was developed by Kenneth W. Iliff and Lawrence W. Taylor Jr., at the NASA Flight Research Center. The technique is thoroughly described in references 5 and 6. The computer program used at the AFFTC is but one version using the Newton-Raphson technique and the comments in this report on the Newton-Raphson method pertain only to this specific version. In this section, a brief discussion of the basic algorithm is given, along with the main features of the program.

The Newton-Raphson program used for this study is a maximum likelihood estimator which uses a modification of the Newton-Raphson algorithm to identify the unknown coefficients in a set of linear differential equations. The equations of motion mechanized by the Newton-Raphson program are listed in Figure 1.

The technique computes time histories using an initial set of derivatives (usually wind tunnel), and compares these calculated time histories with flight measured time histories. From this comparison a mean squared error is obtained and put in the form of a cost function,  $J$ . The object of the Newton-Raphson algorithm is to vary the unknown coefficients (stability and control derivatives) in the equations of motion in such a way as to reduce the cost function,  $J$  to a minimum. This is equivalent of finding where the gradient of  $J$  ( $\nabla J$ ) is zero. The program relates  $\nabla J$  as a function of the set of unknown coefficients and changes these coefficients, using the Newton-Raphson method, until the gradient is zero. The Newton-Raphson method is an iterative process in which a new estimate of the vector of unknown coefficients is dependent on the old estimate and the derivative of the function at the old value. Therefore, the complete Newton-Raphson algorithm contains the derivative of the function  $\nabla J$  which means that second gradients ( $\nabla^2 J$ ) are involved. This algorithm produces rapid convergence to the minimum of  $J$  usually in from four to six iterations. However, the second gradient of  $J$  is very difficult and time consuming to calculate on a digital computer. Therefore, a modification has been made in the second gradient of  $J$  so that no second order terms are included in the computation. Thus, what is used is a modified Newton-Raphson technique.

The modified Newton-Raphson program contains several weighting features which allow the user to have some control over the matching process. These weighting features account for instrumentation noise in the measured parameters, allow the use of a priori information on the derivatives, and permit any derivative to be fixed if it is not involved in a maneuver.

The  $D_1$  matrix is a diagonal weighting matrix whose elements correspond to the flight state parameters. The purpose of the  $D_1$  matrix is to weight the individual flight parameters so that the program will match each parameter equally to account for the amount of measurement noise in any particular channel. From two to four runs of the program are necessary to determine satisfactory  $D_1$  weightings. Once a set of  $D_1$  weightings has been determined for a particular aircraft, they should not have to be changed for subsequent maneuvers as long as the instrumentation system remains the same.

The program contains an a priori feature which allows the use of independent estimates of the unknown coefficient from wind tunnel, previous flight data, or any other source. These a priori estimates may be used as starting values in the program and, during each iteration, the changes that are made to improve the fit are weighted against the deviation from these starting estimates. The addition of a priori information into the program generally results in the extraction of better overall estimates of derivatives but must be used carefully.

The a priori feature contains a weighting matrix ( $D_2$ ) whose elements correspond to each of the unknown coefficients. These weightings correspond to the relative confidence placed in the starting values of the derivatives. If wind tunnel data are used for the starting values, the  $D_2$  matrix allows the user to account for differences in wind tunnel accuracy for different derivatives. For example, high weighting (high accuracy) for  $C_{L\delta}$ , but low weighting (low accuracy) for  $C_{Np}$ .

The program computes a set of confidence levels for the calculated coefficients. To assess the validity of these coefficients, a Cramer-Rao bound is used which estimates their error covariance matrix of the calculated coefficients. This process is described in detail in reference 6. Confidence levels are discussed further in the section entitled " $D_2$  Weightings and Confidence Levels Study."

#### 4.3 Basic Program Structures and Differences

There are basic program differences between the two methods which should be discussed. The most important difference is the role of the human operator. In the hybrid matching process, the human operator is directly involved in the derivative computation. He manually changes the stability and control derivatives until the desired match between the computed solution and flight data is obtained. He, therefore, supplies all the logic inherent in the hybrid matching process. Although the Newton-Raphson technique does not use the human operator in the actual derivative extraction process, the effective use of the program requires a comparable level of knowledge and experience in the selection of weighting functions and use of the a priori option.

Having the human operator directly involved in the derivative extraction process has important advantages which should be incorporated into any good all-digital technique. These advantages include:

1. The human operator supplies engineering judgement to the program to obtain the desired match between computed and flight data. Good engineering judgement would include eliminating or concentrating less on flight data which contained noise, wild data points, extraneous inputs (wind gusts, etc.), or changes in flight conditions (such as angle of attack) which may occur during a maneuver.
2. The human operator can vary the weighting of individual derivatives throughout a particular maneuver. If pulse type maneuvers are performed which isolate the effects of individual derivatives, the operator can obtain the value of those derivatives at the appropriate time during the maneuver when the effects of the derivatives are most pronounced upon the motion of the vehicle. Thus, control surface derivatives will generally be obtained at the time of the corresponding control surface pulse input. Sideslip and damping derivatives will be most heavily weighted during the free, or SAS-on, oscillation of the vehicle.

3. A level of accuracy can be assigned to individual derivatives and the entire maneuver in general by the human operator. It is important that accuracy levels are known, since many maneuvers do not contain sufficient information, or do not isolate the effects of individual derivatives adequately to give an accurate estimation of the value of the derivative. Also, if a maneuver contains little information about a particular derivative, the operator can hold that derivative at its wind tunnel or estimated value. In this manner, he supplies a priori information to the program.

Thus, the role of an experienced individual is extremely important to a derivative extraction technique. The purpose of developing an all digital extraction technique would be to do the job of the human operator more quickly and more accurately, if possible, while still retaining the logic he supplies.

The Newton-Raphson program contains logic which allows individual measured flight parameters to be weighted in such a manner to account for instrumentation noise. However, wild data points and extraneous inputs may severely degrade the results of the program and must be corrected external to the program.

The Newton-Raphson program does not have provisions for time-varying weighting of derivatives, thus the logic described above is not explicitly available in the program. However, the logic is accomplished to a certain degree in that there is more information available in the maneuver to establish values for the control derivatives at the time of the sharp control inputs.

A measure of the accuracy of individual derivatives (confidence levels) is produced by the Newton-Raphson program. A discussion of the adequacy of these confidence levels is given later in this report. The program does have logic which allows starting values to be assigned to each derivative and assigns an individual weighting to each derivative which reflects the relative confidence in the starting values. This logic allows an individual derivative to vary from its starting value, if sufficient information is contained in a maneuver for that particular derivative, and holds it near its starting value when little information is available.

The mathematical models of the Newton-Raphson and hybrid matching programs differ considerably. Equations of motion for the two programs are contained in Figure 1. The Newton-Raphson program uses three-degree-of-freedom equations which completely uncouple the longitudinal and lateral-directional axes. The program also makes small angle approximations in the  $\alpha$  and  $\beta$  equations. (Compare the Newton-Raphson and hybrid equations in Figure 1.) The hybrid matching mathematical model contains complete five-degree-of-freedom equations (no velocity derivatives) which account for coupling effects between axes. The hybrid model does not assume small angle approximations. The hybrid matching model uses a variable dynamic pressure, while dynamic pressure is a constant in the Newton-Raphson program. Neither program accounts for structural flexibility effects. Thus, for an aircraft with significant aeroelastic effects the derivatives obtained are valid only for the flight condition (dynamic pressure and loading) under investigation. The equations of motion of the Newton-Raphson program are adequate for analyzing most flight test maneuvers because they are usually performed under nearly steady state conditions with little coupling between axes. However, maneuvers which are highly coupled and/or transient in nature or which include large attitude excursions would require complete five-degree-of-freedom equations with variable dynamic pressure.

Both techniques assume linear derivatives. Thus, the derivative obtained is the local slope of the force or moment coefficient with respect to a particular variable. It is a linear value for the flight condition under investigation. In actuality, derivatives may not be linear functions. For example,  $C_{n\beta}$  may be a nonlinear function of  $\beta$ . If  $C_{n\beta}$  is nonlinear in the range of  $\beta$ 's experienced during the flight maneuver investigated, it may be difficult to obtain a good match using a linear function. Another example is  $C_{m\alpha}$  which is often a nonlinear function of angle of attack. If a pitch pulse is performed in a region of nonlinear  $C_{m\alpha}$ , the linear computed response will not match the flight response. There are several options for analyzing maneuvers of this type:

1. A nonlinear function can be programmed into the mathematical model if the form of the function is known.
2. The maneuver can be analyzed in sections (at different  $\alpha$ 's or  $\beta$ 's) to obtain a different derivative value for each section.

3. A single value can be obtained for the entire maneuver which is an average value for the angle of attack (or angle of sideslip) range traversed. Different size input pulses may be performed to obtain the relationship between the derivative value and the amplitude of the state variable.

It is important that the data be recorded accurately. Both programs can account for biases in the data and instrumentation noise. However, data dropouts, large discontinuities, or spikes severely degrade the results in the digital Newton-Raphson analysis. In the hybrid matching technique, the human operator can account for such data discontinuities by ignoring extraneous points except for discontinuities in the control position measurements which are direct inputs to the model. It is important that all flight data not contain phase shifts.

It is important to perform the flight test maneuvers at relatively constant Mach number and angle of attack because derivatives may be strong functions of these parameters. If the Newton-Raphson technique is used, it is doubly important to maintain a constant angle of attack since the lateral-directional coupling equations use constant angle of attack in the computations in addition to the potential derivative variation with  $\alpha$ . Also, relatively constant dynamic pressure is desirable during the maneuver if the airplane under investigation is flexible and/or if the Newton-Raphson program, which assumes constant dynamic pressure, is used. If the hybrid matching program is used, maintaining relatively constant Mach and angle of attack during the maneuver are the only conditions which must be satisfied. That is, the airplane does not need to be at level, 1-g flight when the pulse maneuver is performed. A nicer, more analyzable, pulse will probably result if the initial rotational rates are near zero, however. If the Newton-Raphson program is used, in addition to the conditions of constant Mach number, angle of attack, and dynamic pressure, the small angle approximations contained in the equations must be considered. For example, the term  $\sin \phi$  in the  $\delta$  equation is approximated by the angle  $\phi$  in the Newton-Raphson program.\* If the airplane goes through a large bank angle change when the maneuver is performed, this term will be inaccurate. However, the effect of this term is small when the velocity is large, and the inaccuracies produced by the small angle approximation can possibly be ignored under these conditions.

#### 4.4 Equipment and Manpower Resources

One operator who is familiar with both digital and analog computers (as well as experienced in extracting derivatives) is required to run the hybrid matching program. Training requirements vary from individual to individual, of course, and the learning process never ends. However, it is felt that analyzing approximately 20 test maneuvers would provide sufficient experience to become proficient in derivative extraction using the hybrid technique.

The time to analyze and obtain a set of stability and control derivatives for a particular flight test maneuver, although difficult to assess, may differ considerably between the two programs. The average time required for an experienced operator to obtain a set of derivatives, and accuracy levels for the derivatives, using the hybrid matching program is approximately 45 minutes (including computer setup time for the individual maneuver). The digital computer run time required to analyze one flight maneuver using the Newton-Raphson program is approximately four minutes. An additional 10 to 15 minutes per maneuver is required for setup time. Hence, the time to analyze one maneuver, assuming one entry into the computer, is considerably less for the Newton-Raphson program than for the hybrid matching program. The hybrid program is an on-line operation however, and when results are obtained (in the 45-minute time period) they are final results and are not rerun unless additional test information becomes available (i.e., revised inertias, instrumentation calibrations, etc.). The adequacy of the results of the Newton-Raphson program are not known completely until the time histories of the computed and flight data match are received from the computer. If the results are not adequate (see below), the maneuver must be rerun. Thus, although the actual computer run time is minimal, the total time required to obtain optimum results for some maneuvers may be longer. It should be noted that the time per case for hybrid matching does not change as a function of number of cases. The time per case decreases considerably for the Newton-Raphson program as the number of cases is increased.

\* If the airplane oscillates around a bank angle other than zero, this term can be replaced by  $\phi \sin \phi_{av}$  where  $\phi_{av}$  is the average value of  $\phi$  during the maneuver. Thus only the perturbation of  $\phi$  around the average  $\phi$  will be an approximation.

The above discussion assumes that the weighting matrices used in the Newton-Raphson program have been established for a particular airplane. It also assumes that the source data tapes have been edited and transferred to the proper format and computer language to be compatible with each of the analysis programs. This process, although required only once per test program, has proven to be both frustrating and time consuming.

A level of experience comparable to that needed for hybrid matching is required to effectively use the Newton-Raphson program. Most of the experience required is in establishing and using the weighting matrices and interpreting the results of the program.

Assuming a minimum amount of resubmitting data into the computer, the Newton-Raphson program tends to be less time consuming than the hybrid matching technique. It is, therefore, better suited for processing large quantities of data maneuvers. Hybrid matching is more applicable for programs in which a limited amount of data is processed for each flight than it is for programs in which large amounts of data are processed, or for analyzing maneuvers which are highly coupled or transient in nature requiring complete five-degree-of freedom equations.

## 5.0 Discussion of Flight Test Results

### 5.1 F-111E and X-24A Data

Stability and control derivatives obtained using the Newton-Raphson and hybrid matching techniques are presented, along with wind tunnel data, for the F-111E aircraft and the X-24A lifting body. All derivatives presented in these figures are body axis derivatives. The F-111E data are presented as a function of angle of attack at Mach numbers of 2.0, 1.6, 1.4, 1.2, and 0.8 for a wing sweep of 50 degrees. The X-24A data are presented as a function of angle of attack at Mach numbers of 0.9 and 0.8.

Only lateral-directional data are presented. The F-111E flight test program was a lateral-directional study and no longitudinal maneuvers were performed. In the X-24A flight test program, the lateral-directional mode was of primary concern (as it is with most airplanes) and only a limited amount of longitudinal data was obtained. Both techniques have longitudinal modes which have been successfully used on flight test programs. Since the longitudinal mode is not as complex as the lateral directional mode, it is generally more easily analyzed (except when the airplane has nonlinear derivatives such as  $C_{mq}$ ).

There were many questionable aspects of the F-111E program which caused uncertainties in the extracted derivatives. The wind tunnel data was somewhat questionable since it was rigid model data which had analytically flexibilized corrections applied (for some derivatives these corrections were quite large). Also, wind tunnel data for the clean configuration did not include possible effects of trim control surface setting (such as the effect of elevator deflection on sideslip and aileron derivatives). Accuracy of the recorded flight data was not known. Also, the recorded flight data was of poor quality and contained many wild points. The accuracy of the moments of inertia and their variance with fuel consumption were unknown. Finally, the airplane motions were rather heavily damped with the SAS on. Most of the maneuvers analyzed were SAS-on maneuvers. The accuracy of the extracted derivatives is less under these conditions.

The uncertainties discussed above may explain the scatter which is present in the extracted derivatives for the F-111E, and the lack of comparison with wind tunnel data. They would be expected to have a like effect upon both techniques, however, and it is therefore valid to compare the results of the two techniques with each other without qualification. X-24A data is also presented in this report since more confidence is expressed in the quality of the flight data than in the F-111E data. The uncertainties which were present in the F-111E flight test program were minimized in the X-24A program.

#### 5.1.1 Sideslip Derivatives

##### 5.1.1.1 F-111E

Sideslip derivatives  $C_{l\beta}$  and  $C_{n\beta}$  are shown in figure 3, for 50 degrees of wing sweep.\* The significant fact is that comparison between the two derivatives extraction techniques, except for a few instances, is very good.

\*Side force derivatives are not presented in this report since the location of the lateral accelerometer was not accurately known for the F-111E. Also, these derivatives are secondary derivatives and have minor influence on the airplane's response.



Comparison between the extracted derivatives and wind tunnel data for  $C_{l\beta}$  was not particularly good in many instances. There was an unusual amount of scatter in the flight-derived values of  $C_{l\beta}$  at similar flight conditions. Part of this scatter may be explained by the fact that the airplane was heavily damped in roll with the SAC on, which may have degraded the extracted values some. However, the scatter was repeatable in both extraction techniques.

Scatter in the flight values of  $C_{n\beta}$  was low, and agreement between the two extraction techniques was again good. However, the flight-derived values of  $C_{n\beta}$  were much lower than wind tunnel data in most cases. Note that the wind tunnel data was obtained at Mach numbers of 2.0, 1.2, and 0.8. The wind tunnel data shown in the figures at Mach = 1.0 and 1.4 were interpolated from the Mach = 2.0 data and the Mach = 1.2 data. The wind tunnel data at Mach = 1.2 was obtained from a different wind tunnel than the other data, and gave considerably higher values of  $C_{n\beta}$  than data at the other Mach numbers. Also, flight-derived values of  $C_{n\beta}$  have been lower than wind tunnel data in the transonic region on other flight test programs (including the X-24A program).

#### 5.1.1.2 X-24A

Flight results and wind tunnel data for the X-24A sideslip derivatives are presented in figure 7. Agreement between the two extraction techniques was good in most cases. The comparison of flight and wind tunnel data was good for  $C_{l\beta}$ . As in the case of the F-111E, flight results for  $C_{n\beta}$  at Mach = 0.9 were lower than wind tunnel data.

#### 5.1.2 Aileron Derivatives

##### 5.1.2.1 F-111E

Aileron control derivatives for the F-111E are presented in figure 4. Agreement between the two techniques was good in most cases, except at Mach = 2.0 where the hybrid matching results for  $C_{l\delta_a}$  were consistently higher than the Newton-Raphson results. At all Mach numbers, the flight-derived values of  $C_{l\delta_a}$  for both techniques were somewhat higher than wind tunnel data. It is felt that the position of the horizontal tail may have an effect upon the value of the aileron derivatives. If this effect exists, it is not included in the wind tunnel data. Flight results for  $C_{n\delta_a}$  compare reasonably well with wind tunnel data.

##### 5.1.2.2 X-24A

Flight results and wind tunnel data for the X-24A aileron derivatives are shown in figure 8. Comparison between the results of the two techniques with each other and with wind tunnel data is reasonably good in most cases.

#### 5.1.3 Rudder Derivatives

##### 5.1.3.1 F-111E

Rudder control derivatives for the F-111E are given in figure 5.  $C_{l\delta_r}$  is an extremely ineffective control derivative and very difficult to accurately obtain from flight data. In contrast,  $C_{n\delta_r}$  is a very effective derivative, and flight-derived data should be accurate for maneuvers which contain sharp rudder inputs. In most cases, the results of the two techniques compare very well with each other for this derivative. The comparison between computer and wind tunnel data is good at supersonic Mach numbers. At 0.8 Mach number, computer values are consistently lower than wind tunnel data.

##### 5.1.3.2 X-24A

X-24A rudder derivatives are shown in figure 9. Comparison between the two techniques with each other and with wind tunnel data is good except for a few Newton-Raphson cases at Mach = 0.9 and angles of attack around 12 degrees. In some of these cases, the computed Newton-Raphson response did not match the flight response well at the time of the sharp rudder input. It is felt that if the weighting on  $C_{n\delta_r}$  were increased during this short time period, the match would have improved and the computed value of  $C_{n\delta_r}$  would have increased. Variable derivative weighting logic would possibly be an improvement to the Newton-Raphson program, especially when analyzing pulse-type test maneuvers where the primary effect of the control surfaces is restricted to a small segment of time in the maneuver.

### 3.1.4 Damping Derivatives

Damping derivatives for the F-111E and X-24A are presented in figures 6 and 9. It is extremely difficult to accurately extract damping derivatives from flight data when the data contains the inputs of an effective stability augmentation system. A concentrated effort was not made to obtain F-111E damping derivatives using the hybrid matching technique. The only damping derivative which was obtained (for some maneuvers) was  $C_{Lp}$ , which is the most effective damping derivative for most airplanes. When damping derivatives could not be extracted from a maneuver, they were held at their predicted value in the hybrid matching program. When using the matching program, it is quite obvious when there is insufficient information present to define a particular derivative (very little change in response is observed when the derivative is varied over a wide range).

Numerical values for the damping derivatives are given for all maneuvers analyzed by the Newton-Raphson technique. It is important to understand that these values may be heavily weighted toward the initial starting value of the derivative used in the program. In other words, there is logic in the Newton-Raphson program (as in the hybrid program) which holds a derivative at or near its starting value (which is the predicted or estimated value that the operator enters into the program) if no information is contained in the maneuver for that particular derivative. This is desirable logic to have in the program. However, it is important to differentiate between accurately determine derivative data points which were, in fact, quite close to predictions, and derivative data points which were merely left at the predicted value because there was no information present in the test maneuver. This will be discussed in detail in the next section.

The consistency in the values of  $C_{Lp}$ , and possibly  $C_{np}$ , as a function of angle of attack indicates that these derivatives can probably be determined with reasonable accuracy for both airplanes. The overall scatter in the values of  $C_{Lp}$  and  $C_{np}$ , and the fact that the operator using the hybrid program could determine values for only a few maneuvers, indicates that these derivatives are difficult to extract and accurate values cannot be obtained. Whether or not the consistency in the Newton-Raphson values of  $C_{Lp}$  and  $C_{np}$  was caused by these derivatives being too heavily weighted will be discussed in the next section.

### 3.2 $D_2$ Weightings and Confidence Levels Study

Five F-111E maneuvers at a wing sweep of 50 degrees and 0.8 Mach number which ranged in angle of attack from 8.8 to 18.1 degrees were analyzed extensively in an attempt to understand and validate the a priori ( $D_2$ ) weightings and the confidence levels obtained from the Newton-Raphson program. All derivatives presented in this section will be dimensional and in the principle axis. This is because the program prints out the confidence levels in this form and part of the purpose of this study is to relate the final derivatives to the confidence levels. Each of the five maneuvers was run four times, (1) with a a priori weightings using wind tunnel values as starting derivatives, (2) without a a priori weightings using wind tunnel values as starting derivatives, (3) with a a priori weightings using starting derivatives that were double wind tunnel values, and (4) without a a priori weightings using starting derivatives that were double wind tunnel values.

Figure 11 compares the final derivatives for conditions 1 and 3. Also included on this plot are envelopes representing the data from figure 12 which compares final derivatives for conditions 2 and 4 (without a a priori weighting).

From these comparisons the validity of the  $D_2$  weightings, the validity of the confidence levels, and the relative amount of information contained in the maneuvers for each derivative can be determined.

The major derivatives  $L_B$ ,  $N_B$ ,  $L_{\delta a}$ ,  $N_{\delta a}$ , and  $N_{\delta r}$  show consistent results and good comparisons between final derivatives that started with wind tunnel derivatives and those that started with doubled wind tunnel derivatives (figure 12). This indicates a great deal of information available for these derivatives since consistent results are obtained even without a a priori weightings. The only exceptions would be  $L_B$ ,  $L_{\delta a}$ , and  $N_{\delta a}$  for the maneuver at  $\alpha=8.8$  degrees. This maneuver was a SAS on rudder doublet only (no aileron doublet), and contained less information for these derivatives. This maneuver is discussed in more detail later.

These same derivatives show generally good comparisons (with the exception of the maneuver at  $\alpha=8.8$  degrees) for conditions 1 and 3 with a priori weightings as illustrated in figure 11. In the same figure, envelopes have been drawn representing the no a priori data from figure 12. The data run with a priori weightings generally fell within or close to these envelopes. The fact that the final derivative values in all cases investigated were similar, and the fact that there was consistency as a function of  $\alpha$  indicates that the  $D_2$  weightings are correct for  $L_{\delta}$ ,  $N_{\delta}$ ,  $L_{\delta\alpha}$ ,  $N_{\delta\alpha}$ , and  $N_{\delta r}$ .

The relatively ineffective control derivative  $L_{\delta r}$  has a great deal of scatter as a function of  $\alpha$  without a priori weighting (figure 12) which indicates that very little information was contained in the maneuvers for this derivative. In figure 11, final  $L_{\delta r}$  points that started with wind tunnel values, compare well with final points that used starting values that were double wind tunnel. All points fell within or close to the envelope of no a priori data. However, because the data are severely scattered even with a priori weighting it is felt that the  $D_2$  weighting on  $L_{\delta r}$  should be increased.

The damping derivatives  $N_p$  and  $L_p$  show consistent results with  $\alpha$  and with the two different starting values without a priori weightings in figure 12. This means that information was available for those two derivatives in the maneuvers analyzed. A priori weighting seemed to increase the scatter between the final results for the two different starting values considerably in the values for  $N_p$  (figure 11), so it looks like the  $D_2$  weighting for this derivative should be reduced. Figure 3 also shows that the matched values for  $L_p$  that used double wind tunnel derivatives for starting values are biased from the no a priori envelope. This indicates that the  $D_2$  weightings should probably be reduced for this derivative. It is apparent that the  $D_2$  weighting is too large since the matched derivatives under condition 3 are staying close to the starting values and incorrectly biasing the results from the no a priori envelope.

The damping derivatives  $N_r$  and  $L_r$  show a great deal of scatter with  $\alpha$  without a priori weightings (figure 12), indicating little or no information probably because  $r$  is small. With a priori weighting (figure 11) the data are still very scattered with  $\alpha$  and the matched derivatives run under condition 1 do not compare well with those run under condition 3. Therefore, the  $D_2$  weightings for  $N_r$  and  $L_r$  should be increased to give more consistent results and hold the matched values closer to the starting numbers since little information is available.

Confidence levels obtained for the five maneuvers are shown in figure 12. Confidence levels obtained from the version of the Newton-Raphson program used in this study are valid only when a priori is not used. If a priori weighting is used, the confidence levels obtained are influenced by the weighting factor which is assigned to the derivative and are not solely a measure of the amount of information contained in the maneuver for that derivative. A recent version of the Newton-Raphson program has been developed (by NASA-FRC) in which confidence levels can also be obtained when the a priori option is used. Also in this version of the program, confidence levels are given in non-dimensional form. These are significant improvements to the program.

Confidence levels shown in the figures are values obtained from the Newton-Raphson program multiplied by a factor of ten. This is necessary since the confidence levels are only a relative measure of the accuracy of each derivative. Experience has shown that multiplying the confidence levels of the program by a number that is between 5 to 10 converts that values to meaningful numbers that can be associated with derivative values.

Comments obtained by visual inspection of the resultant time histories of each of the five maneuvers are listed below. These comments should be useful in analyzing and determining the validity of the confidence levels.

<u>Maneuver</u> <u><math>\alpha</math></u>	<u>Type of</u> <u>Maneuver</u>	<u>SAS</u>	<u>Quality of Match</u>
8.8	$\delta r$ only	ON	Good overall match
9.1	$\delta r$ only	OFF	Very good overall match
14.7/10.0	$\delta r, \delta a$	ON	Good P match, fair $\beta$ match, poor R match
18.0	$\delta r, \delta a$	ON	Good overall match
18.1	$\delta r, \delta a$	ON	Fair overall match - $C_{L\delta r}$ Appears too high and $C_{N\delta r}$ appears too low

The maneuver at  $\alpha=8.8$  degrees was a good overall match but was a SAS on rudder doublet only (no aileron doublet was performed during the maneuver). Thus, the ailerons were only moving through the SAS commands, and the resulting aileron derivatives should be less accurate than those obtained from aileron doublets. Also, since the ailerons of the F-111 produce larger  $\beta$  excursions and more roll rate than the rudders, one would expect  $L_{\beta}$ ,  $L_p$ , and probably  $N_p$  to be less accurate for this maneuver. And indeed, the confidence levels for  $L_{\beta}$ ,  $L_p$ ,  $N_p$ ,  $L_{\delta a}$ , and  $N_{\delta a}$  are large for this maneuver in comparison to the other maneuvers.

The maneuver at  $\alpha=9.1$  degrees was a SAS off rudder doublet only. (Since the ailerons did not move during this SAS off maneuver, aileron derivatives were held fixed and are therefore, not presented). Since this was a very good SAS off match, one would expect all the derivatives, and especially the damping derivatives, to be more accurate for this maneuver. This is verified by the confidence levels which are, for all derivatives, lower for this maneuver than any other maneuver.

There was a poor match of yaw rate for the maneuver at  $\alpha=10$  degrees (14 degrees for  $L_{\beta}$ ), indicating that  $N_{\beta}$ ,  $N_{\delta a}$ ,  $N_{\delta r}$ ,  $N_r$ , and  $N_p$  may not be accurate for this maneuver.  $N_{\delta r}$  and  $N_r$  do not compare well with the other maneuvers when plotted as a function of  $\alpha$  as in figure 12. Confidence levels for  $N_{\delta a}$ ,  $N_{\delta r}$ , and  $N_r$  are comparatively large for this maneuver, but do not seem to be as large as they should considering the poor quality of the match of yaw rate.

The maneuver at  $\alpha=18$  degrees gave a good overall match, and confidence levels for all derivatives were indeed low.

The maneuver at  $\alpha=18.1$  degrees was viewed as a fair match and confidence levels were also generally fair. In particular,  $L_{\delta r}$  was felt to be high and  $N_{\delta r}$  low (by looking at the printed time-history of the match).  $L_{\delta r}$  was higher and  $N_{\delta r}$  was lower, for this maneuver than for the maneuver at  $\alpha=18.0$  degrees which gave a good match. However, confidence levels for these derivatives were not as large as it would seem they should be.

In summary, confidence levels for the five maneuvers analyzed seemed to be a representative estimate of the accuracy of the associated derivatives in most instances. However, in a few instances where parameters were poorly matched, confidence levels were not as large as it seemed they should have been. Although more investigation in this area is necessary before complete confidence can be given to the confidence levels produced by the Newton-Raphson program, preliminary results obtained from this small study are encouraging.

## 6.0 Conclusions

Flight derived values of the derivatives obtained using all-digital Newton-Raphson technique and the hybrid matching technique agreed well with each other for most cases analyzed. This indicates that if accurate input data are supplied to the two programs, and the right types of maneuvers are analyzed, both programs are capable of extracting accurate derivatives from flight test data.

The results of the two programs did not compare well with wind tunnel predictions in several instances. For example, there was definite disagreement between flight values and wind tunnel predictions of  $C_{D\delta}$  in the transonic region.

Final derivative values obtained from the Newton-Raphson program are relatively insensitive to starting values if a priori weighting is not assigned to the derivatives. If a priori is used, final values may be sensitive to starting values.

Confidence levels produced by the Newton-Raphson program seem to be a representative estimate of the accuracy of the associated derivatives in most instances. More extensive evaluation of these confidence levels is needed however.

At the present time, both techniques require a fairly extensive knowledge of the method being used and could produce misleading or meaningless results if applied by an inexperienced operator.

## References

1. Kirsten, Paul W., Wind Tunnel and Flight Test Stability and Control Derivatives for the X-24A Lifting Body, FTC-TD-71-7, Air Force Flight Test Center, Edwards AFB, California, April 1972.
2. Lauber, Larry F., Captain USAF, Hofeldt, John H., First Lieutenant USAF, and Ulmer, Lon C., A Hybrid Computer Program to Obtain Stability Derivatives from Flight Test Data, FTC-TIM-70-1011, Air Force Flight Test Center, Edwards AFB, California, February 1971.
3. Rappy, John M., First Lieutenant USAF, and Berry, Donald T., Determination of Stability Derivatives from Flight Test Data by Means of High Speed Repetitive Operation Analog Matching, FTC-TDR-64-8, Air Force Flight Test Center, Edwards AFB, California, May 1964.
4. Hood, Frank C., Gobert, Don O., and Winters, Charles P., F-111E Flying Qualities Tests, FTC-TR-72-44, Air Force Flight Test Center, Edwards AFB, California, November 1972.
5. Taylor, Lawrence W., Jr., and Iliff, Kenneth W., Systems Identification Using a Modified Newton-Raphson Method-- a Fortran Program, NASA-TN-D-6734, NASA, May 1972.
6. Iliff, Kenneth W., and Taylor, Lawrence W., Jr., Determination of Stability Derivatives from Flight Data Using a Newton-Raphson Minimization Technique, NASA-TN-D-6759, NASA Flight Research Center, Edwards, California, March 1972.
7. Kirsten, Paul W., and Ash, Lawrence G., A Comparison and Evaluation of Two Methods of Extracting Stability Derivatives From Flight Test Data, AFFTC-TD-73-5, Air Force Flight Test Center, Edwards AFB, California, May 1974.

## Acknowledgement

The authors wish to acknowledge Dr. Kenneth W. Iliff and Mr. Alexander G. Sim of NASA FRC for their advice and help in the understanding and writing of the theory of the Newton-Raphson program; Mr. Richard G. Hector for his aid in adapting the Newton-Raphson program for use at the AFFTC and for providing the interface between the F-111E flight data tapes and the two matching programs; Mr. Christopher Nagy who did part of the F-111E hybrid matching work; and Mr. Lon C. Ulmer and Mr. John Potter for their assistance in the operation of the hybrid matching program.

## HYBRID MATCHING EQUATIONS OF MOTION

## Rotational Acceleration Equations

$$\begin{aligned} I_{xx}\dot{p}_b - I_{xz}\dot{r}_b &= (I_{yy} - I_{zz})q_b r_b + I_{xz}p_b q_b \\ &+ \bar{q}Sb[C_{l_\beta} \cdot \beta + C_{l_{\delta a}} \cdot \delta a + C_{l_{\delta r}} \cdot \delta r] \\ &+ \frac{\bar{q}Sb^2}{2V_t} [C_{l_p} \cdot p_b + C_{l_r} \cdot r_b] \end{aligned}$$

$$\begin{aligned} I_{yy}\dot{q}_b &= (I_{zz} - I_{xx})p_b r_b + I_{xz}(r_b^2 - p_b^2) + \bar{q}S\bar{c}[C_{m_\theta} + C_{m_\alpha} \cdot \alpha + C_{m_{\delta e}} \cdot \delta e] \\ &+ \frac{\bar{q}S\bar{c}^2}{2V_t} \cdot C_{m_q} \cdot q_b \end{aligned}$$

$$\begin{aligned} -I_{xz}\dot{p}_b + I_{zz}\dot{r}_b &= (I_{xx} - I_{yy})p_b q_b - I_{xz}q_b r_b \\ &+ \bar{q}Sb[C_{n_\beta} \cdot \beta + C_{n_{\delta a}} \cdot \delta a + C_{n_{\delta r}} \cdot \delta r] \\ &+ \frac{\bar{q}Sb^2}{2V_t} [C_{n_r} \cdot r_b + C_{n_p} \cdot p_b] \end{aligned}$$

For:  $I_{xy} = I_{yz} = 0$ .

## Angle of Attack

$$\begin{aligned} \dot{\alpha} &= q_b + \frac{1}{\cos \alpha \cos \beta} \left[ \frac{g}{V_t} (\cos \theta \cos \phi - p_b \sin \beta) \right] \\ &- \frac{\bar{q}S}{V_{t,m} \cos \alpha \cos \beta} [C_{N_\theta} + C_{N_\alpha} \cdot \alpha + C_{N_{\delta e}} \cdot \delta e] . \end{aligned}$$

## Sideslip Angle

$$\begin{aligned} \dot{\beta} &= p_b \sin \alpha - r_b \cos \alpha + \frac{1}{\cos \beta} \left[ \frac{g}{V_t} (\cos \theta \sin \phi) - \frac{g}{V_t} (\sin \theta \sin \beta) \right] \\ &+ \frac{\bar{q}S}{V_{t,m} \cos \beta} [C_{y_\beta} \cdot \beta + C_{y_{\delta a}} \cdot \delta a + C_{y_{\delta r}} \cdot \delta r] . \end{aligned}$$

## Normal Acceleration

$$a_{z_b}(g's) = \frac{\bar{q}S}{mg} [C_{N_\theta} + C_{N_\alpha} \cdot \alpha + C_{N_{\delta e}} \cdot \delta e] .$$

## Lateral Acceleration

$$a_{y_b}(g's) = \frac{\bar{q}S}{mg} [C_{y_\beta} \cdot \beta + C_{y_{\delta a}} \cdot \delta a + C_{y_{\delta r}} \cdot \delta r] .$$

Fig.1 Hybrid and Newton-Raphson equations of motion

*Euler Angle Transformations*

$$\dot{\psi} = \frac{q_b \sin \phi + r_b \cos \phi}{\cos \theta}$$

$$\dot{\theta} = q_b \cos \phi - r_b \sin \phi$$

$$\dot{\phi} = p_b + (q_b \sin \phi + r_b \cos \phi) (\tan \theta) .$$

*Equations of Motion Mechanized in the Modified Newton-Raphson Computer Program*

For the lateral-directional mechanization,

$$\begin{aligned} \dot{p} = & \frac{I_{xz}}{I_x} \dot{r} + L_p p + L_r r + L_\beta \beta + L_{\delta_a} \delta_a + L_{\delta_r} \delta_r \\ & + L_{\delta_{c_1}} \delta_{c_1} + L_{\delta_{c_2}} \delta_{c_2} + L_{\delta_0} \delta_0 \end{aligned}$$

$$\begin{aligned} \dot{r} = & \frac{I_{xz}}{I_z} \dot{p} + N_p p + N_r r + N_\beta \beta + N_{\delta_a} \delta_a + N_{\delta_r} \delta_r \\ & + N_{\delta_{c_1}} \delta_{c_1} + N_{\delta_{c_2}} \delta_{c_2} + N_{\delta_0} \delta_0 \end{aligned}$$

$$\begin{aligned} \dot{\beta} = & p \sin \alpha - r \cos \alpha + Y_\beta \beta + \phi g/V \cos \theta \\ & + Y_{\delta_a} \delta_a + Y_{\delta_r} \delta_r + Y_{\delta_{c_1}} \delta_{c_1} + Y_{\delta_{c_2}} \delta_{c_2} + Y_{\delta_0} \delta_0 \end{aligned}$$

$$\dot{\phi} = p + r \tan \theta$$

$$a_y = Y_\beta \beta + Y_{\delta_a} \delta_a + Y_{\delta_r} \delta_r + Y_{\delta_{c_1}} \delta_{c_1} + Y_{\delta_{c_2}} \delta_{c_2} + Y_{\delta_0} \delta_0 .$$

For the longitudinal mode,

$$\begin{aligned} \dot{q} = & M_q q + M_\alpha \alpha + M_V V + M_{\delta_e} \delta_e + M_{\delta_c} \delta_c + M_{\delta_{c_1}} \delta_{c_1} \\ & + M_{\delta_{c_2}} \delta_{c_2} + M_{\delta_0} \delta_0 \end{aligned}$$

$$\begin{aligned} \dot{\alpha} = & \dot{q} + N_q q + N_\alpha \alpha + N_V V + N_\theta \theta + N_{\delta_e} \delta_e + N_{\delta_c} \delta_c \\ & + N_{\delta_{c_1}} \delta_{c_1} + N_{\delta_{c_2}} \delta_{c_2} + N_{\delta_0} \delta_0 + g/V \end{aligned}$$

$$\begin{aligned} \dot{V} = & X_q q + X_\alpha \alpha + X_V V + X_\theta \theta + X_{\delta_e} \delta_e + X_{\delta_c} \delta_c \\ & + X_{\delta_{c_1}} \delta_{c_1} + X_{\delta_{c_2}} \delta_{c_2} + X_{\delta_0} \delta_0 \end{aligned}$$

$$\dot{\theta} = q .$$

$\delta_c$ ,  $\delta_{c_1}$ , and  $\delta_{c_2}$  are additional control inputs and should be used if necessary.

$\delta_0$  represents a bias term in the state equations so that the initial slopes of the state parameters may be adjusted by the program when necessary.

Figure 1 Concluded

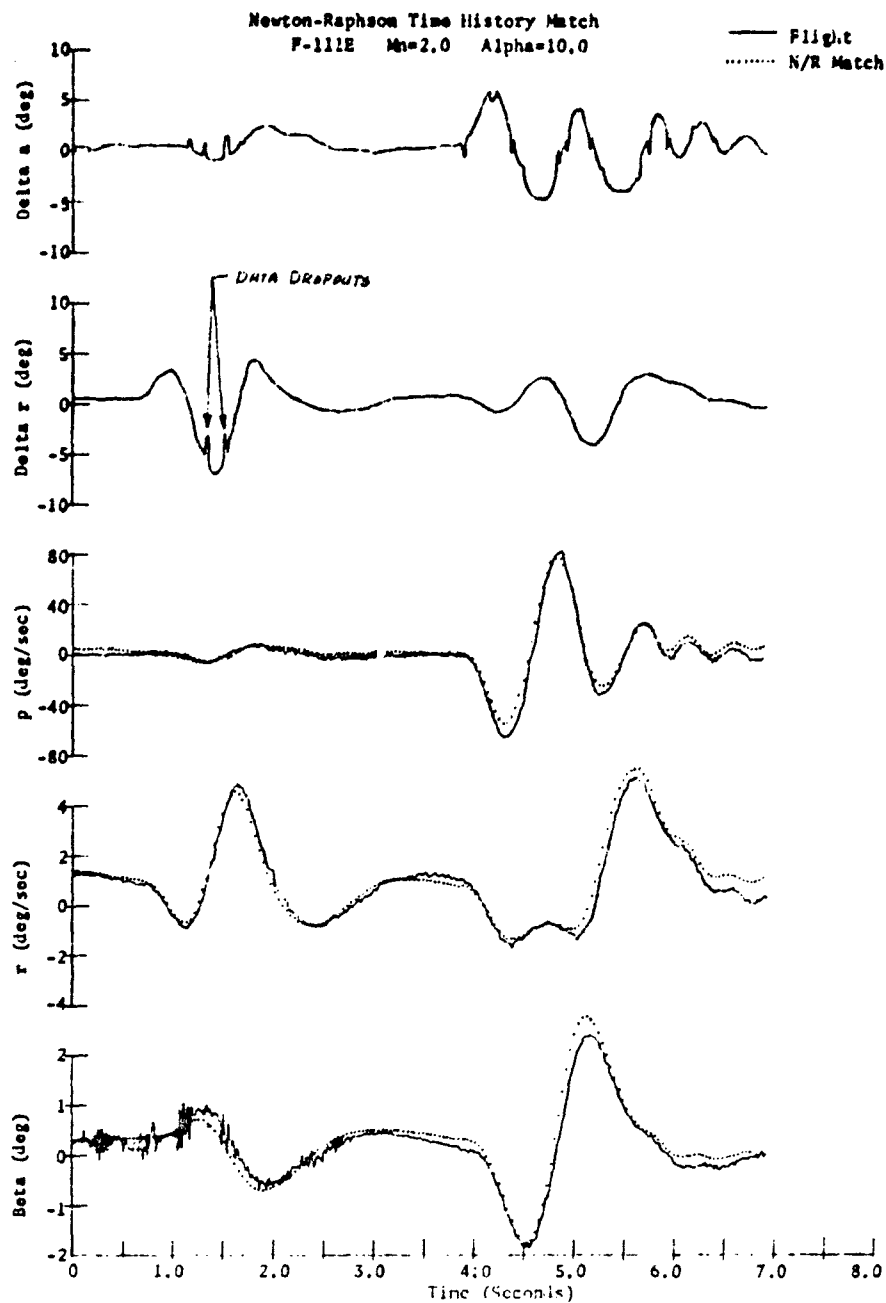


Figure 2 Desirable Lateral-Directional Flight Test Maneuver



Open Symbols - Hybrid Matching  
 Closed Symbols - Newton-Raphson  
 — Wind Tunnel Data  
 --- Interpolated Wind Tunnel Data

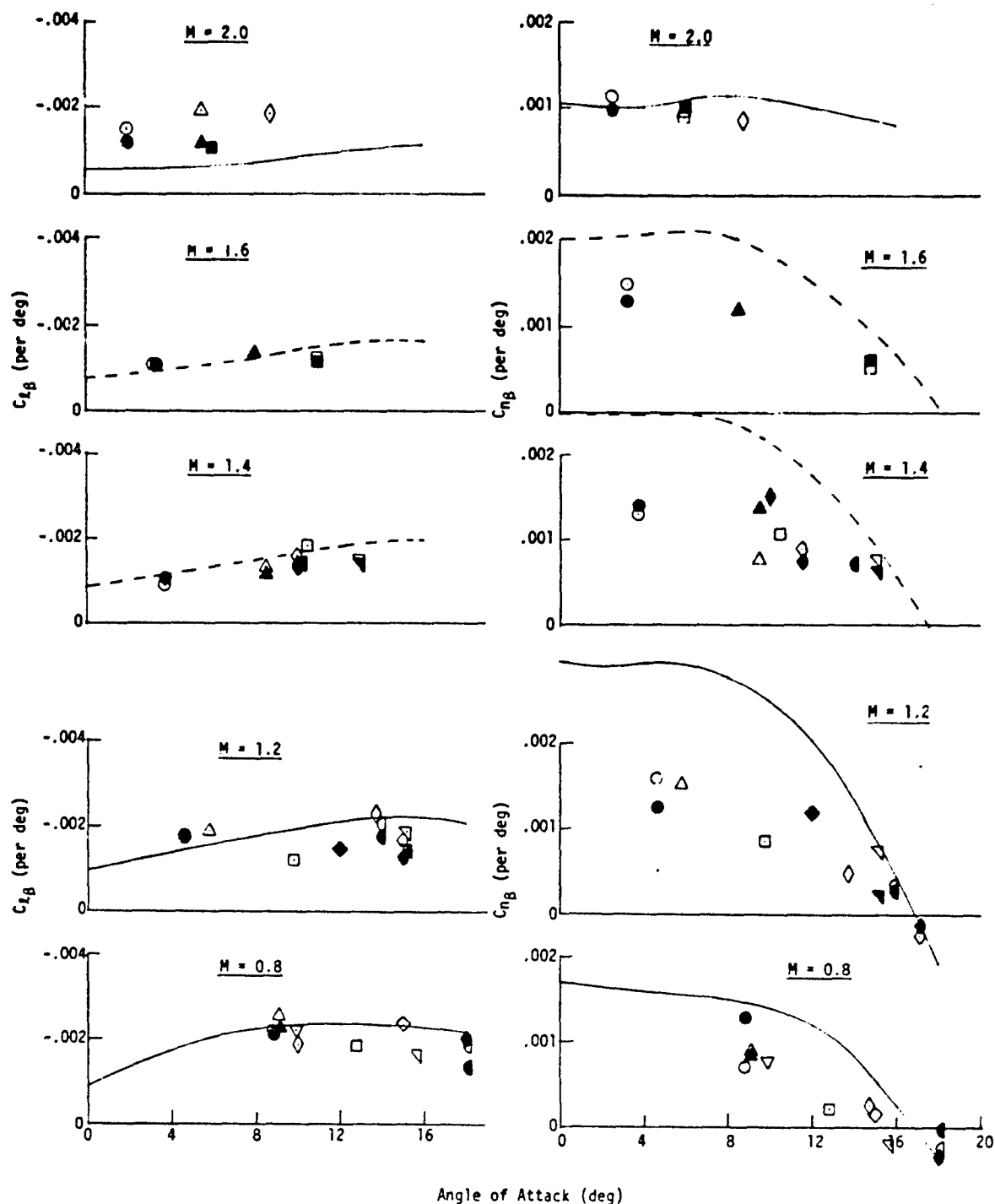


Figure 3. F-111E Sideslip Derivatives -  $A = 50^\circ$

Open Symbols - Hybrid Matching  
 Closed Symbols - Newton-Raphson  
 ——— Wind Tunnel Data  
 - - - Interpolated Wind Tunnel Data

Note: For F-111E Data, Positive  $\delta a$  is defined as producing left roll rate.

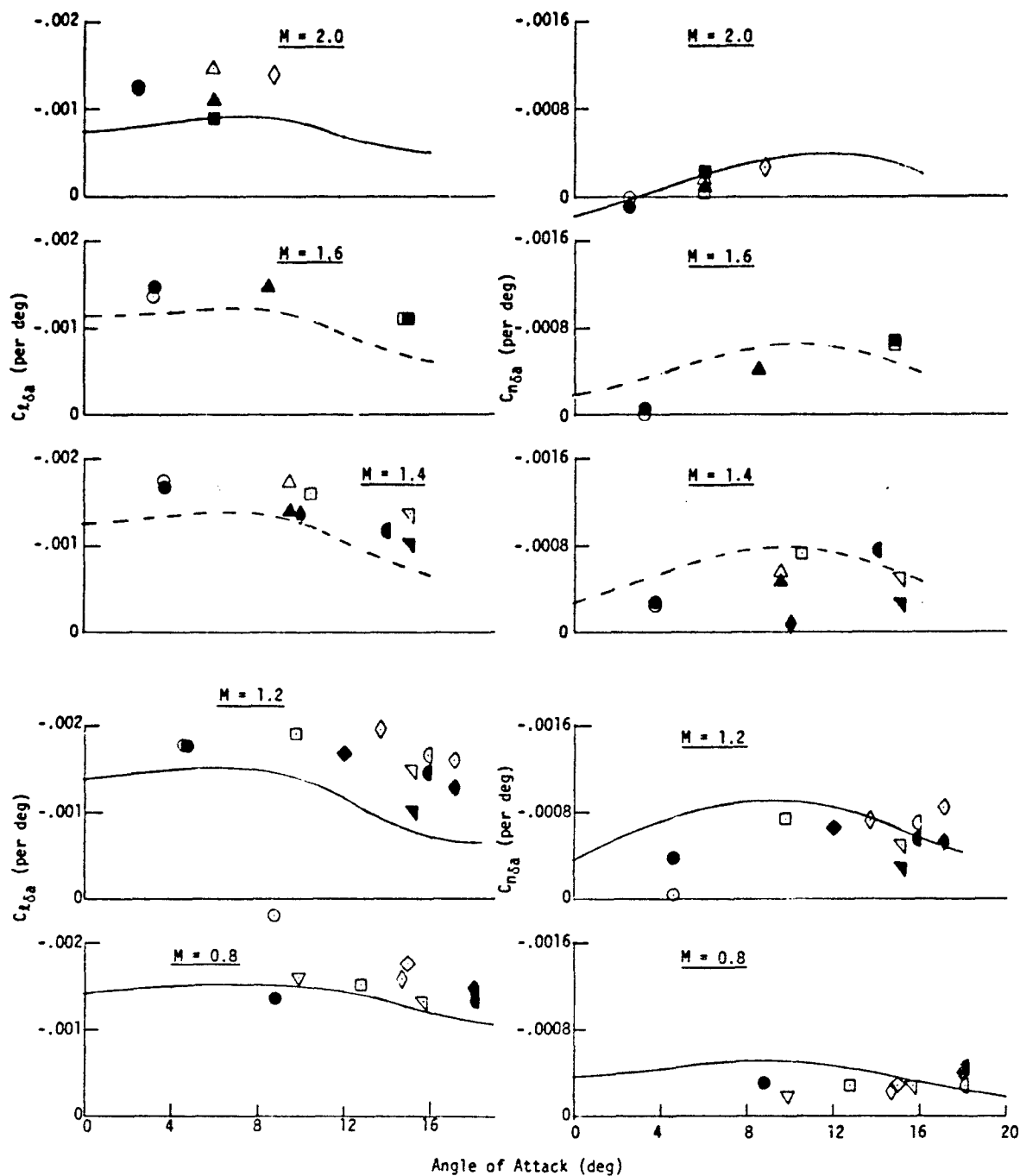


Figure 4. F-111E Aileron Derivatives -  $A = 50^\circ$

Open Symbols - Hybrid Matching  
 Closed Symbols - Newton-Raphson  
 ——— Wind Tunnel Data  
 - - - Interpolated Wind Tunnel Data

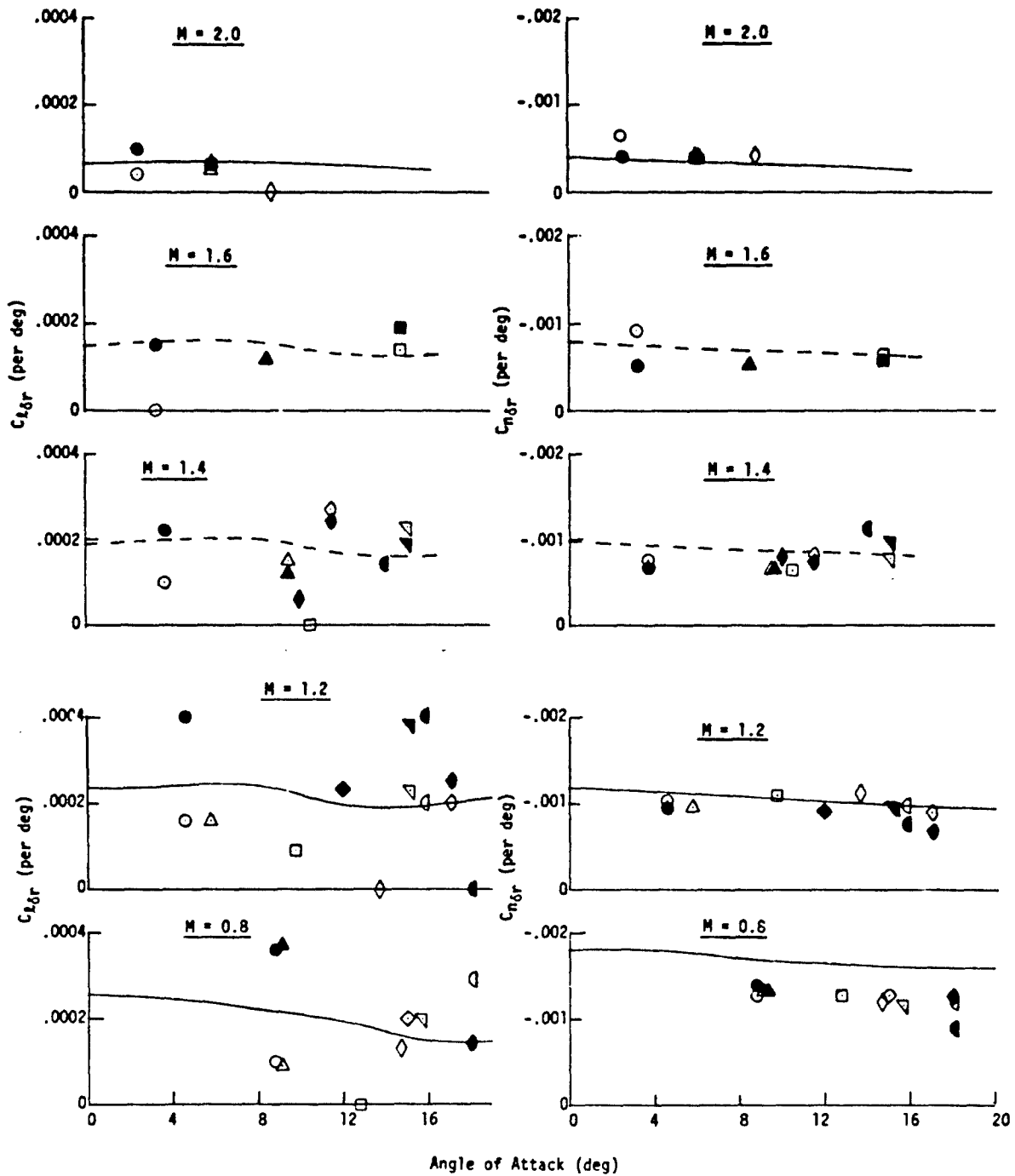


Figure 5. F-111E Rudder Derivatives -  $\Lambda = 50^\circ$

Open Symbols - Hybrid Matching  
 Closed Symbols - Newton-Raphson  
 — Theoretical Data

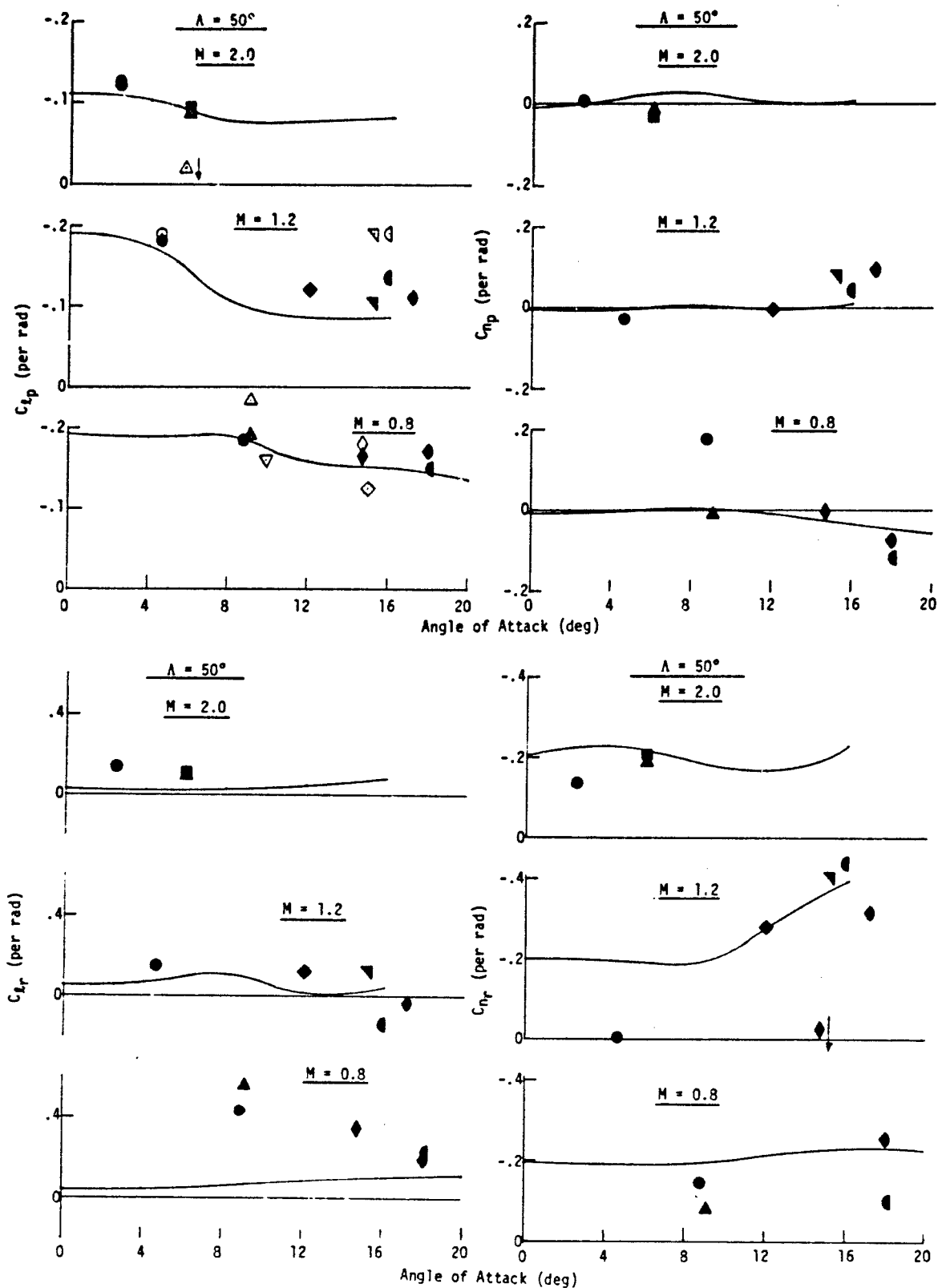


Figure 6. F-111E Damping Derivatives

Open Symbols - Hybrid Matching  
 Closed Symbols - Newton-Raphson  
 — Wind Tunnel Data

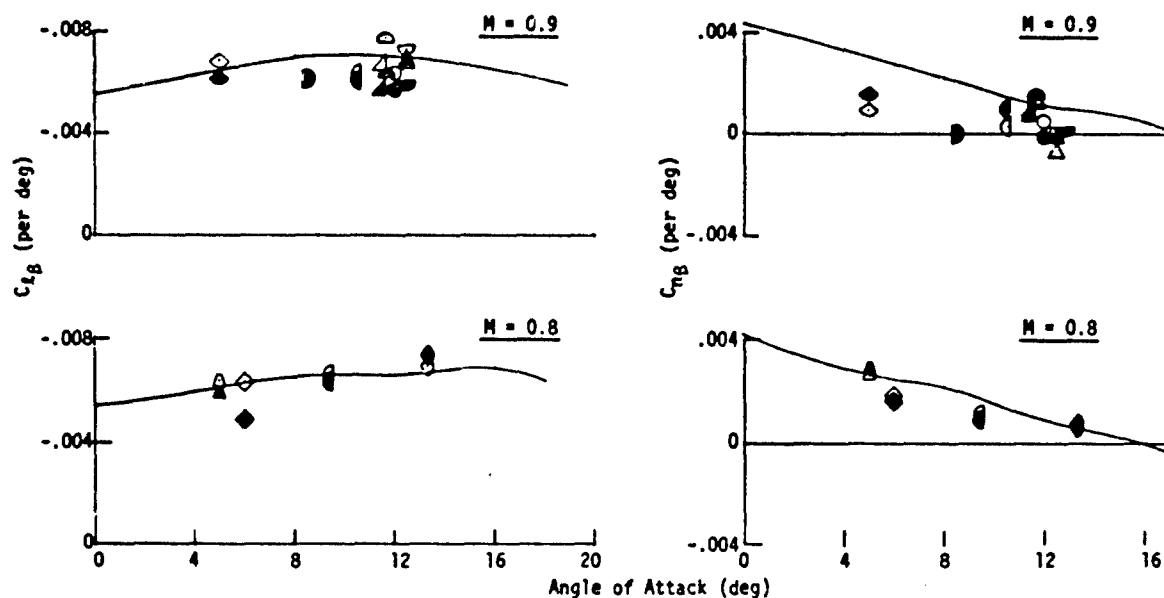


Figure 7. X-24A Sideslip Derivatives

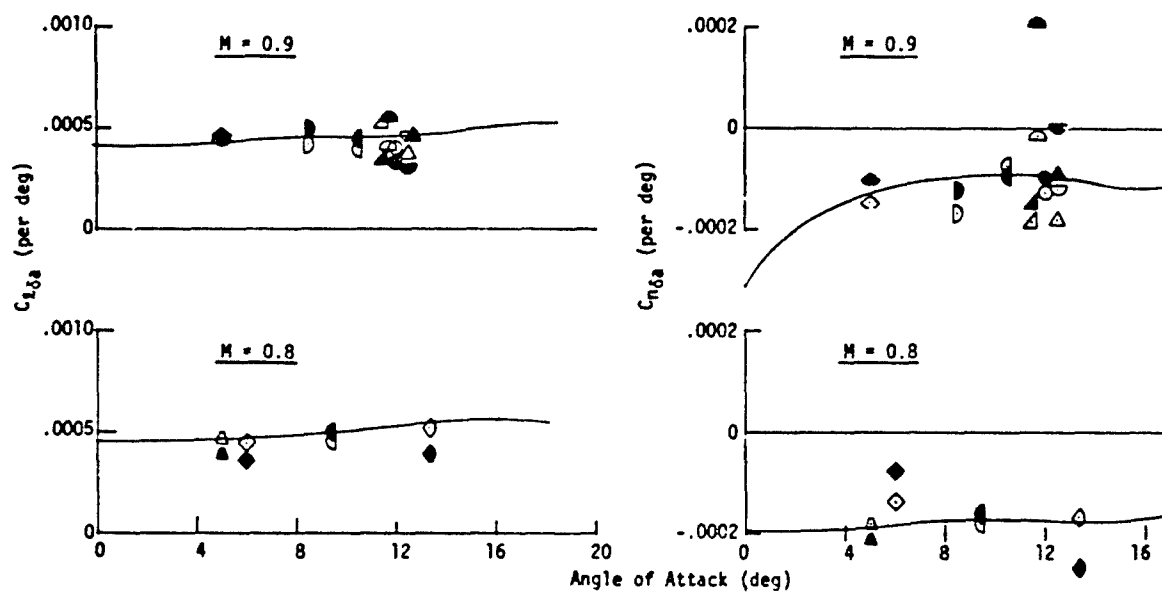


Figure 8. X-24A Aileron Derivatives

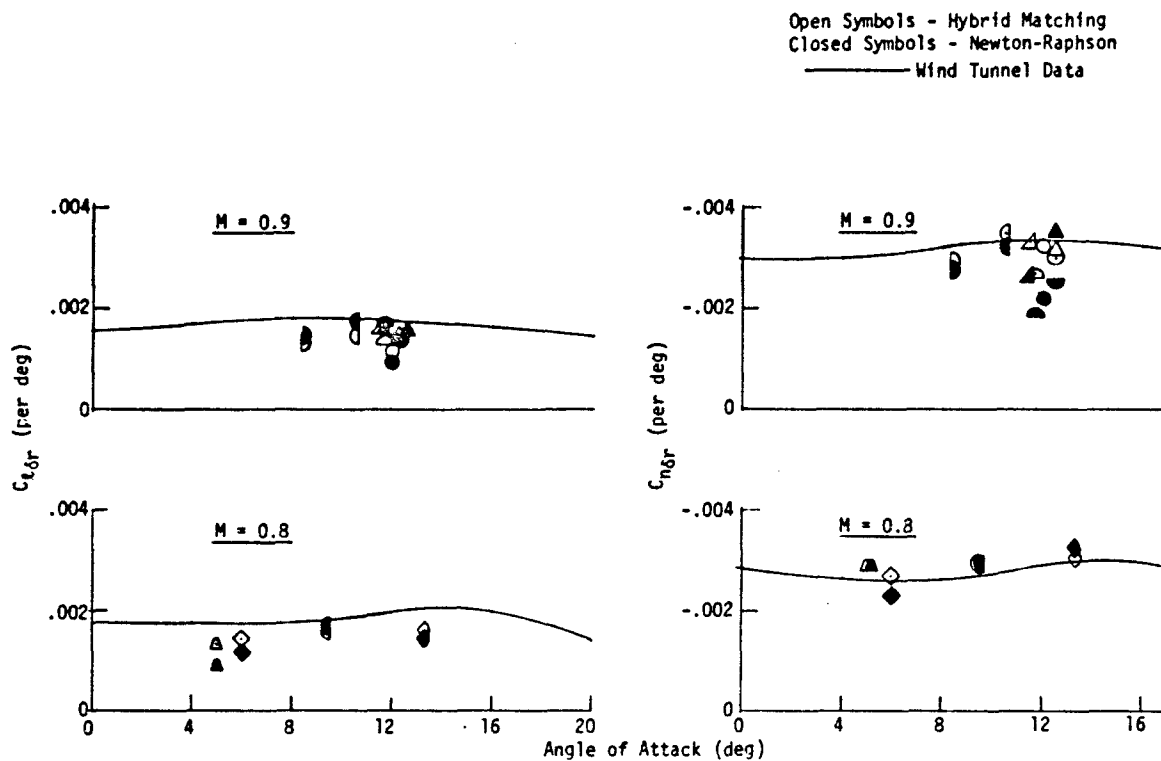


Figure 9. X-24A Rudder Derivatives

Open Symbols - Hybrid Matching  
 Closed Symbols - Newton-Raphson  
 --- Theoretical Data

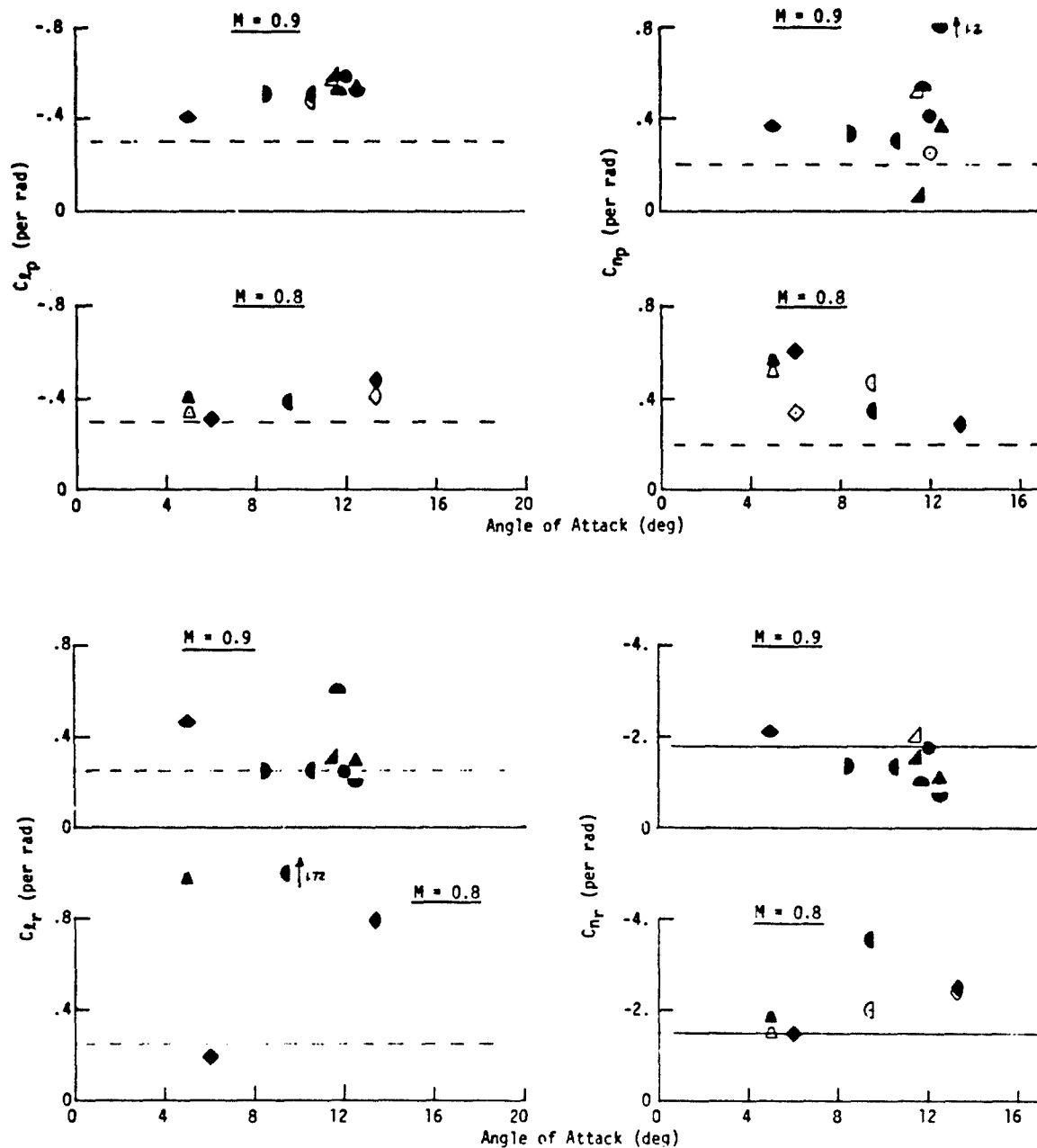
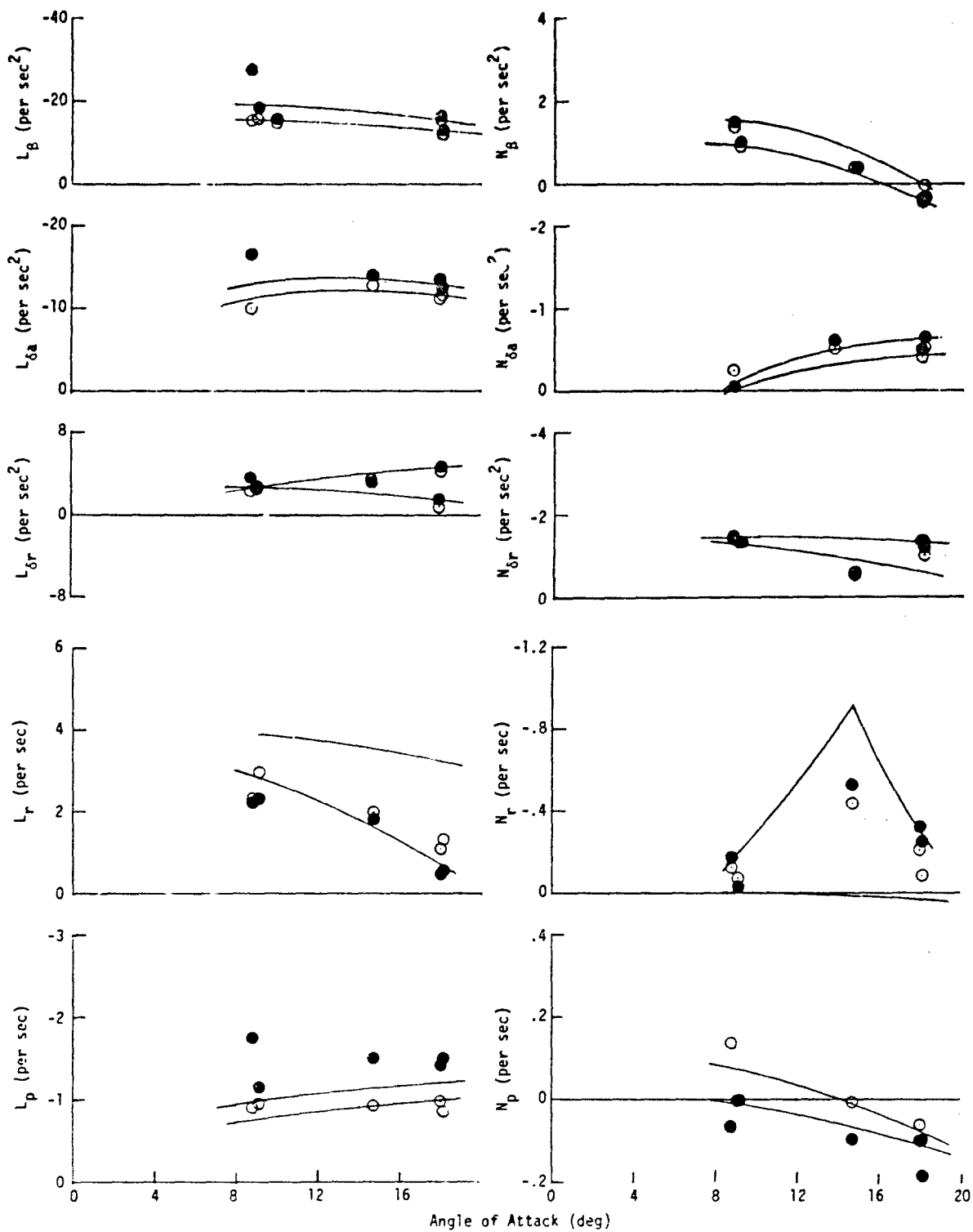


Figure 10. X-24A Damping Derivatives

All data run with a priori

F-111E,  $\Lambda=50^\circ$ ,  $M=0.8$   
Principle Axis

- Uses wind tunnel values for starting values.  
● Uses double wind tunnel values for starting values.

Figure 11.  $D_2$  and Variance Number Study



F-111E,  $\Lambda=50^\circ$ ,  $M=0.8$   
Principle Axis

All data run without a priori

- Uses wind tunnel values for starting values.  
● Uses double wind tunnel values for starting values.

I Confidence Levels

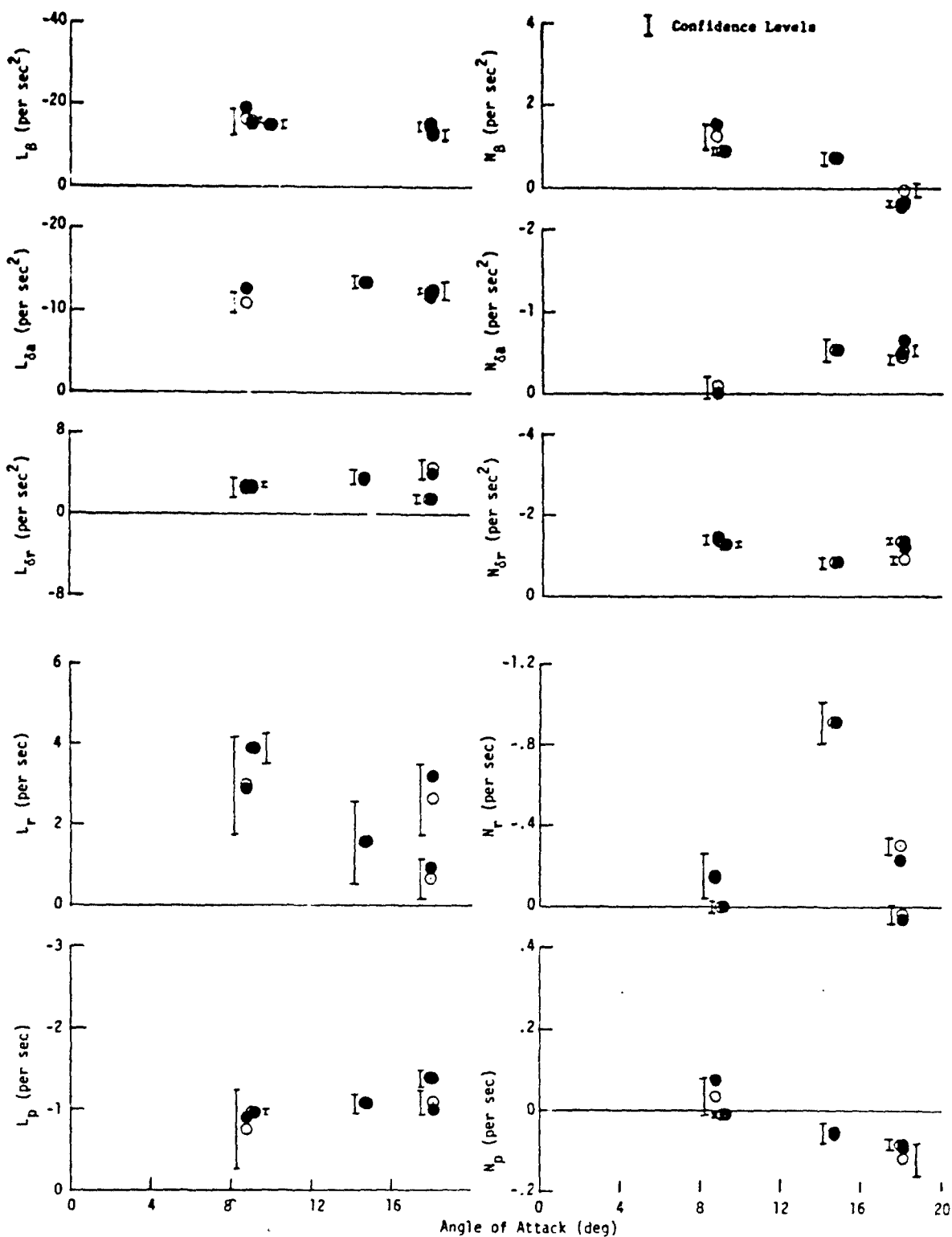


Figure 12.  $D_2$  and Variance Number Study

## ESTIMATION OF THE AIRCRAFT STATE IN NON-STEADY FLIGHT

by

J.A. Mulder

Department of Aeronautical Engineering  
Delft University of Technology  
Delft  
The Netherlands

## SUMMARY

Kalman filtering and smoothing and maximum likelihood estimation techniques have been applied to the problem of estimating the aircraft state in non-steady flight from onboard noisy inertial and barometric measurements. Applied to actual flight test data the estimation schemes yielded similar results.

## 1. INTRODUCTION

In many flight test problems airspeed and angle of attack must accurately be known. Airspeed can be determined from barometric measurements. This, however, introduces measurement errors due to the limited accuracy of the barometric transducers.

The angle of attack is usually measured by means of a vane. The vane is positioned on a boom some distance ahead of the wing. This reduces the magnitude of local aircraft induced air velocities. Nevertheless in many cases the difference between the local direction of the air flow and the direction of the undisturbed flow is not negligible. Thus the necessity arises for the calibration of the vane in a series of steady straight flights. In steady straight flight conditions the aircraft pitch angle can be measured by means of a pendulum while the flightpath angle follows from the change of altitude during a given time interval. The difference between the pitch angle and the flightpath angle is considered to represent the "real" value of the angle of attack and thus a calibration of the vane is possible.

The situation becomes more complex in case the local direction of the airflow is significantly influenced by engine power or engine thrust. This may be experienced particularly when flight testing STOL or VTOL aircraft.

Airspeed and angle of attack are of prime importance when measuring aircraft performance in quasi-steady and non-steady flight conditions. In those flight conditions several corrections have to be applied additionally to the measured value of the angle of attack, Ref. 1. Besides it remains at least questionable whether the calibrations in steady straight flight conditions apply equally well to quasi-steady and non-steady flight conditions.

The problems mentioned above can be circumvented when in addition to the barometric variables several inertial variables are measured in flight. Airspeed and angle of attack may then be derived from the components of the aircraft state vector which can be calculated from the measurements by applying so called state trajectory estimation techniques as described in Ref. 4, 5 and 6.

The possibility of circumventing the task of directly measuring the angle of attack by means of a vane has first been mentioned in Ref. 2. In Ref. 3 the trajectory of the state vector has been calculated by applying regression analysis. In Ref. 4 least squares estimation has been used to this end. The application of an identical algorithm, maximum likelihood estimation, has been reported in Ref. 5. In Ref. 6 the state trajectory estimation problem has been solved by applying the Kalman filtering and smoothing algorithms.

In this paper the estimation techniques described in Ref. 5 and Ref. 6, i.e. maximum likelihood estimation and Kalman filtering and smoothing have been applied to measurements in one non-steady flight test manoeuvre and the results have been compared.

The shape of the nominally symmetric flight test manoeuvre is the subject of Ref. 10. Starting from an approximately steady straight and horizontal flight condition the aircraft, Fig. 1, is accelerated quasi-steady through the speed range of interest.

Once in every period of 30 seconds a dynamic manoeuvre is executed after which the acceleration proceeds in quasi-steady flight. Applying the techniques described in Ref. 7 both performance and handling characteristics are to be derived from the measurements during one manoeuvre.

The paper is organized as follows. In Chapter 3 the mathematical model is presented of the motion of an aircraft in an atmosphere which has been assumed to move uniformly with respect to earth. Some aspects of the instrumentation system are described in Chapter 4. Chapter 5 provides a brief discussion of the estimation schemes applied to the state trajectory estimation problem. In Chapter 6 the experimental results are discussed. Final conclusions are drawn in Chapter 7.

## 2. NOTATION

$a$	kinematic acceleration
$A$	specific force, quantity sensed by an accelerometer
$\Delta A_{z_0}$	zeroshift of the $A_{z_0}$ accelerometer
$E$	mathematical expectation operator
$f$	vector function in (3-1)
$g$	acceleration due to gravity
$h$	vector function in (3-2)
$L$	likelihood function
$p$	probability density function
$\Delta p_c$	impact pressure
$p_s$	static pressure of the undisturbed airflow
$\Delta p_s$	$p_s - p_s(t_0)$
$\Omega_B$	angular velocity about $Z_B$ axis
$R$	variance matrix of measurement noise, radial distance from the earth's centre.
$t$	time
$t_i$	time of $i$ th measurement
$v$	vector of measurement noise
$V$	speed vector
$w$	vector of plant noise
$W$	wind vector
$x$	state vector
$x^a$	augmented state vector
$y$	observation vector
$\Delta z_T(i)$	$\int_{t_0}^{t_i} v_{z_T} dt$
$\alpha$	angle of attack
$\beta$	parameter vector
$\beta^a$	augmented parameter vector
$\gamma^a$	flightpath angle with respect to the atmosphere
$\delta_{ij}$	Kronecker delta
$\theta$	pitch angle
$\lambda$	geographic latitude
$\mu$	geographic longitude
$\phi$	roll angle
$\psi$	heading angle
$\omega^e$	earth's rate of rotation

## superscripts

$a$	with respect to air
$\sim$	estimated quantity
$\cdot$	time derivative
$T$	vector or matrix transpose
$-1$	matrix inverse
$-$	average quantity

## subscripts

$V_{X_T}$	component of vector $V$ along the axis $X_T$ of the reference frame $F_T$
$V_T$	components of vector $V$ are along the axes of $F_T$
$m$	measured quantity

## Reference frames

The origin of  $V_Y$ ,  $V_T$  and of  $V_B$  is in the center of gravity of the aircraft.  $V_Y$ ,  $V_T$  and  $V_B$  are rectangular and righthanded, see Fig. 2.

- $V_Y$  The axis  $X_Y$  and  $Z_Y$  are in the plane through the aircraft's center of gravity and the earth's axis of rotation. The positive direction of  $Z_Y$  is to the earth's center. The positive direction of the  $X_Y$  axis is to the North.
- $V_T$   $Z_T$  coincides with the  $Z_Y$  axis.  $X_T$  is in the plane through  $X_B$  and  $Z_T$ .
- $V_B$  Body fixed reference frame.  $X_B$  and  $Z_B$  are in the plane of symmetry of the aircraft. The positive direction of  $Y_B$  is to starboard.  $X_B$  is parallel to the mean aerodynamic chord.

## 3. THE SYSTEM AND OBSERVATION MODEL

The kinematical relations of the aircraft motion relative to a spherical and rotating earth are well known, Ref. 11. The following set of simplified relations have been used in the present formulation of the state trajectory estimation problem.

$$\dot{V}_{x_T}^a = a_{x_T} - \bar{R}\omega^2 \cos \bar{\psi} \sin \bar{\lambda} \cos \bar{\lambda}$$

$$\dot{V}_{z_T}^a = a_{z_T} - \{2\omega^2 \sin \bar{\psi} \cos \bar{\lambda} + \frac{1}{R} (V_{x_T}^a + W_{x_T})\} (V_{x_T}^a + W_{x_T}) - \bar{R}\omega^2 \cos^2 \bar{\lambda}$$

$$\dot{\Delta z_T} = V_{z_T}$$

$$\dot{\theta} = q_B \cos \varphi - r_B \sin \varphi + \omega^2 \sin \bar{\psi} \cos \bar{\lambda} + \frac{1}{R} (V_{x_T}^a + W_{x_T})$$

The kinematical accelerations  $a_{x_T}$  and  $a_{z_T}$  can be derived from:

$$a_{x_T} = A_{x_B} \cos \theta + A_{y_B} \sin \theta \sin \varphi + A_{z_B} \sin \theta \cos \varphi$$

$$a_{z_T} = -A_{x_B} \sin \theta + A_{y_B} \cos \theta \sin \varphi + A_{z_B} \cos \theta \cos \varphi + g$$

The set of first order differential equations represent a system:

$$\dot{x} = f(x, u, \theta) \quad (3-1)$$

in which the state vector  $x$  is defined by:

$$x = \text{col} \{V_{x_T}^a, V_{z_T}, \Delta z_T, \theta\}$$

and the input vector  $u$  by:

$$u = \text{col} \{A_{x_B}, A_{y_B}, A_{z_B}, q_B, r_B, \varphi\}$$

$\theta$  denotes a vector of unknown parameters which is defined in Chapter 4.

In the derivation of (3-1) from the general expressions in Ref. 11 the following assumptions were made.

- In the course of a non-steady manoeuvre as described in the Introduction the variations of  $R$ ,  $\lambda$  and  $\mu$  are small enough as to permit the substitution of average values  $\bar{R}$ ,  $\bar{\lambda}$  and  $\bar{\mu}$ .
- $W_T$ , the velocity of the atmosphere relative to the earth can be assumed to be constant along the trajectory of a non-steady manoeuvre.
- As mentioned in the Introduction, the non-steady manoeuvre is nominally symmetric. This may be deduced also from the time histories of the "asymmetric components"  $A_{y_B}$ ,  $r_B$  and  $\varphi$  of the input vector  $u$ , Fig. 3. It is therefore reasonable to assume that  $V_{y_T}^a$  is small compared to  $V^a$  and changes of  $\psi$  are small enough as to permit the substitution of an average heading angle  $\bar{\psi}$ .
- For reasons to be stated below, the trajectory of the manoeuvre is selected to be parallel to the atmospheric isobars, hence:

$$W_{y_T} = 0$$

The observation model of (3-1) can be written as:

$$y = h(x) \quad (3-2)$$

In (3-2)  $y$  denotes an observation vector defined by

$$y = \text{col} \{V^a, \Delta z_T\}$$

The components of the observation vector  $y$  can be derived from the impact pressure  $\Delta p_i$  and change of static air pressure  $\Delta p_s$  which are measured very accurately in the instrumentation system, Ref. 8 and 9.

The calculation of  $V^a$  from  $\Delta p_i$  is straight forward and need not be commented upon.

$\Delta p_s$  denotes the change of static air pressure relative to the static air pressure at the initial position of the aircraft at time  $t = t_0$ . Consequently  $\Delta p_s$  represents the vertical distance to a surface of constant static air pressure through the starting point of the non-steady manoeuvre. In principle the change of altitude deduced from  $\Delta p_s$  differs from  $\Delta z_T$  depending on the topography of the surface of constant static air pressure mentioned above.

However, in practice this difference is thought to be negligible because of the following reasons:

- The distance travelled through in the course of a non-steady manoeuvre (app. 30 to 40 km) is small compared to the scale of horizontal atmospheric pressure distributions.
- The trajectory is selected to be approximately parallel to the isobars which can be accomplished by consulting meteorological information prior to executing the flight tests.

Airspeed  $V^a$  can be expressed as follows:

$$V^a = (V_{xT}^2 + V_{yT}^2 + V_{zT}^2)^{1/2} \quad (3-3)$$

Denoting the vertical component of the constant wind by  $W_{zT}$ ,  $V_{zT}^a$  can be written as:

$$V_{zT}^a = V_{zT} - W_{zT}$$

$W_{zT}$  is very small. In the case of anti-cyclonic pressure (high pressure) distributions  $W_{zT}$  is positive and called subsidence. The magnitude of subsidence is in the order of 0.1 m/sec, Ref. 12.

Because the non-steady manoeuvre is nominally symmetric  $V_{yT}^a$  is small and (3-3) may be written as:

$$V^a = (V_{xT}^2 + V_{zT}^2)^{1/2} + (V_{xT}^2 + V_{zT}^2)^{-1/2} (V_{yT}^2 - V_{zT}W_{zT}) = (V_{xT}^2 + V_{zT}^2)^{1/2}$$

which completes the description of the system and observation model.

The flightpath angle with respect to the surrounding air mass  $\gamma^a$  is defined as:

$$\gamma^a = - \arcsin \frac{V_{zT}^a}{V^a}$$

Because  $W_{zT}$  is very small compared to  $V^a$ :

$$\gamma^a = - \arcsin \frac{V_{zT}}{V^a} \quad (3-4)$$

In nominally symmetrical steady as well as non-steady flight conditions the angle of attack  $\alpha$  may be calculated from the components of the state-vector of the system (3-1) by:

$$\alpha = \theta - \gamma^a = \theta + \arcsin \frac{V_{zT}}{(V_{xT}^2 + V_{zT}^2)^{1/2}} \quad (3-5)$$

#### 4. THE INSTRUMENTATION SYSTEM

A detailed description of the instrumentation system employed is presented in Ref. 8 and 9. The system comprises several high accuracy inertial and barometric transducers. Analog signals from the transducers are conditioned to range from zero to 10.000 mV dc and successively filtered by identical fourth order filters. The dc outputs of the filters are sampled and digitized by an analog to digital converter at a rate of 20 per second. The resolution of the analog to digital converter amounts to 0.01% of full scale i.e. 1 mV.

The random errors of the measurements of the "symmetrical components" of the input vector  $u$  are in the order of the resolution of the instrumentation system. In Ref. 8, by comparing the results of several calibrations, zeroshifts could be detected in the order of several mV's.

The random errors of the barometric measurements amount to several mV's due to the limited accuracy of barometric transducers compared to the accuracy of inertial transducers.

It is shown in Ref. 9 the zero outputs of the barometric transducers vary considerably as a function of time. In contrast to the inertial transducers, however, the zeroshifts of the barometric transducers are easily measured in flight before and after every measuring run and can subsequently be corrected for.

In Ref. 13 it is shown that the trajectory of the state vector  $x$  is particularly sensitive to zeroshifts of the  $A_{zB}$  accelerometer and the  $q_B$  rate gyro.

These zeroshifts have therefore to be modelled as the components of an unknown parameter vector  $\beta$  defined as:

$$\beta = \text{col} \{ \Delta A_{x0}, \Delta q_0 \} \quad (4-1)$$

in order to avoid unallowable model errors.

### 5. SOLUTION OF THE STATE TRAJECTORY ESTIMATION PROBLEM

The state trajectory estimation problem can be formulated as a statistical estimation problem. The nonlinear dynamic system (3-1) is observed according to the observation model (3-2). At discrete instants of time  $t_i$ ,  $i = 0, \dots, N$ , measurements are made of the components of the input vector  $u$  and the observation vector  $y$ . These measurements are corrupted by measurement errors which are assumed to be additive.

$$u_m(i) = u(i) + w(i)$$

$$y_m(i) = y(i) + v(i)$$

The assumption is made that  $w(i)$  and  $v(i)$ ,  $i = 0, \dots, N$ , can adequately be represented by zero-mean gaussian random sequences according to:

$$E \{ w(i) \} = 0$$

$$E \{ w(i) w^T(i) \} = \delta_{ij} Q$$

$$E \{ v(i) \} = 0$$

$$E \{ v(i) v^T(i) \} = \delta_{ij} R$$

The components of  $x$  at times  $t_i$  and additionally the components of the parameter vector  $\beta$  have to be estimated in some optimal way from the noisy measurements of  $u(i)$  and  $y(i)$ .

Two different algorithm's have been applied

- The extended Kalman filter followed by a fixed interval smoothing algorithm, corresponding to Table 9.4-3 and 9.5-3 of Ref. 15.
- The maximum likelihood estimation scheme as described in Ref. 16.

Based on the review presented in Ref. 14 both algorithms are briefly discussed in Section 5.1 and 5.2.

#### 5.1 EXTENDED KALMAN FILTERING AND FIXED INTERVAL SMOOTHING

The parameter vector  $\beta$  is assumed to be constant in the course of one flight test manoeuvre,

$$\dot{\beta} = 0 \quad (5-1)$$

(3-1) and (5-1) can then be written as:

$$\dot{x}^* = f^*(x^*, u) \quad (5-2)$$

in which  $x^*$  denotes an augmented state vector:

$$x^* = \text{col} \{ x^T, \beta^T \}$$

The time interval between two successive measurements,  $\Delta t$  is assumed to be small enough as to permit the discretization of (5-2) which may then be written as:

$$x^*(i+1) = \phi(x^*(i), u(i)) \quad (5-3)$$

$w(i)$  is very small because  $u(i)$  is measured very accurately. Then  $w(i)$  may be interpreted as plant noise entering additively into the system (5-3) according to:

$$x^*(i+1) = \phi(x^*(i), u_m(i)) - \frac{\partial \phi}{\partial u} (x^*(i), u_m(i)) \cdot w(i) \quad (5-4)$$

Apart from modelling the input vector measurement noise, the plant noise is considered to account also for differences between the model and the actual process.

When  $x^*(0)$  is assumed to be a gaussian random variable with variance matrix  $P^*(0|0)$  it is shown in Ref. 14 that following from the assumptions stated above the aposteriori probability density function is gaussian and can be written as:

$$\begin{aligned} p(x^*(0), x^*(1), \dots, x^*(N) | y_m(1), y_m(2), \dots, y_m(N)) = \\ C \cdot \exp \{ -\frac{1}{2} [x^*(0) - E(x^*(0))]^T P^{-1}(0|0) [x^* - E(x^*(0))] \\ + \sum_{i=1}^N [y_m(i) - h(x^*(i))]^T R^{-1} [y_m(i) - h(x^*(i))] + \sum_{i=0}^N w^T(i) Q^{-1} w(i) \} \end{aligned} \quad (5-5)$$

in which  $C$  is a normalizing constant.

The most probable estimate of the sequence  $x^*(0), x^*(1), \dots, x^*(N)$  is obtained by maximizing the a posteriori density function, or identically minimizing

$$\begin{aligned} & [x^*(0) - \hat{x}(x^*(0))]^T P^{-1}(0|0) [x^*(0) - \hat{x}(x^*(0))] + \\ & \sum_{i=1}^N [y_m(i) - h(x^*(i))]^T R^{-1} [y_m(i) - h(x^*(i))] + \sum_{i=0}^N w^T(i) Q^{-1} w(i) \end{aligned}$$

with respect to the sequence  $x^*(0), x^*(1), \dots, x^*(N)$  subject to the constraint (5-4). This constitutes a problem in optimal control theory which can be reformulated as a nonlinear two point boundary value problem. In the linear case, the solution is provided by the Kalman filtering and smoothing algorithms, i.e. in case (5-4) and (3-2) are linear. In the nonlinear case (5-4) and (3-2) may be linearized about some nominal trajectory. Application of the Kalman filtering and smoothing algorithms then results in an approximate solution of the problem of maximizing the a posteriori probability density function.

In applying the Kalman filter the sequences of estimates  $\hat{x}^*(i|i)$  and  $\hat{x}^*(i+1|i)$  are generated, i.e. the estimates of  $x^*(i)$  and  $x^*(i+1)$  based on the measurements of  $y$  up to and including  $t_i$ . In case these estimates are utilized as nominal conditions in (5-4) and (3-2) the Kalman filter is indicated as "extended Kalman filter". Subsequent application of the fixed interval smoothing algorithm yields the sequence  $\hat{x}^*(i|N)$ , i.e. the estimates of  $x^*(i)$  based on all measurements. This sequence constitutes the approximate solution mentioned above.

## 5.2 MAXIMUM LIKELIHOOD ESTIMATION

Two important characteristic features of the state trajectory estimation problem stated above can be formulated as:

- the mathematical model described in Chapter 3 is very accurate,
- the components of the input vector  $u$  are measured very precisely.

Therefore it seems in this case reasonable to assume the plant noise to be small enough as to be neglected. This assumption simplifies the estimation problem considerably. It is shown in Ref. 16 the likelihood function  $L$  may now be written as:

$$\begin{aligned} L &= p(y_m(1), y_m(2), \dots, y_m(N) | \beta^*) = \\ &= D \exp \left\{ -\frac{1}{2} \sum_{i=1}^N [y_m(i) - h(x(i))]^T R^{-1} [y_m(i) - h(x(i))] \right\} \end{aligned} \quad (5-6)$$

in which  $D$  denotes a normalizing constant.

The augmented parameter vector  $\beta^*$  is defined as

$$\beta^* = \text{col} \{ V_{xT}^a(0), V_{zT}(0), \Delta z_T(0), \theta(0), \Delta A_{z0}, \Delta q_0 \}$$

The maximum likelihood estimate of  $\beta^*$  can be obtained by maximizing the likelihood function  $L$ , or identically minimizing

$$\sum_{i=1}^N [y_m(i) - h(x(i))]^T R^{-1} [y_m(i) - h(x(i))]$$

with respect to  $\beta^*$  subject to the constraint (3-1). This constitutes a nonlinear optimization problem which may be solved iteratively in several ways. Here the "modified Newton-Raphson" algorithm described in Ref. 16 has been used.

Once an estimate of  $\beta^*$  has been obtained the maximum likelihood estimate of the state follows directly by numerically integrating (3-1) which, because the estimate of  $\beta^*$  is based on all measurements, results in the sequence  $\hat{x}(i|N)$ .

## 6. EXPERIMENTAL RESULTS

The algorithms described in Chapter 5, i.e. extended Kalman filtering, fixed interval smoothing and maximum likelihood estimation have been applied to the measurements in one non-steady flight test manoeuvre. The shape of the non-steady manoeuvre is the subject of Ref. 10 and has been briefly discussed in the Introduction. The time histories of several variables representing the components of the input vector  $u$  of the system (3-1) are presented in Fig. 3.

When applying the extended Kalman filtering and fixed interval smoothing algorithms the estimate of the initial augmented state vector and in addition the variance matrices  $P(0|0)$ ,  $Q$  and  $R$  have to be specified.

The estimate of the initial augmented state vector is defined by:

$$\hat{\beta}^*(0|0) = \text{col} \{ \hat{V}_{xT}^a(0|0), \hat{V}_{zT}(0|0), \hat{\Delta z}_T(0|0), \hat{\theta}(0|0), \hat{\Delta A}_{z0}(0|0), \hat{\Delta q}_0(0|0) \} \quad (6-1)$$

The non-steady flight test manoeuvre starts from a condition of nominally steady, straight and approximately horizontal flight. Initial estimates of  $V_{xT}^a$ ,  $V_{zT}$  and  $\Delta z_T$  may then be calculated from the initial barometric measurements according to:

$$\hat{\theta}_{z_T}^A(0|0) = v_{z_T}^A(0)$$

$$\hat{v}_{z_T}^A(0|0) = (\Delta z_{T_M}(t_i) - \Delta z_{T_M}(0)) / (t_i - t_0)$$

$$\hat{\Delta z_T}(0|0) = \Delta z_{T_M}(0)$$

in which  $t_i - t_0$  refers to the initial period of steady straight flight.

Nominally steady straight flight conditions imply the kinematical accelerations  $a_{z_T}$  and  $\dot{a}_{z_T}$  to be approximately zero.

A reasonable estimate of  $\theta(0)$  may then be deduced from the relevant expressions in Chapter 3:

$$\hat{\theta}(0|0) = -\arctg(\Lambda_{z_{B_M}}(0)/\Lambda_{z_{B_M}}(0))$$

The zeroshifts  $\Delta\Lambda_{z_0}$  and  $\Delta q_0$  cannot be directly measured in flight prior to the execution of the flight test manoeuvre. Therefore, because no a priori information is available the initial estimates of  $\Delta\Lambda_{z_0}$  and  $\Delta q_0$  are put equal to zero:

$$\hat{\Delta\Lambda_{z_0}}(0|0) = 0$$

$$\hat{\Delta q_0}(0|0) = 0$$

The variance matrices  $P^*(0|0)$ ,  $Q$  and  $R$  have been assumed to be diagonal. Reasonable estimates of the diagonal elements of these matrices may be obtained by consulting the general description of the instrumentation system and the results of several laboratory calibrations in Ref. 8 and 9. The resulting numerical values have been listed in Table 1.

When applying the maximum likelihood algorithm an initial augmented parameter vector  $\beta_0^*$  and variance matrix  $R$  have to be specified.

From the discussion above and the definition of  $\beta^*$  in Chapter 5 it follows  $\beta_0^*$  can be put equal to  $\hat{\beta}^*(0|0)$ .

The elements of the variance matrix  $R$  indicate the accuracy of the barometric measurements of airspeed  $V^A$  and change of altitude  $\Delta z_T$  during quasi-steady flight conditions. In the non-steady parts of the flight test manoeuvre these accuracies are reduced considerably because of

- a) the dynamic response of the air pressure tubes,
- b) the parasite sensitivity of the barometric transducers to accelerations.

The additional errors introduced into the barometric measurements in non-steady flight conditions depend on the non-steady motion of the aircraft and can therefore not be represented by independent random processes.

For these reasons it was decided to neglect the barometric measurements during the non-steady parts of the flight test manoeuvre.

Application of the extended Kalman filter, the fixed interval smoothing algorithm and the maximum likelihood estimation algorithm yield corresponding results i.e. estimates of the components of the state vector during the manoeuvre and in addition estimates of the unknown parameters.

The time history of the state vector  $x$  resulting from the application of the maximum likelihood estimation algorithm is presented in Fig. 4. Starting from the initial parameter vector  $\beta_0$  convergence was achieved within 10 iterations. The related residuals are shown in Fig. 5. Fig. 5 clearly illustrates the non-randomness of the errors introduced into the barometric measurements during the non-steady parts of the flight test manoeuvre. The extended Kalman filter yields a similar result, Fig. 6.

The results of the extended Kalman filter, the fixed interval smoothing algorithm and the maximum likelihood estimation algorithm have been compared in Fig. 7 and 8. With respect to Fig. 7 it should be remarked that because the zeroshifts have been assumed to be constant in the course of one flight test manoeuvre the final estimates of  $\Delta\Lambda_{z_0}$  and  $\Delta q_0$  resulting from the extended Kalman filter are not altered by subsequent application of the smoothing algorithm. From the state vector airspeed  $V^A$ , flightpath angle  $\gamma^A$  and angle of attack  $\alpha$  can be derived by applying (3-3), (3-4) and (3-5). In Fig. 9 the resulting time histories are compared.

From Fig. 8 and Fig. 9 it follows that subsequent application of the smoothing algorithm reduces considerably the differences between the results of the extended Kalman filter and the maximum likelihood estimation algorithm.

## 7. CONCLUSIONS

Two different estimation schemes i.e. the extended Kalman filter and fixed interval smoothing and the maximum likelihood estimation algorithm have been applied to the problem of estimating the aircraft state trajectory during a non-steady flight test manoeuvre.

When applying the extended Kalman filter and fixed interval smoothing algorithm the state trajectory estimation problem is linearized about a nominal trajectory. The result therefore constitutes an approximate solution to the problem.



It has been argued that due to the quality of the measurements of the components of the input vector (i.e. the outputs of the inertial transducers) and the accuracy of the mathematical model the plant noise could be assumed to be small enough as to be neglected. This simplifies the state trajectory estimation problem considerably. An exact solution to this simplified estimation problem is provided by the maximum likelihood estimation algorithm.

The results obtained from both estimation schemes closely correspond to each other. This may be best illustrated by the estimated time histories of air speed  $V^a$  and angle of attack  $\alpha$ . As mentioned in the Introduction, these variables are of prime importance in aircraft flight testing. From Fig. 9 follows the differences between the results of both estimation schemes are in the order of  $0.25 \text{ m sec}^{-1}$  in the case of  $V^a$  and  $0.001 \text{ rad}$  or  $0.06^\circ$  in the case of  $\alpha$ .

These closely corresponding results indicate that when applying high accuracy instrumentation techniques both estimation schemes provide an accurate solution to the aircraft state trajectory estimation problem.

#### ACKNOWLEDGEMENT

The author wishes to acknowledge the assistance of Mr. P.J. Verkerk of Delft University of Technology in carrying out the computations.

#### 8. REFERENCES

1. W.R. Simpson, "The development of dynamic flight test techniques for the extraction of aircraft performance", AIAA Paper 72-785, 1972.
2. O.H. Gerlach, "Analysis of a possible method for the measurement of performance and stability and control characteristics of an aircraft in non-steady symmetric flights", in Dutch with summary in English, Report VTH-117, Department of Aeronautical Engineering, Delft University of Technology, 1964.
3. R.J.A.W. Hosman, "A method to derive angle of pitch, flightpath angle and angle of attack from measurements in non-steady flight", Report VTH-156, Department of Aeronautical Engineering, Delft University of Technology, 1971.
4. R.C. Wingrove, "Applications of a technique for estimating aircraft states from recorded flight test data", AIAA Paper 72-965, 1972.
5. J.A. Mulder, "Aircraft performance measurements in non-steady flights", proceedings 3rd IFAC symposium on "Identification and system parameter estimation", Delft-The Hague, 1973.
6. H.L. Jonkers, "Application of the Kalman filter to flightpath reconstruction from flight test data including estimation of instrumental bias errors", Report VTH-162, Department of Aeronautical Engineering, Delft University of Technology, to be published.
7. O.H. Gerlach, "The determination of stability derivatives and performance characteristics from dynamic manoeuvres", Report VTH-163, Department of Aeronautical Engineering, Delft University of Technology, 1971.  
Also in AGARD Conference Proceedings No. 85 on "Flight test techniques", 1972.
8. H.L. Jonkers, J.A. Mulder, K. van Woerkom, "Measurements in non-steady flight: instrumentation and analysis", proceedings of the 7th International Aerospace Instrumentation symposium, Cranfield, England, 1972.
9. R.J.A.W. Hosman, "Advanced flight test instrumentation: design and calibration", Memorandum M-222, Department of Aeronautical Engineering, Delft University of Technology, 1974.
10. H.W. Kleingeld, "Design and evaluation of a symmetric flight test manoeuvre for the estimation of performance, stability and control characteristics", Miscellaneous paper MP-74-029, National Aerospace Laboratory (NLR), 1974.
11. B. Etkin, "Dynamics of flight", John Wiley and Sons, 1959.
12. J.J. Haltiner, F.L. Martin, "Dynamical and physical meteorology", McGraw-Hill, 1957.
13. J.A. Mulder, "Some aspects of performance measurements in non-steady flight", Deutsche Luft- und Raumfahrt Mitteilung 73-25, 1973.
14. H.W. Sorenson, "Comparison of Kalman, Bayesian and maximum likelihood estimation techniques", AGARDograph 139 on "Theory and applications of Kalman filtering", 1970.
15. A.P. Sage, J.L. Melsa, "Estimation theory with applications to communication and control", McGraw-Hill, 1971.
16. R.D. Grove, R.L. Bowles, S.C. Mayhew, "A procedure for estimation stability and control parameters from flight test data by using maximum likelihood methods employing a real-time digital system", NASA TN D-6735.

$$\begin{aligned}\text{diag } P^0(0|0) &= ((1)^2, (2)^2, (1)^2, (1 \cdot 10^{-1})^2, (2 \cdot 10^{-2})^2, (1 \cdot 10^{-4})^2) \\ \text{diag } Q &= ((4 \cdot 10^{-3})^2, (2 \cdot 10^{-3})^2, (6 \cdot 10^{-3})^2, (5 \cdot 10^{-5})^2, (1 \cdot 10^{-4})^2, (5 \cdot 10^{-4})^2) \\ \text{diag } R &= ((5 \cdot 10^{-1})^2, (1)^2)\end{aligned}$$

Table 1. Numerical values of the elements of the variance matrices of the estimate initial augmented state, the plant noise and the measurement noise.

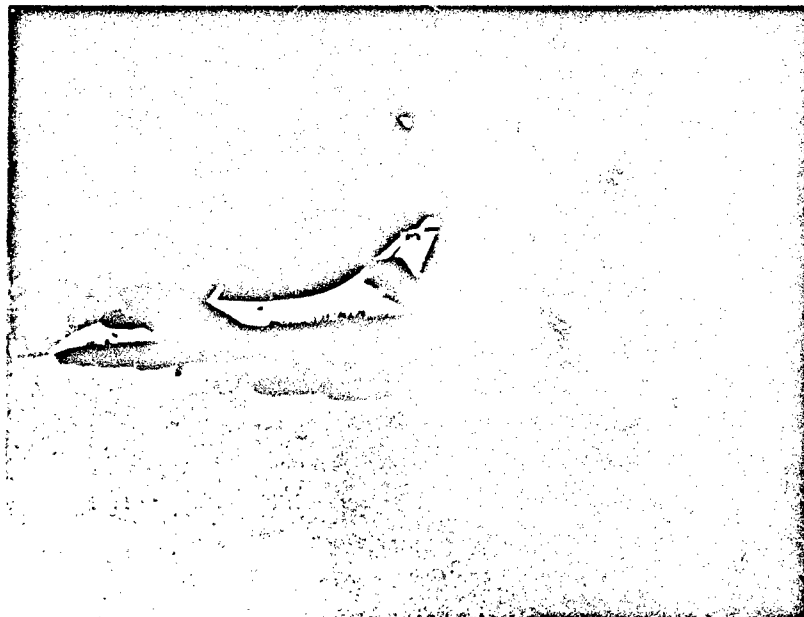


Fig. 1. The Hawker Hunter mk VII laboratory aircraft of the National Aerospace Laboratory (NLR). Note static pressure trailing cone.

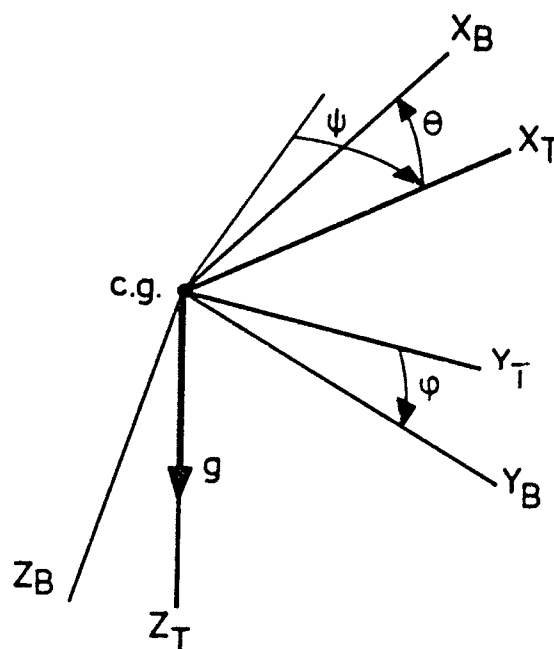


Fig. 2. Definition of the vehicle carried vertical reference frame  $F_T$  and body fixed reference frame  $F_B$ .

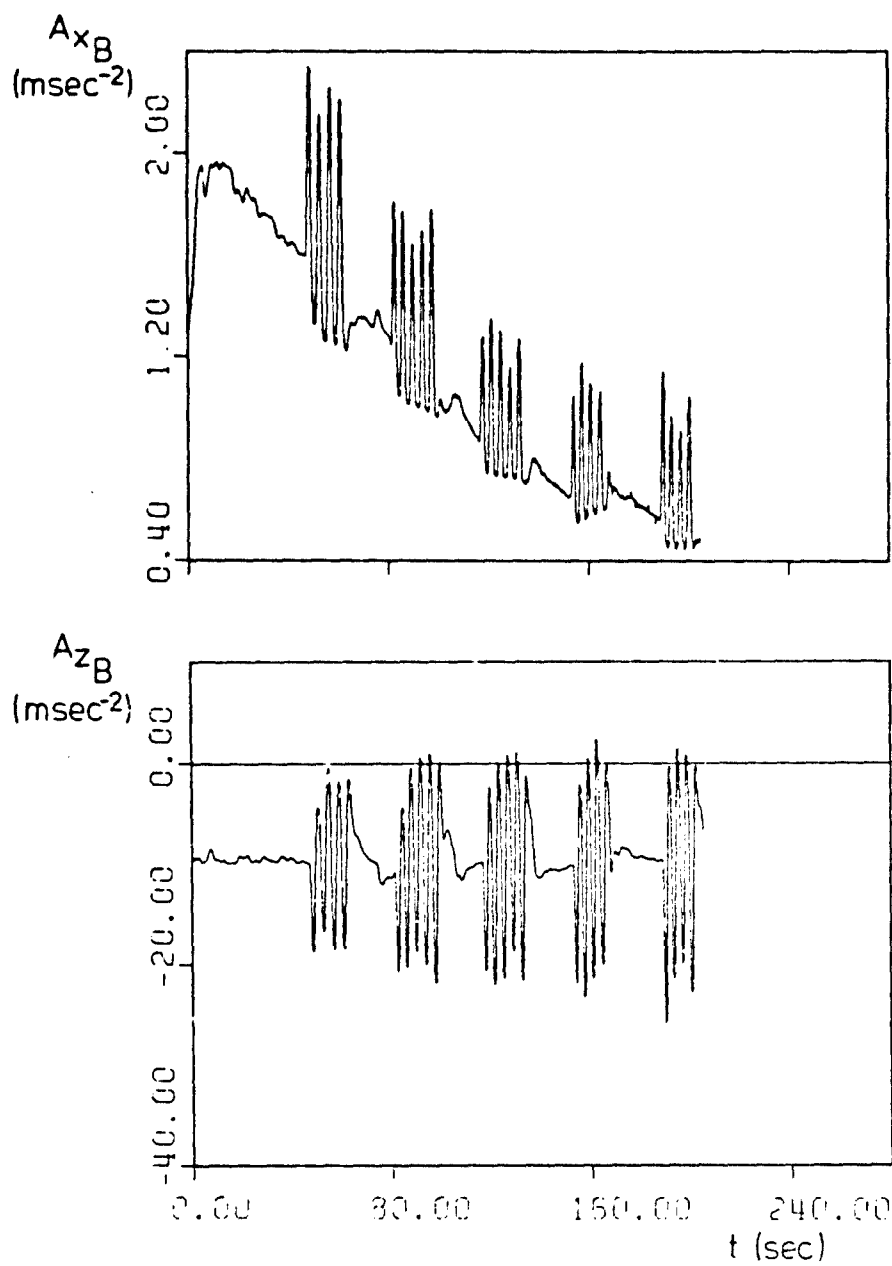


Fig. 3. "Symmetrical components" and "asymmetrical components" of the input vector  $u$  during the nominally symmetric non-steady flight test manoeuvre.

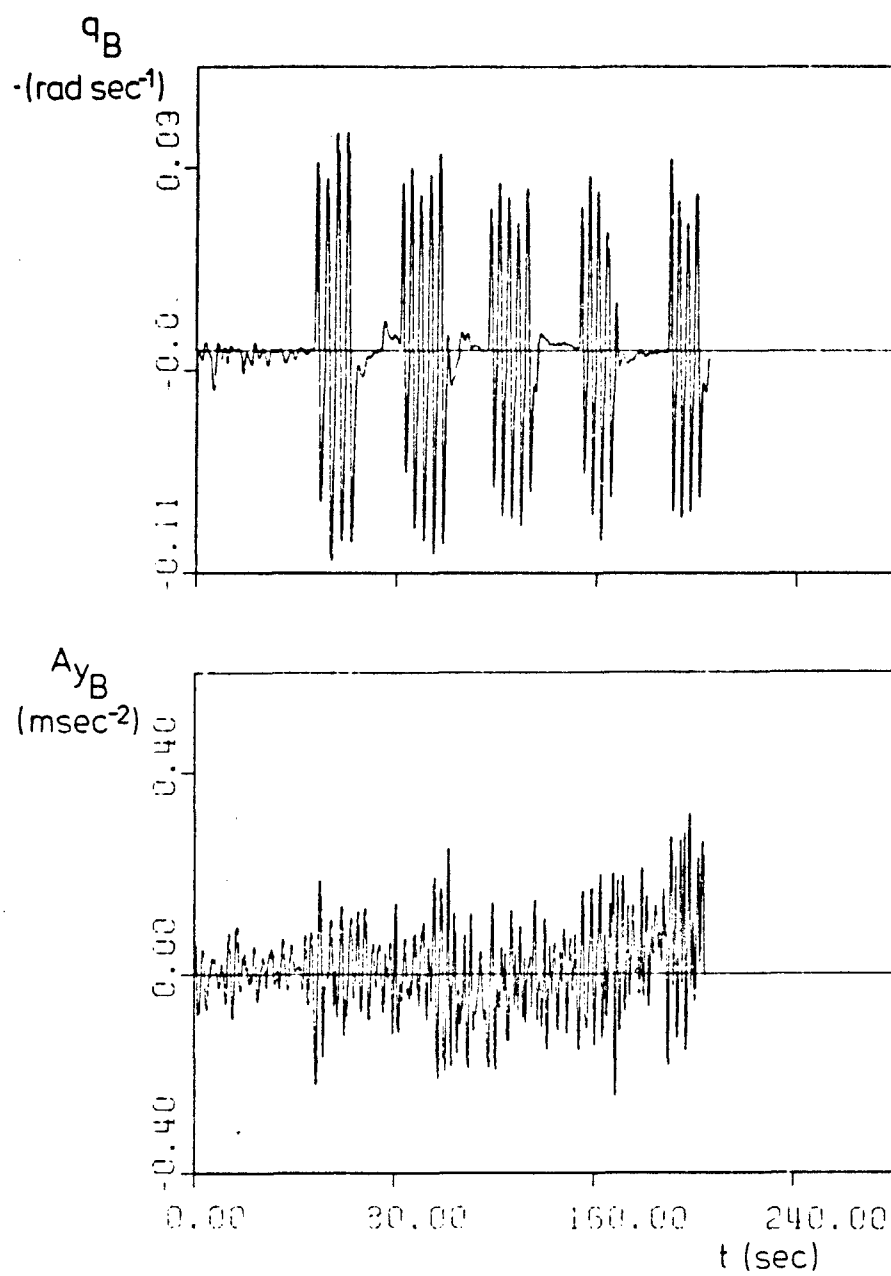


Fig. 3 continued.

19-12

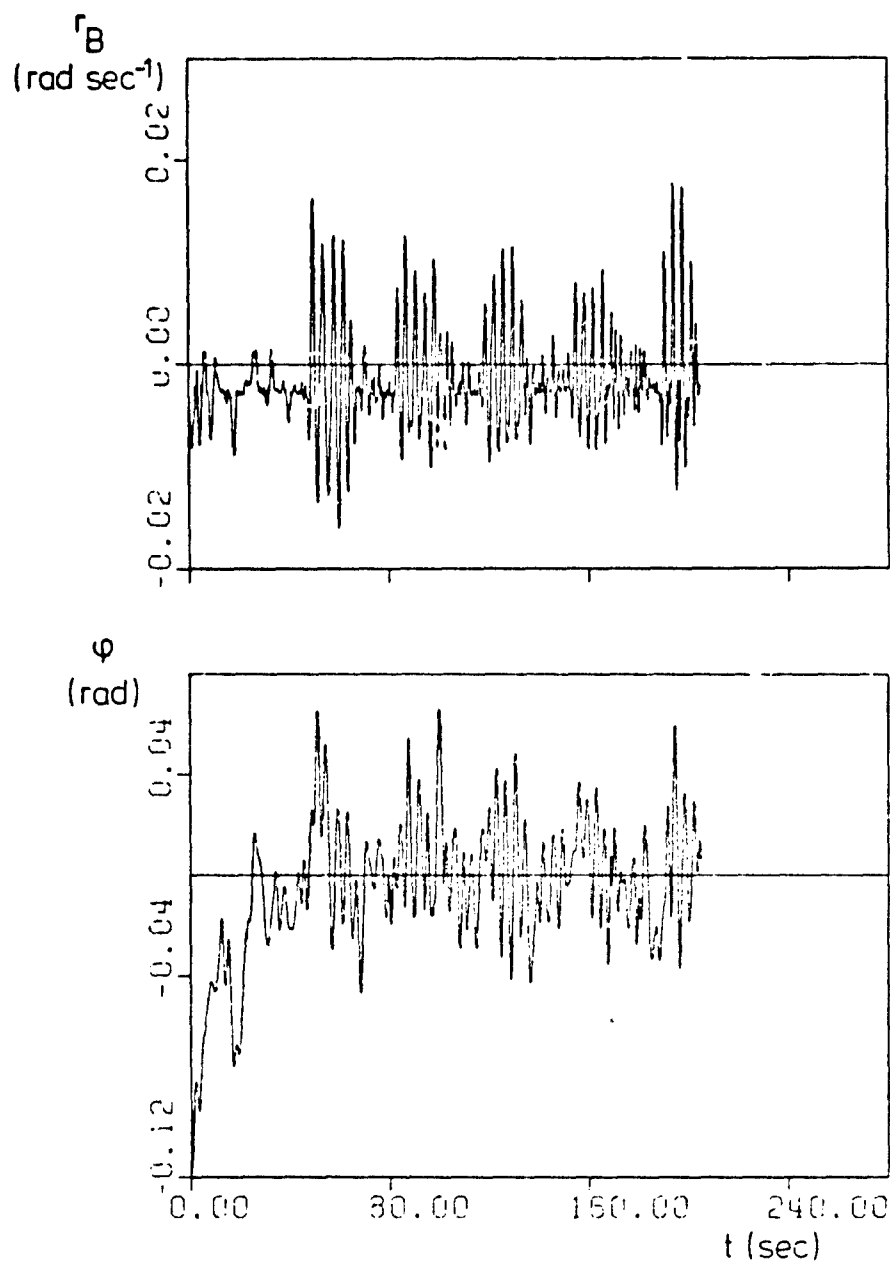


Fig. 3 continued.

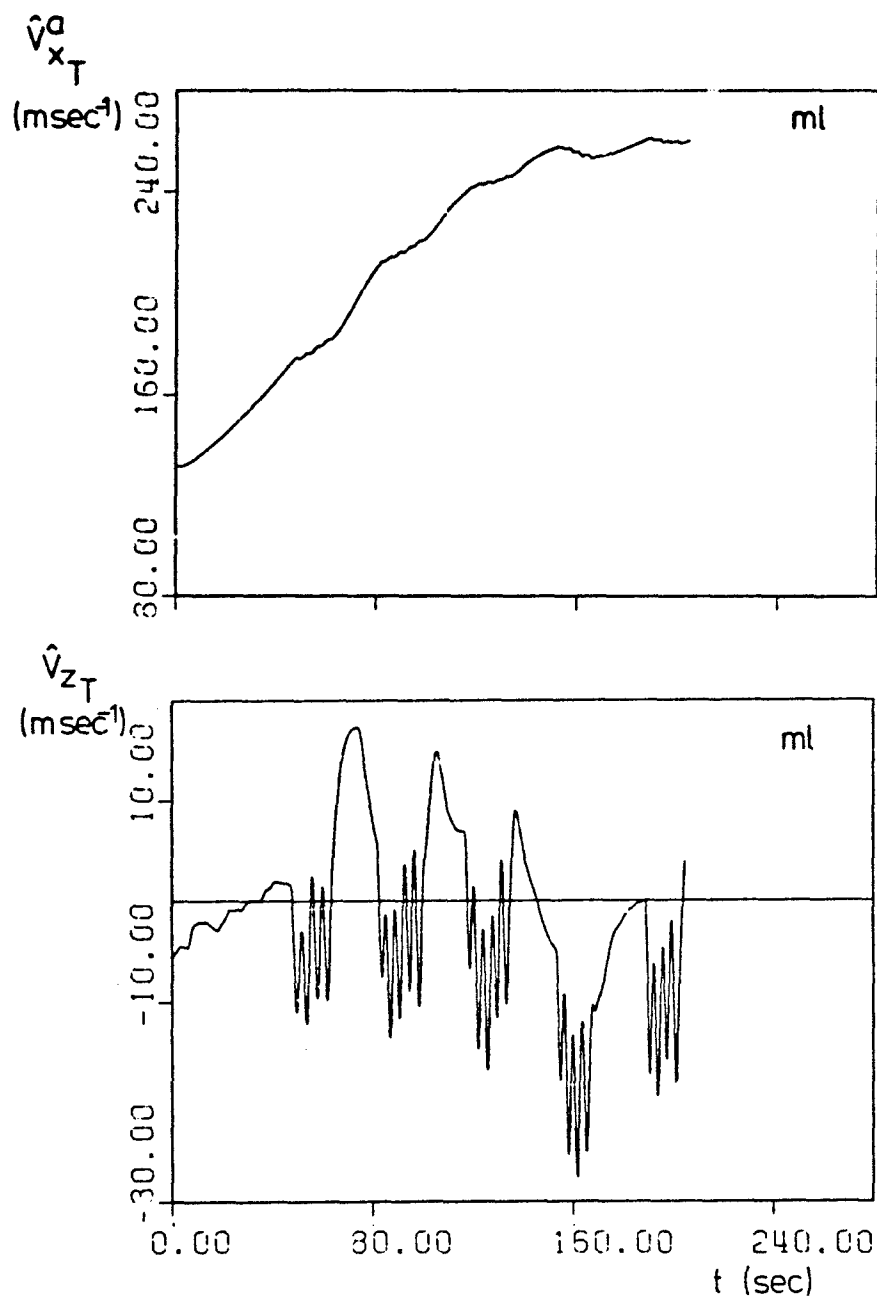


Fig. 4. Maximum likelihood estimate of the state vector  $x$  during the non-steady manoeuvre.

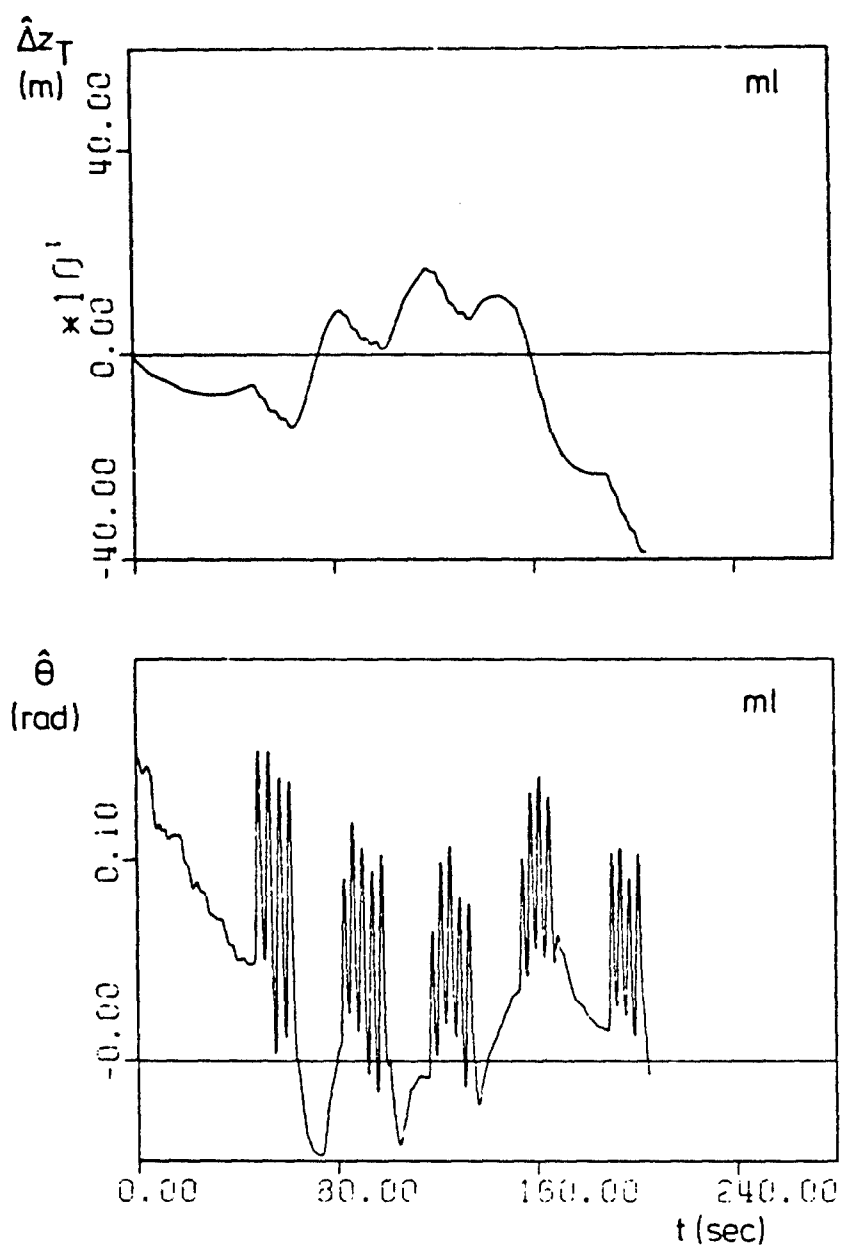


Fig. 4 continued.

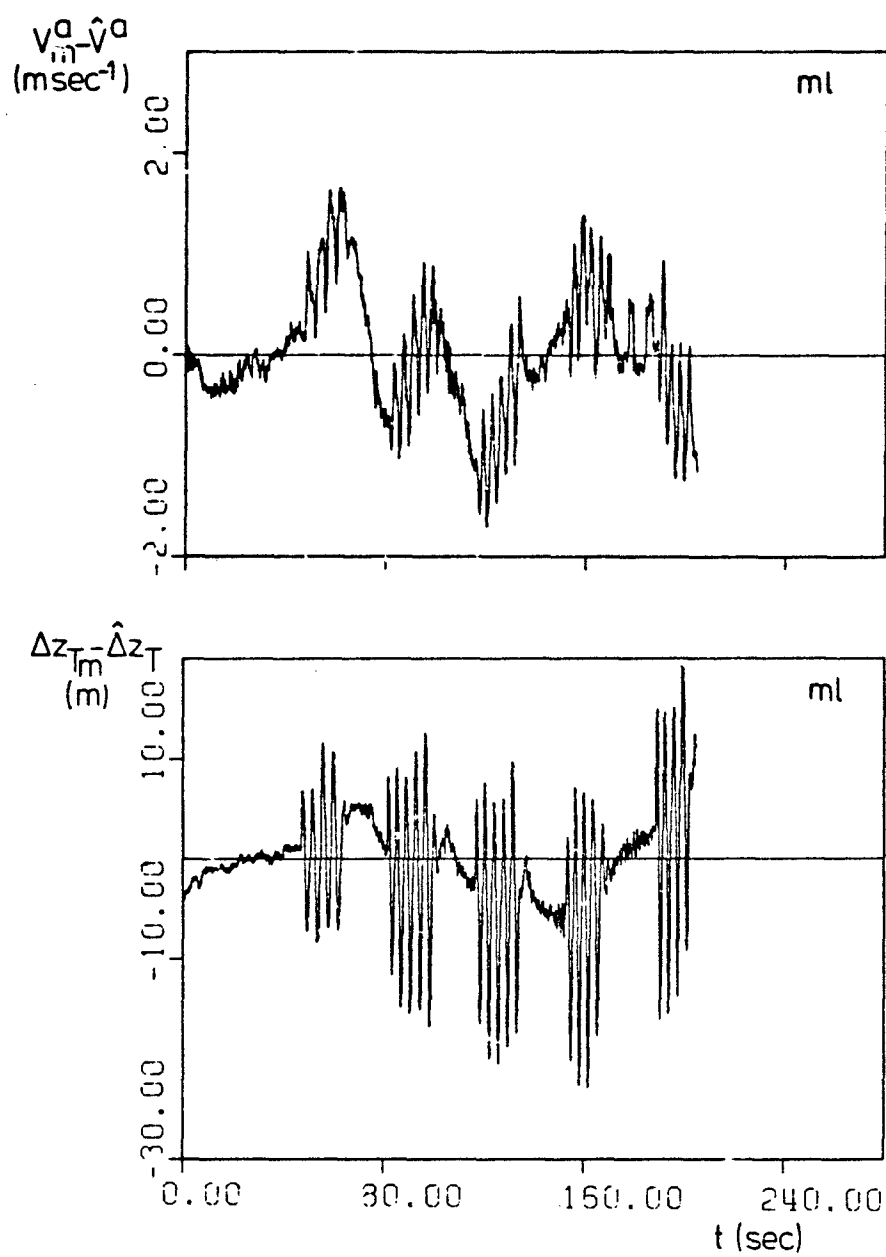


Fig. 5. Residuals resulting from application of the maximum likelihood estimation algorithm.



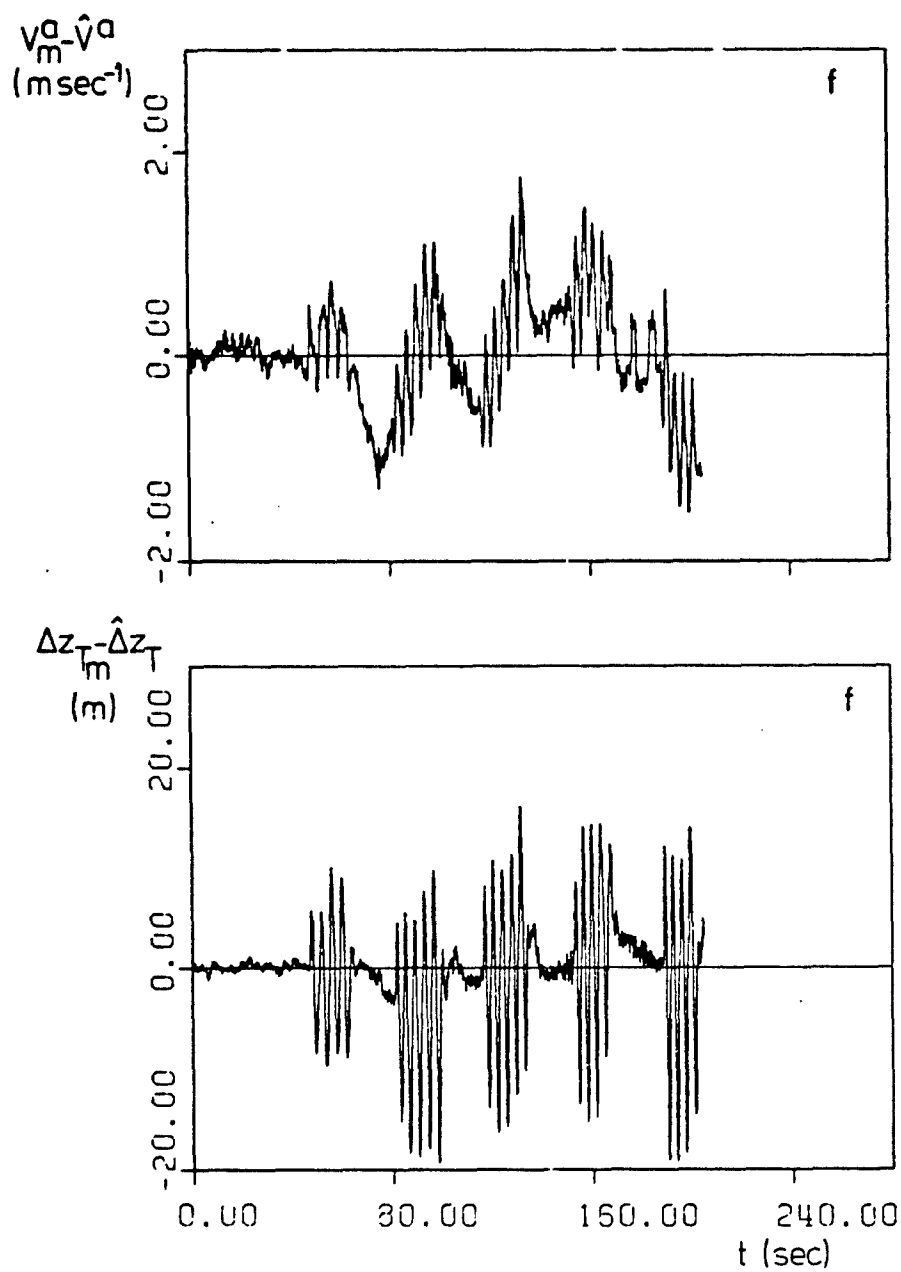


Fig. 6. Residuals (innovations) resulting from application of the extended Kalman filtering algorithm.

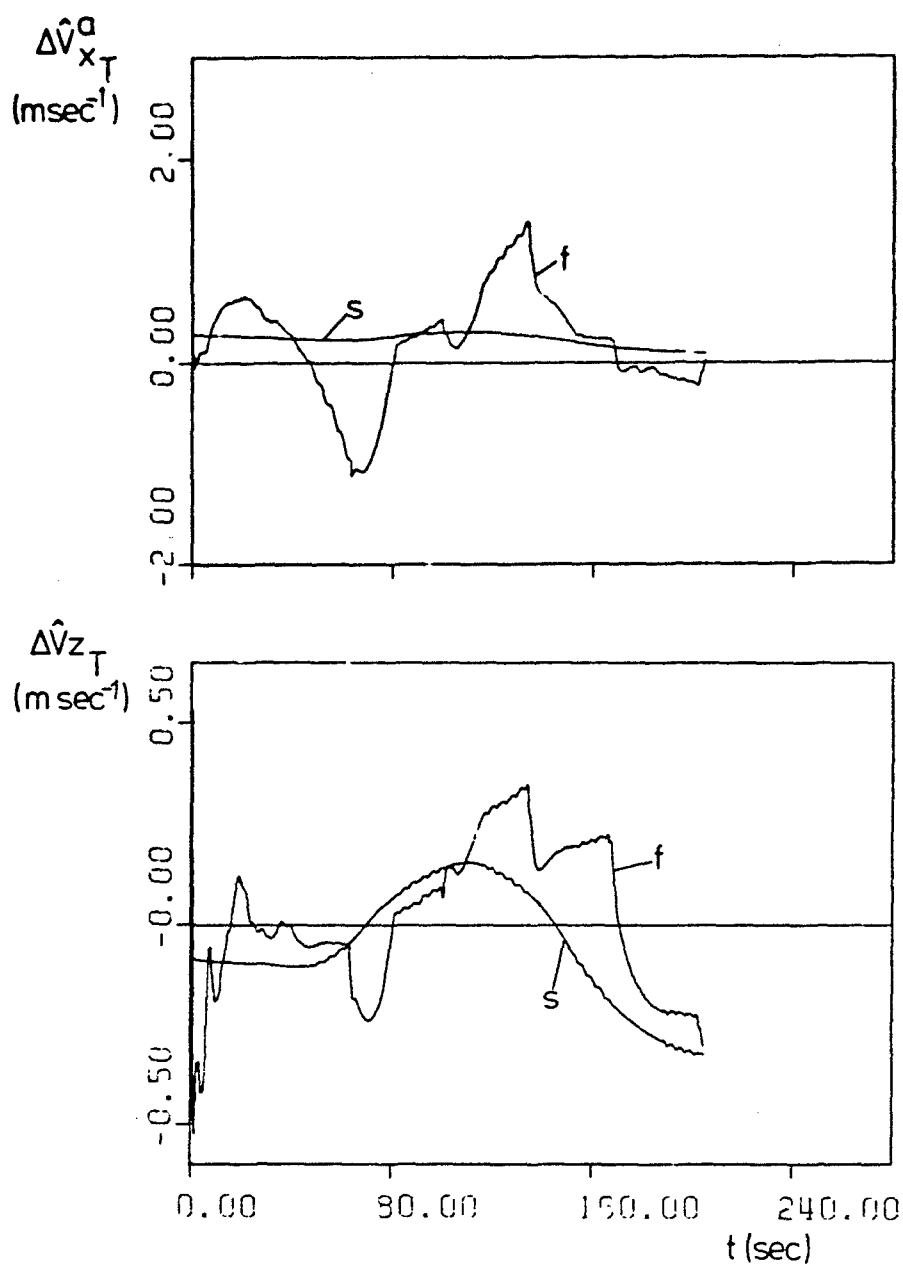


Fig. 7. Difference between extended Kalman filter and maximum likelihood estimates (f) and fixed interval smoothing and maximum likelihood estimates (s) of the state vector  $x$ .

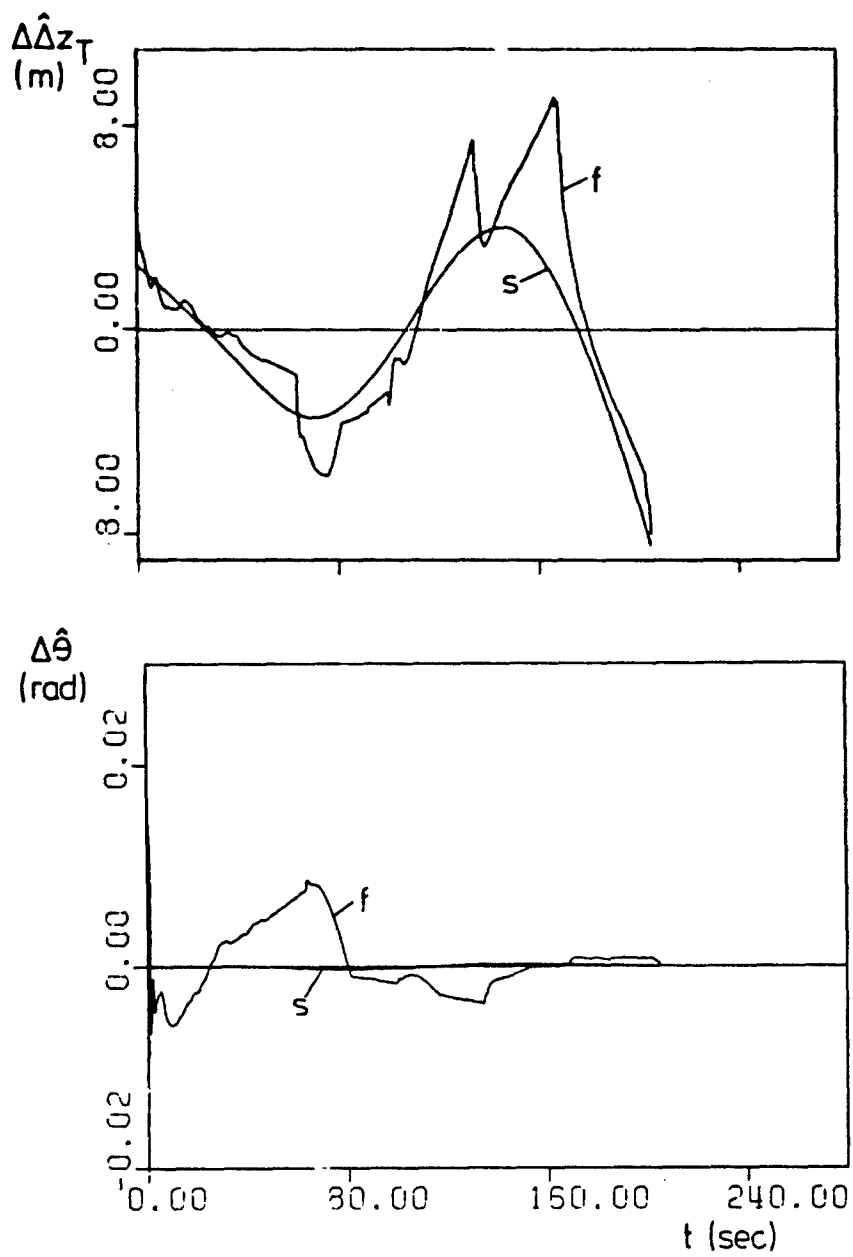


Fig. 7 continued.

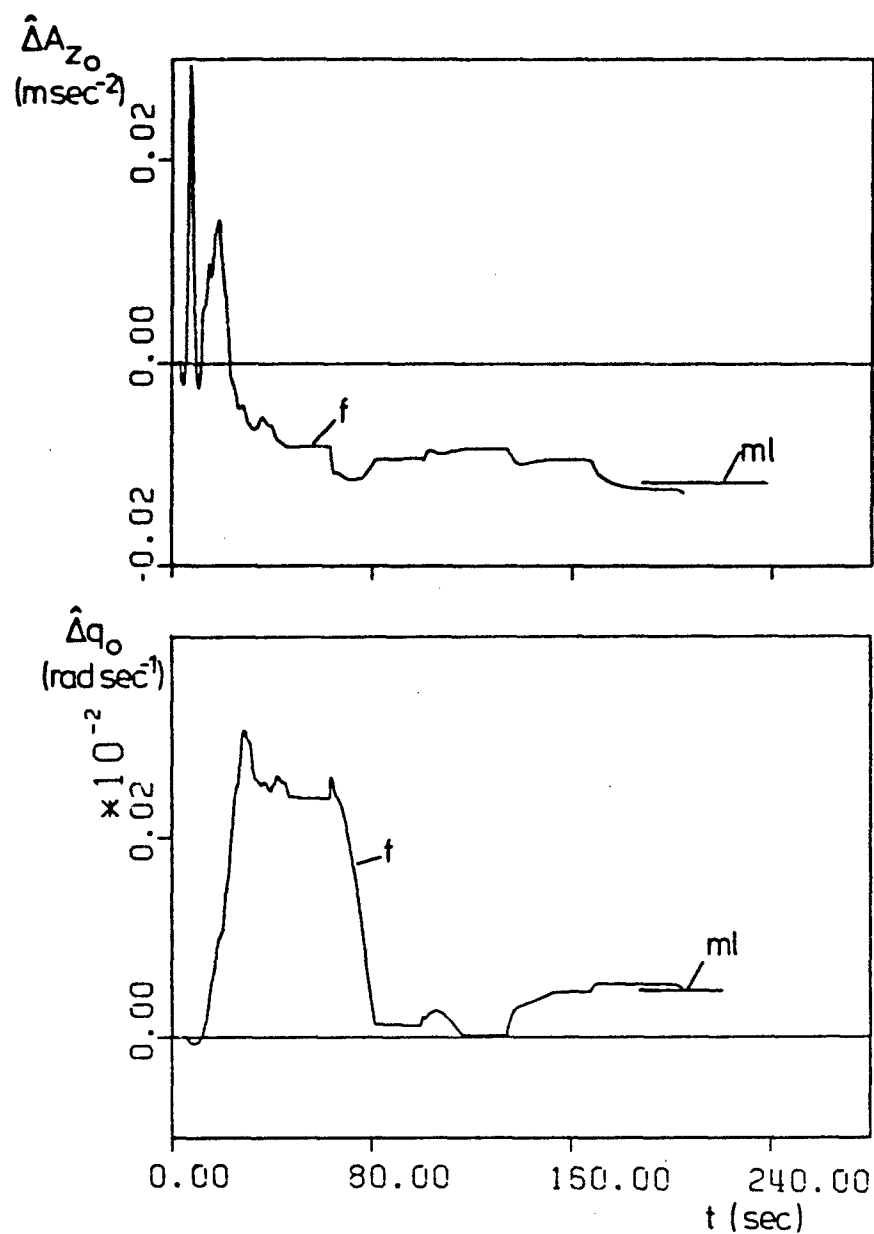


Fig. 8. Extended Kalman filter estimates of the zeroshifts compared to the corresponding results from the maximum likelihood estimation algorithm.

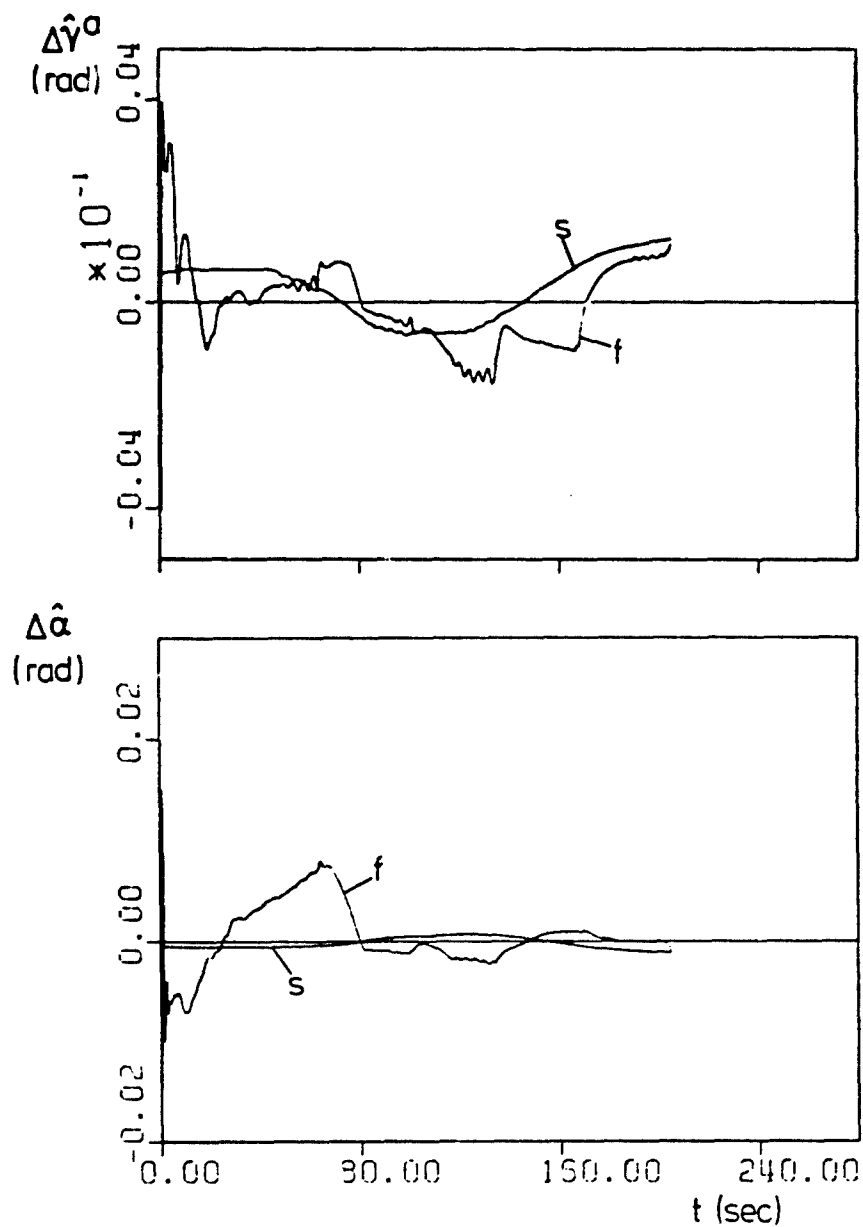


Fig. 9. Difference between extended Kalman filter and maximum likelihood estimates (f) and fixed interval smoothing and maximum likelihood estimates (s) of flightpath angle, angle of attack and airspeed.

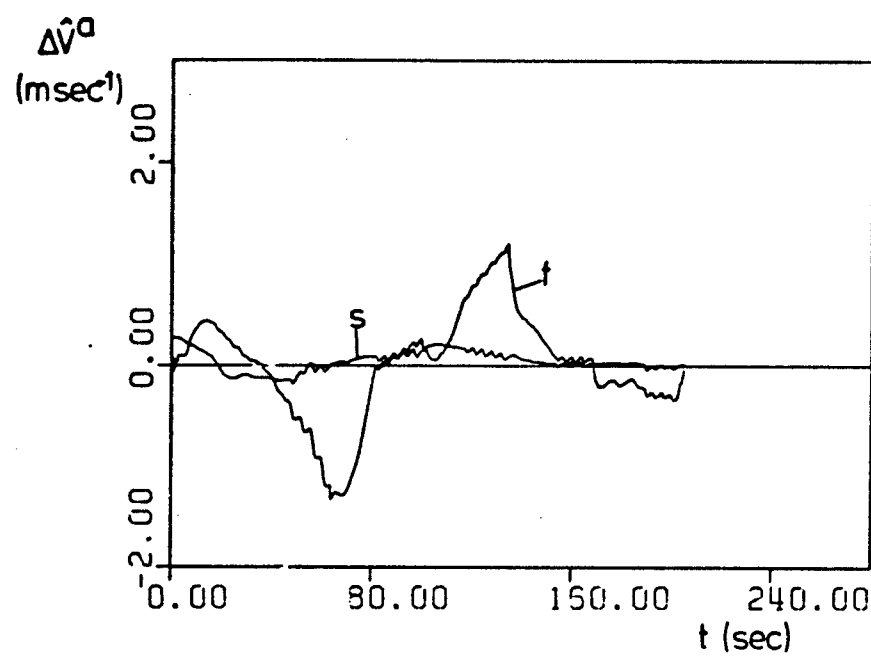


Fig. 9 continued.

# DETERMINATION OF STABILITY DERIVATIVES FROM FLIGHT TEST RESULTS

## BY MEANS OF THE REGRESSION ANALYSIS

by  
HEINZ FRIEDRICH  
DORNIER GMBH  
D-7990 FRIEDRICHSHAFEN  
POSTFACH 317

### SUMMARY

First some fundamental remarks about the analysing method, the regression analysis, are made. Then briefly the method is described and some test results with simulated data are given.

The experiences with the regression analysis gained from flight tests with the aircrafts Dornier Do 31 and Fiat G91-T3 are discussed in detail. With these experiences the possibilities of the method are discussed and improvements by using a Kalman filter are shown.

Finally, for each equation of motion an example with good results is represented.

### 1. FUNDAMENTAL REMARKS ABOUT THE ANALYSING METHOD

At first, some fundamental remarks about the analysing method seem to be necessary. Thereby also the system inherent advantages and disadvantages will be expressed.

Indeed the term "regression analysis" is not correct. It describes only a part of the method, but surely the most important one regarding the mathematics. The method deals with a direct analysis, i.e. the solution of the equation of motion. This sort of method is known as "equation error" method or "equation of motion" method. All these methods determine one value from the equation of motion and all other values must be known from the configuration or from measurements. Consequently, these are simple methods with a closed solution in one step. They are distinguished by the value which is determined and its further processing.

These methods use the physically most obvious way and so a solution without iteration and without coupling of equations of motion is obtained. But there is an important disadvantage, all state parameters are needed and measurement errors are not considered. Therefore many variables must be measured with high accuracy.

In the past, it was tried to overcome this deficiency by means of integration or transformation of the equation system. Here another way is taken. In each equation of motion the aerodynamic coefficient is assumed as unknown. This reduces the difficulties in the first step. The difficulties are now in the second step, i.e. the determination of the stability derivatives from the aerodynamic coefficients. This is done with the regression technique. Therefore, the whole method is called "regression analysis".

## 2. DESCRIPTION OF THE METHOD

The method will not be described in detail. This has already been done in [1]. In the following only the approach will be summarized.

1. Step: The aerodynamic coefficients are determined from the equations of motion (fig. 1).
2. Step: The stability derivatives are determined from the aerodynamic coefficient (fig. 2).

Figure 1 contains the equations of motion used here, and figure 2 shows the aerodynamic coefficients as functions of the stability derivatives and the state variables. The left parts of the equations in fig. 2 were determined in the first step. The state variables are measured. The unknowns are the stability derivatives.

Since each one of these equations can be solved with one observation and each flight test consists of many observations, the stability derivatives can be determined with statistical methods, i.e. with the method of least squares. With the linear equation, this is a problem of the general, linear regression, as it is shown in a general form in fig. 3. The solution of this relatively simple problem leads to the wellknown normal equations (fig. 4). The normal equations are solved as shown in fig. 5.

The computer program has no numerical difficulties. Additional computed parameters facilitate the discussion of the results. Details - as already mentioned - can be seen in [1].

So all stability derivatives from one flight condition are obtained in one single run of the computer program. Another advantage is that the method runs as closed program completely independent of the experience and of the skill of the user.

But there are also grave disadvantages. First the aforementioned difficulty to need many measurements with high accuracy. This fact is additionally complicated, because all variables must have enough motion to get the stability derivatives. In fact, the mathematical statistics require as much random motion as possible.

A further disadvantage is the fact that each observation is considered separately. This leads to great difficulties with phase errors. A correction is impossible, since the motions have to be stochastic.

Consequently, the method implies an extreme alternative, either to get all derivatives in a relatively simple way or else to obtain bad results. So in practical application failures are expected. But generally, the flight test analysis keeps involving failures. However, our activities - which were discussed at another point of the meeting - show, that in flight test analysis several methods should be applied simultaneously. And always the regression analysis should be included, since it requires only a little time for flight testing and analysis and it checks the measured values. This will be illustrated in the following.

## 3. TESTS WITH SIMULATOR DATA

The digital computer program "regression analysis" was tested with simulator data. These tests also are described in detail in [1]. Here only a few important results are stated.

To begin with the most important result: The method found exactly the stability derivatives programmed in the simulator. Fig. 6 shows the deviations for a data set with 14 000 observations. These deviations can all be explained by peculiarities and inaccuracies of the analog computer program. For details see [1].

The test data came from a simulated flight with more motion than in a real flight, in order to detect all derivatives. With the regression analysis, the means of the state variables are determined and then the



derivatives to these means are calculated. When coefficients are programmed in the simulator as non-linear functions, the values of the tangent are calculated.

In fig. 7 the influence of the number of observations on the quality of the results is shown. The figure is typical for stability derivatives. For more than 10 000 observations, practically the interval remains constant. For less than 3 000 observations, some results show already important deviations. Consequently, with a scan frequency of 40 to 50 Hertz, a flight time of only 1 to 5 minutes is required for the analysis.

Also the influence of additional or lacking components was tested. Fig. 8 shows a typical test of supposed but not existing components. The simulation program has no relation between the drag  $C_D$  and the aileron deflection  $\xi$  or angle of sideslip  $\beta$ . Therefore, the stability derivatives  $C_{D\beta}$  and  $C_{D\xi}$  must be zero. According to fig. 8 this result was obtained, as the little values are insignificant. But the most important result of this test is the fact that the surplus variables do not affect the existing derivatives. So we can include any supposed influences into the analysis without changing the regression coefficients or impairing the quality of the regression - as it is shown in the multiple correlation coefficient.

In the contrary, the multiple correlation coefficient shows, whether all influences have been considered (fig. 9). In fig. 9 in the sideforce equation the most important variable, the angle of sideslip  $\beta$ , was not considered. Of course, now the complete analysis was wrong. But the lacking of a component was shown in the bad multiple correlation coefficient.

Thus the tests show that the method can easily be used with very short flight time. Moreover, it has proved that the method is very well suited to find not expected influences or, in turn, to prove that supposed influences are not existing.

#### 4. RESULTS OF FLIGHT TEST ANALYSIS

Now let's talk about the practical application. Three different flight test periods were analysed, flight tests with the conventional version of the Do 31 and with a Fiat G91-T3. The tests with the G 91 were carried out in two periods. Fig. 10 to 15 summarize the results, that is one figure for each equation of motion.

First some general remarks to the flight tests. The first analysing trials were made with flight tests from the Do 31. As expected, they did not show the same good results as the test data from simulation. With these tests only the regression technique was tested. The deficiencies of the equation methods were suppressed, as the aerodynamic coefficients directly came from the simulation. In the flight tests, however, these deficiencies were fully present.

The results of this first analysing period mainly were used to test the data acquisition equipment and the measurements. (Here, this important aspect with the application of the regression analysis cannot be discussed. For details see [3]). This test was used to improve and to expand the test equipment.

Thus, the second test period was realized with an improved data acquisition system. But now, another type of aircraft was used, instead of the transport aircraft Do 31, now the light fighter Fiat G91-T3. We then experienced the wellknown effect of being faced with completely different problems. The first test period with the G 91 did not show any improvement in the results, on the contrary, partly they were even worse. The discussion of the measurements by means of regression analysis showed an impairment of the signals for the incidence  $\alpha$  and the sideslip  $\beta$  which could not yet be explained. Furthermore there were considerable phase errors, caused by electronic filters, which are required for damping the aircraft vibrations. Against the phase errors the filters were adjusted so that all signals showed approximately the same time error. Then the second test period with the G 91 showed an amazing success of this rough phase correction.

Now let's discuss the figures. Fig. 10 represents the results of the lift equation. It shows the improvement in the second period with the G 91. Also this figure illustrates the known problems with  $\dot{\alpha}$ -derivatives. Of course, these influence the whole equation of motion, particularly the derivative  $C_{L\dot{\alpha}}$ .

Fig. 11 contains the results for the drag equation. Here, the results of the first period G 91 were so good that the second period did not show any improvement. In the second test period it can be seen, how an error in  $C_{D0}$  is compensated by an opposite error in  $C_{D\dot{\alpha}}$ .

For the results of the pitch motion (fig. 12) the same is true as for the lift. There is again the bad influence of  $\dot{\alpha}$ . In the pitching moment, the improvement from the first test period to the second is even more distinct.

Now the lateral motion. Fig. 13 shows the sideforce derivatives. Clearly it is to see the impairment of the sideslip signal from the G 91 compared to the Do 31. Also the influence of the phase correction clearly can be recognized.

For the results of the roll equation in fig. 14 the same is true as for the sideforce. Here also the impairment in the sideslip signal of the G 91 can be seen. And there is also a considerable influence by phase correction.

Finally, fig. 15 represents the derivatives of the yaw motion. Here are the same tendencies as already for the sideforce and for the roll motion.

With the results in fig. 10 to 15, the following forecast (fig. 16) can be made for the chances of flight test analysis with regression analysis. The determination of  $C_{D0}$ ,  $C_{D\dot{\alpha}}$  and  $C_{Y\dot{\alpha}}$  has very good chances. However, there are only small chances for the derivatives  $C_{L\dot{\alpha}}$ ,  $C_{m\dot{\alpha}}$ ,  $C_{l\dot{\alpha}}$ ,  $C_{l\dot{\alpha}}$  and  $C_{n\dot{\alpha}}$ , and very likely no chance for  $\dot{\alpha}$ -derivatives. The difficulties with  $\dot{\alpha}$  explain the small chances for  $C_{L\dot{\alpha}}$  and  $C_{m\dot{\alpha}}$ . The difficulties with  $C_{l\dot{\alpha}}$  and  $C_{n\dot{\alpha}}$  are unexpected. It is supposed they are caused by errors of measurements.

## 5. FUTURE ACTIVITIES

Of course the aim of future activities is an improvement of the results. For an equation error method, this means always an improvement of the test equipment. As already mentioned above, just the regression analysis is very well suited for measurement discussion.

But, we took an additional way for the improvement. The large improvements which have been realized already with a rough phase correction seems to promise success with a prefiltering of the measurements.

Fig. 17 shows the most obvious way of the analysis using the Kalman filtering. The further processing by means of the regression analysis is represented by a dotted line. On principle, it is possible to apply the Kalman method in this way. But this requires an iteration, since the aircraft model enters into the filter algorithm, and the most essential part of the model - the model of aerodynamics - is the result of the whole analysis. However, the main difficulties lies in the very complex equations of the external forces and moments which would require an extensive calculation and programming with considerable sources of errors.

Finally, the setup according to fig. 18 was selected. This makes reasonable use of the redundancy in the measurement vector. Thus we get a considerably simpler form of the dynamic equations. The state variables are the same as in the initial setup. However, as given function of time-parameters of our dynamic system the corresponding measurements of the translational and rotational accelerations are introduced into the equations of motion, instead of the aerodynamic forces and moments as function of state variables, aerodynamic coefficients and control deflections. But the aircraft motions must be sufficiently slow in re-

lation to the data acquisition frequency. This permits to integrate the differential equations over an acquisition cycle with constant values of the accelerations.

An important point of this way is the aircraft model (i.e. the aerodynamics) will not be used. This seems reasonable for data filtering as a prefilter before regression analysis. Now the aircraft model to be analyzed in a later step, do not enter the filter. So the Kalman filtering becomes a closed task in the total work of analysing.

It is also attempted to use the Kalman method to filter out quantitatively still unknown systematic errors, such as zero shift, calibration errors, installation errors. Since these activities are not yet concluded, they cannot be discussed here. However, the filter is already programmed. The program is just now in the test phase. The test results are promising for the future. But the adjustment of all parameters is very hard and requires a long time. A first report with the filter program soon will be published as a study for the German Ministry of Defense.

## 6. FINAL REMARK

In the preceding sections the regression method was very critically analyzed. To show the possibilities of the method, for each equation of motion an example with good results finally is given.

It is represented

- in fig. 19 an example from the degree of freedom lift
- in fig. 20 an example from the degree of freedom drag
- in fig. 21 an example from the degree of freedom pitch
- in fig. 22 an example from the degree of freedom sideforce
- in fig. 23 an example from the degree of freedom roll
- in fig. 24 an example from the degree of freedom yaw.

These results need no explanation. They show that also an equation error method in connection with good measuring technique and with statistical methods can supply useful results with relatively low efforts.

## 7. REFERENCES

- [1] H. Friedrich  
Ermittlung der Stabilitätsderivativa aus Flugversuchsergebnissen mit Hilfe der Regressionsanalyse  
Vortrag Nr. 53 der DGLR-Jahrestagung 1969  
  
Übersetzt ins Englische:  
Determining Stability Derivations from Flight Test Results with Aid of Regression Analysis  
Air Force Systems Command, Wright-Patterson AFB, Ohio, Foreign Technology Div.  
Avail: NTIS CSCL 04/3
- [2] K.W. Smillie  
An Introduction to Regression and Correlation  
Academic Press, London and New York, 1966
- [3] U. von Meier, H. Ruf, H. Friedrich, W. Kohl, H.-J. Murser, H. Wönnenberg  
Vergleich von Verfahren zur Durchführung und Auswertung von Flugversuchen zur Bestimmung von Eigenschaften und Leistungen moderner Strahlflugzeuge  
Forschungsbericht aus der Wehrtechnik, BWg-FBWT 73-12, Dezember 1972



	Additional Components	$C_{D\alpha}$	$C_{D\beta}$	$C_{D\gamma}$	Multiple Correlation Coefficient R (%)
Theory	-	1.10	-	-	-
Test Results	-	1.005	-	-	99.99
Test Results with Add. Components	$\beta, \delta$	1.005	-0.00005	-0.00005	99.99

Fig. 8: Test with Additional Components

	Lacking Component	$C_{D\beta}$	$C_{D\gamma}$	$C_{D\delta}$	$C_{D\epsilon}$	Multiple Correlation Coefficient R (%)
Theory	-	-0.024	0.108	0.168	0.077	100
Test Results	-	-0.027	0.1063	0.1675	0.0761	100
Test Results with Lacking Components	$\beta$	-	1.430	-1.030	0.0035	92.97

Fig. 9: Test with a Lacking Component

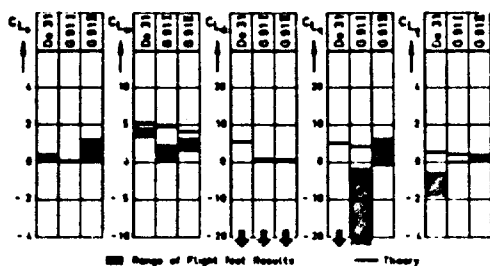


Fig. 10: Flight Test Results Lift-Equation

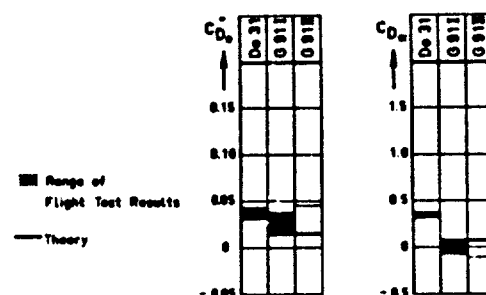


Fig. 11: Flight Test Results Drag-Equation

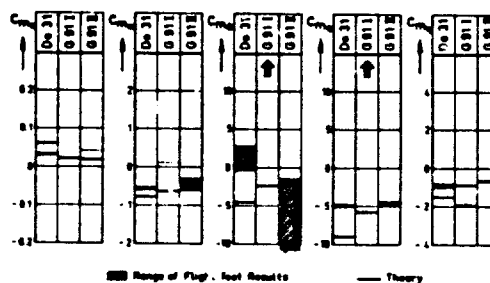


Fig. 12: Flight Test Results Pitch-Equation

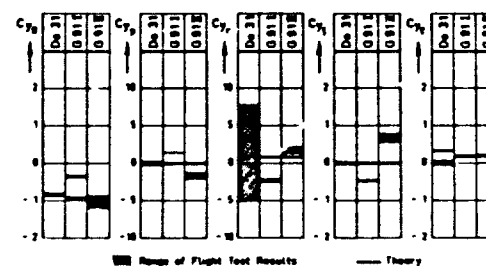


Fig. 13: Flight Test Results Sideforce-Equation

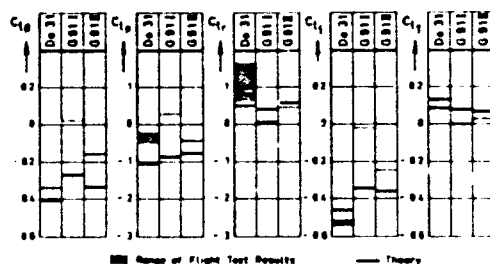


Fig. 14: Flight Test Results Roll-Equation

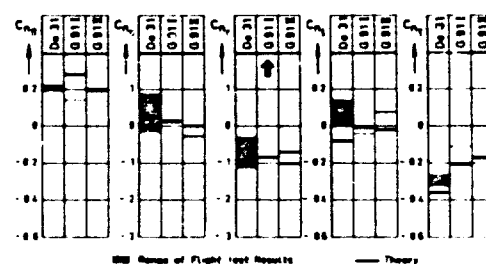


Fig. 15: Flight Test Results Yaw-Equation

	$\alpha$	$\dot{\alpha}$	$q$	$\dot{q}$
$C_L$				
$C_D$				
$C_m$				

	$\beta$	$p$	$r$	$\dot{\beta}$	$\dot{\gamma}$
$C_y$					
$C_l$					
$C_n$					

■ VERY GOOD CHANCE  
 □ GOOD CHANCE  
 ▨ SMALL CHANCE  
 □ NO CHANCE

Fig. 16: Chance to get good Results

	$C_{L\alpha}$	$C_{L\dot{\alpha}}$	$C_{Lq}$	$C_{L\dot{q}}$
Theory	0.2	5.3	1.05	5.15
Result	0.264	4.23	-12.8	4.7

Fig. 19: Regression Analysis of the Lift Equation

	$C_{m\alpha}$	$C_{m\dot{\alpha}}$	$C_{mq}$	$C_{m\dot{q}}$
Theory	0.02	-0.50	-1.0	-4.4
Result	0.045	-0.500	-41.3	-4.42

Fig. 21: Regression Analysis of the Pitch-Equation

	$C_{l\alpha}$	$C_{l\dot{\alpha}}$	$C_{lp}$	$C_{lr}$	$C_{l\dot{\beta}}$	$C_{l\dot{\gamma}}$
Theory	0	-0.335	-0.77	0.50	-0.36	0.063
Result	0.0039	-0.151	-0.400	0.467	-0.244	0.019

Fig. 23: Regression Analysis of the Roll-Equation

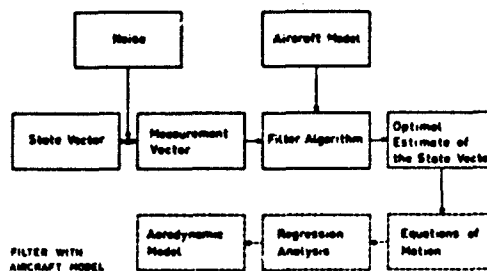


Fig. 17: Parameter Identification with Kalman Filter and Regression

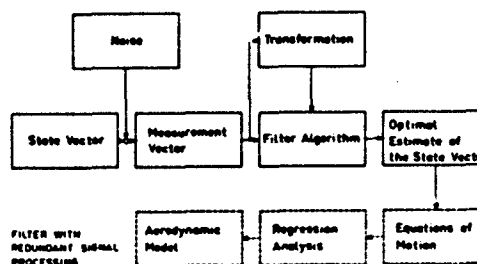


Fig. 18: Parameter Identification with Kalman Filter and Regression

	$C_{D\alpha}$	$C_{D\dot{\alpha}}$
Theory	0.015	0.074
Result	0.014	0.081

Fig. 20: Regression Analysis of the Drag Equation

	$C_{y\alpha}$	$C_{y\dot{\alpha}}$	$C_{yp}$	$C_{yr}$	$C_{y\dot{\beta}}$	$C_{y\dot{\gamma}}$
Theory	0	-0.93	-0.085	0.74	0	0.185
Result	0.008	-0.894	-1.229	1.117	0.504	0.173

Fig. 22: Regression Analysis of the Sideforce-Equation

	$C_{n\alpha}$	$C_{n\dot{\alpha}}$	$C_{np}$	$C_{nr}$	$C_{n\dot{\beta}}$	$C_{n\dot{\gamma}}$
Theory	0	0.19	0	-0.71	-0.02	-0.169
Result	0	0.191	-0.339	-1.044	0.082	-0.172

Fig. 24: Regression Analysis of the Yaw-Equation

MODEL STRUCTURE DETERMINATION AND PARAMETER IDENTIFICATION  
FOR NONLINEAR AERODYNAMIC FLIGHT REGIMES

by

W. Earl Hall, Jr.\*  
Narendra K. Gupta\*\*  
James S. Tyler, Jr.†

SYSTEMS CONTROL, INC.  
1801 Page Mill Road  
Palo Alto, Ca 94304

- \* Program Manager, System Identification and Estimation Division
- \*\*Research Engineer, System Identification and Estimation Division
- † General Manager, Aeronautical and Marine Sector

---

This work was sponsored by the Office of Naval Research  
under Contract N00014-72-C-0328

---

ABSTRACT

A new development for the identification of nonlinear stall/spin regime air dynamic forces and moments is presented, with applications to simulated and flight test response data. This development is a two-step method. The first step is the application of an algorithm which determines the order and coefficients of polynomial expansions of the nonlinear aerodynamic forces and moments which characterize the stall/post-stall flight regime. The second step is the use of a nonlinear six degree-of-freedom maximum likelihood algorithm which accurately estimates the values of the polynomial coefficients. This method has been applied to simulated and flight test data for a twin engine swept wing fighter aircraft. Suggested approaches to more general nonlinear flight regime identification are given.

## 1.0 INTRODUCTION

The stall/post-stall/spin high angle-of-attack operating regime of advanced high performance aircraft is currently recognized as a critical area of the flight envelope which requires more precise definition [1]. The complexity of the dynamic and aerodynamic interactions which characterize such regimes necessitates advanced testing and analysis methods. One of these methods is that of system identification in which flight data from the critical regimes is processed to isolate and quantify the significant aerodynamic contributions.

System identification is emerging as a powerful technology for exploiting test data to significantly improve and increase fundamental knowledge of aircraft dynamics. Such knowledge is essential for more quantitative approaches to handling qualities evaluation, aerodynamic modeling for real time simulations, and verification of analytical and wind tunnel estimates of aerodynamic parameters. In general, system identification consists of at least two phases. The first is the analytical model determination stage wherein the equations and aerodynamic parameters are selected which are to represent the system response. The second phase is the estimation of the parameters of that model from response test data of the system under study. This latter phase is called parameter identification.

For most aircraft testing, the first phase is not a significant issue, since the assumption of a linear, usually longitudinally/laterally decoupled, model is made. This assumption reduces the system identification problem to one of the estimation of the parameters of the linearized models. For transition or extreme flight conditions, however, the assumption of linearity of dynamic and aerodynamic forces and moments may not be accurate. Examples are VTOL aircraft landing or take-off responses and high angle-of-attack aircraft maneuvers. In such regimes, it may be necessary to expand the aerodynamic effects in some type of nonlinear function, usually polynomials in independent flight variables such as angle-of-attack or sideslip angle. It may, in addition, be necessary to retain certain nonlinear dynamic terms to account for inertial cross-coupling effects.

The requirement for nonlinear models thus places stringent demands on the model determination phase of system identification. There are two basic reasons for this. First, a complete mathematical model of the nonlinear responses places severe computational demands on parameter identification algorithms. Hence, the model generally must be reduced in order. Secondly, even if unlimited computer facilities are available, the problem of overparameterization will severely degrade the applicability of the data processing results. Overparameterization is the allowance of more parameters to explain the data than are actually required. The result is excessive computer time, possible algorithm divergences, and incorrect parameter estimates. It is thus necessary in the model determination phase to estimate which terms of a polynomial are actually significant to the response, and to use the parameter identification phase to estimate the value of these terms.

This paper presents a method for performing the system identification task to high angle-of-attack flight data. The method consists of a model determination algorithm for estimating which nonlinear parameters significantly affect aircraft responses and a nonlinear six degree-of-freedom maximum likelihood identification algorithm for identifying accurately the values of the selected nonlinear terms. This method has been applied to simulated responses of an advanced swept wing fighter and to the flight test responses for that fighter.

## 2.0 THE INTEGRATED PARAMETER IDENTIFICATION PROCESS

### 2.1 Requirements for Identification

Aircraft parameter identification is the process of extracting numerical values for the aerodynamic stability and control coefficients from a set of flight test data (e.g., a time history of the flight control inputs and the resulting aircraft response variables). Although the fundamental theoretical basis of identification has existed for over 75 years, practical application of this technology to aircraft flight testing has been attempted only over the last three decades. Most of this application has been limited to identification of low order linear aircraft mathematical models, at low angles-of-attack and Mach number.

There are three principal elements of aircraft parameter identification: (1) the data processing algorithms (identification method), (2) the aircraft instrumentation, and (3) the flight control inputs (Figure 1). These elements are highly interactive.

In order to develop a comprehensive identification technology for application to the high angle-of-attack flight regime, a method of approach has been implemented which integrates these interactive elements. As diagrammed in Figure 2, this method of approach is composed of two basic phases. Phase 1 is a detailed simulation of a high performance aircraft [1]. Phase 2 is the application of advanced parameter identification methods to determine the effects of inputs and measurement errors on the algorithms in processing high angle-of-attack data. Phase 3 is the application of the results of Phases 1 and 2 to the specification and evaluation of high angle-of-attack flight tests [2].

Phase 2 of this procedure involves the critical elements of (1) model and parameter selection, (2) parameter estimation, and (3) model verification. The fundamental complexity of these three elements requires a strong reliance on information available from wind tunnel data and knowledge of aircraft physics. This requirement, however, must be satisfied with caution because of the difficulty of translating the inherently limited capability of wind tunnels and aerodynamic theory to the complex maneuvers and flow interaction at high angles-of-attack. The particular value of such prior information is the manner in which it can be used to formulate the possible types of forces and moments (reserving isolation of the specific nonlinear effects for post-flight analysis). This specification of nonlinear effects is the model determination phase. The parameter identification is the quantification of the specific aerodynamic terms selected by the model determination phase. Model verification is the application of various techniques to increase confidence that the identified model adequately represents the aircraft responses. Such techniques include the calculation of the confidence levels of the estimates, consistency with results of previous wind tunnel and flight tests, and the ability of the identified model to predict responses of the aircraft with different inputs.

The combination of the simulation phase and the identification phase may be performed to validate the estimation procedures, to specify control inputs, instrumentation, and critical flight configuration. These latter two specifications are directly applicable to the design of flight tests for the subject aircraft.



## 2.2 Techniques for Simulation, Model Determination, and Parameter Identification

In this section, we review the techniques which have been developed for implementation of the integrated parameter identification process.

### 2.2.1 Simulation

The simulation objective is to provide a controlled data base for isolating potential identification problems which might arise from actual flight test data. Requirements for inputs and instrumentation, for example, may be specified from such simulations prior to the flight tests. Such requirements may be difficult to individually detect from any specific set of flight data due to the complex response and data iterations which exist in any actual system.

As demonstrated in Reference [1], nonlinear high angle-of-attack responses may be simulated, at least qualitatively, by digital techniques. In particular, responses such as pitch up and yaw departure (due to unstable  $C_{np}$ ) are strongly dependent on wind tunnel measurable static nonlinearities and these critical regions can be predicted for flight conditions simulated by the wind tunnel configuration. Unfortunately, many flight conditions may only be approximated in wind tunnels and, in fact, some aerodynamic (and dynamic) nonlinearities may not be detected from such tests due to scaling or tunnel model support limitations. In addition, high performance maneuvers may induce non-tunnel reproducible interactions between the pilot, the flow fields, and the aircraft.

The simulation described in Reference [1] was designed as a generator of data which is characteristic of that from the responses of high performance aircraft. The characteristics of this simulation are summarized in Table 1. The simulation was subsequently compared with reported results of the stall/spin tests of a swept wing fighter aircraft [3]. Responses such as pitch-up, yaw departure, and spin were obtained with the simulation. In addition, it was found that wing rock would be simulated, and that the roll, sideslip, and aileron deflection amplitudes and angle-of-attack occurrence were comparable with that recorded in the flight test. However, the frequency of the simulation was 7.5 seconds compared to 4.5 seconds for the actual test. This frequency discrepancy was ascribed to uncertainties in the parameters of the aircraft being tested, the pilot responses of the tests, and the differences between the wind tunnel and actual values of dynamic derivatives such as  $C_{\dot{\alpha}}$ . Based on the correlation of the simulated responses with this and other actual responses, the simulation was deemed acceptable as a generator of typical data. Further extensive correlation of the simulation was beyond the scope of the program development.

As discussed in [1,2], the simulation used to generate data is an extensive and detailed representation of the aircraft and data error sources. Both the dynamic equations and the measurements are nonlinear. The simulation aspect of the errors reported here is unique in the application of identification algorithms to simulated data. Typical approaches assume a polynomial form for nonlinear parameter variation, generate the time history data with this model, and then attempt to reconstruct the polynomial from the data [10-12]. Such an approach is certainly useful for testing of a program, but may tend to place more confidence in the effectiveness of an algorithm than is justified. This follows because identification of the same functional form which generates the data disregards the modeling error which may occur by approximating the actual function (unknown) by an assumed or a priori function. The approach used in this work is to generate the data by an aerodynamic model which is of higher order than the model which is identified (e.g., data is in "table look-up format"). Hence, the integrated parameter identification process of Figure 2 contains the element of modeling-error effects explicitly.

### 2.2.2 Model Structure Determination

Having determined an analytical, a priori form for the aerodynamic forces and moments, and selected the principal axis systems, the framework is established for estimating the structure and parameters appropriate to a given data length. Polynomials are chosen as the basis of the identification model for this work. This is itself an assumption about the physics of the aircraft aerodynamics. The assumption is historically based on the dependence between force and moment coefficients and independent variables ( $\alpha$  or  $\delta$ , for example) which is observed in wind tunnels. Recent work in England [13] has demonstrated the validity of such approximations with actual aircraft responses in the subsonic regime. Mathematically, polynomial representations result from series expansions about some reference point (e.g., trim) and herein lies the inherent assumption of the polynomial approximation. Specifically, it is assumed that there are continuous derivatives or rates of changes of derivatives (to an arbitrarily high order). In the transonic regime especially, such continuity may be violated, forcing discontinuous representations. For this work, continuity is assumed.

Wind tunnel test results (and any other information about the physics of the maneuvers) are used to define all the possibilities of the polynomial functions for the forces and moments. Then, the actual response data obtained is used to specify which of these functions are most probable. The goal is to identify only those polynomial coefficients which are required to reproduce the actual force or moment characteristics. This addition to the integrated parameter identification process is diagrammed in Figure 3. Flight tests are conducted for particular conditions and inputs. The data from these tests is then used as the basis for selecting the functional forms required to reproduce the data. The data is passed through a filter, (denoted as the optimal subset regression program) which gives variables which might be required to reproduce the forces and moment characteristics which generate the data. These variables may correspond to the coefficients of powers of the independent variables (say,  $\alpha$  or  $\delta$ ). In general, the number of terms allowed is dictated by expected significance from a priori considerations. Of these possible required terms, the filter selects the most significant. The model defined by these significant variables is then passed to the identification program.

The optimal subset regression algorithm adds and deletes variables to a particular model in an iterative manner (see Appendix). Estimates of previously ignored parameters are incorporated and evaluated by two criteria, as follows:

1. Of all possible variables  $\theta$ , is  $\theta_1$  the most highly correlated with  $y$  of variables not in the regression?
2. If  $\theta_1$  is added to the regression, is its contribution to the "fit" significant relative to variables  $\theta_{i-1}, \theta_{i-2}, \dots, \theta_1$  which have already been used? Does the significance of  $\theta_{i-1}, \dots, \theta_1$  diminish because  $\theta_1$  is included?

These questions are answered within the framework of statistical hypothesis testing. The algorithm uses statistical hypothesis testing techniques based on the Fisher F ratio (e.g., F-tests). Formally, this ratio measures the reduction in fit error with the current model relative to the error due to noise and model uncertainties. A "total" F-ratio measures the entire model fit relative to error and a "partial" F-ratio measures the incremental improvement in fit due to addition or deletion of a parameter in the model. A generalized flow chart is shown in Figure 4. Starting with a list of possible variables, the algorithm enters the variable with the highest partial correlation to the observations  $y$ . The contribution of this variable to reducing fit error is made, and a new variable entered. Subsequent tests add and delete variables to improve the "fit". The final subset of  $\theta$  which results from the procedure is one within confidence bounds set by the user (say, 95% or 99%).

The algorithm not only identifies the most significant parameters, but also finds least square estimates of their true values. In general, these estimates will be in error (biased due to measurement noise and high order modeling errors). As such, they can be used for start up values of the maximum likelihood algorithm to reduce computation time and improve convergence, but may not be considered as final estimates themselves. As an added check on the validity of the determined model, the program computes the residuals,  $y - \hat{y}$ , on the final pass. This provides an evaluation of the adequacy of the model (whose values yield  $\hat{y}$ ) compared to the "true" process (whose values give  $y$ ). Ideally, these residuals will be white Gaussian.

The following assumptions are made for the present application of the subset regression algorithm:

Mass and inertia of the aircraft are known. This assumption is based on the extensive weight and balance data available for modern aircraft. In actual test conditions, however, there may be marked differences between the current aircraft configuration and the baseline calculations (e.g., unsymmetrical loadings, addition of weapons and instrumentation, etc.). This assumption, therefore, requires evaluation of such effects to determine their importance.

Aircraft rate (rotary) functions are assumed to vary only with  $\alpha$  and  $\beta$ . This assumption limits the model structure to lower Mach numbers and aircraft loadings. Specifically, the terms  $C_{m\dot{\alpha}}$ ,  $C_{n\dot{\beta}}$ , and  $C_{l\dot{\beta}}$  are not considered separately from  $C_{m\alpha}$ ,  $C_{n\beta}$ , and  $C_{l\beta}$ . At extreme conditions, this assumption is questionable. The basic reason for allowing use of this assumption is that the data base [1] does not have the aircraft rate and velocity vector rate terms explicitly separated. In general, extreme inputs would be required to separate these contributions in actual flight tests. It must be noted that the regression model structure can be easily modified to include terms such as  $C_{n\dot{\beta}}$  if required.

The general expansion for any specific force or moment coefficient is

$$C = C_0(\bar{\alpha}, \bar{\beta}) + \sum_i EC_{i\alpha}(1)\alpha^i + \sum_j EC_{j\beta}(1)\beta^j + \sum_{ij} EC_{ij\alpha\beta}(1)\alpha^i\beta^j$$

where  $\bar{\alpha}$  and  $\bar{\beta}$  are reference angle-of-attack and sideslip angle, respectively. The specific coefficients for which such an expansion is used are listed in Table 2.

Primary emphasis is placed on the static coefficient structure for the modeling tasks here. All static terms could minimally be expressed as linear combinations of  $(C_{i\alpha} + C_{j\beta})^n$ , where  $n=1,2,3$ . In addition, the coefficients of  $C_m$  could be expanded to  $\alpha^9$  and  $C_n$  to  $\beta^5$ . Control effectiveness coefficients and dynamic coefficients were generally limited to first order expansions in  $\alpha$  only. These expansions were decided upon after initial experimentation with the programs. It was found that higher than first order terms in  $\alpha$  were usually not required on the basis of the regression analysis. In general, these control effectiveness and dynamic terms are difficult to identify from acceptable inputs.

An important aspect of the regression program is that the coefficients are not serial. Thus, if intermediate coefficients were not necessary (e.g., such as  $C_{\alpha^2\beta}$ ), they are not included. (The maximum likelihood program will automatically eliminate terms not specified by the regression).

These assumptions and expansions will be used with an equation error formulation of the six degree-of-freedom representation of the aircraft. Details of this representation are discussed in Reference [2].

### 2.2.3 Parameter Identification Procedure

The extraction of aerodynamic derivatives from flight data has received considerable attention during the last three decades and the most recent efforts are given in Refs. [14-15]. Earlier techniques were mostly manual or analog requiring subjective judgment by operators [16]. These methods are suitable for simple linear systems under very ideal conditions.

More recently, with the availability of fast digital computing machines and efficient computation algorithms, many powerful digital methods have been developed. Examples of digital methods are various equation error methods [17-18], output error methods [19-31], Kalman filter/smoothing approach [11] and the maximum likelihood technique [2,10,32-34].

Output error methods, which include gradient methods and modified Newton-Raphson, were motivated by earlier curve fitting techniques. These methods may not work well if there is high process noise or if the weighting matrix in the criterion function is improperly chosen. The equation error methods minimize the difference between the left hand side and the right hand side of the state equations. Examples of this method are various forms of least square, correlation methods, and instrumental variable approach. Since these methods do not account for measurement noise, the estimates are biased in the presence of this type of error. In the Kalman filter/smoothing approach, the parameters are converted into state variables. The Kalman filter and smoother are developed for this new state vector starting from a priori values of states and parameters and their covariances. This method gives biased estimates even for linear systems and requires a priori knowledge of measurement and process noise covariances.

The maximum likelihood technique solves many of the problems mentioned above. By considering unknown elements of process noise and measurement noise covariances and other instrumentation errors as parameters, it considers these noise sources and also estimates them, if not known a priori. The method determines parameter values, which maximize the likelihood function of the parameters given the measurements and any a priori information. The likelihood function has the same form as the conditional probability of the observations given the parameters. It is customary to work with the logarithm of the likelihood function. The method, as applied to parameter identification in nonlinear dynamic systems with measurement and process noise is a combination of two steps:

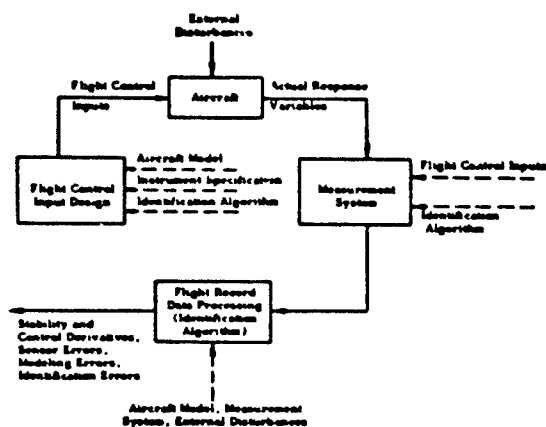


Fig. 1 Interdependence of Modeling, Input Design, a Measurement System, and Data Processing Algorithms

Table 1 Characteristics of Aircraft Data Simulation

Dynamic Equations	Six degree-of-freedom coupled nonlinear equations including engine gyroscopic effects, non-symmetric mass loading effects, and asymmetric thrust. Euler angles obtained from integrating direction cosine matrix. [ref. 4,5]
Aerodynamic Data	Tabular data from wind tunnel tests of a model of subject aircraft [ref. 6,7]. Data consisted of complete static and dynamic forces and moment coefficients for angle-of-attack range $(-10 \leq \alpha \leq 10^\circ)$ , and sideslip $(-40 \leq \beta \leq 40^\circ)$ . Lagrangian formulae used for interpolation when integrating equations.
Measurement System	Detailed model of position, rate, and acceleration gyro, angle-of-attack and sideslip vane, accelerometers, and pitot tube. All measurements subjected to random error-bias error, scale factor error, white noise. [ref. 8]
Control System	Detailed model of the SAS of subject aircraft. [ref. 9] Autopilot used to emulate pilot responses.
Random Disturbances	Random angle-of-attack and sideslip disturbances to simulate gusts. Random variation of normal lift coefficient to simulate buffet.

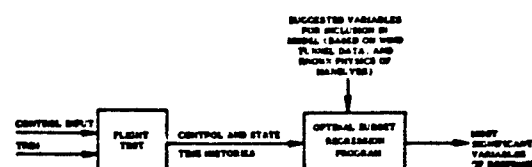


Fig. 3 Model Determination

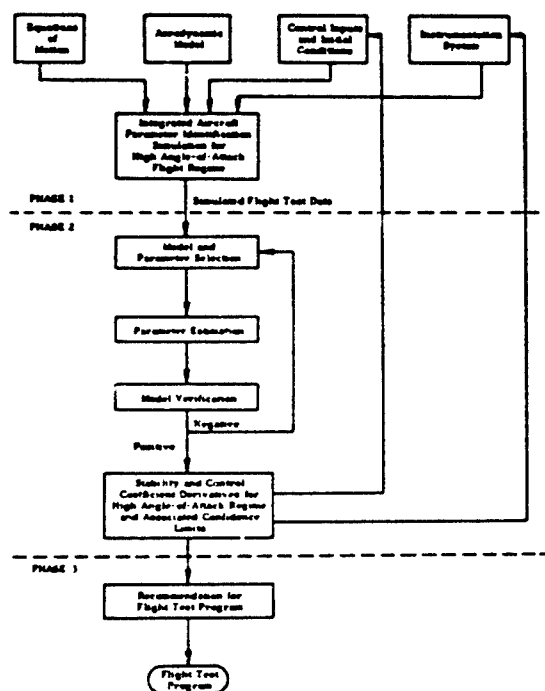


Fig. 2 Implementation of the Design of an Integrated Parameter Identification Process for High Angle-of-Attack Application

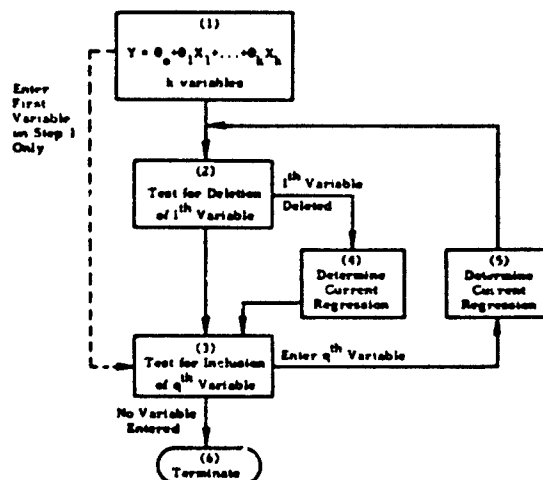


Fig. 4 Generalized Flow Chart of the Subset Regression Algorithm

Table 2 Coefficients Which are Expanded for High Angle-of-Attack Aerodynamic Models

EQUATION	STATIC COEFFICIENT	CONTROL EFFECTIVENESS	DYNAMIC COEFFICIENT
$\dot{u}$	$C_{\dot{u}}(\alpha, \beta)$	$C_{\dot{u} \delta}$	$C_{\dot{u} \dot{\alpha}}$
$\dot{v}$	$C_{\dot{v}}(\alpha, \beta)$	$C_{\dot{v} \delta}$ , $C_{\dot{v} \dot{\alpha}}$	$C_{\dot{v} \dot{\alpha}}$
$\dot{w}$	$C_{\dot{w}}(\alpha, \beta)$	$C_{\dot{w} \delta}$	$C_{\dot{w} \dot{\alpha}}$
$\dot{p}$	$C_{\dot{p}}(\alpha, \beta)$	$C_{\dot{p} \delta}$ , $C_{\dot{p} \dot{\alpha}}$	$C_{\dot{p} \dot{\alpha}}$ , $C_{\dot{p} \dot{\beta}}$
$\dot{q}$	$C_{\dot{q}}(\alpha, \beta)$	$C_{\dot{q} \delta}$	$C_{\dot{q} \dot{\alpha}}$
$\dot{r}$	$C_{\dot{r}}(\alpha, \beta)$	$C_{\dot{r} \delta}$ , $C_{\dot{r} \dot{\alpha}}$	$C_{\dot{r} \dot{\alpha}}$ , $C_{\dot{r} \dot{\beta}}$

1. A Kalman filter for state and its covariance.
2. A Gauss-Newton method for parameter estimates, and associated covariances; also unknown noise statistics.

Figure 5 is a flow chart of the procedure steps. The details of the above steps are given in Ref. [2]. In addition to estimating the parameters in the state and measurement equations, it also determines the covariance of errors in parameter estimates. If the model, whose parameters are identified, is a true representation of the system in the region of operation and the sampling rate is high, the maximum likelihood method gives unbiased estimates of parameters for long data records. With increasing amounts of data, the estimates converge to their true value almost certainly. It can be shown that the technique extracts all information about the parameters from data; in other words, the method is efficient.

The maximum likelihood identification program is combined with the model structure determination algorithm as shown in Figure 6. The process is shown for simulated data, although, as will be discussed, it has also been applied to flight test data.

The computational requirements of maximum likelihood make it very desirable to concentrate as much as possible on estimates of only those parameters which can be estimated well from the available data. Since the computation requirements are roughly proportional to both the number of parameters and the number of model states propagated, estimating parameters ill-specified by the data increases computation with only, at best, marginal increases in useful results. In fact, overparameterization can actually decrease the quality of all the estimates.

First, many parameters can be isolated by examination of the data. If it is apparent that there is only minor excitation and, hence, little information corresponding to a particular identification model state, the state equation for that model and its associated parameters can be removed from the identification procedure. Either a constant or a measured time history of that state can then be substituted in the remaining state equations where there is cross-coupling to the removed state. This technique can be applied in much parameter estimation work involving aircraft where the longitudinal and lateral degrees of freedom can frequently be decoupled for inputs confined to one plane or the other.

Isolation of a reduced set of significant parameters by equation elimination can generally be applied before using the subset regression on the data. After regressing the data, if the results for a particular equation reveal a low F-ratio for the overall fit, below approximately 100, or if all the included variable coefficients have F values below 100, (an F-value of 100 corresponds to a 95% parameter estimate confidence (2 sigma) of about  $\pm 20\%$ ) that equation also can reasonably be eliminated in the maximum likelihood optimization procedure.

Further development of the parameter subset for maximum likelihood estimation based on regression estimate F-values is also desirable. Experimentation reveals that both less computation and better estimates result if maximum likelihood is used to refine estimates of only those parameters whose F-value is more than 4% of the maximum parameter F-value for a particular equation. The 4% cutoff corresponds to parameter estimate confidence five times less than those of the "best" parameter estimate. Attempts to identify more parameters with the maximum likelihood procedure may overparameterize the fit to the given data, resulting in poorer overall estimates of the parameters when compared to the estimates obtained with a smaller parameter set.

If the parameters remaining after insignificant modes have been eliminated, the regression subset is decomposed into two parts. The first part is those terms which are "significant" by the various F-tests. The regression estimated values of these terms are defined more precisely by the maximum likelihood algorithm. The second part consists of terms which are "insignificant", but for which numerical values have been estimated. Because these latter estimates do constitute additional information about the system, they are used as fixed values in the maximum likelihood algorithm. Hence, all regression estimates are used for the maximum likelihood identification; one subset as a priori start-up values and the other subset as fixed values. The reason for including the non-zero values of the "insignificant" subset is that these regression estimates, though not perfect, should be closer to the actual value than an estimate of zero. The estimates of "identified" parameters improve if the estimates of "non-identified" parameters are better.

Table 3 presents the parameter sets for the two demonstration examples, a lateral case and a longitudinal case. Included in the sets used for maximum likelihood estimation in addition to the parameters selected by statistical means are the constant terms for each state equation and the bias on sideslip angle,  $\delta$ , measurement. These additional parameters do not have the F-value statistic for significance ranking, but are nevertheless felt to be potentially important enough to be included. In the case of constant terms, the value is that of the primary aerodynamic coefficient values ( $C_L, C_m, C_u, C_x, C_y, C_z$ ) at the mean  $\alpha$  and  $\delta$  for the experiment data. Thus, the final rule in determining the parameter set should always be the judgment of the user.

### 2.3 Input Design

The model determination and parameter identification aspects of the integrated parameter identification procedure requires careful design of flight tests, in particular, it is necessary to make a good choice of inputs and the instrumentation.

It has long been realized that the ultimate success of a flight test program depends also on the choice of inputs used to excite the desired motions of the aircraft. Good inputs could enhance parameter identifiability and improve confidences on parameter estimates. This is especially true for parameter identification of aircraft models at high angles-of-attack where the aerodynamic derivatives are expanded as polynomials in angle-of-attack and sideslip angle. This leads to a large number of unknown parameters. In addition, there are many other considerations for choosing inputs for specific flight tests [35,36].

The aircraft equations of motion are nonlinear at high angles-of-attack. Stall, wing rock and other phenomena observed in this region cannot be explained by linear models. Under these circumstances, it is possible to consider an aircraft model in which the aerodynamic stability and control coefficients are slowly varying functions of aircraft states, in particular, angle-of-attack  $\alpha$  and sideslip angle  $\delta$ . Usually, the form of these functions is not known a priori.

For very small changes in  $\alpha$  and  $\delta$  during a maneuver, a model assuming constant values of aerodynamic derivatives may be adequate. The techniques, described in Ref. [2], for the design of optimal inputs for linear dynamic systems, can be used to specify inputs for identification of local values of functions representing the stability and control coefficients. It is necessary that there be only small excursions in these states which have maximum effect on parameters being identified.

Many methods have been suggested to design inputs which would give good identifiability of stability and control coefficients over a range of states. One way could be to carry out flight test around many angles-of-attack and sideslip angles covering the range of interest. Inputs based on linear models are designed at each of these points, as explained above. This would give an accurate description of each aerodynamic derivative, but may be practically infeasible because:

1. It would require excessive flight testing time and data processing time.
2. It would require carrying out flight tests in regions where the trim conditions cannot be reached or the airplane is unstable and/or unsafe.

A better scheme is to approximate the nonlinear aerodynamic derivatives by polynomials (or some other truncated series of complete functions) in independent variables. Each unknown nonlinear function in the equations of motion is thus replaced by a set of parameters. These parameters can be identified in a variety of ways. The aerodynamic derivatives are determined from a knowledge of the coefficients of terms in the polynomial expansions.

For small ranges of  $\alpha$  and  $\beta$ , it is possible to determine all the polynomial coefficients in one single experiment. The inputs should have sufficient amplitude so that the motions occur in more or less the entire range of  $\alpha$  and  $\beta$  under consideration. The technique for determining the amplitude is given in Ref. [2]. The amplitude depends on the order of the polynomial, accuracy desired, duration of the experiment and a priori estimate of the coefficients of the polynomial.

To determine aerodynamic derivatives over a wide range of angle-of-attack ( $0 < \alpha < 30^\circ$ ) and sideslip angle ( $-20^\circ < \beta < 20^\circ$ ), it is necessary to perform experiments starting at different  $\alpha, \beta$  trim conditions. The results of these separate experiments are put together to obtain all coefficients in the polynomial. The algorithm of [2, Appendix C] finds the trim conditions and the duration of the experiment at each trim condition to produce a good estimate of the nonlinear function over the entire range of interest. It is possible to put constraints of infeasible operation over a region. The technique considers regions where the stability augmentation system (SAS) is required for pilot safety but deteriorates parameter estimates.

A semi-empirical technique is useful in the design of input signals for identifying parameters in complicated systems with known characteristics. As a first step, analytic inputs are designed based on simplified models. State time histories are generated and inputs are evaluated based on a more accurate but complex model. This would give information about poorly identifiable directions in the parameter space and about poorly excited modes. This is usually done using simple programs which are not necessarily recommended for data reduction from actual flight tests. It is noted that input evaluation can be done without generating simulation data and going through the identification process. In the implementation used here, the optimal subset regression program is used to determine identifiable directions resulting from a certain input. A knowledge of the deficiencies in the chosen input, together with known system behavior, is used to modify the input. The process is repeated until an acceptable input is obtained.

It has been found in this work that, in general, the optimal inputs for high angle-of-attack regimes are those which put the most energy at the known nonlinearities. Examples will be given in the next section.

### 3.0 APPLICATION TO SIMULATED DATA

The preceding sections have presented an overview of the integrated parameter identification process. In this section, we discuss the application of this process to the simulated data of Section 2.1.1.

#### 3.1 "Model Building from Data"

##### 3.1.1 Lateral-Directional Response Application of the Subset Regression Method - Usefulness of Linear Models

One of the first steps in evaluation of the subset regression program was the lateral directional response analysis. This case is considered more important and difficult than the longitudinal tests. Most of the reported incidences of degraded stall/post-stall responses occur in roll or sideslip and multiple nonlinearities characterize the regime.

A number of small perturbation tests were performed for this case. It was determined that severe or complicated control time histories were not warranted for flight tests at high angle-of-attack (due to the basically unstable character of responses in the regime). The fundamental aspect of these examples was to determine the adequacy of a linear model at several angles-of-attack, as opposed to a polynomial model requiring more complicated inputs. These results are shown in Tables 4 and 5.

Note that there is roll-pitch coupling at  $15^\circ$  angle-of-attack for the aileron doublet example. This departure from linearity occurs because of the pitch instability at the point. In each case,  $C_{l_0} = 0$ , which indicated zero rolling moment at trim. In addition, the wind tunnel results indicated  $C_{l_p} = 0$  at  $\alpha = 15^\circ$  which was substantiated by the model structure determination program. At least 98% of the moment variation in each case was explained by using  $C_{l_\beta}$ ,  $C_{l_{\dot{\beta}}}$  and  $C_{l_{\ddot{\beta}}}$ , with the other terms being much less significant. Again, in each case  $C_{n_0} = 0$ , indicating a zero yawing moment at trim. The  $C_{n_\beta}$  coefficient as verified by the known data, changed sign (from positive to negative) between  $\alpha = 1^\circ$  and  $\alpha = 25^\circ$ . As in the aileron doublet case, at least 98% of the yawing moment variation could be explained by using simply  $C_{n_\beta}$ ,  $C_{n_{\dot{\beta}}}$  and  $C_{n_{\ddot{\beta}}}$ . A linear model seems quite adequate in this case where the critical sign change in  $C_{n_\beta}$  was found by this approach.

Thus, a linear model may explain perturbation input aircraft responses, even in a "nonlinear" regime. The linear model is here shown to indeed be adequate as a point-wise definition of the aerodynamic model. This indicates the possibilities of using linear input designs for high angle-of-attack regimes. This conclusion, however, must be approached with caution. At high angles-of-attack, it may be difficult to hold trim and to conduct even perturbation maneuvers at constant angle-of-attack. Not only inherent instability, but also buffet may make such inputs difficult, at best. The important conclusion which can be attained is that the regression program can be used to delineate those regions where linear or nonlinear aerodynamic modeling is required.

### 3.1.2 Static Pitching Moment Characteristics - Input Design for Nonlinear Systems

One of the most important phenomena of the stall/post-stall regime is "pitch-up". Its principal cause is the positive  $C_{m\alpha}$  which occurs close to stall [1]. Unlike most lateral aerodynamic nonlinearities, the affected mode is the relatively simple short period response which can be conceptually treated as a second order system whose stiffness is controlled by  $C_{m\alpha}$ .

The primary objective is to investigate the following questions:

1. What flight test conditions are required to determine the presence of  $C_{m\alpha} > 0$ ?
2. What order polynomial is required to represent the  $C_m$  versus  $\alpha$  characteristic over the test regime?

In order to resolve these issues, several initial conditions and inputs were applied to the F-4 simulation and the subsequent responses passed through the subset regression program. Since the principal effect of the aerodynamic nonlinearity was known to be on pitch (short period) response, pitch acceleration is used as the regression variable.

Initial conditions and inputs used were the following:

1. Trim at  $1^\circ$ ,  $10^\circ$ ,  $20^\circ$  angle-of-attack, doublet stabilator  $1^\circ$ ,  $2^\circ$ ,  $5^\circ$ , respectively.
2. Trim at  $10^\circ$  angle-of-attack, ramp stabilator ( $1^\circ/\text{sec}$ ).
3. Trim at  $13^\circ$  angle-of-attack, sinusoidal stabilator ( $5^\circ$  and  $10^\circ$  amplitudes).

The results of perturbation inputs in anticipated linear regimes were first developed [1]. These regimes were low angle-of-attack ( $\alpha=1^\circ$ ), pre-stall ( $\alpha=10^\circ$ ) and post-stall ( $\alpha=20^\circ$ ). The data from these maneuvers was passed to the subset regression program. The resulting coefficient model was evaluated on the basis of the quantitative "fit" of the response from the estimated model to the actual simulation response. The results are shown in Table 6.

The next series of longitudinal inputs case were made with a stabilator ramp of  $1^\circ/\text{sec}$  to slowly push the aircraft from the linear regime through the known nonlinear  $C_m$  versus  $\alpha$  characteristics at about  $15^\circ$  (starting from  $10^\circ$ ). In addition, sinusoidal inputs were used.

The basic result of these runs was that the  $C_m$  versus  $\alpha$  nonlinear characteristics required data replication for successful determination. Only the last series of runs provided this replication. The physical reason for this requirement is based on the negative spring interpretation of the static moment characteristic. If the initial rates and accelerations with which the aircraft enters the unstable region are too low, the response to a doublet or step would be unstable, forcing the response to a stable region. If the initial accelerations are too high, the aircraft inertia overwhelms the static moment and the data doesn't reflect the nonlinearity. Although several sets of initial conditions and time-varying inputs may exist for isolating the characteristics, no extensive experimentation was performed with other than a sinusoidal stabilator input.

First a  $10^\circ$  amplitude sine wave input at a trim angle-of-attack of  $13.5^\circ$  was tried. The data from this run was passed through the regression program for two maximum allowable polynomials--a fifth order and a ninth order. Compared with the (known) simulation  $C_m$  versus  $\alpha$ , this input did not come acceptably close to the "true" value.

Then, a new input with half the amplitude and frequency was applied. Passing the data of this new input through the regression program, again with two polynomial possibilities, produced the result shown in Figure 7. Clearly, a higher order polynomial can be identified (locally) using this input.

This numerical experimentation demonstrates that the combined use of a detailed simulation, the subset regression routine, and knowledge of the physics of the aircraft response, can help design highly efficient high angle-of-attack flight tests. Other demonstrations of this input design technique are given in Ref. [2].

### 3.1.3 The "Best" Model

The subset regression approach is an elegant and efficient means of model structure estimation. As with most data processing aids, however, its use must be moderated with engineering judgment. Extensive use of the technique, as with any analytical approach repeatedly applied to physical problems, allows formulation of certain guidelines which facilitate such judgment. Such guidelines usually have a basis in theory, but are not easily quantified.

One such guideline is discussed in Ref. [37], the Akaike final value prediction theorem. This criterion states that, for certain types of systems, there is an optimal number of parameters which describe a model structure. A plot of this criterion function versus number of parameters has a unique extremum (i.e., in a quadratic sense) which is at the optimal number of parameters [10]. It is also shown that fit error, the residuals of the estimated versus actual output time history, is not satisfactory since fit errors (as also measured by  $R^2$ , the multiple coefficient) as a criterion, do not possess a unique minimum.

Fit error criteria tend to approach an asymptotic value as the number of parameters is increased. The eventual insensitivity of the fit error to increase in number of parameters, as parameters are added, is due to the continuing reduction of degrees-of-freedom (e.g., number of observations less number of parameters). Fundamentally, when the number of data points equals the number of parameters, the regression curve passes exactly through these points. No further improvement is then possible. Noise will, of course, allow more parameters to be entered (since point-by-point fit no longer occurs), but these parameters tend to fit the noise, not the process.

The Akaike criterion is a function of fit error, but also weights this error with the number of degrees-of-freedom. For the regression, a similar function of fit error is the F-ratio, the ratio of "fit goodness" to fit error, weighted by the degrees-of-freedom. The concept of F-ratio is detailed in Ref. [2] and its importance to this work is significant.

### Table 3 Parameter Set Decomposition

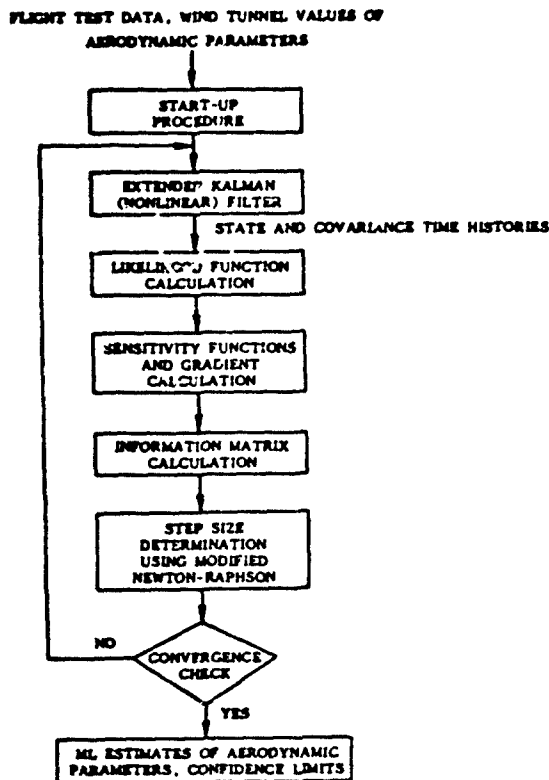


Fig. 5 Flow Chart of Maximum Likelihood Identification Program

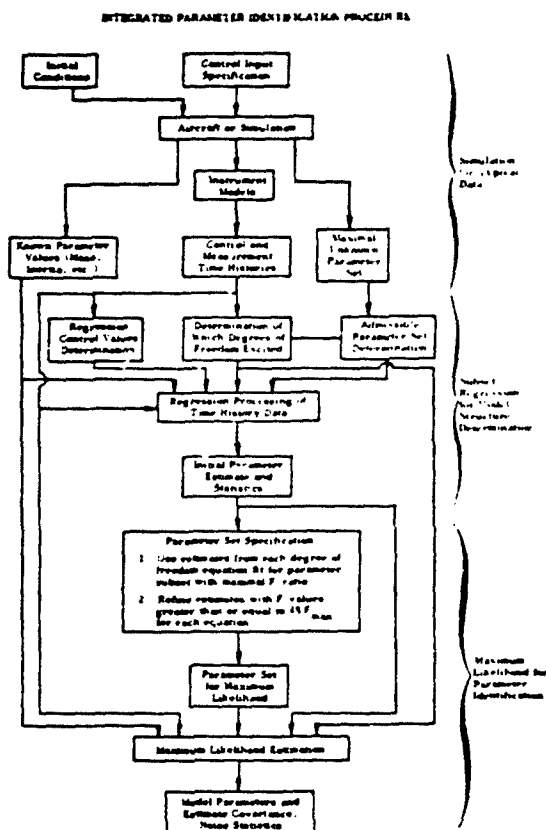


Fig. 6 Operational Flow Chart of Integrated Parameter Identification Process

**Lateral Response**

**Parameter Estimates Refined by Maximum Likelihood**

$C_1$   
 $C_2$   
 $C_3$   
 $C_4$   
 $C_5$   
 $C_6$   
 $C_7$   
 $C_8$   
 $C_9$   
 $C_{10}$

**Other Non-Zero Regression Parameter Estimates Used in Maximum Likelihood**

$C_1$   
 $C_2$   
 $C_3$   
 $C_4$   
 $C_5$   
 $C_6$   
 $C_7$   
 $C_8$   
 $C_9$   
 $C_{10}$

**Longitudinal Response**

**Parameter Estimates Refined by Maximum Likelihood**

$C_1$   
 $C_2$   
 $C_3$   
 $C_4$   
 $C_5$   
 $C_6$   
 $C_7$   
 $C_8$   
 $C_9$   
 $C_{10}$

**Other Non-Zero Regression Parameter Estimates Used in Maximum Likelihood**

$C_1$   
 $C_2$   
 $C_3$   
 $C_4$   
 $C_5$   
 $C_6$   
 $C_7$   
 $C_8$   
 $C_9$   
 $C_{10}$

Table 4 Aileron Doublet ( $+5^\circ$  over 2 second period, 10 sec data length)

ANGLE OF ATTACK	MODEL REQUIRED TO EXPLAIN AT LEAST 99% OF $C_L$ VARIATION
5°	$C_L = C_{L_\beta} \beta + C_{L_{\delta_A}} \delta_A + C_{L_p} p$
15°	$C_L = C_{L_\beta} \beta + C_{L_{\delta_A}} \delta_A + C_{L_{\dot{\alpha}^2}} \dot{\alpha}^2 \beta^2$
25°	$C_L = C_{L_\beta} \beta + C_{L_{\delta_A}} \delta_A + C_{L_p} p + C_{L_r} r$

Table 5 Rudder Doublet ( $+5^\circ$  over 2 second period, 10 second data length)

ANGLE OF ATTACK	MODEL REQUIRED TO EXPLAIN: AT LEAST 99% OF $C_n$ VARIATION
5°	$C_n = C_{n\delta_r} \delta_r + C_{n\beta} \beta + C_{n_r} r$
15°	$C_n = C_{n\delta_r} \delta_r + C_{n\beta} \beta + C_{n_r} r + C_{n_p} p$
25°	$C_n = C_{n\delta_r} \delta_r + C_{n\beta} \beta + C_{n_r} r$

Table 6 Stabilator Doublet (these results are a compilation of several experiments)

ANGLE OF ATTACK	MODEL
$\alpha = 1^\circ$	<p><math>\Delta 1^\circ</math> stabilator doublet, 7 second data length</p> <p><math>C_m = C_{m_0} + C_{m_\alpha} \alpha + C_{m_{\alpha^2}} \alpha^2 + C_{m_{\dot{\alpha}}} \dot{\alpha} + C_{m_q} q</math> matched (virtually) 100% of pitching moment variation</p>
$\alpha = 10^\circ$	<p><math>\Delta 1^\circ</math> stabilator doublet, 7 second data length</p> <p><math>C_m = C_{m_0} + C_{m_\alpha} \alpha + C_{m_{\alpha^2}} \alpha^2 + C_{m_{\dot{\alpha}}} \dot{\alpha} + C_{m_q} q</math> matched 99.8% of pitching moment variation</p>
$\alpha = 20^\circ$	<p><math>\Delta 5^\circ</math> stabilator doublet, 7 second data length</p> <p><math>C_m = C_{m_0} + C_{m_\alpha} \alpha + C_{m_{\alpha^2}} \alpha^2 + C_{m_{\dot{\alpha}}} \dot{\alpha} + C_{m_q} q</math> matched 99.1% of pitching moment variation</p>

That the F-ratio is a measure of the "optimal number" of parameters is shown in Figure 8, corresponding to an example to be discussed in more detail in Section 4. Its placement here is to emphasize the need, based on a criterion other than fit error, to evaluate model suitability. As shown,  $R^2$  is a monotonically increasing function of the number of parameters. The F-ratio, however, has a maximum with seven parameters (obtained after deleting one variable of small significance).

In general, it has been found that the subset F-ratio will have local maxima, beyond the first, as parameters are added. This result is shown in Figure 9. The first general criterion used for selecting parameters to be identified is to delete all parameters included in the regression past the first maximum.

A second guideline to further optimize the regression subset for maximum likelihood application is to select only parameters whose contribution is a certain percentage of the most significant parameter, as discussed in Section 3.1.2.

### 3.2 Identification in the Stall/Post-Stall High Angle-of-Attack Regime

In this section, evaluation of the integrated parameter identification process is carried out using simulated aircraft flight test data. State and measurement model equations used in this maximum likelihood procedure are detailed in Ref. [2]. Nine state equations and eight measurement equations containing thirty-three nonlinear, aerodynamic coefficients compose the identification mode. (Each of these coefficients are further expanded.)

In the identification procedure, the subset regression program is used on the simulated flight test data to identify the model structure and give initial estimates of the selected aerodynamic coefficient polynomial expansion parameters. The maximum likelihood program is then used to refine the parameter estimates obtained from the regression analysis to yield the final parameter estimates and a measure of confidence associated with those estimates. The detailed flow chart of the entire process was illustrated in Figure 5.

In addition to evaluating the identification procedure on a variety of simulated flight test experiments, investigations were also carried out to assess the effects of different levels of measurement noise, process noise, control input variations, identified parameter set size, and data length.

The identifiability of the stall/post-stall regime is the prime objective of the applications conducted for the identification process. This angle-of-attack regime (10° to 25° and beyond) is characterized by multiple nonlinearities in the pitching, roll, and yaw moments and forces. The central objective of this application is that resolution of the identifiability problems for this range is the prime requisite for any high angle-of-attack identification procedure.

The evaluation procedure which has been determined is based on the following considerations:

1. Selection of Inputs: Not all inputs will sufficiently excite the aircraft to induce nonlinear forces and moments. These results were noted in Section 3. A standard set of inputs was selected for this purpose.
2. Selection of Data Length: In general, the longer the data length, the better will be the identification accuracy of those parameters which can be identified. At high angles-of-attack, however, the amplitude of responses may prohibit extensive time at a particular flight condition. This consideration led to a data length of 10 seconds, with a sample rate of 10/sec.
3. Selection of Primary Coefficients: The coefficients which affect aircraft response may be classified as primary or secondary. Primary coefficients are those which most affect aircraft response and which are of greatest interest to the test engineers. Secondary coefficients are those which have, in general, smaller effects on aircraft response, but which, for certain requirements (e.g., SAS or handling quality studies), may be of interest. For the applications discussed here, the static force and moment coefficients are considered primary (e.g.,  $C_x, C_y, C_z, C_m, C_n, C_l$ ). The subset regression program is the essential step in the definition of primary or secondary coefficients.

Tabular summaries of the selected test conditions, inputs and noise levels are given in Ref. [2].

#### 3.2.1 Lateral-Directional Parameter Identification in the High Angle-of-Attack Stall/Post Stall Regime ( $\alpha=17.5^\circ$ )

In the baseline lateral case, control inputs are chosen to excite the lateral-directional modes of the aircraft. Applied controls are a half period sine wave pulse in rudder,  $\delta_r$ , of 10° amplitude and period duration of 2.5 seconds followed by a full period sine wave doublet in ailerons of 7° amplitude and period duration of 2.5 seconds. Total data length is 10 seconds real time, sampled every 0.1 seconds to give 100 points for each measured variable. Initial flight conditions are  $\alpha=17.5^\circ$ ,  $\beta=0^\circ$ , and all rates zero. The baseline runs are corrupted by measurement noise [2]. Twelve parameters are selected by the subset regression program for this baseline case.

Figures 10-12 are time history plots of measurements and various aerodynamic coefficients showing actual values and estimated values with  $\pm 2\sigma$  confidence limits. The most prominent characteristic of both demonstration cases is the excellent measurement estimate fits to the actual data. Estimate  $2\sigma$  confidence limits bracket the measurement noise induced variations of the actual data.

Estimate fits to the nonlinear aerodynamic coefficients reveal a range from excellent estimates to fairly significant biased estimates. For the lateral motion case, the major coefficient estimates,  $C_l, C_n$ , and  $C_y$  are very good; again, with confidence limits bracketing actual data most of the time.

Estimates of control derivatives such as  $C_{n\delta_r}, C_{n\delta_a}$  and  $C_{l\delta_a}$  tend to be biased, however. The two prime reasons for the biased estimates are:



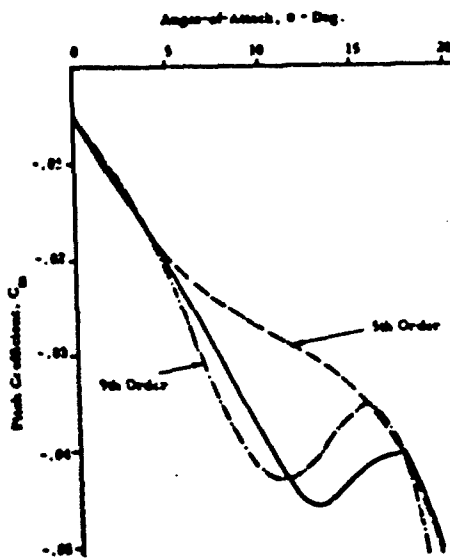


Fig. 7 Effect of Polynomial Order on  $C_p$  Extraction from Simulated Data ( $10^\circ \delta$ )

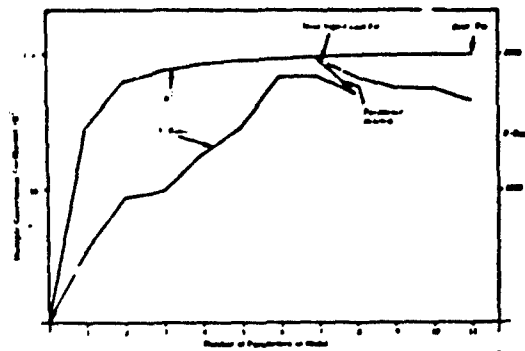


Fig. 8 Multiple Correlation Coefficient ( $R^2$ ) and F-Ratio Variation as Parameters are Added to Model (Longitudinal Case)

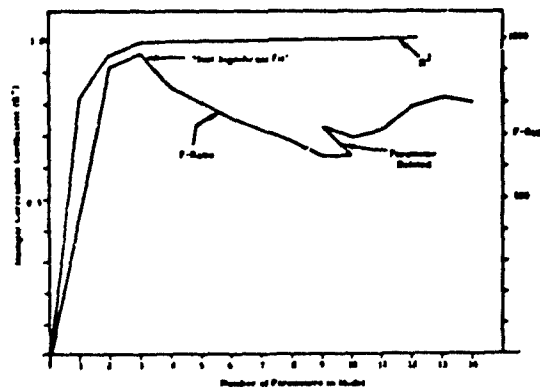
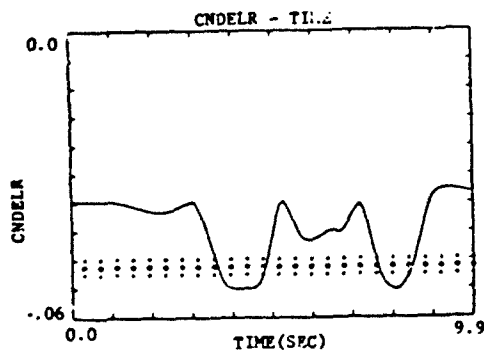
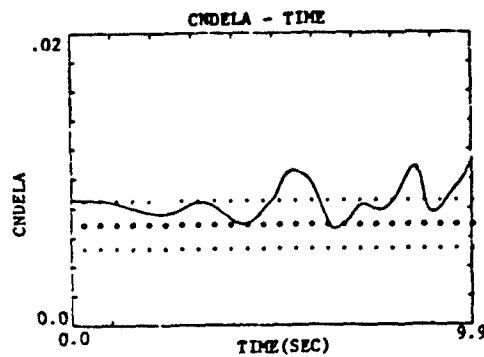
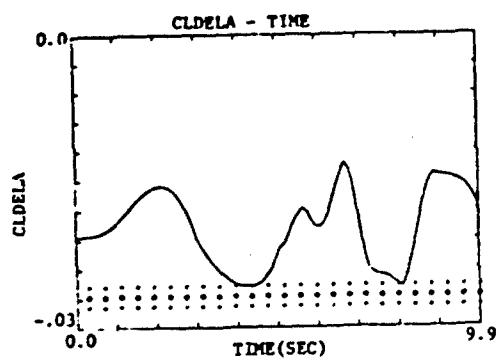


Fig. 9 Multiple Correlation Coefficient ( $R^2$ ) and F-Ratio Variation as Parameters are Added to Model (Lateral Case)



— Response  
 + + + Estimated (with  
 2σ bounds)

Fig. 10 Lateral Control Effectiveness Coefficient Response (Simulated or Estimated) to Combined Aileron/Rudder Input

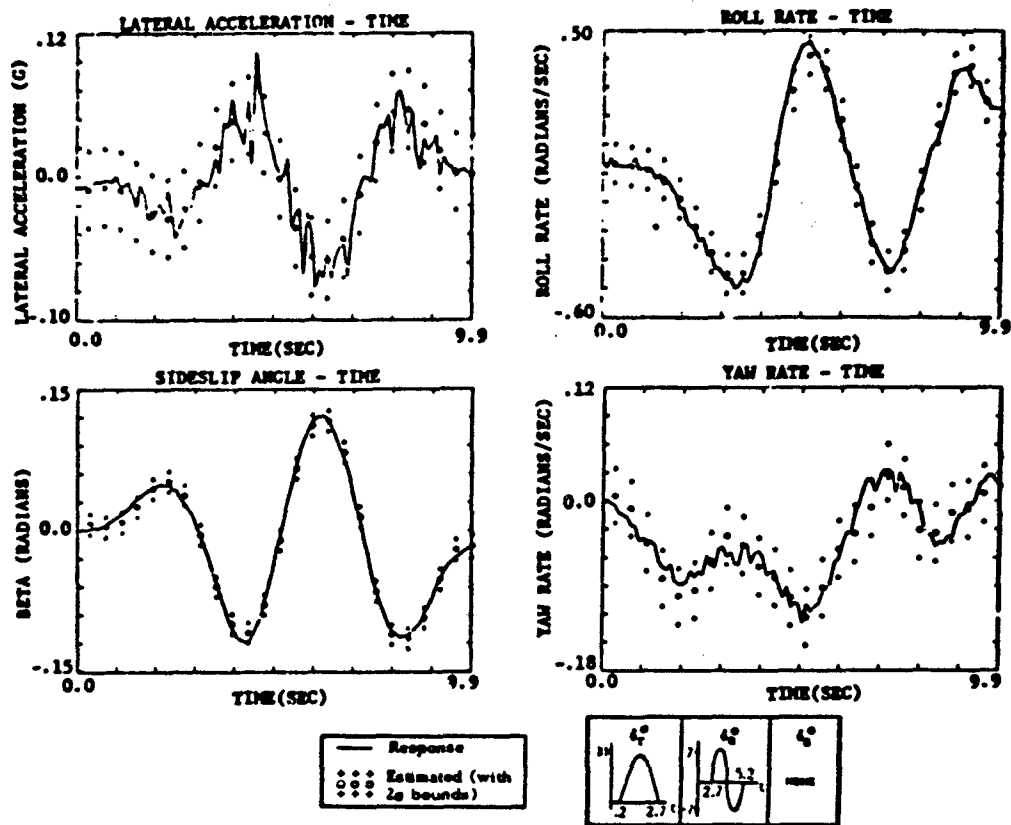


Fig. 11 Lateral Measured and Estimated Response to Combined Aileron/Rudder Input

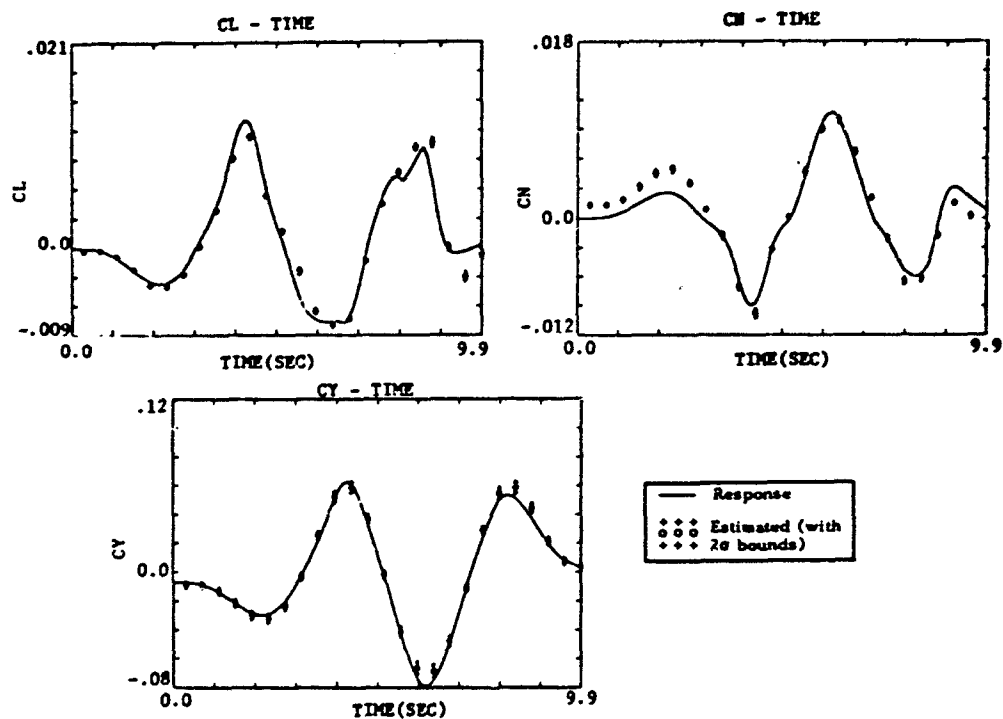


Fig. 12 Lateral Static Coefficient Response (Simulated or Estimated) to Combined Aileron/Rudder Input

1. Modeling errors due to higher order variation of actual coefficients with  $\alpha$  and  $\delta$  than allowed for in coefficient model polynomial expansion.
2. Low amount of information about control derivatives available as a result of short time of control application.

Examination of regression and maximum likelihood results produced the following conclusions.

1. Final maximum likelihood F-values are higher than a priori values, indicating improvement in estimate quality over regression results.
2. F-value ordering indicates relative parameter significance remains close to regression, lending confidence to using the regression for parameter set specification.
3. F-values from the regression and a priori maximum likelihood results are of the same order of magnitude.

Significant improvements in control effectiveness of parameter estimates are achievable by modifying the inputs and increasing the data length [2].

In general, the effect of increased noise, whether process or measurement, on parameter estimates is to decrease the confidence in the estimates. As mentioned, the baseline lateral case does include instrumentation measurement noise. This same case was simulated with increased measurement and process noise (e.g., gusts). In all cases, the estimates were still good, with the expected widening of the confidence intervals [2]. Because of this, no attempt was made to actually identify the process noise in the simulated data.

### 3.3 Longitudinal Results

The longitudinal mode with inputs to excite pitch rate, vertical velocity, and longitudinal velocity is a fundamental aspect of this effort. The stabilator (elevator) input for the baseline longitudinal case is a continuous sine wave superimposed on the initial, constant stabilator angle. With a period of 4 seconds, the input is designed to be approximately at the short period mode frequency of the aircraft and, therefore, yield the most possible information about the parameters governing that mode. Amplitude of the input is  $4^\circ$ . Again, the data length is 10 seconds real time and there are 100 sample points. A second case is also a sinusoidal stabilator input, but with smaller amplitude of  $2^\circ$ . A third case was also generated in which a coupled response was generated in which longitudinal and lateral inputs were simultaneously applied. A total of 31 parameters were identified for this latter case.

Results for these three inputs are shown in Figure 13. It is seen that whereas the  $4^\circ$  stabilator oscillation is very poor at the limits of the test angle-of-attack range, the  $2^\circ$  stabilator and coupled inputs are much better.

One objective of parameter identification techniques is the ability to use model parameter values estimated from one set of data to predict the responses of a different set of data. Of course, the operating range of the data to be predicted should not extend beyond the valid limits of the parameter estimates, but within that constraint, the predicted response should closely approximate the measured response. For the model to be of engineering utility, it must not only be able to reproduce the data upon which it is based, but also be able to closely match responses to different inputs.

Figures 14-15 show the predicted and actual response of the aircraft using parameter estimates from previous lateral/longitudinal coupled response estimates. The inputs for this case, however, are considerably different in form and amplitude from those used to generate previous estimates.

Although the measurement estimate fits for the prediction are not quite as good as the original parameter estimation data fit, the correspondence is, nevertheless, more than satisfactory. An assessment of this relatively simple 31 parameter estimate model must be that it is successful in quite faithfully reproducing the far more complex simulation of real aircraft flight characteristics.

## 4.0 FLIGHT TEST DATA

### 4.1 High Angle-of-Attack Longitudinal Flight Data for a Swept Wing Fighter

The high angle-of-attack results reported here are for flights conducted by the U.S. Air Force [3] on a swept wing fighter aircraft at 40,000 ft. altitude. Only Record 14 from Flight Test 165 is used for the extraction of longitudinal and lateral stability and control coefficients at high angles-of-attack. In this record, the elevator was used to increase the angle-of-attack steadily from about  $15^\circ$  to over  $40^\circ$  over a 20 second period. The airplane stalls at about  $25^\circ$  and finally the unstable lateral motions produce a rolling departure. The thrust of the engines during this maneuver is assumed constant. There are measurements of linear accelerations, angles and angular rates.

First, the subset regression is used to determine a set of relevant aerodynamic derivatives which define the model structure. The angular rates were differentiated numerically to obtain angular accelerations required for the subset regression. To simplify the problem, the aerodynamic derivatives are expanded only as selected functions of angle-of-attack,  $\alpha$ , and sideslip angle,  $\beta$ . The set of functional variables allowed for each moment and force coefficient was discussed previously.

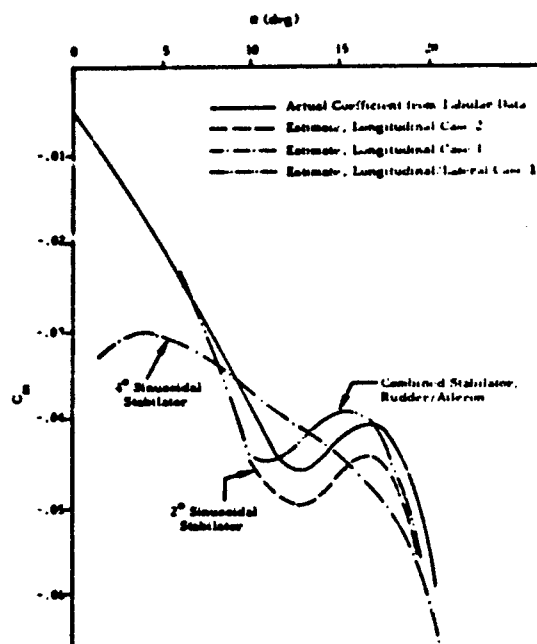
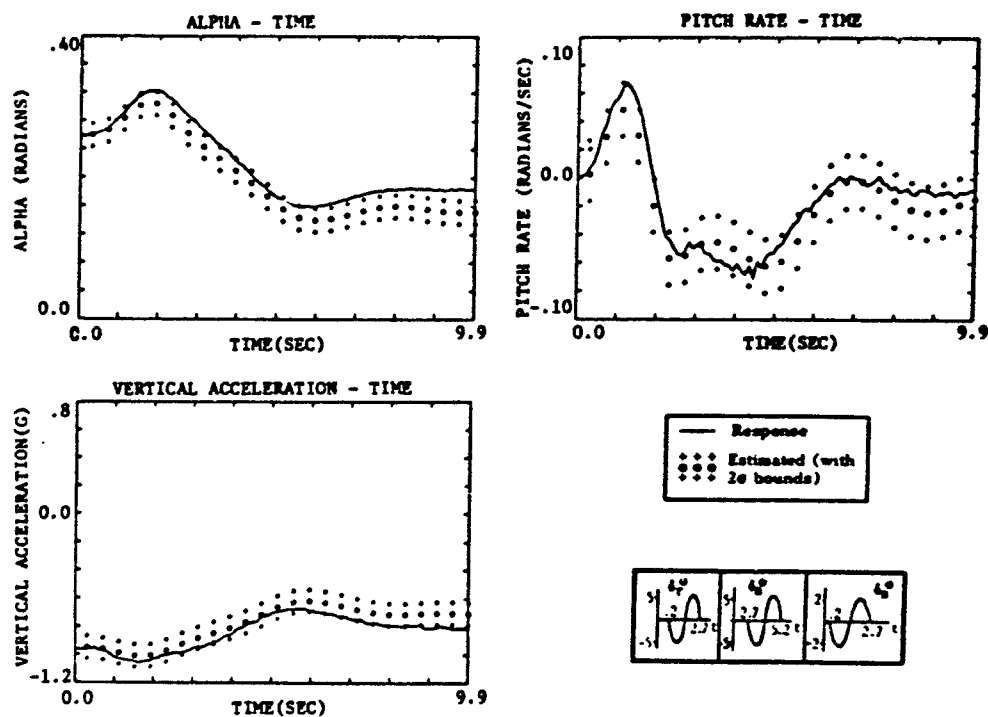
Fig. 13 Estimate of  $C_m$  vs.  $\alpha$  for Different Inputs

Fig. 14 Longitudinal Predicted and Simulated Response to a Combined Stabilator/Aileron/Rudder Input

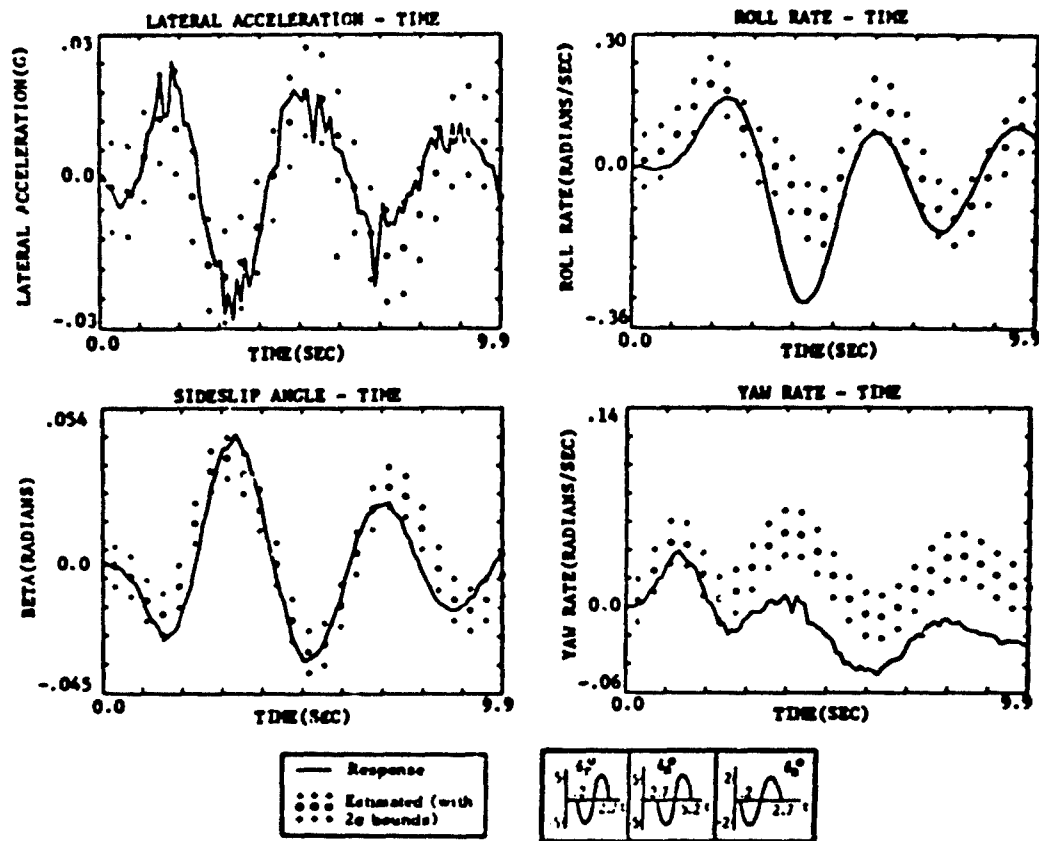


Fig. 15 Lateral Predicted and Simulated Response to a Combined Stabilator/Aileron/Rudder Input

Adequate expansions of forces and moments for the longitudinal motions from the subset regression program are:

$$C_x = C_{x_0} + C_{x_\alpha} \alpha^2 + C_{x_\alpha^4} \alpha^4 + C_{x_\beta} \beta + C_{x_q} q$$

$$C_z = C_{z_0} + C_{z_\alpha} \alpha + C_{z_\alpha^2} \alpha^2 + C_{z_\beta^2} \beta^2 + C_{z_q} q + C_{z_\delta} \delta + C_{z_\alpha \delta} \alpha \delta$$

$$C_m = C_{m_0} + C_{m_\alpha} \alpha + C_{m_\alpha^2} \alpha^2 + C_{m_\alpha^3} \alpha^3 + C_{m_\beta} \beta + C_{m_q} q + C_{m_\delta} \delta$$

There are several important things about these expansions. The order of expansion in terms of angle-of-attack is different for each coefficient. Also, in the expansion for  $C_x$ , the fourth order expansion term must be included while the third order expansion term is not. There is a significant coupling in the longitudinal motions from variations in the sideslip angle. The expansion of the control coefficient is different for the three moment and force coefficients. The model representation selected by the optimal subset regression program is used with the maximum likelihood approach for the estimation of parameters. The starting values of the parameters are taken from the results of the regression. The time history plots of the measurements of angle-of-attack, pitch rate, fore-aft acceleration and vertical acceleration and the predicted values of the measurements based on the identified parameter values are given in Figure 16.

The identified coefficient  $C_m$  is shown in Figure 17. The wind tunnel values of  $C_m$  as a function of angle-of-attack, at zero sideslip angle are also shown. Note that the identified values are for the average sideslip angle encountered in the maneuver.

#### 4.2 High Angle-of-Attack Lateral Flight Data for a Swept Wing Fighter

The first 15 seconds of data from the selected model for the aircraft lateral direction motions are used. There are nonlinear terms in the model, the lateral force and moment coefficients being adequately described by the following equations:

$$C_l = C_{l_0} + C_{l_\beta} \beta + C_{l_{\alpha^2 \beta}} \alpha^2 \beta + C_{l_r} r$$

$$C_n = C_{n_0} + C_{n_{\alpha \beta}} \alpha \beta + C_{n_\beta} \beta$$

$$C_y = C_{y_0} + C_{y_\beta^3} \beta^3 + C_{y_{\alpha \beta}} \alpha \beta + C_{y_{\alpha \delta r}} \alpha \delta r + C_{y_{\alpha p}} \alpha p$$

Notice that at the high angle-of-attack, the lateral controls are almost ineffective. The lateral motion can be adequately explained by an unstable system driven by its coupling with the longitudinal motions.

Most of the estimates did not change very much from the regression values. The time history plots of the measured outputs and predicted outputs are compared in Figure 18. Next, the coefficients  $C_{y_\beta}$  and  $C_{n_\beta}$  are plotted as a function of angle-of-attack. The comparison of the identified values and the wind tunnel values [7] is shown in Figure 19. The identified values are plotted over the range of angle-of-attack encountered in the flight test. These two coefficients are important because they determine the lateral stability of the aircraft at high angles-of-attack.

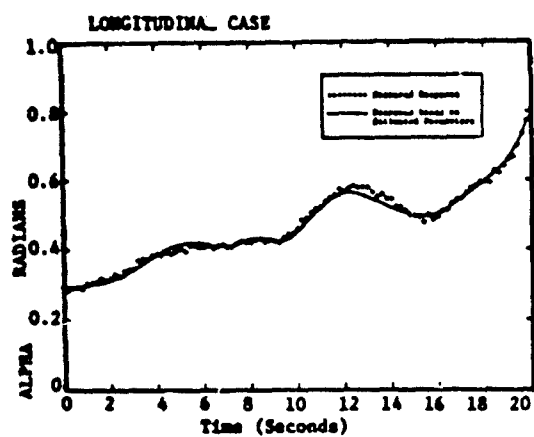
## 5.0 SUMMARY AND CONCLUSION

### 5.1 The Integrated Parameter Identification Procedure

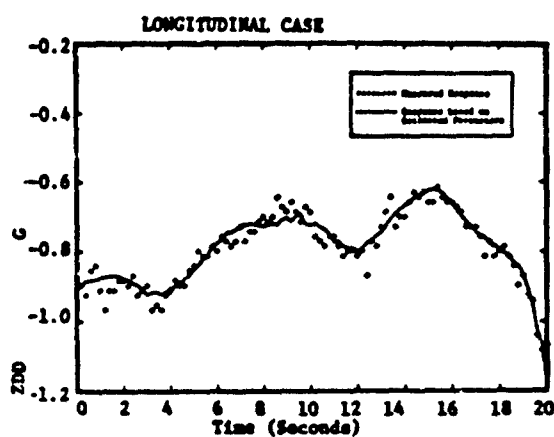
The basic objective of the integrated parameter identification procedure is to most fully exploit the theoretical and computational versatility of the maximum likelihood method to yield a practical data processing tool. Because the likelihood function contains all unknown parameter information if the model is correct, primary emphasis has been placed on specifying the best possible model estimate. This specification is achieved with an algorithm based on subset regression.

Application of this model determination program demonstrates a significant improvement in maximum likelihood efficiency, both in required computation and in accuracy of results. The improvement in performance of the entire process is based on the following characteristics of the regression method:

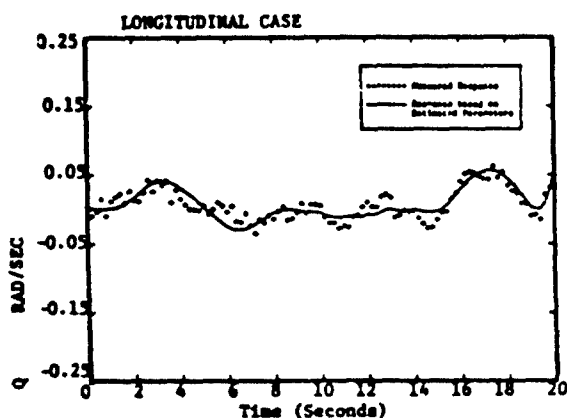
1. The subset regression method selects parameters on their ability to match the measured response. By selecting the optimum number of variables to accomplish this match, the most significant variables are isolated.
2. The method yields a priori estimates from the data above, and does not itself require initial estimates. Though usually biased, the estimates given by the program are frequently better than a priori estimates from other sources.
3. The method gives significance evaluations on the estimated parameters, which serves an essential role in final selection of a model structure to be used in the maximum likelihood algorithm.



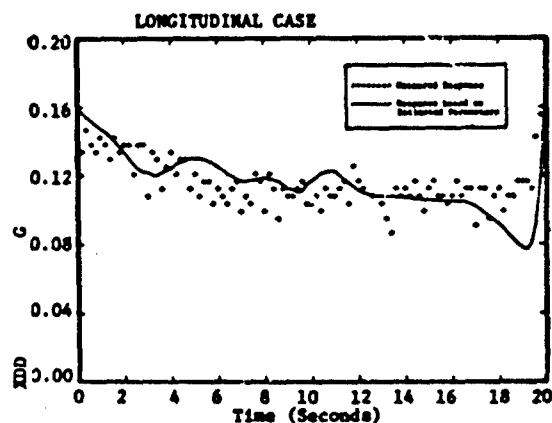
Measured Angle-of-Attack Compared to Response Based on Estimated Parameters



Measured Vertical Acceleration Compared to Response Based on Estimated Parameters



Measured Pitch Response Compared to Response Based on Estimated Parameters



Measured Longitudinal Acceleration Response Compared to Response Based on Estimated Parameters

Fig. 16 Parameter Identification from Longitudinal Response of a Swept Wing Fighter (Flight Test Data)

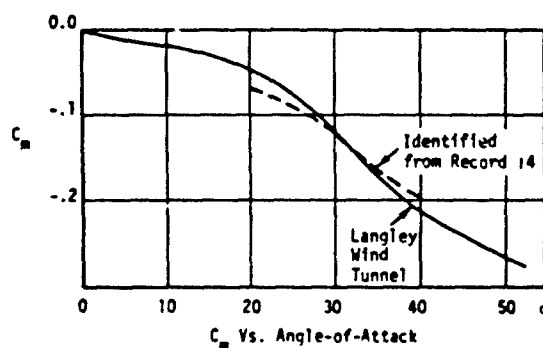
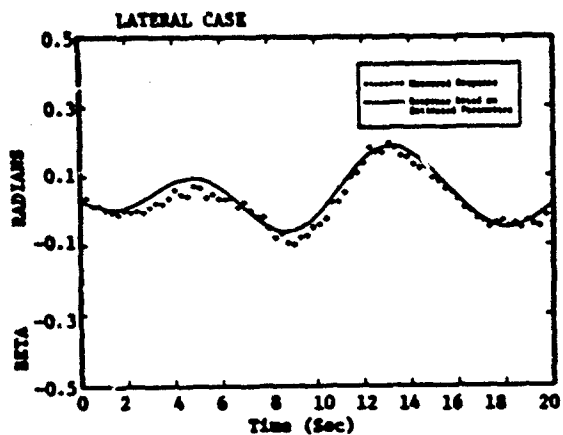
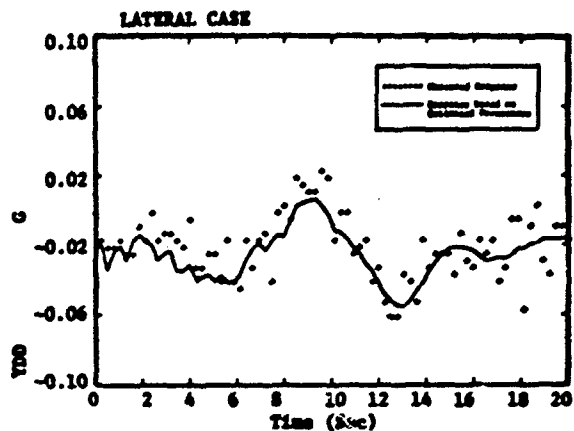


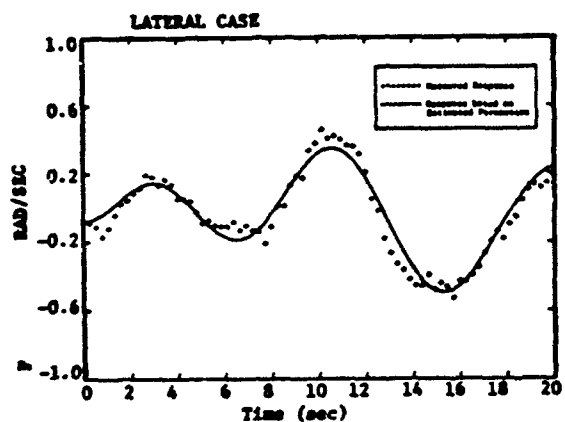
Fig. 17 Identified Coefficients from Longitudinal Responses



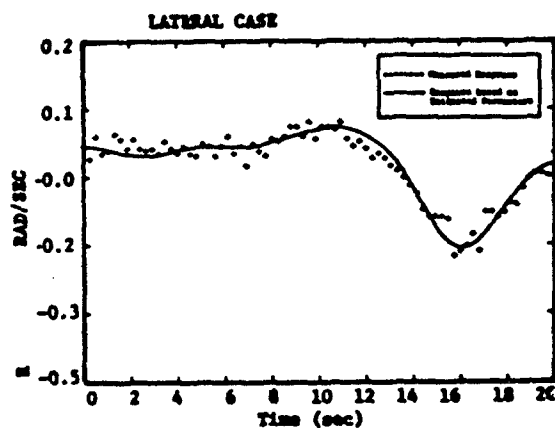
Measured Sideslip Response Compared to Response of Identified Model



Measured Lateral Acceleration Response of Identified Model

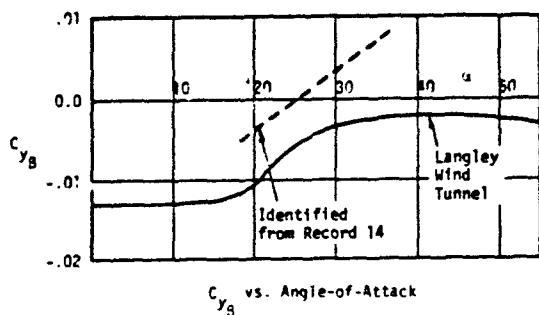


Measured Roll Rate Response of Identified Model

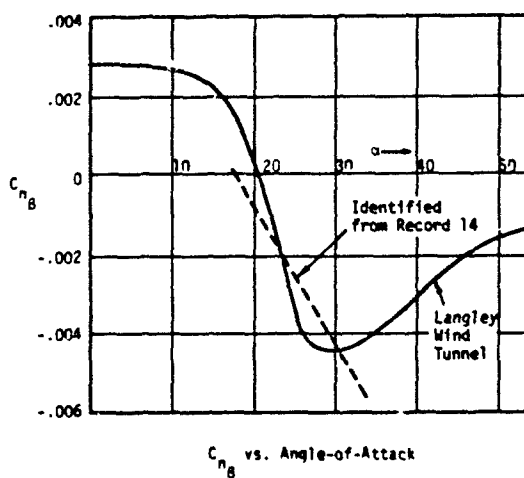


Measured Yaw Rate Response of Identified Model

Fig. 18 Parameter Identification from Longitudinal Response of a Swept Wing Fighter (Flight Test Data)



$C_y$  vs. Angle-of-Attack



$C_n$  vs. Angle-of-Attack

Fig. 19 Identified Coefficients from Lateral Responses



4. The computational requirements of the regression algorithm are modest, and the algorithm can be used quickly not only to evaluate input designs, but also effects of measurement errors.

The implementation of the maximum likelihood for this work can accept either linear or nonlinear aerodynamic expansions of the force and moment coefficients. Further, this algorithm can process parameters for only one dynamic equation or all six. The program includes calculations of parameter significance level.

### 5.2 Application to Simulated and Flight Test Data for the High Angle-of-Attack Stall/Post-Stall Regime

The evaluation of the integrated parameter identification process has been conducted with simulation and flight data. The simulation is highly nonlinear and of much higher order than the identification models used.

The main conclusion of applying the identification procedure to the simulated data is the predominance of linear aerodynamic models required, even for "nonlinear" regimes. This is generally true for small perturbations about steady state conditions. Recognizing that such conditions may not be attainable, nonlinear models are required for large inputs where angle-of-attack and sideslip are simultaneously excited, such as would be obtained for large amplitude sinusoidal inputs or special maneuvers. The regression step is essential since it indicates whether or not nonlinear contributions are required. The ability to recognize and identify such nonlinear terms is requisite for determination of coefficients such as  $C_m$  and  $C_n$ . This is demonstrated with both simulated and flight data of a swept wing fighter aircraft. Both types of data give similar linear and nonlinear aerodynamic models.

Primary emphasis has been placed on the identification of static force and moment coefficients. Greatest errors have been found in estimates of the dynamic rate derivatives and control effectiveness derivatives. These errors are attributed to the relatively low rates which were obtained for inputs to identify the important static derivatives. Inputs may be modified, using input design algorithms discussed in the paper, to improve the estimation of these derivatives. It must be noted that the errors of the dynamic derivatives which were obtained could not be found by comparing time history matches of the measurement of rate, as these were excellent in all cases. Only with comparison of the actual parameter time histories were these errors observed.

Techniques for improving parameter estimates include input design and increased data length (where possible). Such modifications have a significant effect on flight test planning and should be available for identification of important but difficult to excite parameters. The integrated parameter identification process as developed in this work is amenable to such flight test design, using procedures detailed in Ref. [2].

The confidence established in the procedure led to evaluation of the identification results by a prediction criterion. Specifically, the parameter estimates from a specific lateral maneuver with one input are used to predict the response of the simulation to another input (for roughly the same flight regime). This prediction capability was verified with excellent results.

In summary, it is concluded that the application of the integrated parameter identification process developed for the high angle-of-attack stall/post-stall regime offers significant improvements in the ability to identify not only parameters, but also the entire system structure and parameters. Primary interest now lies in input design for testing of aircraft in such regimes.

## APPENDIX A

### Model Structure Determination by Stepwise Regression

The stepwise regression technique has been used in statistics to determine a set of independent variables which determine the value of the dependent variable to a specified accuracy. The same technique can be used to determine the model structure of a nonlinear dynamic system, which is linear in parameters, in particular the high angle-of-attack problem. With measurements of accelerations and state variables, the equations of motion can be written as

$$y = X\theta + \epsilon \quad (A.1)$$

where  $y$  is an  $m \times 1$  vector of accelerations,  $X$  is an  $m \times p$  matrix of state variables and nonlinear functions of state variables,  $\theta$  is a  $p \times 1$  vector of parameters and  $\epsilon$  is the residual. The set of important parameters is determined by performing a correlation analysis between  $y$  and  $X$ . The parameters are included in the regression equation one at a time until the entire model is determined (see Kendall and Stuart [38] for details).

At any point in the analysis the regression equation  $y = X\theta + \epsilon$  can be partitioned as

$$y = X_1\theta_1 + X_2\theta_2 + \epsilon \quad (A.2)$$

where  $X_1$  includes  $q$  variables and  $X_2$  contains  $p-q$  variables. Then

$$y - X_1\theta_1 = X_2\theta_2 + \epsilon \quad (A.3)$$

which shows that an estimate of  $\theta_2$  could be obtained by regressing the residuals from the regression of  $y$  on  $X_1$  (which estimates  $\theta_1$ ). Then the vector  $y - X_1\theta_1$  is regarded as a new observation, say  $y^{(1)}$ , which may be regressed on  $X_2$  to estimate  $\theta_2$ . This decomposition can be applied to each possible subset of variables,  $X_1$ , "bringing in" new variables from the right to left hand side of Eq. (A.3). The requirement on "bringing in" new variables may be satisfied by examining the significance of each variable.

The  $F$  test may be used to determine the significance of a single parameter by noting that the estimate  $s^2$  of the variance  $\sigma^2$  is distributed as  $\sigma^2 \chi^2_{m-p}$ . Hence,  $s^2/\sigma^2 \sim (\chi^2_{m-p})/(m-p)$ . Then for the parameter  $\theta_1$ ,

$$\frac{\hat{\theta}_1 - \theta_1}{s_{\theta_1}} = \frac{(\hat{\theta}_1 - \theta_1)/\sigma_{\theta_1}}{s_{\theta_1}/\sigma_{\theta_1}} \quad (A.4)$$

where  $s_{\theta_1}$  is the standard error of  $\theta_1$ , which is

$$s_{\theta_1} = \sqrt{s_{11}} \quad (A.5)$$

where  $s_{11}$  is the 1<sup>th</sup> diagonal term of  $(X^T X)^{-1}$ .

Since  $(\hat{\theta}_1 - \theta_1)/\sigma_1 \sim n(0,1)$ , it follows that, by definition of Student's  $t$  distribution that

$$\frac{\hat{\theta}_1 - \theta_1}{s_{\theta_1}} = t_{m-p} \quad (A.6)$$

In particular, it is desired to test the hypothesis  $\theta_1 = 0$  (i.e.,  $y$  does not depend on  $\theta$ ), the statistic  $t = \hat{\theta}_1/s_{\theta_1}$  is used. It is shown in [37] that the  $F$  distribution with 1 and  $(m-p)$  degrees-of-freedom is equivalent to the  $t^2$  distribution with  $m-p$  degrees-of-freedom. Hence, the significance of individual regression coefficients,  $\theta$ , is determined from  $F$  ratios

$$F = \hat{\theta}_1^2/s_{\theta_1}^2 \quad (A.7)$$

If the ratio (A.7) indicates a variable is not significant, then the variable is deleted. To bring in another variable, the partial correlation coefficients of all other parameters are examined. To form the  $F$  ratio for these coefficients

$$r_{y\bar{x}_j}^2 = \frac{(\hat{\theta}_j/s_{\theta_j})^2}{(\hat{\theta}_j/s_{\theta_j})^2 + (m-q)} \quad (A.8)$$

where  $q$  is the number of variables already in the regression. The corresponding  $F$  test is

$$F_j = \frac{r_{y\bar{x}_j}^2 (m-q)}{1 - r_{y\bar{x}_j}^2} \quad (A.9)$$

The variable ( $F$  ratio with 1 and  $m-q$  degrees of freedom), is calculated for each of the remaining variables. The variable with the highest value is then brought into regression. This process is repeated until all relevant parameters are included in the regression.

#### ACKNOWLEDGEMENT

The authors wish to cite the significant contributions to SCI project engineers in the accomplishment of this effort. Mr. Richard Smith and Mr. Richard Mohr were instrumental in the aircraft analysis, and development and integration of the algorithms reported in this paper. In addition, many useful interpretations of the results are based on discussions with Professor Raman Mehra of Harvard University. Finally, this work has been greatly enhanced by technical discussions with the ONR contract monitor, Mr. David S. Siegel.

#### REFERENCES

1. Hall, Jr., W.E., "Identification of Aircraft Stability and Control Derivatives for the High Angle-of-Attack Regime", Technical Report No. 1, prepared for the Office of Naval Research under Contract N00014-73-C-0328, June 1973.
2. Hall, Jr., W.E., Gupta, N.K., Smith, R.G., "Identification of Aircraft Stability and Control Derivatives for the High Angle-of-Attack Regime", Technical Report No. 2, prepared for the Office of Naval Research, 1974.
3. McElroy, C.E., Sharp, P.S., "Stall/Near Stall Investigation of the F-4E Aircraft," Air Force Flight Test Center, Edwards Air Force Base, FIC-SD070-20, Oct. 1970.
4. Thelander, J.A., "Aircraft Motion Analysis," FDL-TDR-64-70, 1964.
5. Etkin, E., Dynamics of Atmospheric Flight, John Wiley and Sons (1971); (also Dynamics of Flight, John Wiley (1959)).
6. Grafton, S.C., Libbey, C.E., "Dynamic Stability Derivatives of a Twin Jet Fighter for Angles-of-Attack from -10° to 110° and Sideslip Angles from -40° to 40°," NASA TND-6425, August 1971.
7. Anglin, E.L., "Static Force Tests of a Model of a Twin Jet Fighter Airplane for Angles-of-Attack from -10° to 110° and Sideslip Angles from -40° to 40°," NASA TND-6425, August 1971.
8. Sorensen, J.A., "Analysis of Instrumentation Error Effects on the Identification Accuracy of Aircraft Parameters", NASA CR-112121, May 1972.
9. Private Communication, Capt. David Carlton, Edwards, Air Force Base, 7 July 1972.
10. Stepner, D.E., Mehra, R.K., "Maximum Likelihood Identification and Optimal Input Design for Identifying Aircraft Stability and Control Derivatives", NASA CR-220, March 1973.
11. Chen, R.T.N., Eulrich, B.J., Lebacqz, J.V., "Development of Advanced Techniques for the Identification of V/STOL Aircraft Stability and Control Parameters", CAL Report No. BM-2820-F-1, August 1971.
12. Holmes, J.E., "Limitations in the Acquisition of Nonlinear Aerodynamic Coefficients from Free Oscillation Data by Means of the Chapman-Kirk Technique", presented at AIAA Guid. and Cont. Conf., Aug. 1972.
13. Ross, A.J., "Investigation of Nonlinear Motion Experience on a Slender-Wing Research Aircraft", Journal of Aircraft, Vol. 9, No. 9, Sept. 1972, pp. 625-631.
14. NASA Symposium, Parameter Estimation Techniques and Applications in Aircraft Flight Testing, Edwards Flight Research Center, April 24 & 25, 1973.
15. Astrom, K.J. and Eykhoff, P., "System Identification - A Survey", Automatica, Vol. 7, pp. 123-162, Pergamon Press, 1971.

16. Wolcovich, C.H., Iliff, K.W., and Gilyard, G.B., "Flight Test Experience in Aircraft Parameter Identification", Presented at AGARD Symp. on Stability & Control, Braunschweig, Germany, April 1972.
17. DiFranco, D., "In-Flight Parameter Identification by the Equation-of-Motion Technique--Application to the Variability Stability T-33 Airplane", Cornell Aeronautical Laboratory Report No. TC-1921-F-3, 15 December 1965.
18. Gerlach, O.H., "Determination of Performance and Stability Parameters from Non-Steady Flight Test Manuevers", SAE National Bus. Aircraft Meeting, Wichita, Kansas, March 1970.
19. Goodwin, G.C., "Application of Curvature Methods to Parameter and State Estimation", Proc. IEEE, Vol. 16, No. 6, June 1969.
20. Taylor, L., et al., "A Comparison of Newton-Raphson and Other Methods for Determining Stability Derivatives from Flight Data", Third Tech. Workshop on Dynamic Stability Problems, Ames Research Center, 1965; also presented at AIAA Third Flight Test, Sim. and Support Conf., Houston, Texas, March 1969.
21. Bellman, R., et al., "Quasilinearization, System Identification, and Prediction", RAND Corporation, RM-3812, August 1967.
22. Kumar, K.S.P. and Shridhar, R., "On the Identification of Control Systems by the Quasilinearization Method", IEEE Trans., Vol. AC-10, pp. 151-154, April 1964.
23. Larson, D., "Identification of Parameters by Method of Quasilinearization", CAL Report 164, May 1968.
24. Denery, D.G., "An Identification Algorithm Which is Insensitive to Initial Parameter Estimates", AIAA Eighth Aerospace Science Conference, January 1970.
25. Young, P.C., "Process Parameter Estimation and Adaptive Control", In Theory of Self-Adaptive Control Systems, P. Hammond, ed., Plenum Press, New York, 1966.
26. Schalow, R.D., "Quasilinearization and Parameter Estimation Accuracy", Ph.D. Thesis, Syracuse Univ., 1967.
27. Dolbin, B., "A Differential Correction Method for the Identification of Airplane Parameters from Flight Test Data", University of Buffalo, Masters Thesis, December 1968.
28. Lason, L.S., et al., "The Conjugate Gradient Method for Optimal Control Problems", IEEE Trans., G-AL, Vol. 12, No. 2, April 1967.
29. Suit, W.T., "Aerodynamic Parameters of the Navion Airplane Extracted from Flight Data," NASA TN D-6643, March 1972.
30. Steinmetz, G.S., Parrish, R.V., and Bowles, R.L., "Longitudinal Stability and Control Derivatives of a Jet Fighter Airplane Extracted from Flight Test Data by Utilizing Maximum Likelihood Estimation", NASA TN D-6532, March 1972.
31. Tyler, J.S., Powell, J.D., and Mehra, R.K., "The Use of Smoothing and Other Advanced Techniques for VTOL Aircraft Parameter Identification", Final Report to Cornell Aeronautical Laboratory under Naval Air Systems Command Contract No. N00019-69-C 0534, June 1970.
32. Astrom, K.J. and Wenmark, S., "Numerical Identification of Stationary Time Series", Sixth International Instruments and Measurements Congress, Stockholm, September 1965.
33. Kashyap, R.L., "Maximum Likelihood Identification of Stochastic Linear Dynamic Systems", IEEE Trans. AC, February 1970.
34. Mehra, R.K., "Identification of Stochastic Linear Dynamic Systems Using Kalman Filter Representation", AIAA Journal, Vol. 9, No. 1, Jan. 1971.
35. Gupta, N.K. and Hall, W.E., "Input Design for Identification of Aircraft Stability and Control Coefficients", Technical Report 6991-01, Systems Control, Inc., Palo Alto, Calif., March, 1974; also NASA CR - to be published.
36. Mehra, R.K. and Gupta, N.K., "Status of Input Design for Aircraft Parameter Identification", paper presented at AGARD Specialist's Conf. on Methods for Aircraft State and Parameter Estimation, NASA Langley Research Center, Hampton, Virginia, Nov. 5, 1974.
37. Akaike, H., "Statistical Predictor Identification", Ann. Inst. Statist. Math., Vol. 22, 1970.
38. Kendall, M.G. and Stuart, A., The Advanced Theory of Statistics, Vol. I and II, 2nd Edition, Charles Griffin and Company, Ltd., London, 1967.

# IMPORTANCE OF HELICOPTER DYNAMICS TO THE MATHEMATICAL MODEL OF THE HELICOPTER

by

William F. White, Jr.  
Langley Directorate  
U.S. Army Air Mobility R&D Laboratory  
NASA Langley Research Center  
Hampton, Virginia 23665

## SUMMARY

A mathematical model of the helicopter requires appropriate representation of the constituent elements of rotor dynamics. General-purpose programs that model a variety of configurations for a broad range of operating conditions often result in varying and incompatible levels of sophistication. Analysis of specific dynamic problems facilitates the identification of configuration parameters that determine system behavior. For the present analysis, the nonlinear equations of a torsionally rigid hingeless rotor are linearized about an equilibrium condition to determine flap-lag stability characteristics in hover. A collocation method is used to obtain the coupled natural frequencies and modes. These modes allow exact treatment of the effect of elastic coupling which more than compensates for the destabilizing inertial coupling. The sensitivity of damping to the number of modes was found to be small and reasonable accuracy was obtained using the first flapwise and edgewise coupled modes. The range of destabilizing precone was found to be small.

## NOTATION

$a$	Lift curve slope
$\bar{C}_{d0}$	Ratio of drag coefficient to lift curve slope, $C_{d0}/a_r \bar{a}$
$c$	Blade chord
$E$	Young's modulus
$e$	Distance between mass and elastic axis
$e_a$	Distance between area centroid of tensile member and elastic axis
$G$	Dimensionless generalized mass or shear modulus of elasticity
$I_1, I_2$	Cross-section area moments of inertia
$J$	Torsional stiffness constant
$k_a$	Polar radius of gyration of cross-sectional mass about elastic axis
$k_{a1}, k_{a2}$	Principal mass radii of gyration
$k_a$	Polar radius of gyration of cross-sectional area effective in carrying tension
$L_x, L_y$	Aerodynamic loading per unit length
$M$	Number of blade modes
$m$	Mass per unit length
$n$	Number of blade stations
$Q$	Dimensionless generalized force
$q$	Generalized coordinates
$R$	Blade radius
$T$	Blade tension
$u, v, w$	Elastic displacements of a point on the elastic axis, parallel to the $x, y, z$ coordinate system
$x, y, z$	Undeformed coordinate system, $x$ coincident with elastic axis of the undeformed blade
$\beta_p$	Blade precone
$\beta_1$	Dimensionless flapwise modal displacement

$\gamma$	Lock number
$c_1$	Dimensionless edgewise modal displacement
$\theta$	Local blade pitch angle
$\kappa$	Dimensionless mass, $m/m_r$
$A_1, A_2$	Dimensionless bending stiffness
$\bar{A}_1, \bar{A}_2, \bar{A}_{12}$	Generalized bending stiffness
$v$	Inflow velocity
$\xi$	Dimensionless radial coordinate $x/R$
$\sigma$	Solidity
$\sigma_w, \sigma_v$	Real part of flapwise and edgewise eigenvalues
$\hat{\sigma}_p$	Ratio of the real part of edgewise eigenvalues to the corresponding eigenvalue at zero precone
$\hat{\sigma}_\theta$	Ratio of the real part of edgewise eigenvalues to the corresponding eigenvalue at zero pitch
$\tau$	Dimensionless time, $\Omega t$
$\phi$	Elastic torsional deflection
$\Omega$	Rotor angular velocity
$\bar{\omega}$	Dimensionless natural frequency, $\omega/\Omega$
$\bar{\omega}_{E0}$	Dimensionless first edgewise frequency for zero pitch angle
$\bar{\omega}_{B0}$	Dimensionless first flapwise frequency for zero pitch angle
$( )'$	$\partial/\partial x$ or $\partial/\partial \xi$
$( )''$	$\partial^2/\partial x^2$ or $\partial^2/\partial \xi^2$
$( )_0$	Equilibrium quantity
$( )^*$	Nondimensionalized by $\Omega$ for frequencies, $R$ for displacements, $\Omega R$ for velocities, and $m\Omega^2 R$ for forces per unit length
$( )_r$	Reference quantity

## 1. INTRODUCTION

As fixed-wing vehicles have progressed from low subsonic to the hypersonic flight regime, appropriate analyses have evolved to assist in predicting and understanding the associated aeroelastic instabilities. In the case of helicopter rotors, parallel development of a mathematical model is far from complete. While most helicopter instabilities are understood reasonably well when viewed as general physical phenomena, they are not as amenable to analysis as their fixed-wing counterparts. This is due in part to an aerodynamic environment of exquisite intractability. In dealing with the flow fields associated with helicopter rotors, the analyses developed for fixed wings must be drastically modified or abandoned altogether.

Structural dynamics of helicopter rotors differ significantly from their fixed-wing counterparts. Varied design practice generates numerous root boundary conditions with varying geometric and elastic properties. Inplane flexibility manifests itself by adding additional degrees of freedom and as a potential source of inter-modal coupling. Rotation leads to complicated inertia loads which must be regarded as a potential source of stiffness and coupling between degrees of freedom. Geometric design parameters such as droop, sweep, precone, hub offsets, and noncoincident mass, tension, pitch, and elastic axes may significantly alter rotor dynamic characteristics. Rotor blades are typically very complex structures having highly nonuniform elastic, inertial, and geometric distributions. In general, the equations which describe the flapwise, edgewise, and torsional characteristics of such blades are nonlinear integro-differential equations.<sup>1-3</sup> The nonlinearities arise from aerodynamic and inertial terms, and periodic terms arise when cyclic pitch changes are imposed. In forward flight, additional nonlinear and periodic terms of aerodynamic origin arise.

The substructuring of helicopter dynamic stability and loads analyses is generally based on advance ratio since it is an important determinant of the aerodynamic forces. At high advance ratio periodic aerodynamic and structural terms may significantly influence rotor stability. Thus, when periodic terms are important, methods such as Floquet theory must be used to accurately determine rotor stability.

An additional substructuring of helicopter dynamics is the number of degrees of freedom, denoted by hub constraint. When the hub is fixed only a single blade analysis is necessary to define rotor stability.

The single blade with a fixed hub is important for several reasons. Most importantly, the dynamic behavior of a single blade is the basic building block for more complex problems. For instabilities which depend on rotor/fuselage coupling, such as air or ground resonance, a knowledge of isolated blade dynamics is useful. Furthermore, methods for improving rotor blade stability are also likely to prove effective for improving the stability of coupled rotor/fuselage dynamics. The single blade analysis is often subject to further reduction by uncoupling or suppressing the flapwise, edgewise, and torsional degrees of freedom in various combinations. With hub fixity relaxed, all blades are intercoupled with themselves and the helicopter fuselage. This class of problems emphasizes the dynamic coupling between rotor and fuselage degrees of freedom. Air and ground resonance are important subdivisions in this category. An additional consideration is the coupling of the rotor with feedback control systems. For hover or low advance ratios, standard control system synthesis techniques are applicable.

In recent years a considerable amount of rotor aeroelastic research has focused on specific instabilities.<sup>4</sup> These analyses provide insight into the physical characteristics of numerous types of instabilities and provide the basis for general-purpose helicopter mathematical models. Several general-purpose simulation models exist in the Army's inventory of computer programs. These programs have been developed to predict performance, handling qualities, rotor dynamics, and loads. Limited success has been obtained for specific rotor configurations. Emphasis on modeling a variety of configurations for a broad range of flight conditions has resulted in varying and incompatible levels of sophistication. The aeroelastic module is generally based on modeling requirements for rotor loads. A major deficiency is the inability to accurately determine hingeless rotor stability boundaries.

In recent years the hingeless rotor has become an increasingly attractive concept. The advantage of this system is the large moment capability which can be transmitted directly to the aircraft. The resulting high control power and angular damping substantially improve flying qualities and maneuverability. However, a greater potential for instability exists due to strong dynamic coupling inherent in the cantilever configuration. Recent research and flight-test experience<sup>5-7</sup> has revealed that hingeless rotor stability is significantly influenced by elastic and inertial coupling terms.

## 2. FLAP-LAG STABILITY OF HINGELESS ROTORS

For the present analysis, the equations of motion for combined bending are obtained by extension of the method of Houbolt and Brooks.<sup>8</sup> The assumptions used in deriving this system of equations are briefly outlined: (a) The elastic blade is cantilevered to a rigid hub and rotating at constant speed. (b) The blade is torsionally rigid. (c) Precone is assumed to be a small angle. (d) The elastic axis is a straight line. (e) The pitch axis is coincident with the elastic axis. (f) The mass and tension axes have negligible offset from the elastic axis. (g) The blade cross section is symmetric about the major principal axis. (h) Hover flight is assumed and cyclic pitch change is negligible. (i) Two-dimensional quasi-steady aerodynamic loads are used with radial flow, apparent mass, and stall effects neglected. (j) Structural damping is neglected.

Figure 1 depicts the deformed position of the elastic axis as a general space curve. Equations (A-1) and (A-2) of Appendix A are the flapwise and edgewise equations of motion for appropriate values of the applied loading. The applied loadings for small precone and negligible chordwise offsets are

$$\begin{aligned} p_x(x,t) &= m\Omega^2 x + 2m\dot{\Omega}\dot{v} \\ p_y(x,t) &= L_y - m\ddot{v} + m\Omega^2 v + 2m\Omega\delta_p \dot{v} - 2m\Omega\dot{u} \\ p_z(x,t) &= L_z - m\ddot{u} - m\Omega^2 \beta_p x - 2m\Omega\delta_p \dot{v} \\ q_y(x,t) &= q_z(x,t) = 0 \end{aligned} \quad (1)$$

Substituting Equation (1) into Equations (A-1) and (A-2) of Appendix A and differentiating twice yields the coupled flapwise-edgewise equations of motion.

$$\begin{aligned} &[(EI_1 \cos^2 \theta + EI_2 \sin^2 \theta)w'' + (EI_2 - EI_1) \sin \theta \cos \theta v'']'' \\ &\quad - (Tw')' + m\ddot{u} + m\Omega^2 \beta_p x + 2m\Omega\delta_p \dot{v} = L_z \\ &[(EI_1 \sin^2 \theta + EI_2 \cos^2 \theta)v'' + (EI_2 - EI_1) \sin \theta \cos \theta w'']'' \\ &\quad - (Tv')' + m\ddot{v} - m\Omega^2 v + 2m\Omega\dot{u} - 2m\Omega\delta_p \dot{v} = L_y \end{aligned} \quad (2)$$

where

$$-T' - m(\Omega^2 x + 2\Omega\dot{v}) = 0 \quad (3)$$

$$u = -\frac{1}{2} \int_0^x [(w')^2 + (v')^2] dx \quad (4)$$

Equation (3) represents the apparent shortening effect due to combined transverse bending. The equations of motion are expressed in dimensionless form by dividing by  $m_r \Omega^2 R$ . Dimensionless displacements  $\bar{u}$ ,  $\bar{v}$ ,  $\bar{w}$  are based on rotor radius  $R$ , and the independent variables become  $\xi = x/R$  and  $\tau = \Omega t$ . The dimensionless equations are:

$$-\bar{T}' - \kappa(\xi + \dot{\bar{v}}) = 0$$

$$\begin{aligned}
(\bar{A}_1 \ddot{w}'' + \bar{A}_{12} \ddot{w}''')'' - (\bar{w}')' + \kappa \ddot{w} - \bar{L}_z - \kappa \beta_p \xi - 2\kappa \beta_p \dot{\bar{v}} \\
(\bar{A}_2 \ddot{w}'' + \bar{A}_{12} \ddot{w}''')'' - (\bar{v}')' + \kappa \ddot{v} - \kappa \bar{v} = \bar{L}_y + 2\kappa \beta_p \dot{\bar{v}} - 2\kappa \dot{\bar{u}}
\end{aligned} \quad (5)$$

where

$$\begin{aligned}
\bar{A}_1 &= A_1 \cos^2 \theta + A_2 \sin^2 \theta \\
\bar{A}_2 &= A_1 \sin^2 \theta + A_2 \cos^2 \theta \\
\bar{A}_{12} &= (A_2 - A_1) \sin \theta \cos \theta \\
A_1 &= \frac{EI_1}{m_r \Omega^2 R^4} \quad A_2 = \frac{EI_2}{m_r \Omega^2 R^4} \\
\bar{T} &= \frac{T}{m_r \Omega^2 R^2} \quad \kappa = \frac{m}{m_r}
\end{aligned}$$

The dimensionless aerodynamic forces per unit length denoted by  $\bar{L}_y$  and  $\bar{L}_z$  may be obtained from the two-dimensional quasi-steady relations of Reference 3 as

$$\begin{aligned}
\bar{L}_y &= -\frac{\gamma}{8} \bar{a} c [\theta \xi \bar{v} - \bar{v}^2 + \bar{c}_{d0} \xi^2 + (\theta \bar{v} + 2\xi \bar{c}_{d0}) \dot{\bar{v}} + (\theta \xi - 2\bar{v}) \dot{\bar{w}}] \\
\bar{L}_z &= \frac{\gamma}{8} \bar{a} c [\theta \xi^2 - \xi \bar{v} + (2\theta \xi - \bar{v}) \dot{\bar{v}} - \xi \dot{\bar{w}}]
\end{aligned} \quad (6)$$

Note that higher order effects<sup>10</sup> due to elastic deflections are neglected. The quantity  $\bar{v}$  is the local dimensionless inflow velocity for a hovering rotor. The inflow is approximated by combined blade element and momentum theory<sup>11</sup> as

$$\bar{v} = \sqrt{\left(\frac{a_r \bar{a} \theta}{16}\right)^2 + \frac{a_r \bar{a} \theta \xi \theta}{8}} - \frac{a_r \bar{a} \theta}{16} \quad (7)$$

Equation (5) may be simplified by substitution of Equations (3) and (4) to eliminate  $\bar{u}$  and  $\bar{T}$ . The resulting equations are:

$$\begin{aligned}
(\bar{A}_1 \ddot{w}'' + \bar{A}_{12} \ddot{w}''')'' - [\bar{w}'] \int_{\xi}^1 \kappa (\xi + 2\dot{\bar{v}}) d\xi + \kappa \ddot{w} - \bar{L}_z - \kappa \beta_p \xi - 2\kappa \beta_p \dot{\bar{v}} \\
(\bar{A}_2 \ddot{w}'' + \bar{A}_{12} \ddot{w}''')'' - [\bar{v}'] \int_{\xi}^1 \kappa (\xi + 2\dot{\bar{v}}) d\xi + \kappa \ddot{v} - \kappa \bar{v} = \bar{L}_y + 2\kappa \beta_p \dot{\bar{v}} + 2\kappa \int_0^{\xi} (\bar{v}' \dot{\bar{v}} + \bar{w}' \dot{\bar{w}}) d\xi
\end{aligned} \quad (8)$$

These equations may be linearized about an equilibrium operating condition to retain the essential features of the nonlinear coupling, and the resulting equations are simplified by expansion in terms of the free vibration modes. For the present analysis, these modes are defined as the coupled rotating modes (Appendix A). The displacements and loads consist of equilibrium and perturbation components.

$$\begin{aligned}
\bar{w}(\xi, \tau) &= w_0(\xi) + w(\xi, \tau) \\
\bar{v}(\xi, \tau) &= v_0(\xi) + v(\xi, \tau) \\
\bar{L}_y(\xi, \tau) &= L_{y0}(\xi) + L_y(\xi, \tau) \\
\bar{L}_z(\xi, \tau) &= L_{z0}(\xi) + L_z(\xi, \tau)
\end{aligned} \quad (9)$$

where the dimensionless equilibrium and perturbation quantities in Equation (9) are now written without a bar. Substituting Equation (9) into (8) and neglecting higher order products of perturbation quantities yields the equilibrium and perturbation equations.

$$\begin{aligned}
(\bar{A}_1 w_0'' + \bar{A}_{12} w_0''')'' - [w_0'] \int_{\xi}^1 \kappa \xi d\xi = L_{z0} - \kappa \beta_p \xi \\
(\bar{A}_2 v_0'' + \bar{A}_{12} v_0''')'' - [v_0'] \int_{\xi}^1 \kappa \xi d\xi = L_{y0}
\end{aligned} \quad (10)$$

$$\begin{aligned}
(\bar{A}_1 w'' + \bar{A}_{12} w''')'' - [w' \int_{\xi}^1 \kappa \xi d\xi]' + \kappa w - L_s - 2\beta_p \kappa w - 2\kappa w_0' + 2w_0'' \int_{\xi}^1 \kappa \xi d\xi \\
(\bar{A}_2 v'' + \bar{A}_{12} v''')'' - [v' \int_{\xi}^1 \kappa \xi d\xi]' + \kappa v - \kappa v = L_y + 2\beta_p \kappa v - 2\kappa v_0' + 2v_0'' \int_{\xi}^1 \kappa \xi d\xi + 2\kappa \int_0^{\xi} (v_0' \dot{v}' + w_0' \dot{w}') d\xi
\end{aligned} \quad (11)$$

The displacement at a radial station  $\xi$  is expressed as a superposition of the contributions of the various modes

$$\begin{aligned}
w(\xi, \tau) &= \sum_{j=1}^M \beta_j(\xi) q_j(\tau) \\
v(\xi, \tau) &= \sum_{j=1}^M \zeta_j(\xi) q_j(\tau) \\
v_0(\xi) &= \sum_{j=1}^M A_{0j} \zeta_j(\xi) \\
w_0(\xi) &= \sum_{j=1}^M A_{0j} \beta_j(\xi)
\end{aligned} \quad (12)$$

The linearized perturbation equations may be simplified by substituting Equation (12), and applying the orthogonality relation given by Equation (A-7) of Appendix A. The perturbation equations in matrix form are

$$[G] \{\ddot{q}\} + [\omega^2 G] \{q\} = \{0\} \quad (13)$$

where

$$G_{ij} = \int_0^1 \kappa [\beta_i^2 + \zeta_i^2] d\xi \quad (14)$$

$$Q_{ij} = [C_{ij} + S_{ij}] \dot{q}_j \quad (15)$$

$$\begin{aligned}
C_{ij} = \int_0^1 \left\{ -\frac{\gamma_{\tau} \bar{\kappa}}{6} (\theta \bar{v} + 2\bar{\xi} \bar{c}_{d0}) \zeta_i \zeta_j + [2\beta_p \kappa - \frac{\gamma_{\tau} \bar{\kappa}}{6} (\theta \bar{\xi} - 2\bar{v})] \zeta_i \beta_j \right. \\
\left. - [2\beta_p \kappa + \frac{\gamma_{\tau} \bar{\kappa}}{6} (\bar{v} - 2\theta \bar{\xi})] \beta_i \zeta_j - \frac{\gamma_{\tau} \bar{\kappa}}{6} \bar{\xi} \beta_i \beta_j \right\} d\xi
\end{aligned} \quad (16)$$

$$S_{ij} = \sum_{k=1}^M S_{ikj} A_{0k} \quad (17)$$

$$\begin{aligned}
S_{ikj} = 2 \int_0^1 \beta_i \beta_k'' \left( \int_{\xi}^1 \kappa \zeta_j d\xi \right) d\xi + 2 \int_0^1 \zeta_i \zeta_k'' \left( \int_{\xi}^1 \kappa \zeta_j d\xi \right) d\xi + 2 \int_0^1 \kappa \zeta_i \left[ \int_0^{\xi} (\zeta_k' \zeta_j' \right. \\
\left. + \beta_k' \beta_j') d\xi \right] d\xi - 2 \int_0^1 \kappa \beta_i \beta_k' \zeta_j d\xi - 2 \int_0^1 \kappa \zeta_i \zeta_k' \beta_j d\xi
\end{aligned} \quad (18)$$

The coefficients  $A_{0k}$  may be obtained from Equation (10). Defining  $D_{ij} = -(C_{ij} + S_{ij})$ , Equation (13) is written in matrix form as

$$[G] \{\ddot{q}\} + [D] \{\dot{q}\} + [\omega^2 G] \{q\} = \{0\} \quad (19)$$



Assuming

$$q = \hat{q} e^{\lambda t} \quad (20)$$

Equation (19) may be expressed in conventional eigenvalue form as

$$[K] \{\hat{q}\} = \lambda [L] \{\hat{q}\} \quad (21)$$

where

$$[K] = \begin{bmatrix} -[C]^{-1} [D] & -[C]^{-1} [\bar{\omega}^2 C] \\ [L] & [0] \end{bmatrix} \quad (22)$$

### 3. DISCUSSION OF RESULTS

Stability characteristics of the coupled flapwise-edge-wise bending oscillations of a cantilever blade may be determined from Equation (21) for known operating conditions and blade properties. For the present analysis, the spanwise variations of dimensionless mass and stiffness are illustrated in Figure 2. The amplitudes of these distributions are varied to obtain the desired blade frequencies for a specified rotor speed, radius, and collective pitch. Figure 3 illustrates the typical variation of the flapwise-edge-wise natural frequencies with rotor speed. These natural frequencies are obtained from Equation (A-5) using 20 equally spaced radial stations for  $R = 6.985$  meters.

Stability characteristics of the coupled flapwise-edge-wise bending oscillations of a hingeless blade without precone in a hovering flight condition are shown in Figure 4. The results are presented as a locus of roots of Equation (21) with increasing pitch angle for the first flapwise and edge-wise modes. Loci for several configurations having various inplane frequencies are presented. It is convenient to classify rotors in terms of the first edge-wise and flapwise frequencies at zero pitch. These dimensionless frequencies are denoted by  $\omega_{E0}$  and  $\omega_{F0}$ . The flapwise mode is typically well damped and the inherently low edge-wise damping is substantially increased for higher pitch angles. This is consistent with the results of Reference 12 for a rigid blade model with appropriate root restraint springs to approximate the elastic coupling. The modal solution avoids the difficulty of having to assume the degree of elastic coupling. For specified geometric, inertial, and elastic properties, Equation (A-5) is used to determine the appropriate elastic coupling.

The influence of the number of modes on first edge-wise modal damping is given in Table 1. The sensitivity of damping to the number of modes is relatively small and reasonable accuracy may be obtained using the first flapwise and edge-wise coupled modes.

The Coriolis and centrifugal terms given by  $S_{ij}$  in Equation (18) tend to destabilize the edge-wise degree of freedom. The influence of  $S_{ij}$  on the dimensionless edge-wise damping is illustrated in Figure 5. The effect of blade precone on the dimensionless edge-wise damping is shown in Figure 6. In general, precone is stabilizing except for small positive increments.

### 4. CONCLUSIONS

1. Conventional linear equations of motion yield unconservative results for the coupled flapwise-edge-wise stability of cantilevered, torsionally rigid rotor blades. The coupled flapwise-edge-wise equations can be linearized about an equilibrium operating condition to retain the effect of the inertial coupling terms. The edge-wise damping is dependent on these terms.
2. The sensitivity of flapwise and edge-wise damping to the number of modes was found to be small. Accurate results can be obtained using the first flapwise and edge-wise coupled modes.
3. The use of coupled rotating modes avoids the difficulty of having to assume the degree of elastic coupling. These modes allow exact treatment of elastic coupling which more than compensates for the destabilizing inertial coupling. Thus, flapwise-edge-wise oscillations of nonuniform blades in hover were found to be stable over a wide range of parameters.
4. Precone was found to be stabilizing except for small positive increments.
5. The collocation method<sup>13</sup> used to determine the coupled flapwise-edge-wise modes is easily extended to the calculation of coupled flapwise, edge-wise, and torsional modes.

### APPENDIX A — NATURAL FREQUENCIES AND MODES OF HINGELESS ROTOR BLADES

This Appendix formulates a numerical solution for the natural frequencies and modal functions of a nonuniform rotor blade. The blade is idealized as a rotating cantilevered beam which has nonuniform properties and arbitrary twist. The term "twist" is used to define a variable orientation along the length of the beam of the principal axes relative to the plane of rotation. Twist, chordwise offsets, and pitch will cause the beam to have coupled flapwise, edge-wise, and torsional displacements. Solutions of the equations which describe the behavior of such a beam and the associated orthogonality relationships are obtained.

The integrating matrix developed by Hunter in Reference 13 is the basis for the method of solution. The integrating matrix  $[L]$  is a means of numerically integrating a function that is expressed in terms of the values of the function at specified increments of the independent variable. It is derived by expressing the integrand as a polynomial in the form of Newton's forward-difference interpolation formula. Integrating matrices based upon polynomials of degrees one to seven are given in Reference 13. Solutions of the equations of motion are developed entirely in matrix notation. First, the integro-differential equations, which

are linear homogeneous equations having variable coefficients, are expressed in matrix form. The matrix equations are then integrated using the integrating matrix [L] as an operator. Next, the constants of integration are evaluated by applying the boundary conditions, and the resulting matrix equations are expressed in standard eigenvalue form. Solutions of this eigenvalue problem may be obtained by conventional methods.

For the present analysis, the equations of motion for combined bending and torsion are obtained by extension of the method of Houbolt and Brooks.<sup>8</sup> The principal assumptions used in deriving this system of equations are briefly outlined: (a) The elastic blade is cantilevered to a rigid hub and rotating at constant speed. (b) The blade elasticity is adequately described by the conventional bending and torsion characteristics described in Reference 8. Shear deformation and rotary inertia are negligible. Furthermore, the effects of the additional section constants  $B_1$  and  $B_2$  described therein are considered to be negligible. (c) The elastic axis of the undeformed blade is a straight line. (d) The pitch axis is coincident with the elastic axis of the undeformed blade. (e) The blade cross section is symmetric about the major principal axis. (f) Cyclic pitch, precone, sweep, and higher order inertial and elastic terms are assumed to have a negligible effect on the blade frequencies and modes.

Figure 1 depicts the deformed position of the elastic axis as a general space curve. The applied loadings are shown acting at a point  $P_1$  which is located at a radial distance ( $\eta$ ) from the axis of rotation. The bending moments at point P produced by the applied loadings at  $P_1$  are equated to the elastic restoring moments<sup>8</sup> to yield

$$(EI_1 \cos^2 \theta + EI_2 \sin^2 \theta)w'' + (EI_2 - EI_1)\cos \theta \sin \theta v'' - T_{e_a} \sin \theta - T_{e_a} \phi \cos \theta = \int_x^R (-p_x(w_1 - w) + p_x(\eta - x) + q_y) d\eta \quad (A-1)$$

$$(EI_2 - EI_1)\cos \theta \sin \theta w'' + (EI_1 \sin^2 \theta + EI_2 \cos^2 \theta)v'' - T_{e_a} \cos \theta + T_{e_a} \phi \sin \theta = \int_x^R (-p_x(v_1 - v) + p_y(\eta - x) + q_z) d\eta \quad (A-2)$$

$$(GJ + Tk_a^2)\phi' + Tk_a^2\theta' + \int_x^R T_{e_a}(w'' \cos \theta - v'' \sin \theta) d\eta = \int_x^R (q_x + q_y v' + q_z w') d\eta \quad (A-3)$$

The applied loadings (in vacuum) may be obtained from Reference 8 as

$$\begin{aligned} p_x(x,t) &= -T' = m\Omega^2 x \\ p_y(x,t) &= -m\ddot{u} + m\ddot{\phi} \sin \theta + m\Omega^2 v \\ &\quad + m\Omega^2(\cos \theta - \phi \sin \theta) \\ p_z(x,t) &= -m\ddot{u} - m\ddot{\phi} \cos \theta \\ q_x(x,t) &= -m\Omega^2 e v \sin \theta + m(\ddot{v} \sin \theta - \ddot{u} \cos \theta) \\ &\quad - m\Omega^2(k_{m2}^2 - k_{m1}^2)(\sin \theta \cos \theta + \phi \cos 2\theta) \\ &\quad - m k_{m2}^2 \ddot{\phi} \\ q_y(x,t) &= m\Omega^2 e x(\sin \theta + \phi \cos \theta) \\ q_z(x,t) &= -m\Omega^2 e x(\cos \theta - \phi \sin \theta) \end{aligned} \quad (A-4)$$

Substituting the applied loading given by Equation (A-4) into Equations (A-1), (A-2), and (A-3) and deleting steady-state terms yields the free vibration equations. Application of the integrating matrix [L] yields the corresponding eigenvalue problem.

$$[G] \{\phi\} = \omega^2 [H] \{\phi\} \quad (A-5)$$

where

$$\{\phi\} = \begin{bmatrix} \frac{w''}{v''} \\ \phi' \end{bmatrix}$$

$$[G] = \begin{bmatrix} G_{1v} & G_{1\phi} & G_{1\psi} \\ G_{2v} & G_{2\phi} & G_{2\psi} \\ G_{3v} & G_{3\phi} & G_{3\psi} \end{bmatrix}, \quad [H] = \begin{bmatrix} H_{1v} & H_{1\phi} & H_{1\psi} \\ H_{2v} & H_{2\phi} & H_{2\psi} \\ H_{3v} & H_{3\phi} & H_{3\psi} \end{bmatrix}$$

The partitions of  $[G]$  and  $[H]$  are  $(n+1)$  matrices defined as follows:

$$[G_{1v}] = \{EI_1 \cos^2 \theta + EI_2 \sin^2 \theta\} + \Omega^2 [P_3(mx)] [F]^2$$

$$[G_{2v}] = \{(EI_2 - EI_1) \cos \theta \sin \theta\}$$

$$[G_{3v}] = -\Omega^2 [L] [e_a \cos \theta] [P_2(mx)] + \Omega^2 [L] [m \cos \theta] [F]$$

$$[G_{1\phi}] = \{(EI_2 - EI_1) \cos \theta\}$$

$$[G_{2\phi}] = \{EI_1 \sin^2 \theta + EI_2 \cos^2 \theta\} - \Omega^2 [P_1] [m] + \Omega^2 [P_3(mx)] [F]^2$$

$$[G_{3\phi}] = \Omega^2 [L] [e_a \sin \theta] [P_2(mx)] + \Omega^2 [L] [m \cos \theta] [F]^2$$

$$- \Omega^2 [L] [m \sin \theta] [F]$$

$$[G_{1\psi}] = -\Omega^2 [P_2(mx)] [e_a \cos \theta] [F] + \Omega^2 [L] [m \cos \theta] [F]$$

$$[G_{2\psi}] = \Omega^2 [P_2(mx)] [e_a \sin \theta] [F] - \Omega^2 [x] [L] [m \sin \theta] [F]$$

$$[G_{3\psi}] = [G_{\psi}] + \Omega^2 [k_a^2] [P_2(mx)] + \Omega^2 [L] [m(k_{m2}^2 - k_{m1}^2) \cos 2\theta] [F]$$

$$[H_{1v}] = [P_1] [m] [F]^2$$

$$[H_{2v}] = [0]$$

$$[H_{3v}] = [L] [m \cos \theta] [F]^2$$

$$[H_{1\phi}] = [0]$$

$$[H_{2\phi}] = [P_1] [m] [F]^2$$

$$[H_{3\phi}] = -[L] [m \sin \theta] [F]^2$$

$$[H_{1\psi}] = [P_1] [m \cos \theta] [F]$$

$$[H_{2\psi}] = -[P_1] [m \sin \theta] [F]$$

$$[H_{3\psi}] = [L] [mk_a^2] [F]$$

where

$$[P_1] = [L] [x] - [x] [L]$$

$$[P_2(f)] = \text{diag } [L] [f]$$

$$[P_3(f)] = [L] [f] - [P_2(f)]$$

$$[F] = ([B] - [I]) [L]$$

$$[B] = \begin{bmatrix} 0 & 0 & \dots & \dots & 0 & 1 \\ 0 & \dots & \dots & \dots & 0 & 1 \\ \vdots & & & & \vdots & \\ \vdots & & & & \vdots & \\ 0 & \dots & \dots & \dots & 0 & 1 \end{bmatrix}$$

Solutions of Equation (A-5) define the natural frequencies and associated modal functions. The first element in each of the above matrices corresponds to the tip value. The 1,  $n+1$ , and  $2n+1$  rows and columns of the dynamic matrix  $[G]^{-1}[H]$  are deleted prior to iteration. The modal deflections are determined from the eigenvectors of Equation (A-5) as

$$\begin{Bmatrix} w \\ v \\ \phi \end{Bmatrix} = \begin{bmatrix} [F]^2 & & \\ & [F]^2 & \\ & & [F] \end{bmatrix} \begin{Bmatrix} w'' \\ v'' \\ \phi' \end{Bmatrix} \quad (A-6)$$

The orthogonality relation for these modes may be derived from Equations (A-1), (A-2), and (A-3) by application of cantilever-free boundary conditions. The orthogonality relation is

$$\int_0^R [mw_1'v_1' + mv_1'v_1' + mk^2\phi_1\phi_1 + m\epsilon \cos\theta\phi_1w_1 - m\epsilon \sin\theta\phi_1v_1 - m\epsilon \sin\theta v_1\phi_1 + m\epsilon \cos\theta w_1\phi_1] dx = 0 \quad i \neq j \quad (A-7)$$

#### REFERENCES

1. Friedman, P., and Tong, P., "Dynamic Nonlinear Elastic Stability of Helicopter Rotor Blades in Hover and Forward Flight." NASA CR-114485, May 1972.
2. Hodges, D. H., "Nonlinear Bending and Torsion of Rotating Beams With Application to Linear Stability of Hingeless Helicopter Rotors." Ph. D. Thesis, Stanford University, December 1972.
3. Hodges, D. H., and Ormiston, "Nonlinear Equations for Bending of Rotating Beams With Application to Linear Flap-Lag Stability of Hingeless Rotors." NASA TM X-2770, 1973.
4. Loewy, R. G., "Review of Rotary-Wing V/STOL Dynamic and Aeroelastic Problems." Journal of the American Helicopter Society, Vol. 14, No. 3, July 1969, pp. 3-23.
5. Reichert, G., and Huber, H., "Influence of Elastic Coupling Effects on the Handling Qualities of a Hingeless Rotor Helicopter." 39th AGARD Flight Mechanics Panel Meeting, Hampton, Virginia, September 1971.
6. Huber, H. B., "Effect of Torsion-Flap-Lag Coupling on Hingeless Rotor Stability." Paper presented at the 29th Annual National Forum of the American Helicopter Society, May 1973.
7. Hansford, R. E., and Simons, I. A., "Torsion-Flap-Lag Coupling on Helicopter Rotor Blades." Journal of the American Helicopter Society, Vol. 18, No. 4, October 1973, pp. 2-12.
8. Houbolt, J. C., and Brooks, G. W., "Differential Equations of Motion for Combined Flapwise Bending, Chordwise Bending, and Torsion of Twisted, Nonuniform Rotor Blades." NACA Technical Report 1346, 1958.
9. Bisplinghoff, R. L., Ashley, H., and Holfman, R. L., "Aeroelasticity." Addison-Wesley, Reading, Massachusetts, 1955.
10. Peters, D. A., and Ormiston, R. A., "The Effects of Second Order Blade Bending on the Angle of Attack of Hingeless Rotor Blades." Journal of the American Helicopter Society, Vol. 18, No. 4, October 1973, pp. 45-48.
11. Gessow, A., and Meyers, G. C., "Aerodynamics of the Helicopter." Frederick Ungar Publishing Company, New York, 1967.
12. Ormiston, R. A., and Hodges, D. H., "Linear Flap-Lag Dynamics of Hingeless Helicopter Rotor Blades in Hover." Journal of the American Helicopter Society, Vol. 17, No. 2, April 1972, pp. 2-14.
13. Hunter, W. F., "Integrating Matrix Method for Determining the Natural Vibration Characteristics of Propeller Blades." NASA Technical Note D-6064, 1970.

TABLE 1. EFFECT OF THE NUMBER OF MODES ON FIRST FLAP AND LAG MODE  
DAMPING AT  $\theta = 0.3$ ,  $\bar{\omega}_{\zeta_0} = 0.664$ ,  $\bar{\omega}_{\beta_0} = 1.104$ ,  $n = 20$

M	Mode type	$\sigma_v/(\sigma_v)_{M=2}$	$\sigma_w/(\sigma_w)_{M=2}$
2	1st lag & 1st flap	1.000	1.000
3	2nd flap	1.0112	1.006
4	2nd lag	1.0128	1.005
5	3rd flap	1.0131	1.006

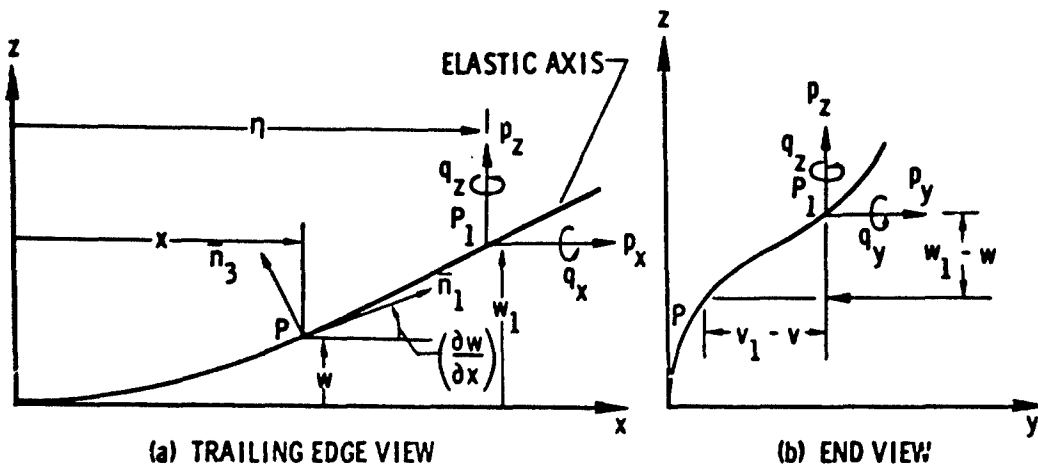


Figure 1. Equilibrium of forces and moments.

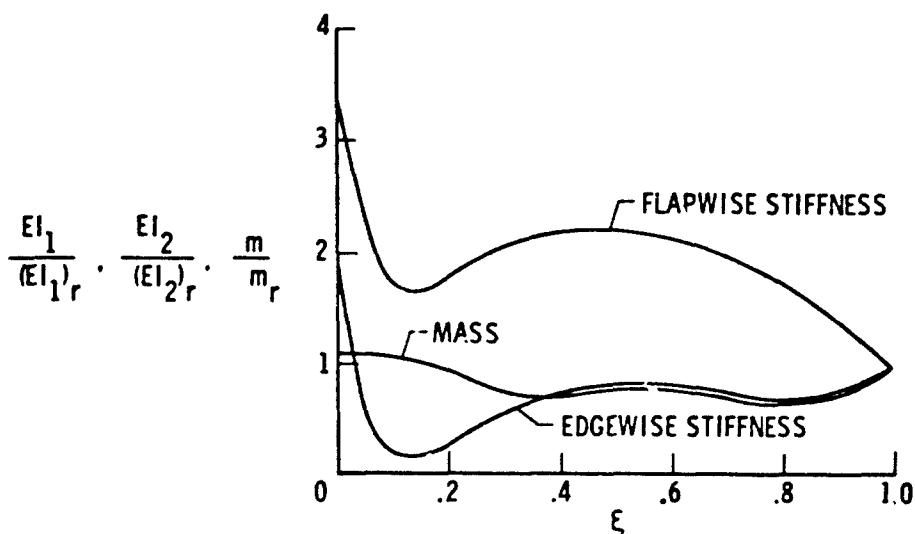


Figure 2. Spanwise variation of dimensionless blade mass and stiffness.

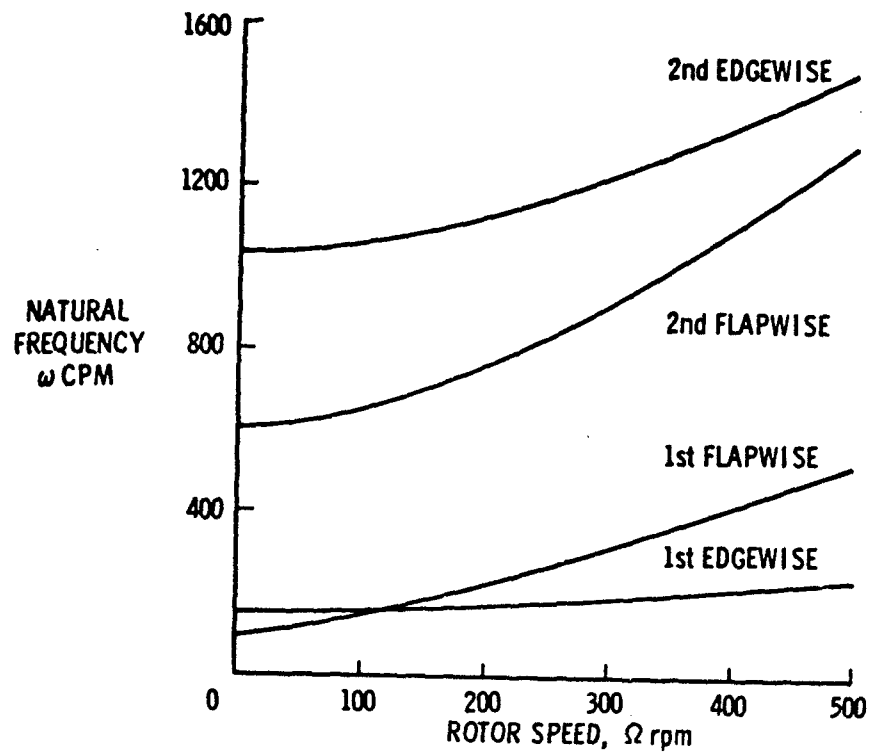


Figure 3. Variation of blade natural frequencies with rotor speed,  $R = 6.985$  meters,  $\delta = 0.0$  radian,  $n = 20$ .

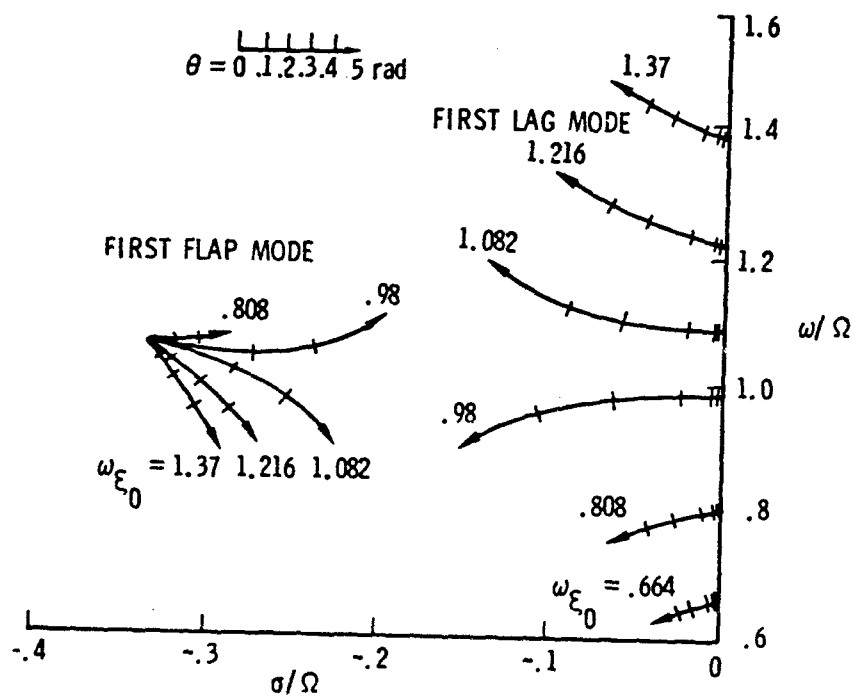


Figure 4. Locus of roots with increasing pitch angle for first flap and lag modes,  $\gamma_r = 5.0$ ,  $\sigma = 0.05$ ,  $C_{d_0} = 0.01$ ,  $\omega_{B_0} = 1.104$ ,  $M = 3$ .

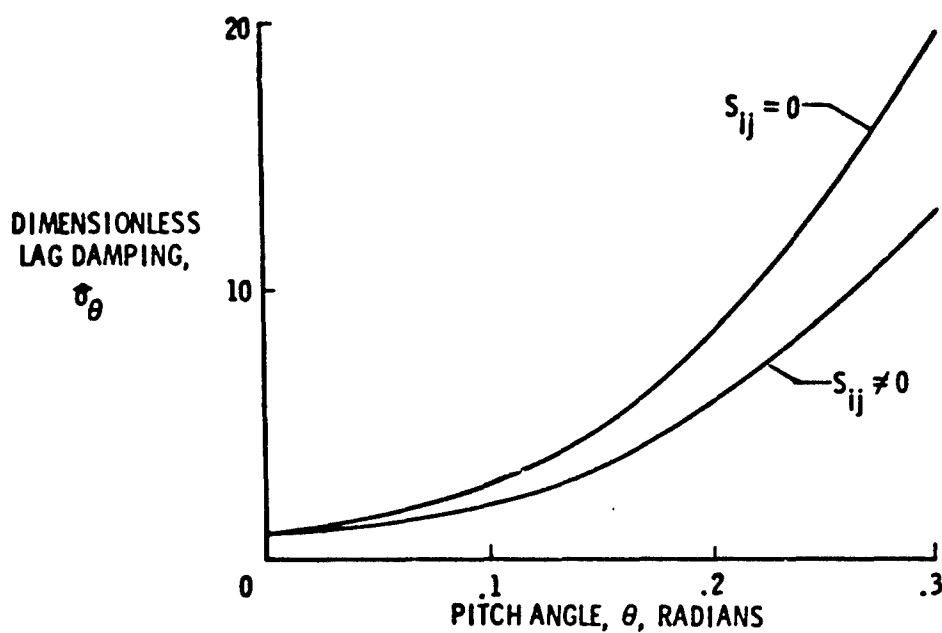


Figure 5. Effect of nonlinear terms on first lag mode damping,  $\gamma_r = 5.0$ ,  $\sigma = 0.05$ ,  $C_{d0} = 0.01$ ,  $\bar{\omega}_{\xi 0} = 0.664$ ,  $\bar{\omega}_{\beta 0} = 1.104$ ,  $M = 3$ .

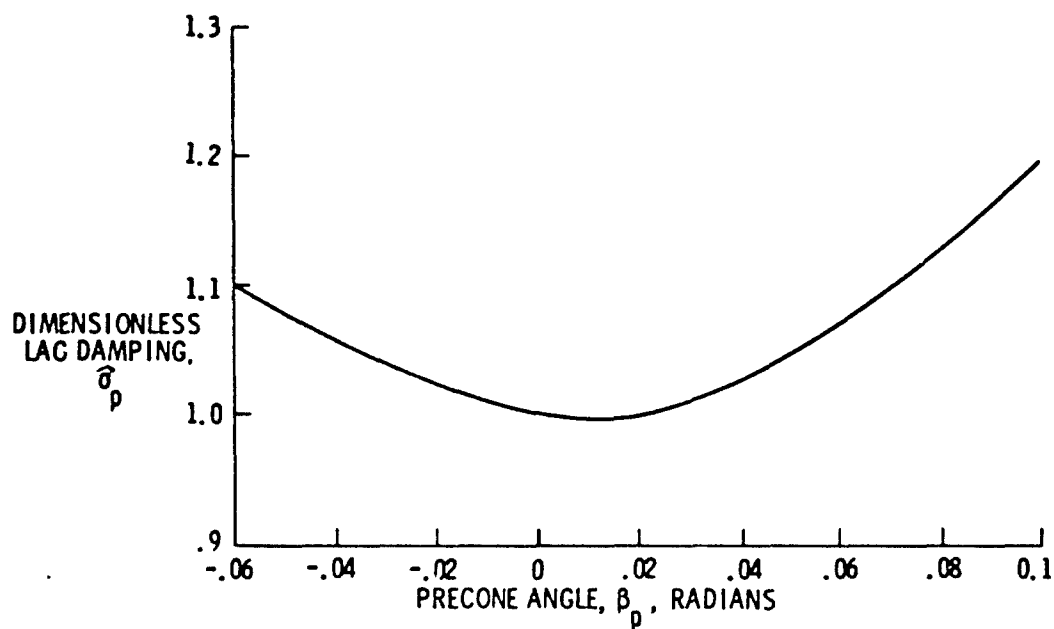


Figure 6. Effect of precone on first lag mode damping,  $\gamma_r = 5.0$ ,  $\sigma = 0.05$ ,  $C_{d0} = 0.01$ ,  $\bar{\omega}_{\xi 0} = 1.216$ ,  $\bar{\omega}_{\beta 0} = 1.104$ ,  $\theta = 0.1$ ,  $M = 3$ .

# ESTIMATES OF THE STABILITY DERIVATIVES OF A HELICOPTER AND A V/STOL AIRCRAFT FROM FLIGHT DATA

by

D.G. Gould and W.S. Hindson  
Flight Research Laboratory  
National Aeronautical Establishment  
National Research Council of Canada

## SUMMARY

Stability derivatives for the Bell 205 helicopter have been derived from flight data using a least squares quasilinearization technique. The aircraft model, which included a first order representation of rotor response characteristics was based on fundamental parameters descriptive of the particular design. A conglomerate analysis procedure which produced estimates based on data from several similar manoeuvres was used to increase the confidence in the results observed.

Data from the CL-84 V/STOL aircraft were also analyzed, indicating the validity of certain *a priori* longitudinal stability derivatives for the aircraft, and yielding estimates of others. The results indicate the need to use a more elaborate modelling technique, such as was used for the Bell 205, which takes into account the particular complexities of the aircraft.

## 1.0 INTRODUCTION

The real concern of the engineer in applying modern analytical techniques to system identification problems is not so much in the quantitative minimization of the fit error, but rather in obtaining reliable parameter estimates of general applicability. This calls for the use at every opportunity of good engineering judgment in the application of these techniques, particularly in cases where advance knowledge about the system is lacking. Tending to act in opposition to this requirement is the increasing necessity for specialist mathematical analysts to implement what may appear to the practical aeronautical engineer as formidably complex identification techniques. However, it is suggested that a reduced analytical sophistication may in some cases be an acceptable tradeoff for increased participation by the engineer in the identification process.

In this paper, some of the significant means of exercising this engineering judgment in lieu of mathematical complexity are discussed by way of examples of extracting model parameters descriptive of a helicopter and a V/STOL aircraft from flight measurements of responses. The choice of mathematical model, considerations in obtaining convergence, the use of parameter and state vector weighting, and a practical method to allow for process noise by expanding the data base, and thereby increasing the confidence in the reliability of the results are the subjects of this presentation.

In the case of the helicopter this work was undertaken to assist design of a high gain full authority multichannel autopilot for the aircraft, shown in Figure 1, which is under development as an airborne simulator (Ref. 1). The parameter extraction effort for the CL-84 V/STOL aircraft shown in Figure 2 was performed to assess the validity of certain significant *a priori* stability derivatives to model the small perturbation longitudinal handling characteristics of the aircraft in support of the Tripartite V/STOL Instrument Flight Test program reported in part in References 2 and 3.

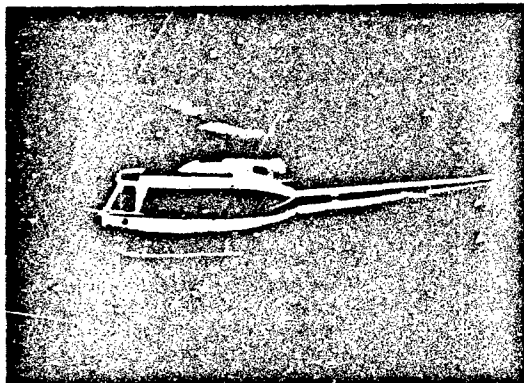


Fig. 1: Bell 205A1 Helicopter

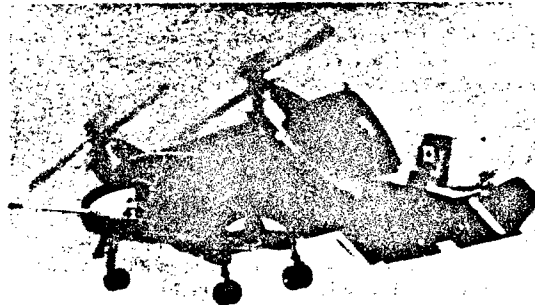


Fig. 2: CL-84 Tilt Wing V/STOL Aircraft



## 2.0 ANALYSIS METHOD

The classical method of least squares (Ref. 4) applied to the linear or non-linear parameter identification problem provides the basis for most of the parameter identification techniques in use today. In its simplest form, the method is generally termed quasi-linearization, but employing slightly different assumptions, it is also equivalent to the modified Newton-Raphson technique.

### 2.1 Least Squares Quasilinearization Technique

Consider the linear or non-linear system modelled by the equation set

$$F(X_i, U_j, \lambda_k) = 0 \quad 2.1.1$$

the solution of which is  $X_i(U_j, \lambda_k)$

where the only constraint imposed is that the column parameter vector  $\lambda_k$  be constant over the time period of interest. In this representation,  $U_j$  is a known system vector forcing function and  $X_i$  is the column state vector describing the response of the system.

To the first order, the change in system response,  $X_i$ , due to a small change in the parameter vector,  $\lambda_k$ , is

$$X_i(U_j, \lambda_k + \Delta \lambda_k) = X_i(U_j, \lambda_k) + \frac{\partial X_i(U_j, \lambda_k)}{\partial \lambda_k} \Delta \lambda_k \quad 2.1.2$$

The corresponding value of the cost function is

$$J = \int_0^t \left\{ [Y_i - X_i(U_j, \lambda_k) - \frac{\partial X_i(U_j, \lambda_k)}{\partial \lambda_k} \Delta \lambda_k]^T \right. \\ \left. W_{ii} [Y_i - X_i(U_j, \lambda_k) - \frac{\partial X_i(U_j, \lambda_k)}{\partial \lambda_k} \Delta \lambda_k] \right\} dt \quad 2.1.3$$

where  $Y_i$  is the column vector of observed states and  $W_{ii}$  is a weighting matrix reflecting the relative accuracy in measurement of the state variables. It may also reflect the relative importance assigned to the observed state variables if, for example, it is desired to arrive at final estimates with emphasis on the response of only one or two of the state variables. With the assumption that an extremum in  $J$  has been reached, then  $\frac{\partial J}{\partial \Delta \lambda_k} = 0$  yields a recursive relationship for successive changes in the parameter vector in order to minimize the cost function:

$$\Delta \lambda_k = \left[ \int_0^t \left\{ \left[ \frac{\partial X_i(U_j, \lambda_k)}{\partial \lambda_k} \right]^T W_{ii} \left[ \frac{\partial X_i(U_j, \lambda_k)}{\partial \lambda_k} \right] \right\} dt \right]^{-1} \cdot \\ \left[ \int_0^t \left\{ \left[ \frac{\partial X_i(U_j, \lambda_k)}{\partial \lambda_k} \right]^T W_{ii} [Y_i - X_i(U_j, \lambda_k)] \right\} dt \right] \quad 2.1.4$$

It should be noted, although it is not the case of present interest, that if the parameter sensitivity functions,  $\frac{\partial X_i}{\partial \lambda_k}$ , are independent of  $\lambda_k$  Equation 2.1.2 is exact, Equation 2.1.4 is an explicit expression, and iterative solutions are not required. In the present analysis, since 2.1.1 is a set of first order differential equations (linear or non-linear) the sensitivity functions are dependent on  $\lambda_k$  and iterative solutions are necessary.

Although the formulation is classical, the recent success of this method is a result of modern computing capabilities which now permit calculation of the parameter sensitivity directly from the modelling Equation 2.1.1.

### 2.2 The Problem of Obtaining Convergence

It is usually the case, when dealing with aircraft response measurements, that the recursion relationship as given by Equation 2.1.4 does not result in successive parameter changes that converge. There are a number of reasons for this behaviour, the most common one being that the equations of 2.1.4 are poorly conditioned usually because of an approximate linear relationship (in the time histories) among the state variables and/or among the parameter sensitivity functions. This problem can be alleviated but often not eliminated by a careful choice of control inputs (the system vector forcing functions). This difficulty has been allowed for in these tests through the use of simultaneous unco-ordinated (i.e. dissimilar) inputs from the two governing cockpit controls, each containing as broad a range of exciting frequencies as possible.

It is also true that the ability to obtain convergence may be highly dependent on the accuracy of the initial estimates with which the iteration is begun. For conventional aircraft, good estimates of the aerodynamic parameters are usually available from wind tunnel tests or theoretical prediction. If the aircraft is a helicopter or other V/STOL vehicle, this favourable situation is usually lacking for various reasons associated with the complexity of interfering aircraft components, and the difficulty of performing good wind tunnel tests.

An equation error starting technique proposed by Denery in Reference 5 can assist in obtaining convergence by reducing the sensitivity of the analysis to initial parameter estimates. By using first the observed values of the state variables in the calculation of the sensitivity functions, the analysis is controlled until the response of the iterating model improves, conceptually to a point from which monotonic convergence to the absolute minimal cost function can be initiated. Although this will result in biased estimates of the parameters if continued, if the calculated model response is then used as is correctly required in Equations 2.1.4, the bias due to this procedure is removed and proper results are obtained. This technique was used with some success in the work reported here, but it has been found that the choice of initial parameters estimates still remains very critical.

It has been our experience, that the procedure which most consistently gives convergent behaviour is one where significant weight is given to the original estimates of some of the parameters.

It has also been found that inclusion of any independent constraints among the parameters which can be formulated can contribute significantly to convergence. This will be discussed further in a later section.

### 2.3 Inclusion of *A Priori* Estimates

In the event that fairly reliable estimates of some parameters are known, it is possible to control the amount of departure from these first estimates during the course of the iterations through an additional term in the cost function of the form (Ref. 6)

$$(\lambda_k - \lambda_{k_0})^T D_{kk} (\lambda_k - \lambda_{k_0}) \quad 2.3.1$$

With this additional term the Expression 2.1.4 for  $\Delta\lambda_k$  becomes

$$\Delta\lambda_k = \left[ \int_0^t \left\{ \left[ \frac{\partial X_i}{\partial \lambda_k} \right]^T W_{ii} \left[ \frac{\partial X_i}{\partial \lambda_k} \right] dt + D_{kk} \right\}^{-1} \right. \\ \left. \left[ \int_0^t \left\{ \left[ \frac{\partial X_i}{\partial \lambda_k} \right]^T W_{ii} [Y_i - X_i] dt - D_{kk} (\lambda_k - \lambda_{k_0}) \right\} \right] \right] \quad 2.3.2$$

This expression allows for the calculation of successive changes in the parameter vector from the initial estimates in order to minimize the cost function which now includes Expression 2.3.1.

The practical effect of the *a priori* weight matrix  $D_{kk}$  is twofold. It ensures that certain parameters emerging from the iteration will retain realistic values based on previously known independent information or other justification. Secondly, it improves conditioning of the sensitivity function product matrix requiring inversion in the recursion equation by contributing a controllable amount to the diagonal elements.

As discussed in Reference 7, a statistical interpretation can be made of the weighting matrices  $W_{ii}$  and  $D_{kk}$ , relating them to the measurement noise characteristics of the state vector elements, and the statistical properties of the initial estimates. While there is justification of this approach provided that the statistical assumptions can be validated, this is often not the case, particularly if one attempts to account for the effect of unknown random atmospheric disturbances by this means. The procedure adopted here sets the weighting matrices according to engineering judgment based on the conditions of the test and the quality of *a priori* information available. A method to allow for the process noise due to unknown atmospheric inputs, and to some extent modelling deficiencies, is discussed in a later section.

## 3.0 DEVELOPMENT OF THE SYSTEM MODEL

### 3.1 In Terms of Stability Derivatives

In the field of flight dynamics, the classical means whereby the aircraft equations of motion have been made tractable has been through linearization and small perturbation simplifications. This resulted in the classical aerodynamic stability derivatives contained in two three-degree-of-freedom sets of decoupled equations. Although not nowadays necessary, this approach is still valid, and for many reasons it is useful to consider for V/STOL aircraft and helicopters. However, the fundamental meaning and relative importance of the stability derivatives may require special interpretation.

Following this convention, the lateral directional response of the single rotor Bell 205A helicopter was first modelled as follows:

$$\begin{aligned}
 \dot{P} &= L_P \dot{P} + L_P P + L_R R + L_V V & + L_{\delta a} \delta \dot{a} + L_{\delta a} \delta a + L_{\delta r} \delta r \\
 \dot{R} &= N_P \dot{P} + N_P P + N_R R + N_V V & + N_{\delta a} \delta \dot{a} + N_{\delta a} \delta a + N_{\delta r} \delta r \\
 \dot{V} &= Y_P \dot{P} + (Y_P + Y_P) P + (Y_R - u_0) R + Y_V V + g\theta & + Y_{\delta a} \delta \dot{a} + Y_{\delta a} \delta a + Y_{\delta r} \delta r \\
 \dot{\phi} &= P
 \end{aligned}
 \tag{3.1.1}$$

The quantities  $P$ ,  $R$ ,  $V$ , and  $\phi$ , namely the roll rate, yaw rate, lateral velocity and bank angle represent the state vector  $X_1$ ;  $\delta \dot{a}$ ,  $\delta a$  and  $\delta r$  represent the known system vector forcing function  $U_1$ ; while the parameter vector consists of the twenty one aerodynamic stability derivatives  $L_P$ ,  $L_P$ ,  $L_R$ ,  $\dots$ ,  $Y_{\delta a}$ ,  $Y_{\delta r}$ .

The  $\delta \dot{a}$  and  $\dot{P}$  time derivatives are retained as first order approximations to the lag in main rotor response and the lag in side-wash at the tail rotor resulting from the changing lateral force of the main rotor. This constitutes what is considered to be valid modelling for the simple seesaw type of rotor system which was involved, at least for the range of frequencies of interest in this investigation. The identification of the rotor response time constant, which as a first estimate is simply one quarter of the rotor fundamental period, is equivalent to incorporation of a single rotor degree of freedom contributing to the three-degree-of-freedom lateral-directional response.

The parameter vector can be reduced to eighteen modified stability derivatives which contain the  $\dot{P}$  derivatives in order to present the problem in the more recognized linear form

$$[\dot{X}] = [F][X] + [B][U]$$

where  $[F]$  is the matrix containing the response or state vector derivatives and  $[B]$  contains the control derivatives.

Using intuitive initial estimates of the stability derivatives where it was not possible to obtain preliminary estimates from a cursory examination of the flight data, a solution was attempted which also incorporated the equation error starting technique of Denery. It was found that the solutions often did not converge, and so it was concluded that the freedom of some of the parameters would have to be restrained by using the *a priori* weight technique. With sufficient *a priori* weight on some of the more significant derivatives such as the damping derivatives, convergent solutions were obtained but some of the derivative estimates resulting were physically unrealistic. And quite different estimates resulted from small changes in the first estimates of those parameters which had high *a priori* weights. Since the *a priori* information available was not such that much confidence could be placed on the accuracy of any of the first estimates of the derivatives, this brute force stability derivative approach was rejected, and a formulation in terms of more fundamental parameters was sought, but still retaining algebraic relation to the basic linearized stability derivative form.

Proceeding in the same fashion for the response of the helicopter in the longitudinal plane

$$\begin{aligned}
 \dot{U} &= X_U \dot{U} + X_U U + X_W \dot{W} + X_W W + X_Q \dot{Q} + (X_Q - W_0) Q - g\theta \\
 &+ X_{\delta c} \delta \dot{c} + X_{\delta c} \delta c + X_{\delta s} \delta \dot{s} + X_{\delta s} \delta s \\
 \dot{W} &= Z_U \dot{U} + Z_U U + Z_W \dot{W} + Z_W W + Z_Q \dot{Q} + (Z_Q + U_0) Q \\
 &+ Z_{\delta c} \delta \dot{c} + Z_{\delta c} \delta c + Z_{\delta s} \delta \dot{s} + Z_{\delta s} \delta s \\
 \dot{Q} &= M_U \dot{U} + M_U U + M_W \dot{W} + M_W W + M_Q \dot{Q} + M_Q Q \\
 &+ M_{\delta c} \delta \dot{c} + M_{\delta c} \delta c + M_{\delta s} \delta \dot{s} + M_{\delta s} \delta s \\
 \dot{\theta} &= Q
 \end{aligned}
 \tag{3.1.2}$$

In a fashion similar to that employed for the lateral-directional modelling, the  $\delta \dot{s}$  and the state vector time rate of change derivatives are used as first order approximations to the lag in main rotor response, and the  $U$  in downwash at the horizontal tail resulting from the changing normal force of the main rotor.

Without very reliable initial estimates for at least some of the thirty stability derivatives contained in the parameter vector, it would be very unlikely that convergent solutions could be obtained because of poor conditioning in the sensitivity function matrix, and even in the event solutions were obtained, many of the stability derivative estimates would be physically unrealistic and of little value to the engineer.

### 3.2 In Terms of More Fundamental Parameters

The procedure adopted for the results given in this paper, and in considerably more detail in References 8 and 9 expresses the stability derivatives in terms of the aerodynamic forces and moments acting on the major components of the aircraft, moment arms and inertial parameters. For example, the total derivatives  $X_W$  and  $Z_W$  are broken into elements associated with the major helicopter components as follows:

$$X_W = X_{WMR} + X_{WTR} + X_{WFT} + X_{WFUS} \quad 3.2.1$$

$$Z_W = (1 - e_{TR} - e_{FT}) Z_{WMR} + Z_{WTR} + Z_{WFT} + Z_{WFUS}$$

where the subscripts MR, TR, FT and FUS refer to the main rotor, tail rotor, fixed tail and fuselage respectively. The terms  $e_{TR}$  and  $e_{FT}$  represent down-wash factors at the tail rotor and fixed tail resulting when the  $Z$  force on the main rotor is changed. The corresponding pitching moment derivative,  $M_W$  is

$$M_W = \frac{m}{I_{yy}} \left[ -h_{MR} X_{WMR} + (e_{TR} l_{TR} + e_{FT} l_{FT}) Z_{WMR} - l_{TR} Z_{WTR} - l_{FT} Z_{WFT} + l_{FUS} Z_{WFUS} \right] \quad 3.2.2$$

where  $m$  is the helicopter mass,  $I_{yy}$  is the pitching moment of inertia, and  $h_{MR}$ ,  $l_{TR}$ ,  $l_{FT}$ ,  $l_{FUS}$  represent the moment arms from the reference axes to the effective aerodynamic centres of the main rotor, tail rotor, fixed tail and fuselage, respectively.

Similar expressions were developed for each of the stability derivatives of the Equation 3.1.2 in terms of new parameters such as those in the above expressions. Thirty-three new parameters, designated  $P_i$ , were used in the expressions for the thirty stability derivatives, designated  $R_m$ . The algebraic constraints provided by these expressions make it such that a change in one parameter  $P_i$ , say  $X_{WMR}$ , not only changes  $X_W$  but also changes  $M_W$ . Furthermore, most of these new parameters ( $h_{MR}$ ,  $l_{TR}$ ,  $l_{FT}$  - etc.) could be estimated *a priori* and the confidence in the estimates established for use in setting the elements of an *a priori* weight vector.

The sensitivity functions with respect to the original stability derivatives,

$$\frac{\partial X_i}{\partial R_m}$$

were calculated from the sets of sensitivity equations obtained by taking derivatives of the Equation Set 3.1.2 with respect to the parameters  $R_m$  appearing in these equations. The partial derivatives

$$\frac{\partial R_m}{\partial P_i}$$

expressing the sensitivity of each of the stability derivatives to the parameters  $P_i$ , were obtained from the expressions such as 3.2.1 and 3.2.2 and the sensitivity functions with respect to the new set of parameters  $P_i$  calculated from

$$\frac{\partial X_i}{\partial P_i} = \sum_{m=1}^{30} \frac{\partial R_m}{\partial P_i} \cdot \frac{\partial X_i}{\partial R_m} \quad 3.2.3$$

The method is similar for the lateral-directional response. The 21 stability derivatives ( $L_p$ ,  $L_r$ , ...,  $Y_{\dot{\delta}}$ ) can be written in terms of 19 fundamental parameters descriptive of the characteristics of the components assumed to be contributing to the aerodynamic forces and moments. This procedure is equivalent to the classical method of estimating stability derivatives from basic aerodynamic and design data. The reader is directed to References 8 and 9 for a detailed description of the modelling assumptions employed for the 205 helicopter.

Algebraic complexity is introduced using this procedure, but it has the very significant advantage of providing constraints on the variations among the different parameters. Moreover, the fundamental parameters themselves are in several cases moment arms to aerodynamic centres, aircraft mass and moment of inertia parameters, rotor response time lag, etc, which although not known precisely, allow reliable initial estimates to be made and permit *a priori* weighting to restrict changes in these parameters within physically realistic limits.

### 3.3 CL-84 Modelling

The argument for using the fundamental parameter modelling technique, found to be necessary for the helicopter, can be made even more strongly for this aircraft. Particularly in the powered lift flight regime, this aircraft is dominated by an unusual complexity of aerodynamics and flight control mixing. It is very likely that reliable information of a design nature could only be extracted after applying significant aerodynamic and engineering experience relating to this particular aircraft in order to form a satisfactory model. Even at that point, unusual engineering related difficulties are likely to occur in applying the identification procedures which

result from the high vibration environment and the complex aerodynamic flow field to which even the boom mounted sensors are subjected. In addition, the effects of atmospheric disturbances become of longer and more significant duration in the flight record at the low airspeeds involved.

Nevertheless, unlike the case of the helicopter, there did exist from wind tunnel tests and other independent flight information prior estimates of some of the conventional stability derivatives. Since information of a handling qualities nature was sought in relation to a precise small perturbation instrument flying task, it was of interest to apply the basic longitudinal stability derivative representation given by Equations 3.1.2, except that for the results reported here the derivatives with respect to the time rate of change of the state observation vector were not used. In the most fundamental sense, it would be thought that a simplified modelling and identification procedure would have some validity if it could satisfactorily reproduce the flight response using close to these *a priori* values, and at the same time yield physically realistic values of the other derivatives.

In order to assist the identification procedure by constraining the variations in some of the derivatives in a manner similar to the fundamental parameter formulation in the previous section, the normal and longitudinal accelerations were added to the state vector. The model described in Equations 3.1.2 is now extended to include

$$A_X = X_U U + X_W W + X_Q Q + X_\theta \theta + X_{\dot{\theta}} \dot{\theta} + X_{\dot{\theta}_c} \dot{\theta}_c + X_{\dot{\theta}_s} \dot{\theta}_s + X_{\dot{\theta}_e} \dot{\theta}_e$$

$$A_Z = Z_U U + Z_W W + Z_Q Q + Z_\theta \theta + Z_{\dot{\theta}} \dot{\theta} + Z_{\dot{\theta}_c} \dot{\theta}_c + Z_{\dot{\theta}_s} \dot{\theta}_s + Z_{\dot{\theta}_e} \dot{\theta}_e$$

where the  $\dot{\theta}$  derivatives are a result of the stability augmentation system.

These expressions contribute to the elements of the sensitivity function product matrix

$$\left[ \frac{\partial X_i(U, \lambda_k)}{\partial \lambda_k} \right]^T [W_{ii}] \left[ \frac{\partial X_i(U, \lambda_k)}{\partial \lambda_k} \right]$$

to an extent allowed by their respective components in the state vector weighting matrix  $[W_{ii}]$ .

The advantage of introducing these constraints is apparent in the identities

$$\dot{U} = A_U - W_U Q$$

$$\dot{W} = A_W + U_W Q$$

### 3.4 Method Used to Reduce the Influence of Process Noise

Process noise commonly is said to be the result of unknown random inputs to the system, and also the effect of errors in the mathematical model chosen to describe the system. The former will generally consist of unknown small atmospheric disturbances occurring during the test, and which may be of nearly the same period as the duration of the test. Consequently, as implied in Section 2.3, it is often not meaningful to think of these disturbances in a statistical sense. Moreover, even if the best possible model is chosen for the system, bias will exist in the iterated parameters as the algorithm seeks to improve a particular fit. This can itself be considered a form of modelling error. While more advanced techniques do exist (Ref. 10) which can account more analytically for process noise, the procedure adopted here is thought to adequately allow for these effects from a practical point of view for most situations.

The procedure simply involves extending the data base from which the parameters are calculated by including a number of similar but independent runs for which the same model parameters are expected. These additional data appear as an additional dimension in the state and control input vectors in the computation, contributing in an additive manner to the cost function and sensitivity function matrix. The result is a single set of model parameters best fitting several runs which may differ to an unknown extent in terms of atmospheric turbulence, and the peculiarities of the exciting control inputs.

## 4.0 RESULTS

### 4.1 Bell 205 (UH1H) Helicopter

The procedures just outlined have been used to obtain 21 lateral-directional and 30 longitudinal stability derivatives of the Bell 205 helicopter from the identification of 19 and 33 more fundamental parameters respectively.

The observed responses used in the cost functions were roll rate, yaw rate and lateral velocity for the lateral-directional tests, and longitudinal velocity, normal velocity, pitch rate and normal acceleration for the longitudinal tests. In both cases, a quasilinearization procedure similar to that described in Section 2 was used to first remove the unknown biases from the measurements of the Euler angles and their rates prior to formation of the observed state response vector. This procedure is described in Reference 8. The observations of linear velocity were obtained from an on-board real time calculation of wideband inertial body axis velocities, the reliability of which had been independently verified.

The two sets of control inputs, lateral cyclic and tail rotor collective, and longitudinal cyclic and main rotor collective were measured at the pilot's control, and their unfiltered time rates of change calculated directly for inclusion in the vector forcing functions.

Several tests each with about ten to fifteen seconds of random excitation were performed in ostensibly smooth atmospheric conditions for each of three different speeds, 40, 70 and 100 knots. The 70 knot results are presented here.

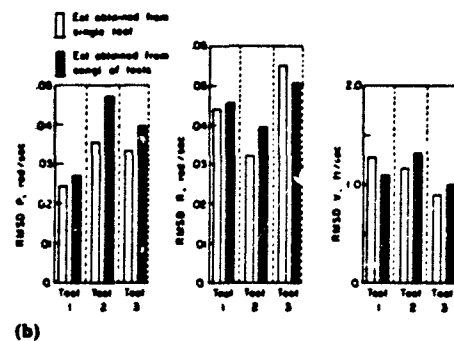
#### 4.1.1 Lateral-Directional Estimates

The estimates obtained for 10 dominant lateral-directional stability derivatives are given in Figure 3 for three tests all performed from the same reference flight condition. The results are all physically realistic indicating the success of the fundamental parameter formulation which allowed use of the *a priori* weight technique with confidence. Although one would expect closely similar results from each of the runs, there are some significant variations among some of the estimates, for example the roll damping derivative,  $L_p$ . The most likely causes of these differences are thought to be the existence of small unknown atmospheric disturbances and peculiarities in the response resulting from the particular characteristics of the control inputs which were of course different from run to run.

	Values obtained from analysis of Separate Tests			Values Obtained from anal. of Tests
	1	2	3	
$L_p$	-0.820	-0.823	-0.822	-0.806
$M_p$	-0.048	-0.022	-0.009	-0.037
$L_r$	0.122	0.106	0.200	0.174
$M_r$	-1.363	-1.029	-1.264	-1.303
$L_v$	-0.0964	-0.0137	-0.0147	-0.0147
$M_v$	0.0100	0.0162	0.0146	0.0177
$L_{\dot{\phi}}$	0.183	0.178	0.101	0.164
$M_{\dot{\phi}}$	0.024	0.024	0.020	0.025
$L_{\dot{\psi}}$	-0.234	-0.218	-0.269	-0.280
$M_{\dot{\psi}}$	0.661	0.467	0.431	0.463

ESTIMATED VALUES OF LATERAL-DIRECTIONAL  
ROTARY DERIVATIVES, 70 KNOTS

(a)



(b)

Fig. 3: Bell 205 Helicopter

When the data base was expanded to simultaneously include all these runs in a conglomerate analysis, the results shown in the last column of Table 1 were obtained. As shown in Figure 4 for a typical run, these estimates produced a quality of fit nearly as well as when the run was treated separately. Figure 3 indicates how the root mean square errors for the fitted parameters varied for the three runs separately, and as part of the conglomerate. While the penalty for demanding that a common set of derivatives be found which fits all runs is an increase in the cost function, the increase is small and it is argued that the confidence in using the results for more general applicability is considerably enhanced.

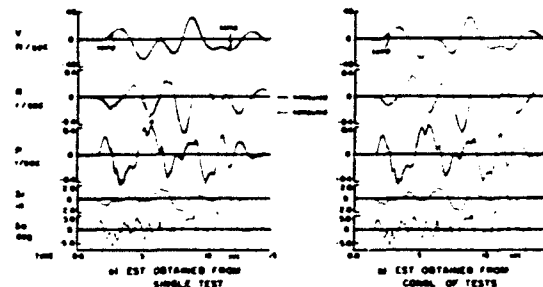


Fig. 4: Quality of Fit Achieved with Bell 205  
Lateral-Directional Results

#### 4.1.2 Longitudinal Estimates

Some of the results of the longitudinal analysis for the helicopter are presented in Figure 5 for the reference flight condition occurring at 70 knots. Again there is physical realism in the results, bearing in mind that the flight vehicle is a helicopter (for example,  $X_0$  is unusually high because of the flapping rotor), but there remains a variability among estimates obtained from separate runs.

To better illustrate the effects of the conglomerate analysis, the total weighted root mean square error for all fitted parameters is plotted in the same figure for the runs treated separately and together at successive iteration steps. All runs were started at step zero with the same set of initial estimates. The dashed line represents the global weighted root mean square error across all four runs, and it is seen to have converged quickly to nearly its final value by iteration Step 2. At the same time, the dispersion in fit error among the runs treated separately and together of course decreases, and carries on for the separate runs to their own minima by Step 5. It could be said that the separate minima achieved, and the variability in the final estimates together reflect the peculiarities of these runs. However, while the total global fit error remains nearly constant for the conglomerate case after Step 2, it is seen that the conglomerate dispersion is decreased and the error distributed to a closely equivalent level across all four runs. It is this effect which supports the proposition made earlier that possible errors due to process noise have been reduced. While this process noise is not

	SEPARATE RUNS				CONGRUATE
	1	2	3	4	
$X_0$	0.0080	0.0022	0.0008	0.0000	0.0017
$X_1$	0.0004	0.0008	0.0010	0.0010	0.0009
$X_2$	2.65	3.56	2.25	2.30	2.46
$X_3$	0.3048	0.0008	0.0008	0.0008	0.0077
$X_4$	1.680	1.537	1.750	1.666	1.536
$X_5$	0.49	0.506	0.728	0.775	0.66
$X_6$	0.66	0.94	0.721	0.646	0.66
$Z_0$	0.30	0.06	0.023	0.234	0.009
$Z_1$	0.942	0.925	0.893	0.721	0.876
$Z_2$	0.30	1.0	2.3	0.20	1.40
$Z_3$	0.087	0.04	0.020	0.0099	0.076
$Z_4$	0.75	0.75	0.441	0.650	0.650
$Z_5$	0.050	0.027	0.037	0.007	0.008
$Z_6$	35.7	36.7	36.4	32.6	36.4
$W_0$	0.0040	0.0030	0.0037	0.0026	0.0060
$W_1$	0.0048	0.0039	0.0036	0.0030	0.0049
$W_2$	0.402	0.067	0.020	0.450	0.046
$W_3$	0.0009	0.0008	0.0008	0.0013	0.0022
$W_4$	0.0142	0.000	0.006	0.0119	0.0067
$W_5$	0.061	0.25	0.086	0.077	0.061
$W_6$	0.16	0.38	0.059	0.068	0.160

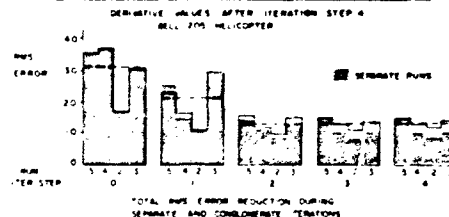


Fig. 5: Effects of Conglomerate Analysis

identified, and it is inevitably true that deficiencies remain in the mathematical model, the confidence with which the engineer can apply these results in a more general sense is considerably increased.

Figure 6 shows the quality of fit which is achieved for a typical run treated separately and in a conglomerate fashion. Again the differences are not great, and are plausibly attributable to control input peculiarities and/or unknown atmospheric disturbances.

#### 4.2 CL-84 V/STOL Aircraft

A brute force stability derivative technique employing the representation given in Equations 3.1.2 was used with flight data from the aircraft in its wing angle 40 degrees (relative to horizontal datum) configuration shown approximately in Figure 2. The test procedure was identical to that described earlier for the helicopter, except that the reference flight condition was at a nominal steady descent angle of nine degrees referred to still air. The corresponding airspeed in this configuration is approximately forty knots.

The results of two different analyses of the single test available with the aircraft in this configuration (with stability augmentation) are shown in Figure 7.

The ability of the *a priori* values to model the response when only the longitudinal, normal and angular pitch velocities were used in the state observation vector is indicated in Column 2. With the exception of  $X_{\dot{u}}$  to be discussed later, the response damping derivatives and where applicable, the control input derivatives have remained close to their *a priori* values. Five iterations were performed with high relative weights on all the *a priori* values. The other derivatives, notably the control derivatives for which there were no *a priori* initial estimates readily available, have all attained reasonable values. Shown in the same figure are the root mean square errors in the observed parameters using these results. The longitudinal and normal accelerations calculated using these derivatives do not fit well, however.

When the longitudinal and normal accelerations are included in the state response vector, and the high weights on the *a priori* values retained, the results are as shown in Column 3. Although more of the derivatives have departed from their *a priori* values, there is still reasonable correspondence. It may be significant that the *a priori* values available did not relate precisely to the reference condition used in the flight tests.

The quality of fit achieved with the results not incorporating  $A_{\dot{u}}$  and  $A_{\dot{w}}$  are shown in Figure 8. The poor resolution of the data and lack of response in longitudinal velocity assuredly contribute to the discrepancies in these derivatives seen in the Table. With  $A_{\dot{u}}$  and  $A_{\dot{w}}$  included, the results in Figure 9 are obtained. While it is tempting to release some of the weighted parameters in order to further reduce the fit errors which are particularly visible in the accelerations, there would be no basis for confidence of the new values obtained without other corroborating flight data. This was done, and although good fits were obtained, physically unrealistic values resulted. For example, in attempting to fit  $A_{\dot{u}}$ , the algorithm tends to identify an unjustifiably large value of  $X_{\dot{u}}$ , while the more correct derivative which likely should be identified is  $X_{\dot{q}}$ . This difficulty is probably a result of the high value of pitch damping due mainly to the stability augmentation system, and could perhaps be alleviated by extending the analysis used here to also identify an appropriate  $W_0$  as appearing in Equations 3.1.2, thereby separating  $X_{\dot{q}}$ .

While the extent of the stability derivative model assumed is obviously limited, all of the fitting discrepancies are not necessarily a result of this modelling simplification. The extended influence of atmospheric turbulence at the low flight speed of the test (40 kts), and the distinct likelihood of both static and dynamic position errors for the pitot-static system and the boom mounted and angle of attack vane from

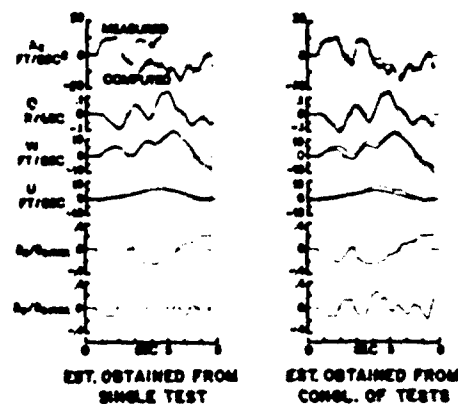


Fig. 6: Quality of Fit Achieved with Bell 206 Longitudinal Results

	1	2 (1306)	3 (2256)
	LEVEL FLIGHT A PRIORI VALUE	$A_{\dot{u}}$ $A_{\dot{w}}$ NOT INCLUDED	$A_{\dot{u}}$ $A_{\dot{w}}$ INCLUDED
$X_u$	-0.342	-0.368	-0.331
$X_w$	-0.395	0.02	-0.02
$X_{\dot{u}}$		0.622	0.660
$X_{\dot{w}}$		0.089	0.307
$Z_u$	-0.313	-0.377	-0.642
$Z_w$	-0.130	-0.130	-0.146
$Z_q$	-3.63	-3.62	-3.59
$Z_{\dot{u}}$		-1.19	-1.08
$Z_{\dot{w}}$	0.67	-0.642	0.90
$M_u$	-0.0096	-0.064	-0.078
$M_w$	-0.01	-0.009	-0.009
$M_q$	-4.68	-4.68	-4.00
$M_{\dot{u}}$	-1.80	-1.79	-1.24
$M_{\dot{w}}$		0.054	0.050
$M_{\dot{q}}$	0.375	0.319	0.340

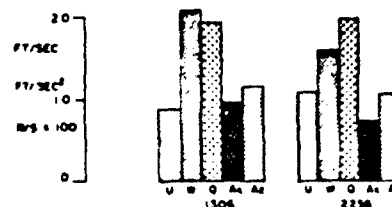


Fig. 7: CL-84 Stability Derivative Estimates with Stability Augmentation-Wing 40

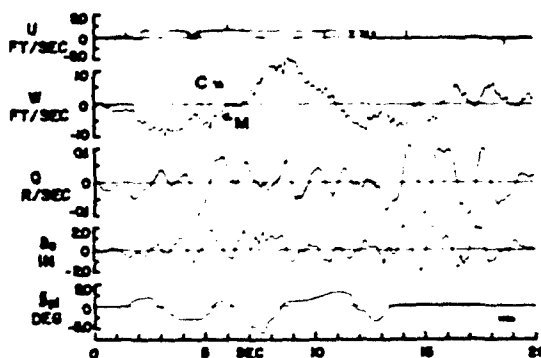


Fig. 8: CL-84 Results Without Accelerations Included in State Observation Vector

which linear velocities were derived present unusual uncertainties in comparison with tests with conventional aircraft.

However, as a result of this analysis, the *a priori* values available for the stability derivatives have been verified approximately, and additional derivatives deduced, notably  $X_{\dot{\delta}_R}$ ,  $Z_{\dot{\delta}_R}$ , and  $M_{\dot{\delta}_R}$ . Of equal use is the information made available to the engineer during the course of the analysis relating to deficiencies in the model assumed and the identification of particular improvements needed to be incorporated.

### 5.0 CONCLUSION

Stability derivatives for the Bell 205 helicopter have been derived for both lateral-directional and longitudinal degrees of freedom. The success of the analysis depended on formulation of the stability derivatives in terms of more fundamental parameters peculiar to the specifics of the aircraft. The confidence in the more general applicability of the results was obtained by determining a single set of derivatives best fitting the information contained in several separate runs from the same reference flight condition. In this way, the effects of unknown atmospheric turbulence, and of peculiarities in the control inputs were reduced.

Data from the CL-84 aircraft have been analysed to assess the validity of existing conventional stability derivatives for the aircraft. While there is general correspondence with the previously available data and additional derivatives have been obtained, it is apparent that this simplified stability derivative modelling technique is deficient in being able to more accurately describe the response. Formulation of the aircraft model in more complex terms peculiar to the aircraft is considered a requirement in order to obtain reliable system information.

It is proposed that a logical analytical sophistication, which appears to be lagging the advancements in identification techniques, is the more fundamental formulation of system models. Not only is this now analytically tractable, it also yields more basic and meaningful information, and may in some cases such as those described here be of absolute necessity.

### REFERENCES

- Hindson, W.S.  
Roderick, W.E.  
Lum, K. *Progress in the Development of a Versatile Airborne V/STOL Simulator.* National Research Council of Canada, DME/NAE Quarterly Bulletin 1974(1).
- Barrett, J.N.  
White, R.G. *The Flight Development of Electronic Displays for V/STOL Approach Guidance.* AGARD Conference on the Guidance and Control of V/STOL Aircraft and Helicopters at Night and in Poor Visibility, May 1974.
- Gold, T.  
Walchli, R.M. *Head Up Display for All-Weather Approach and Landing of Tilt-Wing V/STOL Aircraft.* AIAA Paper No. 74-952, August 1974.
- Swertling, P. *Modern State Estimation Methods from the Viewpoint of the Method of Least Squares.* IEEE Transaction on Automatic Control, Vol. AC 16, No. 6, December 1971.
- Denery, D.G. *An Identification Algorithm Which Is Insensitive to Initial Parameter Estimates.* AIAA Paper No. 70-34, January 1970.
- Iliff, K.W.  
Taylor, L.W. *Determination of Stability Derivatives from Flight Data Using a Newton-Raphson Minimization Technique.* NASA TN D-6579, March 1972.
- Taylor, L.W. *A New Criterion for Modelling Systems. Parameter Estimation Techniques and Applications in Aircraft Flight Testing.* NASA TN D-7467, April 1974.
- Gould, D.G.  
Hindson, W.S. *Estimates of the Lateral-Directional Stability Derivatives of a Helicopter from Flight Measurements.* National Research Council of Canada, Aero. Report LR-572, December 1973.
- Gould, D.G.  
Hindson, W.S. *Estimates of the Longitudinal Stability Derivatives of a Helicopter from Flight Measurements.* National Research Council of Canada, Aero. Report - to be published.
- Chen, R.T.  
Eulrich, B.J.  
Lebacqz, J.W. *Development of Advanced Techniques for the Identification of V/STOL Aircraft: Stability and Control Parameters.* CALSPAN Report No. BM-2820-F-1, August 1971.

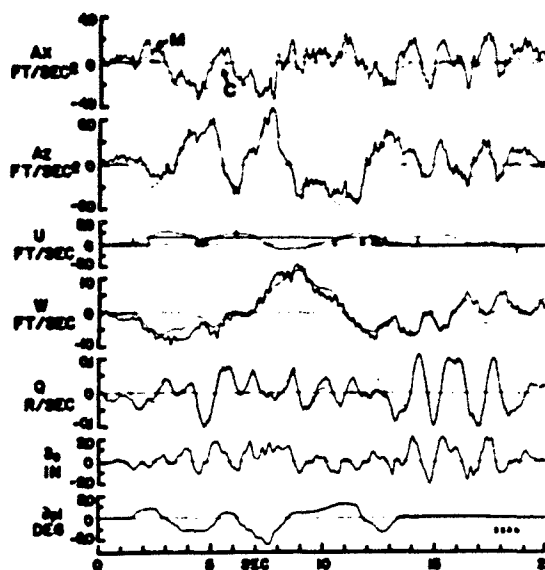


Fig. 9: CL-84 Results with  $A_1$ ,  $A_2$  Included in State Observation Vector



# ROTORCRAFT DERIVATIVE IDENTIFICATION FROM ANALYTICAL MODELS AND FLIGHT TEST DATA\*

John A. Molusis  
Aeromechanics Branch  
Sikorsky Aircraft  
Division of United Aircraft Corporation

## SUMMARY

A general procedure is presented for systematic development of rotorcraft models for use in systems identification, which includes fuselage and rotor degrees of freedom (DOF). Formulations for rigid blade flap and lag as well as the normal mode representation of an elastic blade are developed for hingeless and articulated rotor systems. The method of multiblade coordinates is used to obtain linear constant coefficient state variable models of various levels of approximation. Two of the approximate models, a 6 DOF and a 9 DOF, are identified from a nonlinear articulated helicopter computer simulation. The results demonstrate the accuracy attainable for each model.

Advanced statistical system identification methods and algorithms are reviewed. A least squares method used with an optimum data filter and an extended Kalman filter are both used to identify 6 DOF derivatives from helicopter flight test data. Derivative and time history comparisons are made and correlated with analytic model derivatives.

The results outline the status of rotorcraft modeling and systems identification and indicate areas that require further investigation.

## INTRODUCTION

A need exists for methods that will enable systematic correlation and improvement of existing rotorcraft analytic prediction methods. For example, analytic models generally predict incorrectly the unstable Dutch roll characteristics associated with some helicopters at high speeds. Also, many existing analytic models do not predict the correct gain values of pitch rate feedback which cause the rotor tip path plane to become unstable. In addition to these problems, requirements exist for more accurate control, gust alleviation, and improved handling qualities of current and future rotorcraft. These are among the motivating factors for pursuing the identification of derivatives from rotorcraft flight test data.

Successful identification of derivatives from rotorcraft flight data requires three fundamental steps. First, the modeling requirements and the important degrees of freedom of the problem must be defined. Second, a computationally efficient yet accurate identification algorithm is required to treat both measurement and process noise. Third, the proposed method must be applied to flight test data and a complete evaluation must be conducted through correlation with flight data and analytic prediction. Iteration on these three steps is required until the modeling, algorithm, and correlation all yield satisfactory results. This paper is concerned with each of these three steps, with particular emphasis on the rotorcraft modeling problem.

A general procedure is presented for development of rotorcraft models. The models vary in complexity and are dependent on the number of blades and rotor type. A large number of models are developed to approximate the rotor and fuselage degrees of freedom, which range from an 18 DOF flap-lag-fuselage model to a first order representation of the rotor. The 6 degree of freedom quasi-static fuselage model is also considered.

The need for including rotor degrees of freedom in rotorcraft derivative identification was established in Reference 1, which shows that identified 6-DOF helicopter derivatives only approximate the conventional quasi-static values. This is a direct result of not including the rotor degrees of freedom in the identification. Reference 2 discusses the results of identification of both a 6 DOF rigid body model and a 9 DOF rotor and fuselage model from a nonlinear computer simulation of a helicopter. The results demonstrate that the 9 DOF identified model represents short period time histories considerably better than does the 6 DOF model. These studies indicate the need to investigate the general rotorcraft modeling problem and determine the accuracy in identified derivatives that can be obtained for the various approximate models.

The modeling problem is considered in two parts. The first part discusses the method for transforming rotorcraft equations of motion into various approximate constant coefficient models of the rotor and fuselage. Both hingeless and articulated rotors are considered. The second part gives results of a nonlinear computer simulation study that investigated the derivative accuracy obtainable for two approximate constant coefficient linear models using system identification from input/output data.

\*Part of this research was supported by USAAMRDL Langley Directorate and NASA, LRC, Hampton, Va.

A number of studies reported in the literature discuss the problem of rotorcraft modeling. Hohenemser in Reference 3 was probably the first to formulate the rigid body quasi-static derivative model for rotorcraft. The quasi-static derivative assumption is based on the fact that the rotor degrees of freedom are of higher frequency than the fuselage. As a result, the contribution of the rotor can be lumped into the fuselage to form a 6 degree of freedom derivative model. This approximate model is generally satisfactory for low-frequency handling qualities studies and for preliminary aircraft stability and control assessment. Such a model is generally not acceptable for high-frequency transient predictions or high-gain feedback studies. The question of adequate hingeless rotor modeling in flight dynamics is treated in References 4 and 5, which conclude that for low-advance ratios, first flap bending is required. References 6 and 7 consider the multiblade coordinate representation of rotor dynamics and determine the regions in which the constant coefficient multiblade coordinate model is a good representation of the periodic coefficient rotating coordinate model. A further approximation is presented in Reference 8, in which a flapping rotor is represented by a first-order rotor model.

Rotorcraft modeling requirements for accurate derivative identification from input/output data remain to be answered. In particular, this paper addresses the question of how accurately derivatives can be identified for the various approximate models. In addition, a generalized procedure is presented for development of constant coefficient models for the rotor and fuselage of both hingeless and articulated rotors. Both rigid blade flapping and blade flexibility are considered.

The second fundamental step necessary for accurate identification of rotorcraft derivatives from flight data is the requirement for a computationally efficient yet accurate algorithm. A review of methods for parameter and state estimation is presented, with particular emphasis on advance statistical methods of identification. These include (1) maximum likelihood (ML), (2) maximum a posteriori parameter estimation (MAP-parameter) and (3) maximum a posteriori state estimation (MAP-state). Approximate methods of solution are discussed for each of these methods. The solutions all result in a Kalman filter, with the ML and MAP-parameter estimation methods requiring an iterative algorithm, such as quasi-linearization; and the MAP-state estimation method resulting in an extended Kalman filter or second-order filter. The method used for application to flight test data is the extended Kalman filter. The effect of various data filters is examined, using both the extended Kalman filter and a least squares method.

The third fundamental step necessary for accurate identification is application to flight test data and correlation with analytic prediction methods. The flight test applications presented use a 6 degree of freedom identification model. The flight data used are from a CH-53A helicopter at 100 knot trim condition, and the identified derivatives are correlated with derivatives obtained from a nonlinear helicopter analytic computer model that includes fuselage and blade flapping degree of freedom.

The three fundamental steps are reported in this paper. The results conclude the first iteration in the development of a successful procedure for obtaining rotorcraft derivatives from flight test data.

#### ROTORCRAFT MODELING

The rotorcraft modeling problem is difficult because of the large number of degrees of freedom that occur both in the nonrotating and rotating axes and because of the complexity in the aerodynamics. The most important degrees of freedom required to describe the rigid aircraft motion are the rigid body and the flapping rotor, but inplane (lag), torsion, higher blade modes, or air mass dynamics may be required for particular studies or for investigation of rotor instability problems. Figure 1 summarizes various degrees of freedom that may contribute to vehicle motion.

Low-frequency rigid-body flight dynamics can be modeled adequately with 6 degrees of freedom, but transient data contain both body and rotor motions. Identification using only 6 degrees of freedom results in derivatives that are only approximations of conventional quasi-static derivatives. Accurate rigid body derivatives can be obtained by first identifying the derivatives of a larger model, which includes the fuselage and separate rotor degrees of freedom, and then reducing this model to 6 DOF quasi-static derivatives. In addition, the individual derivative contributions from the rotor degrees of freedom can be obtained from the larger fuselage and rotor model.

The rotorcraft modeling problem is discussed in the following sections, with emphasis on developing a simple and accurate characterization of the rotor for use in system identification.

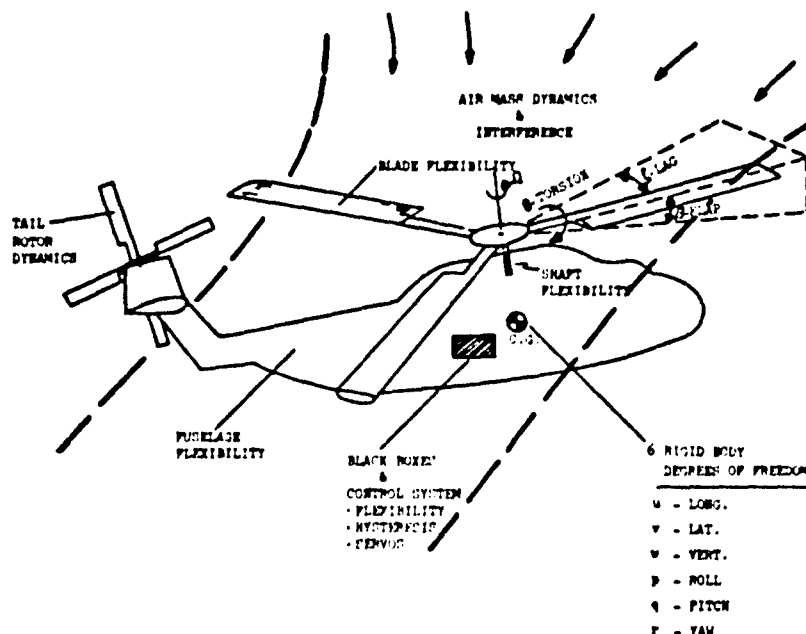


Figure 1. - Illustrative Diagram of a Rotorcraft Showing the Degrees of Freedom Which Describe the Total Vehicle Motion.

#### Rotor Characterization

Four basic rotor system types can be classified: (1) articulated, (2) semi-rigid (teetering), (3) hingeless, and (4) rigid (including propellers). Reference 9 discusses typical rotor configurations for each of the rotor systems. Each rotor system is distinguished according to the blade natural frequency in the flapping and in-plane directions. An articulated rotor system consists of rigid blade flap and lag motion, and a hingeless rotor consists of elastic deflection in the flatwise and inplane directions. This characterization is shown in Figure 2, obtained from Reference 9. Frequencies for several rotorcraft have been superimposed on this figure. The significance of this characterization for rotorcraft is that the four basic rotor concepts can be treated comparably, with the difference appearing in the natural frequency of the blade motion.

- ⊙ CH-53A (Sikorsky)
- ⊙ AH-64 (Sikorsky)
- ⊙ AH-64 (Lockheed)
- ⊙ UH-1 (Bell)
- ⊙ HO-4S (Bell)
- ⊙ WS-13 (Westland)

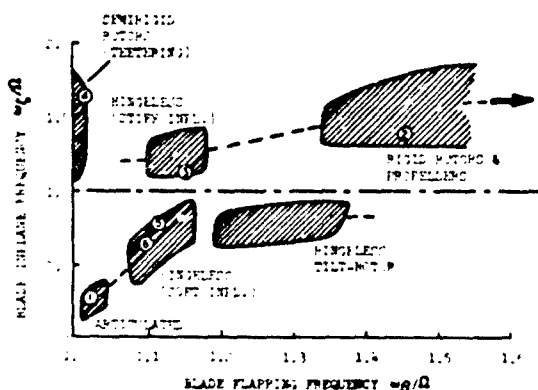


Figure 2. Rotor Characterization by Flapping and Inplane Natural Frequency Showing Location for Typical Rotorcraft.

#### Transformation of Rotating to Fixed Axes

The nonlinear equations of motion of a rotorcraft in forward flight contain coefficients that are periodic with rotor azimuth and result from asymmetric rotor aerodynamic loading in forward flight. Linearization of the nonlinear equations result in linear equations with periodic coefficients. The rotor state variables for blade flap motion can be represented conveniently in the fixed-axes system by a multiblade coordinate transformation. This transformation is of the fourier type and is given by equation (1)

$$\begin{aligned}
s_0 &= 1/N_b \sum_{i=1}^{N_b} s_i \\
s_{nc} &= 2/N_b \sum_{i=1}^{N_b} s_i \cos n \psi_i \\
s_{ns} &= 2/N_b \sum_{i=1}^{N_b} s_i \sin n \psi_i \\
s_d &= 1/N_b \sum_{i=1}^{N_b} s_i (-1)^i \quad ; N_b \text{ even only}
\end{aligned} \tag{1}$$

The flapping motion of the  $i$ th blade is then

$$s_i = s_0 + \sum_{n=1}^k (s_{nc} \cos n \psi_i + s_{ns} \sin n \psi_i) + s_d (-1)^i \tag{2}$$

where

$$k = \begin{cases} 1/2 (N_b - 1), & N_b \text{ odd} \\ 1/2 (N_b - 2), & N_b \text{ even} \end{cases}$$

The coordinates to the left of the equal sign in equation (1) are now in the nonrotating axes system. When transforming the periodic coefficient equations, an additional fourier operation is made in the equations, as discussed in Reference 7. This second operation eliminates many of the periodic coefficients from the equations in the nonrotating system and results in constant coefficients plus higher order harmonic terms. The constant coefficient approximation is then obtained by using the time-averaged coefficients in the nonrotating frame.

The procedure for accomplishing this transformation will be shown for both articulated and hingeless rotor systems. The state variable notation will be used whenever convenient, and the number of rotor modes will in general depend on the degrees of freedom chosen for the model.

Generalized modeling procedure for articulated rotors. The nonlinear equations of motion of a rotorcraft can be written in state notation according to equation (3), where  $\underline{x}_1$  represents the state vector of fuselage variables in the nonrotating axis, and  $\underline{x}_2^R$  represents the rotor state variables in the rotating axis.

$$\begin{aligned}
\dot{\underline{x}}_1 &= f_1(\underline{x}_1, \underline{x}_2^R, \underline{u}, t) \\
\dot{\underline{x}}_2^R &= f_2(\underline{x}_1, \underline{x}_2^R, \underline{u}, t)
\end{aligned} \tag{3}$$

The superscript  $R$  implies that the state vector is in the rotating axis system, and the variable  $t$  represents the fact that the equations contain terms that are periodic with period  $t_1$ . The vector  $\underline{u}$  represents the control input vector.

Linearization of equation (3) results in linear equations with periodic coefficients, as shown in equation (4).

$$\begin{aligned}
\dot{\underline{x}}_1 &= F_{11}(t)\underline{x}_1 + F_{12}(t)\underline{x}_2^R + G_1(t)\underline{u} \\
\dot{\underline{x}}_2^R &= F_{21}(t)\underline{x}_1 + F_{22}(t)\underline{x}_2^R + G_2(t)\underline{u}
\end{aligned} \tag{4}$$

The matrix arrays  $F_{ij}(t)$  represents periodic coefficient functions of period  $t_1$ . This periodicity is denoted by  $t$ .

Transformation to the nonrotating axis is accomplished by the transformation given in equation (5)

$$\underline{x}_2^R = T(t) \underline{x}_2 \tag{5}$$

where the state vector  $\underline{x}_2$ , without the superscript, represents coordinates in the nonrotating axis. The matrix  $T(t)$  represents a transformation that will generally be periodic. Substitution of equation (5) into equation (4) results in equation (6).

$$\begin{aligned}
\dot{\underline{x}}_1 &= F_{11}(t)\underline{x}_1 + F_{12}(t) T \underline{x}_2 + G_1(t)\underline{u} \\
\dot{\underline{x}}_2 &= T^{-1} F_{21}(t)\underline{x}_1 + T^{-1} (F_{22}(t) T - \dot{T}) \underline{x}_2 + T^{-1} G_2(t)\underline{u}
\end{aligned} \tag{6}$$

The variable  $t$  has been dropped for simplicity in the transformation matrix  $T(t)$ . Equation (6) is now in the nonrotating axis system, and the coefficients are periodic with period  $t_1$ . The transformation matrix  $T(t)$  is generally chosen to satisfy the transformation given by equation (1) which results in multiblade coordinates.

The constant coefficient approximation is then obtained by averaging the periodic coefficients over one period. The resulting constant coefficient equations in the nonrotating axis system are given by equation (7), where the coefficients  $A_{1j}$  and  $B_1$  represent the average value of the appropriate terms in equation (6).

$$\begin{aligned}\dot{\underline{x}}_1 &= A_{11}\underline{x}_1 + A_{12}\underline{x}_2 + B_1 u \\ \dot{\underline{x}}_2 &= A_{21}\underline{x}_1 + A_{22}\underline{x}_2 + B_2 u\end{aligned}\quad (7)$$

Equation (7) represents a suitable form for use in rotorcraft derivative identification. The actual number of rotor coordinates used will depend on the number of blades, the degree of approximation desired, and the number of modes used to represent the rotor. This will be discussed further in a subsequent section.

Associated with equation (7) will be a set of measurement equations. These are given by equation (8):

$$\begin{aligned}\underline{z}_1 &= H_1 \underline{x}_2 \\ \underline{z}_2^R &= H_2 \underline{x}_2^R = H_2 T(t) \underline{x}_2\end{aligned}\quad (8)$$

The matrix  $H_1$  and  $H_2$  represents the relationship between state variables and measurements and is generally known. For an articulated rotor,  $\underline{z}_2^R$  will represent the vector of blade flap and lag angles measured in the rotating axis. The formulation above is nonstochastic, so additive measurement noise is not included in equation (8) and process noise is absent in equation (7). The stochastic formulation will be treated later.

A convenient alternative formulation for rotorcraft is to transform the rotor states of equation (7) to normal coordinates  $\underline{y}_2$ . This is accomplished by the transformation in equation (9), in which  $M_2$  represents the modal matrix associated with rotor state variables  $\underline{x}_2$ :

$$\underline{x}_2 = M_2 \underline{y}_2 \quad (9)$$

This results in equation (10) in which  $A_{22}$  is a diagonal matrix of eigenvalues:

$$\begin{aligned}\dot{\underline{x}}_1 &= A_{11} \underline{x}_1 + A_{12} \underline{y}_2 + B_1 u \\ \dot{\underline{y}}_2 &= A_{21} \underline{x}_1 + A_{22} \underline{y}_2 + B_2' u\end{aligned}\quad (10)$$

where

$$A_{12} = A_{12} M_2, \quad A_{21} = M_2^{-1} A_{21}, \quad A_{22} = M_2^{-1} A_{22} M_2$$

and  $B_2' = M_2^{-1} B_2$ . The measurement equations are now given by equation (11):

$$\begin{aligned}\underline{z}_1 &= H_1 \underline{x}_1 \\ \underline{z}_2^R &= H_2 T(t) M_2 \underline{y}_2\end{aligned}\quad (11)$$

Equations (10) and (11) represent an alternative form for use in derivative identification. This form is particularly convenient, because the identification can be treated in two stages. In the first stage, spike inputs into the controls of a rotorcraft will permit simple inspection of the rotor measurements to obtain the frequency and damping of the rotor modes along with the modal matrix  $M_2$ . Although the details of this procedure will not be given here, use of a zero phase shift band-pass digital filter and free response data resulting from spike inputs enables determination of the matrices  $M_2$ ,  $A_{22}$  and  $B_2'$ . The second stage is then to identify the remaining elements of the matrices  $A_{11}$ ,  $A_{12}$ ,  $B_1$  and  $A_{21}$ , using the identification algorithm to be discussed in a subsequent section. The first stage permits accurate determination of the rotor, because the rotor modes all lie near the imaginary axis (low damping) for rotorcraft and can be accurately separated with a bandpass digital filter, such as the one developed by Martin and Graham in Reference 10.

Generalized modeling procedure for hingeless rotors. Hingeless rotor systems can be modeled using the normal mode representation of an elastic blade. This assumption is based on the fact that the deflection along a blade can be approximated as the product of mode shapes and time functions (participation factors). The inplane, vertical, and torsional deflections of a flexible blade can be written as

$$\begin{bmatrix} y(r,t) \\ z(r,t) \\ \theta(r,t) \end{bmatrix} = \sum_{n=1}^{nm} \begin{bmatrix} \gamma_n(r) \\ z_n(r) \\ \theta_n(r) \end{bmatrix} \delta_n(t) \quad (12)$$

where  $y(r,t)$ ,  $z(r,t)$  and  $\theta(r,t)$  represent the inplane, vertical, and torsional deflections in the shaft axis system as a function of blade span  $r$  and time  $t$ , and  $nm$  equals the number of modes. The matrix on the right of the equal sign in equation (12) is the matrix of mode shapes and depends on blade span  $r$ . The participation factors  $\delta_n(t)$  are independent of blade span and depend only on time. The participation factors are the solution to equation (13).

$$\ddot{\delta}_n + 2\zeta_n \omega_n \dot{\delta}_n + \omega_n^2 \delta_n = \frac{F_n}{I_n} \quad (13)$$

The structural damping and natural frequency of each mode are given by  $\zeta_n$  and  $\omega_n$  respectively. The generalized forces are denoted by  $F_n(\cdot)$ . The parentheses denote that  $F_n$  is a function of aerodynamics, participation factors, control inputs, and all state variables.  $I_n$  represents the generalized inertia associated with each mode.

Equations (12) and (13) can be used to describe the motion of each blade in the rotating system. Rather than use equation (12), a more convenient form can be obtained by writing the bending moment at a radial station  $r_1$  in terms of the participation factors. This is shown in equation (14):

$$\begin{bmatrix} I_{BM}(r_1,t) \\ V_{BM}(r_1,t) \\ T_{BM}(r_1,t) \end{bmatrix} = \sum_{n=1}^{nm} \begin{bmatrix} I_{BM_n}(r_1) \\ V_{BM_n}(r_1) \\ T_{BM_n}(r_1) \end{bmatrix} \delta_n(t) \quad (14)$$

where  $V_{BM}(r_1, t)$ ,  $I_{BM}(r_1, t)$ , and  $T_{BM}(r_1, t)$  represent the vertical, inplane, and torsional bending moment at radial station  $r_1$ . The load coefficients are given by  $V_{BM_n}(r_1)$ ,  $I_{BM_n}(r_1)$ , and  $T_{BM_n}(r_1)$  and are independent of time. The load

coefficients will depend generally on the blade mode shapes, mass and inertia distribution, rotor rotational speed, and natural frequency of the modes. The development of equation (14) can be found in Reference 11. Equation (13) and (14) will be used to represent the rotor degrees of freedom and measurement equations respectively. Equation (14) is more convenient than equation (12) for the measurement equation, since blade bending moments can be measured readily with strain gage instrumentation.

The participation factors  $\delta_n$  in equation (13) represent the generalized coordinates in the inplane and out-of-plane shaft axis. Since the blade bending moments are measured in the blade axis and not the shaft axis, the measurement equation must transform the inplane and out-of-plane coordinates to blade bending coordinates. This transformation is shown in state variable notation in equation (15):

$$\underline{z}_2^R(r_1,t) = H_2(\theta_R, t) \underline{x}_2^R(r_1, t) \quad (15)$$

where  $\underline{x}_2^R(r_1, t)$  represents the state vector of inplane and out-of-plane bending moments and  $H_2(\theta_R, t)$  represents the appropriate transformation to convert to the blade bending moments  $\underline{z}_2^R(r_1, t)$  at radial station  $r_1$ . Generally  $H_2(\theta_R, t)$  will be a function of geometric blade pitch angle  $\theta_R$  and hub geometry and can assume to be known.

Equations (13) and (15) can be combined with the rigid body equations to form the rotorcraft equations of motion given by equation (16) and measurement equations given by equation (17):

$$\begin{aligned} \dot{\underline{x}}_1 &= f_1(\underline{x}_1, \delta_n(t), \underline{u}, t) \\ \ddot{\delta}_n + 2\zeta_n \omega_n \dot{\delta}_n + \omega_n^2 \delta_n &= \frac{F_n}{I_n}(\underline{x}_1, \delta_n, \underline{u}, t) \end{aligned} \quad (16)$$

$$\begin{aligned} \underline{z}_1 &= H_1 \underline{x}_1 \\ \underline{z}_2^R &= H_2(\theta_R, t) \underline{x}_2^R(r_1, t) \\ &= H_2(\theta_R, t) M(r_1) \underline{x}_2^R(t) \end{aligned} \quad (17)$$

where  $M(r_1)$  represents the load coefficients with respect to the inplane and out-of-plane coordinates, and  $\delta_n$  is represented by the state vector  $\underline{x}_2^R(t)$ .

Linearization of equation (16) and conversion of the generalized coordinates  $\theta$  to state variables  $x_2^R$  results in linear equations with periodic coefficients. The linearized equations are given by equation (18) and the measurements by equation (19).

$$\begin{aligned}\dot{x}_1 &= F_{11}(t)x_1 + F_{12}(t)x_2^R + G_1(t)u \\ \dot{x}_2^R &= F_{21}(t)x_1 + F_{22}(t)x_2^R + G_2(t)u\end{aligned}\quad (18)$$

$$\begin{aligned}z_1 &= H_1 x_1 \\ z_2^R(r_1, t) &= H_2(\theta_R, t)M(r_1)x_2^R(t)\end{aligned}\quad (19)$$

The superscript R in equations (18) and (19) indicate that the coordinates are in the rotating reference axis, and the variable  $r_1$  in equation (19) indicates that the blade bending measurement  $z_2^R(r_1, t)$  is at blade radial station  $r_1$ .

Equations (18) and (19) represent the state variable description of a rotorcraft with flexible blades. The rotor state measurements are given by equation (19), which contains the unknown load coefficient matrix  $M(r_1)$ . Since this matrix cannot be uniquely determined in an identification, a transformation is required to remove  $M(r_1)$  from the measurement equation, as shown in equation (20).

$$\bar{x}_2^R(r_1, t) = M(r_1)x_2^R(t) \quad (20)$$

Substitution of equation (20) into equations (18) and (19) results in equations (21) and (22)

$$\begin{aligned}\dot{x}_1 &= F_{11}(t)x_1 + F'_{12}(t)\bar{x}_2^R(r_1, t) + G_1(t)u \\ \dot{\bar{x}}_2^R(r_1, t) &= F'_{21}(t)x_1 + F'_{22}(t)\bar{x}_2^R(r_1, t) + G'_2(t)u\end{aligned}\quad (21)$$

$$\begin{aligned}z_1 &= H_1 x_1 \\ z_2^R(r_1, t) &= H_2(\theta_R, t)\bar{x}_2^R(r_1, t)\end{aligned}\quad (22)$$

where  $F'_{12}(t) = F_{12}(t)M^{-1}(r_1)$ ,  $F'_{21}(t) = M(r_1)F_{21}(t)$ ,  
 $F'_{22}(t) = M(r_1)F_{22}(t)M^{-1}(r_1)$  and  $G'_2(t) = M(r_1)G_2(t)$ .

The rotorcraft equations (21) and (22) are now identical in structure with the periodic coefficient equations of the articulated rotor development given by equations (4) and (8). Thus, equations (21) and (22), which are periodic, can now be transformed into constant coefficient equations in the nonrotating axis, using the multiblade coordinate transformation given by equation (5). This results in equations of the structure given by equations (7) and (8) for multiblade coordinates and equations (10) and (11) for normal coordinates.

The rotorcraft derivatives can be identified from input/output data, using either equations (7) and (8) or equations (10) and (11). The procedure outlined in the last section for obtaining rotor eigenvalues and eigenvectors from free response data is also applicable to the elastic formulation presented in this section.

#### Rotor State Variables in Nonrotating System and Further Approximations

The number of state variables required to represent the rotor degrees of freedom in the nonrotating frame equals the number of state variables required in the rotating frame. Thus, a 3-bladed flapping rotor requires 3 DOF in the nonrotating frame, and a 6-bladed rotor requires 6 DOF.

Figure 3 lists the coordinates for a flapping rotor in rotating and non-rotating frames of reference. The number of degrees of freedom is the same for both the rotating and nonrotating frame, and the differential coning mode  $\theta_d$  appears only in rotor systems consisting of even numbers of blades.

The transformation accounts for the motions of all blades. For a 3-bladed rotor, the degrees of freedom are coning,  $\theta_o$ , (all blades flap together); rotor tilting in pitch,  $\theta_{1c}$ , (cosine-flapping); and rotor tilting in roll,  $\theta_{1s}$ , (sine-flapping). Adding a fourth blade adds a differential coning mode in which blades 1 and 3 flap in one direction and blades 2 and 4 flap in the other direction. Adding more blades adds degrees of freedom that warp the tip path plane.

Number of Blades	Rotating Coordinates	Nonrotating Coordinates
1	$\delta_1$	$\delta_0$
2	$\delta_1, \delta_2$	$\delta_0, \delta_4$
3	$\delta_1, i = 1, 2, 3$	$\delta_0, \delta_{1C}, \delta_{1S}$
4	$\delta_1, i = 1, 2, \dots, 4$	$\delta_0, \delta_{1C}, \delta_{1S}, \delta_4$
5	$\delta_1, i = 1, 2, \dots, 5$	$\delta_0, \delta_{1C}, \delta_{1S}, \delta_{2C}, \delta_{2S}$
6	$\delta_1, i = 1, 2, \dots, 6$	$\delta_0, \delta_{1C}, \delta_{1S}, \delta_{2C}, \delta_{2S}, \delta_4$
7	$\delta_1, i = 1, 2, \dots, 7$	$\delta_0, \delta_{1C}, \delta_{1S}, \delta_{2C}, \delta_{2S}, \delta_{3C}, \delta_{3S}$

Coordinates  $\delta_1$  (differential coning),  $\delta_{1C}$  (warp cosine), and  $\delta_{1S}$  (warp sine) are reactionless modes, since at hover they do not produce a net reaction at the hub. For this reason, these modes can often be neglected for open-loop flight dynamics studies.

- Notes: (1) Number DOF's the same in both rotating and nonrotating system.  
 (2)  $\delta_4$ , differential coning, appears only for even bladed rotors.  
 (3) Gimbaled rotors require modification of the coordinates due to hub accent carryover.

Figure 3. Description of Coordinates for a Flapping Rotor in the Rotating and Nonrotating System for Various Rotor Systems with Different Number of Blades.

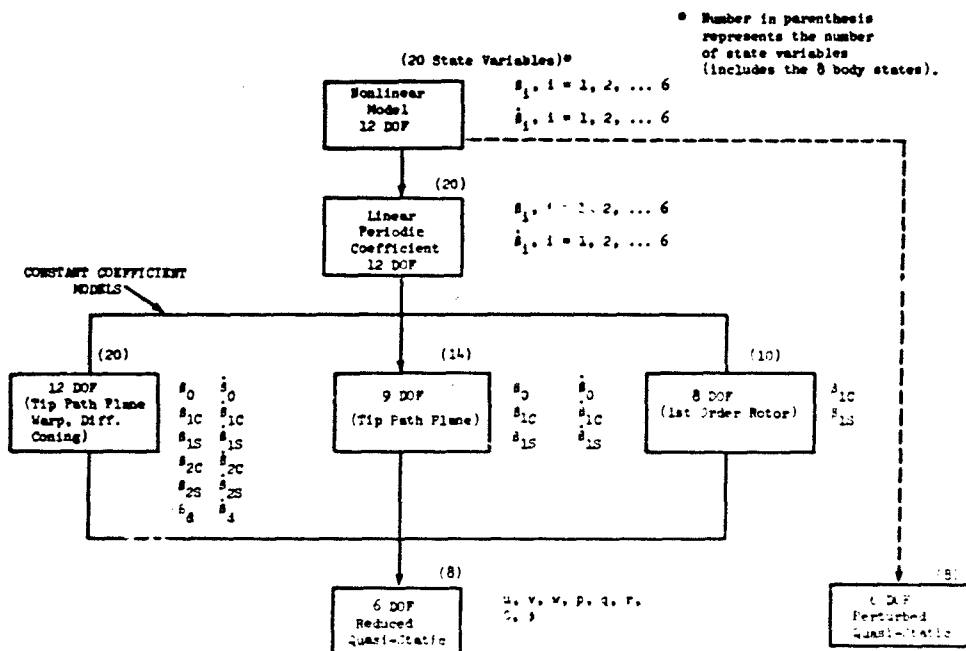


Figure 4. Rotorcraft Analytic Models Showing the State Variables Required to Describe the Rotor Flapping Degrees of Freedom. (6 Bladed Rotor Assumed).

Figure 4 shows typical analytic models for a 6-bladed rotor that can be used in rotorcraft flight dynamics studies. The models shown include only flapping degree of freedom for the rotor. The state variables for each model are indicated, and the three reactionless modes are ignored in the 9 DOF model. The models consist of 6 body degrees of freedom and the appropriate number of rotor degrees of freedom. The 8 DOF model uses a first-order representation for the rotor and is the same model described in Reference 8. This is the simplest model that includes the rotor degrees of freedom separately and models accurately the first-flap regressing mode.

Typical characteristic roots for a 6-bladed flapping rotor in the nonrotating frame are shown in Figure 5. The 6 body degrees of freedom are of low frequency, and the rotor roots are generally of higher frequency. The most important rotor root with regard to rigid body motion is the flap regressing mode, but the other rotor roots will generally be of significance for high-gain feedback investigations.



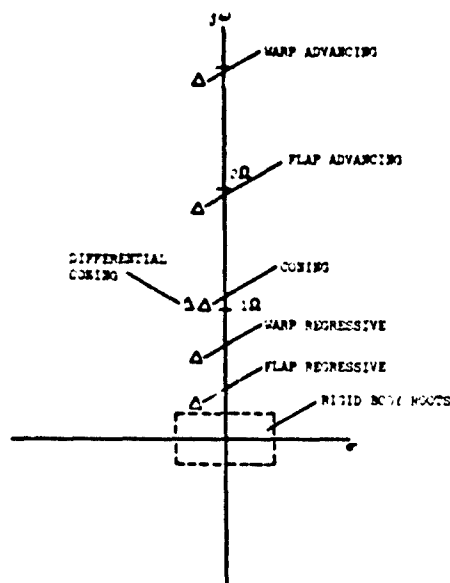


Figure 5. Illustrative Diagram Showing Typical Characteristic Root Location for a Six-Bladed Flapping Rotor.

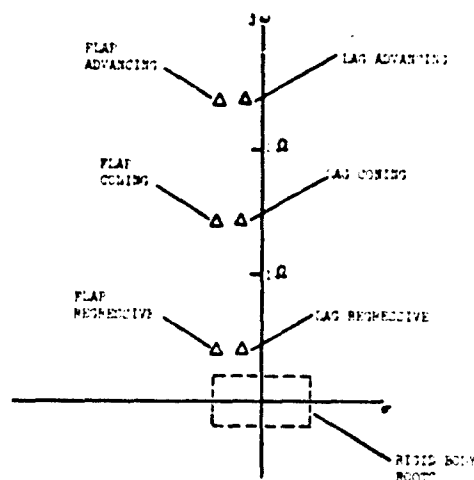


Figure 6. Illustrative Diagram Showing Typical Characteristic Root Location for Flap and Lag DOF for a Three-Bladed Hingeless (Rigid) Rotor.

In addition to the flapping motion, high-gain feedback studies may require inclusion of the rotor inplane degree of freedom. Inplane degree of freedom generally does not introduce a significant net reaction at the hub and is usually ignored for most flight dynamics studies. High-gain feedback studies may require this mode for accurate rotor stability boundary prediction and for studies concerned with the effect of feedback on air resonance. In addition, the inplane mode may cause errors in identified derivatives if not modeled in the identification process.

Figure 6 shows typical rotor inplane and flapping characteristic roots in the nonrotating system for a 3-bladed stiff rotor system. Thus, 3 DOF for inplane and 3 DOF for flapping motion would be required for representation of the rotor in the nonrotating system. Systems identification of this model would require 12 DOF: 6 DOF for the body, 3 DOF for flapping, and 3 DOF for inplane.

Figure 7 shows alternative models of various levels of approximation for a rotorcraft which include both flap and inplane degree of freedom. The constant coefficient models consist of flap-lag and flap-only representations of the rotor. The 10 DOF first-order rotor flap-lag model contains a first-order representation for both flap and lag degree of freedom similar to the 8 DOF first-order rotor flap model discussed previously. This model retains the lower frequency flap-regressing and lag-regressing characteristic roots.

The 9 DOF flap and 8 DOF first-order rotor flap model are included in this figure, since the typical rotorcraft will contain both flap and lag degrees of freedom, and it would be desirable to use only the flapping degrees of freedom in the identification. Whether the presence of lag DOF will degrade system-identified derivatives needs further investigation.

Also shown in Figure 7 is the quasi-static 6 DOF model obtained directly by perturbing the nonlinear model. This model may or may not have the identical derivative values as the reduced quasi-static model shown in Figure 7. A difference in derivatives could arise if the linear constant coefficient models, which include separate rotor degrees of freedom, are not good representations of the nonlinear model. This problem will be discussed in a subsequent section.

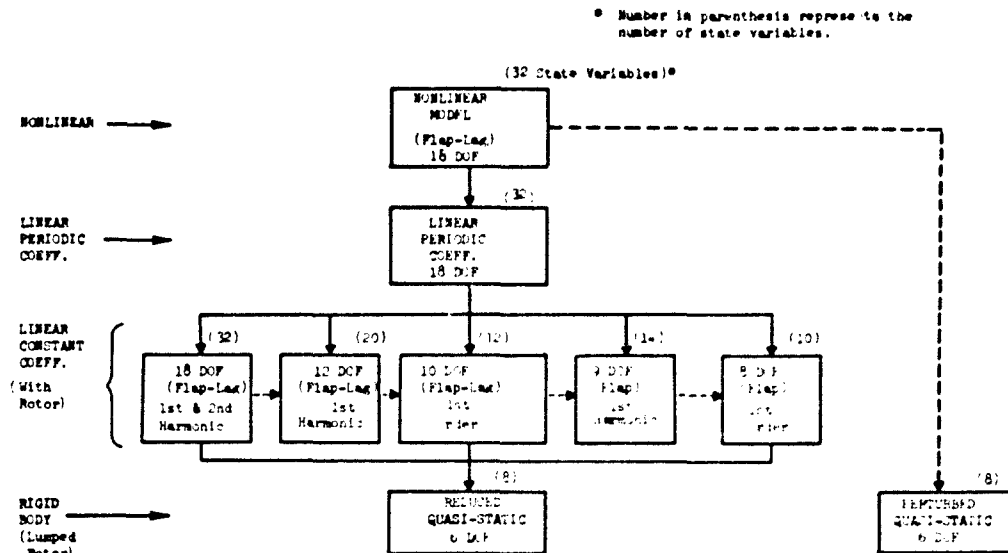


Figure 7. Rotorcraft Analytic Models Including Flap and Lag DOF for a 6-Bladed Rotor.

#### Reduction to Quasi-Static and First Order Rotor Models

The linear constant coefficient models, which include separate body and rotor degrees of freedom, can be reduced to a 6-DOF rigid body quasi-static model. This is accomplished by first partitioning the model into separate rotor and body degrees of freedom. This is shown in Table 1, where  $x_1$  represents the state vector of body variables, and  $x_2$  represents the state vector of rotor variables. The rotor degrees of freedom are lumped into the body degree of freedom by setting  $\dot{x}_2 = 0$ , solving for  $x_2$  from equation (2), and substituting the resulting expression for  $x_2$  into equation (1). The quasi-static derivative model is shown in equation (5) of Table I.

This technique can be used for reducing any linear model with separate rotor degrees of freedom to the conventional quasi-static derivative model. This model will be referred to as the reduced quasi-static model.

Table 2 shows the procedure for reducing the body with separate rotor degrees of freedom to the first-order rotor representation discussed previously. The rotor state variables are represented by the vector  $x_2$ . The coefficients circled in the derivative matrix of Table 2 are usually smaller than the other coefficients and can be neglected. This approximation results in a second-order equation for coning, as shown in equation (3), and two first-order equations for flapping, as shown in equation (4) of Table 2. The coning equation yields estimates of the damping and frequency of the coning mode and, since the natural frequency is much greater than the flap-regressing mode, the coning mode can be ignored. The first-order representation of equation (4) yields an accurate estimate of the flap regressing mode.

REDUCTION TO QUASI-STATIC DERIVATIVE		
Rigid Body DOF:	$\dot{x}_1 = A_{11} x_1 + A_{12} x_2 + B_1 u$	(1)
Rotor DOF:	$\dot{x}_2 = A_{21} x_1 + A_{22} x_2 + B_2 u$	(2)
Let	$\dot{x}_2 = 0$	(3)
	$x_2 = -A_{22}^{-1} A_{21} x_1 - A_{22}^{-1} B_2 u$	(4)
Substitute Equation (4) into equation (1) results in		
	$\dot{x}_1 = \underbrace{(A_{11} - A_{12} A_{22}^{-1} A_{21})}_{\text{Quasi-Static Stability Derivative Matrix, } A_{11}'} x_1 + \underbrace{(B_1 - A_{12} A_{22}^{-1} B_2)}_{\text{Quasi-Static Control Derivative Matrix, } B_{11}'} u$	(5)

Table 1. Method to Reduce Rotorcraft Linear Rotor/Body Models to the Quasi-Static Derivative Model.

REDUCED TO FIRST ORDER MODEL

(1)

$$\dot{\theta} = A_{\text{rot}} \theta + B_{\text{rot}} \delta$$

(2)

$$\begin{bmatrix} \dot{\theta}_0 \\ \dot{\theta}_{1C} \\ \dot{\theta}_{1S} \\ \dot{\theta}_{1L} \end{bmatrix} = \begin{bmatrix} 0 & 1 & 0 & 0 & 0 & 0 \\ a_{11} & a_{12} & a_{13} & a_{14} & a_{15} & a_{16} \\ 0 & 0 & 0 & 1 & 0 & 0 \\ a_{21} & a_{22} & a_{23} & a_{24} & a_{25} & a_{26} \\ 0 & 0 & 0 & 0 & 0 & 1 \\ a_{31} & a_{32} & a_{33} & a_{34} & a_{35} & a_{36} \end{bmatrix} \begin{bmatrix} \theta_0 \\ \theta_{1C} \\ \theta_{1S} \\ \theta_{1L} \end{bmatrix} + \begin{bmatrix} 0 \\ a_{17} \\ 0 \\ a_{27} \\ 0 \\ a_{37} \end{bmatrix} \delta$$

Neglect  $\dot{\theta}_{1C} = 0$

Coming Eq.:  $\dot{\theta}_0 = a_{11} \theta_0 + a_{12} \dot{\theta}_0$  (3)

First Order

Rotor (Flap):  $\begin{bmatrix} \dot{\theta}_{1C} \\ \dot{\theta}_{1S} \end{bmatrix} = \begin{bmatrix} a_{14} & a_{16} \\ a_{24} & a_{26} \end{bmatrix}^{-1} \cdot \begin{bmatrix} a_{17} & a_{15} \\ a_{27} & a_{25} \end{bmatrix} \cdot \begin{bmatrix} \theta_{1C} \\ \theta_{1S} \end{bmatrix}$  (4)

At Hover:

$$\begin{bmatrix} \dot{\theta}_{1C} \\ \dot{\theta}_{1S} \end{bmatrix} = \begin{bmatrix} -c_{\theta_0} & \omega_a(1-c^2)/b \\ -\omega_a(1-c^2)/b & -c_{\theta_0} \end{bmatrix} \begin{bmatrix} \theta_{1C} \\ \theta_{1S} \end{bmatrix}$$

Table 2. Method for Deriving First Order Rotor Model From Rotor-Body Models.

Also shown in Table 2 is the form of the first-order rotor model for the hover condition which is particularly simple due to the symmetry of the rotor.

This concludes the discussion of rotorcraft modeling. This section has considered the modeling problem in considerable depth and is necessary, since the ultimate goal of using system identification is to correlate flight-identified derivatives with analytic prediction to isolate and remove model deficiencies. To accomplish this, the approximations used in formulating the derivative model must be clearly understood. Also, the most suitable model to be used will depend on the particular problem or investigation at hand.

#### COMPUTER MODEL STUDIES

This section discusses the results of several studies in which derivative models were identified from a computer simulation of a helicopter. Both a 6-DOF linear model which contains 60 derivatives and a 9-DOF linear model which contains 144 derivatives were identified from a nonlinear simulation of a rotorcraft. The results demonstrate the degree of accuracy that can be obtained for the various identified models. Three separate computer studies are discussed, and some of the results were published previously in References 1, 2 and 12. In each case, a least squares method was used to identify the derivatives from transient input/output data. Since the computer simulation contains no state variable measurement noise, the least squares method yields unbiased estimates of the derivatives, provided that all modes are properly excited. Thus, the results of this section are not hindered by approximate identification algorithms as is in-flight data identification.

##### Linear and Nonlinear 6-DOF Study

Reference 1 presented a study of derivative identification from a 6-DOF linear computer simulation of an S-61 helicopter, in which it was shown that all 60 derivatives could be identified to six significant figures. It was found that two maneuvers generated by pulse inputs and lasting six seconds each were sufficient to excite all modes properly for successful identification.

Reference 1 also presented results of a 6-DOF linear derivative identification from a nonlinear coaxial rotor helicopter simulation. It was found that the identified derivatives only approximate the conventional quasi-static derivatives. Table 3 compares the quasi-static and 6-DOF system identified derivatives for many of the primary derivatives from this study. It is apparent that the system identified derivatives only approximate the quasi-static values. Some derivatives are accurately identified, while others differ by as much as 100%. These differences are a direct result of using only

Longitudinal Derivatives			Lateral Directional Derivatives		
	Quasi-Static	6 DOF System Ident.		Quasi-Static	6 DOF System Ident.
$X_u$	-.031	-.002	$Y_v$	-.139	-.108
$X_0$	-33.7	-31.2	$Y_r$	-134.0	-134.5
$Z_u$	-1.22	-1.13	$L_v$	-.038	-.012
$Z_0$	133.6	135.9	$L_r$	-7.96	-2.78
$M_u$	.012	.011	$L_p$	.252	2.08
$M_0$	-.013	-.024	$M_v$	.011	.012
$N_u$	-3.98	-1.26	$N_r$	-.450	-.536
$X_{\beta 1s}$	-.310	-.019	$N_p$	-.705	-.378
$M_{\beta 1s}$	.672	.364	$Y_{A1s}$	.532	.254
$Z_{\beta c}$	-6.94	-6.38	$L_{A1s}$	2.02	.939
$N_{\beta c}$	.480	.213	$M_{A1s}$	.185	.110

Table 3. Comparison of Quasi-Static and 6-DOF System Identified Derivatives from a Nonlinear Helicopter Computer Simulation (Coaxial Rotor, 80 Kts).

conventional 6-DOF perturbed quasi-static derivative model, also diagramed in Figure 4. Only a 3-DOF tip path plane representation for the rotor was used in these studies. Since the rotor has 6 blades, the correct number of modes is 6 which includes differential coning, warp sine, and warp cosine.

**Tip path plane resolver.** Two methods are available for resolving rotating coordinates  $\beta_1$  to the nonrotating axes system. The first method is the fourier transformation given in equation (1). The second method makes use of a Kalman filter, which for an isotropic rotor is essentially equation (1) passed through a first-order low-pass filter. The Kalman filter method is shown in Reference 12 and was found to be superior to the fourier method when the flapping measurements are contaminated with noise and thus is the superior method for use with flight test data. The Kalman filter method can be made to approach the fourier resolver of equation (1) by letting the effective time constant of the Kalman filter approach zero. Thus, all studies of identification from the computer used the Kalman filter to estimate the tip path plane coordinates. Reference 12 discusses this technique in detail.

**Identified derivative models.** Figure 8 shows a block diagram of the procedure

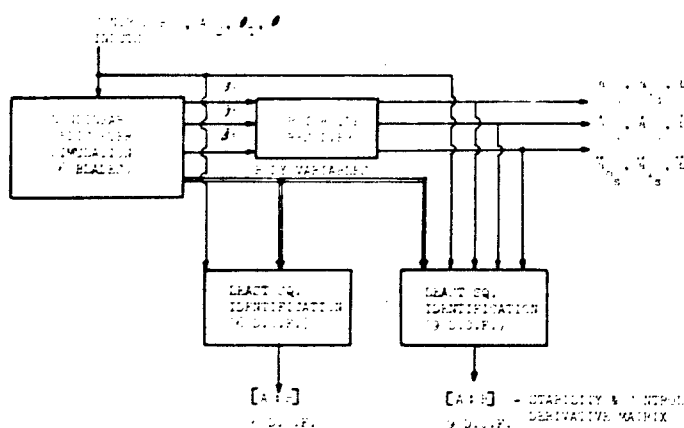


Figure 8. Procedure Used to Identify 6 and 9-DOF Linear Derivatives from Nonlinear Computer Simulation.

6-DOF in the identification model, which should include separate rotor degrees of freedom. Although the quasi-static and system identified derivatives show different values, the characteristic roots were found to be similar for the two models.

#### Nonlinear 6-DOF and 9-DOF Study

Reference 2 presents results of a study in which both 6-DOF and 9-DOF linear derivative models were identified from a nonlinear computer simulation of a CH-53A helicopter. The nonlinear model contained 6 blades with flapping degree of freedom and 6 degrees of freedom for the rigid body. The rotor was simulated with full nonlinear aerodynamics, and uniform inflow filtered with a first-order lag was used for the air mass dynamics.

The nonlinear simulation represents the 12-DOF nonlinear model, as indicated in Figure 4. The least squares identification method was used to obtain a 9-DOF linear and a 6-DOF system identified model. In addition, the 9-DOF model was reduced to the 6-DOF reduced quasi-static model, as indicated in Figure 4. The 6-DOF models can thus be compared directly with the

conventional 6-DOF perturbed quasi-static derivative model, also diagramed in Figure 4. Only a 3-DOF tip path plane representation for the rotor was used in these studies. Since the rotor has 6 blades, the correct number of modes is 6 which includes differential coning, warp sine, and warp cosine.

Figure 8 shows a block diagram of the procedure used to identify the 9-DOF and 6-DOF linear models. The nonlinear model was excited with pulse-type inputs, and 22 maneuvers of 4 seconds duration were used in the identification. A sampling rate of .0135 second was used throughout the study. The 9-DOF identified derivative array resulting from this study is shown in Table 4. Table 5 compares the 6-DOF perturbed quasi-static derivatives, the 6-DOF reduced derivatives obtained from the 9-DOF identified model, and the 6-DOF identified derivatives. This comparison shows that the 6-DOF reduced derivatives agree closely with the 6-DOF perturbed quasi-static values. The 6-DOF identified derivatives in some cases show errors of 100%, whereas the 6-DOF reduced derivatives are a much better representation of the perturbed quasi-static values.



Longitudinal Derivatives				Lateral Directional Derivatives			
	Quasi-Static	9 DOF Reduced to 6 DOF	6 DOF Identified		Quasi-Static	9 DOF Reduced to 6 DOF	6 DOF Identified
$K_V$	.0064	.0064	-.0004	$L_V$	-.023	-.024	-.017
$K_\phi$	-.579	-.644	.018	$L_\psi$	-1.59	-1.70	-1.27
$K_\delta$	.0017	.0021	-.0012	$L_\eta$	-1.02	-1.21	.85
$K_\zeta$	.212	.232	.092	$L_F$	.395	.250	.743
$K_{\delta 1s}$	-.096	-.101	-.077	$L_{A1s}$	.390	.422	.378
$K_{\delta 0}$	.075	.079	.056	$L_{OT}$	.066	.065	.073
$Z_V$	-.880	-1.30	-.877	$Z_F$	.0072	.0070	.0079
$Z_\psi$	-.028	-.029	-.031	$F_F$	-.742	-.718	-.63
$Z_{\delta 0}$	-7.14	-10.03	-8.72	$F_\psi$	-.085	-.100	.0025
		*		$F_{OT}$	-.0896	-.0899	-.0890
$X_\phi$	-.0458	-.0148	-.0283	$Y_V$	-.081	-.068	-.054
$X_\psi$	.074	.128	.113	$Y_\psi$	5.22	5.10	5.69
$X_\zeta$	-1.78	-1.43	-1.17	$Y_{A1s}$	.614	.677	.602
$X_{\delta 1s}$	.365	.209	.226				

\* 9 DOF Identified Reduced to 6 DOF

Table 5. Comparison of Quasi-Static, 6-DOF Reduced and 6-DOF Identified Derivatives from a Nonlinear Helicopter Computer Simulation. (CH-53A, 33,500 lbs, 100 kts).

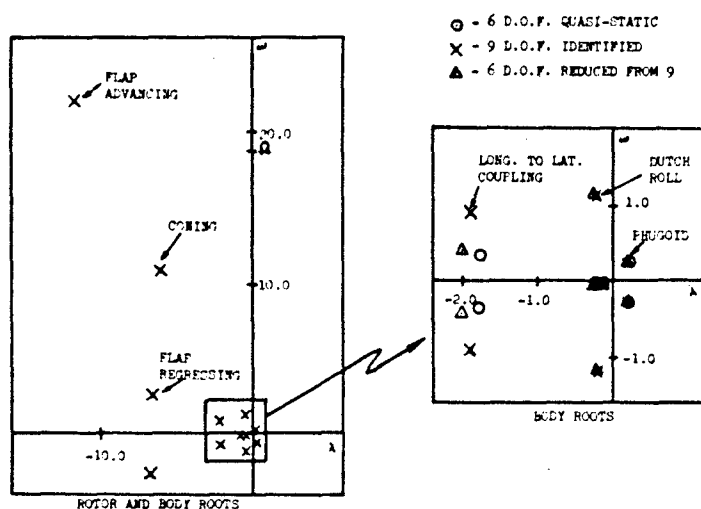


Figure 9. Characteristic Roots from the Various Linear Models Obtained from the Non-linear Simulation Showing Root Location for Rotor Modes, and Low Frequency Body Modes.

The characteristic roots for the rotor degrees of freedom are shown in Figure 9. Also shown are the 6-DOF quasi-static and 6-DOF reduced roots. The low frequency body roots show excellent agreement for the three models. Time histories and further characteristic root comparisons can be found in References 2 and 12. An anomaly is noted in the location of the frequency of the coning root. The coning root is expected to have a natural frequency approximately equal to the rotor rotational speed, 19.3 radians/sec. The coning root shown in Figure 9, however, is at 11 radian/sec. This lower than expected frequency is a result of selecting the effective Kalman resolver cutoff frequency to be  $\omega_c = 15.96$ . Additional studies were conducted with larger cutoff frequencies, and it was found that the coning root approached the rotor rotational speed. The most important root with regard to rigid body dynamics is the flap regressing mode, which is of much lower frequency and thus not affected by the Kalman resolver.

The 6-DOF reduced derivatives of Table 5 show slight discrepancies when compared with the perturbed quasi-static values. These discrepancies most likely result from (1) nonlinearities in the nonlinear model, which are not modeled in the 9-DOF linear model, (2) absence of the differential coning, warp sine, and warp cosine modes, (3) absence of the first-order air mass dynamics (time constant = .256 secs.), (4) effective filtering in the Kalman resolver, and (5) approximation of the periodic coefficient model by constant coefficients. Although the exact reason for the discrepancy requires further investigation, the improvement in the 6-DOF reduced derivatives is clearly shown when compared with the 6-DOF identified derivatives.

**Evaluation of derivative accuracy.** Several tests must be made to evaluate the accuracy of the linear 9-DOF identified derivative array. Although this procedure can be applied to any of the linear models that include separate rotor degrees of freedom, the technique will be discussed using the 9-DOF model identified from the CH-53A nonlinear computer simulation shown in Table 4.

The 9-DOF model approximates the larger 12-DOF periodic coefficient model discussed previously. It is necessary therefore to make several tests with this array and compare them with the nonlinear simulation from which the array was obtained. These tests consist of evaluating (1) the reduced 6-DOF model, (2) the elements of the 9-DOF array, and (3) transient response data. All these tests can be made by perturbing the nonlinear model and the linear 9-DOF model in the conventional manner required to obtain quasi-static derivatives, and then recording the complete derivative time plot. A sample result of this perturbation is shown in Figure 10. The transient response shown in Figure 10 represents the body pitch acceleration due to a 1-unit change in roll rate ( $M_p = \Delta q / \Delta p$ ). The solid line is obtained from the nonlinear model and the dashed line from the 9-DOF linear model. The conventional 6-DOF quasi-static derivative is shown by the circle symbol, and the triangle represents the 6-DOF reduced derivative which is in good agreement with the conventional quasi-static derivative. The diamond symbol represents the 9-DOF identified coefficient and is in good agreement with the initial response ( $t=0$ ) of the nonlinear transient. Finally a comparison of the transient response of the

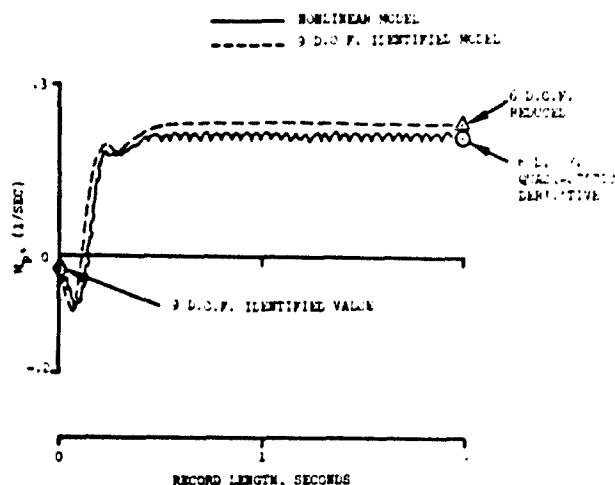


Figure 10. Derivative Time Plot Obtained by Perturbing the Nonlinear Model and the 9-DOF Linear Model, Showing Method to Check the Validity of System Identified Derivatives.

nonlinear and 9-DOF model due to a perturbation in  $p$  demonstrates that the rotor dynamics are correctly identified. The above procedure should be applied to all the derivative time plots for a complete check of the 9-DOF model accuracy.

#### Alternative Method to Obtain Linear 9-DOF Model From a Nonlinear Simulation

The previous section discussed the physical interpretation of the various derivative models (6-DOF quasi-static, 6-DOF reduced, 9-DOF). This interpretation suggests a method for obtaining derivative values from the nonlinear model by perturbing only the body state variables. Three steps are required and will be discussed with the aid of Figure 11.

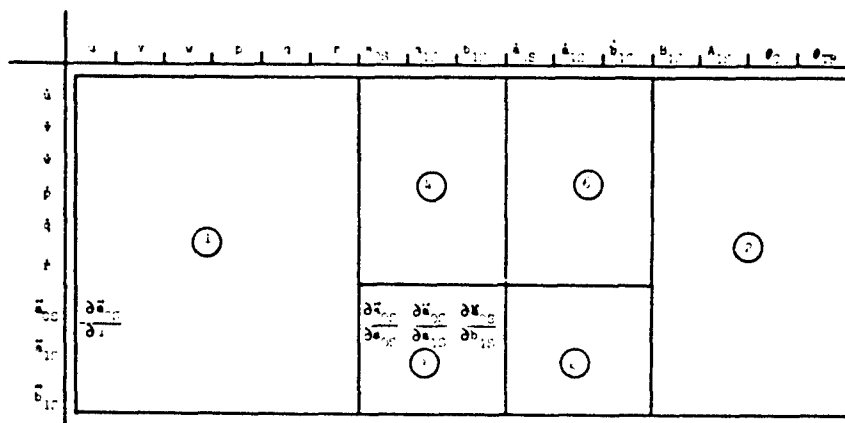


Figure 11. Nine DOF Derivative Array Partitioned into 6 Areas Demonstrating Method to Obtain Full Derivative Array by Perturbing Only the Body Variables of a Nonlinear Simulation.

**Step 1.** Figure 11 shows the array for the 9-DOF derivative model. This array is positioned into 6 areas. Derivatives in area blocks (1) and (2) of Figure 11 can be obtained by independently perturbing each column in these blocks. A time plot in the form of Figure 9 is obtained for each derivative. The value at  $t=0$  for each plot is then the appropriate derivative for blocks (1) and (2). The quasi-static tip path plane change must be saved for each perturbation and is used to obtain block areas (3) and (4). Also the derivative time plots (Figure 10) must be saved and are used to obtain blocks (5) and (6).

**Step 2.** Block (3) and (4) can be obtained one row at a time by using the quasi-static tip path plane change due to each perturbation from step 1. For example, the coning derivatives in block (3) of Figure 11 can be obtained from the  $\Delta u$  perturbation of step 1 by forming the equation:

$$\ddot{a}_{0s} = \left( \frac{\partial \ddot{a}_{0s}}{\partial u} \right) \Delta u + \left( \frac{\partial \ddot{a}_{0s}}{\partial a_{0s}} \right) \Delta a_{0s} + \left( \frac{\partial \ddot{a}_{0s}}{\partial a_{1s}} \right) \Delta a_{1s} + \left( \frac{\partial \ddot{a}_{0s}}{\partial b_{1s}} \right) \Delta b_{1s} \quad (23)$$

where  $\Delta a_{0s}$ ,  $\Delta a_{1s}$ , and  $\Delta b_{1s}$  become the tip path plane change due to a  $\Delta u = 1$  perturbation obtained from step 1 and  $\left( \frac{\partial \ddot{a}_{0s}}{\partial u} \right)$  is known from step 1.

Equation (23) represents one equation in the three unknown derivatives  $\frac{\partial \ddot{a}_{0s}}{\partial a_{0s}}$ ,  $\frac{\partial \ddot{a}_{0s}}{\partial a_{1s}}$  and  $\frac{\partial \ddot{a}_{0s}}{\partial b_{1s}}$ . Two more equations can be obtained from the  $\Delta v$  and  $\Delta w$  perturbation to yield 3 equations with 3 unknowns that can be solved for the 3 unknown coning derivatives.

Since the 9-DOF model is only an approximation of a more complicated model, the remaining perturbation variables  $p$ ,  $q$ ,  $r$ ,  $B_{1s}$ , and  $A_{1s}$ , and  $\theta_c$  can be used to obtain 6 more equations. This will provide 9 equations in 3 unknowns and can be solved using a simple least squares fit. This procedure will guarantee the rotor derivatives that yield the best possible approximation to conventional quasi-static values when the 9-DOF model is reduced to the 6-DOF reduced model.

This procedure should be repeated for each row of blocks (3) and (4) to obtain all rotor static derivatives.

**Step 3.** Blocks (5) and (6) of Figure 11 represent derivatives associated with the rotor rate state variables  $\dot{a}_{0s}$ ,  $\dot{a}_{1s}$ , and  $\dot{b}_{1s}$ . The derivatives for these blocks can be obtained by using the transient derivative time plots saved from the first step. Each row of blocks (5) and (6) must be determined separately. This is done by using the derivative time plots (one is shown in Figure 10) for each perturbation and determining the 3 rate derivatives of a row by a least squares fit. The resulting solution will provide the rotor rate derivatives that best match the transient rotor behavior.

The least squares curve fit is required in the above procedure, because  $a_{0s}$ ,  $a_{1s}$ ,  $b_{1s}$ ,  $\dot{a}_{0s}$ ,  $\dot{a}_{1s}$ , and  $\dot{b}_{1s}$  are difficult to perturb independently in a nonlinear simulation. An alternative procedure that may be acceptable would be to perturb the rotor flapping variables  $\beta_i$  according to equation (1). This would result in the appropriate independent perturbation of the rotor state variables in the nonrotating system.

The least squares method discussed above is a simple and effective method for obtaining linear derivatives for large rotor/body models and can be extended to obtain models of order larger than the 9-DOF model discussed.

#### Empirical Correction to 6-DOF Identified Derivatives

The 6-DOF identified derivatives in many cases were found to differ from the quasi-static values. This difference arises because the rotor degrees of freedom are not modeled in the identification. An empirical procedure based on a nonlinear simulation can be used to correct flight identified derivatives to approximate quasi-static values. This correction amounts to a correction factor multiplied by the system identified derivative, as shown in equation (24).

$$\begin{array}{lcl} \text{Approx.} & & \\ \text{Quasi-static} & \text{6-DOF} & \\ \text{Derivative} & = \text{Flight} & \times \text{Correction} \\ \text{(Flight Test)} & \text{Identified} & \text{Factor} \\ & \text{Derivative} & \end{array} \quad (24)$$

The correction factor can be obtained from a nonlinear simulation and is shown in equation (25)

$$\begin{array}{lcl} \text{Correction} & & \\ \text{Factor} & = & \frac{\text{Computer Quasi-static Derivative}}{\text{Computer System Identified Derivative}} \end{array} \quad (25)$$



The validity of this correction factor depends upon the computer model having rotor response similar to flight data. Although this procedure depends on how well the nonlinear model represents the flight vehicle, the correction factor will yield a much better representation of the quasi-static definition. Examples of this correction applied to flight identified derivatives will be shown in a subsequent section.

#### DERIVATIVE IDENTIFICATION METHODS

This section discusses many of the methods available for helicopter derivative identification. Particular emphasis is given to the advanced statistical methods for identification, since both measurement noise and process noise are included in the problem.

Identification techniques can be classified as equation error methods, output error methods, or advanced statistical methods. Equation error methods yield biased derivative estimates when measurement noise is present. Output error methods yield biased derivative estimates when process noise is present. Advanced statistical methods include both measurement noise and process noise as part of the formulation. Table 6 lists the 3 classifications and shows 7 methods available for derivative identification. The least squares method (Method 1) yields biased derivatives when measurement noise is present, but this method is the only one in Table 6 that has an exact closed form solution. All the other methods require algorithms that are iteratively applied or approximate. The least squares method must be used with high-quality data filters to obtain reasonable accuracy in the identified derivatives. Using digital and optimum filtering of the data provides acceptable quality data in many cases. Results obtained using the least squares method with various data filters will be discussed in a subsequent section. The least squares method has the advantage of efficient and simple computer computation for problems described by large derivative arrays, whereas the other methods of Table 6 are computationally inefficient.

METHODS FOR AIRCRAFT STATE AND PARAMETER ESTIMATION			
CLASSIFICATION	METHOD	CRITERIA	SOLUTION
Equation Error	1. Least Squares (Regression)	$J = \text{Quadratic Function of Equation Error}$	Closed Form Using Method 1.
Output Error	2. Gradient	$J = \text{Quadratic Function of Output Error}$	Iterative Using Method 2, 3 or 4
	3. Conjugate Gradient		
	4. Quasilinearization Modified Newton-Raphson		
Advanced Statistical	5. Max. Likelihood (ML)	$p(x/p)$	Iterative using Method 2, 3 or 4
	6. Max. A Posteriori Parameter Estimation (MAP-Parameter)	$p(x/p)$	
	7. Max. A Posteriori State Estimation (MAP-State)	$p(x_p, x/s)$	Sequential Using . Invariant Embedding (Extended Kalman Filter) . 2nd Order Filter . Filter/Smoothing Methods

Notes: a) Method 6 is related to Method 5 by Bayes' Rule. (A priori information available).

b) Methods 5, 6 and 7 reduce to criteria of Method 1 when measurement noise is absent.

Table 6. Summary of Methods for Aircraft State and Parameter Estimation.

The output error techniques shown in Table 6 include gradient, conjugate gradient, and quasilinearization (modified Newton-Raphson) methods. The difficulty in using these methods in the helicopter identification problem is that they attempt to curve fit the response of the derivative model to the test data. Since the helicopter contains large amounts of process noise and is almost always unstable in the longitudinal mode, the error between the derivative model and flight data is expected to diverge after four or five seconds of data, even with the correct derivatives in the linear derivative model. The output error methods are formulated to provide a best match to the test data, so the derivatives will be incorrectly adjusted to minimize the fit error.

The advanced statistical methods in Table 6 are formulated to include both process noise and measurement noise and represent the correct formulation for the helicopter derivative identification problem. These methods will be discussed in the following sections.

### Advanced Statistical Methods

The advanced statistical methods treat process noise and measurement noise as random disturbances with assumed probability distributions. The noise statistics are assumed to be gaussian with known mean and variance, although this assumption is not required. The formulation of the derivative identification problem is applicable using the 3 advanced statistical methods of Table 6.

The differential equations of motion for the derivative model can be expressed as

$$\dot{\underline{x}} = f(\underline{x}, \underline{x}_p, \underline{u}) + \underline{w} \quad (26)$$

where  $\underline{x}$  is an  $n \times 1$  vector of state variables  
 $\underline{x}_p$  is an  $p \times 1$  vector of parameters (derivatives)  
 $\underline{u}$  is an  $m \times 1$  vector of control inputs  
 $f$  is an  $n \times 1$  vector expressing the nonlinear functional relationship of the state and input vector  
 $\underline{w}$  is an  $n \times 1$  zero mean white gaussian process noise vector.

The measurement equations can be expressed as

$$\underline{z} = h(\underline{x}) + \underline{n} \quad (27)$$

where  $\underline{z}$  is an  $r \times 1$  vector of physical measurements  
 $h$  is an  $r \times 1$  vector of nonlinear functional relationships of the state variables  
 $\underline{n}$  is an  $r \times 1$  zero mean white gaussian measurement noise vector.

If the equations of motion described by equation (26) are linear, they may be written as

$$\dot{\underline{x}} = \underline{A}\underline{x} + \underline{B}\underline{u} + \underline{w} \quad (28)$$

and the measurement equations become

$$\underline{z} = \underline{H}\underline{x} + \underline{n} \quad (29)$$

The stability and control derivatives are contained in the parameter vector  $\underline{x}_p$  for both the linear and nonlinear formulation. The problem is to identify the parameters  $\underline{x}_p$  in the differential equation (26), given measurements of the system state variables by equation (27). To determine the unknown parameters (derivatives) of equation (26), a criteria must be specified which measures the goodness with which the unknown derivatives are identified. This criterion differentiates the three statistical methods of Table 6. The difference between methods 5, 6, and 7 of Table 6 is found in the criteria and the method chosen for solution. These methods along with solutions will be discussed briefly below for the continuous-time formulation with noise covariance assumed to be known.

Maximum Likelihood (ML). The ML estimate of the unknown derivatives is obtained by maximizing the conditional probability density of  $\underline{z}$  given  $\underline{x}_p$  and is obtained by

$$\text{Max}_{\underline{x}_p} p(\underline{z}/\underline{x}_p) \quad (30)$$

This problem reduces to the equivalent formulation below and is discussed in Reference 13 for the continuous case and Reference 14 for the discrete case.

Determine the parameters  $\underline{x}_p$  that minimize

$$J = 1/2 \int_{t_0}^{t_f} (\underline{z} - \underline{H}\underline{x})^T \underline{R}^{-1} (\underline{z} - \underline{H}\underline{x}) dt \quad (31)$$

Subject to the Kalman filter equations

$$\dot{\underline{K}} = \underline{P}\underline{R}^{-1}\underline{H}^T \quad (32)$$

$$\dot{\underline{x}} = \underline{A}\underline{x} + \underline{B}\underline{u} + \underline{K}(\underline{z} - \underline{H}\underline{x}) \quad (33)$$

$$\dot{\underline{P}} = \underline{A}\underline{P} + \underline{P}\underline{A}^T + \underline{Q} - \underline{P}\underline{H}^T \underline{R}^{-1} \underline{H}\underline{P} \quad (34)$$

This optimization problem is simplified by assuming that the covariance equation (34) rapidly reaches a steady value and thus is removed from the formulation. The problem now becomes that of minimizing equation (31) with respect to the parameters  $\underline{x}_p$  and  $\underline{K}$  (Kalman gain), subject to constraint equation (33).

This simplified problem can then be solved using a quasi-linearization or suitable computational algorithm. This approach requires that the Kalman gain has reached steady value. Unstable systems may violate this assumption, so the covariance

equations must be included as additional constraints in the optimization problem. Since most rotorcraft are unstable without automatic flight control systems, the optimization problem must include the covariance constraint equations. This is computationally prohibitive for large derivative models, such as rotorcraft.

Maximum A Posteriori Parameter Estimation (MAP - parameter). The MAP-parameter estimate of the unknown derivatives is obtained by maximizing the conditional probability density of  $\underline{x}_p$  given  $\underline{z}$  and is obtained by:

$$\text{Max}_{\underline{x}_p} p(\underline{x}_p/\underline{z}) \quad (35)$$

This criterion is related to the ML criterion by Bayes' rule:

$$p(\underline{x}_p/\underline{z}) = p(\underline{z}/\underline{x}_p) p(\underline{x}_p)/p(\underline{z}) \quad (36)$$

This changes the criterion by adding the term

$$1/2(\underline{x}_p(t_0) - \underline{\bar{x}}_p)^T P_p^{-1} (\underline{x}_p(t_0) - \underline{\bar{x}}_p) \quad (37)$$

to the performance index of equation (31). The criteria now includes a priori estimates of the parameters  $\underline{x}_p$  and variance in the estimate of the parameters  $P_p$ . The constraint equations remain the same, and a similar computational technique is required for a solution.

Maximum A Posteriori State Estimation (MAP - state). The MAP-state estimate of the unknown parameters is obtained by treating the parameters as state variables and maximizing the conditional probability density of  $\underline{x}$  and  $\underline{x}_p$  given  $\underline{z}$ . This is expressed in equation (38).

$$\text{Max}_{\underline{x}, \underline{x}_p} p(\underline{x}, \underline{x}_p/\underline{z}) \quad (38)$$

Using Bayes' rule this is written as

$$\text{Max}_{\underline{x}, \underline{x}_p} p(\underline{z}/\underline{x}, \underline{x}_p) p(\underline{x}, \underline{x}_p)/p(\underline{z}) \quad (39)$$

This criterion is shown in Reference 15 to reduce to an equivalent optimization problem as follows.

Determine the initial conditions  $\underline{x}_p(t_0)$ ,  $\underline{x}(t_0)$  and process noise  $\underline{w}(t)$  that minimize the quadratic performance criteria

$$\begin{aligned} J = & 1/2 \int_{t_0}^{t_f} (\underline{z} - H\underline{x})^T R^{-1} (\underline{z} - H\underline{x}) dt + 1/2 \int_{t_0}^{t_f} \underline{w}^T Q^{-1} \underline{w} dt \\ & + 1/2 (\underline{x}(t_0) - \underline{\bar{x}}_0)^T P_0^{-1} (\underline{x}(t_0) - \underline{\bar{x}}_0) \\ & + 1/2 (\underline{x}_p(t_0) - \underline{\bar{x}}_p)^T P_p^{-1} (\underline{x}_p(t_0) - \underline{\bar{x}}_p) \end{aligned} \quad (40)$$

subject to the differential constraint equation

$$\dot{\underline{x}} = A\underline{x} + B\underline{u} + \underline{w} \quad (41)$$

The resulting solution for  $\underline{x}_p(t_0)$  represents the MAP-state estimate of the unknown parameters.

The solution to the formulation given in equations (40) and (41) is obtained by first obtaining the necessary equations that minimize equation (40), using the maximum principle or taking first variations. The necessary conditions result in a two-point boundary value problem that can be solved by the invariant imbedding technique (Reference 15) or by assuming a solution  $\underline{x} = \underline{\hat{x}} - P\underline{\lambda}$  as is done in Reference 1. The resulting recursive solution is approximate and requires a reasonably good a priori derivative estimate to assure that the linearizations made to obtain the solutions are valid.

The recursive solution reduces to the extended Kalman filter if the measurement equations are linearized. The extended Kalman filter solution has a similar structure to the solution obtained for the ML method. The extended Kalman filter solution is given in equations (42) through (46):

$$\dot{\underline{\hat{x}}} = A\underline{\hat{x}} + B\underline{u} + PH^T R^{-1} (\underline{z} - H\underline{\hat{x}}) \quad (42)$$

$$\dot{\underline{\hat{x}}}_p = P_{p1} H^T R^{-1} (\underline{z} - H\underline{\hat{x}}) \quad (43)$$

$$\dot{P} = AP + PA^T - PH^T R^{-1} HP + Q + A_p P_{p1} + (A_p P_{p1})^T \quad (44)$$

$$\dot{P}_{p1} = P_{p1} A^T + P_{pp} A_p^T - P_{p1} H^T R^{-1} HP \quad (45)$$

$$\dot{P}_{pp} = -P_{p1} H^T R^{-1} H P_{p1}^T \quad (46)$$

where  $A = \frac{\partial f}{\partial \underline{x}}$ ,  $A_p = \frac{\partial f}{\partial \underline{x}_p}$  and  $H = \frac{\partial h}{\partial \underline{x}}$  represent linearizations about the current state  $\underline{\hat{x}}$  and parameter estimate,  $\underline{\hat{x}}_p$ .

Equations (42) and (43) provide estimates of the state and parameter vector, respectively, while equations (44) and (46) give the covariance for the state and parameter, respectively. Equation (45) yields the cross covariance between the state and parameters.

The similarity between the ML solution and the MAP-state solution is seen by comparing equation (33) with equation (42) and equation (34) with equation (44). In the ML method, the solution is obtained by a Kalman filter. The parameters and Kalman gain are iterated to minimize the performance index of equation (31). In the MAP-state method, the parameters and state are obtained recursively with a Kalman filter for the state and parameters.

The ML performance index of equation (31) with constraint equations (32), (33), and (34) can be shown to be similar to the MAP-state performance index of equation (40) with constraint equation (41). This relationship is shown in Reference 13.

#### Practical Considerations in Using the Extended Kalman Filter

Two methods are used for derivative identification in this paper: a least squares method and the extended Kalman filter. Before application of these methods, the data must be processed to remove high-frequency signals and bias errors. In addition, the measurement noise should be minimized when using the least squares method, since measurement noise results in biased estimates. These and other considerations are discussed below along with the overall method used to obtain derivatives from helicopter flight data.

Identification of derivatives. The overall flow diagram of the method used for derivative identification in this paper is shown in Figure 12. Several maneuvers about a specified trim are used in the identification to assure that sufficient data are used in the process. The derivatives are identified to yield the best array that simultaneously matches the independent maneuvers. This approach modifies the performance criteria of equation (40) to read

$$J = \sum_{i=1}^{NM} \left\{ \frac{1}{2} \int_{t_0}^{t_f} (\underline{z} - H\underline{x})^T R^{-1} (\underline{z} - H\underline{x}) dt + \frac{1}{2} \int_{t_0}^{t_f} \underline{w}^T Q^{-1} \underline{w} dt + \frac{1}{2} (\underline{x}(t_0) - \underline{\hat{x}}_0)^T P_0^{-1} (\underline{x}(t_0) - \underline{\hat{x}}_0) + \frac{1}{2} (\underline{x}_p(t_0) - \underline{\hat{x}}_p)^T P_p^{-1} (\underline{x}_p(t_0) - \underline{\hat{x}}_p) \right\} \quad (47)$$

Where the summation is from 1 to NM maneuvers. Solution of this problem requires slight modification in the solution given in equations (42) through (46) and is presented in References 1 and 16. This approach couples the maneuvers and is similar to ensemble averaging.

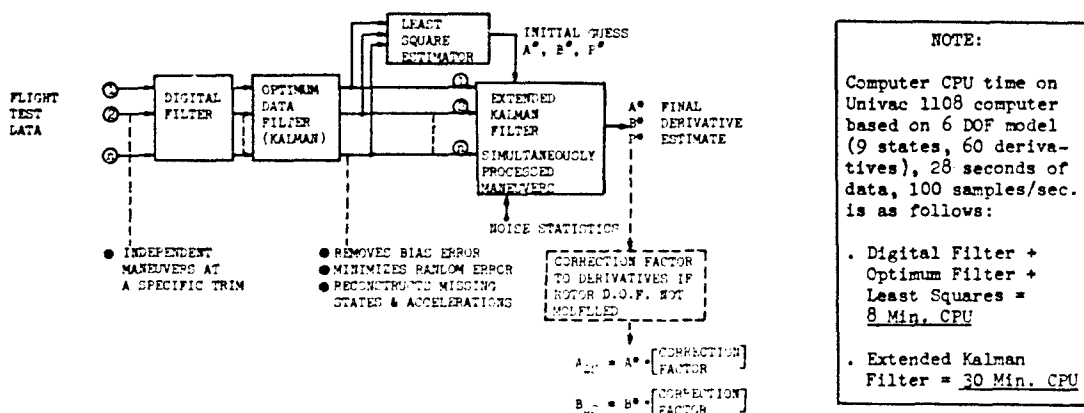


Figure 12. Overall Method Used to Identify 6-DOF Derivatives From Flight Test Data.

As shown in Figure 12, the data are first passed through a digital filter to remove high-frequency contamination. (Helicopter flight data are contaminated with frequencies of large magnitudes at 1 per rev intervals and at all modes of vibration.) The digital filter suppresses this high frequency contamination without introducing phase shift in the data. A Martin-Graham filter described in Reference 10 is used for the digital filter.

The data are then processed with a Kalman filter, which (1) removes bias error in the data, (2) minimizes errors in the state variables, and (3) reproduces state variables and accelerations that are not available. The equations used in the Kalman filter are the known Euler equations and inertial terms in the general rigid-body equations of motion. The equations used are presented in Reference 16 and consist of 22 state variables (15 state variables are the biases to be determined) and 15 measurements. The equations do not include any of the aerodynamic derivatives.

The data are then used with the least squares method, and the derivatives are identified. The identified derivatives are used as a priori estimates for the multi-maneuver extended Kalman filter. The number of state variables for the extended Kalman filter will depend on the number of maneuvers used and the model size chosen.

An extensive study is described in Reference 16 which examined various filters and methods for the a priori estimate for use with the extended Kalman filter. The results of this study will be discussed in a subsequent section.

In a previous section, the modeling requirements for helicopter derivative identification were discussed. It was found that considerable errors in the identified derivatives result if the rotor degrees of freedom are not modeled as independent degrees of freedom. If the derivative model contains only the rigid-body degrees of freedom, a correction factor is required to convert the identified derivatives to the quasi-static values. The identification of derivatives from helicopter flight data in this paper is conducted with a 6-DOF rigid-body model and thus requires a correction factor, which is indicated in Figure 12. Results using this correction factor will be discussed in the flight data identification section.

Evaluating the flight identified derivatives. Once the derivatives have been identified, the standard procedure for assessing their accuracy is to simulate the derivative model with the flight data inputs and compare the time history response with the flight data. Helicopters generally have unstable longitudinal characteristic roots, so a derivative model identified with perfect accuracy will diverge from the flight data, due to small errors in initial conditions, modeling terms, or wind disturbances. Therefore, when testing the accuracy of identified derivatives, only short data segments (typically 4 to 6 secs) can be used with confidence. In addition data not used in the identification should be used for comparison, since comparing against data used in the identification is not a conclusive test.

An alternative method is available for comparing time history data that do not diverge with an unstable model. This is done by multiplying each of the measured state variables and inputs by the appropriate derivative and summing the result. The resulting reconstructed acceleration can be compared directly with the flight measured acceleration. This approach also has the advantage of allowing assessment of the individual contributions of each derivative and provides a measure of whether sufficient signal-to-noise ratio exists to identify each derivative accurately.

Flight test methods have been used in the past to isolate certain of the control derivatives or characteristic roots. For example, the Dutch roll mode can be obtained by visual inspection of test data from most helicopters by using the pitch stability augmentation to stabilize the instability in pitch and exciting the Dutch roll with a small spike input in the pedals or lateral cyclic input. Also pulse inputs cause acceleration changes and the ratio of acceleration change to pulse input can be used to estimate the control derivatives. These and other specialized testing procedures can be used as checks on the accuracy of the system identified derivatives.

#### APPLICATIONS TO FLIGHT DATA

The method described in the previous sections and shown in Figure 12 was applied to the following rotorcraft: (1) CH-53A, (2) CH-54B, and (3) a coaxial hingeless rotor helicopter. In addition, the effects of different data filters and a priori derivative estimates were examined to assess their impact on the identified derivatives, using the least squares method and the extended Kalman filter. The detailed investigations for some of these studies are documented in References 2, 16, and 17, and the results are summarized herein. All these studies use a 6-DOF derivative model in the identification. The actual form of the model used is given in Reference 16. As indicated in Figure 12, a correction factor is required to correct for absence of rotor degrees of freedom in the model.

##### Application to CH-53A

The CH-53A is a 6-bladed articulated rotor helicopter. The flight test data from the CH-53A were obtained from a handling qualities flight test program conducted for the U. S. Navy by Sikorsky Aircraft. The test data selected were from an aft center-of-gravity condition, 35000-lb aircraft at 100 knots trim airspeed. The data consist of time history responses to pulsed control inputs. Six maneuvers of 6 seconds duration sampled 100 times a second were used in this study. Four maneuvers were used in the identification process, and two maneuvers were selected to assess the ability of the identified derivative model to predict data not used in the identification.

Effects of different data filters on identified derivatives. Three filters were investigated to determine their effects when used with both the least squares and extended Kalman filter derivative estimators: (1) a first-order low pass filter with cutoff frequency of 10 Hz, (2) a Martin-Graham digital filter with cutoff frequency of

3.0 Hz and termination frequency of 4.9 Hz, and (3) an optimum data filter (extended Kalman filter) with data processed first by the digital filter. The third filter is the one described in Figure 12 and is the method found to be most accurate. The criterion used to determine the most accurate filter is as follows. Time histories were generated from each of the identified derivative arrays and compared with the four maneuvers of flight test data used in the identification and with the two maneuvers not used in the identification. The root mean square (RMS) error between the test data and derivative model time histories for all state variables and accelerations were computed, and the total RMS error (RMS summation of all states and accelerations) was computed for each maneuver. The total RMS errors for the four maneuvers used in the identification and the total RMS errors for the two maneuvers not used in the identification were computed. The above total RMS errors for each filter were compared, and the filtering method that yielded the smallest RMS error was considered to be the most accurate.

The results of the three filters using the least squares derivative estimator

Raw Data Filter	RMS Error* in Test Data and Time Histories From Identified Derivative Model	
	Maneuvers 1, 2, 3, 4 (Used in the Identification)	Maneuvers 5, 6 (Not used in the Identification)
First Order	47.3	70.6
Digital	29.3	34.0
Kalman	19.2	19.4

\* Total RMS error obtained for all channels for the maneuvers shown

Table 7. Results of Filtering on RMS Error Time History Match for the Least Square Identified Derivative Model.

Raw Data Filter	RMS Error* in Test Data and Time Histories From Identified Derivative Model	
	Maneuvers 1, 2, 3, 4 (Used in the Identification)	Maneuvers 5, 6 (Not used in the Identification)
First Order	19.4	27.8
Digital	20.1	19.8
Kalman	18.9	19.9

\* Total RMS error obtained for all channels for the maneuvers shown

Table 8. Results of Filtering on RMS Error Time History Match for the Extended Kalman Filter Identified Derivative Model.

contamination, and the improvement in RMS error over the low-pass filter is significant for both the least squares and extended Kalman filter identification method. Thus, flight data should be filtered to remove high-frequency contamination regardless of the identification method used.

A significant finding from this study is that the least squares method used with the Kalman data filter yields an RMS error nearly as accurate as the extended Kalman filter derivative identification method. This is important, since the least squares method used with the Kalman data filter is computationally more efficient than the extended Kalman filter derivative identification method. Also, the least square method is practical for identification problems with large derivative arrays, whereas the extended Kalman filter becomes increasingly more inefficient.

Table 9 compares the lateral directional derivatives for the least squares method and extended Kalman filter method of derivative identification. Both methods used the Kalman data filter. Also shown in Table 9 are the derivative values obtained from a nonlinear analytic computer program. For the most part, the derivatives from the least squares method and extended Kalman filter method are comparable, with neither showing better accuracy. The analytic derivatives show good correlation for some

are shown in Table 7, and the results using the extended Kalman filter are shown in Table 8. Table 7 shows the improvement in RMS error when using the Kalman filter for the least squares derivative identification method. The data used in the identification process and the data not used in the identification process have the smallest RMS error when the Kalman technique for filtering data is used. This is as expected, since the Kalman filter provides the best estimates of the state variables of the three filtering methods. Since the least square method yields biased derivatives when measurement noise is present, the filtering method that gives the most accurate state variable estimate should perform best.

Table 8 gives results of using the extended Kalman filter derivative estimation method. Again, the data filter yielding the best results is the Kalman filter, but the digital filter results in an RMS error nearly as good as the Kalman filter. This is as expected, since this derivative estimator is formulated to include measurement noise.

The digital and Kalman filter both remove high frequency

derivatives and poor correlation for others. The longitudinal derivatives were found to show poor correlation for many important derivatives. This was also found to be true with the computer model studies discussed earlier. The lateral directional derivatives generally are identified more accurately, so a meaningful comparison such as in Table 9 can be made.

Derivative	Units	Least Squares Method	Extended Kalman Filter Method	Analytic Prediction (Quasi-Static)
$L_v$	1/sec	-.0052	-.0051	-.023
$L_p$	1/sec	-.1855	-.155	-1.59
$L_r$	1/sec	1.74	1.32	-1.02
$L_{\dot{\delta}_a}$	1/sec	.862	.79	.395
$L_{\dot{\delta}_a}$	1/sec <sup>2</sup> -deg	.199	.214	.390
$L_{\dot{\delta}_r}$	1/sec <sup>2</sup> -deg	.084	.069	.067
$N_v$	1/ft-sec	.0040	.0049	.0072
$N_p$	1/sec	-.786	-.756	-.742
$N_r$	1/sec	-.041	-.110	-.085
$N_{\dot{\delta}_a}$	1/sec <sup>2</sup> -deg	-.097	-.095	-.0895
$Y_v$	1/sec	.0029	-.047	-.081
$Y_p$	ft/sec	20.8	20.46	9.22
$Y_{\dot{\delta}_a}$	ft/sec <sup>2</sup> -deg	.642	.559	.614

\* Flight data was first filtered with the Kalman data filter.

Table 9. Comparison of the Lateral Directional Derivatives Identified from Flight Data Using the Least Squares and Extended Kalman Filter Methods. Derivatives from Analytic Prediction Also Shown. (CH-53A, 100 kts, 35000 lbs.)

Effect of a priori derivative guess on extended Kalman filter. The least squares derivatives and an arbitrary derivative guess were both used to initialize the extended Kalman filter derivative identification method. The arbitrary guess consists of setting all derivatives to zero, except for some of the control derivatives that could easily be estimated from the flight data. The derivative values for the arbitrary guess are given in Reference 16. Both the digital filter and Kalman data filter were used. The RMS errors between the identified derivative model time histories and flight data are presented in Table 10. The RMS errors are shown to be slightly improved when using the least squares a priori derivative guess.

Raw Data Filter	Initial Derivative Guess	RMS Error* in Test Data and Time Histories from Identified Derivative Model	
		Maneuvers 1, 2, 3, 4 (Used in the Identification)	Maneuvers 5, 6 (Not Used in the Identification)
Digital	Arbitrary	20.1	19.8
Digital	Least Square	16.0	17.8
Kalman	Arbitrary	18.9	19.9
Kalman	Least Square	17.8	19.7

\* Total RMS error obtained for all channels for the maneuvers shown.

\*\* Kalman data filter was used with the Least Square method.

Table 10. Results of A Priori Derivative Estimate on RMS Error Time History Match Using the Extended Kalman Filter.

#### Correction of Derivatives to Quasi-Static Values

The derivative model identified from flight data did not include separate degrees of freedom to represent the rotor. Thus, it is necessary to convert the identified 6-DOF derivatives to quasi-static values, as discussed in a previous section.

Table 11 shows the flight identified derivatives both with and without the correction, along with the analytic model quasi-static derivatives. Table 11 shows that the correction factor yields flight identified derivatives more representative of analytic prediction. This is particularly true for the lateral directional derivatives. The longitudinal derivatives are poorly represented. This was also true for the computer model studies examined previously.

Longitudinal Derivatives	Analytic Prediction (Quasi-Static)	Flight Identified (Corrected to Quasi-Static)	Flight Identified (Uncorrected)	Lateral Directional Derivatives	Analytic Prediction (Quasi-Static)	Flight Identified (Corrected to Quasi-Static)	Flight Identified (Uncorrected)
$M_u$	.0064	-.0010	.0001	$L_v$	-.0013	-.0021	-.0010
$M_q$	-.579	-.176	.006	$L_p$	-1.59	-1.11	-.887
$M_w$	.0017	-.0013	.0009	$L_r$	-1.08	-1.55	1.29
$N_u$	.010	-.011	-.115	$L_{\dot{r}}$	.395	.227	.406
$N_{\dot{w}}$	-.094	-.041	-.0391	$L_{A\dot{w}}$	.390	.130	.2231
$M_{\dot{w}}$	.0747	.055	.0407	$L_{\dot{w}}$	.0000	.0000	.0734
$Z_u$	-.080	-.093	-.390	$N_v$	.0070	.0044	.0044
$Z_w$	-.117	.009	.099	$N_r$	-.742	-1.11	-.876
$Z_{\dot{w}}$	-7.14	-4.16	-5.090	$N_p$	-.005	-	-.000
$X_u$	-.0458	-.006	-.108	$N_{\dot{r}}$	-.0090	-.0001	-.0000
$X_w$	.074	-.035	-.054	$Y_v$	-.081	-.157	-.106
$X_p$	-1.07	-6.9	-5.856	$Y_p$	.0000	.0000	.0000
$X_{\dot{w}}$	.000	.000	.0000	$Y_{A\dot{w}}$	.000	.000	.0000

Table 11. Comparison of Analytically Predicted Derivatives, Flight Identified (Corrected to Quasi-Static) and Flight Identified (Uncorrected) (CH-53A, 100 kts).

The 6-DOF flight identification is consistent with the identification results found from the nonlinear computer studies. That is, the 6-DOF identified derivatives are only approximations of quasi-static derivatives. The degree of accuracy is unknown and difficult to assess by time history match, because the 6-DOF model is approximate and the system is unstable. The correction factor used on the flight-identified derivatives provides corrected flight identified derivatives that are better approximations of the flight vehicle quasi-static derivatives than are the corresponding computer identified derivatives of the computer quasi-static derivatives.

#### Time History Comparisons and Characteristic Roots

The flight identified derivative model was simulated with the inputs used to generate the actual flight test data. This was done for all six maneuvers. The complete results can be found in Reference 16, and several of the comparisons are shown in Figures 13a and 13b. Many of the time histories matched well, but others provided a poor match to the flight data. The effect of the blade degree of freedom is clearly seen in the acceleration data.

The pitch attitude and longitudinal and vertical velocity comparisons shown in Figure 13a provide a reasonably good match, yet the longitudinal derivatives were known to be in error. This demonstrates that the derivative accuracy of a 6-DOF model cannot be assessed by comparing time history data. Time history match with test data will only be meaningful if all the significant modes of a rotorcraft are included in the model. This fact explains why rotorcraft model investigations and computer model identification must be conducted. Comparisons for a maneuver that was not used in the identification are shown in Figure 13b. The acceleration data shown in Figure 13b also show the high frequency rotor degrees of freedom.

The characteristic roots of the flight identified derivatives and the analytic model roots are presented in Figure 14. The characteristic root locations are shown to be in good agreement for low frequency roots, even though the longitudinal derivatives are considerably different. Roots are also presented in Figure 15 for results of identification at 150 knots. The Dutch roll mode is known to be unstable at this condition. The flight identified roots correctly predict this, but the analytic model roots are in error.



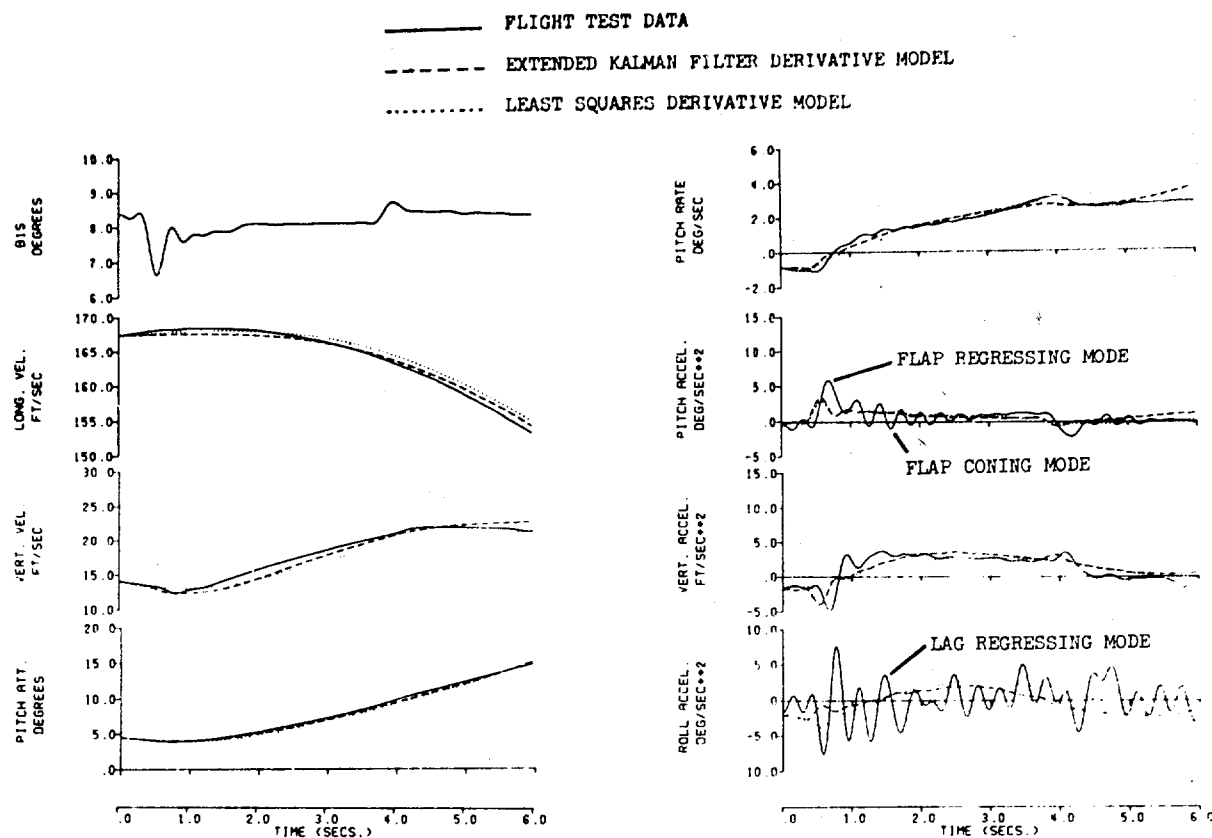


Figure 13a. Time History Comparison of 6-DOF Identified Derivative Models vs. Flight Test Data Used in the Identification. (Longitudinal Cyclic Input, CH-53A, 100 kts)

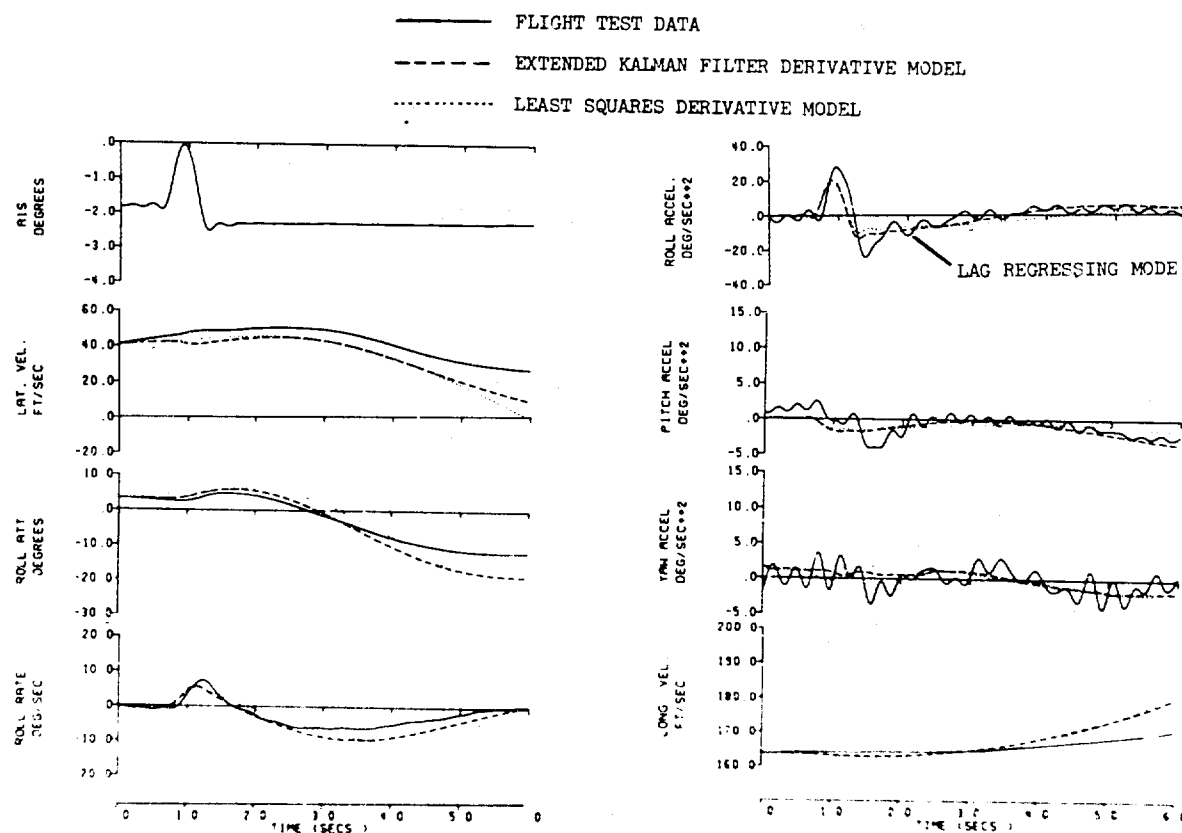


Figure 13b. Time History Comparison of 6-DOF Identified Derivative Models vs. Flight Test Data Not Used in the Identification. (Lateral Cyclic Input, CH-53A, 100 kts)

■ FLIGHT TEST DATA (6 DOF IDENTIFIED)  
○ THEORY (9 DOF IDENTIFIED)

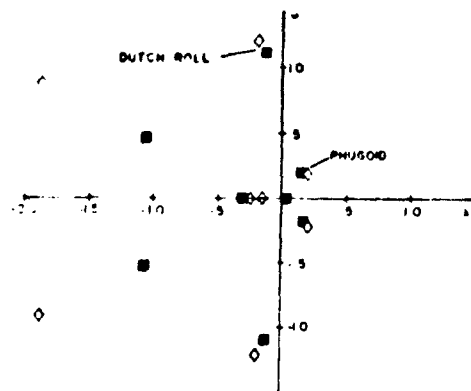


Figure 14. Characteristic Roots Identified from Flight Data by the Kalman Filter Method vs. Analytic Model Roots (CH-53A, 100 kts, AFCS Off).

■ FLIGHT TEST DATA (6 DOF IDENTIFIED)  
○ THEORY (9 DOF IDENTIFIED)

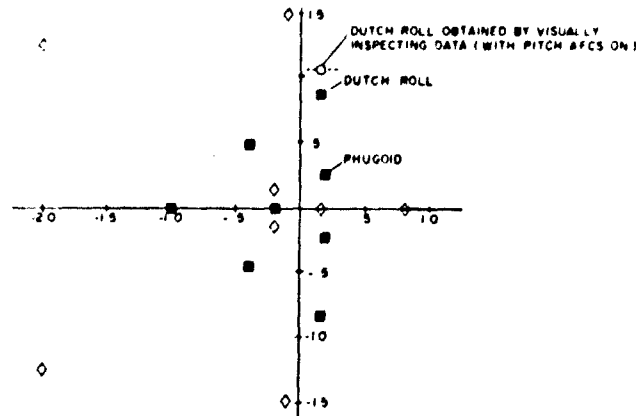


Figure 15. Characteristic Roots Identified from Flight Data by the Kalman Filter Method vs. Analytic Model Roots (CH-53A, 150 kts, AFCS Off).

#### Further Applications

The 6-DOF identification method of Figure 12 was also applied to a CH-54B at 45 knots airspeed and the ABC coaxial hingeless rotor helicopter. The CH-54B resulted in similar conclusions regarding 6-DOF modeling.

Application to the ABC resulted in several different conclusions. The flight data used for the ABC identification were taken at 25 knots. At this condition, the motion of hingeless rotor helicopters is generally dominated by several static derivatives. In particular, the derivatives  $M_{\dot{\eta}}$  and  $M_{\dot{\omega}}$  contribute to much of the motion in pitch. The data used consisted of many low-frequency control inputs, so the time history response was accurately represented by a rigid body model. This fact allows accurate identification of many of the static derivatives. The conclusion reached from this study is that a 6-DOF model is more accurately identified from flight data if low frequencies dominate the response. This is as expected, since the rigid body model is accurate only for low-frequency motion.

#### CONCLUSIONS

A general procedure has been presented for systematic development of rotorcraft models with articulated or hingeless rotors for use in systems identification. It was demonstrated that many approximate models which include the rotor and fuselage degrees of freedom can be developed for use in systems identification. In general, the simple models are dimensionally smaller, but result in identified derivatives with less accuracy. It was shown that the least squares identification method used on a nonlinear simulation is valuable in determining the number of rotor degrees of freedom that should be included in the model. A nonlinear computer simulation of an articulated rotor helicopter with 6 fuselage DOF, 6 blades with flapping DOF, and uniform first-order inflow dynamics was used to examine the accuracy attainable for a 6-DOF and 9-DOF linear identified derivative model. The results show that the 9-DOF model with 6 fuselage and 3 rotor degrees of freedom yield more than 50% of the identified derivatives to within 10% of the true value. The 6-DOF fuselage model results in considerable errors for many of the identified derivatives. The 6-DOF lateral directional derivatives were found to be more accurate than the longitudinal derivatives, with 40% of the lateral derivatives within 10% of the true value. These results demonstrate the importance of selecting an accurate model for use in identification.

An alternative model that may provide acceptable derivative accuracy is the first-order rotor representation for blade flap and lag developed in this paper. The approximations used to develop this model were shown, and the derivative accuracy attainable with this model needs further examination. Identification without lag DOF in the model will result in further errors in identified derivatives. Thus, further studies of the accuracy attainable for the various approximate models developed in this paper should be conducted using a nonlinear computer simulation. The nonlinear model should include at least blade flap and lag and first-order air mass dynamics.

The normal mode representation for hingeless rotor systems was shown to reduce to the same model structure as articulated rotor systems. An examination is required of the accuracy attainable using the normal mode formulation. The least squares method used with a nonlinear rotorcraft simulation should be used to assess this approximation.

The advanced statistical methods applicable to rotorcraft identification include the (1) maximum likelihood, (2) maximum a posteriori - parameter, and (3) maximum a posteriori - state estimation methods. The criterion for these three methods for the continuous formulation is similar: the primary difference is in the algorithm selected for solution. The many degrees of freedom (8 to 12) required in rotorcraft identification make computation efficiency a primary concern. The two-stage method of simple flight test experiments to determine the rotor model, followed by a standard identification, can considerably reduce the computational requirements, thus permitting use of the advanced statistical methods.

Six-DOF identification from flight test data confirms the results of computer model studies. The lateral directional derivatives were clearly superior in accuracy to the longitudinal. The correction factor applied to the 6-DOF flight identified derivatives to account for absence of the rotor DOF was shown to improve accuracy further.

Six-DOF flight identification may provide models acceptable for simulation purposes, but the accuracy is generally not good enough for correlation. The flight identified characteristic roots were found to be accurate for the low frequency modes, even with derivatives of questionable accuracy.

The least squares (LS) method used with the optimum data filter resulted in flight identified derivatives of nearly the same quality as the extended Kalman filter. This conclusion may not hold for higher measurement noise levels typical at higher airspeeds. The computational simplicity of the LS method, combined with a simple optimum filter, makes this approach worthy of consideration in problems with large derivative arrays.

Rotorcraft modeling, identification algorithms, and flight test applications with correlation have been addressed. Continued applications using the approximate models developed and procedures presented in this paper are necessary before derivatives of the required accuracy can be identified from rotorcraft flight test data.

#### REFERENCES

1. Molusis, J. A.: "Helicopter Stability Derivative Extraction and Data Processing Using Kalman Filtering Techniques," presented at the 28th Annual National Forum of the American Helicopter Society, Washington D. C., Preprint No. 641, May 1972.
2. Molusis, J. and Briczinski S.: "Helicopter Derivative Identification from Analytic Models and Flight Test Data," presented at a symposium held at Flight Research Center Edwards, California, entitled Parameter Estimation Techniques and Applications in Aircraft Flight Testing, April 24-25, 1973. (NASA TN D-7647 pp 175-186, April 1974).
3. Hohenemser, K.: "Dynamic Stability of a Helicopter with Hinged Rotor Blades," September 1939, NACA TM No. 907, p. 2.
4. Curtiss, H. C. Jr. and Shupe N. K.: "A Stability and Control Theory for Hingeless Rotors," presented at the 27th Annual National Forum of the American Helicopter Society, Washington, D. C., May 1971.
5. Hohenemser, K. H., and Yin, S. H.: "On the Question of Adequate Hingeless Rotor Modeling in Flight Dynamics," presented at the 29th Annual National Forum of the American Helicopter Society, Washington, D. C., Preprint No. 732, May 1973.
6. Peters, D. A. and Hohenemser K. H.: "Application of the Floquet Transition Matrix to Problems of Lifting Rotor Stability," Journal of the American Helicopter Society, April, 1971, pp. 25-33.
7. Biggers, J. C.: "Some Approximations to the Flapping Stability of Helicopter Rotors," presented at the AHS/NASA-Ames Specialists' Meeting on Rotorcraft Dynamics, Feb. 13-15, 1974.
8. Hohenemser, K. H. and Yin, S. K.: "On the Use of First Order Rotor Dynamics in Multiblade Coordinates," presented at the 30th Annual National Forum of the American Helicopter Society, Washington, D. C., preprint No. 831, May 1974.
9. Huber, H.: "Parametric Trends & Optimization - Preliminary Selection of Configuration - Prototype Design & Manufacture," AGARD Lecture Series No. 63 on Helicopter Aerodynamics and Dynamics, March 1973.
10. Graham, R. J.: "Determination and Analysis of Numerical Smoothing Weights," NASA TR R-179, December 1963.
11. Davis, J. M., Bennett, R. L., and Blankenship, B. L.: "Rotorcraft Flight Simulation with Aeroelastic Rotor and Improved Aerodynamic Representation," USAAMRDL-TR-74-10A, Volume I, June 1974, pp. 3-22 to 3-25.
12. Briczinski, S. and Cooper, D.: "Flight Investigation of Rotor/Vehicle State Feedback," Final Report of NASA Contract NAS1-11563, to be published.

13. Reid, D. B.: "Optimal Inputs for System Identification," SUDAAR No. 440, May 1972.
14. Mehra, R. K., Stepner, D. B., and Tyler, J. S.: "A Generalized Method for the Identification of Aircraft Stability and Control Derivatives," JACC 1973, paper 16-3.
15. Sage, A. P. and Melsa, J. L., System Identification, Academic Press, New York and London, 1971.
16. Molusis, J. A.: "Analytical Study to Define a Helicopter Stability Derivative Extraction Method," NASA CR-132371-Vol. I and NASA CR-132372-Volume II, May 1973.
17. Molusis, J. A.: "Helicopter Stability Derivative Extraction from Flight Data Using the Bayesian Approach to Estimation," Journal of the American Helicopter Society, 1973.

## NOTATION

$A, A_{ij}$	Matrix of stability derivatives, subscripts $ij$ indicate partitioned matrix
$A^*, A^*$	Initial and final stability derivative matrices respectively (Fig. 12)
$A_p$	Matrix used in the extended Kalman filter formulation, $A_p = \frac{\partial f}{\partial x_p}$
$A_{QS}$	Quasi-static stability derivative matrix defined in Eq. 5 of Table 1
$A_{1S}$	Rotor lateral cyclic pitch control input, positive for right stick deflection, degrees (scalar)
$a_{ij}$	Elements of the rotor stability derivative matrix $A_{22}$ (Table 2)
$a_{OS}, a_{1S}$	Coning and cosine component of first harmonic flapping respectively w.r.t. shaft axis, radians
$B, B_1, B_2$	Matrix of control derivatives, subscripts 1 and 2 indicate partitioned matrix
$B^*, B^*$	Initial and final control derivative matrices respectively (Fig. 12)
$B_{QS}$	Quasi-static control derivative matrix defined in Eq. 5 of Table 1
$B_{1S}$	Rotor longitudinal cyclic pitch control input, positive for forward stick deflection, degrees (scalar)
$b_{1S}$	Sine component of first harmonic flapping w.r.t. shaft axis, radians
$F_{ij}(t)$	Periodic coefficient stability derivative matrices appearing in linearized rotorcraft equations of motion, $t$ denotes periodicity (Eq. 4)
$F_n()$	Generalized forces appearing in elastic blade solution for $n$ th mode response (scalar)
$f, f_1, f_2$	Nonlinear vector equations of motion relating state vector and control inputs to the time derivative of the state, subscripts 1 and 2 indicate the fuselage and rotor respectively.
$G_1(t), G_2(t)$	Periodic coefficient control derivative matrices appearing in linearized rotorcraft equations of motion, $t$ denotes periodicity (Eq. 4)
$h(x)$	Nonlinear vector equations relating the measurements to the state vector (Eq. 27)
$H, H_1, H_2$	Matrix relating measurements and state vector, subscripts 1 and 2 indicate the fuselage and rotor respectively
$H_2(\theta_R, t)$	Matrix transforming the inplane/out of plane bending moments in the shaft axis to blade bending moments
$I_n$	Generalized inertia associated with the $n$ th mode of a rotor blade (scalar)
$I_{BM}(r_1, t), I_{BM_n}(r_1)$	Inplane bending moment and load coefficient respectively at blade radial station $r_1$ in the shaft axis (scalar)
$J$	Quadratic performance criteria (scalar)
$K$	Kalman gain matrix found in the Kalman filter equations

$L( )$	Normalized rolling moment derivative of the rigid body, $\partial \dot{p} / \partial ( )$ (scalar)
$M( )$	Normalized pitching moment derivative of the rigid body, $\partial \dot{q} / \partial ( )$ (scalar)
$M(r_1)$	Matrix of load coefficients associated with the blade bending moments in the shaft axis
$M_2$	Matrix of eigenvectors associated with the rotor degrees of freedom
$\text{Max}_{x_p} p(x_p/z)$	Implies maximization of the conditional probability density $p(x_p/z)$ w.r.t. $x_p$
$nm$	Number of modes used to represent the blade elastic response
$\underline{n}$	Random white gaussian measurement noise vector
$N( )$	Normalized yawing moment derivative of the rigid body, $\partial \dot{r} / \partial ( )$ (scalar)
$N_b$	Number of blades (scalar)
$NM$	Number of simultaneous maneuvers used to identify derivatives (scalar)
$p$	Body roll rate, radians/sec
$P, P_o$	Covariance of the error in the state vector estimate, subscript o denotes initial; $P = E((\underline{x} - \hat{\underline{x}})(\underline{x} - \hat{\underline{x}})^T)$ , where E denotes expected value
$P_{1p}$	Covariance of the state vector and parameter vector
$P_p, P_{p_o}$	Covariance of the error in the parameter vector estimate, subscript o denotes initial
$P^o, P^*$	Covariance in the initial and final derivative estimate (Fig. 12)
$p(x_p/z)$	Conditional probability density function of $x_p$ given $z$ (assumed gaussian)
$q$	Body pitch rate, radians/sec
$Q$	Process noise intensity matrix $Q = \Delta t \cdot E(\underline{w} \underline{w}^T)$
$r$	Body yaw rate, radians/sec
$r, r_1$	Blade radial station
$R$	Measurement noise intensity matrix $R = \Delta t \cdot E(\underline{n} \underline{n}^T)$
$t, t_o, t_f$	Time, initial time and final time respectively, secs
$T(t)$	Periodic coefficient matrix which transforms coordinates in the rotating axis to the nonrotating axis
$T_{BM}(r_1, t), T_{BM_n}(r_1)$	Torsional bending moment and load coefficient respectively at blade radial station $r_1$ in the shaft axis (scalar)
$u$	Longitudinal velocity in the body axis, positive forward, ft/sec
$\underline{u}$	Vector of control inputs
$v$	Lateral velocity in the body axis, positive to the right, ft/sec
$V_{BM}(r_1, t), V_{BM_n}(r_1)$	Vertical bending moment and load coefficient respectively at blade radial station $r_1$ in the shaft axis (scalar)
$w$	Vertical velocity in the body axis, positive down, ft/sec
$\underline{w}$	Random white gaussian process noise
$X( )$	Normalized longitudinal force derivative of the rigid body $\partial \dot{u} / \partial ( )$ (scalar)
$\underline{x}, \underline{x}_1, \underline{x}_2$	State vector of rotor and body variables, state vector of body variables, and state vector of rotor variables respectively in the nonrotating axis
$\underline{x}_2^R$	State vector of rotor variables in the rotating axis

$\underline{x}_p$	State vector of parameters which include stability and control derivatives
$\underline{x}_0, \underline{x}_p$	Initial estimate in the state and parameter vector respectively
$\underline{x}(t_0), \underline{x}_p(t_0)$	Initial value of the state and parameter vector respectively
$\hat{\underline{x}}, \hat{\underline{x}}_p$	Current estimate of the state and parameter vector as given by the Kalman filter
$\underline{x}_2^R(r, t)$	State vector of rotating coordinates as a function of blade radial station $r$
$\underline{y}_2$	State vector of normal coordinates for the rotor state variables
$y(r, t), y_n(r)$	Inplane blade deflection and mode shapes respectively as a function of blade radial station $r$ in the shaft axis
$\underline{y}(\ )$	Normalized lateral force derivative of the rigid body, $\partial \dot{y} / \partial (\ )$
$\underline{z}, \underline{z}_1, \underline{z}_2^R$	Vector of fuselage and rotating state measurements, vector of fuselage state measurements, and vector of rotating state measurements respectively.
$z(r, t), z_n(r)$	Vertical blade deflection and mode shapes respectively as a function of blade radial station $r$ in the shaft axis
$\underline{z}_2^R(r_1, t)$	Measurement vector of blade bending moments at radial station $r_1$ in the blade axis
$\underline{z}(\ )$	Normalized vertical force derivative of the rigid body, $\partial \dot{z} / \partial (\ )$ (scalar)
$\beta_i$	Rotor blade flapping of $i$ th blade in the rotating axis, radians
$\beta_0, \beta_d$	Coning and differential coning coordinates respectively in the nonrotating axis, radians
$\beta_{nc}, \beta_{ns}$	Cosine and sine coordinates respectively in the nonrotating axis for the $n$ th harmonic, radians
$\Delta(\ )$	Indicates a perturbation of quantity in parenthesis
$\delta_n$	Generalized coordinate associated with the $n$ th mode shape of an elastic blade
$\zeta$	Blade lag angle in Figure 1 and damping ratio in Table 2
$\zeta_n$	Damping ratio associated with $n$ th mode shape
$\theta, \phi$	Fuselage pitch and roll attitude respectively in inertial axis, radian
$\theta(r, t), \theta_n(r)$	Torsional blade deflection and mode shapes respectively as a function of blade radial station $r$ in the shaft axis
$\theta_{TR}, \theta_T$	Tail rotor collective pitch angle, radians
$\theta_0, \theta_c$	Main rotor collective pitch angle, radians
$\theta_R$	Blade geometric pitch angle, radians
$\lambda, \sigma$	Real axis in the complex plane
$\underline{\lambda}$	Adjoint vector resulting from application of the maximum principle
$A_{ij}$	Matrices resulting when transforming state equations to normal form (Eq. 10)
$\phi_i$	Phase angle for each blade in the disk of the rotor, $\phi_i = \Omega t + \phi_i$ where $\phi_i$ represents the azimuthal angle of each blade, radians
$\mu$	Imaginary axis in the complex plane
$\omega_n$	Natural frequency associated with the $n$ th mode shape, rad/sec
$\omega_c / \Omega, \omega_s / \Omega$	Natural frequency of the inplane and flapping 1st blade mode respectively normalized by rotor rotational speed
$\Omega$	Rotor rotational speed, radians/sec (scalar)

## Special symbols.

$(\dot{\phantom{x}})$	Denotes time derivative, $\frac{d(\phantom{x})}{dt}$
$(\phantom{x})^{-1}$	Denotes matrix inversion
$(\phantom{x})^T$	Denotes matrix transpose
$(\hat{\phantom{x}})$	Denotes current Kalman filter estimate
$(\bar{\phantom{x}})$	A bar below a lower case variable denotes a vector and all upper case variables are matrices except where noted in the list of symbols
$\partial(\phantom{x})/\partial(\phantom{x})$	Denotes partial derivative of numerator w.r.t. denominator

ROTOR SYSTEMS RESEARCH AIRCRAFT (RSRA)  
REQUIREMENTS FOR, AND CONTRIBUTIONS TO, ROTORCRAFT STATE ESTIMATION  
AND PARAMETER IDENTIFICATION

by

Gregory W. Condon  
Langley Directorate  
U.S. Army Air Mobility R&D Laboratory  
NASA Langley Research Center  
Hampton, Virginia 23665

**SUMMARY**

The National Aeronautics and Space Administration and the United States Army have jointly contracted for the development of two Rotor Systems Research Aircraft (RSRA). These flight research vehicles are being designed specifically to provide the United States Government with the capabilities necessary for the effective and efficient in-flight test and verification of promising new rotor concepts and supporting technology developments. The research mission and unique features of the RSRA will require the new and expanded application of state estimation and parameter identification technology and will provide heretofore unavailable flight capabilities with which to expand the state of the art of the parameter identification technology. This paper will present the RSRA requirements for, and possible contributions to, rotorcraft state estimation and parameter identification technology. The intent of this paper is to engender the timely consideration of the RSRA in the current and future developments of this technology.

**SYMBOLS**

A, B, C, D, E, F	Transmission mounting reactive forces in the body axis system, lb
$a_{TX}, a_{TY}, a_{TZ}$	Inertial accelerations of the transmission in the body axis system, ft/sec <sup>2</sup>
$a_{WX}, a_{WY}, a_{WZ}$	Inertial accelerations of the wing in the body axis system, ft/sec <sup>2</sup>
$a_X, a_Y, a_Z$	Inertial accelerations of the body in the body axis system, ft/sec <sup>2</sup>
H, I, J, K, L, M	Wing mounting reactive forces in the body axis system, lb
$I_{TXX}, I_{TTY}, I_{TZZ}$	Transmission principal moments of inertia, slug-ft <sup>2</sup>
$I_{WXX}, I_{WYY}, I_{WZZ}$	Wing principal moments of inertia, slug-ft <sup>2</sup>
$i_T$	Transmission incidence with respect to the longitudinal body axis, radians
$i_W$	Wing incidence with respect to longitudinal body axis, radians
L, M, N	Body aerodynamic moments in the body axis system, ft-lb
$L_{IT}, M_{IT}, N_{IT}$	Transmission inertia moments in the body axis system, ft-lb
$L_{IW}, M_{IW}, N_{IW}$	Wing inertia moments in the wing principal axis system, ft-lb
$L_{IW}, M_{IW}, N_{IW}$	Wing inertia moments in the body axis system, ft-lb
$L_R, M_R, N_R$	Rotor moments at the hub in the body axis system, ft-lb
$L_W, M_W$	Wing aerodynamic moments at the wing pivot in the body axis system, ft-lb
$m_T$	Mass of the transmission, slugs
$m_W$	Mass of the wing, slugs
P, Q, R	Angular velocity components of the body expressed in the body axis system, rad/sec <sup>2</sup>
$Q_T$	Sum of the engine and tail rotor drive-shaft torques, ft-lb
V	Airspeed, knots
X, Y, Z	Body aerodynamic forces in the body axis system, lb
$X_{IT}, Y_{IT}, Z_{IT}$	Transmission inertia forces in the body axis system, lb
$X_{IW}, Y_{IW}, Z_{IW}$	Wing inertia forces in the body axis system, lb
$X_R, Y_R, Z_R$	Rotor forces at the hub in the body axis system, lb



$X_W, Z_W$	Wing aerodynamic forces at the wing pivot in the body axis system, lb
$x_t, y_t, z_t$	Rotor mounting geometry dimensions in the transmission principal axis system, ft
$x_W, z_W$	Distances from the wing pivot axis to the wing center of gravity in the wing principal axis system, ft
$x_1, y_1, z_1$	Wing mounting geometry dimensions in the wing principal axis system, ft
$z_R$	Distance from the rotor hub to the transmission center of gravity along the shaft, ft
$\alpha$	Fuselage angle of attack, radians
$\beta$	Fuselage sideslip angle, radians
$\beta'$	Wing-tilt mechanism angular deflection, radians
$\delta$	Control deflection, radians
$\underline{\delta}$	Longitudinal, lateral, directional, collective stick deflections, inches

## 1. INTRODUCTION

There are many new rotor concepts and supporting research efforts in various stages of development that have the potential capability of alleviating some of the limitations associated with current rotorcraft. These rotor concepts and technology developments must, in the final analysis, be flight tested in order to quantify their performance and characteristics in the real and dynamic environment of flight. In the past, flight testing has been accomplished by either modifying an existing vehicle or building a new vehicle. In addition to being quite expensive, this approach has resulted in severe restrictions on the test envelope, measurement accuracy, and in some cases flight safety.

In order to overcome these shortcomings, the United States Army and the National Aeronautics and Space Administration have contracted with Sikorsky Aircraft for the development of two Rotor Systems Research Aircraft (RSRA). These flight research vehicles are being specially designed with the inherent capabilities necessary for effective and efficient in-flight test and verification of promising new rotor concepts and supporting technology developments.

Of prime importance to successful completion of the flight research mission is the accurate estimation of the state of the research rotor system or technology development under test and of the parameters depicting its characteristics. In general, the desired quantitative measures may be of aerodynamic, structural, or performance states or characteristics. These quantitative measures will be used to evaluate system performance, to verify and provide impetus for improved prediction techniques, to develop control system laws, and for ground-based simulation.

The unique research mission and several of the unique features of the RSRA air vehicle will require the unique or expanded application of state estimation and parameter identification techniques as regards rotorcraft. In addition, the RSRA possesses several unique capabilities heretofore unavailable with which to expand the state of the art of rotorcraft parameter identification technology.

This paper will outline the RSRA concept, describe the RSRA flight research capabilities, and present the RSRA requirements for and possible contributions to rotorcraft state estimation and parameter identification technology. The objective of this paper is to engender the timely consideration of the RSRA in the current and future developments of this technology.

## 2. ROTOR SYSTEMS RESEARCH AIRCRAFT

In order for the RSRA to be an effective tool with which to conduct rotorcraft flight research for a broad spectrum of research rotors and research tasks, certain capabilities are necessary. The vehicle must be able to provide a flight and rotor test envelope that is sufficiently broad to encompass the expected envelopes of future rotor systems under both trim and transient conditions. The flight control capabilities must be sufficiently versatile in order to exploit this broad test envelope for a multitude of research tasks and to provide accurate and repeatable test conditions, both trim and transient, throughout the envelope. The success of the RSRA as a research tool will depend greatly on the ability to measure accurately the appropriate vehicle and rotor parameters that define the pertinent characteristics of the rotor or supporting research development under examination.

### 2.1 Airframe

The RSRA must be able to provide a broad envelope of rotor and flight test conditions in order to permit the systematic mapping of the characteristics of the candidate research rotors throughout their operating envelopes under both trim and transient conditions. Hence, the RSRA airframe must possess the capabilities necessary to generate, above some airspeed, reactive forces and moments of sufficient magnitude to exercise the candidate research rotors throughout their operating envelopes. As shown in Figure 1, a variable incidence wing will provide a force to react the rotor trim lift. High-speed flaps will generate transient reactive lift on the rotor about the trim rotor lift. In the longitudinal axis, auxiliary thrust engines will provide a force to react the rotor trim drag and high-speed drag brakes will react the rotor trim propulsive force and generate transient reactive longitudinal force. In addition to being required to generate forces to react the rotor forces, the RSRA, as shown in Figure 1, will generate trim and transient moments to react the rotor moments. An elevator, ailerons, and a rudder will provide this capability. The platform, that is, the fixed-wing airplane, force and moment generation capabilities are shown in Figure 2. Hence

th: RSRA has a full set of rotorcraft control surfaces, that is, a main rotor and a tail rotor; and a full set of airplane controls, that is, a variable-incidence wing, propulsive engines, flaps, drag brakes, ailerons, elevator, and a rudder.

The physical characteristics of the RSRA are shown on Figure 3 and listed in Table 1. As shown in Figure 4, the RSRA will be flown as a helicopter, an airplane, and a compound helicopter. The performance characteristics are listed in Table 2.

Flight operation of the RSRA will require the identification of the stability and control derivatives for all three baseline configurations and hence the application of stability and control derivative extraction technology applicable to both airplanes and helicopters. The compound helicopter configuration will require the application of the combined technology.

## 2.2 Flight Control System

The flight control system must possess sufficient capabilities and versatility to effectively utilize the broad test envelope for many and varied research tasks and to provide accurate and repeatable test conditions, both trim and transient, throughout this envelope. The required flight control capabilities and versatility will be provided by the RSRA fly-by-wire flight control system. The fly-by-wire flight control system exercises control of the control surfaces through an on-line backup mechanical flight control system. This backup mechanical system provides a highly reliable flight control capability suitable for acceptable flight operation of the RSRA throughout its flight envelope; the fly-by-wire flight control system provides the flight control capability and versatility required for the research mission.

Figure 5 shows the functional layout of the mechanical flight control system for each axis of the primary and secondary flight controls. The control system in the pitch, roll, and yaw axes provides the safety pilot with integrated control of the rotorcraft and airplane control surfaces. For example, the safety pilot's longitudinal stick exercises control of the elevator deflection and longitudinal cyclic pitch according to the ratio selected in the control phasing unit. The selection of the control phasing setting and, therefore, the relative contribution of the rotor and airplane controls is based upon achieving acceptable control effectiveness throughout the RSRA flight regime. The control system provides direct control of collective pitch, wing tilt, flap deflection, and drag brake deflection. The mechanical flight control system also has an analog stability augmentation system for the three angular degrees of freedom.

Figure 6 shows the functional layout of the fly-by-wire flight control system for each axis of control. The system exercises control of the main rotor, tail rotor, elevator, ailerons, rudder, flaps, and drag brakes. Control commands are calculated in the digital computer controller based upon the programmed control laws and input variables, the input variables consisting of pilot control positions and rotor and fuselage states. Control surface commands are input through force feel actuators and series actuators. In pitch and roll, control command inputs through the force feel actuators provide integrated control of the rotor and airplane surfaces according to the setting of the control phasing unit. The series actuators, in both the rotor and airplane control runs, provide the capability to input control commands to the rotor and the airplane control surfaces independently and, therefore, for example, to react rotor moments with airplane moments. This independence of control of the airplane and helicopter control surface motions allows the independent optimization of the airplane and helicopter control inputs in order to enhance the ability to identify stability and control derivatives for the compound helicopter configuration. This capability is not available through the mechanical flight control system since the airplane and helicopter control surface motions are related according to the setting of the control phasing unit.

Time-variant dependent control of the rotor and the airplane surfaces can be achieved by inputting time-variant dependent control commands to the series actuators. This capability is not available through the force feel actuator since the fly-by-wire flight control system does not exercise control of the control phasing units. The series actuators in each control channel (rotor or airplane) are comprised of a low-speed large-authority actuator for use in generating trim inputs and high-speed, low-authority actuator for use in generating transient inputs. In yaw, control commands are input through the force feel actuators to provide integrated control of the rudder and tail rotor according to the setting of the control phasing unit. High-speed, low-authority series actuators are provided for use in directional stability augmentation. In the collective channel, force feel actuators are utilized to input control commands; high-speed low-authority series actuators are used for stability augmentation. High-speed, limited-authority series actuators are utilized to input control commands to the flaps and drag brakes.

The core of the fly-by-wire flight control system (see Fig. 7) is the Teledyne Systems Company TDY-43 general-purpose flight-qualified digital computer, the characteristics of which are listed in Table 3. The 16K of memory coupled with the basic processor computational speed and accuracy provides the capability to handle relatively complex and sophisticated control tasks.

A control panel (see Fig. 8) located in the cockpit provides the pilots with the in-flight control and monitoring capabilities necessary to fully utilize the functions implemented in the fly-by-wire system. The system provides five basic functions: stability augmentation, autopilot, control stick force feel, automatic control inputs, and research control modes. The stability augmentation and autopilot systems are utilized by either the safety or evaluation pilots to facilitate the normal flight of the RSRA and the setting of trim conditions prior to engaging the research control modes. The force feel system is used during all aspects of RSRA flight by either the safety pilot or the evaluation pilot in order to provide force feel characteristics on the control sticks to improve the vehicle handling qualities. The automatic control input feature provides a repeatable pulse or step input, the characteristics of which are precisely defined as stored in memory. The desired axis and, where appropriate, the desired control device (main rotor or elevator in pitch, main rotor or ailerons in roll, tail rotor and rudder in yaw, main rotor or flaps in vertical, and drag brakes in the longitudinal) are selected by the pilot. Since the shape of the automatic pulse input is under software control, this input can be defined by any arbitrarily shaped function within the capabilities of the control system to reproduce this motion at the control surface. Hence, this feature provides the capability to study individually, for each control surface, optimal control inputs for enhancing the ability to identify stability and control derivatives from flight-test data.

The research versatility of the RSRA is provided by utilization of the research control modes. Three basic modes are provided: manual, automatic, and auto/manual, and form the basic format within which the control laws to be utilized for the research mission will be implemented. In the manual mode, all of the RSRA control surfaces are under the manual control of the evaluation pilot. For example, this mode will be utilized in the helicopter configuration to accomplish handling qualities research using the RSRA as a six-degree-of-freedom variable stability, in-flight simulator. In the manual/auto mode, several of the RSRA control surfaces, or degrees of freedom, are under the manual control of the evaluation pilot, the remaining control surfaces or degrees of freedom under the automatic control of the fly-by-wire system. For example, as shown in Figure 9, the evaluation pilot could exercise manual control of the rotor under test while the fly-by-wire system utilized the five-degree-of-freedom fixed-wing controls to automatically simulate a fuselage of different aerodynamic and mass/inertia properties, thus simulating a range of fuselage characteristics for a given rotor system under test. This control task is the case that was used to size the flight computer computational capability. In the automatic mode, all of the RSRA control surfaces are under the control of the fly-by-wire flight control system. This mode will be utilized in the helicopter simulation configuration for the automatic control and indexing of rotor test conditions. For example, the fly-by-wire system would step main rotor collective pitch over a range of values as stored in an array in memory while holding cyclic pitch constant and maintaining the vehicle flight path and airspeed constant by use of the fixed-wing control surfaces. This flight control capability coupled with the platform force and moment generation capability permits mapping of rotor performance over a broad range of each variable, independently of the other variables and in a precise and repeatable manner.

The automatic control input feature only permitted the input of control surface motions for one control surface at a time. The automatic mode provides the capability to independently input control surface motions simultaneously to any combination of the control surfaces. Hence, the capability exists to study any combination of optimum control inputs for enhancing the ability to identify stability and control derivatives from flight-test data.

Peripheral to the flight computer is a Program Monitor and Control Unit (PMCU). This unit, shown in Figure 7, is under the control of the third crewman, the flight engineer, and provides the in-flight capability to modify and/or observe the operational software; in particular to slow any of the 128 constants located in memory by 0 to 200 percent of their value, to display the contents of any memory location, accumulator, index register or special register, and to initiate a printout on the onboard printer. For example, the pulse duration of the preprogrammed automatic control inputs may be defined by one of the 128 constants and therefore changed in flight. It will also be used on the ground to load and verify programs and to check out or debug the program in a continuous or step-by-step mode.

The fly-by-wire control commands interface with the mechanical flight control system through the Actuator Control and Monitor Unit (ACMU) which provides the circuitry required for control of the electrically-input force feel and series actuators and for monitoring of their operation.

The Failure Monitor Unit (FMU) monitors the safety pilot primary control stick motions and the main rotor longitudinal pitch, elevator, collective, and flaps series actuator commands for "hardovers" — exceedance of their respective rate and amplitude envelopes — and upon detection of a hardover disengages the fly-by-wire flight control system.

In order to utilize the fly-by-wire flight control system to provide accurate and repeatable test conditions, both trim and transient, for the many and varied research tasks envisioned for the RSRA, comprehensive rotor and vehicle state information must be available in the flight computer. This state information is derived from input signals supplied by aircraft mounted sensors. The particular input signals for the flight computer and the characteristics of the corresponding channel of the computer input are as specified in Table 4. The sensor characteristics are compatible with those specified for the research instrumentation system and listed in Table 5.

The RSRA has two unique measurement systems that provide heretofore unavailable state information with which to achieve direct setting and control of test conditions: a rotor force and moment measurement system and a wing force and moment measurement system. As depicted in Figure 10, each system is mounted to the airframe on load cells. The output signals are sent to the flight computer where the forces and moments are estimated on-line and hence are available for use in control by the fly-by-wire system or for display to the pilot. The details to these systems will be discussed in the following section on research instrumentation.

### 2.3 Research Instrumentation

Successful flight research is greatly dependent upon the ability to accurately measure and record the appropriate data from which to estimate the states and parameters defining the characteristics of interest. This is best accomplished if the system for obtaining each measurement is designed as an integral part of, and permanently incorporated into, the vehicle, and if the data recording system is specifically designed for the flight research role. This philosophy has been applied to the measurement systems for the RSRA. The data recording system is the Piloted Aircraft Data System (PADS), a new and versatile data collection system designed at Langley Research Center (LRC) specifically for aeronautical flight research programs including rotorcraft.

A schematic of the research instrumentation system for the RSRA is shown as Figure 11. The data recording system is comprised of two PADS. Each PADS provides up to 104 PCM channels for use in recording up to 10 Hz data, and up to 40 constant bandwidth FM channels for use in recording up to 400 Hz data. In addition, one channel is provided for recording voice and events and one channel for recording PCM time code for use in correlating measurements recorded onboard and measurements telemetered to the ground station. The telemetry capability provides for up to 104 channels for PCM data and 10 channels for FM data to be telemetered from the number 1 PADS. The PCM uses a nine-bit analog to digital converter to provide an accuracy of  $\pm 0.2$  percent of full scale for  $\pm 5$  volt inputs and  $\pm 0.5$  percent full scale for  $\pm 10$  millivolt inputs. The CBW-FM subsystem is comprised of voltage controlled oscillators and mixer-amplifiers, the root sum squared error being less than or equal to 2 percent full scale. The signal conditioner provides

a root sum squared error of less than or equal to 0.5 percent full scale. The ground station provides for real-time display and hard-copy recording of a limited number of selected channels of data, for recording on tape all of the telemetered data channels and for off-line data editing, reformatting, and generation of a digital tape for use in automatic data processing.

The research instrumentation system as configured on the delivered vehicles will provide the measurements listed in Table 5. Hence, there will be 140 spare channels of PCM and 74 spare channels of FM for use in recording data from sensors to be installed in the future for particular research programs. A 192-channel slipring assembly mounted on the main rotor shaft provides the capability to transmit to the PADS, for recording on these spare channels, rotor information required for future research programs. For example, Molusis and Brucsinaki<sup>1</sup> have pointed out the importance of the contribution of the rotor degrees of freedom to the short-term high-frequency accelerations of the body due to rotor transients and the resultant necessity for using a nine-degree-of-freedom rotor/body model in order to properly represent this short-term response. The slipring assembly provides the capability to record the rotor information for identification of such a model.

The baseline measurements listed in Table 5 are provided by standard flight research sensors which measure attitudes, rates, control surface positions, airspeed, and so forth, and by RSRA peculiar measurements systems which measure subsystem flight loads. The standard flight research measurements are provided by state-of-the-art, off-the-shelf sensors. The characteristics of the transducers are listed in Table 5. It is to be noted that the choice of sensors has been based upon flight research requirements in general, and in order to provide sufficiently accurate data for a particular research program it may be necessary to change sensors. For example, in gathering data for stability derivative extraction research it may be necessary to replace the rate gyros with sensors of greater sensitivity over a smaller range in order to increase the accuracy of the measurements.

The RSRA-peculiar force and moment measurement systems provide the capability to measure flight loads for particular subsystems of interest and thereby provide a breakdown of the contribution of each of these systems to the total flight loads experienced by the aircraft. In general, the subsystems are mounted to the airframe on load cells in configurations so as to most accurately provide the data necessary to define the particular flight loads of interest for that subsystem. The main rotor transmission is mounted to the airframe, as shown in Figure 10, by six uniaxial load cells, the outputs of which will be utilized to estimate all of the three-axis force and moments on the main rotor. That is,

- Main rotor longitudinal force
- Main rotor side force
- Main rotor vertical force
- Main rotor pitching moment
- Main rotor rolling moment
- Main rotor yawing moment

The wing is mounted to the airframe, as shown in Figure 10, with a biaxial load cell at each of the two pivot points and with an uniaxial load cell incorporated in each of the two wing-tilt actuators. The load cell outputs will be used in estimating:

- Wing lift
- Wing drag
- Wing pitching moment
- Wing rolling moment

Each auxiliary thrust TF-34 engine is mounted to the airframe as shown in Figure 12, with the uniaxial load cell output used in estimating the auxiliary engine thrust. The tail rotor is mounted to the airframe as shown in Figure 12 with the uniaxial load cell output used in estimating the tail rotor thrust.

The capability to measure in-flight the forces and moments generated by the rotor will provide the necessary data with which to correlate directly the outputs of analytical rotor models. In the past, the forces and moments generated by the rotor had to be inferred from measured body motions and inertia characteristics and from measured/estimated aerodynamic characteristics of the fuselage. In addition, the capability to automatically control the vehicle state with the fixed-wing control surfaces provides the capability to independently vary the rotor states or rotor controls and thereby quantify their individual relationships with the rotor forces and moments. These capabilities should provide strong impetus for the development and verification of rotor models.

The output signals of the main rotor and wing loads cells are supplied as inputs to the fly-by-wire system computer wherein the force and moments are estimated on-line and hence are available for use in control by the fly-by-wire system or for display to the pilot. The main rotor forces and moments will be estimated using Equations (1) through (6) in Appendix A. The forces are resolved in an axis system, as shown in Figure 13, at the center of the rotor hub and parallel to the body axis system. It is to be noted that transmission inertia loads, shaft engine torque, tail rotor torque, system geometry, and interactions are accounted for in the equations. The interactions will be neglected for the in-flight system. It is expected that due to the small load cell deflections (~ 0.001 inch) these interactions will be sufficiently small and that acceptable accuracy will be achieved for the in-flight system. The results of calibration will be utilized in calculating the load cell forces from load cell output signals. The wing forces and moments will be estimated using Equations (7) through (12) in Appendix A. The wing forces are resolved in an axis system, as shown in Figure 14, at the midpoint between the pivot hinges and parallel to the body axis system. The equations account for the same factors as do the equations for the rotor and additionally account for the variable-wing incidence.

The output signals of each load cell for the main rotor, wing, auxiliary engines, and tail rotor measurement systems are recorded on PADS. These signals will be utilized in off-line estimating of the forces and moments for data purposes. In order to provide the greatest possible accuracy for data purposes, the forces and moments will be estimated using the equations of Appendix A to include the interactions. Subsequent paragraphs describe the interactions and the method of determination.

The load cells are state-of-the-art, off-the-shelf transducers with the characteristics as listed in Table 5. In order to minimize errors due to load cell inaccuracies, load cells have been chosen with as small a range as possible within the constraints of the expected in-flight loads for the particular rotor and within the availability of off-the-shelf transducers. Different rotors may require load cells of different sensitivity and range.

An accuracy analysis has been conducted by Dr. Ping Tchong of Old Dominion University, Norfolk, Virginia, for the on-line (flight computer) rotor force and moment measurement system and the results are shown in Table 6. The one- $\sigma$  accuracies quoted are for the values of forces and moments estimated in the flight computer. The errors quoted are random errors resulting from nonlinearities, hysteresis, resolution, sensitivity drift, zero shift, and noise in the measurement system to include the sensors. The one- $\sigma$  accuracies do not include random errors due to hysteresis, friction, and alternate load paths (such as hydraulic lines) in the mounting system. These inaccuracies will be quantified during calibration of the mounting system. The fixture for calibrating the four RSRA peculiar force and moment measurement systems is shown as Figure 15. The system will permit the application of calibrating forces and moments independent of one another or in combination with one another stepped over approximately 75 percent of the full range of loads. The calibration procedure will be in general accordance with the procedure discussed in Reference 2 and will permit the quantification of all the first- and second-order interactions in the load cell balance mounting thereby eliminating these effects including their nonlinearity, in the estimation of the applied forces and moments by the off-line system (PADS).

### 3.0 CONCLUDING REMARKS

The unique research mission and several of the unique features of the RSRA will require the new and expanded application of state estimation and parameter identification technology as regards rotorcraft. The identification of stability and control parameters for the RSRA needs to include the stability derivatives associated with the rotor degrees of freedom and the control derivatives associated with the combined helicopter and airplane control surfaces. The RSRA will provide unique state estimation capabilities in the form of measurements of the flight loads for the main rotor, wing, auxiliary propulsion, and tail rotor subsystems.

Due to unique airframe, flight control, and instrumentation system capabilities, the RSRA is an ideal vehicle with which to conduct flight development studies on rotorcraft stability and control derivative identification technology. The automatic flight control capabilities include prescribed independent inputs to each control surface, individually or concurrently, and provide accurate, repeatable test conditions. The instrumentation system provides accurate measurement of the pertinent vehicle and rotor states to include the flight loads on the rotor, wing, auxiliary propulsion, and tail rotor subsystems.

### 4.0 REFERENCES

1. Molusis, John, and Briczinski, Stan: Helicopter Derivative Identification From Analytical Models and Flight Test Data. Symposium on Parameter Estimation Techniques and Applications in Aircraft Flight Testing. NASA TN D-7647, April 1974.
2. Hansen, Raymond M.: Evaluation and Calibration of Wire-Strain-Gage Wind Tunnel Balances Under Load. AGARD Report 13, February 1956.

### APPENDIX A

#### A.1 Rotor Force and Moment Estimation

The forces and moments on the main rotor transmission are resolved in an axis syst. with the origin at the center of the rotor hub and parallel to the aircraft body axis system. The rotor forces and moments are determined by solving Newton's laws in this moving coordinate system. Figure 13 was used to derive the equations that follow:

$$\begin{bmatrix} X_R \\ Y_R \\ Z_R \\ L_R \\ M_R \\ Q_R \end{bmatrix} = \begin{bmatrix} -X_{IT} \\ -Y_{IT} \\ -Z_{IT} \\ -L_{IT} + f_6 Y_{IT} - Q_T \\ -M_{IT} + f_5 Z_{IT} - f_6 X_{IT} \\ -N_{IT} - f_5 Y_{IT} \end{bmatrix} + \begin{bmatrix} 0 & 0 & 0 & 0 & 0 & 1 \\ 0 & 0 & 0 & -1 & 1 & 0 \\ -1 & -1 & -1 & 0 & 0 & 0 \\ \frac{y_t}{2} & -\frac{y_t}{2} & 0 & f_4 & -f_3 & 0 \\ f_1 & f_1 & -f_2 & 0 & 0 & f_3 \\ 0 & 0 & 0 & -f_1 & -f_2 & 0 \end{bmatrix} \begin{bmatrix} A \\ B \\ C \\ D \\ E \\ F \end{bmatrix} + \begin{bmatrix} \text{Interactions} \\ \text{Interactions} \\ \text{Interactions} \\ \text{Interactions} \\ \text{Interactions} \\ \text{Interactions} \end{bmatrix} \quad (1)$$

Where:

$$X_{IT} = m_t a_{TX} \quad (2a)$$

$$Y_{IT} = m_t a_{TY} \quad (2b)$$

$$Z_{IT} = m_t a_{TZ} \quad (2c)$$

$$L_{IT} = I_{TXX} \dot{\theta} + (I_{TZZ} - I_{TXX}) \dot{\theta} \quad (2d)$$

$$M_{TY} = I_{TTY} \dot{\theta} + (I_{YXX} - I_{TZZ}) q r \quad (3b)$$

$$M_{TZ} = I_{TZZ} \dot{\theta} + (I_{TTY} - I_{YXX}) p q \quad (3c)$$

$$f_1 = \frac{x_T}{2} \cos i_T + (z_R + z_T) \sin i_T \quad (4a)$$

$$f_2 = \frac{x_T}{2} \cos i_T - (z_R + z_T) \sin i_T \quad (4b)$$

$$f_3 = (z_R + z_T) \cos i_T + \frac{x_T}{2} \sin i_T \quad (5a)$$

$$f_4 = (z_R + z_T) \cos i_T - \frac{x_T}{2} \sin i_T \quad (5b)$$

$$f_5 = z_R \sin i_T \quad (6a)$$

$$f_6 = z_R \cos i_T \quad (6b)$$

The interaction terms for each force and moment represent the cross-coupling effects of the load cell reaction forces and will be defined by static calibration of the balance mounting.

#### A.2 Wing Force and Moment Estimation

The forces and moments on the wing are resolved in an axis system with origin on the wing hinge line halfway between the pivot points and parallel to the body axis system. The wing forces are determined by solving Newton's laws in this moving coordinate system. Figure 14 was used to derive the equations which follow:

$$\begin{bmatrix} X_W \\ Z_W \\ M_W \\ L_W \end{bmatrix} = \begin{bmatrix} -X_{IW} \\ -Z_{IW} \\ -M_{IW} + f_{10} Z_{IW} + f_{11} X_{IW} \\ -L_{IW} - f_{11} Y_{IW} \end{bmatrix} + \begin{bmatrix} \sin \beta' & \sin \beta' & 0 & 0 & -1 & -1 \\ -\cos \beta' & -\cos \beta' & -1 & -1 & 0 & 0 \\ -f_{12} & -f_{12} & 0 & 0 & 0 & 0 \\ -\frac{y_1}{2} \cos \beta' & \frac{y_1}{2} \cos \beta' & -\frac{y_2}{2} & \frac{y_2}{2} & 0 & 0 \end{bmatrix} \begin{bmatrix} H \\ I \\ J \\ K \\ L \\ M \end{bmatrix} + \begin{bmatrix} \Sigma \text{ Interactions} \\ \Sigma \text{ Interactions} \\ \Sigma \text{ Interactions} \\ \Sigma \text{ Interactions} \end{bmatrix} \quad (7)$$

Where:

$$X_{IW} = m_W a_{WX} \quad (8a)$$

$$Z_{IW} = m_W a_{WZ} \quad (8b)$$

$$L_{IW}^i = (\dot{\theta} \cos i_W - \dot{\theta} \sin i_W) I_{WXX} + (I_{WZZ} - I_{WYY})(p \cos i_W - r \sin i_W)(r \cos i_W + p \sin i_W) \quad (9a)$$

$$M_{IW}^i = \dot{\theta} I_{WYY} + (I_{WXX} - I_{WZZ}) q(r \cos i_W + p \sin i_W) \quad (9b)$$

$$L_{IW} = L_{IW}^i \cos i_W \quad (10a)$$

$$M_{IW} = M_{IW}^i \quad (10b)$$

$$f_{10} = x_W \cos i_W + z_W \sin i_W \quad (11a)$$

$$f_{11} = x_W \sin i_W - z_W \cos i_W \quad (11b)$$

$$f_{12} = x_1 \cos (i_W - \beta') \quad (12)$$

The interaction terms for each force and moment represent the cross-coupling effects of the load cell reaction forces and will be defined by static calibration of the balance mounting.

TABLE 1. RSRA DESIGN CONFIGURATION CHARACTERISTICS

Stress gross weight	26,200 lb	
Design gross weight, compound mission	26,200 lb	
Gross weight, hover mission	18,400 lb	
Weight empty, compound configuration	20,968 lb	
Weight empty, helicopter configuration	14,633 lb	
Main rotor system (Sikorsky H-3)		
Diameter	62 ft	
Number of blades	5	
Chord	1.32 ft	
Normal tip speed	660 ft/sec	
Blade twist	-8°	
Tail rotor system (Sikorsky H-3)		
Diameter	10.6 ft	
Number of blades	5	
Chord	0.612 ft	
Normal tip speed	689 ft/sec	
Blade twist	0°	
Wing		
Area	369 sq ft	
Span	44.8 ft	
Airfoil section	NACA 63 <sub>2</sub> 415	
Aspect ratio	5.45	
Variable-incidence range	-9° to +15°	
Taper	0.62	
Lower horizontal stabilizer (except helicopter)		
Area	98.1 sq ft	
Span	25.0 ft	
Chord (mean)	3.93 ft	
Elevator area	12.5 sq ft	
Incidence (coupled to wing tilt)	+8°	
Upper horizontal stabilizer		
Area	Except helicopter 17.2 sq ft	Helicopter 35.4 sq ft
Span	8.58 ft	13.25 ft
Chord (mean)	2.04 ft	2.78 ft
Vertical stabilizer		
Area	101.1 sq ft	
Span	15.9 ft	
Chord (mean)	6.83 ft	
Rudder (area)	24.8 sq ft	
Turboshaft engines		
Type	T58-GE (2)	
Military rating, SLS	1400 hp	
Main gearbox (Sikorsky H-3)		
Power rating, 30 minutes	2500 hp	
Turbofan engines		
Type	TF-34-GE-400(2)	
Military rating, SLS, static	8159 lb	
Military rating, SLS, 300 knots	5340 lb	

TABLE 2. RSRA PERFORMANCE REQUIREMENTS

Item	Requirement
Hover OGE (helicopter)	SL 95° F
Hover payload	2000 lb
Speed	300 kt @ mil pwr
Helicopter simulation speed envelope	120 - 200 kt
Wing design lift	
Clean	DCW @ 150 kt
With flap	DCW @ 120 kt
Stall margin	10 percent

TABLE 3. TDY-43 FLIGHT COMPUTER CHARACTERISTICS

Memory	Core, 16K x 16, 1.3 $\mu$ s cycle
Computation process	Parallel
Formats	
Data	Fixed point, fractional binary, 2's complement
Word length	16 bits
Instruction	Single address, single instruction
Addressing	Immediate direct, relative, indexed, and indirect
Addressing range	To 65K words
Instructions	70
Clock frequency	3 MHz
Registers	Dual 8-register file
Execution speeds (direct, relative, indexed)	
Add/subtract	2.67 $\mu$ s
Multiply	6.00 $\mu$ s
Divide	8.67 $\mu$ s
DP add/subtract	5.33 $\mu$ s
Input/output	4 synchro inputs 13 ac inputs (2nd order filters) 34 dc inputs (2nd order filters) 39 dc inputs (single pole filters) 35 dc inputs (unfiltered) 62 dc outputs (single pole filters) 64 28 Vdc discrete inputs 31 28 Vdc discrete outputs
Interrupts	8 (3 dedicated internally)
Real-time clock	16 bits; program accessible 0.1 msec resolution 6.5536 seconds range
BITE	Memory check Instruction check Wrap-around I/O check Reset timer

TABLE 4. FLY-BY-WIRE FLIGHT CONTROL SYSTEM INPUTS

Signal	Conversion range	Accuracy	Minimum conversion per second	Signal	Conversion range	Accuracy	Minimum conversion per second
Pitch attitude	$\pm 90$ deg	$\pm .2$ deg	20	Vertical acceleration	$\pm 4$ g's	$\pm .24$ fps <sup>2</sup>	40
Roll attitude	$\pm 180$ deg	$\pm .2$ deg	20	Airspeed	0 to 360 kts	$\pm .7$ kts	40
Heading	$\pm 180$ deg	$\pm .2$ deg	20	Fuselage angle of attack	$\pm 40$ deg	$\pm .1$ deg	20
Pitch rate	$\pm 40$ deg/sec	$\pm .1$ deg	40	Sideslip angle	$\pm 15$ deg	$\pm .1$ deg	20
Roll rate	$\pm 40$ deg/sec	$\pm .1$ deg/sec	40	Drag brake position	0 to 60 deg	$\pm .12$ deg	20
Yaw rate	$\pm 40$ deg/sec	$\pm .1$ deg/sec	40	Wing incidence	$\pm 25$ deg	$\pm .05$ deg	20
Pitch acceleration	$\pm 75$ deg/sec <sup>2</sup>	$\pm .13$ deg/sec <sup>2</sup>	40	Stabilator incidence	$\pm 25$ deg	$\pm .05$ deg	20
Roll acceleration	$\pm 150$ deg/sec <sup>2</sup>	$\pm .27$ deg/sec <sup>2</sup>	40	Flap deflection	$\pm 25$ deg	$\pm .05$ deg	20
Yaw acceleration	$\pm 75$ deg/sec <sup>2</sup>	$\pm .13$ deg/sec <sup>2</sup>	40	Aileron deflection	$\pm 25$ deg	$\pm .05$ deg	20
Longitudinal acceleration	$\pm 2$ g's	$\pm .12$ fps <sup>2</sup>	40				
Lateral acceleration	$\pm 2$ g's	$\pm .12$ fps <sup>2</sup>	40				



TABLE 4. TDY-43 FLIGHT COMPUTER CHARACTERISTICS — Concluded

Signal	Conversion range	Accuracy	Minimum conversion per second	Signal	Conversion range	Accuracy	Minimum conversion per second
Rudder deflection	$\pm 50$ deg	$\pm .10$ deg	20	Copilot pedal control	0 to 100%	$\pm .2\%$	40
Elevator deflection	$\pm 50$ deg	$\pm .2$ deg	20	Longitudinal control phasing	0 to 100%	$\pm .2\%$	20
Collective mixer input	0 to 100%	$\pm .2\%$	20	Lateral control phasing	0 to 100%	$\pm .2\%$	20
Pitch mixer input	0 to 100%	$\pm .2\%$	20	Directional control phasing	0 to 100%	$\pm .2\%$	20
Roll mixer input	0 to 100%	$\pm .2\%$	20	Longitudinal cyclic series trim actuator position	0 to 100%	$\pm .2\%$	20
Auxiliary engine No. 1 thrust	0 to 100%	$\pm .2\%$	20	Lateral cyclic series trim actuator position	0 to 100%	$\pm .2\%$	20
Auxiliary engine No. 2 thrust	0 to 100%	$\pm .2\%$	20	Elevator series trim actuator position	0 to 100%	$\pm .2\%$	20
Pilot longitudinal FFS trim control	0 to 100%	$\pm .2\%$	20	Aileron series trim actuator position	0 to 100%	$\pm .2\%$	20
Copilot longitudinal FFS trim control	0 to 100%	$\pm .2\%$	20	Load cell A	$\pm 35,000$ lb	$\pm 70$ lb	20
Pilot lateral FFS trim control	0 to 100%	$\pm .2\%$	20	Load cell B	$\pm 25,000$ lb	$\pm 50$ lb	20
Copilot lateral FFS trim control	0 to 100%	$\pm .2\%$	20	Load cell C	$\pm 25,000$ lb	$\pm 50$ lb	20
Pilot collective FFS trim control	0 to 100%	$\pm .2\%$	20	Load cell D	$\pm 25,000$ lb	$\pm 50$ lb	20
Copilot collective FFS trim control	0 to 100%	$\pm .2\%$	20	Load cell E	$\pm 25,000$ lb	$\pm 50$ lb	20
Pilot pedal FFS trim control	0 to 100%	$\pm .2\%$	20	Load cell F	$\pm 8,000$ lb	$\pm 16$ lb	20
Copilot pedal FFS trim control	0 to 100%	$\pm .2\%$	20	Load cell J	$\pm 28,000$ lb	$\pm 40$ lb	20
Pilot lateral control	0 to 100%	$\pm .2\%$	40	Load cell K	$\pm 28,000$ lb	$\pm 40$ lb	20
Copilot lateral control	0 to 100%	$\pm .2\%$	40	Load cell L	$\pm 12,000$ lb	$\pm 16$ lb	20
Pilot longitudinal control	0 to 100%	$\pm .2\%$	40	Load cell M	$\pm 12,000$ lb	$\pm 17$ lb	20
Copilot longitudinal control	0 to 100%	$\pm .2\%$	40	Load cell N	$\pm 25,000$ lb	$\pm .2\%$ of full scale	20
Pilot collective control	0 to 100%	$\pm .2\%$	40	Load cell I	$\pm 25,000$ lb	$\pm .2\%$ of full scale	20
Copilot collective control	0 to 100%	$\pm .2\%$	40	Barometric altitude	-1,000 to +19,000	$\pm 20$ ft	20
Pilot pedal control	0 to 100%	$\pm .2\%$	40	Outside air temperature	$\pm 60^\circ$ C	$\pm .12^\circ$ C	20
				Rotor rpm	0 to 100%	$\pm .2\%$	20
				Rotor azimuth	0 to $360^\circ$	$\pm .2$ deg	40
				Rotor blade flapping	-30 to +30 deg	$\pm .1$ deg	40
				Rotor blade lead lag	-60 to +60 deg	$\pm .12$ deg	40
				Pitch at blade cuff	-10 to +30 deg	$\pm .1$ deg	40
				Spare input (16)	-10 to +10 Vdc	$\pm .2\%$	20
				Spare input (20)	-10 to +10 Vdc	$\pm .2\%$	40

TABLE 5. RESEARCH INSTRUMENTATION MEASUREMENTS

Measurement	Transducer			Measurement full scale	PCM/FM	Frequency response
	Type	Accuracy	Full scale			
Rotor lift cell "A"	Load cell	+1%	35,000 lb	43,500 lb	PCM	10
Rotor lift cell "B"	Load cell	+1%	25,000 lb	34,900 lb	PCM	10
Rotor lift cell "C"	Load cell	+1%	25,000 lb	34,900 lb	PCM	10
Main rotor torque drive shaft	S.G.	+1%	2400 $\mu$ in./in.	65,000 ft lb	PCM	10
Transmission torque cell "D"	Load cell	+1%	25,000 lb	25,000 lb	PCM	10
Transmission torque cell "E"	Load cell	+1%	25,000 lb	25,000 lb	PCM	10
Long. force cell "F"	Load cell	+1%	8,000 lb	10,400 lb	PCM	10-30
MR rpm	Photo cell	TBD	120Z	120Z	PCM	10
MR azimuth 1/72 per rev.	Photo cell	TBD	1/72/rev.	72/rev.	FM	300
MR blade flap $\beta$	Linear gener.	TBD	360°	-5.5° +20°	FM	30
MR blade hunt $\gamma$		TBD	360°	-3° +20°	FM	30
MR blade pitch $\theta$		TBD	360°	-6.5° +20.4°	FM	30
Rt. lat. servo position	Pot.	+1%	6 in.	100Z	PCM	10
Lt. lat. servo position	Pot.	+1%	6 in.	100Z	PCM	10
Long. servo position	Pot.	+1%	6 in.	100Z	PCM	10
Airspeed (swiveling probe)	TBD	TBD	400 kts	400 kts	PCM	6
Pitch attitude	Gyro	TBD	+82°	+30°	PCM	10
Roll attitude	Gyro	TBD	360°	+90°	PCM	10
Yaw attitude	Gyro	TBD	360°	+30°	PCM	10
Pitch rate	Gyro	+1%	75°/sec	60°/sec	PCM	10
Roll rate	Gyro	+1%	150°/sec	90°/sec	PCM	10
Yaw rate	Gyro	+1%	75°/sec	60°/sec	PCM	10
Pitch acceleration	Gyro	+1%	+75°/sec <sup>2</sup>	+30°/sec <sup>2</sup>	PCM	10
Roll acceleration	Gyro	+1%	+150°/sec <sup>2</sup>	+30°/sec <sup>2</sup>	PCM	10
Yaw acceleration	Gyro	+1%	+75°/sec <sup>2</sup>	+30°/sec <sup>2</sup>	PCM	10
Vertical linear accel.	Accel.	+1%	-1 +4G	-1 +4G	PCM	10
Lateral linear accel.	Accel.	+1%	+0.5G	+0.5G	PCM	10
Longitudinal linear accel.	Accel.	+1%	+0.5G	+0.5G	PCM	10
Angle of attack	Pot.	+1%	+60°	+40°	PCM	10
Sideslip	Pot.	+1%	+60°	+40°	PCM	10
Drag brake position	Pot.	+1%	TBD	0-100Z	PCM	10
Wing pitch actuator cell "H"	Load cell	+1%	25,000 lb	31,300 lb	PCM	10
Wing pitch actuator cell "I"	Load cell	+1%	25,000 lb	31,300 lb	PCM	10
Wing pivot point cell "J"	Load cell	+1%	20,000 lb	28,000 lb	PCM	10
Wing pivot point cell "K"	Load cell	+1%	20,000 lb	28,000 lb	PCM	10
Wing pivot point cell "L"	Load cell	+1%	8,000 lb	10,000 lb	PCM	10
Wing pivot point cell "M"	Load cell	+1%	8,000 lb	10,000 lb	PCM	10
Wing incidence angle	Pot.	+1%	TBD	-9° +15°	PCM	10
Right aileron position	Pot.	+1%	TBD	0-100Z	PCM	10
Right flap position	Pot.	+1%	TBD	0-100Z	PCM	10
Antitorque cell "N"	Load cell	+1%	5,000 lb	5,000 lb	FM	10-30
Tail drive shaft Q	S.G.	+1%	2400 $\mu$ in./in.	1200 ft-lb	PCM	10
Horiz. stab. elevator pos.	Pot.	+1%	TBD	0-100Z	PCM	10
Rudder position	Pot.	+1%	TBD	0-100Z	PCM	10
Left engine aux. thrust	Load cell	+1%	5,000 lb	3800 lb	PCM	10
Right engine aux. thrust	Load cell		5,000 lb	3800 lb	PCM	10
Pilot's lat. control pos.	Pot.	+1%	TBD	0-100Z	PCM	10
Copilot's lat. control pos.	Pot.	+1%	TBD	0-100Z	PCM	10
Pilot's long. control pos.	Pot.	+1%	TBD	0-100Z	PCM	10
Copilot's long. control pos.	Pot.	+1%	TBD	0-100Z	PCM	10
Pilot's coll. control pos.	Pot.	+1%	TBD	0-100Z	PCM	10
Copilot's coll. control pos.	Pot.	+1%	TBD	0-100Z	PCM	10
Antitorque control pos.	Pot.	+1%	TBD	0-100Z	PCM	10
Lateral control stick force	S.G.	TBD	2400 $\mu$ in./in.	25 lb	PCM	10
Long. control stick force	S.G.	TBD	2400 $\mu$ in./in.	25 lb	PCM	10
Coll. control stick force	S.G.	TBD	2400 $\mu$ in./in.	25 lb	PCM	10
Anti Q control force	S.G.	TBD	2400 $\mu$ in./in.	75 lb	PCM	10
Pitch phasing unit pos.	Pot.	TBD	TBD	0-100Z	PCM	10
Roll phasing unit pos.	Pot.	TBD	TBD	0-100Z	PCM	10
Yaw phasing unit pos.	Pot.	TBD	TBD	0-100Z	PCM	10
Helo. long. servo series trim	Pot.	TBD	TBD	0-100Z	PCM	10
Stab. series trim control pos.	Pot.	TBD	TBD	0-100Z	PCM	10
Helo. lat. servo ser. trim pos.	Pot.	TBD	TBD	0-100Z	PCM	10
Roll series trim control pos.	Pot.	TBD	TBD	0-100Z	PCM	10
No. 1 eng. T-58 torque	Press.	+1%	150 psi	75 psi	PCM	10
No. 2 eng. T-58 torque	Press.	+1%	150 psi	75 psi	PCM	10
Main rotor push rod	S.G.	+3%	2400 $\mu$ in./in.	1500 lb	FM	100
Altitude	Press.	+1%	TBD	-1000, +15,000	PCM	QS
OAT	Res.	+0.5%	+60° C	+60° C	PCM	QS
Rate of climb	Press.	TBD	+6000 fpm	+6000 fpm	PCM	QS
Stabilizer position	Pot.	+1%	TBD	+8°	PCM	10

TBD: To be determined.

QS: Quasi-static.

S.G.: Strain gage.

TABLE 6. ROTOR FLIGHT LOADS MEASUREMENT SYSTEM ACCURACY

Force/moment component	Range	Accuracy (1σ)
Vertical force (lb)	-3K/ +48.8K	+313/ +152
Longitudinal force (lb)	+10K	+71
Lateral force (lb)	+10K	+110
Pitching moment (ft-lb)	+24K	+796/ +421
Rolling moment (ft-lb)	+12K	+669/ +507
Yawing moment (ft-lb)	-3K/ +65K	+424/ +220

● 1-g. STRAIGHT AND LEVEL FLIGHT ABOVE 120 KNOTS

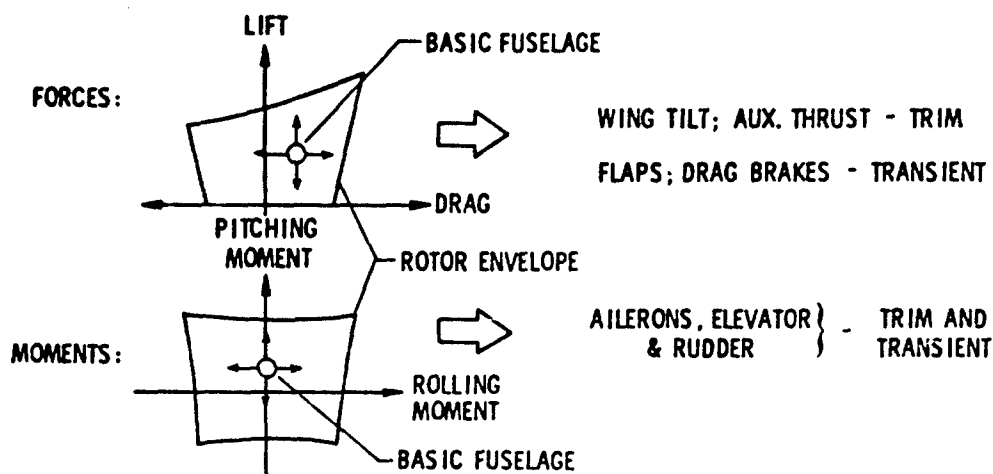


Figure 1. Control surface requirements based upon rotor test envelope requirement.

COMPOUND HELICOPTER, 1-g. STRAIGHT AND LEVEL FLIGHT CAPABILITY

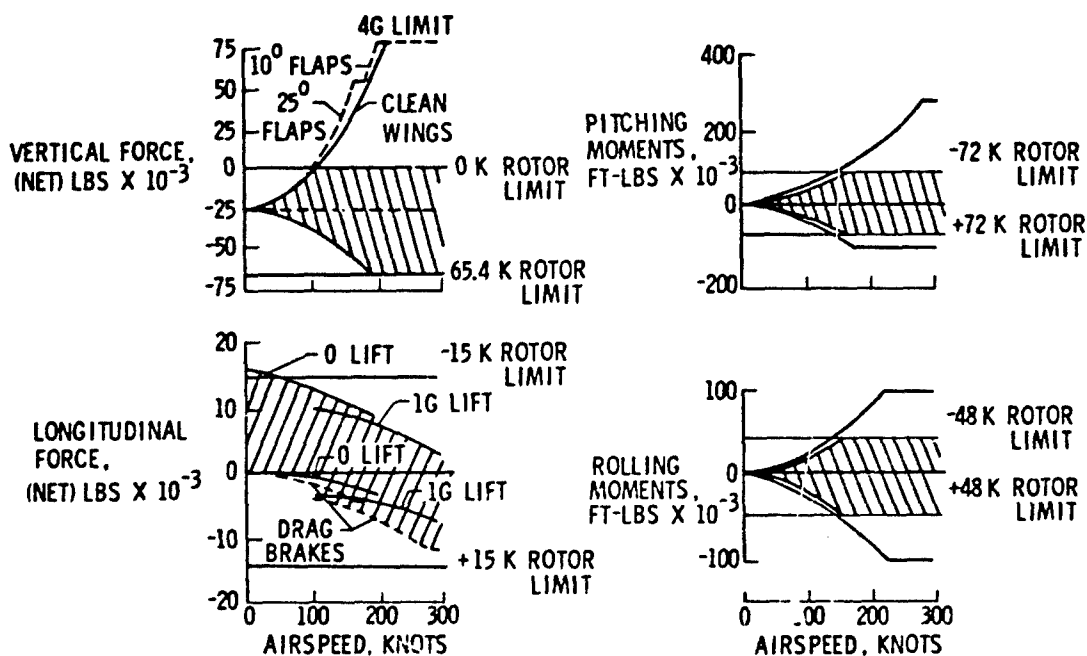


Figure 2. RSRA platform force and moment generation capability.

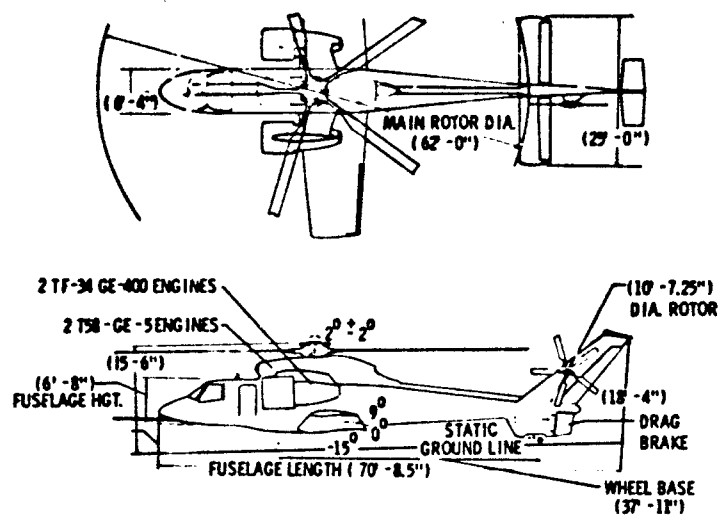


Figure 3. RSRA physical characteristics.

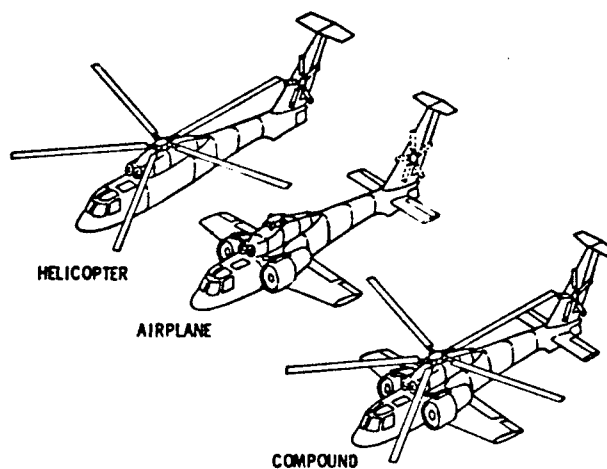


Figure 4. RSRA flight configuration.

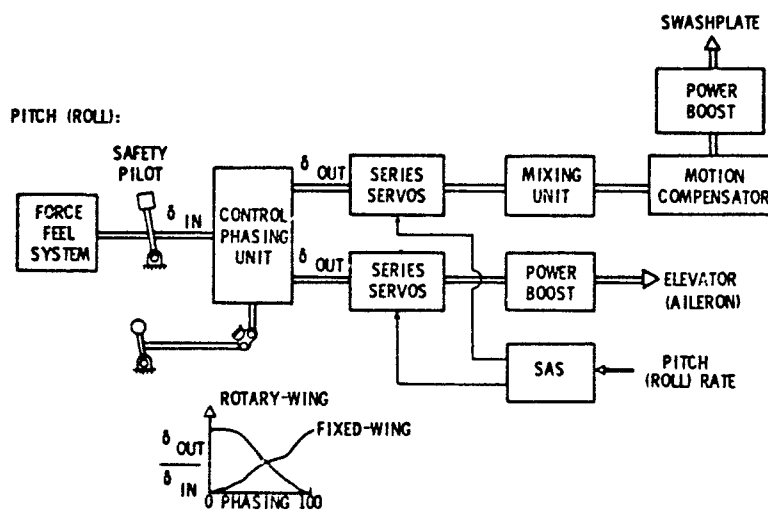


Figure 5. Mechanical flight control system functional layout.

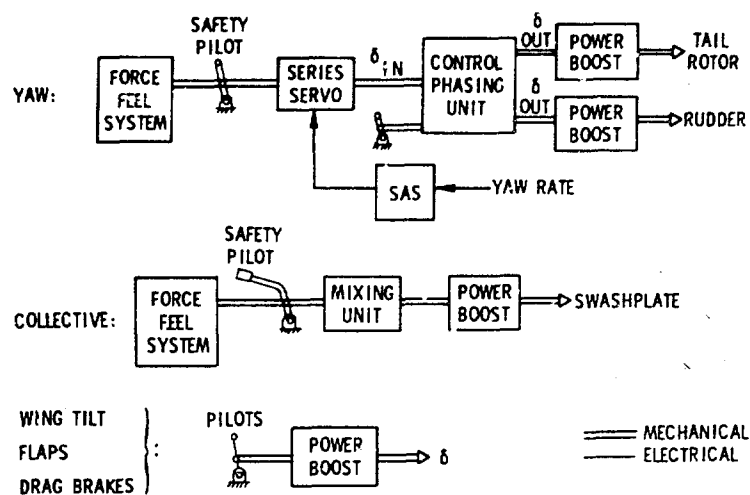


Figure 5. Concluded.

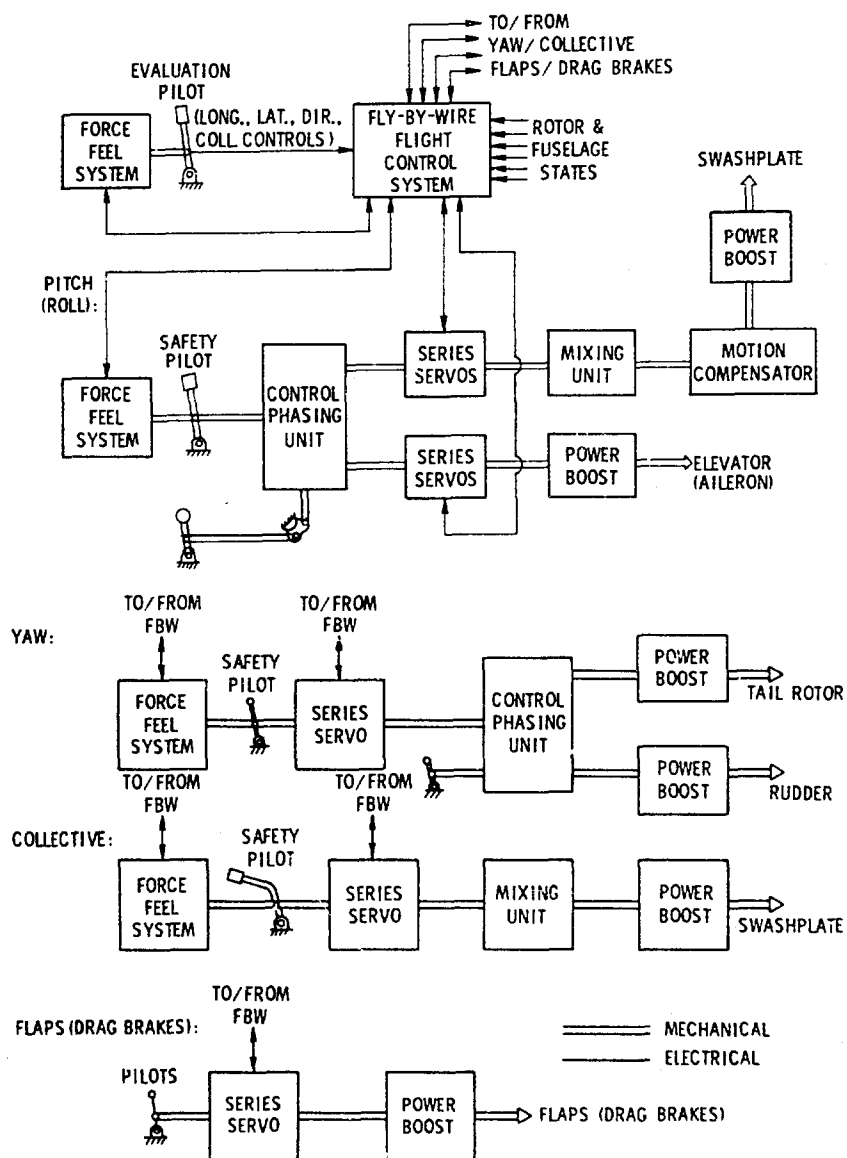


Figure 6. Fly-by-wire flight control system interface with mechanical flight control system.



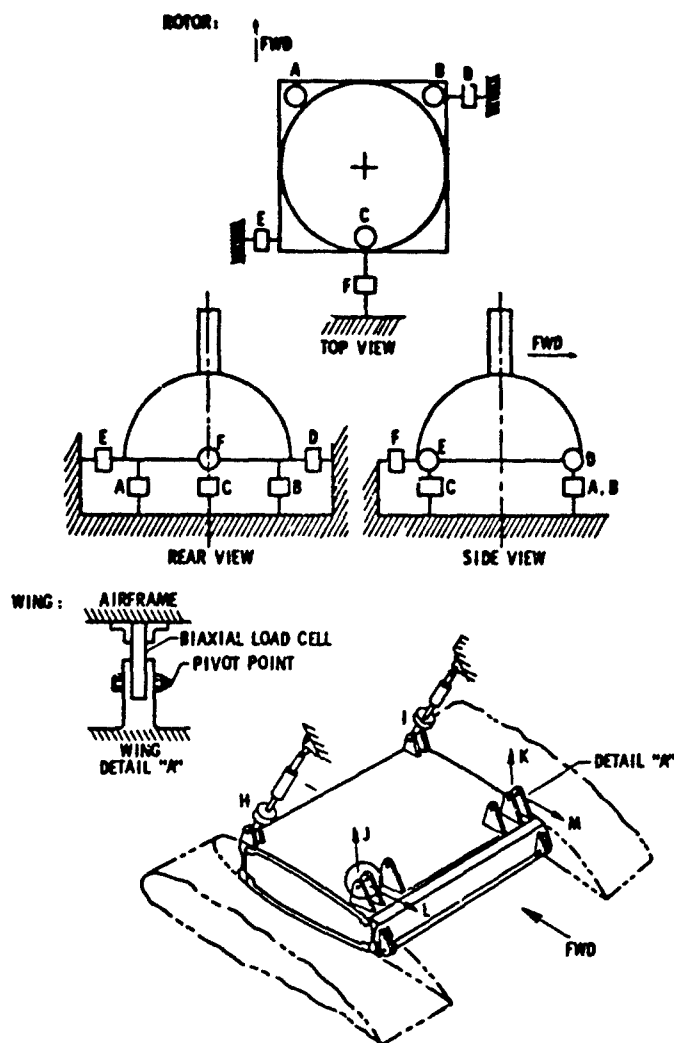


Figure 10. Rotor and wing flight loads measurement systems configuration.

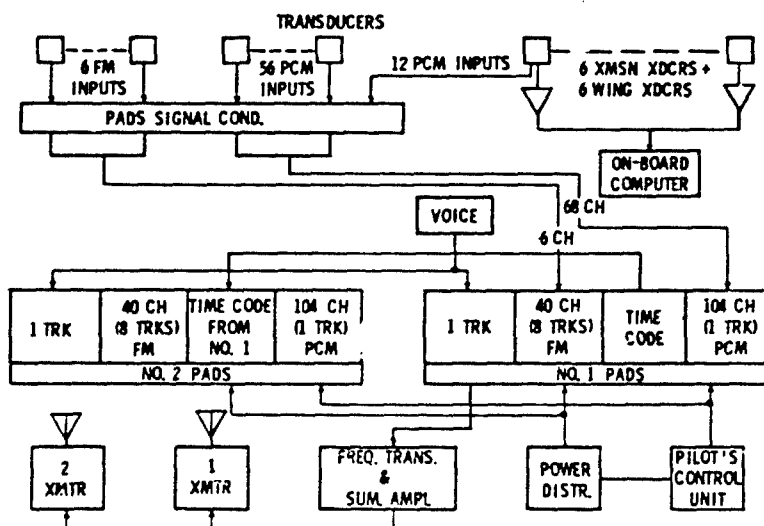


Figure 11. Research instrumentation system schematic.

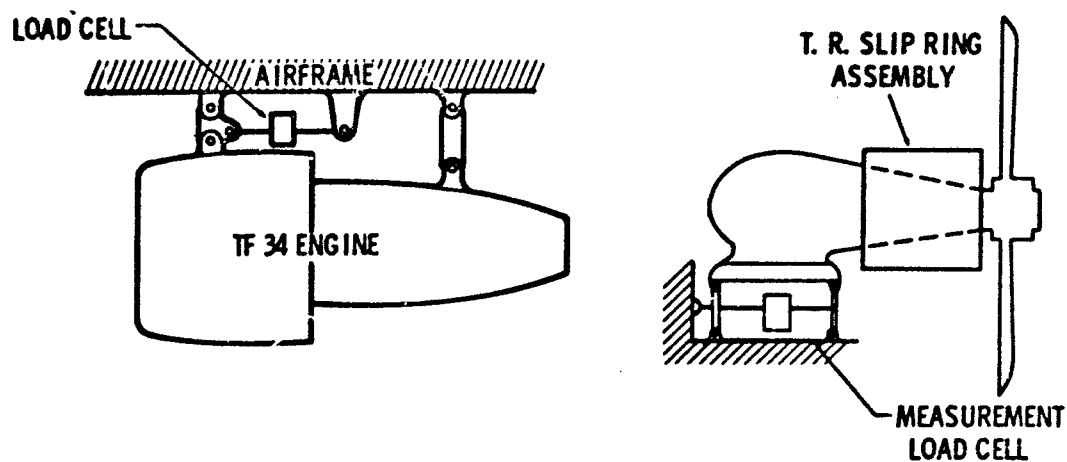


Figure 12. Auxiliary propulsion and tail rotor flight loads measurement systems configuration.

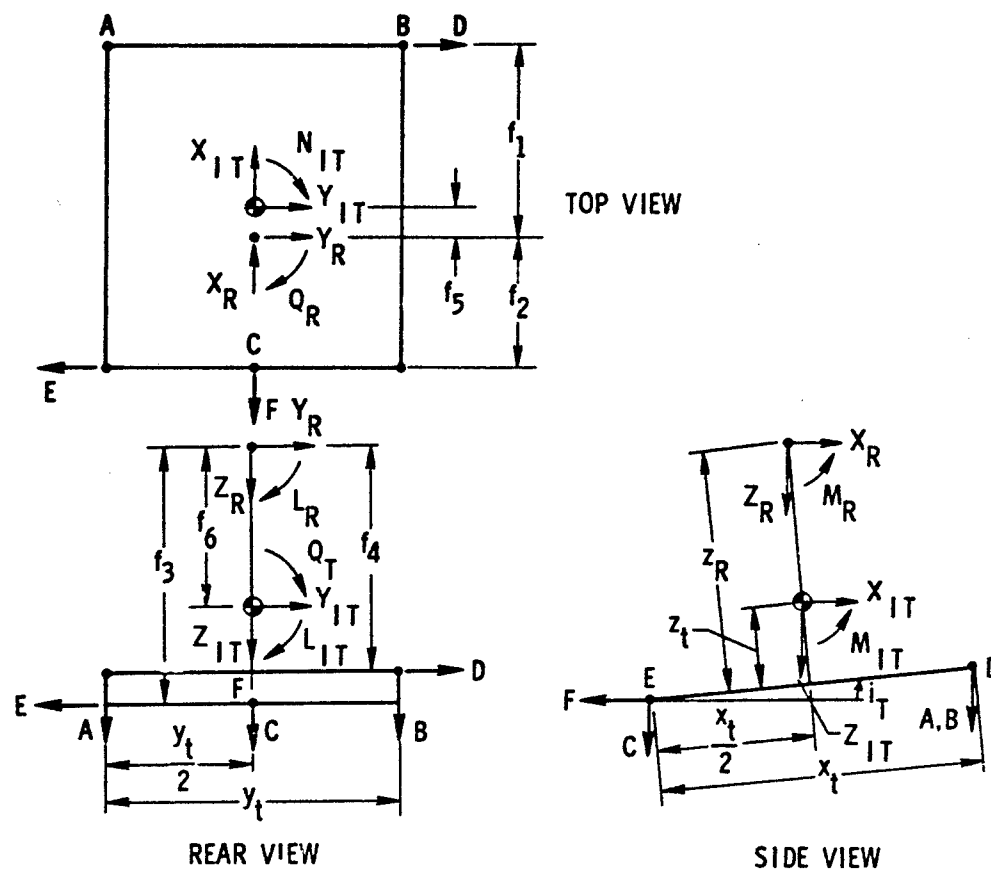


Figure 13. Rotor flight loads measurement system geometry.



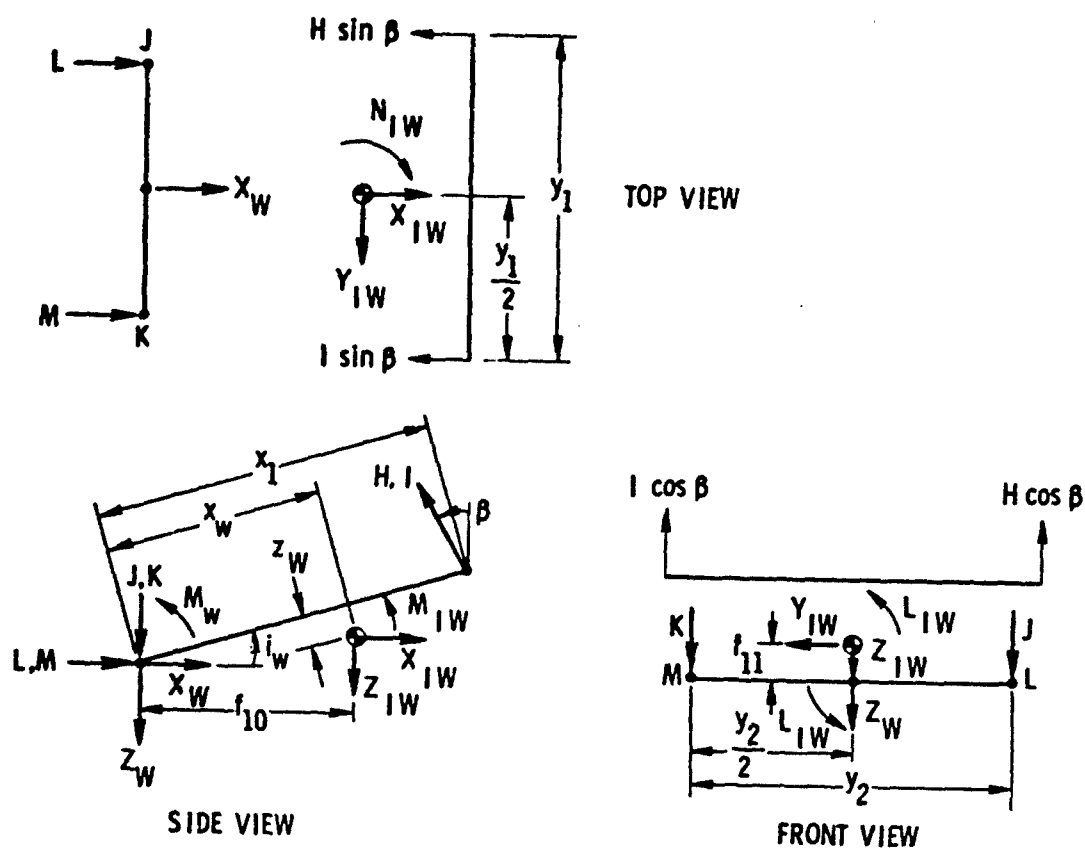


Figure 14. Wing flight loads measurement system geometry.

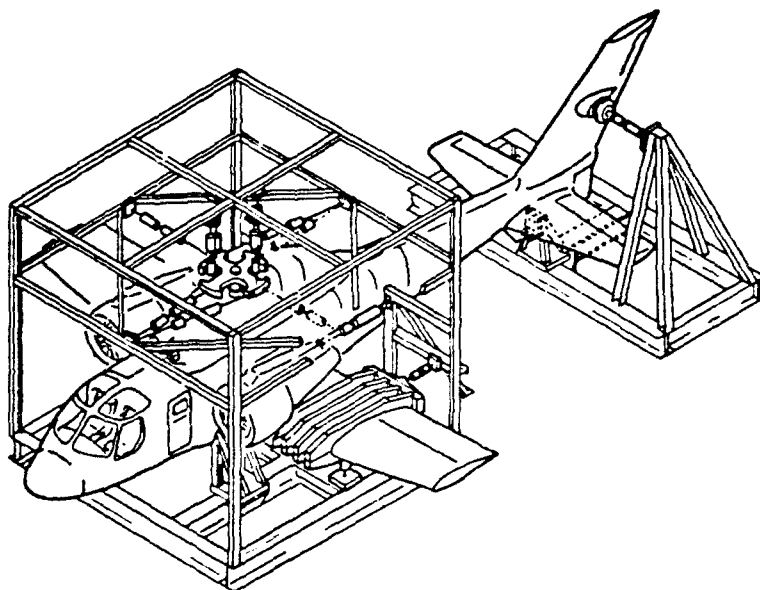


Figure 15. Flight loads measurement systems calibration fixture.

## COMMENTS ON COMPUTATION OF AIRCRAFT FLIGHT CHARACTERISTICS

by

C.L. Livingston,  
Group Engineer, Stability & Control,  
Bell Helicopter Company,  
Fort Worth, Texas 76101, USA

A digital computer program (C81) is used to compute performance, dynamics, and loads of a wide variety of aircraft shown in Figure 1. Figure 2 shows some of the configurations which have been simulated on C81. The configuration simulated depends upon the values specified in the input data card deck and the program logic control switch settings.

The computer program was initially designed to solve for helicopter rotor loads in steady and maneuvering flight. Fuselage aerodynamics and a quasistatic dynamic flight stability section were added next. Gust penetration by the rotor disk was simulated for ramp, sine-squared, and later vortex gusts. The rotor dynamic model was restructured into the present normal modes model so that rotor transient response can be computed. Auxiliary propulsion (jets or propellers), drag brake, store drop and improved aerodynamic interference equations were added also. Figure 3 summarizes the major features of the current program which is fully documented in USAAMRDL TR 74-10 (3 volumes), "Rotorcraft Flight Simulation with Aeroelastic Rotor and Improved Aerodynamic Representation", June, 1974, by J.M. Davis, R.L. Bennett, and B.L. Blankenship. The control linkage array enables the control surfaces of all the configurations shown in Figure 2 to be connected to the pilot's controls and phased with each other or mast tilt as necessary. Wake tables can be used when a very detailed rotor induced velocity distribution as a function of rotor thrust, advance ratio, and inflow ratio is determined from a separate analysis. Separate wake tables are available to represent impingement from each rotor on each aerodynamic surface. The simplified wake interference equations which are integral to the program are usually adequate for most performance and stability analyses.

The computer program solves for the equilibrium solution of the force and moment equations first. This trim solution may be obtained in accelerated or unaccelerated flight, regardless of the flight path angle or power required as long as a realistic trajectory is specified. The trim solution provides control positions and performance data. Rotor loads are also available if requested.

Either the small perturbation theory stability data or maneuver sections of the program may be entered once trim is established. The maneuver section computes response and loads to disturbances caused by control motion, gusts, weapon recoil, store drop, throttle chop, etc. At any point in the maneuver, both stability and rotor loads data are available upon request. The stability section uses quasistatic rotor aerodynamics and computes the eigenvalues and eigenvectors to the characteristic equations of motion. Up to 14 degrees of freedom may be specified: 6 rigid body, 2 flapping for each rotor and 2 pylon deflections for each pylon. The number of degrees of freedom to be used is specified in the input data - from two, uncoupled, 3 by 3 matrices for longitudinal and lateral-directional flight modes, up to the fully coupled 14 by 14 matrix. Transfer functions of attitude response to control displacement are calculated as well as phase angles and magnitudes for direct plotting of Bode diagrams. Figure 4 summarizes these modes of C81 operation.

A typical time history of a cyclic pull up in autorotation is shown in Figure 5. To compute this with C81, the initial autorotational trim is computed, the maneuver section entered, and the flight test measured control motions are input. C81 then computes the response of the helicopter, which is shown in the figure as a solid line. Flight test measured values are shown as open circles. Notice that the calculated loads either agree with or have peaks higher than measured in flight test. This is typical of the results of flight test comparisons and the conservative difference assures adequate strength of first designs of components.

Use of the normal mode approach for representing aeroelastic rotor loads resulted in an improvement in the prediction of pitch link oscillatory loads. Figure 6 compares measured and calculated loads for different weight and store configurations. Loads were computed with and without bearing friction and compare quite well with measured data.

Figure 7 illustrates one of many features of the maneuver section of the program. The "g-tracker" feature computes the control motions necessary to produce the time history of normal acceleration which is specified in the input data. The variation of all other flight parameters and loads during the resulting maneuver may then be plotted. The rapid change in  $g$  of Figure 7 excites the short period mode of the example helicopter. The inherent damping and frequency is clearly shown and can serve as a check on the frequency and damping computed by small perturbation theory used in the stability analysis.

The possible linkages between the pilot controls and the control surfaces of the helicopter are shown in Figure 8. For fixed wing aircraft, the collective control can become the throttle and the rotor swashplate angles become ailerons, elevator and rudder. Both fixed wing control surfaces and rotor controls may be connected by linear or non-linear linkages for compound aircraft such as autogyros, winged helicopters with auxiliary propulsion, or tilt-rotor helicopters.

The degrees of freedom and force and moment equations used in the linear stability analysis are indicated on Figure 9. The user of C81 can select which degrees of freedom to use for any problem by appropriate input data switches (0 or  $\neq 0$ ). Also shown on this figure are the two most frequently used representations: the uncoupled longitudinal and lateral-directional equations and the fully coupled  $6 \times 6$  flight-path equations. Degrees of freedom not used are treated quasistatically; that is, after the perturbation in the stability variable of interest is made, all degrees of freedom not used in the stability matrix are allowed to seek new equilibrium values caused by the changes forces and moments. The resulting derivatives are total derivatives and include the partial derivatives of all excluded degrees of freedom.

The C81 program is used in the design stage to compute performance, stability, and loads data. The capability to compute maneuver data enables realistic design loads to maneuvers called out in customer specification requirements. Stability and transfer function data allow rapid design of stabilization systems and determination of design trade-offs involved when stability actuator authority is varied. Response to gusts include the diminished loads caused by aircraft response. If the "autopilot" feature is used, the required autopilot actuator authority can be determined at a glance, as well as maximum and minimum variations of all flight parameters and loads.

## PROGRAM USES

- I. Performance
  - A. Thrust, Power, Attitude
  - B. Free-Flight, Wind Tunnel
- II. Rotor Dynamics
  - A. Loads
  - B. Stability
- III. Stability & Control
  - A. Stick Fixed
  - B. Forced Response

Figure 1

## POSSIBLE C81 CONFIGURATIONS

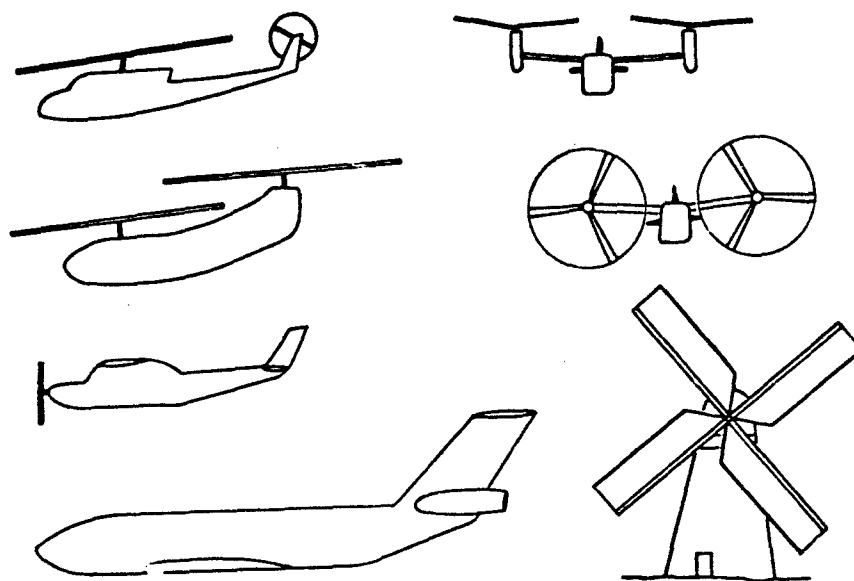


Figure 2

## C81 MATHEMATICAL MODELS

- I. 2 Rotors
  - A. Aeroelastic and/or Quasistatic
  - B. Up to 7 Blades each
  - C. Any Hub Type - Rigid, Articulated, Teetering
- II. Rigid Fuselage
  - A. Large Angle Aerodynamics
- III. 6 Aerodynamics Lifting Surfaces
  - A. Wing (separate left and right hand panels)
  - B. 4 Surfaces
  - C. No Small Angle Assumptions
- IV. Control Linkage
- V. Wake Table
- VI. Flight Constants

Figure 3

## MODES OF OPERATION

- I. Trim ( $\Sigma F = 0$ )
  - A. Control Settings
  - B. Performance
  - C. Rotor Loads
- II. Maneuver (Num. Integration)
  - A. Forced Response
  - B. Nonlinearities
- III. STAB (Small Perturbation)
  - A. Stick Fixed
  - B. Transfer Functions

Figure 4

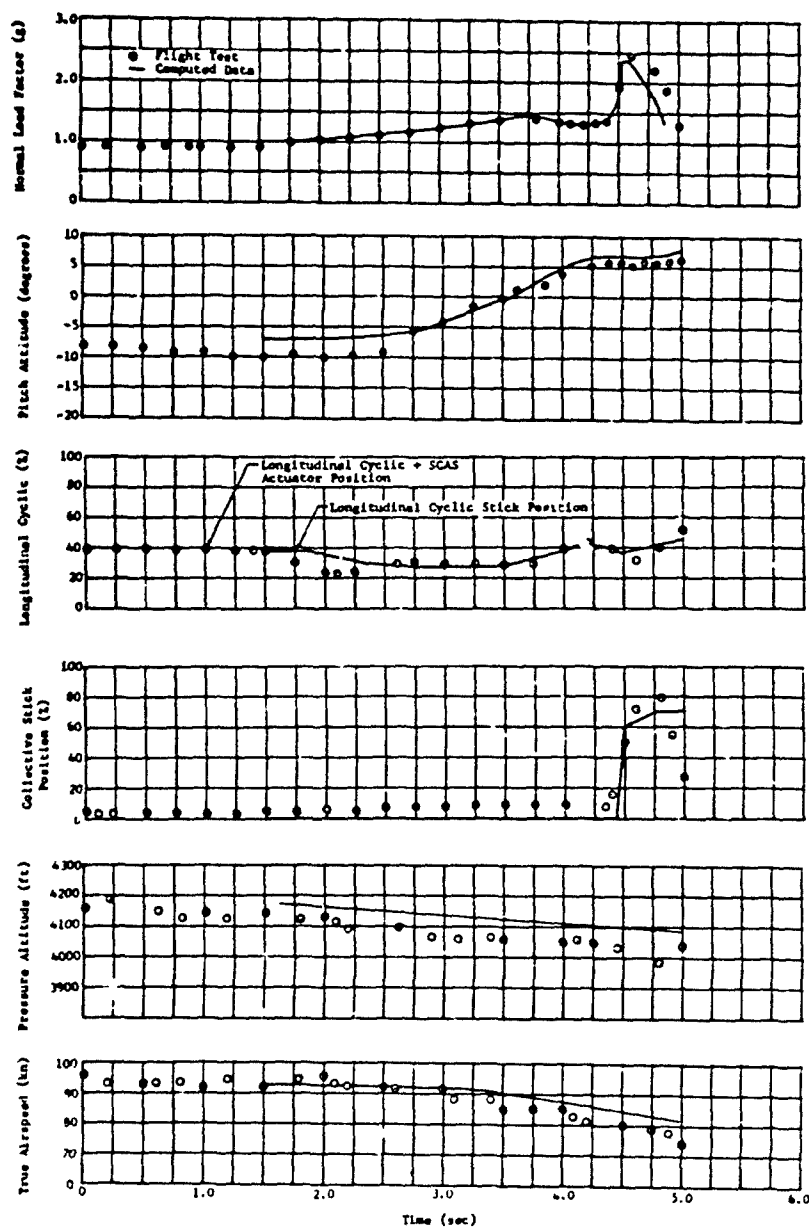


Fig.5 Time histories of symmetric pullup from autorotation, counter 775

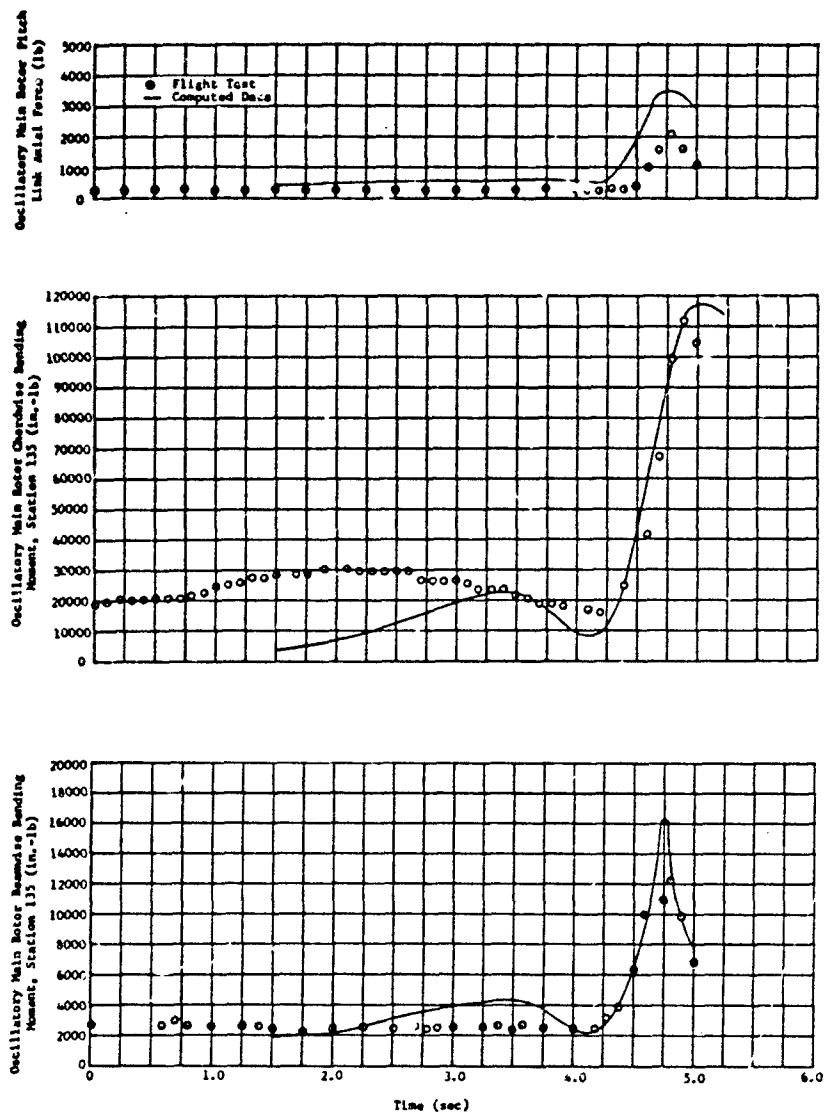


Fig 5 Concluded

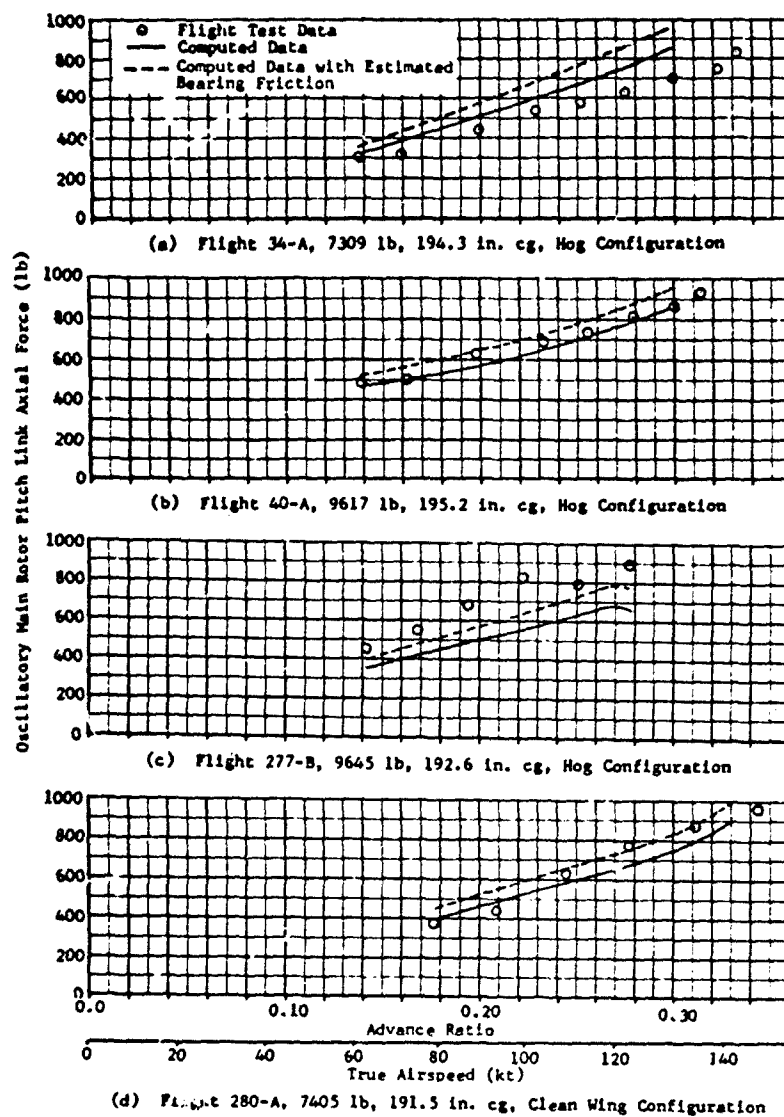


Fig.6 Comparison of measured and computed oscillatory main rotor pitch link axial force

## PILOT SIMULATION

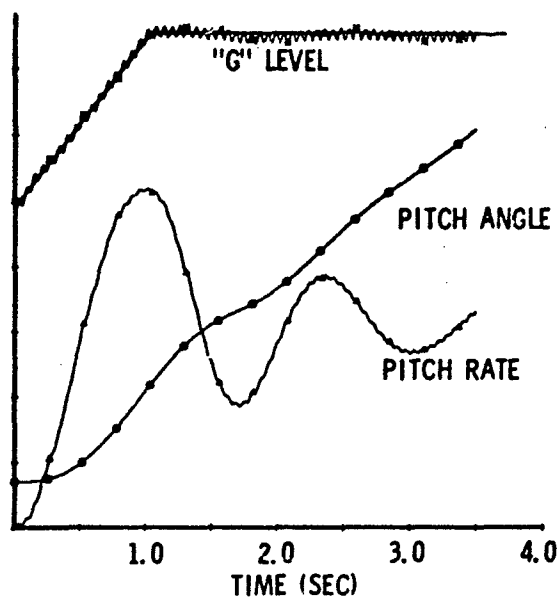


Figure 7

## SUMMARY OF ROTOR CONTROL LINKAGES

Controlled Angle	Independent Control			
	Collective Stick	F/A Cyclic Stick	Lat. Cyclic Stick	Pedal
Rotor 1 Collective	Basic (S, T, C)	XCRT(2) (T)	XCRT(5) (C)	XCRT(10) (C)
Rotor 1 F/A Cyclic		Basic (S, T, C)	XCRT(7) (C)	XCRT(11) (C)
Rotor 1 Lat. Cyclic			Basic (S, T, C)	XCRT(13) (T)
Rotor 2 Collective	XCRT(1) (T, C)	XCRT(3) (T)	XCRT(6) (C)	Basic (S, C)
Rotor 2 F/A Cyclic		XCRT(4) (T, C)	XCRT(8) (C)	XCRT(12) (C)
Rotor 2 Lat. Cyclic			XCRT(9) (T, C)	XCRT(14) (T)

S = Single-Main-Rotor  
 T = Tandem Rotors  
 C = Composite for Side-by-Side Rotors

Figure 8



		CG Deg. of Freedom						Rotor Deg. of Freedom		Pylon Deg. of Freedom	
		Long.			Lat.			main	tail	main	tail
		u	w	q	v	p	r				
CG Forces and Moments	X										
	Z										
	M										
	Y										
	L										
	N										
Rotor Moments	Main										
	Tail										
Pylon Moments	Main										
	Tail										

(a) Basic Stability Analysis Matrix

		Long.	Lat.	Rotor		Pylon	
CG Forces and Moments	Long.						
	Lat.						
Rotor Moments	Main						
	Tail						
Pylon Moments	Main						
	Tail						

IPL (29) = 0  
IPL (30) = 0  
IPL (31) = 0

(b) Uncoupled Fuselage (Two 3x3 Matrices)

Note:

Cross-hatched area represents Degrees of Freedom used in each case.


IPL (29) ≠ 0  
IPL (30) = 0  
IPL (31) = 0

(c) Coupled Fuselage (One 6x6 Matrix)

Fig.9 Schematic of matrices used in the stability analysis

# THE EFFICIENT APPLICATION OF DIGITAL IDENTIFICATION TECHNIQUES TO FLIGHT DATA FROM A VARIABLE STABILITY V/STOL AIRCRAFT

By

J. Victor Lebacqz  
X-22A Project Engineer  
Flight Research Department  
Calspan Corporation  
Buffalo, New York 14221

## SUMMARY

A prerequisite in the use of response-feedback variable stability aircraft to obtain flying qualities data is an accurate method for estimating stability and control parameters from flight data. It is necessary, however, that such methods be efficient and cost-effective to minimize the effort and expense spent performing the estimation. This paper discusses the application of a digital identification technique based on Kalman filter theory to flight data from flying qualities experiments using the variable stability X-22A V/STOL research aircraft. The emphasis of the discussion is on practical aspects of identifying efficiently data covering a wide range of dynamic characteristics; particular attention is paid to the elimination of adjustments in the technique for each data run and the use of particular pilot control inputs to maximize identifiability. Results are presented for a variety of simulated dynamics.

## INTRODUCTION

In general, experimental flying qualities investigations seek to correlate dynamic characteristics of an aircraft to pilot ratings of the suitability of the characteristics for the performance of a prescribed task. Variable stability aircraft incorporate electronic implementation of control laws that vary the dynamic characteristics of the aircraft in a prescribed manner. The most prevalent mechanization of this capability, and the one used in the X-22A V/STOL variable stability aircraft, is the response-feedback system. With this technique, response variables of the aircraft are sensed directly and used to command control deflections proportionally, thereby changing the closed-loop aircraft characteristics; by varying the matrix of feedback gains, a wide variety of aircraft characteristics can be simulated for piloted evaluations. Unlike a ground simulator or model-following variable stability aircraft, however, the resulting dynamic characteristics are not accurately known a priori; it is therefore mandatory to have an accurate and efficient means of identifying the characteristics obtained from flight records.

Since the inception of variable stability aircraft in the early 1950's by the NACA and Cornell Aeronautical Laboratory (now Calspan Corporation), this problem of identification of the dynamics of the simulated aircraft, both for calibration purposes and for the correlation of pilot ratings with the achieved dynamic configurations, has been of extreme theoretical and practical concern. Early methods included various analytic treatments based on hand measurement of recorded responses to prescribed inputs and the matching of responses with the outputs of an analog computer (References 1 and 2). With the advent of the digital computer, it became feasible to handle large amounts of data that might require numerical analyses. This capability led first to equation-error techniques (Reference 3) and then to response-error methods (References 4, 5, and 6), which were applied with various degrees of success to the aircraft identification problem. As is by now well known, however, accurate identification of aircraft parameters generally requires advanced methods that can treat both equation errors (process noise) and response errors (measurement noise). Methods which have this capability include techniques which maximize a classical, non-Bayesian likelihood function (Reference 7) or which extend Kalman filter (Bayesian maximum likelihood) theory to nonlinear situations (References 8, 9).

This paper discusses the application of the identification technique developed in Reference 9 to flight data from the X-22A variable stability V/STOL aircraft (Figure 1). The X-22A aircraft is a unique research tool which is capable of reproducing a wide range of vehicle dynamic characteristics at many fixed-operating STOL flight conditions as well as through a complete V/STOL transition (120 kts  $\rightarrow$  0 kts). To date, the aircraft has been used in two STOL and one V/STOL flight experiments. The first STOL experiment investigated longitudinal short-term dynamic characteristics for landing approach (References 10, 11), and the second studied lateral-directional dynamic characteristics and roll control power requirements for landing approach (References 12, 13). The V/STOL experiment, currently underway, is concerned with the control, guidance, and display requirements for descending decelerating VTOL instrument approaches and landings (References 14, 15). The plethora of dynamic situations simulated in these programs, coupled with the relative inaccuracy of aerodynamic data for the basic aircraft and the requirements for accurate yet economically efficient identification, provides an extensive data base for the evaluation of the practical usefulness of an advanced identification technique.

The organization of this paper is as follows. A brief review of the identification technique and a summary of the X-22A data acquisition and handling procedures are given in the next two sections. The succeeding two sections describe the selection of the a priori information needed by the algorithms and review recent theoretical aspects of designing control inputs to enhance identifiability. Representative results from the lateral-directional STOL program are then presented, followed by preliminary results from approximated control input designs obtained in the third program. A few remarks and recommendations conclude the paper.

### IDENTIFICATION TECHNIQUE

The identification techniques used on the X-22A flight data are:

- A classical least-squares equation-error method, which can be used by itself but which generally provides initial estimates for
- A Bayesian maximum-likelihood estimator, using a recursive, locally iterated Kalman filter.

As is generally known, equation-error techniques lead in theory to biased parameter estimates in the presence of measurement noise. In practice, modern gyros and air sensors have good signal-to-noise ratios, and in fact equation-error techniques often provide sufficiently accurate results (Reference 16); experience with X-22A data analyses has shown that damping ratios of oscillatory motions tend to be underestimated but that frequencies are generally quite accurate using equation-error derivative estimates. The primary advantage of the equation-error technique is that it is rapid and inexpensive, and that it is sufficiently accurate given the quality of the X-22A sensors to provide good initial estimates for the locally iterated Kalman filter.

The development of this version of a Kalman filter for aircraft identification has been described in detail elsewhere (References 9, 17) and hence will be reviewed only briefly here. The central idea is to obtain a suboptimal minimum variance estimate of the parameters (and states) from the measured data for generally nonlinear systems by extension of Kalman filter theory. To this end, we consider an augmented state consisting of the aircraft states and the parameters to be identified; the resulting state equation is, of course, nonlinear even if the unaugmented state equation is linear, and therefore some form of approximation to the optimal nonlinear filter is required. A common approximation is to use an extended Kalman filter to estimate the states; this technique, however, has been shown to yield biased estimates, the cause for which may be viewed as inaccuracies in the reference trajectory about which the linearization takes place. To improve the reference trajectory, therefore, a locally iterated filter-smoother is used (References 9, 18, 19), which is possible because of the recursive nature of the technique. This procedure updates the reference trajectory between every two time points through alternate one-stage extended Kalman filtering and one-stage smoothing, the iterations continuing until there is negligible change in the reference trajectory between successive iterations. It can be shown formally that this procedure reduces the bias caused by state and measurement nonlinearities (Reference 9).

The salient features of this identification technique may be summarized as follows (Reference 20):

1. The technique seeks minimum variance estimates (i.e., the conditional mean) of general systems described by nonlinear state and measurement equations including both process and measurement noise. The formulation of the algorithms is predicated on this generality; hence for example, the implicit nonlinearity introduced by augmenting the state with the parameters to be identified does not compromise the formulation.
2. The technique is recursive in nature. It is theoretically possible to apply the algorithms on line in real time, although this capability is not included at present in the X-22A data acquisition equipment.
3. The technique as currently employed on the X-22A programs does not estimate the measurement and process noise covariances. Methods which directly maximize the likelihood function do perform this estimation well for linear systems (Reference 7), and the lack of this capability is somewhat of a drawback of the technique. For the application of the technique to X-22A flying qualities flight data, however, the deficiency is minor, as (1) the model structure is generally well defined and calibration flight records are obtained in relatively smooth air, both of which decrease the process noise in the system, and (2) the quality of the data acquisition procedures and measuring sensors is high enough to obtain valid a priori measurement noise statistics from the flight records. The determination of the process and measurement noise covariances for the X-22A is discussed in more detail in a later section.

### DATA ACQUISITION EQUIPMENT AND PROCEDURES

The data acquisition systems and procedures used for X-22A flight programs are described in References 21 and 22, and only those aspects which bear on identification of the flight records are repeated here.

A schematic of the digital data acquisition system is shown in Figure 2. Sensors in the aircraft measure all pertinent quantities, such as rigid body responses, control deflections, and variable stability system command signals. This information is sampled 200 times per second and telemetered via an L-band pulse-code-modulated telemetry link to a mobile ground station, where it is decoded and recorded on line on the "bit-stream" recorder. For post flight data analyses, the bit-stream information is processed through the digital mini-computer to produce an IBM 370/65 compatible digital tape.

The data on this digital tape are then processed and edited to be compatible with the identification computer programs. In the first X-22A flight program, the data were initially digitally filtered by a third-order Butterworth filter in order to reduce the sampling rate to the 1/0.08 samples/second of the identification technique without introducing aliasing errors. It was ascertained experimentally, however, that this filtering is not necessary; hence, on the succeeding programs, no digital or other filtering of the telemetered data was performed.

#### ALGORITHM INPUT INFORMATION

The purpose in using a Bayesian, rather than non-Bayesian, maximum likelihood estimator is to make use of known information concerning the qualities of the measurements or initial parameter estimates rather than estimating them along with the actual parameter values. The following a priori information is therefore required to initiate the Kalman filter algorithm:

1. Initial estimates of the parameters
2. Variances of the initial estimates
3. Measurement noise variances
4. Process noise variances

Thorough discussions of the selection of these values are given in References 10, 12, 20, and 22, and hence only a brief qualitative summary is given here. The primary point of importance is that, although the performance of the algorithm can be improved by "optimizing" this information for each data set, it is necessary to seek compromise values whenever possible if doing so makes the identification process more efficient and hence economical.

As was mentioned earlier, the least-squares equation-error method is used to provide initial estimates for the Kalman filter algorithm. In addition to the parameter estimates, the equation-error method also provides estimates of their variances; these variances, however, are incorrect absolutely (too small) and relatively (wrong indications of relative accuracy). It is preferable theoretically, therefore, to compute the initial variance estimates by an independent method. As is discussed in References 9 and 20, one such method is to compute the Cramer-Rao lower bounds on the variances, which are functions of the control inputs as well as the parameter values, and multiply them all by a large factor. Experimental experience has shown, however, that multiplying the equation-error variances equally by an arbitrary, large factor (i.e. 100) appears to provide adequate results (hence indicating relative insensitivity of the technique to the initial ratios of the variances), and thereby eliminates an additional computational step.

The measurement noise statistics are obtained by visual examination of the flight records. This estimate is then checked qualitatively by comparing plots of the residual sequences of the filter operation with the assumed noise statistics, and readjusting the statistics if required. The X-22A data acquisition system provides data with excellent signal-to-noise ratios in general, and therefore this method of estimating the measurement noise variances is sufficiently precise. Again, in the interests of rapid and efficient identification procedures, the measurement noise statistics are kept the same for all data records if possible.

The most difficult choice of required a priori information is that of the process noise statistics. To some degree, the process noise covariance matrix  $Q$  is a "fiddle parameter" in the algorithm which may be used to improve its performance for a given data record. On the other hand, the requirement for rapid post-flight identification as nearly automatic as possible leads to a desire to hold these statistics at a fixed value for all flight records. To make this tradeoff, then, it is important to define precisely what the sources of process noise might be. For the X-22A data, there are essentially three sources of process noise:

1. Gust or turbulence inputs
2. The variable stability system
3. Modeling errors

Of these, the gust inputs are of the least significance for the records that are analyzed, because the majority of calibration identification records are obtained in turbulence-free air to facilitate rapid checks on the frequency and damping of prevalent rigid-body modes of motion. The variable stability system is the source of "noise" both as a result of its dynamics not being included in the model and through its operation on noisy measurement signals. Modeling errors are primarily a result of the fundamental restriction that we seek the best linear model for the aircraft dynamics that will fit the data, as most flying qualities parameters are defined in terms of linear systems.

For identification of the X-22A data, it is assumed that one set of process noise statistics is acceptable for all configurations save those which involve the de-augmentation of several stability derivatives (in which case the linear model becomes a poor approximation), and this set is used for the rapid processing of the data. The values of the statistics are selected primarily by iteration on early data sets to achieve adequate performance, and then held constant. A more complete description of this procedure is given in References 20 and 22.

#### IDENTIFIABILITY OF DATA

Perhaps the most important aspect of maximizing the efficiency of the identification process concerns choosing control inputs to enhance the "identifiability" of the desired parameters from the data. The best identification performance possible, in the sense of minimum mean square estimation error, is given by the Cramer-Rao lower bound on the variances, which is a direct function of the characteristics of the input. A fairly sizable body of literature has therefore developed concerning "optimal" input designs which are predicated on minimizing some scalar indication of these bounds (References 23, 24) or maximizing a similar scalar measure from the Fisher information matrix, the elements of which are the sensitivities (Reference 25). The difficulty with these designs is that the question of what is being optimized becomes important: in all cases, some scalar must be chosen for optimization, since there is no defined "optimal" for

a matrix. In addition, the design problem formulated this way is a fixed interval optimization problem, and hence does not indicate the amount of data necessary to achieve a desired accuracy, which is an important question from a flight-test-conduct point of view. A recent reformulation of the input design problem by Chen appears theoretically to offer a more useful result (Reference 26).

Chen formulates the problem as a time-optimal control problem subject to constraints on the maximum allowable variances. With this formulation, the design procedure yields a "bang-bang" control for many applications, with the switching intervals being dependent on the system parameters; this characteristic is exploited in the use of less expensive "suboptimal" designs, in which the switching points are chosen by recursively computing the Cramer-Rao lower bounds on the variances and using their time-rates-of-change as switching indicators. The input designs using this new approach are compared in Reference 26 to other designs, and the results appear to demonstrate increased identifiability.

On the three X-22A flight programs, three different approaches to input design for identification have been followed. The first program used simple elevator stick doublet inputs, since angle of attack stability and pitch rate damping were the primary variations between configurations, and this simple input provides good sensitivities for these derivatives. The second program involved variation of a majority of the lateral-directional derivatives, however, and a single simple input could not provide sufficient identifiability. On this program, therefore, an attempt was made to have the pilots put in "switching" inputs in both roll and yaw, with the frequency requested as being close to the natural frequencies of the simulated aircraft. This approach generally provides good identifiability (Reference 20), although the fact that the pilot may tend to act as a feedback controller can rapidly degrade the identifiability, since then the inputs become linearly related to at least one aircraft output. On the third program, these "switching" pilot inputs were again used, and, in addition, an attempt was made to implement a suboptimal time-optimal input design based on the results of Reference 26.

To check on the "goodness" of the inputs, two alternatives are available. First, as we have discussed, the Cramer-Rao lower bound may be calculated for the record using the estimated stability derivatives. In a relative sense between several records, however, it is not necessary to perform this additional calculation. If we assume that the identification technique approaches an efficient estimator (unbiased, minimum variance), then the final variance of the parameters computed by the technique should approach the Cramer-Rao lower bound (Reference 9); therefore, a comparison of the magnitudes of the diagonal terms in the final covariance matrix provides some indication of the identifiability. It is also instructive to normalize this matrix and examine the normalized covariances between the parameters, as high values (e.g.,  $\sim 0.9$ ) indicate a strong degree of linear dependence.

#### APPLICATION TO FLIGHT DATA

##### Representative Results: Lateral-Directional Dynamics

To provide an indication of the quality of the results obtained with this identification technique, representative time history matches from the second flight program are given in Figures 3-5. Results from the first program are given in Reference 10, and a more detailed presentation from the second program is given in Reference 12.

The second X-22A flight program investigated lateral-directional flying qualities and roll control power requirements for STOL landing approach. Primary variables in the experiment were roll mode time constant, Dutch roll frequency, and the roll-to-sideslip ratio, out of which seven base dynamic configurations were selected; for each of these, yaw due to aileron was varied, and, for selected cases, the available roll control power was electrically limited. To achieve these dynamic configurations, all of the roll and yaw moment derivatives of the X-22A were changed by the variable stability system, and a large quantity of resulting calibration configurations were generated whose characteristics had to be determined from flight calibration records.

The identification of these data was performed using a set of equations which included nonlinear kinematic terms and linear expansions of the aerodynamics (see Reference 12). The results shown in the figures span the range of dynamics investigated in the experiment. Configuration 1 in Figure 3 has highly augmented roll damping and de-augmented directional stiffness; Configuration 4 in Figure 4 has augmented directional stiffness, approximately the same roll damping as the X-22A, and de-augmented dihedral effect; Configuration 6 in Figure 5 is similar to Configuration 4 except that the roll damping is de-augmented.

The results shown in these figures were obtained by the "production line" techniques dictated by the exigencies of a flight program as discussed earlier; that is, a set of measurement and process noise statistics selected by iteration during the early calibration data analyses were used uniformly. The initial covariance matrix of the estimates was also obtained by simply multiplying the equation-error variances by a constant factor; the factor used for these data was  $10^3$ , which did not precipitate filter instability in these cases and yet ensured sufficient filter gain.

##### Effect of Initial Estimates

Although, for good signal-to-noise characteristics of the measurements, the equation-error technique provides initial parameter estimates that are quite accurate, it is nonetheless useful to ascertain if the locally iterated filter smoother algorithm can be shown to provide good results regardless of the initial estimates. Figure 6 gives the results of identifying the same data as in Figure 4, but with the initial estimates set at zero. The initial variances, measurement noise statistics, and process noise statistics are identical. As can be seen, the final derivative estimates and modal characteristics are identical. This demonstrated insensitivity to the initial estimates and resulting decrease in non-uniqueness problems is extremely valuable to the "production line" identification required on flying qualities programs, as it eliminates the need for any "optimal" processing of the data prior to identification.

### Effect of Control Inputs

As we have discussed, the time histories of the control inputs are very important to obtain valid identification results. Figures 7 and 8 show time histories of two calibration records from the current flight program; the configurations are approximately the same, and involve attitude and rate augmentation added to the basic X-22A dynamics. As can be seen by referring to the figures, two types of control inputs were used. In Figure 7, the pilot was told to use longitudinal stick inputs with switching at intervals which were near what he judged the characteristic period to be. In Figure 8, a unique feature of the variable stability system which permits automatic implementation of "perfect" step, pulse, or doublet inputs was used to provide an approximation to an input designed using a suboptimal variation of the procedure discussed in Reference 26. The design called for switching intervals of approximately 3.8 seconds, but the actual interval implemented was unfortunately more on the order of 4.5 seconds, and so this example does not quite provide the "best" results that might be expected.

Both of these control inputs represent attempts to enhance identifiability in the sense of providing both small variances and covariances of the final estimates. On this basis, they are quite successful. The only significant normalized covariances ( $\sigma_{ij} > .5$ ) for either are listed below for the derivatives affected:

$i, j$	$\sigma_{ij}$	
	Manual	Auto
$M_\theta, M_w$	-0.92	-0.74
$M_{\dot{\theta}}, M_{\dot{q}}$	-0.65	-0.46
$M_w, M_u$	-0.29	-0.50

For both of these data sets, the only high covariances are between the  $M_w$  and  $M_\theta$  estimates, which is a result of the configuration having attitude augmentation. The fact that the remainder are low indicates a lack of linear dependence between the parameters themselves as well as the states, which is necessary for good identifiability (Reference 9).

With respect to the variances of the final estimates, it would be expected that the automatic input would provide somewhat smaller ones, since the input design procedure is predicated on picking desired values for the variances. The table below gives the desired accuracy of some of the derivatives used in the suboptimal input design (Reference 26), the final variances achieved with the automatic input approximation to this design, and the variances achieved with the manual input:

$i$	$\sigma_{ii}$		
	Desired	Auto	Manual
$M_u$	.0005	.0011	.0013
$M_w$	.0005	.00055	.001
$M_{\dot{q}}$	.10	.03	.03
$M_\theta$	.50	.09	.12
$M_{\dot{\theta}}$	.03	.0045	.0045
$X_u$	.05	.01	.009
$X_w$	.01	.006	.007
$X_{\dot{\theta}}$	.10	.001	.055
$Z_u$	.20	.025	.024
$Z_w$	.02	.014	.021
$Z_{\dot{\theta}}$	.50	.005	.12

The final variance estimates for both input types are within the desired values except  $M_u$ , although in general the automatic input designed on a suboptimal basis provides increased accuracy.

These variances and normalized covariances are extremely useful in a relative sense for determining identifiability, but care must be taken in the interpretation of the variances as indicators of absolute accuracy. To illustrate this point, the derivative estimates from these two data sets are compared in the table below; in addition, the sums of the two sigma values of the variance estimates are given for comparison with the differences.

Derivative	Manual	Auto	$2\sigma_{man} + 2\sigma_{auto}$
$M_u$	-.00249	-.0233	.004
$M_w$	-.0280	-.0128	.003
$M_q$	-1.276	-1.231	.12
$M_\theta$	-2.595*	-5.474*	.48
$M_{\dot{s}_{ss}}$	.368	.45	.018
$X_u$	-.224	-.193	.038
$X_w$	.023	.034	.028
$X_{\dot{s}_{ss}}$	.014	.084	.11
$Z_u$	-.230	-.176	.10
$Z_w$	-.439	-.464	.07
$Z_{\dot{s}_{ss}}$	.59	.81	.25

\*Not comparable: different amounts of attitude augmentation.

Note particularly that while the differences in the force derivative estimates ( $X_i$  and  $Z_i$ ) are correctly predicted by the variance estimates, those in some of the moment estimates are not. This discrepancy is a result of the correlations between these estimates as given in a previous table; it is clear that low correlations are necessary for the variance estimates to have meaning in an absolute sense between records. A refinement to the design technique of Reference 26 which would constrain the covariances as well as the variances might alleviate some of this difficulty.

These examples, and previous experimental experience discussed in Reference 20, indicate that it is possible to provide inputs that enhance identifiability in actual flight experience, given a little forethought. It is particularly encouraging to find that pilots can be instructed to use inputs which approach "optimal" designs in efficacy.

#### Equation-Error Estimates

For completeness, the time history matches of the equation-error technique estimates for the same data as in Figure 8 are given in Figure 9. As was discussed previously, the X-22A measurement system provides data with excellent signal-to-noise ratios, and hence the equation-error estimates generally are quite accurate, which can be seen in Figure 9; the derivative estimates are compared in the table below.

Derivatives	Eq'n Error	Kal. Filter
$M_u$	-.0149	-.0233
$M_w$	-.0105	-.0128
$M_q$	-1.027	-1.231
$M_\theta$	-4.942	-5.474
$M_{\dot{s}_{ss}}$	.402	.450
$X_u$	-.169	-.193
$X_w$	-.053	-.034
$X_{\dot{s}_{ss}}$	.063	.084
$Z_u$	-.235	-.176
$Z_w$	-.410	-.464
$Z_{\dot{s}_{ss}}$	.32	.81

This fortunate circumstance allows "quick looks" at calibration records in an economical fashion to ascertain whether the achieved dynamics are close to those desired, since the equation-error technique is less expensive to use than the Kalman filter. In the example of Figure 9, in fact, the equation-error and final filter results generally are within 20% of each other, a fact which is partially a result of the well designed input.

#### CONCLUDING REMARKS

This paper has discussed the application of digital identification techniques, and in particular a Bayesian maximum likelihood method based on Kalman filter theory, to actual flight data from the variable stability X-22A aircraft. In the course of the three flying qualities programs conducted with this aircraft, a large quantity of dynamic situations have been simulated and the resulting flight records analyzed (e.g. over 300 records on the second program alone); the emphasis of the paper has therefore been on the practical aspects of identifying many data efficiently and economically. Based on this experience in applying the technique, a general conclusion that can be drawn is that it provides a useful and efficient tool for identifying stability and control derivatives from flight data, and that, in fact, it can be applied in a "production line" fashion required during a flight program with little loss in accuracy.

With respect to the results discussed in this paper, specific conclusions that are pertinent are:

- The locally iterated filter-smoother algorithm developed for nonlinear systems provides very good identification results for the quasilinear (linear aerodynamics) systems discussed in this paper.
- The technique appears to offer the advantage of insensitivity to the initial parameter estimates for X-22A data, thereby eliminating any necessity for data processing prior to identification.
- The required input information to the algorithm (i.e., the covariance matrices) may be held essentially constant for "production line" identification during a flight program after an initial iteration period.
- The control input time histories are very critical to good identification results. Pilot inputs which attempt "switching" near characteristic frequencies provide good identifiability. Inputs which approximate the suboptimal designs developed in Reference 26 further enhance identifiability.

#### ACKNOWLEDGMENTS

The development of the identification technique described in this paper was supported by the Naval Air Systems Command under Contract N00019-69-C-0534. X-22A flight programs are supported by the X-22A Steering Group chaired by the Naval Air Systems Command, and have been performed under contracts N00019-72-C-0044, N00019-72-C-0417, and N00019-73-C-0504. The author is grateful to Dr. R.T.N. Chen, whose technical insight has been particularly helpful, and to Mr. C.L. Mesiah and Mr. J.W. Lyons, who perform all the computer programming for X-22A programs.

#### REFERENCES

1. Neal, T.P.: Frequency and Damping from Time Histories Maximum-Slope Method. *Journal of Aircraft*, Volume 4, No. 1, January-February 1967.
2. Hall, G.W.: A Method for Matching Flight Test Records with the Output of an Analog Computer. Paper presented at the National Electronics Conference, December 1969.
3. DiFranco, D.A.: In-Flight Parameter Identification by the Equations of Motion Technique -- Application to the Variable Stability T-33 Airplane. *Calspan Report No. TC-1921-F-3*, December 1965.
4. Larson, D.B.: Identification of Parameters by the Method of Quasilinearization. *Calspan Report No. 164*, 1968.
5. Hall, G.W., Larson, D.B., and Martino, P.A.: A Quasilinearization Method for Determining Lateral-Directional Modal Parameters from Digitally Recorded Flight Test Data. *Calspan Report No. TM-2832-F-1*, April 1970.
6. Grove, R.D., Bowles, K.L., and Mayhew, S.C.: A Procedure for Estimating Stability and Control Parameters from Flight Test Data by Using Maximum Likelihood Methods Employing a Real-Time Digital System. *NASA TND-6735*, May 1972.
7. Mehra, R.K., Stepner, D.E., and Tyler, J.S.: A Generalized Method for the Identification of Aircraft Stability and Control Derivatives from Flight Test Data. Paper 16-4 presented at 1972 JACC, August 1972.
8. Molusis, J.A.: Analytical Study to Define a Helicopter Stability Derivative Extraction Method, Vol. 1. *NASA CR 132371*, May 1973.
9. Chen, R.T.N., Eulrich, B.J., and Lebacqz, J.V.: Development of Advanced Techniques for the Identification of V/STOL Aircraft Stability and Control Parameters. *Calspan Report No. BM-2820-B-1*, August 1971.
10. Smith, R.E., Lebacqz, J.V., and Schuler, J.M.: Flight Investigation of Various Longitudinal Short-Term Dynamics for STOL Landing Approach Using the X-22A Variable Stability Aircraft. *Calspan Report No. TB-3011-F-2*, January 1973.
11. Schuler, J.M., Smith, R.E., and Lebacqz, J.V.: An Experimental Investigation of STOL Longitudinal Flying Qualities in the Landing Approach Using the Variable Stability X-22A Aircraft. Preprint No. 642, 28th Annual Forum of American Helicopter Society, Washington, D.C., May 1972.
12. Smith, R.E., Lebacqz, J.V. and Radford, R.C.: Flight Investigation of Lateral-Directional Flying Qualities and Control Power Requirements for STOL Landing Approach Using the X-22A Aircraft. *Calspan Report No. AK-S130-F-1*, February 1974.
13. Lebacqz, J.V., Radford, R.C., and Smith, R.E.: An Experimental Investigation of STOL Lateral-Directional Flying Qualities and Roll Control Power Requirements Using the Variable Stability X-22A Aircraft. Paper presented at the 30th Annual Forum of the American Helicopter Society, Preprint No. 841, May 1974.
14. Chen, R.T.N., Lebacqz, J.V., and Aiken, E.W.: A Preliminary Look at Flight Director Design Philosophies for Application to a VTOL Landing Approach Flight Experiment. Paper presented at the 10th Annual Conference on Manual Control, 9-11 April 1974.



15. Lebacqz, J.V., and E.W. Aiken: The X-22A Task III Flight Program: Control, Guidance, and Display Requirements for Accelerating Descending VTOL Instrument Approaches. Paper presented at the Advanced Aircrew Display Symposium, Naval Air Test Center, Patuxent River, Md., April 1974.
16. Wingrove, R.C.: Estimation of Longitudinal Aerodynamic Coefficients and Comparison with Wind-Tunnel Values. Paper presented at NASA Symposium on Parameter Estimation, April 1973, reproduced in: Parameter Estimation Techniques and Applications in Aircraft Flight Testing, NASA TN D-7647, April 1974.
17. Chen, R.T.N., and Eulrich, B.J.: Parameter and Model Identification of Nonlinear Dynamical Systems Using a Suboptimal Fixed-Point Smoothing Algorithm. Paper presented at 1971 JACC, August 1971.
18. Wishner, R.P. et. al.: A Comparison of Three Nonlinear Filters. Automatica, Vol. 5, pp. 487-497, 1969.
19. Jarwinski, A.H.: Stochastic Processes and Filtering Theory. Academic Press, 1970.
20. Lebacqz, J.V.: Application of A Kalman Filter Identification Technique to Flight Data from the X-22A Variable Stability V/STOL Aircraft. Paper presented at NASA Symposium on Parameter Estimation, April 1973, reproduced in: Parameter Estimation Techniques and Applications in Aircraft Flight Testing, NASA TN D-7647, April 1974.
21. Beilman, J.L.: An Integrated System of Airborne and Ground-Based Instrumentation for Flying Qualities Research with the X-22A Airplane. Paper presented at the 7th International Aerospace Instrumentation Symposium, March 1972.
22. Lebacqz, J.V., Smith R.E., and Radford, R.C.: A Review of the X-22A Variable Stability Aircraft and Research Facility. Calspan Report No. AK-5130-F-2, February 1974.
23. Goodwin, G.C.: Input Synthesis for Minimum Covariance State and Parameter Estimation. Electronics Letters, Volume 5, No. 21, 16 October 1969.
24. Reid, D.B.: Optimal Inputs for System Identification. NASA CR-128173, May 1972.
25. Mehra, R.K.: Optimal Inputs for Linear System Identification. Proc. JACC 1972, pp. 811-820, August 1972.
26. Chen R.T.N.: Input Design for Parameter Identification -- Part I: A New Formulation and a Practical Solution. Paper presented at the 1974 JACC, June 18-21, 1974.

#### NOTATION

$I_x$	moment of inertia about body x-axis, ft-lb sec <sup>2</sup>
$I_y$	moment of inertia about body y-axis, ft-lb sec <sup>2</sup>
$I_z$	moment of inertia about body z-axis, ft-lb sec <sup>2</sup>
$I_{xz}$	product of inertia in body axis, ft-lb sec <sup>2</sup>
$L_{\dot{\alpha}}$	$= (1/I_x) \partial L / \partial \dot{\alpha}$ , dimensional roll moment derivative, (rad/sec <sup>2</sup> ) / ( )
$L'_{\dot{\alpha}}$	$= (1 - I_{xz}^2 / I_x I_z) (L_{\dot{\alpha}} + \frac{I_{xz}}{I_x} N_{\dot{\alpha}})$ , (rad/sec <sup>2</sup> ) / ( )
$M_{\dot{\alpha}}$	$= (1/I_y) \partial M / \partial \dot{\alpha}$ , dimensional pitch moment derivative, (rad/sec <sup>2</sup> ) / ( )
$N_{\dot{\alpha}}$	$= (1/I_z) \partial N / \partial \dot{\alpha}$ , dimensional yaw moment derivative, (rad/sec <sup>2</sup> ) / ( )
$N'_{\dot{\alpha}}$	$= (1 - I_{xz}^2 / I_x I_z) (N_{\dot{\alpha}} + \frac{I_{xz}}{I_z} L_{\dot{\alpha}})$ , (rad/sec <sup>2</sup> ) / ( )
$n_y$	body y-axis acceleration, 57.3 ft/sec <sup>2</sup>
$p$	body axis roll rate, deg/sec
$q$	body axis pitch rate, deg/sec
$r$	body axis yaw rate, deg/sec
$t$	time, seconds
$u$	body x-axis velocity, ft/sec
$v$	true velocity, ft/sec
$w$	body z-axis velocity, ft/sec
$X_{\dot{\alpha}}$	$= (1/M) \partial X / \partial \dot{\alpha}$ , dimensional x-force derivative, (ft/sec <sup>2</sup> ) / ( )
$Y_{\dot{\alpha}}$	$= (1/M) \partial Y / \partial \dot{\alpha}$ , dimensional y-force derivative, (ft/sec <sup>2</sup> ) / ( )
$Z_{\dot{\alpha}}$	$= (1/M) \partial Z / \partial \dot{\alpha}$ , dimensional z-force derivative, (ft/sec <sup>2</sup> ) / ( )
$\alpha$	angle of attack, degrees
$\beta$	angle of sideslip, degrees
$S_{ES}$	longitudinal stick position, positive aft, inches
$S_{AS}$	lateral stick position, positive right, inches
$S_{RP}$	rudder pedal position, positive right, inches

- $\zeta$  damping ratio of Dutch roll characteristic response  
 $\theta$  pitch attitude, degrees  
 $\sigma_r$  variance of ( ) in units of ( )  
 $\tau_r$  roll mode time constant, seconds  
 $\phi$  roll attitude, degrees  
 $|a/b|$  magnitude of roll-to-sideslip ratio in Dutch roll component  
 $\omega_d$  Dutch roll undamped natural frequency, rad/sec  
 $\dot{(\ )}$  time rate of change of ( ), ( )/sec

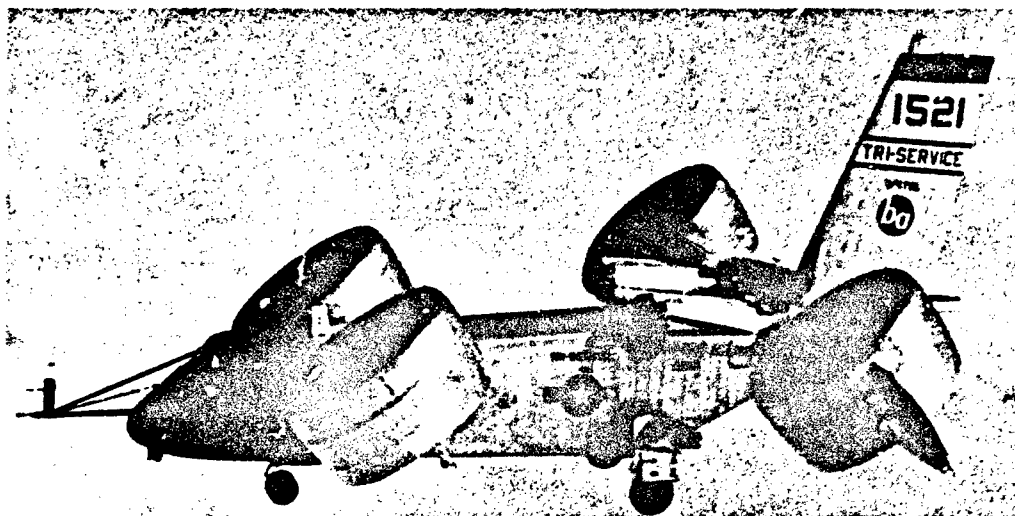


Figure 1. Variable Stability X-22A V/STOL Aircraft

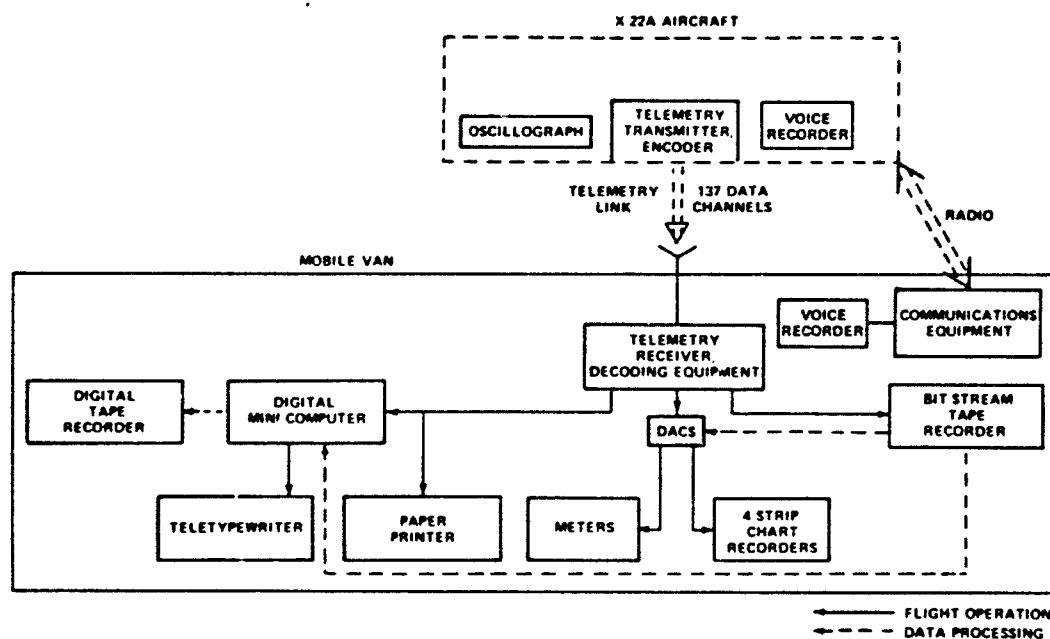


Figure 2. Schematic Diagram of Digital Data Acquisition System

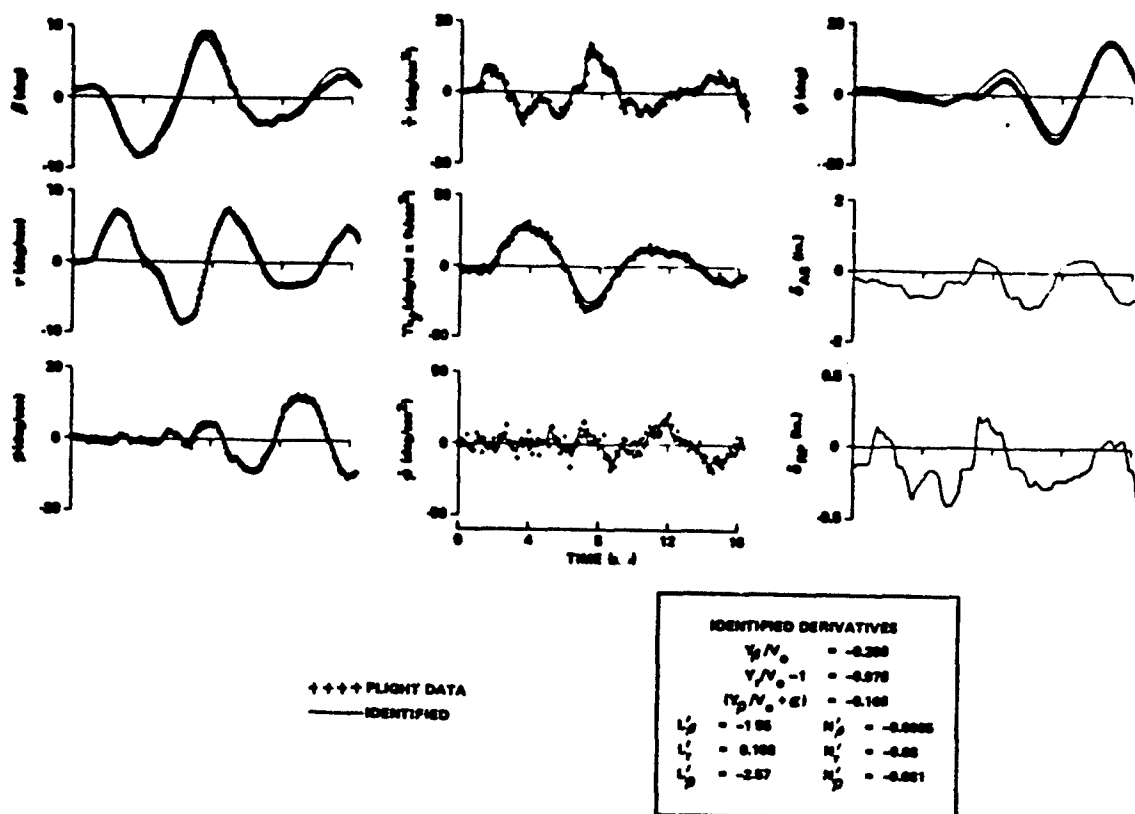


Figure 3. Identification of Configuration 1

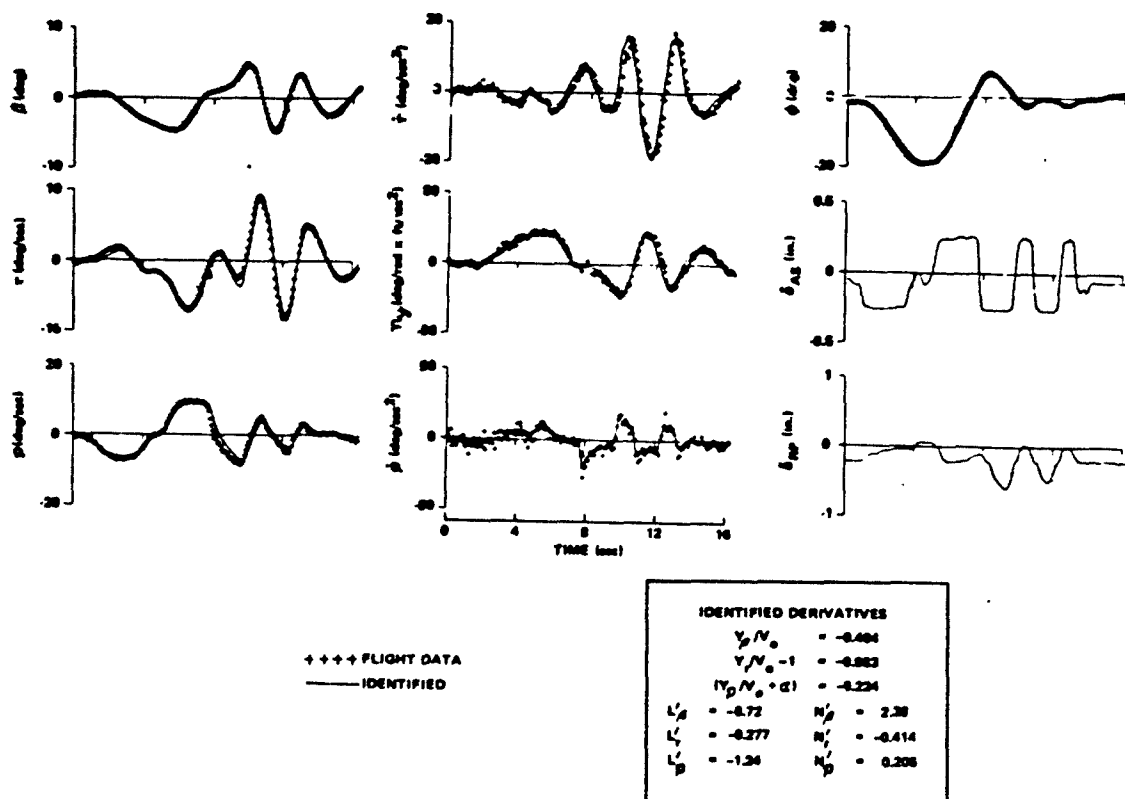


Figure 4. Identification of Configuration 4

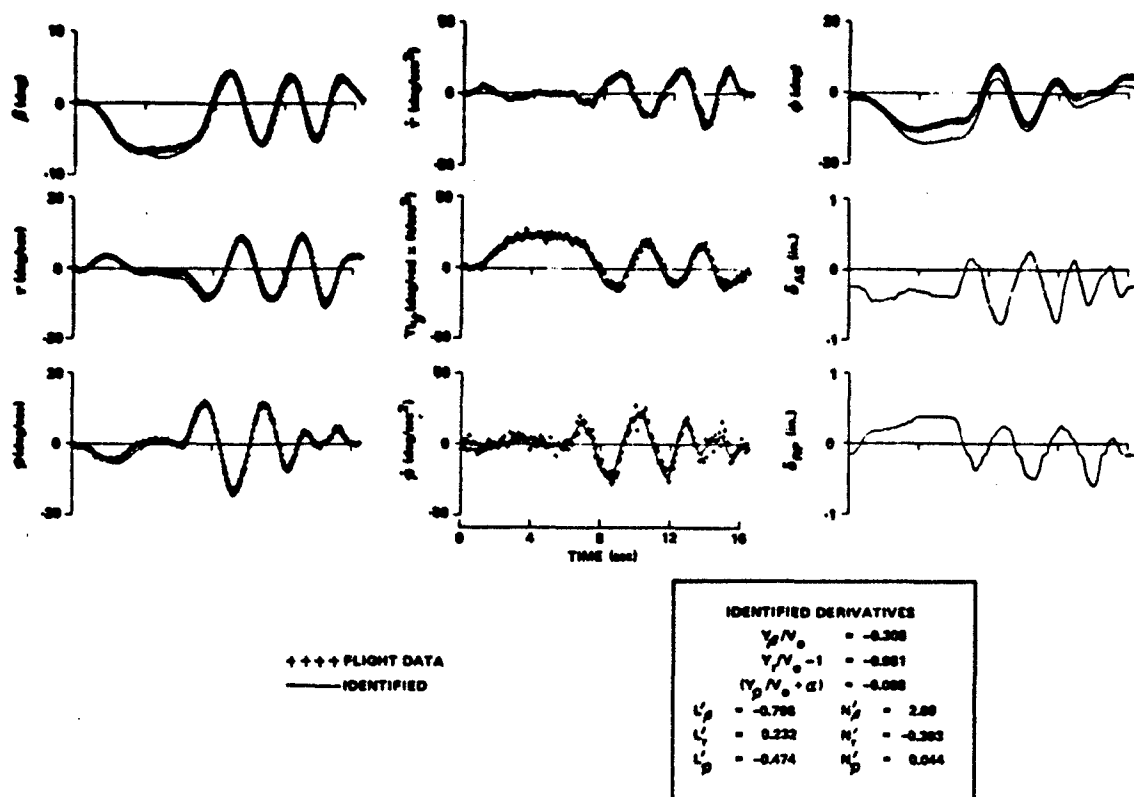


Figure 5. Identification of Configuration 6

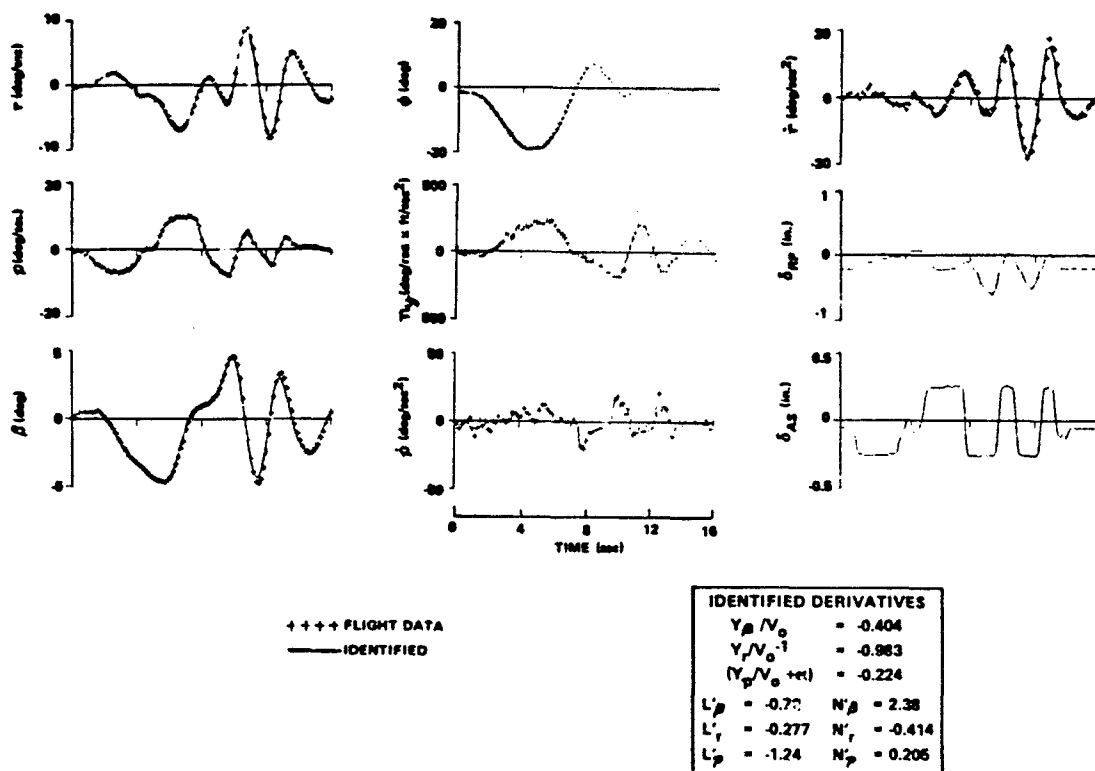


Figure 6. Identification of Configuration 4 With Initial Estimates at Zero

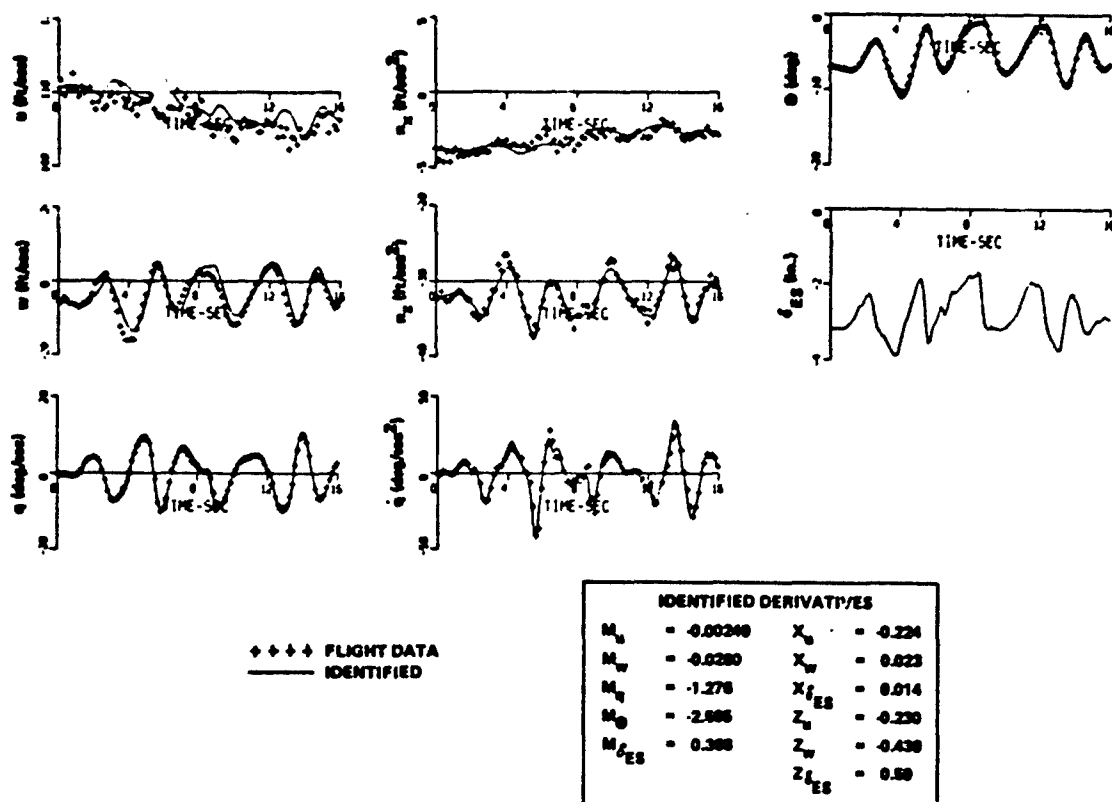


Figure 7. Manual Longitudinal Input

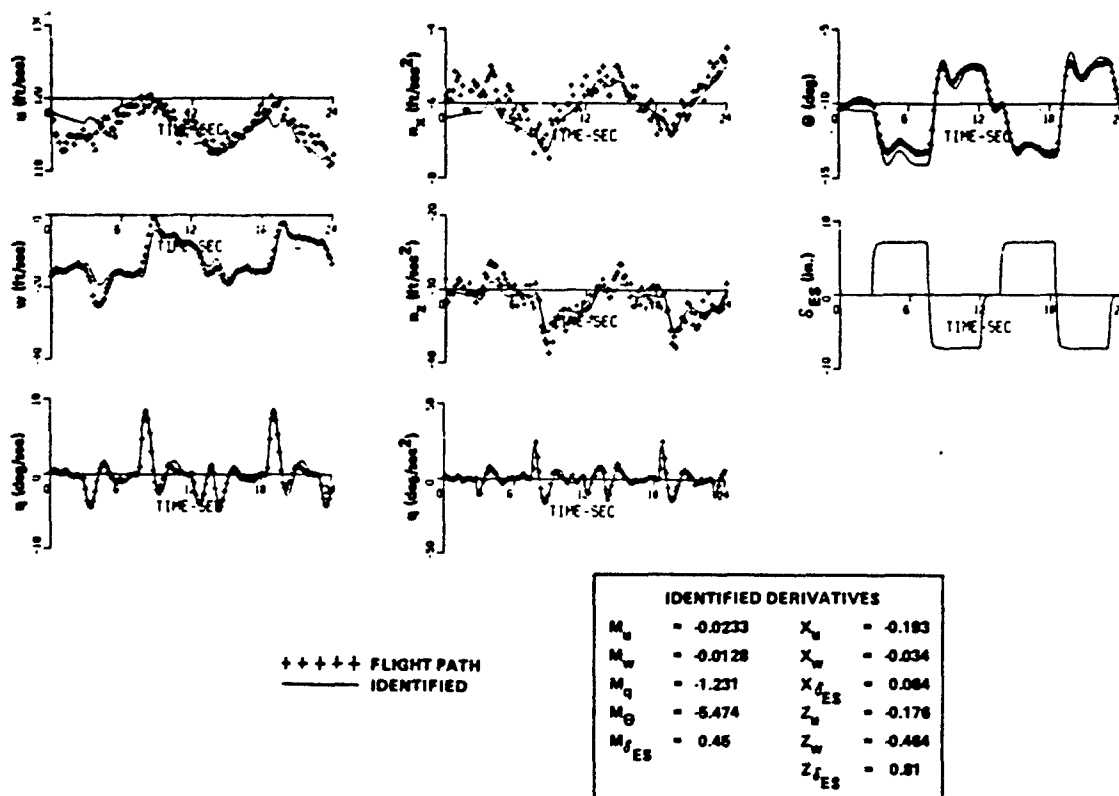
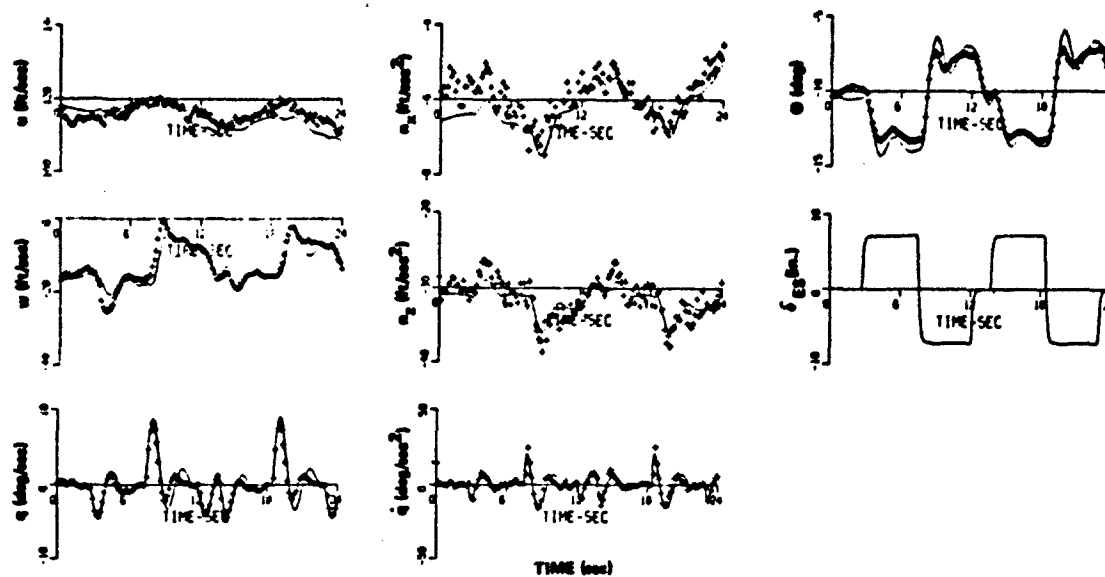


Figure 8. Automatic Longitudinal Input



++++ FLIGHT DATA  
 \_\_\_\_\_ IDENTIFIED

IDENTIFIED DERIVATIVES			
$M_u$	= -0.0149	$X_u$	= -0.189
$M_w$	= -0.0106	$X_w$	= -0.063
$M_q$	= -1.027	$X_{\dot{q}}$	= 0.063
$M_{\dot{q}}$	= 0.402	$Z_u$	= -0.335
$M_{\ddot{q}}$	= -4.942	$Z_w$	= -0.410
		$Z_{\dot{q}}$	= 0.32

Figure 9. Equation-Error Estimates for Data of Figure 8

PARAMETER ESTIMATION OF POWERED-LIFT STOL AIRCRAFT CHARACTERISTICS  
INCLUDING TURBULENCE AND GROUND EFFECTS

Rodney C. Wingrove  
Ames Research Center, NASA  
Moffett Field, California, 94035

### SUMMARY

This paper considers the estimation of longitudinal aerodynamic coefficients from data recorded during flight tests of a powered-lift STOL aircraft. First, a comparison is made between the coefficient values determined by the regression and quasilinearization identification techniques from records taken during elevator pulse maneuvers. The results show that for these tests the regression method provides less scatter in coefficient estimates and provides better correlation with the predicted values. Special techniques are then developed which allow identification of the coefficients from records taken during landing maneuvers in which the aircraft encounters turbulence while flying in ground effect. Flight test results are presented to illustrate the effects of air turbulence and ground proximity on the estimated coefficient values.

### NOMENCLATURE

$a_y$	pitching acceleration, rad/sec <sup>2</sup>	T	thrust term
$a_x$	acceleration measured along X-axis, g units	u	velocity along X-axis, m/sec
$a_z$	acceleration measured along Z-axis, g units	V	total velocity, m/sec
$\bar{c}$	mean aerodynamic chord, m	w	velocity along Z-axis, m/sec
C	aerodynamic coefficient	x	vector of state variables
g	acceleration of gravity, m/sec <sup>2</sup>	$\alpha$	angle-of-attack, rad
h	height-above-ground-level, m	$\delta$	elevator deflection, rad
$I_{yy}$	inertia about the Y-axis	$\theta$	pitch angle, rad
K	constant parameter	$\rho$	atmospheric density
M	aircraft weight	$\sigma$	standard deviation (rms)
q	pitching rate, rad/sec	-	free air value, out-of-ground effect
Q	dynamic pressure	^	estimated value
S	aircraft wing area, m <sup>2</sup>		

### 1. INTRODUCTION

NASA is conducting a rather broad research program on powered-lift concepts for future use with jet STOL transport aircraft. As part of this program a C-8A Buffalo aircraft has been modified with an augmented jet-flap system (ref. 1). This aircraft has been undergoing flight tests to determine the in-flight aerodynamic performance and handling qualities. In support of this program a study has been made to evaluate the use of parameter identification techniques in determining the aerodynamic coefficient values from the recorded flight data.

Several identification methods are available from previous studies (refs. 2-10) to identify the aircraft parameters from the records taken where the aircraft is excited only by elevator inputs in calm air. These previous methods, however, are generally unable to treat the problems associated with identification of the aircraft parameters during landing maneuvers where there are significant external disturbances due to the air turbulence and ground proximity.

In this investigation two different parameter identification techniques have been applied to data recorded during pulse-type maneuvers where the aircraft dynamics are excited by elevator inputs. This paper will review the accuracy in determining the coefficient values using these different identification techniques. Special techniques are then applied to data recorded during landing maneuvers where the aircraft is excited by the combination of air turbulence, ground proximity, and the pilot's normal control actions. This paper reviews the development of these special techniques and presents results which illustrate the effects of air turbulence and ground proximity on the estimated coefficient values.

The intent of the paper is to present the genesis of each of the problems and the identification algorithms used in the problem solution along with a discussion of some of the more important findings.

## 2. AIRCRAFT AND INSTRUMENTATION SYSTEM

The results in this paper were obtained from flight test data recorded during test maneuvers with an augmented jet-flap STOL research aircraft (ref. 1). This vehicle (fig. 1) is a high-wing STOL aircraft powered by two turbofan engines mounted in nacelles located under the wing. The relatively cold flow from the front fans is ducted to augmentor jet flaps. The engine exhaust is directed through nozzles, one on each side of the nacelles, to provide vectored propulsive lift.

The flight test instrumentation included a nose boom with a pitot-static system and vanes, body-mounted accelerometers and rate gyros, vertical gyros, position transducers on the control surfaces, pressure and temperature transducers to measure the propulsive characteristics, and a radar altimeter to measure height-above-ground-level. The vane-measured angle-of-attack,  $\alpha$ , has been corrected to account for angular rates and for upwash (as a function of height-above-ground). The pitching angular acceleration,  $\ddot{\theta}$ , has been derived from the pitch rate signal. The linear accelerations,  $a_z$  and  $a_x$ , have been obtained from the body mounted accelerometer signals and corrected (to the aircraft center-of-gravity) to account for angular accelerations. The flight data were obtained with an airborne digital recorder and then processed at discrete points, 10 points/sec, on a ground based digital computer.

## 3. COMPARISON OF ESTIMATION TECHNIQUES

This section will review some estimation results for standard pulse-type maneuvers in which the aircraft is relatively free from turbulence effects and is above ground proximity effects. Emphasis will be to compare results from the different identification techniques and to gain some understanding of their relative accuracy in estimating the values for the aerodynamic coefficients.

Several previous studies (refs. 2-10) have compared different identification algorithms for estimating aircraft parameters and have found that the results may depend on the technique used. These identification techniques generally fall into two categories: equation error and output error. With noise in the measured aircraft states, the equation error technique can produce biased estimates of the coefficient values (refs. 2-4). The output error technique can reduce the bias error; however, it is affected by modeling errors and also may produce the larger standard deviations in the estimated coefficient values (ref. 10). This paper will compare results of both a regression technique (equation error) and a quasilinearization technique (output error).

### 3.1 Identification algorithms

The non-linear equations used to mathematically model the aircraft longitudinal forces and pitching moment were taken as:

$$\hat{a}_x = (QS/M) [\hat{C}_{x_0} + \hat{C}_{x_\alpha} \alpha + \hat{C}_{x_\delta} \delta + \hat{C}_{x_q} (q\bar{c}/2V)] + T_x \quad (1)$$

$$\hat{a}_z = (QS/M) [\hat{C}_{z_0} + \hat{C}_{z_\alpha} \alpha + \hat{C}_{z_\delta} \delta + \hat{C}_{z_q} (q\bar{c}/2V) + \hat{C}_{z_{C_j}} C_j] + T_z \quad (2)$$

$$\hat{a}_m = (QS\bar{c}/I_{yy}) [\hat{C}_{m_0} + \hat{C}_{m_\alpha} \alpha + \hat{C}_{m_\delta} \delta + \hat{C}_{m_q} (q\bar{c}/2V)] + T_m \quad (3)$$

Coefficient terms are included which account for variations in the aircraft angle-of-attack,  $\alpha$ ; elevator deflection,  $\delta$ ; and pitch rate,  $q$ . This model also includes a  $C_j$  term due to the powered-lift function,  $C_j$  ( $C_j$  = thrust of cold air/QS). Using this model the unknown coefficient values have been determined by the regression (also called equations of motion, or least squares) and the quasilinearization (also called modified Newton-Raphson) parameter identification methods. (Reference 10 outlines the details of these techniques as used for the results in this report.)

Regression is a relatively simple technique which determines the coefficient values that minimize the least squares difference between the time histories for each of the measured accelerations,  $a_x$ ,  $a_z$ , and  $a_m$ , and the corresponding model outputs,  $\hat{a}_x$ ,  $\hat{a}_z$ , and  $\hat{a}_m$ . The coefficient values are determined in three independent solutions, eqs. (1)-(3), using the well-known matrix inversion procedure (ref. 7).

Quasilinearization, in contrast to the regression method, integrates the following kinematic equations to obtain estimated time histories of the aircraft states.

$$\dot{\hat{u}} = g(\hat{a}_x - \sin \hat{\theta}) - \hat{q}\hat{w} + \hat{k}_u, \quad \hat{u}(0) = u_0 \quad (4)$$

$$\dot{\hat{w}} = g(\hat{a}_z + \cos \hat{\theta}) + \hat{q}\hat{u} + \hat{k}_w, \quad \hat{w}(0) = w_0 \quad (5)$$

$$\dot{\hat{q}} = \hat{a}_m + \hat{k}_q, \quad \hat{q}(0) = q_0 \quad (6)$$

$$\dot{\hat{\theta}} = \hat{q} + \hat{k}_\theta, \quad \hat{\theta}(0) = \theta_0 \quad (7)$$

This technique determines the coefficient values (and bias terms) that minimize the weighted least squares difference between the time histories of the measured variables,  $a_x$ ,  $a_z$ ,  $a_m$ ,  $u$ ,  $w$ ,  $q$ , and  $\theta$ , and their corresponding estimated values. With this technique, initial estimates for the unknown parameter values are made (e.g., from the regression results) and then the estimates are successively improved in an iterative manner, using the quasilinearization algorithm (refs. 2, 3 and 6).



One primary difference between these two methods is that with the regression method the variables,  $q$ ,  $\alpha$ ,  $V$ , and  $Q$ , in eqs. (1)-(3) are taken as the measured values, whereas, with quasilinearization these variables in eqs. (1)-(3) are represented by the estimated values;  $\hat{q}$ ,  $\hat{\alpha} = \tan^{-1} (\hat{w}/\hat{u})$ ,  $\hat{V} = \sqrt{\hat{u}^2 + \hat{w}^2}$ , and  $\hat{Q} = \rho V^2/2$ .

### 3.2 Comparison of estimated and measured time histories

Figures 2 and 3 present a comparison of measured time histories with those computed using the two identification methods. Figure 2 presents the regression results and fig. 3 presents the quasilinearization results. Values for the rms difference between the measured and estimated data are listed in table 1. Figures 2 and 3 illustrate that the estimated time histories generally fall within the scatter of the measured data. As shown in table 1, the rms fit to the pitching acceleration,  $a_m$ , is about the same for both methods; however, the regression method provides as much as a 30% better fit to the measured linear accelerations,  $a_x$  and  $a_z$ .

### 3.3 Comparison of coefficient values

The coefficient values determined by the two techniques are presented in fig. 4. Also shown (dotted lines) are the corresponding values which have been predicted from other independent sources, such as steady-state flight tests, wind tunnel tests, and theory (refs. 1, 11-13).

In general, the more important coefficients such as  $C_{z_\alpha}$ ,  $C_{x_\alpha}$ ,  $C_{m_\delta}$ , and  $C_{m_q}$ , are in agreement both between the two methods and with the predicted values. The standard deviations (e.g., run-to-run scatter) of these estimated parameters are also relatively small.

Other coefficients, such as  $C_{z_\delta}$ ,  $C_{z_q}$ ,  $C_{x_\delta}$ , and  $C_{x_q}$ , show somewhat more scatter. The inability of either technique to estimate these terms accurately is probably because the influence of these terms on the aircraft forces is small. And also, there is a strong dependency between the elevator deflection,  $\delta$ , and the pitch rate,  $q$ . Previous studies (e.g., refs. 7, 14-16) have also noted the large standard deviation associated with estimating these terms.

For almost all of the coefficients, the regression values have less run-to-run scatter and agree better with the predicted values. A majority of the regression values (with the exceptions noted above) are within about  $\pm 10\%$  of the predicted values.

### 3.4 Discussion of identification techniques

The results presented show that the regression method provides better results than the quasilinearization method. For instance, the regression method provides a better fit to the measured accelerations, less scatter in the estimated coefficient values, and better agreement with the predicted values.

Any errors to be expected with the regression method depend, to a large extent, on the amount of measurement noise. Any noise in the measurement of the variables,  $q$ ,  $\alpha$ ,  $V$ , or  $Q$ , could cause bias errors with the regression method. Although the amount of noise cannot be determined with certainty, the recorded data (e.g., fig. 3b) show very little of what may be termed white or near white measurement noise (e.g., there is a low noise-to-signal ratio). Apparently, for the flight test situations considered in this study, there are no large amounts of measurement noise that could cause significant errors with the regression method.

The errors to be expected with the quasilinearization method are related to inaccuracies in the estimates of the variables,  $\hat{q}$ ,  $\hat{\alpha}$ ,  $\hat{V}$ , and  $\hat{Q}$  (fig. 3b). In particular, any modeling errors (e.g., neglect of higher-order aerodynamic terms and cross-coupling from the lateral-directional mode) will cause inaccuracies in these estimated states. Also, the quasilinearization technique usually has larger standard deviations in the estimated coefficient values because all of the coefficients are determined within one dependent set of equations, eqs. (1)-(7); whereas using the regression method, the coefficients are determined with three independent equations, eqs. (1)-(3).

For this particular application, regression appears to be the better method to use in obtaining the coefficient values. This should not imply that in other situations (i.e., where there may be larger amounts of measurement noise, or where all the states are not directly measured) regression would be the better method to use. Experience has shown that it is good practice to consider both methods utilizing, wherever possible, the advantages of each method.

## 4. PARAMETER IDENTIFICATION IN TURBULENCE

One of the problems in parameter identification during landing maneuvers is to account for the air turbulence which is usually present at low altitudes. Most of the previous studies have considered aircraft parameter identification in the absence of turbulence (refs. 2-10), or have made simplifying assumptions about the noise spectrum of turbulence and its interaction with the airframe (refs. 17-18). In this paper, a state estimation technique (ref. 19) is used to measure the time history of the turbulence gust disturbances. This measured turbulence is then treated as a forcing function in the aerodynamic equations. This technique makes no assumptions about the turbulence noise characteristics and further allows an examination of the manner in which the turbulence interacts with the airframe.

### 4.1 State estimation

The inertial velocities and position of the aircraft have been estimated by a solution of the following kinematic equations:

$$\dot{\hat{\alpha}} = g(a_x - \sin \hat{\theta}) - \dot{q}\hat{u} + \dot{\hat{u}}_{u_0}, \quad u(0) = \hat{u}_{u_0} \quad (8)$$

$$\dot{\hat{\theta}} = g(a_z + \cos \hat{\theta}) + \dot{q}\hat{w} + \dot{\hat{w}}_{w_0}, \quad w(0) = \hat{w}_{w_0} \quad (9)$$

$$\dot{\hat{\theta}} = q + \dot{\hat{q}}_{q_0}, \quad \theta(0) = \hat{\theta}_{\theta_0} \quad (10)$$

$$\dot{\hat{h}} = \hat{u} \sin \hat{\theta} - \hat{w} \cos \hat{\theta} + \dot{\hat{h}}_{h_0}, \quad h(0) = \hat{h}_{h_0} \quad (11)$$

where the unknown constant ( $\hat{K}$ ) terms are determined by quasilinearization. This application of quasilinearization requires no mathematical model of the aerodynamics; rather, the direct measurements of the accelerations,  $a_z$  and  $a_x$ , and the pitching rate,  $q$ , are used in a manner similar to that in a strapped-down inertial system (see ref. 19 for further details and the formulation including lateral motions).

For the landing approach maneuvers in this study, state estimation provides smoothing of the measured states,  $(h, \theta)$ , along with the estimates of the inertial velocities,  $(\hat{u}, \hat{w})$ , and the inertial angle-of-attack,  $\hat{\alpha}_1 = \tan^{-1}(\hat{w}/\hat{u})$ . Figure 5 presents some of the estimated states along with the measured data for a representative landing approach maneuver. The upper portion of the figure illustrates good correlation between the radio altimeter measurement and the estimated height-above-the-runway. The lower portion of the figure compares the estimated inertial angle-of-attack,  $\hat{\alpha}_1$ , and the airflow (vane-measured) angle-of-attack,  $\alpha_a$ . For these representative landing approach maneuvers there seems to be a large random fluctuation of the airflow vane. The difference between the airflow and inertial angle-of-attack provides a measure of turbulence acting on the airframe.

Note: An examination has been made to determine possible errors in the airflow angle-of-attack measured by the vane. As noted previously, the airflow measurement,  $\alpha_a$ , includes corrections for angular rate and upwash (as a function of height-above-ground). It has been found that for flight maneuvers out of turbulence there is excellent agreement between the airflow measurement,  $\alpha_a$ , and the estimate,  $\hat{\alpha}_1$ .

#### 4.2 Interaction of turbulence with the airframe

A necessary consideration in parameter estimation for STOL aircraft, traveling at low speeds, has been to determine the manner in which this measured turbulence interacts with the airframe. The turbulence as measured by the vane located forward of the aircraft will not immediately interact with the major aerodynamic surfaces. A first approximation for this delayed interaction is to use a time shift,  $\Delta t$ , to account for the time it takes for the measured gusts to travel from the vane until they strike the major aerodynamic surfaces.

Noting that the total angle-of-attack at any time consists of both the gust and inertial components, we have

$$\alpha(t) = \underbrace{\text{Measured turbulence shifted by } \Delta t}_{\alpha_{\text{gust}}(t - \Delta t)} + \underbrace{\text{Inertial angle-of-attack}}_{\hat{\alpha}_1(t)} \quad (12)$$

where the turbulence gust component is obtained as the difference between the measured airflow angle-of-attack and the inertial angle-of-attack at the time,  $t - \Delta t$ .

$$\alpha_{\text{gust}}(t - \Delta t) = \alpha_a(t - \Delta t) - \hat{\alpha}_1(t - \Delta t) \quad (13)$$

Figure 6 illustrates the effect of the time shift,  $\Delta t$ , on the rms fit errors,  $\sigma_{a_z}$ ,  $\sigma_{a_x}$ , and  $\sigma_{a_m}$ , for a typical segment of a landing approach maneuver. As shown, there appears to be a different value of time shift,  $\Delta t$ , which will provide a minimum rms fit error to each of the measured terms,  $a_x$ ,  $a_z$ , and  $a_m$ . These values of time shift appear to be reasonable from aerodynamic considerations. The fit error for the linear forces,  $\sigma_{a_z}$  and  $\sigma_{a_x}$ , are minimized if the measured turbulence is delayed by the amount of time required for the gusts to travel from the vane to near the aircraft aerodynamic center ( $\Delta t = 0.4$  sec at  $V = 36$  m/sec). The fit error for the moment term,  $\sigma_{a_m}$ , however, is minimized using the time required for the turbulence to reach the stabilizer ( $\Delta t = 0.7$  sec at  $V = 36$  m/sec).

The relative amounts of rms fit error reduction, with the time delay, also appear reasonable. The linear  $z$  force is strongly affected by angle-of-attack gusts and, as shown by using the appropriate time shift, the rms error,  $\sigma_{a_z}$ , is reduced by about 30%. The moment term and the linear  $x$  force are influenced less with a reduction of about 10% in  $\sigma_{a_m}$  and 5% in  $\sigma_{a_x}$ , by the appropriate choice of time shifts.

A further indication of the importance of time shift becomes apparent in fig. 7 where the effect of  $\Delta t$  on the estimate values for the coefficients,  $\hat{C}_{z_\alpha}$ ,  $\hat{C}_{z_q}$ , and  $\hat{C}_{z_\delta}$ , is shown. Without a time shift (at  $\Delta t = 0$ ) the estimated values are much different than predicted. However, using an appropriate time shift ( $\Delta t = 0.4$  sec) these terms are near their predicted value.

#### 4.3 Discussion of turbulence effects

The appropriate value of time shift is related to the ratio, length/speed. For the linear forces,  $a_z$  and  $a_x$ , the time shift can be taken approximately as:

$$\Delta t = \frac{\text{distance from vane to aircraft A.C.}}{\text{forward airspeed}}$$

For the pitching moment the time shift is approximately:

$$\Delta t = \frac{\text{distance from vane to stabilizer}}{\text{forward airspeed}}$$

With large STOL aircraft flying at low speeds the appropriate time delay will be in the order of seconds. For small aircraft at high speeds, however, the time delay may be quite small.

Previous parameter identification studies, which have included turbulence effects, apparently did not find a requirement to time-correlate the vane-measured turbulence. These previous studies (refs. 17-18) have considered smaller aircraft at higher speeds where the inclusion of the time shift may not be so critical. However, as shown by the results in this paper, the time-dependent interaction of turbulence on the airframe can affect significantly the estimated coefficient values and, therefore, should be considered in each application.

One additional note is that turbulence may, in fact, aid in the identification of some of the parameters. This is because turbulence acts as another forcing function in addition to the usual control input forcing function. The results from this study indicate that some of the aerodynamic coefficients may be determined more accurately from maneuvers in turbulent air (e.g., the aircraft is excited by both gusts and elevator inputs) as compared with maneuvers in clear air (excited by only elevator inputs). For instance, as noted previously, the terms  $\hat{C}_{z_q}$  and  $\hat{C}_{z_\delta}$  are highly correlated and difficult to determine

accurately using elevator pulse maneuvers (fig. 4). However, the estimated values in turbulence are generally found to be near their predicted values (fig. 7).

## 5. PARAMETER IDENTIFICATION OF GROUND EFFECTS

Ground proximity effects are of concern with STOL aircraft because wind tunnel tests and theory have predicted significant changes (both static and dynamic) in the aerodynamic flow field for such high-lift aircraft near the ground (refs. 20-23). These effects on the aerodynamic coefficient values have not yet been determined by accurate in-flight measurements from landing maneuvers. This section reviews a preliminary application of parameter identification to determine the changes in the aerodynamic coefficients due to ground proximity. Parameter identification has been used in two ways. First, it has been used to determine the gross changes in the aerodynamic coefficients due to ground effect. Second, it has been used in the development of a mathematical model which indicates the amount of change in the aerodynamic coefficients as a function of height-above-ground, angle-of-attack, etc.

Representative maneuvers, which have been used to analyze the ground effects, are presented in fig. 8. In each of these runs the pilot controlled the aircraft near a constant angle-of-attack. Maneuvers are shown at different levels of angle-of-attack for different nozzle angle settings (i.e., different levels of aerodynamic and propulsive lift).

### 5.1 Gross effects of ground proximity

The gross effects of ground proximity on the aerodynamic coefficients can be isolated as follows:

$$\Delta C_{L_G} = C_L - [\hat{C}_{L_m}] \quad (14)$$

$$\Delta C_{D_G} = C_D - [\hat{C}_{D_m}] \quad (15)$$

$$\Delta C_{M_G} = C_M - [\hat{C}_{M_m}] \quad (16)$$

where the terms,  $\Delta C_{L_G}$ ,  $\Delta C_{D_G}$ , and  $\Delta C_{M_G}$ , represent the gross changes due to ground effect; the terms,  $C_L$ ,  $C_D$ , and  $C_M$ , are the measured aerodynamic coefficients,

$$C_L = [-(a_z - T_z) \cos \alpha + (a_x - T_x) \sin \alpha] (M/QS) \quad (17)$$

$$C_D = [-(a_z - T_z) \sin \alpha - (a_x - T_x) \cos \alpha] (M/QS) \quad (18)$$

$$C_M = (a_m - T_m) (I_{yy}/QS\bar{c}) \quad (19)$$

and the terms,  $[\hat{C}_{L_m}]$ ,  $[\hat{C}_{D_m}]$ , and  $[\hat{C}_{M_m}]$  are the predicted coefficient values (total sums) derived from parameter identification out of ground effect (as discussed previously).

$$[\hat{C}_{L_m}] = \hat{C}_{L_0} + \hat{C}_{L_\alpha} \alpha + \hat{C}_{L_\delta} \delta + \dots \quad (20)$$

$$[\hat{C}_{D_m}] = \hat{C}_{D_0} + \hat{C}_{D_\alpha} \alpha + \hat{C}_{D_\delta} \delta + \dots \quad (21)$$

$$[\hat{C}_{M_m}] = \hat{C}_{M_0} + \hat{C}_{M_\alpha} \alpha + \hat{C}_{M_\delta} \delta + \dots \quad (22)$$

Figure 9 presents representative results showing the gross changes in aerodynamic coefficients as a function of height-above-ground level. An examination of the data presented in this figure provides insight into some of the variables which influence the changes in the aerodynamic coefficients and also indicates the type of terms which must be included in the mathematical model for ground effect.

First, the magnitude of the ground effects generally vary in an exponential manner as the aircraft nears the ground. This type of variation with height is similar to that noted in most previous studies of ground effect.

Second, the ground effects vary from run to run depending upon the aircraft operating conditions. For run 1 (shown by circle symbols) there is a more positive change in lift and a more negative change in drag as compared with run 2. These differences apparently account for the greater increase in flight path angle and speed near the ground in run 1 as compared with run 2 (fig. 8). For run 1 the ground effect appears "buoyant" enough to cause the aircraft to float up away from the ground; whereas with run 2, the ground effect appears less buoyant, and the aircraft continues to descend to the ground.

Third, fig. 9 shows that the magnitude of the ground effects is somewhat different for descent and ascent (shown by the arrows). This apparent "dynamic" ground effect is illustrated in more detail with fig. 10 where the time history of  $\Delta C_{L_G}$  is presented for the portion of run 1 where the aircraft descends and ascends above ground level. As shown, there is a rather abrupt loss in lift associated with the change from the descending to ascending flight path. This decrease occurs after the passage of the minimum altitude point. Apparently, the effect of the ground plane on the flow field is time-dependent. Near the ground the flow field is effectively straightened, causing a lift loss (see sketch in fig. 10). Such a lift loss, with a time lag, has been predicted from previous small scale dynamic tests (ref. 20); however, it had not yet been verified from actual flight test data.

### 5.2 Mathematical model for ground effect

An examination of the data presented in fig. 9 (and similar data from other runs) gives insight into the form of equations required to model mathematically the changes in the aerodynamic coefficients due to ground proximity. A preliminary mathematical model which is being evaluated is of the form

$$\begin{bmatrix} \Delta \hat{C}_{L_G} \\ \Delta \hat{C}_{D_G} \\ \Delta \hat{C}_{M_G} \end{bmatrix} = e^{-h/\hat{k}_h} [\hat{k}] x \quad (23)$$

where the term  $e^{-h/\hat{k}_h}$  represents the exponential variation of the ground effect with height;  $[\hat{k}]$  represents a matrix (3xn) of unknown constant coefficients; and  $x$  represents a time varying vector (nx1) of state variables which influence the amount of change in the aerodynamic coefficients due to ground effect (e.g., angle-of-attack, rate of descent, etc.).

The parameter which has been found to have the most significant effect on the rms fit error is scale height parameter,  $\hat{k}_h$ . Figure 11 illustrates the relative rms values for  $C_L$ ,  $C_D$ , and  $C_M$  as a function of  $\hat{k}_h$ . As shown in fig. 11, the best fit is obtained, for all three coefficients, with a scale height parameter of  $\hat{k}_h \approx 4.5$  meters (15 ft).

Using the values obtained by parameter identification we can see how each of the variables (e.g.,  $h$ ,  $\alpha$ , etc.) affect the aerodynamic coefficients. As an example, fig. 12 presents the estimated aerodynamic coefficients as a function of angle-of-attack both in and out of ground effect. Ground proximity is shown to cause (1) a slight increase in  $C_L$  at low angles-of-attack along with a slight decrease in the lift curve slope,  $C_{L_\alpha}$ , (2) a reduction of about 30% in  $C_D$ , and (3) a significant shift in the moment,  $C_M$ , with an increase in the static stability,  $-C_{M_0}$ .

The trends, due to ground proximity, found in this flight test study are in general agreement with results found in a wind tunnel study using a similar powered-lift STOL configuration. That is, the wind tunnel tests also show similar changes in lift and lift curve slope, a decrease in drag, and similar shift in moment with increased static stability. However, the magnitude of the changes are somewhat different in the flight tests as compared with the wind tunnel tests. Figure 13 compares the changes due to ground effect,  $\Delta C_{L_G}$ ,  $\Delta C_{D_G}$ , and  $\Delta C_{M_G}$ , as obtained from flight and wind tunnel tests. In comparing these data the height above the ground level has been normalized with respect to the chord length; also  $\Delta C_{L_G}$  and  $\Delta C_{D_G}$  are normalized with respect to their free-air values. As shown, the changes in lift and moment are in general agreement with the wind tunnel, however, the decrease in drag determined in the flight test is about three times greater than the decrease in drag determined in the wind tunnel. Some differences were to be expected between the flight and wind tunnel results because, in the wind tunnel, the angle-of-flow between the ground plane and airframe is not the same as in actual flight; and also, in the wind tunnel there is a boundary layer on the ground plane (for fixed planes), again not the same as in actual flight. Because of the difficulties of accurately duplicating the ground proximity effects (both static and dynamic) from wind tunnel tests alone, it would appear that parameter identification, as used in this study, can be an important tool in the analysis of ground effects for future vehicles.

### 6. CONCLUDING REMARKS

This paper has reviewed some recent flight experience in the identification of longitudinal aerodynamic coefficients for a powered-lift STOL aircraft. Comparisons were made between results obtained by the regression and quasilinearization identification techniques. Also, special techniques were presented for the identification of aerodynamic coefficients when the aircraft encounters air turbulence and ground proximity.

This study shows that for the data analyzed in this investigation the regression method provides better results than the quasilinearization method. The regression method provides a better fit to the

measured accelerations, less scatter in the estimated coefficient values, and better agreement with the predicted values.

The technique for estimating parameters in turbulence involves the use of state estimation, combined with airflow (i.e., vane) measurements, to determine the time history of the gust disturbances. The results show that the measured turbulence must be time-correlated to account for interaction of the gusts along the airframe. Using this technique, the results indicate that some of the aerodynamic coefficients may be determined more accurately from maneuvers in turbulent air (e.g., the aircraft is excited by both gusts and elevator inputs) as compared with maneuvers in clear air (excited by only elevator inputs).

In the estimation of ground proximity effects parameter identification has been used in two ways. First, it has been used to determine the gross changes in the aerodynamic coefficients due to ground effect, and second, it has been used in the development of a mathematical model for ground effect. The results show that ground proximity causes a slight increase in lift, a moderate decrease in drag, and a significant change in pitching moment.

This review illustrates that there are some differences between the results obtained by the various identification methods, but of more importance, is a determination of the form of the aerodynamic equations (i.e., number and type of nonlinear and time-dependent terms) required to model mathematically the aircraft and its interaction with external forces. For this study of STOL aircraft, during landing maneuvers in turbulence, the primary consideration has been to define the form of the mathematical models. Future work appears warranted to investigate the problems of developing the most accurate mathematical models for advanced STOL and V/STOL aircraft. The development of these mathematical models requires an analysis of the recorded flight data along with an understanding of those physical processes which may affect the vehicle dynamics.

#### ACKNOWLEDGEMENTS

The author thanks R. F. Vomaske and D. H. Hickey of Ames Research Center for their aid in obtaining the data used in this paper, and for their suggestions in analyzing the ground effect contributions.

#### REFERENCES

1. Quigley, Hervey C.; Innis, Robert C., and Grossmith, Seth: A Flight Investigation of the STOL Characteristics of an Augmented Jet Flap STOL Research Aircraft. NASA TM X-62,334, 1974.
2. Iliff, K. W.; and Taylor, L. W.: Determination of Stability Derivatives from Flight Data Using a Newton-Raphson Minimization Technique. NASA TN D-6579, 1972.
3. Denery, D. G.: Identification of System Parameters from Input-Output Data with Applications to Air Vehicles. NASA TN D-6468, 1971.
4. Chen, R. T. M.; Eulrich, B. J.; and Lebacqz, V. J.: Development of Advanced Techniques for the Identification of V/STOL Aircraft Stability and Control Parameters. CAL Rept. BM-2820-F-1, Aug. 1971.
5. Mehra, R. K.; Stepner, D. E.; and Tyler, J. S.: A Generalized Method for the Identification of Aircraft Stability and Control Derivatives from Flight Test Data. Proceedings of 1972 Joint Automatic Control Conference, Aug. 1972, pp. 525-534.
6. Grove, Randall D.; Bowles, Roland L.; and Mayhew, Stanley C.: A Procedure for Estimating Stability and Control Parameters from Flight Test Data by Using Maximum Likelihood Methods Employing a Real-Time Digital System. NASA TN D-6735, 1972.
7. Gerlach, O. H.: The Determination of Stability Derivative and Performance Characteristics from Dynamic Maneuvers. AGARD-CP-85, May 1971.
8. Molusis, John A.: Analytical Study to Define a Helicopter Stability Derivative Extraction Method. NASA CR-132371, 1974.
9. Aubrun, Jean-Noël: Nonlinear Systems Identification in the Presence of Non-Uniqueness. NASA TN D-6467, 1971.
10. Wingrove, Rodney C.: Estimation of Longitudinal Aerodynamic Coefficients and Comparison with Wing Tunnel Values. In NASA TN D-7647, 1974, pp. 125-147.
11. Cook, A. M.; and Aiken, T. N.: Low-Speed Aerodynamic Characteristics of a Large-Scale STOL Transport Model with an Augmented Jet Flap. NASA TM X-62,017, 1971.
12. Spitzer, R. E.: Predicted Flight Characteristics of the Augmentor Wing Jet STOL Research Aircraft. NASA CR-114463, 1972.
13. Cleveland, William B.; Vomaske, Richard F.; and Sinclair, S. R. M.: Augmentor Wing Jet STOL Research Aircraft Digital Simulation Model. NASA TM X-62,149, 1972.
14. Suit, W. T.: Aerodynamic Parameters of the Navion Airplane Extracted from Flight Data. NASA TN D-6643, 1972.
15. Steinmetz, George G.; Parrish, Russell V.; and Bowles, Roland L.: Longitudinal Stability and Control Derivatives of a Jet Fighter Airplane Extracted from Flight Test Data by Utilizing Maximum Likelihood Estimation. NASA TN D-6532, 1972.

16. Williams, James L.: Extraction of Longitudinal Aerodynamic Coefficients from Forward-Flight Conditions of a Tilt Wing V/STOL Airplane. NASA TN D-7114, 1972.
17. Iliff, Kenneth W.: Identification of Aircraft Stability and Control Derivatives in the Presence of Turbulence. In NASA TN D-9647, 1974, pp. 77-113.
18. Stepner, David E.; and Mehra, Raman K.: Identification of M2/F3 Stability and Control Derivatives from Flight Data Containing Gust Effects. In NASA TN D-7647, 1974, pp. 115-124.
19. Wingrove, Rodney C.: Applications of a Technique for Estimating Aircraft States from Recorded Flight Test Data. AIAA Paper 72-965, 1972. (Also J. of Aircraft, Vol. 10, No. 5, May 1973, pp. 303-307.)
20. Turner, Thomas R.: Ground Influence on a Model Airfoil with a Jet-Augmented Flap as Determined by Two Techniques, NASA TN D-658, 1961.
21. Gratzner, L. B.; and Mahal, A. S.: Ground Effects in STOL Operations, AIAA Paper No. 71-579, June 1971.
22. Hassell, James L., Jr.; and Judd, Joseph H.: Study of Ground Proximity Effects on Powered-Lift STOL Landing Performance, NASA SP-320, 1972, pp. 199-213.
23. Hickey, David H.: V/STOL Aerodynamics - A Review of the Technology. Presented at the AGARD Fluid Dynamics Panel Specialists Meeting on V/STOL Aerodynamics, Delft, The Netherlands, April 24-26, 1974.

TABLE 1. RMS DIFFERENCE BETWEEN ESTIMATED AND MEASURED TIME HISTORIES

		Regression	Quasilinearization
$\sigma_{\dot{z}}$	g units	0.0127	0.0176
$\sigma_{\dot{x}}$	g units	0.00605	0.00788
$\sigma_{\dot{\theta}}$	deg/sec <sup>2</sup>	0.708	0.726
$\sigma_u$	m/sec	---	0.552
$\sigma_w$	m/sec	---	0.230
$\sigma_q$	deg/sec	---	0.295
$\sigma_\theta$	deg	---	0.630

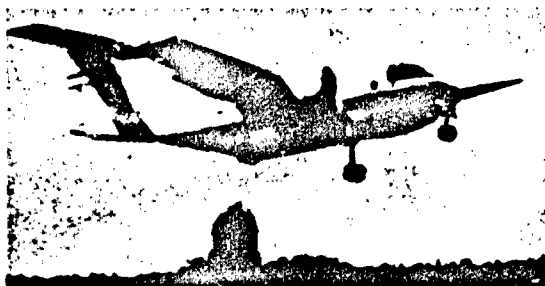


Fig. 1 Augmented jet-flap STOL research aircraft.

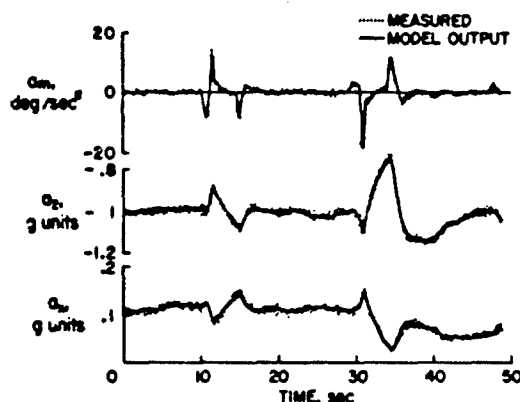
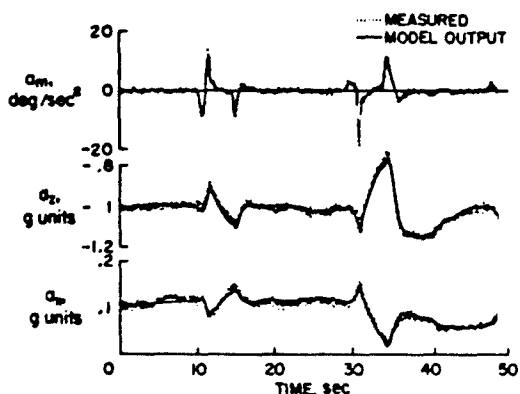
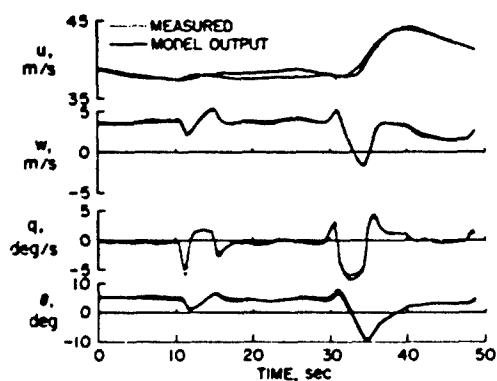


Fig. 2 Estimated model outputs compared with direct measurements; regression method.



(a) Accelerations



(b) Pitch angle and velocities

Fig. 3 Estimated model outputs compared with direct measurements; quasilinearization method.

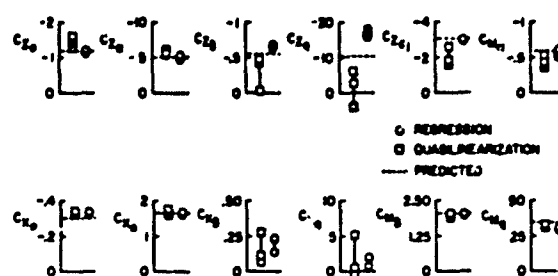
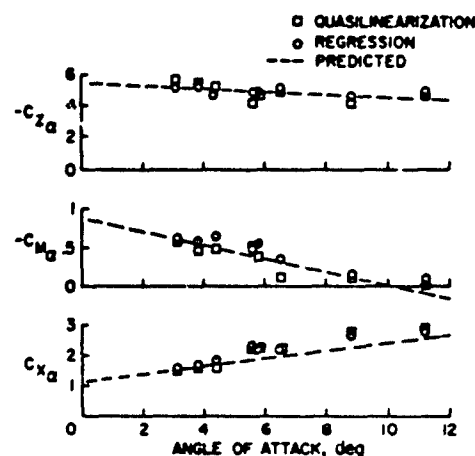
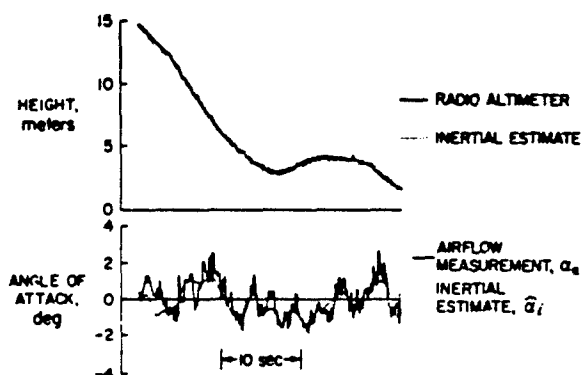
(a) Three pulse maneuvers;  $-2^\circ \leq \alpha \leq 10^\circ$ .(b) Variation with  $\alpha$ .Fig. 4 Comparison of estimated coefficient values; flap =  $67^\circ$ ;  $0.3 \leq C_j \leq 0.4$ .

Fig. 5 Comparison of estimated states with direct measurements.

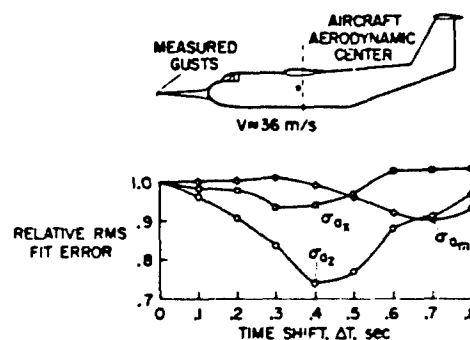


Fig. 6 Time shifting the measured turbulence to minimize the model fit error.

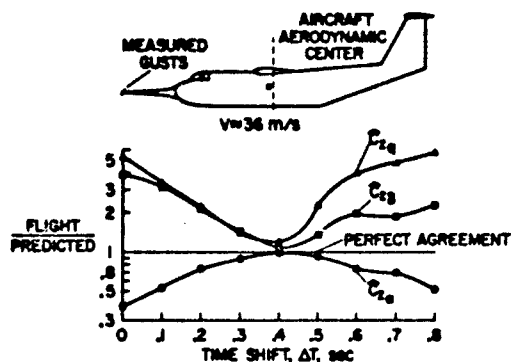


Fig. 7 Effect of time shifting the measured turbulence on the estimated coefficient values.

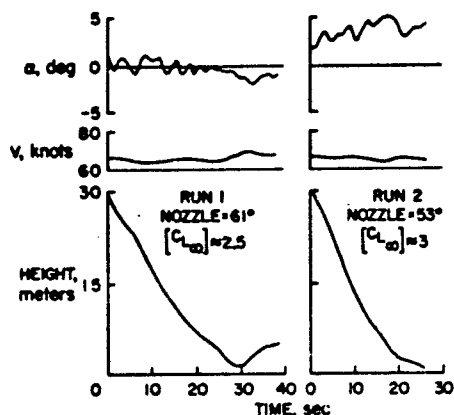


Fig. 8 Landing approach maneuvers used to determine effects of ground proximity.

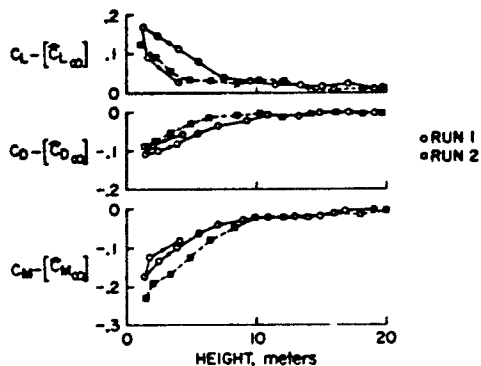


Fig. 9 Gross changes in the aerodynamic coefficients as a function of height-above-ground level.

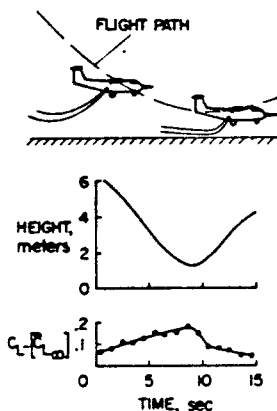


Fig. 10 The time history of changes in lift coefficient due to ground proximity.

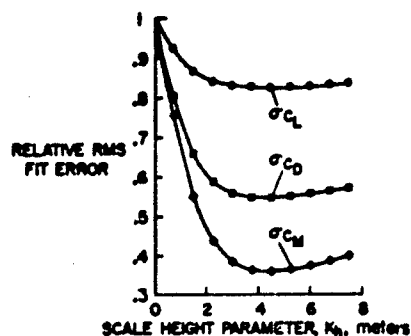


Fig. 11 Effect of the scale height parameter,  $K_h$ , on the model fit error.

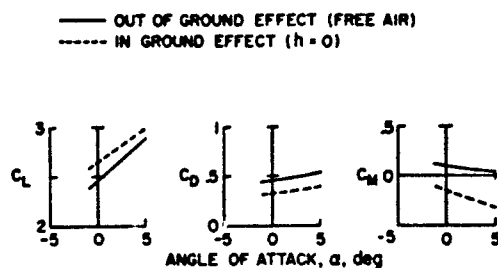


Fig. 12 Measured aerodynamic coefficients, both in and out of ground effect; flap = 67°, nozzle = 60°,  $C_j = 0.5$ .

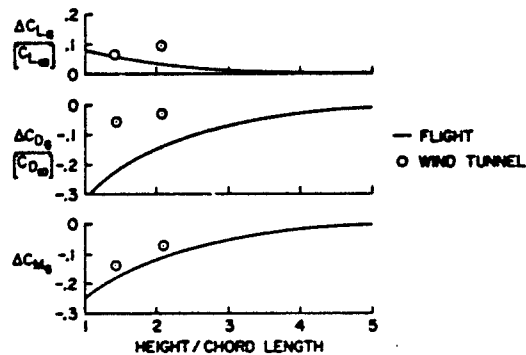


Fig. 13 Comparison of ground effect changes measured in flight and wind tunnel;  $C_{L_m} = 2.5$ .



## ESTIMATION OF ELASTIC AIRCRAFT AERODYNAMIC PARAMETERS

by

Robert C. Schwanz

William R. Wells

Air Force Flight Dynamics Laboratory  
Wright-Patterson Air Force Base, Ohio 45433, USA

## SUMMARY

The importance of including aeroelasticity in aircraft parameter estimation is discussed using the B-52E and C-5A aircraft as examples. A parameter estimation method, employing the modal truncation dynamics math model and the maximum likelihood estimation algorithm, is selected to illustrate the computational difficulties that must be solved. A combined in-house and contractual research program is then outlined that addresses these anticipated problem areas. The aircraft selected for the initial applications of the methods is the B-52E that was flown in the Control Configured Vehicle (CCV) research program of the AF Flight Dynamics Laboratory.

## LIST OF SYMBOLS

<u>Arabic Symbol</u>	<u>Definition</u>
$a_x$	Fore and aft acceleration, inches/second squared.
$a_y$	Side acceleration, inches/second squared.
$a_z$	Vertical acceleration, inches/second squared.
$\bar{b}$	Wing reference span, inches.
$C_D$	Coefficient of drag, Drag/ $qS$ .
$C_L$	Coefficient of lift, Lift/ $qS$ .
$C_L$	Coefficient of rolling moment, Rolling Moment/ $qS\bar{b}$ .
$C_m$	Coefficient of pitching moment, Pitching Moment/ $qS\bar{c}$ .
$C_n$	Coefficient of yawing moment, Yawing Moment/ $qS\bar{b}$ .
$C_y$	Coefficient of side force, Side Force/ $qS$ .
$\bar{c}$	Wing reference chord, inches.
$\hat{p}$	Non-dimensional roll rate, (Roll Rate) $\times (\bar{b}/2U_1)$ .
$q$	Dynamic Pressure, pounds/inches squared.
$\hat{q}$	Non-dimensional pitch rate, (Pitch Rate) $\times (\bar{c}/2U_1)$ .
$\hat{r}$	Non-dimensional yaw rate, (Yaw Rate) $\times (\bar{b}/2U_1)$ .
$S$	Wing reference area, inches squared.
$T_{1/2}$	Time to one-half amplitude, seconds.
$U_1$	Reference forward velocity, inches/second.

<u>Greek Symbol</u>	<u>Definition</u>
$\alpha$	Perturbation angle-of-attack, degree.
$\alpha_1$	Reference (trim) angle-of-attack, degree.
$\dot{\alpha}$	Non-dimensional rate of angle of attack, $\dot{\alpha}\bar{c}/2U_1$ .
$\beta$	Perturbation sideslip angle, degree.
$\delta_a$	Perturbation aileron angle, degree.

Greek Symbol	Definition
$\delta_e$	Perturbation elevator angle, degree.
$\delta_H$	Perturbation stabilizer angle, degree.
$\delta_{H1}$	Reference (trim) stabilizer angle, degree.
$\delta_r$	Perturbation rudder angle, degree.
$\theta$	Pitch attitude, degree.
$\dot{\theta}$	Pitch rate, degree/second.
$\ddot{\theta}$	Pitch acceleration, degree/second squared.
$\phi$	Bank angle, degree.
$\dot{\phi}$	Rate of bank angle change, degree/second.
$\ddot{\phi}$	Acceleration of bank angle change, degree/second squared.
$\omega_d$	Damped frequency of oscillation, Hertz
$\psi$	Heading angle, degree.
$\dot{\psi}$	Rate of heading angle change, degree/second.
$\ddot{\psi}$	Acceleration of heading angle change, degree/second squared.

## 1. INTRODUCTION

During the past decade a substantial research effort has been directed toward the estimation of aerodynamic stability and control parameters from aircraft flight test data. A recent symposium (Reference 1) sponsored by the Flight Research Center of the National Aeronautics and Space Administration highlighted many of the research efforts that have been initiated by the government and industry. Some of the motivations for these recent efforts are the verification of the basic aircraft analytical design methods, the minimization of the expense of stability and control flight test experiments, and the improvement of mathematical models of aircraft that are implemented on the flight simulators.

Most of the parameter estimation results presented to date have emphasized the correlation of flight test data to data measured during wind tunnel tests of rigid aircraft. The reason for this emphasis on rigid aircraft is that most existing parameter estimation methods mathematically model the aircraft as a "rigid" structure, thus eliminating the possibility of explicitly estimating static and dynamic aeroelastic parameters that affect the measured flight data. At the very best, the existing methods can approximately model the vehicle as Quasi Static by assuming the structural distortion occurs instantaneously. Thus, the structural motion is assumed to have the phase of the body-fixed axis system motions such as  $\alpha$ ,  $\beta$ ,  $p$ ,  $q$ ,  $r$ , etc.

If the flight test of a vehicle indicates a Quasi Static behavior, modern methods will estimate vehicle parameters that are a product of the aerodynamic stability and control derivatives of the rigid vehicle modified by a static aeroelastic correction factor. e.g.,  $C_{L_\alpha} = C_{L_\alpha}^{\text{Rigid}} + \Delta C_{L_\alpha}$

The inclusion of even the simplest aeroelastic correction factor complicates the desired design verifications, since the data determined from flight test must then be correlated with wind tunnel measured data that have been modified by analytically determined Quasi Static correction factors.

The objective of this paper is to describe the flexible aircraft parameter estimation research of the Control Criteria Branch of the Air Force Flight Dynamics Laboratory. This work began in 1972 with a study by Schwanz and Wells (Reference 2) that identified the possible combinations of the formulations of elastic aircraft dynamic with the available parameter estimation methods. The results of that study led to the selection of the Modal truncation formulation to describe the aircraft dynamics and the maximum likelihood parameter estimation algorithm. The intent here is to estimate both the aerodynamic parameters of the body-fixed axis system motions (stability and control derivatives) and the aerodynamic parameters of structural motion relative to the body-fixed axis system (generalized aerodynamic forces proportional to position, velocity, and acceleration). As such, the sensors are mathematically modeled to include the structural dynamics motions as well as the body-fixed axis system motions.

## 2. FORMULATION OF THE PROBLEM

A review of the literature indicates that a successful attempt to estimate the aerodynamic parameters of flexible aircraft has not been reported. Consequently, this initial attempt to estimate these parameters is restricted. The linearized equations discussed in this paper describe the symmetric, small disturbance motions of an elastic flight vehicle. Further, the problem is restricted to the initial conditions of steady, non-rotating flight, with the wings level, and with the relative velocity vector of the center of mass parallel to the flat earth. In addition, the following simplifications and assumptions

are employed:

The thrust is assumed to be constant during the perturbation motion and its magnitude determined solely by the initial conditions of flight.

All motions, body-fixed axis system and elastic deformation, are of small perturbation magnitude and are of the same order.

The sensor locations are assumed to be precisely prescribed for some aircraft shape and the signals of the sensors are assumed to be free of bias.

The generalized stiffness, mass, and damping as well as the total mass and inertia of the aircraft are assumed to be known (within some tolerance) by previous measurements or calculations.

The elastic flight vehicle is adequately represented by lumped masses related structurally and aerodynamically by finite element theory as sketched in Figure 1.

Process noise, or atmospheric turbulence, is assumed negligible.

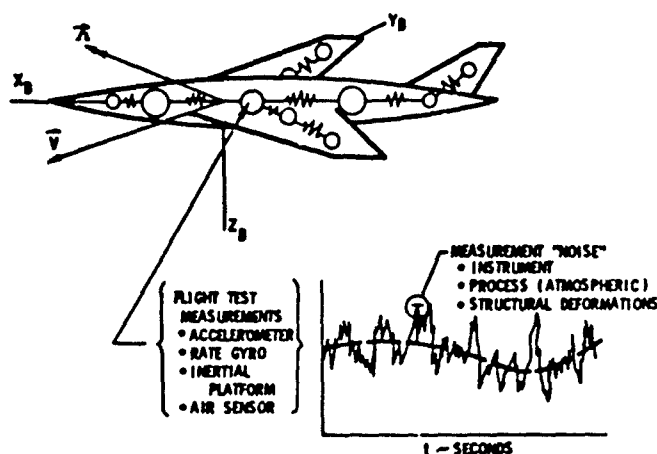


Figure 1. Lumped Mass Representation of a Flexible Aircraft

### 3. EQUATIONS OF MOTION

The linearized equations of motion for flexible aircraft found in the literature are of varied form and are often specialized to a particular problem. However, the many formulations can be divided into six major groups. (Reference 4):

**Exact** - The motion of the structure is determined by eigenvalue (root) and eigenvector (mode shape) solutions of the equations of motion for the elastic aircraft. The mode shape coordinates contain complex numbers. The accuracy of the solution is limited by the existing computerized routines that calculate the complex number eigenvalues and eigenvectors.

**Modal Substitution** - The motions of the structure are assumed to be related to the orthogonal, invacuum eigenvectors (mode shapes). The eigenvectors contain only real numbers.

**Residual Stiffness** - The mode shapes representing the elastic motion in the Modal Substitution formulation are separated into "retained" and "deleted" modes. The deleted modes are represented in the dynamic stability analysis as static elastic aeroelastic corrections, using a correction factor related to the deleted modes and the stiffness matrix of the free-free structure.

**Residual Flexibility** - Similar to the Residual Stiffness formulation, except the static elastic aeroelastic correction is related to the retained modes and the flexibility matrix of the free-free structure.

**Modal Truncation** - The deleted modes of the Residual Stiffness and Residual Flexibility formulations are not represented by any correction factor. This is the most common dynamic aeroelastic formulation reported in the literature.

**Quasi Static** - The motions of the structure are assumed to be in-phase with the rigid body motions. The method is used primarily for the conceptual and preliminary design of handling quality and reduced static stability control systems for elastic aircraft with a wide frequency separation between the axis system motions and the structural deformations.

An illustration of the possible magnitude of the Quasi Static correction factors for a large bomber

aircraft such as the B-52E is presented in the following table. These factors, that modify the primary stability and control derivatives of the B-52E (Reference 5), are theoretically estimated using the Level 2 FLEXSTAB Computer Program System (Reference 6). A cursory examination of the static aeroelastic increments and ratios listed in the table indicates that static aeroelasticity substantially changes the derivatives of the B-52E aircraft. For example,  $C_{m\dot{\alpha}}$  is reduced by a factor of 4 and  $C_{L\dot{\alpha}}$  is reduced by a factor of 2. These order of changes can have a large effect on the dynamics of the aircraft as Mach number, dynamic pressure, or mass distribution are changed.

Table 1. Level 2 FLEXSTAB Estimates of the B-52E Stability and Control Derivatives

	Mach Number		0.569	
	Altitude, feet		4,000	
	Weight, pounds		350,000	
	Center of Mass, % c		29.8	
	Rigid(R)	Elastic(E)	Increment (E-R)	Ratio(E/R)
Trim State				
$\alpha_1$ , degrees	-3.79	-2.28	1.51	0.60
$\delta H_1$ , degrees	1.86	2.27	0.41	1.22
Stability Derivatives				
$C_{L\dot{\alpha}}$ , per degree	0.098	0.072	-0.026	0.73
$C_{m\dot{\alpha}}$ , per degree	-0.0197	-0.0050	0.0147	0.25
$C_{m\dot{\alpha}}$	-19.35	-15.58	3.77	0.81
$C_{m\dot{\delta}}$	-7.56	-7.30	0.26	0.97
$C_{L\dot{\beta}}$ , per degree	-0.0016	-0.0012	0.0004	0.75
$C_{n\dot{\beta}}$ , per degree	0.0023	0.0016	-0.0007	0.70
$C_{L\dot{p}}$	-0.522	-0.261	0.261	0.50
$C_{n\dot{p}}$	-0.153	-0.119	0.034	0.78
Control Power Derivatives				
$C_{m\dot{\delta}_H}$ , per degree	-0.0328	-0.0280	0.0048	0.85
$C_{m\dot{\delta}_a}$ , per degree	-0.0147	-0.0068	0.0079	0.46
$C_{L\dot{\delta}_a}$ , per degree	-0.00079	-0.00045	0.00034	0.57
$C_{n\dot{\delta}_r}$ , per degree	-0.0013	-0.0006	0.0007	0.46

For those cases in which the Quasi Static formulation of the dynamics is inadequate for the design task, the Modal Truncation or Residual Flexibility formulations are most commonly employed. The relative numerical significance of these two formulations can be illustrated using the C-5A Active Lift Distribution Control System (ALDCS) development described in Reference 7. The effect of the rigid airplane, Quasi Static, Modal Truncation, and Residual Flexibility formulations on selected stability and control derivatives of the C-5A and on the center of mass motion parameters of the C-5A are presented in Figures 2 and 3. These data are theoretically estimated by the Level 2 FLEXSTAB System for the cases of 0, 3, 7, and 13 retained inviscid modes and then connected with straight lines to facilitate their visualization.

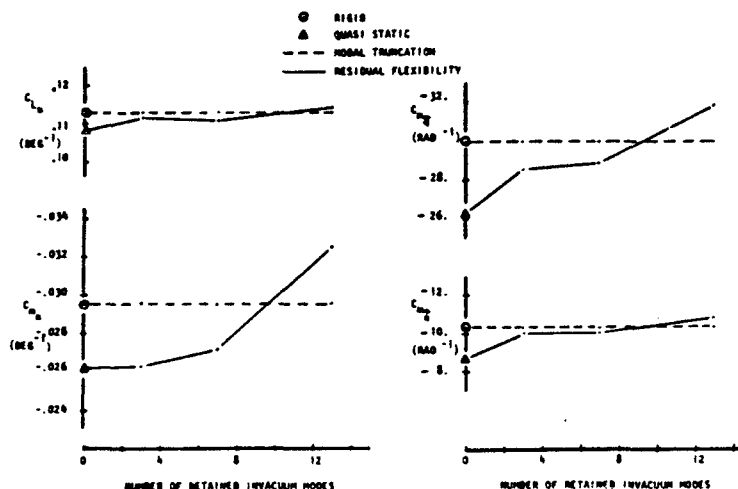


Figure 2. C-5A Longitudinal Stability Derivatives, ALDCS Cruise Design Point 412301

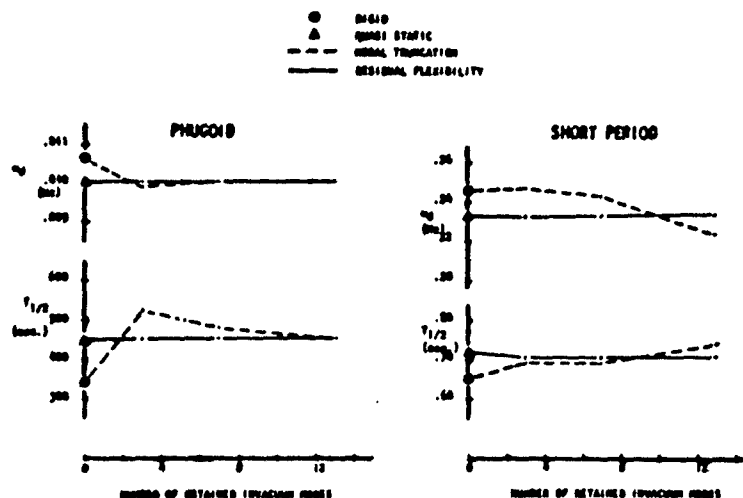


Figure 3. C-5A Center of Mass Dynamics, Unaugmented Aircraft, ALDCS Cruise Design Point 412301

Figure 2 illustrates the effect of static aeroelasticity on the derivatives; the theoretical estimate of the "rigid" C-5A derivatives are presented for contrast. The difference between the rigid and Quasi Static value of the derivative at zero "retained modes" is the elastic increment such as previously presented for the B-52E. Note in particular that the Modal Truncation formulation explicitly employs the rigid airplane derivative values regardless of the number of invacuum modes that are dynamically retained. In contrast, the Residual Flexibility formulation "adjusts" the value of all the derivatives for static elasticity depending upon the number of retained invacuum modes. As shown, the Residual Flexibility numbers vary strongly with the number of retained modes, eventually converging approximately to the Quasi Static value when all the dynamic aeroelastic effects of the invacuum modes are deleted.

Figure 3 illustrates a disadvantage of the Modal Truncation formulation when contrasted to other formulations. As shown, the phugoid and short period dynamics of the C-5A are dependent upon formulation. The most theoretically correct estimates shown in Figure 3 are the Quasi Static solution, at zero number of retained invacuum modes, and the Residual Flexibility solution at the other cases. The number of invacuum modes that must be retained to adequately represent the dynamics of the elastic aircraft in the Modal Truncation formulation is highly dependent upon the problem being analyzed and nearly always is larger than the number required for the Residual Flexibility formulation.

The Modal Truncation formulation has been selected by the Control Criteria Branch for the initial study of flexible airplane parameter estimation. As shown in Figures 2 and 3, its advantage is that the equations of motion for the body-fixed reference axis system contain explicit rigid airplane stability and control derivatives. In addition, it can be shown that the sensor equations of this formulation for the accelerometers are simpler than those of the other elastic airplane dynamics formulations and are also independent of the parameters being estimated. The disadvantage of the formulation is that it requires a substantial number of modes to represent both the static and dynamic aeroelastic effects of the invacuum modes. As examples of the number required, the C-5A Active Lift Distribution Control System (Reference 7) required from 6 to 15 modes, while the B-52E CCV Ride Control System (Reference 8) required as few as 5 to as many as 27 invacuum modes.

The linearized equations of symmetric motion for the elastic airplane may be written (Reference 2):

$$[F_{ij}](\dot{Z}_j) = [B_{ij}](Z_j) + [G_{ik}](\delta_k) + [N_i], \quad i, j = 1, 4 + 2r; \text{ and } k = 1, 2c \quad (1a)$$

$$[Z_j(t=0)] = [Z_j(0)] \quad (1b)$$

where  $[F_{ij}]$ ,  $[B_{ij}]$ , and  $[G_{ik}]$  contain the aerodynamic elements to be estimated.

$[Z_j]$  is the state vector containing axis system motion and structural deformation rates.

$[\delta_k]$  is the control vector of position and rate.

$[N_i]$  is the process noise, such as atmospheric turbulence, and is assumed to be negligible in this analysis.

$r$  is the number of retained invacuum modal coordinates in the Modal truncation formulation.

$c$  is the number of actively moving control surfaces.

## 4. SENSOR AND MEASUREMENT EQUATIONS

The acceleration sensor representations ( $a_L$ ) that are required may be derived (Reference 2) in terms of the states ( $Z_j$ ):

$$\{a_L\} = [N_{Lj}]\{\dot{Z}_j\} + \{g_L\} \quad \begin{matrix} L = 1, L \\ j = 1, 4 + 2r \end{matrix} \quad (2)$$

where  $\{a_L\}$  is the theoretical value of the acceleration measurement at  $L$  number of selected locations on the aircraft.

$\{g_L\}$  is the gravity vector at each accelerometer whose axis is parallel to the  $x$  body axis.

$L$  is the total number of accelerometers.

$[N_{Lj}]$  is of constant value and proportional to either the distance of the accelerometer from the center of mass of the aircraft or to the initial velocity of the aircraft.

In order to duplicate the experimental measurements, the accelerometer representations are augmented:

$$\{y_m\} = [H_{mn}]\{x_n\} \quad \begin{matrix} m = 1, L + 4 \\ n = 1, 4 + 2r + L \end{matrix} \quad (3)$$

where  $\{y_m\}$  is a measurement vector whose ordered elements are forward velocity, vertical velocity, pitch rate, pitch attitude, and then  $L$  number of accelerations.

$\{x_m\}$  is a state vector of  $4 + 2r$  states,  $\{Z_j\}$ , augmented by  $L$  accelerations,  $\{a_L\}$ .

$[H_{mn}]$  is a transformation matrix relating the state vector to the theoretical measurement vector. Its elements are proportional to unity and the slope of the invacuum mode at the location of the rate and attitude gyros.

The experimental measurements,  $\{y_m\}$ , have the same element order as  $\{y_m\}$  and are written (Reference 2):

$$\{y_m\} = [T_{mn}]\{s_n\} + \{n_m\} \quad m, n = 1, L + 4 \quad (4)$$

where  $\{s_n\}$  is the measurement output of the sensors in their local axis systems.

$[T_{mn}]$  is the direction cosine transformation matrix that relates sensor output in the local measurement axis to measurement components in the body fixed axis system of equations (1) and (2).

$\{n_m\}$  is instrument noise in the measurements having the expectancy properties.

$$E\{n_2(t_1)\} = 0$$

$$E\{[n_2(t_1)][n_2(t_j)]^T\} = [R_{1j}\delta_{1j}] \quad i, j = 1, 4 + L$$

In "rigid" airplane parameter estimation problems the transformation  $[T_{mn}]$  is not required, i.e.,  $\{y_m\} \equiv \{s_n\}$ , as the sensor axis system can be installed to be parallel to the body-fixed reference axis system of equations (1) and (2). However, for elastic aircraft, such as the B-52E, sensors on the extremes of the fuselage or wing and tails can have significant angular reorientation from their installed orientation to the orientation during the reference condition of flight. Figure 4 illustrates the effect of wing dihedral on sensor reorientation due to static aeroelasticity. Obviously, perturbation deformations that are measured will also cause some additional reorientation of the measurement axes of the sensors. This additional reorientation is assumed small in the analysis presented herein.

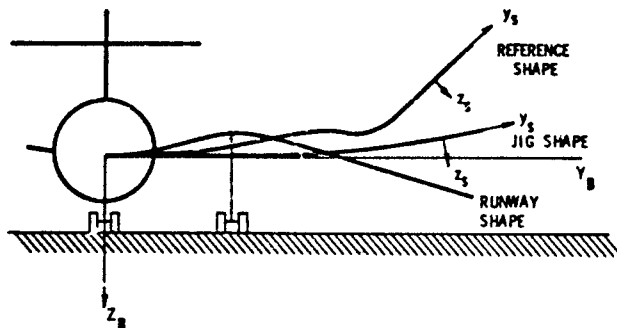


Figure 4. Effect of Vehicle Elasticity on Sensor Measurement Axis Reorientation

## 5. MAXIMUM LIKELIHOOD ESTIMATION

The methods used to estimate the stability and control parameters of rigid aircraft may be characterized (Reference 9) as "Equation Error," "Output Error," and "Advanced Non-linear." The maximum likelihood method falls into the latter characterization along with the extended Kalman filter. The advantages of the advanced methods are that they can be applied to problems which contain both process noise (turbulence-induced aircraft motions) and instrument noise.

The maximum likelihood method has been selected for the analysis presented herein due to its prior success on "rigid" aircraft. In addition, the computer demands of the method serve to identify the areas of major flight testing and computational difficulties prior to an expansion of the work effort to other estimator methods.

The first step in this estimation process is to determine which of the aerodynamic parameters in  $[F_{ij}]$ ,  $[B_{ij}]$ , and  $[G_{ik}]$  are to be estimated. In the case of the flexible aircraft, these parameters are  $b$  in number (Reference 2), where

$$b = 3r^2 + 3rc + 9c + 15r + 20$$

Clearly, for the case of  $r$  and  $c$  moderately large,  $b$  is very large.

The parameters expressed as components of a vector,  $\{p_b\}$  are estimated as (Reference 2):

$$\begin{aligned} \{p_b\} = \{p_b^*\} + \left[ \sum_{i=1}^N [H][A(t_i)]^T [R]^{-1} [H][A(t_i)] \right]^{-1} \\ \cdot \left[ \sum_{i=1}^N [H][A(t_i)]^T [R]^{-1} \{v_m(t_i)\} \right] \end{aligned} \quad (5)$$

where  $N$  is the number of measurements.

$$[R] = \frac{1}{N} \sum_{i=1}^N \{v_m(t_i)\} \{v_m(t_i)\}^T \quad m = 1, L + 4 \quad (6)$$

$$\{v_m(t_i)\} = \{y_m(t_i)\} - \{y_m(t_i)\} \quad m = 1, L + 4 \quad (7)$$

$\{p_b^*\}$  is the initial estimate for  $\{p_b\}$  from theoretical methods such as Level 2 FLEXSTAB.

$[A]$  is the matrix of sensitivity coefficients,

$$[A] = \begin{bmatrix} [\partial Z_j / \partial p_b] \\ [\partial a_z / \partial p_b] \end{bmatrix}$$

The sensitivity coefficients are calculated by differentiating equations (1) and (2) with respect to the parameters  $\{p_b\}$  found in  $[F_{ij}]$ ,  $[B_{ij}]$ , and  $[G_{ik}]$ . This means that the elements of  $[A]$  may be determined by solving a matrix differential equation for  $[\partial Z_j / \partial p_b]$  and an algebraic equation for  $[\partial a_z / \partial p_b]$ , (Reference 2):

$$\begin{aligned} [\partial \dot{Z}_j / \partial p_b] = \frac{d}{dt} [\partial Z_j / \partial p_b] = [F]^{-1} \left[ \left[ \frac{\partial B_{ij}}{\partial p_b} Z_j \right] + [B_{ij}] [\partial Z_j / \partial p_b] \right. \\ \left. + \left[ \frac{\partial G_{ik}}{\partial p_b} \delta_k \right] \right] - [F]^{-1} \left[ \frac{\partial F_{ij}}{\partial p_b} d_j \right] \end{aligned} \quad (8a)$$

$$\text{where } \{d_j\} = [F]^{-1} \{ [B_{jn}] \{Z_n\} + [G_{jk}] \{\delta_k\} \}$$

$$[\partial a_z / \partial p_b] = [M_{zj}] [\partial \dot{Z}_j / \partial p_b] \quad (8b)$$

$$\frac{\partial Z_j}{\partial p_b}(t=0) = \frac{\partial a_z}{\partial p_b}(t=0) = 0 \quad (8c)$$

The solution of equations (8) is substituted into equation (5) to calculate  $\{p_b\}$  where  $\{p_b^*\}$  in equations (1) and (2), and  $\{x_n\}$  and  $\{y_m\}$  are again calculated for all  $t_i$ . The new values for  $\{v(t_i)\}$  from equation (7) are then used to repeat the process to arrive at a second update of  $\{p_b\}$ . The process is repeated until  $\{p_b\}$  converges to its maximum likelihood value as measured by the convergence of  $J(p_b)$ , the performance function:

$$J(p_b) = \det \frac{1}{N} \sum_{i=1}^N v_m(t_i) v_m(t_i)^T$$

## 6. PROBLEMS OF COMPUTATION AND APPLICATION

To date, seven problems of computation and application have been identified by the in-house research:

- Proper input design for excitation of all state components.
- Availability of the direction cosine transformation matrix,  $[T]$ , in equation (4).
- Determination of the optimum number, type, and location of sensors on the aircraft.
- The absence of realistic start-up data for  $\{p_0^*\}$  in equation (5).
- The inversion of large and possibly ill-conditioned matrices in equation (5).
- The integration of a large number of sensitivity equations in equations (8).
- Rational choice for the particular parameter to be included in the analysis.

The excitation of the body-fixed axis motions and important elastic deformations is essential if the signal to noise ratio is to be large enough for optimum parameter extraction from the flight test data. Hopefully, this can be assured by careful selection of precision instrumentation and by well-planned flight tests and by previous analytical simulations using the large digital computer.

The second problem, the calculation of  $[T]$  in equation (4), can be solved using the combined output data of the NASTRAN and the Level 2 FLEXSTAB Computer Program Systems. Other less precise calculations of  $[T]$  are possible from FLEXSTAB alone, provided only dihedral angle changes and aerodynamically significant rotations are of interest. Since  $[T]$  is in part a function of  $\{p_p\}$ , an iterative cycle between a parameter estimation method and Level 2 FLEXSTAB may be required for some applications. For expediency in our restricted in-house effort,  $[T]$  has been assumed to be a diagonal unity matrix.

The determination of the optimum number, type, and location of sensors, has plagued the methods developed for "rigid" aircraft. The inclusion of aeroelasticity effects could conceivably either complicate or alleviate the problem. The complication introduced is the requirement for a larger number of sensors. The alleviation introduced is a more precise representation of the sensor signals in equations (4). Figure 5 presents a fraction of the total number of sensors on the B-52E. The type and location of these sensors is thought to be adequate for the first flight test applications of our in-house method. With these thoughts in mind, the in-house study has assumed that proper air data sensors, rate gyros, and accelerometer measurements are now available. These available sensor signals have been approximated with similar-type sensor signals which have been analytically created by the Level 2 FLEXSTAB programs. Prior to applying the estimation program to actual flight data, the analytical test cases will be corrupted with instrumentation noise and bias to provide insight into the flight test problems.

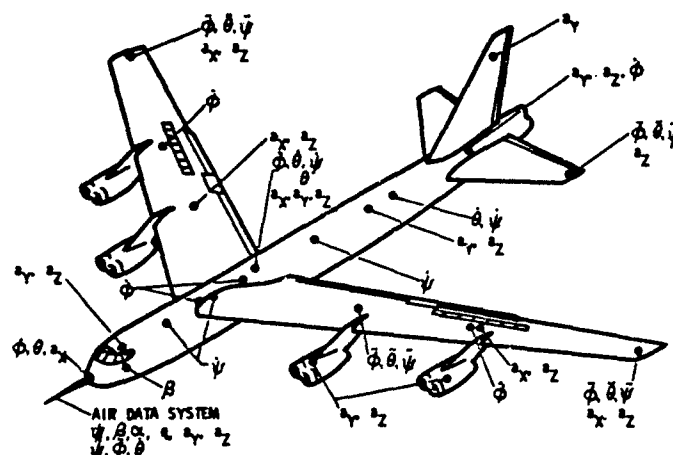


**Figure 5. Sensors Available on NB-52E CCV Aircraft**

The absence of realistic start-up data for  $\{p_0^*\}$  in equation (5) poses a difficult computational problem. Many of the parameters defined in equation (5) may be of small magnitude, difficult to estimate analytically and impossible to measure experimentally during wind tunnel tests of "rigid" and elastic models of the flight vehicle. Fortunately most of the parameters of importance are calculated analytically by existing aeroelastic stability and control methods. Also, the Modal Truncation formulation of the dynamics allows direct inclusions of the available wind tunnel measurements of "rigid" airplane stability and control derivatives. In addition, simpler estimation methods, such as least squares, may also prove of value to estimate  $\{p_0^*\}$ .



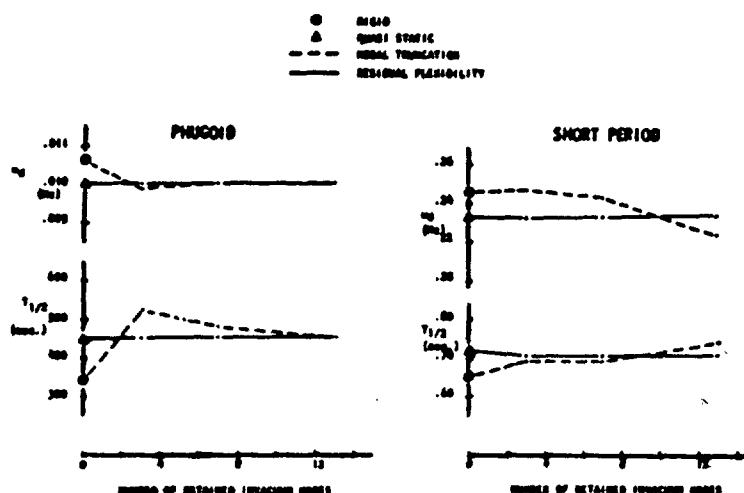


Figure 3. C-5A Center of Mass Dynamics, Unaugmented Aircraft, ALDCS Cruise Design Point 412301

Figure 2 illustrates the effect of static aeroelasticity on the derivatives; the theoretical estimate of the "rigid" C-5A derivatives are presented for contrast. The difference between the rigid and Quasi Static value of the derivative at zero "retained modes" is the elastic increment such as previously presented for the B-52E. Note in particular that the Modal Truncation formulation explicitly employs the rigid airplane derivative values regardless of the number of invacuum modes that are dynamically retained. In contrast, the Residual Flexibility formulation "adjusts" the value of all the derivatives for static elasticity depending upon the number of retained invacuum modes. As shown, the Residual Flexibility numbers vary strongly with the number of retained modes, eventually converging approximately to the Quasi Static value when all the dynamic aeroelastic effects of the invacuum modes are deleted.

Figure 3 illustrates a disadvantage of the Modal Truncation formulation when contrasted to other formulations. As shown, the phugoid and short period dynamics of the C-5A are dependent upon formulation. The most theoretically correct estimates shown in Figure 3 are the Quasi Static solution, at zero number of retained invacuum modes, and the Residual Flexibility solution at the other cases. The number of invacuum modes that must be retained to adequately represent the dynamics of the elastic aircraft in the Modal Truncation formulation is highly dependent upon the problem being analyzed and nearly always is larger than the number required for the Residual Flexibility formulation.

The Modal Truncation formulation has been selected by the Control Criteria Branch for the initial study of flexible airplane parameter estimation. As shown in Figures 2 and 3, its advantage is that the equations of motion for the body-fixed reference axis system contain explicit rigid airplane stability and control derivatives. In addition, it can be shown that the sensor equations of this formulation for the accelerometers are simpler than those of the other elastic airplane dynamics formulations and are also independent of the parameters being estimated. The disadvantage of the formulation is that it requires a substantial number of modes to represent both the static and dynamic aeroelastic effects of the invacuum modes. As examples of the number required, the C-5A Active Lift Distribution Control System (Reference 7) required from 6 to 15 modes, while the B-52E CCV Ride Control System (Reference 8) required as few as 5 to as many as 27 invacuum modes.

The linearized equations of symmetric motion for the elastic airplane may be written (Reference 2):

$$[F_{ij}]\{\ddot{Z}_j\} = [B_{ij}]\{\dot{Z}_j\} + [G_{ik}]\{\delta_k\} + [N_i], \quad i, j = 1, 4 + 2r; \text{ and } k = 1, 2c \quad (1a)$$

$$\{Z_j(t=0)\} = \{Z_j(0)\} \quad (1b)$$

where  $[F_{ij}]$ ,  $[B_{ij}]$ , and  $[G_{ik}]$  contain the aerodynamic elements to be estimated.

$\{Z_j\}$  is the state vector containing axis system motion and structural deformation rates.

$\{\delta_k\}$  is the control vector of position and rate.

$[N_i]$  is the process noise, such as atmospheric turbulence, and is assumed to be negligible in this analysis.

$r$  is the number of retained invacuum modal coordinates in the Modal truncation formulation.

$c$  is the number of actively moving control surfaces.

## 9. REFERENCES

1. Collection of Articles, National Aeronautics and Space Administration, Parameter Estimation Techniques and Applications in Aircraft Flight Testing, NASA TN D-7647, April 1974.
2. Schwanz, R., Wells, W., Air Force Flight Dynamics Laboratory, Estimation of Elastic Aircraft Parameters Using the Maximum Likelihood Method, pages 337-358, Reference 1.
3. Collection of Articles, The American Society of Mechanical Engineers, System Identification of Vibrating Structures, 1972.
4. Schwanz, R. C., Flight Control Division, Air Force Flight Dynamics Laboratory, Formulations of the Equations of Motion of an Elastic Aircraft for Stability and Control and Flight Control Applications, AFFDL-FGC-TM-72-14, August 1972.
5. Dornfeld, G. M., The Boeing Commercial Airplane Company, A Method for Predicting the Stability Characteristics of Control Configured Vehicles, Volume IV - B-52E Demonstration Case and Results, AFFDL-TR-74-91, Volume IV, November 1974.
6. Dusto, A. R., et al., The Boeing Commercial Airplane Company, A Method for Predicting the Stability Characteristics of Control Configured Vehicles, AFFDL-TR-74-91, Volumes I-IV, November 1974.
7. Margrove, W. J., The Lockheed Georgia Company, The C-5A Active Lift Distribution Control System, Paper Presented at NASA Sponsored Symposium on Advanced Control Technology and Its Potential for Future Aircraft, July 1974.
8. Stockdale, C. R., Poyneer, R. D., Flight Control Division, Air Force Flight Dynamics Laboratory, Control Configured Vehicle Ride Control System (CCV RCS), AFFDL-TR-73-83, July 1973.
9. Mehra, R., Taylor, J., Systems Control, Incorporated, Lecture Notes on Parameter Estimation Methods, Presented to AFFDL on 9-12 May 1972.

This Document  
Reproduced From  
Best Available Copy